Stony Brook University

Tumor-targeting Drug Delivery System of Anticancer Agent

A Dissertation Presented

by

Shuyi Chen

to
The Graduate School
in Partial Fulfillment of the
Requirements
for the Degree of

Doctor of Philosophy
in
Chemistry

Stony Brook University

May 2008

Stony Brook University

The Graduate School

Shuyi Chen

We, the dissertation committee for the above candidate for the Doctor of Philosophy degree, hereby recommend acceptance of this dissertation.

Iwao Ojima – Dissertation Advisor
Distinguished Professor, Department of Chemistry

Nicole S. Sampson – Chairperson of Defense
Professor, Department of Chemistry

Robert C. Kerber – Third Member
Professor, Department of Chemistry

George A. Ellestad – Outside Member
Senior Research Scientist, Department of Chemistry
Columbia University

This dissertation is accepted by the Graduate School

Lawrence Martin
Dean of the Graduate School

Abstract of the Dissertation

Tumor-targeting Drug Delivery System of Anticancer Agent

by

Shuyi Chen

Doctor of Philosophy

in

Chemistry

Stony Brook University

2008

Cancer has become the leading cause of death in the U.S. for people under the age of 85. Current cancer chemotherapy relies on the premise that tumor cells are more likely to be killed by the cytotoxic agents because of their rapidly proliferating. Unfortunately, many anticancer drugs cannot differentiate normal cells from tumor cells, which would

cause severe undesirable side effects. Accordingly, tumor-targeting drug delivery systems of anticancer agents have attracted extensive attention in cancer chemotherapy.

A novel molecular missile, where biotin was applied as a tumor-targeting ligand for receptor-mediated endocytosis, was explored for the efficient delivery of the anticancer agent, 2^{nd}-generation taxoid SB-T-1214. To further investigate the tumor-targeting process and drug release mechanism, several fluorescence-labeled drug conjugates were designed and synthesized. The cellular uptakes of these conjugates were assayed in a leukemia cancer cell line "L1210FR" by confocal fluorescence microscopy (CFM). The cytotoxicity of the tumor-targeting drug conjugate was also assayed against several different types of cells.

Additionally, single-walled carbon nanotube (SWNT) was introduced to this biotin-mediated drug delivery system. Functionalized SWNT can serve as efficient drug delivery platform for potential application to tumor-targeting chemotherapy, taking advantage of enhanced permeability and retention (EPR) effect associated with nanomaterials. We have unambiguously demonstrated the occurrence of the designed cancer-specific receptor-mediated endocytosis of the whole conjugate, followed by efficient drug release and binding of the drug to the target protein by confocal fluorescence microscopy (CFM) in the leukemia cell line "L1210FR". The cytotoxicity of these functionalized SWNT conjugates were assayed against several different types of cells. The results have unambiguously demonstrated the occurrence of the designed cancer-specific receptor-mediated endocytosis of the whole conjugate, followed by efficient drug release and binding of the drug to the target microtubules. The conjugate shows the specificity to the cells with their surface over-expressed with the biotin

receptor. The cytotoxicity of the conjugate comes from the released taxoid molecues inside the cells.

Table of Contents

List of Figures……viii

List of Schemes……xii

List of Tables……xiv

List of Abbreviations……xv

Acknowledgements……xix

Chapter I

Anticancer Drug Paclitaxel and β-Lactam Synthon Method

§1.1. INTRODUCTION: CANCER AND CANCER CHEMOTHERAPY 1
§1.2. ANTICANCER DRUG PACLITAXEL 2
§1.2.1. Discovery and Development 2
§1.2.2. The Biological Role of Paclitaxel 2
§1.2.3. The Production of Paclitaxel 5
§1.2.4. Structure-Activity Relationship (SAR) Studies 7
§1.3. β-LACTAM SYNTHON METHOD 8
§1.3.1. Introduction 8
§1.3.2. Results and Discussion 9
§1.3.2.1. Asymmetric Synthesis of Enantiopure β-Lactam *via* Chiral Ester Enolate-Imine Cyclocondensation 9
§1.3.2.2. Synthesis of Enantiopure β-Lactams *via* Staudinger Reaction Followed by Enzymatic Kinetic Resolution 11
§1.3.2.3. Synthesis of 2nd-Generation of Taxoids by β-LSM 13
§1.4. EXPERIMENTAL SECTION 15

Chapter II

Synthesis of C3'-Difluorovinyl Taxoid SB-T-12852

§2.1. INTRODUCTION 25
§2.2. RESULTS AND DISCUSSION 28
§2.2.1. Synthesis of 4-Difluorovinyl β-Lactam 28
§2.2.2. Synthesis of C3'-Difluorovinyl 2nd-Generation Taxoid SB-T-12852 29
§2.2.3. Biological Evaluation of Difluorovinal Taxoid SB-T-12852 29
§2.3. EXPERIMENTAL SECTION 30

Chapter III

Biotin-mediated Endocytosis of Fluorescein-labeled Anticancer Agent

§3.1. INTRODUCTION 34
§3.1.1. Tumor-Targeting Delivery of Cytotoxic Drug 34
§3.1.2. Tumor Recognition Moiety....36
§3.1.3. Cytotoxic Agents as Warhead....41
§3.1.4. Linker Pool....43
§3.2. RATIONAL DESIGN OF TUMOR-SPECIFIC PRODRUG 48
§3.2.1. Previous Achievements of Disulfide-Containing Prodrugs....48
§3.2.2. Novel Disulfide Linkers for Efficient Drug Release 50
§3.2.3. Biotin as Tumor Recognition Moiety 52
§3.2.4. Coupling Ready Warhead....54
§3.2.5. Fluorescent Probes for Evaluation of Intracellular Drug Release 55
§3.3. RESULTS AND DISCUSSION....59
§3.3.1. A New Class of Disulfide Linkers....59
§3.3.1.1. Synthesis of Disulfide-Containing Linkers 60
§3.3.1.2. Kinetic Study of Model Drug Release Profile....57
§3.3.2. Fluorescence-Tagged Molecular Probes....72
§3.3.2.1. Synthesis of Fluorescence-Tagged Molecular Probes....73
§3.3.2.2. *In Vitro* Evaluation of Fluorescence-Tagged Molecular Probes 76
§3.4. EXPERIMENTAL SECTION....83

Chapter IV

Functionalized SWNT (*f*-SWNT) as Transporter for Tumor-targeting Drug Delivery

§4.1. INTRODUCTION 100
§4.1.1. Nanomedicine 100
§4.1.2. Carbon Nanotubes (CNT)....107
§4.1.2.1. Toxicity and Pharmacological Studies of CNT:....108
§4.1.2.2. Surface Chemistry of CNT 110
§4.1.3. Functionalized CNT as Drug Delivery Platform 112
§4.2. RESULTS AND DISCUSSION....116
§4.2.1. Rational Design of *f*-SWNT as Transporter for Drug Delivery 116
§4.2.2. Syntheses and Structure Characterization of *f*-SWNT-based Conjugate....119
§4.2.3. Biological Evaluation of Functionalized *f*-SWNT-based Conjugate....125
§4.3. EXPERIMENTAL SECTION....134
§4.3.1. Syntheses of Functionalized SWNTs....134
§4.3.2. Confocal Microscopy, Flow Cytometry and Cytotoxicity Analysis....137
§4.4. PERSPECTIVE: COMBINATION CHEMOTHERAPY 138

List of Figures

Figure **Page**

Chapter I

Figure 1-1. Structure of Taxol® (paclitaxel) 2
Figure 1-2. The cell cycle and microtubule-targeting anticancer agent....3
Figure 1-3. Microtubule formation and mechanism of action of paclitaxel 4
Figure 1-4. Structure of 10-deacetylbaccatin III (10-DAB III) 5
Figure 1-5. Summary of SAR studies of paclitaxel 7
Figure 1-6. Whitesell's chiral auxiliary....8
Figure 1-7. Competition between direct ring-closure and isomerization 13
Figure 1-8. Taxoid derivatives....13
Figure 1-9. Representatives of 2nd-generation novel taxoids....14

Chapter II

Figure 2-1. Representatives of fluorinated drugs....25
Figure 2-2. Structure of SB-T-12842-4 and SB-T-128221-3 26
Figure 2-3. Structure of difluorovinyl 2nd-generation taxoids SB-T-12851, SB-T-12852, SB-T-12853, and SB-T-12854 27

Chapter III

Figure 3-1. Receptor-mediated endocytosis pathway....35
Figure 3-2. Tumor-activated prodrug 36
Figure 3-3. Tumor recognition moieties 37
Figure 3-4. Mylotarg® (gemtuzumab-ozogamicin) 38
Figure 3-5. DHA-taxoid drug conjugates 39
Figure 3-6. Folic acid-guided formulation with entrapped paclitaxel 39
Figure 3-7. Chemical structure of HPMA-HA-DOX bioconjugate....40
Figure 3-8. Chemical structure of AN-238 41
Figure 3-9. Representative cytotoxic agents commonly used in tumor-targeting drug delivery 42
Figure 3-10. Linker pool 44
Figure 3-11. BR96-Doxorubicin conjugate 45
Figure 3-12. BR96-monomethyl auristatin E (MMAE) conjugate....46
Figure 3-13. HuC242-DM1 conjugate....47
Figure 3-14. C225-paclitaxel conjugates 48
Figure 3-15. Antitumor activity of anti-EGFR mAb-taxoid immunoconjugates against A431 xenografts in SCID mice....49
Figure 3-16. Novel disulfide linkers 50
Figure 3-17. Proposed mechanism for 2nd-generation self-immolative disulfide linker ...51
Figure 3-18. Model reaction for the mechanism-based release profile 52
Figure 3-19. Chemical structure of biotin....53

Figure 3-20. Structure of the hetero-bifunctional intermediate 54
Figure 3-21. Examples of tumor-targeting drug conjugates bearing the novel self-immolative disulfide linkers.....55
Figure 3-22. Subcellular localization of fusion genes highlight organelles of interest with new colors 56
Figure 3-23. Commonly used fluorescent probes: fluorescein and coumarin derivatives 56
Figure 3-24. Fluorescent and flurogenic probes for the internalization and drug release.....57
Figure 3-25. Intracellular release of coumarin from fluorogenic probe biotin-linker-coumarin conjugate (3-53) 58
Figure 3-26. The fluorescence microscopy images of permealized and fixed H-460 cells by FITC-labeled (A) and rhodamine-labeled paclitaxel (B) staining ...58
Figure 3-27. Receptor-mediated endocytosis of the whole drug conjugate and the taxoid release mechanism 59
Figure 3-28. Structure of disulfide linkers with variable lengths 60
Figure 3-29. Utilization the *gem*-dimethyl effect to construct complicated macrocyclic molecules 63
Figure 3-30. Decreasing in angle between the two reacting terminuses when the *gem*-dimethyl functionality was introduced.....63
Figure 3-31. Structure of disulfide linkers with a *gem*-mono/dimethyl functionality on the benzilic position 63
Figure 3-32. Structure of disulfide linkers with substituents on aromatic ring 65
Figure 3-33. Structure of disulfide linkers with different S-S bonds.....65
Figure 3-34. Measurement of model drug release rate constant for disulfide linker (3-4).....68
Figure 3-35. Measurement of pH-dependent drug release profile for disulfide linker (3-4).....69
Figure 3-36. Measurement of *gem*-dimethyl effect on drug release for disulfide linker (3-28).....70
Figure 3-37. Measurement of substituent effect on drug release for disulfide linker (3-31).....72
Figure 3-38. Concentration-dependent cellular uptake of biotin-FITC conjugate (3-49).....77
Figure 3-39. Time-dependent cellular uptake of biotin-FITC conjugate (3-49).....78
Figure 3-40. Confocal fluorescent images and the flow cytometry analysis of L1210FR cells after incubation with biotin-FITC (3-49) under different conditions ...79
Figure 3-41. Epifluorescent image of L1210FR cells that are incubated with biotin-linker-coumarin (3-53) 80
Figure 3-42. Confocal fluorescent image of L1210FR cells that are incubated with prodrug biotin-linker-SB-T-1214-fluorescein conjugate (3-64) 81
Figure 3-43. CFM images and the flow cytometry analysis of different types of cells after incubation with biotin-linker-SB-T-1214-fluorescein (3-64) at the final concentration of 20 μM at 37 ^{o}C for 2 h 82

Chapter IV

Figure 4-1. Physiological characteristics of normal and tumor tissue 102
Figure 4-2. Transendothelial transportation mechanism of Abraxane delivery 103
Figure 4-3. Mechanism of action of lymphotropic superparamagnetic nanoparticles.....104
Figure 4-4. Transmission electron microscopy (TEM) images of semiconductor quantum dots 104
Figure 4-5. Structure of a multifunctional QD probe 105
Figure 4-6. Ten distinguishable emission colors of CdSe/ZnS QDs 105
Figure 4-7. Fluorescence micrographs of QD-stained cells and tissues 106
Figure 4-8. Different structures of graphite 107
Figure 4-9. SEM image of carbon nanotubes (CNTs) 107
Figure 4-10. CNT wrapped with macromolecules and a photo of DNA-functionalized SWNT solution in H_2O 110
Figure 4-11. Confocal fluorescent microscopy images of dual staining of endosomes in HL-60 cells revealed the endocytosis transportation mechanism of fluorescein-labeled SWNTs (SWNT-biotin-SA, on the left). 112
Figure 4-12. Epifluorescence images of Jurkat cells incubated with *f*-CNTs.....115
Figure 4-13. Biodegradable dendrimeric and polymeric drug delivery platforms 116
Figure 4-14. Monovalent binding of a drug (left) *versus* polyvalent binding of a virus (right) on a cell surface 117
Figure 4-15. Schematic illustration of three key steps involved in the tumor-targeting drug delivery of biotin-SWNT-taxoid conjugate (4-12) 119
Figure 4-16. TEM and AFM images of SWNTs 121
Figure 4-17. UV-visible spectra of SWNT-based conjugates 123
Figure 4-18. ATR-IR spectra of biotin-SWNT-FITC conjugate (4-11) 123
Figure 4-19. UV-visible spectra of SWNT and its conjugates 124
Figure 4-20. Photographs of vials containing SWNT conjugates in CH_2Cl_2 125
Figure 4-21. CFM images of L1210FR cells under different conditions 126
Figure 4-22. Comparison of fluorescence intensities of L1210FR cells by flow cytometry upon treatment with pristine SWNT (purple line), SWNT-FITC conjugate (4-4) (blue line) and biotin-SWNT-FITC (4-11) (red line) with the final concentration of 10 μg/mL at 37 °C for 3 h, in each case 127
Figure 4-23. CFM images and the flow cytometry analysis of L1210FR cells after incubation with SWNT-FITC conjugate (4-4) at the final concentration of 10 μg/mL under different conditions for 3 h 128
Figure 4-24. CFM images and the flow cytometry analysis of L1210FR cells after incubation with biotin-SWNT-FITC conjugate (4-11) at the final concentration of 10 μg/mL under different conditions for 3 h.....130
Figure 4-25. CFM images of L1210FR cells treated with biotin-SWNT-SB-T-1214-fluorescein (4-12) (final concentration: 50 μg/mL) at 37 ^{o}C for 3 h, incubated before and after the addition of glutathione ethyl ester 131
Figure 4-26. CFM images and the flow cytometry analysis of different types of cells after incubation with biotin-SWNT-SB-T-1214-fluorescein (4-12) at the final concentration of 50 μg/mL at 37 ^{o}C for 3 h 132

Figure 4-27. Results of MTT cytotoxicity assay of biotin-SWNT-SB-T-1214-fluorescein conjugate (4-12) on different cell lines 133
Figure 4-28. A two-drug combination therapy leads to the complete remission of a mouse model of B-cell lymphoma in all of the treated animals. In contrast, animals treated with either drug alone (rapamycin or doxorubicin) rarely experienced complete remission 139
Figure 4-29. Structure of HPMA copolymer-AGM-DOX conjugate as an example of polymer-drug combination chemotherapy.....140

List of Schemes

Scheme **Page**

Chapter I

Scheme 1-1. The first semisynthesis of paclitaxel....6
Scheme 1-2. Ojima's coupling protocol....6
Scheme 1-3. Retro-synthesis of taxane-based anticancer agents....8
Scheme 1-4. Lithium-chiral ester enolate-imine cyclocondensation....8
Scheme 1-5. [2+2] ketene-imine cycloaddition (Staudinger reaction)....9
Scheme 1-6. Synthesis of Whitesell's chiral auxiliary....9
Scheme 1-7. Synthesis of chiral TIPS-Ester....10
Scheme 1-8. Synthesis of (*3R,4S*)-4-isobutenyl-1-(*tert*-butoxycarbonyl)-3-[(triisopropylsilyl)oxy]azetidin-2-one....10
Scheme 1-9. Proposed mechanism of chiral ester enolate-imine condensation....11
Scheme 1-10. Synthesis of (*3R,4S*)-*cis*-3-ethoxyethoxy-4-phenylazetidin-2-one....12
Scheme 1-11. Synthesis of (*3R,4S*)-4-*iso*-butenyl-1-(*tert*-butoxycarbonyl)-3-[(triisopropylsilyl)oxy]azetidin-2-one....12
Scheme 1-12. Semisynthesis of 2nd-generation taxoid SB-T-1214 (1-23)....14

Chapter II

Scheme 2-1. Representative transformations of *N*-*t*-Boc-3-PO-4-R_f-β-lactams....26
Scheme 2-2. Synthesis of (3*R*, 4*S*)-*N*-Boc-3-TIPSO -4-difluorovinylazetidin-2-one....28
Scheme 2-3. Mechanism of 1,1-difluoroolefins formation....28
Scheme 2-4. Synthesis of C3'-difluorovinyl 2nd-generation taxoid SB-T-12852....29

Chapter III

Scheme 3-1. Preparation of mAb-12136 conjugate....49
Scheme 3-2. Mechanism-based taxoid release profile with ^{19}F NMR....52
Scheme 3-3. Synthesis of 4-fluorophenyl 2-(2-(methyldisulfanyl)phenyl)-acetate (3-4)....60
Scheme 3-4. Synthesis of 4-fluorophenyl 2-((methyldisulfanyl)methyl)-benzoate (3-9)....61
Scheme 3-5. Synthesis of 4-fluorophenyl 2-(2-((methyldisulfanyl)methyl)-phenyl) acetate (3-15)....61
Scheme 3-6. Utilization the *gem*-dimethyl effect to facilitate organic synthesis....62
Scheme 3-7. Synthesis of 4-fluorophenyl 2-(2-(methyldisulfanyl)phenyl) propanoate (3-22)....64
Scheme 3-8. Synthesis of 4-fluorophenyl 2-methyl-2-(2-(methyldisulfanyl)-phenyl)-propanoate (3-26)....64
Scheme 3-9. Original synthetic route towards the coupling-ready warhead conjugate (3-40)....66

Scheme 3-10. Utilization of an allyl-ester protecting group in the synthesis towards the coupling-ready warhead conjugate 66
Scheme 3-11. Synthesis of the coupling-ready warhead conjugate (3-40) with TIPS-ester protecting group....67
Scheme 3-12. Model reaction for rate constant determination using disulfide linker (3-4) 68
Scheme 3-13. Model reaction for drug release with different thiol-initiated fragmentation....69
Scheme 3-14. Model reaction of disulfide linker (3-28) with a *gem*-dimethyl functionality at the benzilic position....70
Scheme 3-15. Model reactions of substituent effect comparison 71
Scheme 3-16. Model reaction of S-S bond polarity comparison using the disulfide linker (3-34) 72
Scheme 3-17. Synthesis of biotin-FITC conjugate (3-49)....73
Scheme 3-18. Synthesis of biotin-linker-coumarin conjugate (3-53)....74
Scheme 3-19. Modification of fluorescein moiety 74
Scheme 3-20. Installation of fluorescein unit (3-57) onto the SB-T-1214 (1-23) 75
Scheme 3-21. Synthesis of the biotin-linker-SB-T-1214-fluorescein conjugate (3-64) 76
Scheme 3-22. Synthesis of biotin-linker-SB-T-1214 conjugate (3-65)....76

Chapter IV

Scheme 4-1. Chemical modification around the sidewalls and the end parts of CNTs 111
Scheme 4-2. Structure of the SWNT-Pt(IV) complex mediated with phospholipids-PEG conjugate....113
Scheme 4-3. Structure of some chemically functionalized SWNTs *via* 1,3-dipolar cycloaddition....114
Scheme 4-4. Structures of three fluorescently labeled *f*-SWNT-based conjugates 118
Scheme 4-5. Synthesis of SWNT-FITC conjugate (4-4). 120
Scheme 4-6. Synthesis of biotin-SWNT-FITC conjugate (4-11) 122
Scheme 4-7. Synthesis of biotin-SWNT-linker-SB-T-1214-fluorescein (4-12)....123

List of Tables

Table **Page**

Chapter II

Table 2-1. *In vitro* cytotoxicity (IC_{50} nM) of fluoro-taxoids 27
Table 2-2. *In vitro* cytotoxicity (IC_{50} nM) of C3'-difluorovinyl taxoids 30

Chapter III

Table 3-1. Mechanism-based taxoid release profile with HPLC analysis 52
Table 3-2. Relative uptake of vitamins in various tumor cell lines 54
Table 3-3. Substituent effects on the aromatic ring for drug release 71
Table 3-4. *In vitro* cytotoxicity of taxol, taxoid (SB-T-1214, 1-23) and biotin-linker-SB-T-1214 (3-65).....83
Table 3-5. IC_{50} value of the biotin-linker-SB-T-1214 (3-65) against different cell lines 83

Chapter IV

Table 4-1. Applications of nanomaterials to healthcare 101
Table 4-2. *In vivo* toxicity studies on different types of carbon nanotubes (CNTs) 109
Table 4-3. IC_{50} value of the biotin-SWNT-SB-T-1214-fluorescein conjugate (4-12) against different cell lines.....133

List of Abbreviations

10-DAB III	10-deacetylbaccatin III
Å	angstrom
Ac	acetyl
AcOH	acetic acid
AGM	aminoglutethimide
AML	acute myelogenous leukemia
Anal	analysis
atm	atmosphere
ATP	adenosine triphosphate
bd	broad doublet
Bn	benzyl
bp	boiling point
br	broad
bs	broad singlet
Boc	*tert*-butoxycarbonyl
t-Bu	*tert*-butyl
n-BuLi	*n*-butyllithium
Bz	benzoyl
Calcd	calculated
CAN	cerium(IV) ammonium nitrate
CDR	complementarity determining region
CFM	confocal fluorescence microscopy
CNT	carbon nanotube
CPT	camptothecin
CVD	chemical vapor deposition
d	doublet
DCC	*N,N*'-dicyclohexylcarbodiimide
DCM	dichloromethane
dd	doublet of doublet
DDS	drug delivery system
de	diastereomeric excess
DHA	docosahexaenoic acid
DIC	*N,N*-diisopropylcarbodiimide
DIPEA	*N,N*-diisopropylethylamine
DM1	methyldithio-maytansinoid
DMAP	4-*N,N*'-dimethylaminopyridine
DMF	*N,N*'-dimethylformamide
DMS	dimethyl sulfide
DMSO	dimethyl sulfoxide
DNA	deoxyribonucleic acid
DOX	doxorubicin
DTPA	diethylentriaminepentaacetic acid
DTT	dithiothreitol
EC_{50}	concentration of drug that produces 50 % effect

EDC.HCl	1-ethyl-3-(3-dimethylaminopropyl)carbodiimide hydrochloride
ee	enantiomeric excess
EE	ethoxyethyl
e.g.	for example
EGFR	epidermal growth factor receptor
EPR	enhanced permeability and retention
eq	equivalent
ESI	electrospray ionization
Et	ethyl
et al.	and others
EtOAc	ethyl acetate
EtOH	ethanol
EVE	ethyl vinyl ether
FDA	Food and Drug Administration
FITC	fluorescein isothiocyanate
F-SWNT	fluorinated single-walled carbon nanotube
f-SWNT	functionalized single-walled carbon nanotube
FTIR	fourier tranform infrared spectroscopy
g	gram
GC	gas chromatography
GI	gastrointestinal
GlcNAc	*N*-acetyl-D-glucosamine
GlcUA	D-glucuronic acid
GSH	glutathione
GSH-OEt	glutathione mono ethyl ester
GTP	guanosine 5'-triphosphate
h	hour
HA	hyaluronic acid
HATU	2-(1H-7-azabenzotriazol-1-yl)-1,1,3,3-tetramethyl uronium hexafluoro phosphate methanaminium
HEX	hexanes
HiPCO	high pressure carbon monoxide
HMPA	hexamethylphosphoramide
HOBT	1-hydrobenzotriazole hydrate
HOSu	*N*-hydroxysuccinimide
HPLC	high performance liquid chromatography
HPMA	*N*-(2-hydroxypropyl)methacrylamide copolymer
HRMS	high resolution mass spectrometry
Hz	hertz
IC_{50}	concentration for 50 % inhibition
i.e.	that is
*i*Pr	isopropyl
IR	infrared spectroscopy
J	coupling constant
K_d	dissociation constant
kDa	kilodalton

kg	kilogram
KHMDS	potassium 1,1,1,3,3,3-hexamethyldisilazide
L	liter
LC	liquid chromatography
LDA	lithium diisopropylamide
LiHMDS	lithium 1,1,1,3,3,3-hexamethyldisilazide
m	multiplet
M	molar or molarity
mAb	monoclonal antibody
MALDI–TOF	matrix-assisted laser desorption ionization time-of-flight
MAPs	microtubule associated proteins
MDR	multi-drug resistance
MDS	methyldisulfanyl
Me	methyl
MeOH	methanol
mg	milligram
MHz	megahertz
min	minute
mL	milliliter
MMAE	monomethyl auristatin E
mM	milimolar
mmol	millimole
mol	mole
mp	melting point
MPA	methylpyridinium acetate
MRI	magnetic resonance imaging
MS	mass spectrometry
MTD	maximum tolerated dose
MWNT	multi-walled carbon nanotube
NaHMDS	sodium 1,1,1,3,3,3-hexamethyldisilazide
NCI	National Cancer Institute
nM	nanomolar
NMO	*N*-methylmorpholine-*N*-oxide
NMR	nuclear magnetic resonance
PABC	*p*-aminobenzyloxycarbonyl
PBS	phosphate buffered saline
PDT	pyridyldithio
PEG	poly(ethylene glycol)
Pgp	P-glycoprotein
Ph	phenyl
PLAP	pig liver acetone powder
PMA	phosphomolybdic acid
PMP	*p*-methoxyphenyl
ppm	parts per million
PSMA	prostate-specific membrane antigen
p-TSA	*p*-toluenesulfonic acid

Py	pyridine
q	quartet
QD	quantum dot
rt	room temperature
s	singlet
SAR	structure-activity relationship
SCID	severe combined immunodeficiency
SPP	*N*-succinimidyl-4-(2-pyridyldithio)pentanoate
SST	somatostatin
SWNT	single-walled carbon nanotube
t	triplet
$t_{1/2}$	half time
TAP	tumor activated prodrug
TBDMS	*tert*-butyldimethylsilyl
TEA	triethylamine
TEM	Transmission electron microscopy
tert	tertiary
TES	triethylsilyl
Tf	triflouromethanesulfonate
TFA	trifluoroacetic acid
THF	tetrahydrofuran
TIPS	triisopropylsilyl
TLC	thin layer chromatography
TMS	trimethylsilyl
TOPO	trioctylphosphine oxide
TTM	tumor-targeting molecule
U.S.	United States
USDA	U.S. Department of Agriculture
U-tube	ultra short carbon nanotube
UV	ultraviolet-visible
wt	weight
[α]	specific optical rotation
β-LSM	β-Lactam Synthon Method
δ	chemical shift
μg	microgram
μL	microliter
μM	micromolar
μm	micrometer
μmol	micromole

Acknowledgments

I would like to first express my true gratitude to my dissertation advisor Professor Iwao Ojima, for his incessant and invaluable guidance during my Ph.D. study. Professor Ojima set the perfect example of scientist with his persistent pursuit of excellence and ingenious insights of research. Professor Ojima's continuous support and never-ending encouragement have brought out the best in me, making my graduate study at Stony Brook the most memorable years of my life.

Besides, I would like to thank the committee members: Professor Nicole S. Sampson and Professor Robert C. Kerber, the chair and third member of my committee, respectively. Their help as well as insightful comments throughout my advancement in the Ph.D. program have been truly invaluable. I would also like to thank Doctor George A. Ellestad from Columbia University, for taking time out of his busy schedule to be the fourth member of my committee.

I would like to thank all the faculty members at Stony Brook University for their valuable classes and discussions. Special thanks go to my collaborators, Professor Stanislaus Wong, Dr. Jin Chen, Xianrui Zhao, and Dr. Jingyi Chen, who have shared their expertise in various disciplines with me and made great contribution in a variety of aspects of my research at Stony Brook.

A special thank go to our NMR specialist, Mr. James Marecek, for his kind assistance in NMR spectroscopy and many insightful discussions on my research. I thank Mrs. Katherine Hughes, Student Affairs Coordinator, for her warm-hearted assistance in a variety of matters during my stay at Stony Brook.

I want to express my true appreciation to all of the past and present members of Professor Ojima's group for their support throughout my Ph.D. study at Stony Brook. I would like to thank Dr. Xinyuan Wu, Dr. Zihao Hua, Dr. Larisa Kuznetsova, Dr. Antonella Pepe, Dr. Wen-Hua Chiou, Dr. Bruno Chapsal, Dr. Qing (Sunny) Huang, Dr. Jin Chen, Dr. Greta Varchi, Dr. Bibia Bennacer, Dr. Hojae Choi, Dr. Claude Commandeur, Dr. Stanislav Jaracz, Dr. Seung Yub Lee, Ilaria Zanardi, Xianrui Zhao, Liang Sun, Yuan Li, Ce Shi, Manisha Das, Stephen Chaterpaul, Gary Yu-Han Teng, Kunal Kumar, Joseph Junior Kaloko, Corey Chi-Feng Lin, and Edison S. Zuniga for their

valuable discussions as well as warm relationships. Special thanks go to Joseph Junior Kaloko for taking his time to carefully proof read this dissertation.

I also want to thank Ms. Yoko Ojima for her gracious hospitality and kindness. Very special thanks go to Mrs. Patricia Marinaccio, our Project Staff Assistant, who is also known as the "Mom" of the Ojima Group. I want to thank her for always being there for me and making me feel like at home when I am away from home.

I am most grateful to my family, especially my wife Yuan Li, for their encouragement, support and love. You believed in me, encouraged me and always, always stood by me.

Finally, I acknowledge financial support from the National Institutes of Health, National Cancer Institute, and the Department of Chemistry at Stony Brook.

Chapter I
Anticancer Drug Paclitaxel and β-Lactam Synthon Method

§ 1.1. Introduction: Cancer and Cancer Chemotherapy

Cancer is a major public health problem worldwide with an estimate of over six million new cases per year. According to "Cancer Facts and Figures 2005", an annual cancer statistics report by the American Cancer Society, cancer has surpassed heart disease and become the leading cause of death in the U.S. for people under the age of 85.[1] In the year 2006, about 1,399,790 new cancer cases are expected to be diagnosed in the united states. It is estimated that 1 in 3 Americans will suffer from cancer in their lifetime and 1 in 5 will die from it.

Cancer is the collective name referring to a group of complex diseases characterized by uncontrolled growth and spread of abnormal cells. These cells can invade other tissues, either by direct growth into adjacent tissue through invasion or by implantation into distant sites by metastasis. Cancer can be caused by both hereditary (hormones, immune conditions, and inherited mutations) and environmental (chemicals, radiation, and viruses) factors, resulting in the damage to DNA and causing mutations to genes that encode for proteins controlling cell division.

Nowadays, cancer can be treated by surgery, radiation therapy, hormonal suppression, chemotherapy and immunotherapy. The choice of therapy depends on the location and grade of the tumor and the stage of the disease, as well as the condition of the patient. Usually, cancer has more than ten years of latency period.[2] Early detection of cancer would greatly increase the survival rate. If the growth of tumor remains localized, cancer is usually treated by surgery or radiation therapy. However, in the cases that cancer has already metastasized, *i.e.* tumor spawns cells that break away from the parent mass and spread to distant sites in body, chemotherapy is the only hope for patients to survive.

In cancer chemotherapy, medicines also known as anticancer drugs are administered to kill the cancer cells. Most chemotherapeutic drugs are taken orally or intravenously. Most often, combination chemotherapy is applied because when two or more drugs are administered at the same time, each drug can target in its own way to attack growing cancer cells and stop the growth cycle. The side effects from chemotherapy are the potential damage of those healthy normal cells, especially fast dividing cells such as those responsible for hair growth and for replacement of the intestinal epithelium. The common side effects in chemotherapy are nausea and vomiting, hair loss, skin rash, fatigue, lowered white blood cell counts, increased susceptibility to infection, bleeding and bruising.

§ 1.2. Anticancer Drug Paclitaxel

§ 1.2.1. Discovery and Development

In the early 1960's, the U. S. National Cancer Institute (NCI) initiated a collaboration program with the U.S. Department of Agriculture (USDA) to screen 35,000 plant species for anticancer activity.[3] In 1966, the U.S. Forest Service sent crude extracts taken from the bark of the pacific yew tree (*Taxus brevifolia*) to the NCI and the initial screenings of these extracts indicated tumor inhibitory properties and potent cytotoxicity against mouse leukemia.[3] However, it took another 5 years for Dr. Wani and co-workers to isolate the pure active component of the extracts and characterized the chemical structure of this compound in 1971.[4] This novel anticancer agent was then named after "Taxol®" (paclitaxel). Between 1960 and 1981, paclitaxel had been proved to be the most attractive and interesting compound from more than 110,000 samples collected and assayed.

Taxol® (paclitaxel), is a natural diterpenoid compound, possessing a tetracyclic framework including an oxetane D-ring with an *N*-benzoylphenylisoserine side chain attached to the C-13 hydroxy group. There are 11 chiral centers and 14 oxygen atoms present in the molecule. The chemical structure of Taxol® (paclitaxel) is shown in Figure 1-1.

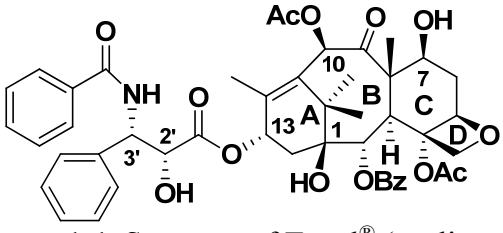

Figure 1-1. Structure of Taxol® (paclitaxel).

§ 1.2.2. The Biological Role of Paclitaxel

It is very important to understand the formation and cellular functions of micruotubules before interpreting the mechanism of action of paclitaxel. Microtubule is a major structural component of the cell and performs critical functions in cellular division and cytoskeleton formation. Paclitaxel was originally thought to be a typical spindle poison similar to the vinca alkaloids.[5] These drugs shared a similar mode of action by inhibiting the polymerization of tubulins to form microtubules, which disrupts the cell division cycle and eventually results in cell apoptosis. However, in 1979, Horwitz and co-workers[6,7,8] discovered that paclitaxel possessed a unique mechanism of action. Instead of inhibiting the tubulin polymerization, paclitaxel actually promoted the polymerization, stabilized the resulting microtubules and prevented depolymerization thereby inhibiting the normal dynamic reorganization of microtubular network required for mitosis, which eventually induced cell apoptosis. Figure 1-2 illustrates the cell cycle and the role of microtubule-targeting anticancer agent.[3]

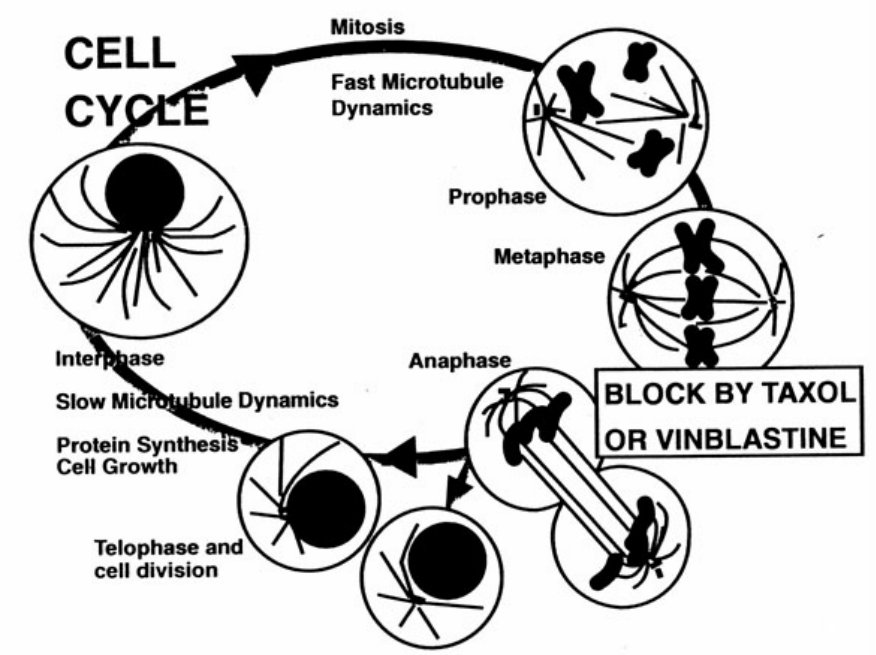

Figure 1-2. The cell cycle and microtubule-targeting anticancer agent.[3]

Cells have a characteristic life cycle that could be divided into two major stages: *interphase* and *Mitosis*, where microtubules and chromosomes rearrange to form two daughter cells. During *interphase*, the size of the cell increases as new proteins are synthesized and the genetic material is duplicated, under slow microtubule dynamics. After passage through critical checkpoints, the cell enters *mitosis*, where the actual cell division occurs. *Mitosis* can be further subdivided into several small phases based on cellular activity. *Prophase* is the first stage, where the duplicated chromatin condenses into chromosomes, each composed of two identical chromatids. At this point, the centrosome splits into two daughter centrosomes, which will constitute the spindle poles of the dividing cell at a later time. Afterward, spindles, which are composed of microtubules, begin to radiate out from each centrosome to enter the nucleus as the nuclear membrane breaks down. The cell cycle enters the stage of the *metaphase,* when the spindles attach themselves onto the sets of chromosomes and help align them along the "equator" of the cell. In the stage of *anaphase*, the pairs of chromosomes slowly separate and are pulled towards their respective centrosomes, facilitated by the contracting microtubules to which they are attached. It is between *metaphase* and *anaphase* that microtubule-targeting agents such as paclitaxel or vinca alkaloids disrupt the regular dynamics required for *mitosis*. As a result of this mitotic block, apoptosis or programmed cell death is eventually induced. As the cycle enters *telophase*, the nuclear envelope reforms around each set of chromosomes and the cell membrane pinches off to form the two daughter cells, which can either enter the quiescent G_0 phase or re-enter the cell cycle.[2]

The mechanism of action of paclitaxel was further investigated by Horwitz[6,7] at the molecular level. They claimed that paclitaxel enhanced the rate, extent, and nucleation phase of tubulin polymerization and stabilized the microtubules. The paclitaxel treated stabilized microtubules were found to be resistant to usual depolymerization conditions

of either low temperature (4 ^{o}C) or 4 mM $CaCl_2$ solution. Figure 1-3 summarizes the process of microtubule formation and the mechanism of action of paclitaxel.[6] Microtubules are primarily composed by the dimerization of two polypeptide subunits, *i.e.* α- and β-tubulin with a molecular weight of about 50 kDa each. In the presence of magnesium ions, guanosine 5'-triphosphate (GTP), and microtubule-associated proteins (MAPs), the α- and β-tubulins form dumbbell-shaped heterodimers, which would grow both along and perpendicular to the axis until the two edges join to form a microtubule composed of 13 protofilaments with an average diameter of about 24 nm. In contrast, paclitaxel binds to the α,β–tubulin heterodimer aggregate in a 1:1 ratio to promote the polymerization and stabilize the resulting microtubules, either in the presence or the absence of GTP, MAPs, and magnesium ion. The microtubule formed is quite different from that produced by MAP induction in that only 12 protofilaments are present with an average diameter of about 22 nm, and is irreversibly stabilized to regular microtubule depolymerization conditions (calcium ions or cooling to 4 ^{o}C).[3]

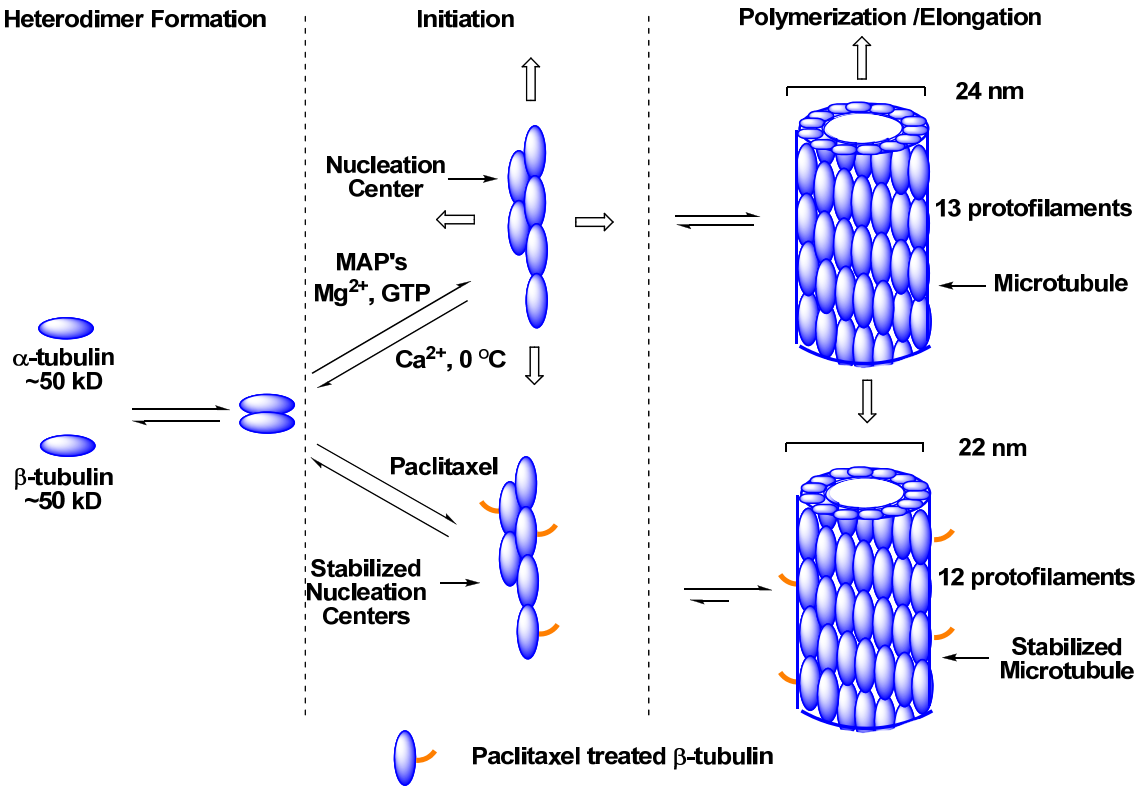

Figure 1-3. Microtubule formation and mechanism of action of paclitaxel.[6]

Paclitaxel has attracted extensive pharmacological and clinical studies due to its unique mechanism of action and novel structure. It has been approved by the U.S. Food and Drug Administration (FDA) for the treatment of different cancer diseases: including ovarian cancer (1992), breast cancer (1994), Kaposi's sarcoma (1997) and lung cancer (1998). Phase II and III clinical trials for other cancers, such as colon, prostate, head and neck cancers, in addition to combination therapy with other chemotherapeutics, are currently in progress.

Taxotere® (docetaxel, a semisynthetic analog of paclitaxel), developed by Rhône-Poulenc Rorer (now Sanofi-Aventis) following from the discoveries of Pierre Potier, was also approved by the FDA for the treatment of breast cancer (1996), non-small cell lung cancer (1999), and most recently for head and neck cancer (2006). Paclitaxel and docetaxel are currently two of the most successful anticancer drugs on the market.

§ 1.2.3. The Production of Paclitaxel

Despite such an overwhelming worldwide medical success, large-scale clinical trials were initially hampered by the limited supply of the drug.[9] Paclitaxel was isolated from the bark of the Pacific yew tree (*Taxus brevifolia*, a slow-growing tree), which made it a limited and non-renewable source.[10] Approximately 3,000 yew trees would be sacrificed to obtain 1 Kg of paclitaxel (0.01% yield). Accordingly, alternative methods of production of paclitaxel had to be explored in order to secure a sustainable supply of this novel anticancer drug.

Chemical approaches have been extensively explored in the past decades. Total syntheses of paclitaxel have been accomplished by six research groups (Holton,[11,12] Nicolaou,[13,14,15,16] Danishefsky,[17] Wender,[18,19] Kuwajima,[20] Mukaiyama[21]). Unfortunately, from a practical point of view, none of these processes offered feasibility in large scale manufacturing.

Fortunately, in 1980, the isolation of 10-deacetylbaccatin III (10 DAB-III) (Figure 1-4) from the leaves of the European yew tree (*Texus baccata*, 1 g/ 1 Kg of fresh leaves), which is a renewable source, provided the long-term supply of paclitaxel and its congeners *via* semisynthesis.[3] 10 DAB-III comprised the complex tetracyclic framework of paclitaxel without the C-13 isoserine side chain. Accordingly, long-term supply of paclitaxel and its analogues were ensured by attaching the chiral C-13 side chain to the properly modified 10 DAB-III baccatin core. Indeed, novel taxoids with superior activity and better pharmacological properties have been explored. Several excellent reviews on this topic have been reported in the literature.[3,22]

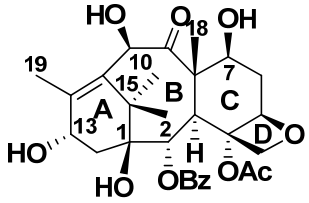

Figure 1-4. Structure of 10-deacetylbaccatin III (10-DAB III).

The first semisynthesis of paclitaxel utilizing 10-DAB III was reported by Potier and Greene in 1988.[23] They found that each of the four hydroxyl groups on the baccatin core exhibited different activities, which allowed for the step-wise protection at C-7 and C-10 positions sequentially, following by the esterification of the C-13 hydroxyl group with (2*R*,3*S*)-*N*-benzoyl-phenylisoserine as shown in Scheme 1-1. The isoserine acid was synthesized in 8 steps with a modest 80 % ee (later improved to 98 %[24,25]), from *trans*-cinnamyl alcohol. However, due to the highly hindered environment at the C-13 hydroxyl group, the esterification of the C-13 hydroxyl group with the protected chiral side chain precursor only gave the protected paclitaxel in 80 % yield based on 50 %

conversion, even under harsh conditions (73 °C, 100 h). Additionally, significant epimerization at the C-2' position was observed.

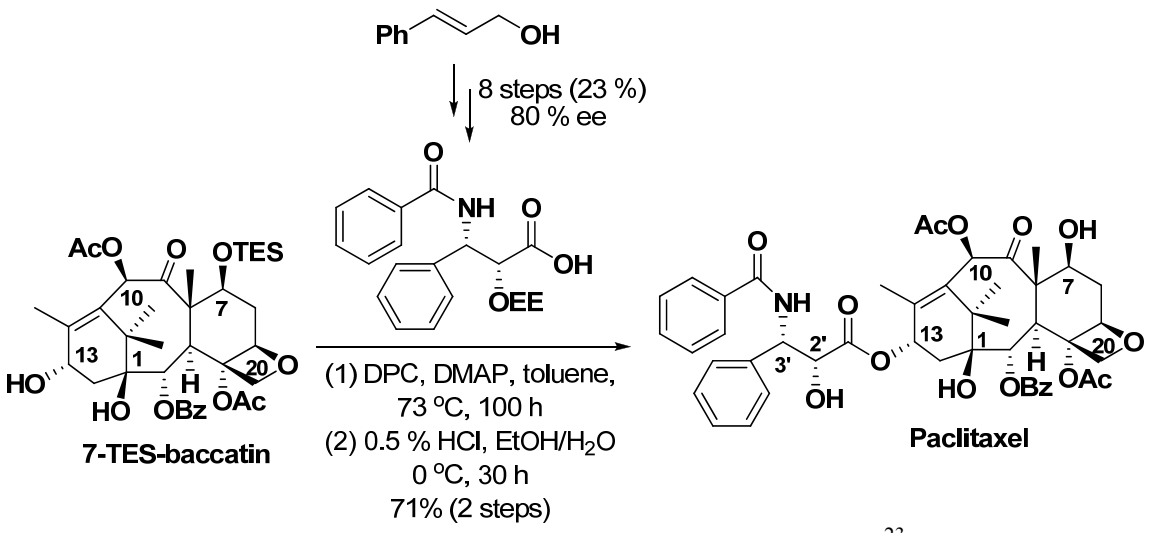

Scheme 1-1. The first semisynthesis of paclitaxel.[23]

Since then, numerous efforts have been made toward the semisyntheses of paclitaxel, *i.e.* Holton oxazinone coupling,[26] Ojima-Holton β-lactam coupling,[27,28] Commercon oxazolidinecarboxylic acid coupling,[29] and Kingston oxazolinecarboxylic acid coupling[30]. Among these coupling methods, the Ojima-Holton β-lactam coupling (Scheme 1-2) has been the most efficient semisynthetic method for the preparation of paclitaxel and other novel taxoids for SAR studies. With this practical and efficient semisynthesis protocol, ring-opening coupling of *N*-acyl-β-lactams with 13-*O*-metalated derivatives of 7-TES-baccatin III in the presence of strong bases, such as NaH, *n*-BuLi, LDA, LiHMDS, NaHMDS, and KHMDS, was realized in excellent yield. The highly enantiopure β-lactam (3*R*,4*S*)-4-phenylazetidin-2-one could be obtained either *via* a highly efficient lithium chiral ester enolate-imine cyclocondensation or [2+2] ketene-imine cycloaddition (Staudinger reaction), which will be covered later in this chapter.

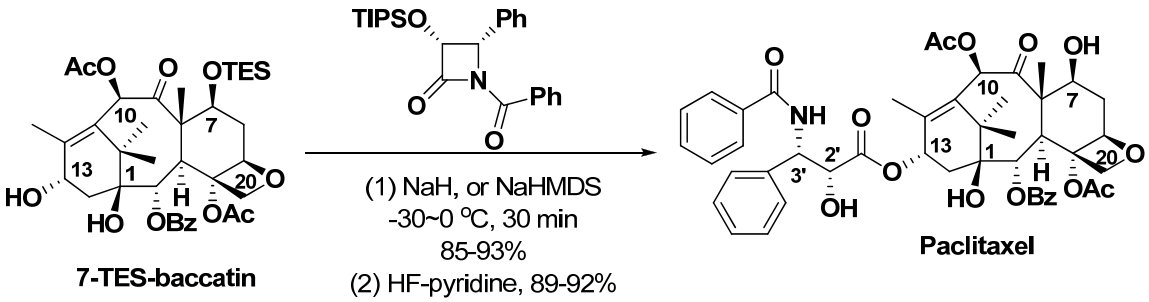

Scheme 1-2. Ojima's coupling protocol.

§ 1.2.4. Structure-Activity Relationship (SAR) Studies

The efficient semisynthesis protocol of paclitaxel was truly critical. It not only assured the sufficient supply of this important anticancer drug, but also offered a practical route to explore the structure-activity relationship (SAR) studies of paclitaxel analogues and the development of new generation taxoids with better pharmacological profiels.[31,32,33] The SAR studies results of paclitaxel are summarized in Figure 1-5.[2]

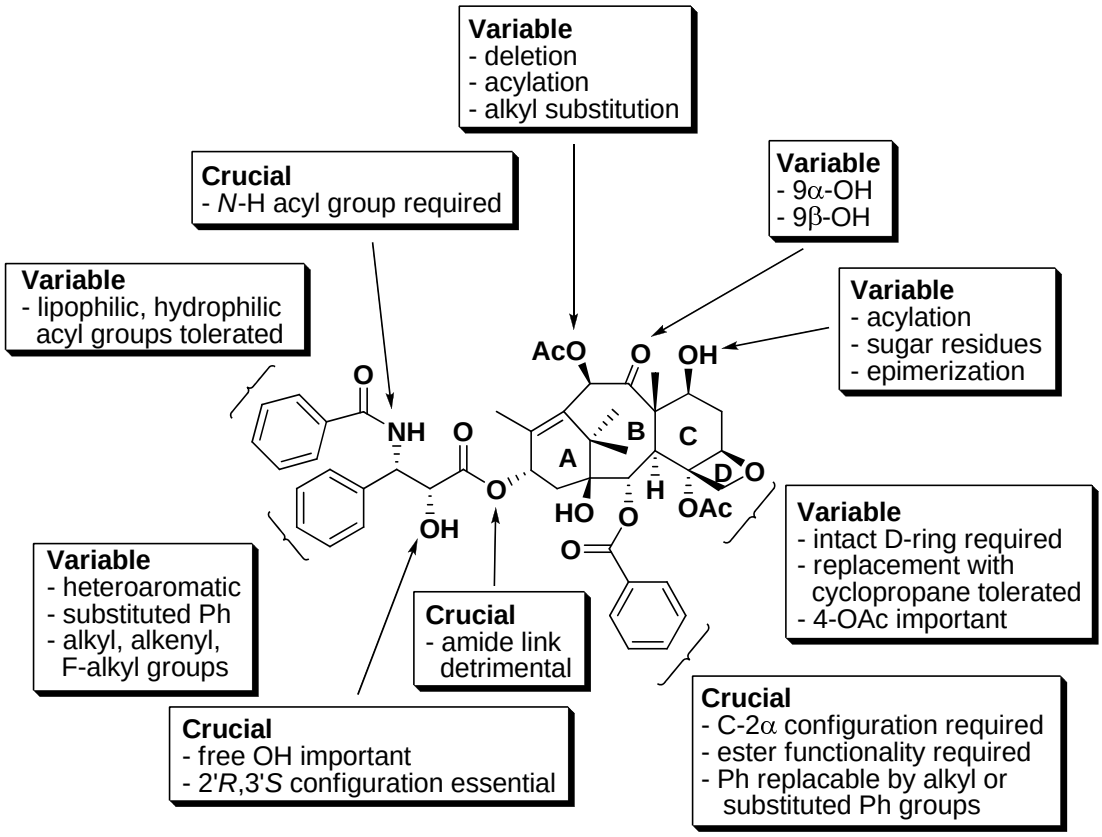

Figure 1-5. Summary of SAR studies of paclitaxel.[2,34]

§ 1.3. β-Lactam Synthon Method (β-LSM)

§ 1.3.1. Introduction

The β-Lactam skeleton has attracted significant research interest in medicinal and synthetic chemistry over the past decades.[35] β-Lactam antibiotics, such as penicillin and cephalosporin, have a long history in combating bacterial infections.[36] Recently, β-lactams have been reported to be versatile intermediates for the syntheses of unnatural amino acid, peptides and peptide turn mimetics,[37] heterocycles[38] and other types of compounds with biological interest.[39] Additionally, through 1980s and 1990s, Ojima *et al.* successfully developed the "*β-lactam Synthon Method (β–LSM)*" and demonstrated that enantiopure β-lactams could also serve as versatile intermediates for the semisynthesis of taxane-based anticancer agents (Scheme 1-3).[40]

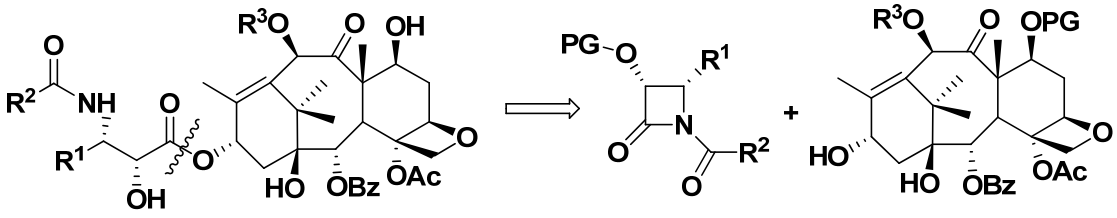

Scheme 1-3. Retro-synthesis of taxane-based anticancer agents.

A variety of synthetic protocols have been reported for the synthesis of β-lactams,[41,42] including hydroxamate cyclization[43] and chromium carbene-imine reaction[44]. Among these approaches, enolate-imine cyclocondensation[27] and ketene-imine cycloaddition (also known as Staudinger reaction)[42] were the two most widely used methods to construct the azetidin-2-one ring. The lithium-chiral ester enolate-imine cyclocondensation protocol (Scheme 1-4), developed by Ojima *et al.* in 1992, involved the use of Whitesell's chiral auxiliary ((-)-*trans*-2-phenylcyclohexanol, Figure 1-6) to control the enantioselectivity, but was then eliminated in the cyclocondensation step. The final β-lactam products were obtained in good yield and high enantiomeric purity.[27]

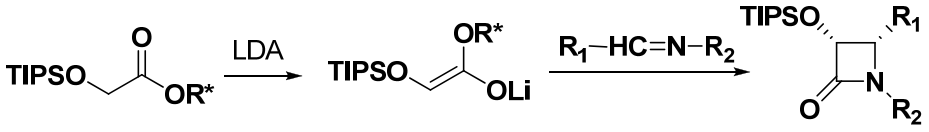

Scheme 1-4. Lithium-chiral ester enolate-imine cyclocondensation.

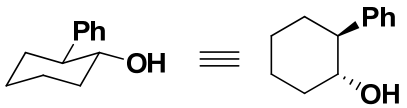

Figure 1-6. Whitesell's chiral auxiliary.

The second widely used method for the construction of the β-lactam skeleton is [2+2] ketene-imine cycloaddition (also known as Staudinger reaction) from readily available Schiff bases and ketenes.[42] The approach is initiated with *in situ* generation of the ketene from an acyl chloride in the presence of base, followed by a nucleophilic attack of imine to the ketene to form a zwitterionic intermediate, which undergoes an electrocyclic conrotatory ring closure to give the racemic azadiene ring (Scheme 1-5).[42] This reaction proceeds without a catalyst and its reaction rate mainly depends on the nucleophilicity of the imine. The racemic products can be separated by enzymatic kinetic resolution with PS-amano lipase. PS-amano lipase preferentially hydrolyzes the acetate moiety at C-3 of the (3*S*,4*R*) enantiomer of racemic β-lactam and affords (+)-β-lactam in high enantiopurity.[45] This reaction is compatible with a large number of functionalities on *N* and C-4 postitions.

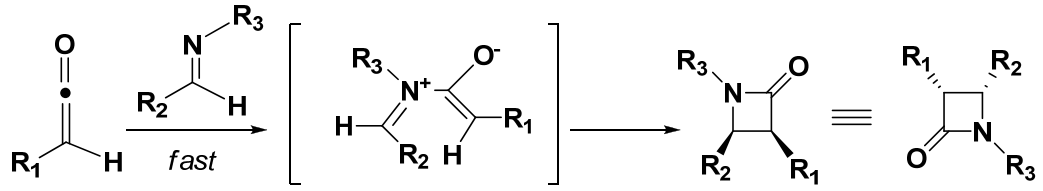

Scheme 1-5. [2+2] ketene-imine cycloaddition (Staudinger reaction).

§ 1.3.2. Results and Discussion

§ 1.3.2.1. Asymmetric Synthesis of Enantiopure β-Lactams *via* Chiral Ester Enolate-Imine Cyclocondensation

In the protocol of chiral ester enolate-imine cyclocondensation, TIPS-ester **(1-7)** was synthesized first. CuI-catalyzed ring opening of cyclohexene oxide with phenylmagnesium bromide provided racemic *trans*-2-phenylcyclohexanol **(1-1)**. After acetylation of the alcohol, enzymatic kinetic resolution of the racemic acetate **(1-2)** using pig liver acetone powder (PLAP) afforded Whitesell's chiral auxiliary **((-)-1-3)**[46] in good yield. (Scheme 1-6)

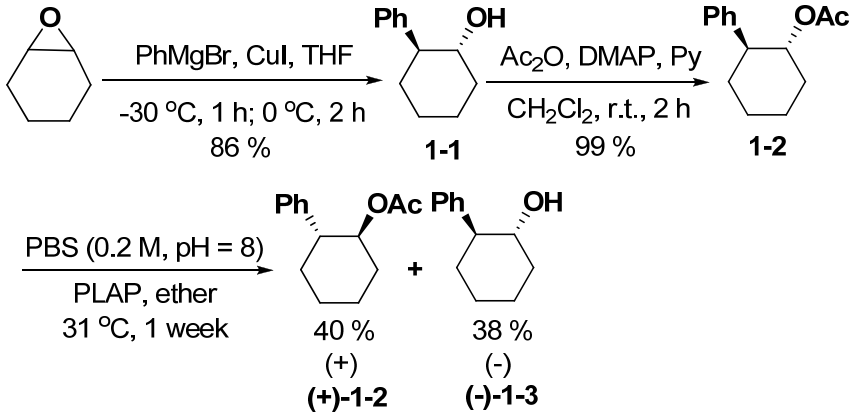

Scheme 1-6. Synthesis of Whitesell's chiral auxiliary.

The reaction of bromoacetic acid with the sodium alkoxide of benzyl alcohol gave benzyloxyacetic acid **(1-4)**, which was then reacted with chiral alcohol **(1-3)** to yield ester **(1-5)**. Hydrogenolysis, followed by TIPS protection of the resulting alcohol gave the chiral TIPS-ester **(1-7)** in good overall yield. (Scheme 1-7)

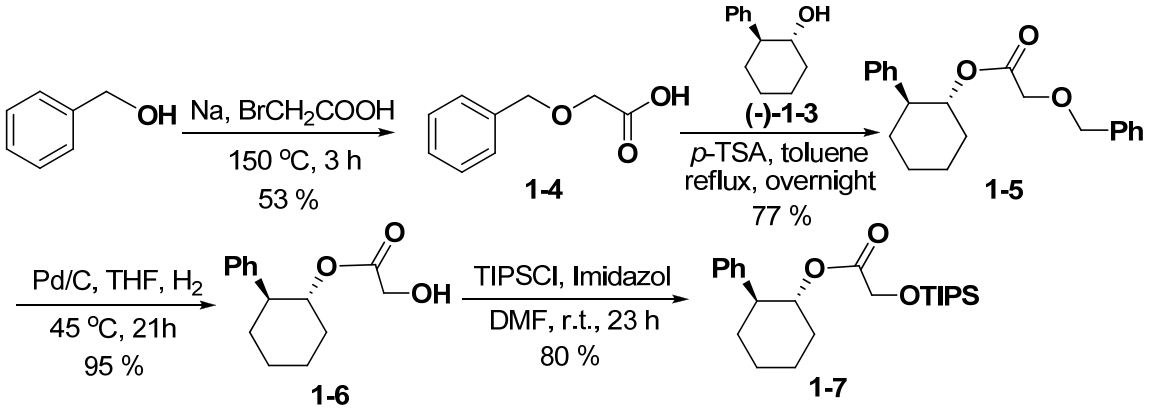

Scheme 1-7. Synthesis of chiral TIPS-Ester.

To synthesize the *p*-methoxyphenyl (PMP) β-lactam **(1-9)**, 3-methylbut-2-enal was first reacted with *p*-anisidine in methylene chloride to generate *N*-*p*-methoxy-phenyl-*iso*-butenylaldimine **(1-8)**. The (*E*)-enolate was prepared by slowly adding TIPS ester **(1-7)** in THF to LDA at very low temperature, and was then reacted with the *N*-*p*-methoxyphenyl-iso-butenaldimine **(1-8)** to yield enantiopure β-lactam **(1-9)**. The *p*-methoxy phenyl group was then removed by ceric ammoniumnitrate (CAN) oxidation in aqueous acetonitrile. Subsequent standard acylation with *tert*-butyldicarbonate anhydride gave the desired β-lactam **(1-11)**. (Scheme 1-8)

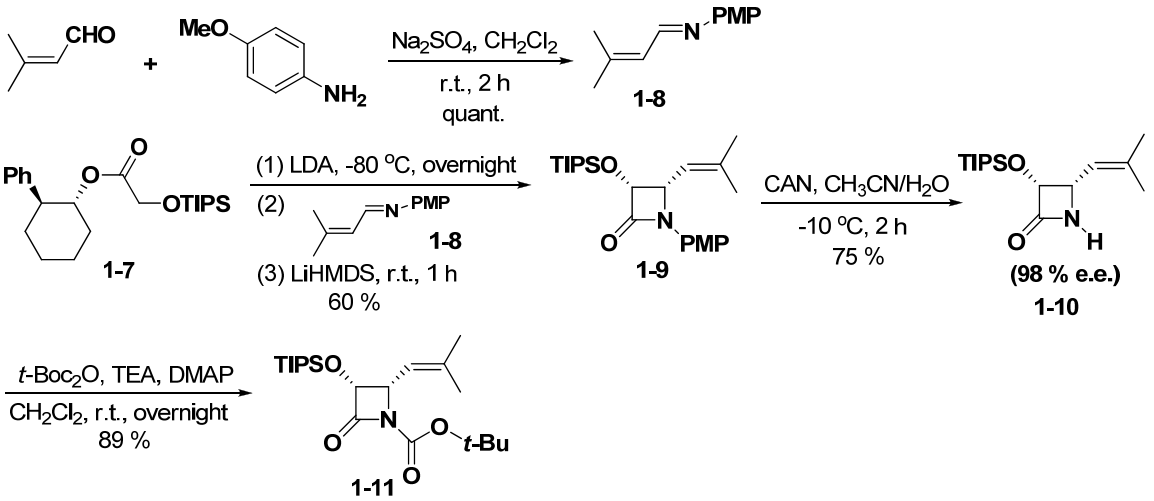

Scheme 1-8. Synthesis of (*3R,4S*)-4-isobutenyl-1-(*tert*-butoxycarbonyl)-3-[(triisopropylsilyl)oxy]azetidin-2-one.

The selective formation of (*3R,4S*)-*cis*-*β*-lactam with high enatiomeric purity could be explained by the 6-membered-ring transition state proposed in Scheme 1-9.[47] At low temperature, (*E*)-enolate was predominantly formed and the initial enolate addition to

imine would occur from the least hindered face, thus forming the enantiopure β-amino ester intermediate, which could be isolated upon quenching the reaction. When warmed up to room temperature, this intermediate cyclized to give the enantiopure β-lactam with release of the chiral auxiliary.

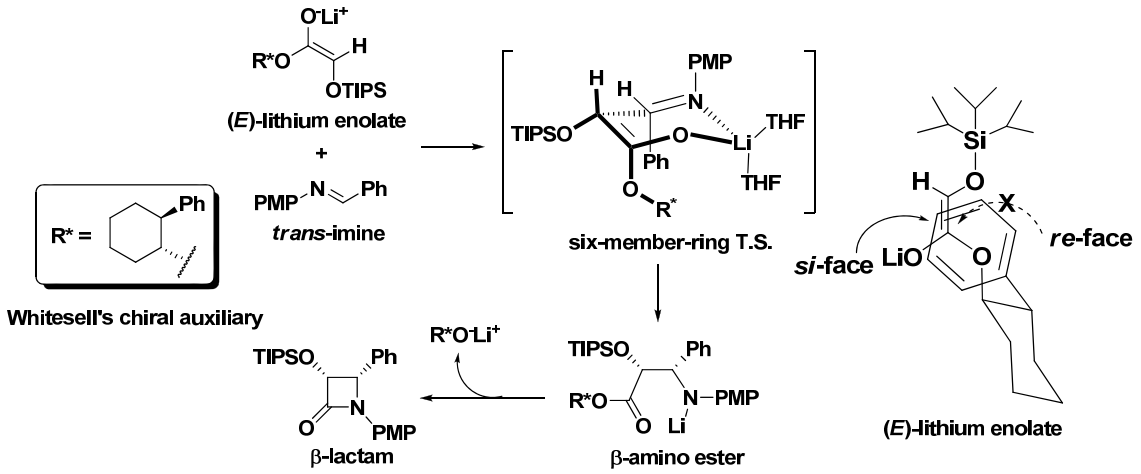

Scheme 1-9. Proposed mechanism of chiral ester enolate-imine condensation.

§ 1.3.2.2. Synthesis of Enantiopure β-Lactams *via* Staudinger Reaction Followed by Enzymatic Kinetic Resolution

Recently, there has been increasing interest in the use of hydrolytic enzymes to produce optically active compounds. In particular, lipases have been widely used for the kinetic resolution of racemic alcohols and carboxylic esters.[45] These lipases also catalyzed highly enantioselective cleavage of the β-lactam ring to yield derivatives of (*2R,3S*)-phenylisoserine in high enantiomeric excess. The resolved enantiomers were important intermediates in the synthesis of the C-13 side chain of paclitaxel. The commercial availability and relative stability of the lipases made them an attractive class of catalysts for affecting industrial-scale kinetic resolution processes.

Acetoxyacetyl chloride, in the present of a tertiary amine, reacted with an imine to give the corresponding racemic β-lactam. It was shown that PS-amano lipase preferentially hydrolyzed the acetate moiety at C-3 of the (*3S,4R*) enantiomer of **(1-13)**.[48] A common approach for improving the biocatalytic reaction rates of water-insoluble substrates was the use of co-solvent. In this case, 10 % CH_3CN was used as co-solvent to improve the rate and the enantioselectivity of the reaction. The *p*-methoxyphenyl group was removed by ceric ammonium nitrate (CAN) oxidation. The acetoxy group was hydrolyzed to give **(1-16)**, which was then protected with EE group (1-ethoxyethyl) to yield **(1-17)**. Since the 1-ethoxyethyl group was relatively small in size, it was anticipated that it would facilitate the coupling reaction of β-lactam to baccatin (Scheme 1-10).

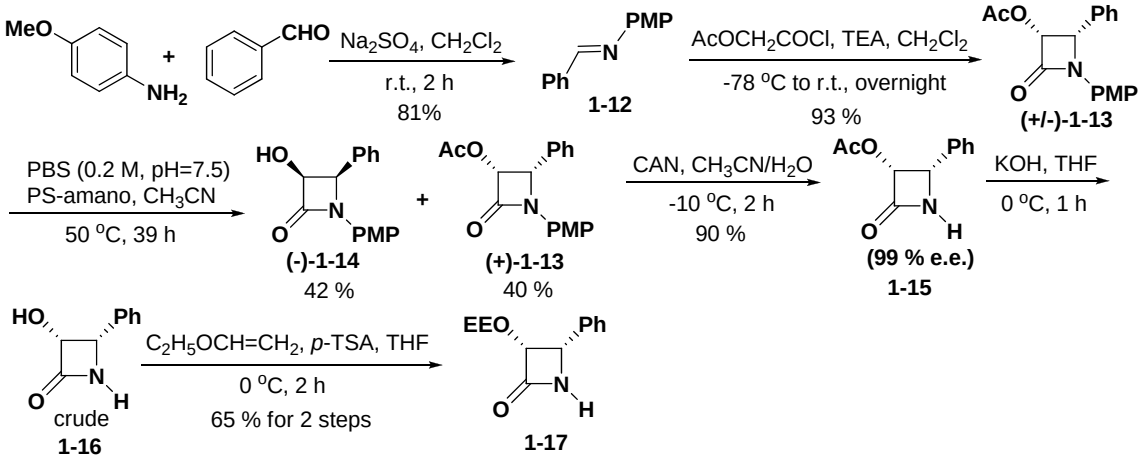

Scheme 1-10. Synthesis of (*3R,4S*)-*cis*-3-ethoxyethoxy-4-phenylazetidin-2-one.

The 4-*iso*-butenyl *β*-lactam can also be synthesized *via* a similar protocol (Scheme 1-11).

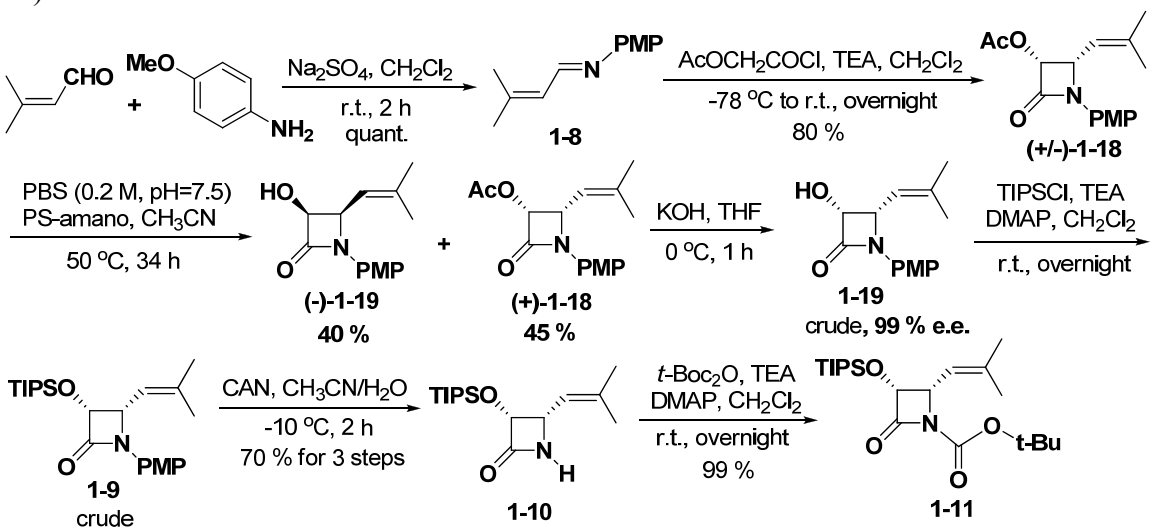

Scheme 1-11. Synthesis of (*3R,4S*)-4-*iso*-butenyl-1-(*tert*-butoxycarbonyl) -3-[(triisopropylsilyl)oxy]azetidin-2-one.

During the [2+2] ketene-imine cycloaddition, competition between the direct ring-closure and the isomerization of the imine in the zwitterionic intermediate controlled the relative stereoselectivity. (Figure 1-7)[49] The ring closure step was obviously affected by the electronic effect of the ketene and imine substituents. Electron-donating ketene substituents and electron-withdrawing imine substituents were found to accelerate the direct ring closure, leading to a preference for *cis*-β-lactam formation.

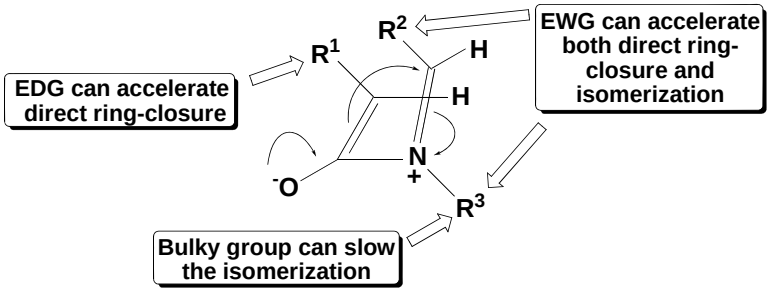

Figure 1-7. Competition between direct ring-closure and isomerization.

§ 1.3.2.3. Synthesis of 2nd-Generation Taxoids by β-LSM

Taxol® (paclitaxel) and its semisynthetic analog Taxotére® (docetaxel) are two of the most important drugs in cancer chemotherapy.[33] Both of the drugs have shown excellent anti-tumor activity against various cancer cell lines, and have been approved by the FDA for the treatment of several different types of cancers. However, recent reports demonstrate that treatment with these drugs often result in various undesired side effects and multi-drug resistance (MDR).[50] Accordingly, it is essential to develop novel taxoids with diminished side effects, superior pharmacological properties, and higher activities against various classes of tumors, especially against drug-resistant human cancers.

Through collaboration with world-leading experts in oncology, pharmacology, cell biology, hematology, and toxicology, extensive structure-activity relationship (SAR) studies on paclitaxel, docetaxel, as well as on a series of highly active 2nd-generation taxoids were explored by Ojima and coworkers, as summarized in Figure 1-8.[51,52,53,54,55,56,57,58]

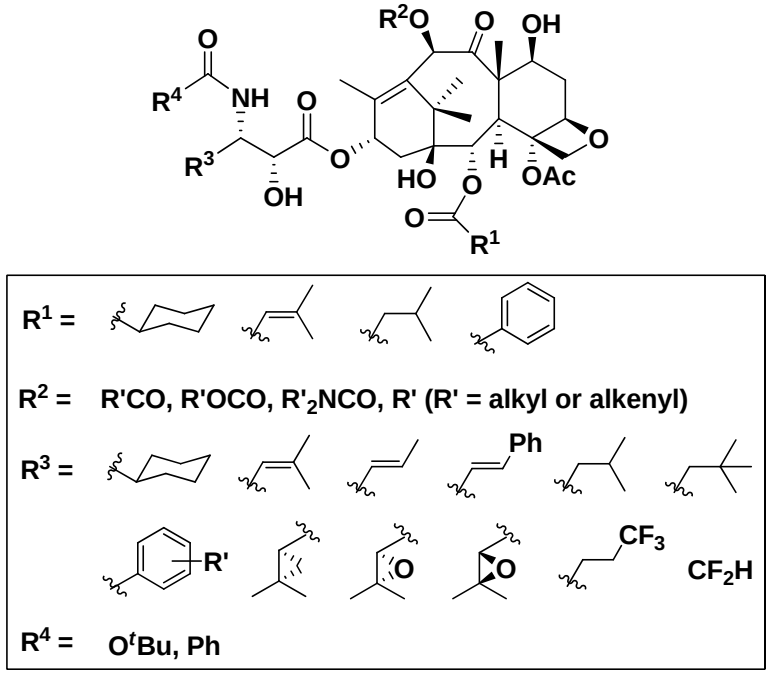

Figure 1-8. Taxoid derivatives.

It has been shown previously that these 2nd-generation taxoids possessed one order of magnitude higher potency than paclitaxel and docetaxel against drug-sensitive cancer cell lines, and 2-3 orders of magnitude higher potency than their parent compounds against drug-resistant cell lines expressing MDR phenotypes. These SAR study have disclosed three key factors responsible for the strong anticancer activity of these novel taxoids: (1) the presence of a *tert*-butoxycarbonyl group at C-3'-*N* instead of benzoyl group; (2) the replacement of C-3' phenyl with an alkenyl or alkyl group; and (3) proper modification at C-10 position. **SB-T-1213**,[59] **SB-T-1214** [59] and **SB-T-101131** (IND5109)[60] are three representatives of these series of taxoids (Figure 1-9).

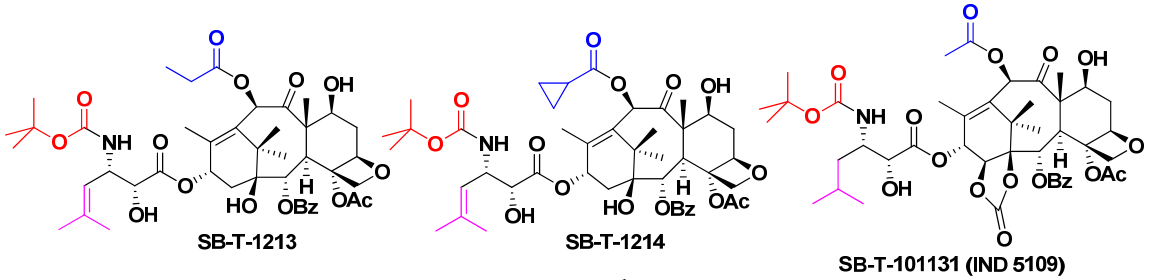

Figure 1-9. Representatives of 2nd-generation novel taxoids.

Scheme 1-12 outlined the semisynthesis of 2nd-generation taxoid SB-T-1214 **(1-23)**.[59] Starting from the natural product 10-DAB III, a selective protection of the C-7 OH using three equivalents of triethylsilyl chloride (TESCl) and 4 equivalents of imidazole in dimethylformamide (DMF) solution gave the desired 7-TES-10-DAB **(1-20)**, which was then treated with lithium bis(trimethylsilyl)amide (LiHMDS) at -40 °C, followed by the addition of cyclopropanyl carbonyl chloride to afford C-10 modified baccatin **(1-21)**. In the presence of LiHMDS, the β-lactam was coupled with modified baccatin **(1-21)** *via* Ojima-Holton coupling protocol to afford protected taxoid **(1-22)**. Following by deprotection of silyl group using HF-pyridine condition gave taxoid SB-T-1214 **(1-23)** in excellent overall yield.

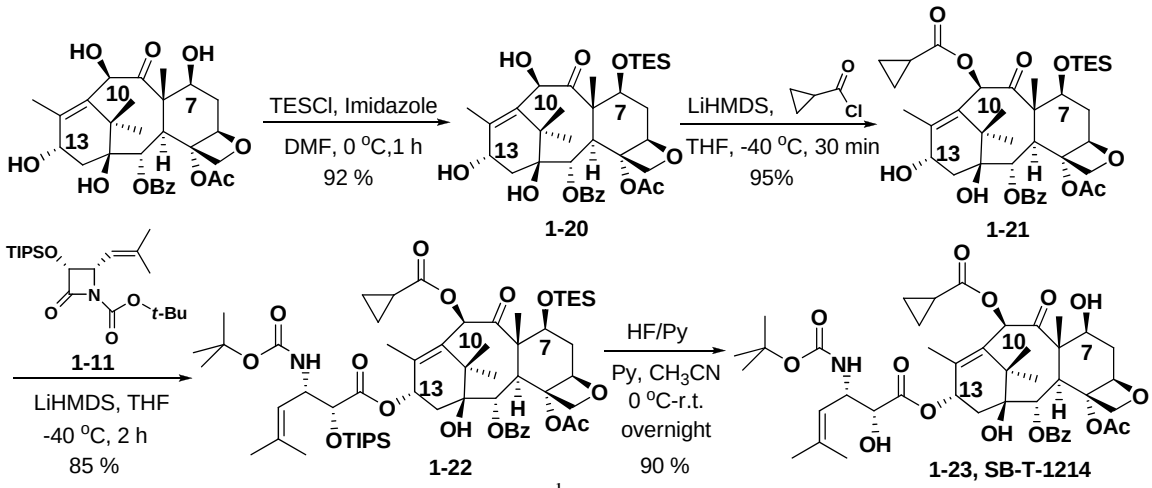

Scheme 1-12. Semisynthesis of 2nd-generation taxoid SB-T-1214 **(1-23)**.

§ 1.4. Experimental Section

General Methods: ^{1}H, ^{13}C and ^{19}F NMR spectra were measured on a Varian 300, 400, 500, or 600 MHz NMR spectrometer. The melting points were measured on a "Uni-melt" capillary melting point apparatus from Arthur H. Thomas Company, Inc.. Optical rotations were measured on a Perkin-Elmer Model 241 polarimeter. High-resolution mass spectrometric analyses were conducted at the Mass Spectrometry Laboratory, University of Illinois at Urbana-Champaign, Urbana, IL. GC-MS analyses were performed on an Agilent 6890 Series GC system equipped with the HP-5HS capillary column, (50 m X 0.25 mm, 0.25 um) and with the Agilent 5973 network mass selective detector. LC-MS analyses were carried out on an Agilent 1100 Series Liquid Chromatograph Mass Spectrometer. IR spectra were measured on a Shimadzu FTIR-8400s spectrophotometer. TLC analyses were performed on Merck DC-alufolien with Kieselgel 60F-254 and were visualized with UV light in 10 % sulfuric acid-EtOH or 10 % PMA-EtOH solution. Column chromatography was carried out on silica gel 60 (Merck; 230-400 mesh ASTM). Chemical purity was determined with a Waters HPLC or shimazu HPLC, using a Phenomenex Curosil-B column, employing CH_3CN/water as the solvent system with a flow rate of 1 mL/min. Chiral HPLC analysis for the determination of enantiomeric excess was carried out with a Waters HPLC assembly, comprising Waters M45 solvent delivery system, Waters Model 680 gradient controller, Water M440 detector (at 254 nm) equipped with a Spectra Physics Model SP4270 integrator. The system uses a DAICEL-CHIRACEL OD chiral column (25 x 0.46 cm i.d.), employing hexane/2-propanol as the solvent system with a flow rate of 1.0 ml/min.

Materials: The chemicals were purchased from Sigma Aldrich Company, Fischer Company or Acros Organic Company. 10-Deacetyl baccatin III (10-DAB III) was donated by Indena, SpA, Italy. Dichloromethane and methanol were dried before use by distillation over calcium hydride under nitrogen or argon. Ether and THF were dried before use by distillation over sodium-benzophenone kept under nitrogen or argon. Toluene and benzene were dried by distillation over sodium metal under nitrogen or argon before use. Dry DMF was purchased from EMD chemical company, and used without further purification. PURE SOLVTM, Innovative technology Inc, provided an alternative source of dry toluene, THF, ether, and dichloromethane. The reaction flasks were dried in a 110 ^{o}C oven and allowed to cool to room temperature in a desiccator over "*Drierite*" (calcium sulfate) and assembled under inert gas nitrogen or argon atmosphere.

Racemic *trans*-2-phenylcyclohexanol [(±)-1-2]:[47]

A solution of phenylmagnesium bromide in 100 mL of THF was prepared from magnesium (4.71g, 0.194 mol) and bromobenzene (20 mL, 0.196 mol) using standard condition. After cooling the Grignard solution to -30 ^{o}C, CuI (1.68 g, 8.82 mmol) was added. The resulting solution was stirred for approximately 10 min, and a solution of cyclohexene oxide **(**13.3 mL, 0.133 mol) in 133 mL of THF was added dropwise over a period of 1 h. The reaction mixture was then allowed to warm up to 0 ºC and stirred for an additional 2 h. The reaction was quenched at 0 ºC with saturated aqueous NH_4Cl solution and extracted with ethyl acetate. The organic layer was washed with saturated

aqueous NH_4Cl solution until there was no longer any color change in the aqueous layer. The combined aqueous layers were extracted with ether and the combined organic layers dried over anhydrous $MgSO_4$, filtered and concentrated *in vacuo*. Recrystallization from hexanes gave white needle solid (20.15 g, 86 %). mp: 57-58 °C. ^{1}H NMR (300 MHz, $CDCl_3$) δ 1.25-1.53 (m, 4 H, H on C2, C4, OH), 1.62 (s, 1 H, H on C6), 1.76 (m, 1 H, H on C3), 1.84 (m, 2 H, H on C3), 2.11 (m, 1 H, H on C6), 2.42 (ddd, *J* = 16.6, 10.8, 5.4 Hz, 1 H, H on C2), 3.64 (ddd, *J* = 16.6, 10.8, 5.4 Hz, 1 H, H on C1), 7.17-7.35 (m, 5 H, H on benzene ring). All data are in agreement with literature values.[47]

Racemic *trans*-2-phenylcyclohexyl acetate [(±)-(1-3)]:[47]
To a solution of 4-dimethylaminopyridine (DMAP) (0.277 g, 3.14 mmol), pyridine (5.00 mL), racemic alcohol **(1-2)** (18.38 g, 0.105 mol) in 15 mL CH_2Cl_2, was added dropwise a solution of acetic anhydride (11 mL) in 18 mL CH_2Cl_2 over a period of 2h. The reaction was then poured into a mixture of 32 mL 6 *N* HCl, 48 mL ice and 100 mL ether. The organic layer was washed with 2 *N* HCl aqueous solution and the combined aqueous layers were extracted with ether. The combined organic layers were washed with saturated aqueous $NaHCO_3$ solution and dried over anhydrous $MgSO_4$, filtered and concentrated *in vacuo* to afford pale yellow oil **(**22.62 g, 99.4 %). ^{1}H NMR (300 MHz, $CDCl_3$) δ 1.35 (m, 1 H, H on C4), 1.41 (m, 1 H, H on C4), 1.46 (m, 1 H, H on C2), 1.56 (m, 1 H, H on C6), 1.74 (s, 3 H, H on CH_3), 1.78 (m, 1 H, H on C3), 1.84 (m, 1 H, H on C3), 1.93 (m, 1 H, H of C6), 2.65 (ddd, *J* = 16.6, 11.0, 5.4 Hz, 1 H, H on C2), 4.98 (ddd, 1 H, H on C1), 7.17-7.35 (m, 5 H, H on benzene ring). All data are in agreement with literature values.[47]

(+)-*trans*-2-Phenylcyclohexyl acetate [(+)-1-3] and (-)-*trans*-2-phenylcyclohexanol [(-)-1-2]:[47]
To 1.2 L of 0.5 M aqueous buffer with pH = 8 (KH_2PO_4/K_2HPO_4) was added racemic acetate **(1-3)** (22.08 g, 0.101 mol) in 85 mL of ether at 31 ºC. After stirring for 30 min, 4.9 g of pig liver acetone powder (PLAP) was added. The mixture was stirred for 7 days at 31 ºC, until ^{1}H NMR of the crude organic layer showed <50/50 ratio of alcohol and acetate. The reaction mixture was quenched by acidifying to pH = 4 with 2 *N* HCl solution. To the resulting mixture was added 200 mL ether with stirring for 1 h. After the PLAP was allowed to settle, the supernatant organic layer was removed (addition of ether and removal of the organic layer was repeated 3 times). The organic and aqueous layers were filtered and the aqueous layer was extracted with ether. The combined organic layers were dried over anhydrous $MgSO_4$, filtered and concentrated *in vacuo*. The residue was purified by flash column chromatography on silica using hexanes and ethyl acetate to afford acetate as yellow oil (8.83 g, 40 %) and pure alcohol as a white solid (8.39 g, 38 %). mp: 63-64 ºC. ^{1}H NMR (300 MHz, $CDCl_3$) δ 1.25-1.53 (m, 4 H, H on C2, C4, OH), 1.62 (s, 1 H, H on C6), 1.76 (m, 1 H, H on C3), 1.84 (m, 2 H, H on C3), 2.11 (m, 1 H, H on C6), 2.42 (ddd, *J* = 16.6, 10.8, 5.4 Hz, 1 H, H on C2), 3.64 (ddd, *J* = 16.6, 10.8, 5.4 Hz, 1 H, H on C1), 7.17-7.35 (m, 5 H, H on benzene ring). All data are in agreement with literature values.[47]

Benzyloxyacetic acid (1-4):[2]
At room temperature, sodium metal (6.75 g, 0.293 mol) was added gradually to benzyl alcohol (110 mL, 1.06 mol) with stirring. After most of the sodium had reacted, the mixture was heated to 150 ºC and complete disappearance of the sodium was observed. At this point, bromoacetic acid (17.74 g, 0.129 mol) in 25 mL of THF was added dropwise. The reaction mixture was stirred at 150 ºC for 3 h and then cooled to room temperature. Cold water was added and the two layers separated. The aqueous layer was carefully extracted with dichloromethane to remove any remaining benzyl alcohol. The water layer was acidified with 10 % HCl to a pH of 2-3 and extracted with ether. The organic layer was then dried over magnesium sulfate, filtered and concentrated *in vacuo*. The oil residue was distilled under reduced pressure to afford **(**10.56 g, 92 %) as colorless oil. bp: 138-140 ºC (0.3 mm Hg); ^{1}H NMR (300 MHz, $CDCl_3$) δ 4.17 (s, 2 H, H on benzyl group), 4.67 (s, 2 H, H on C1), 7.38 (m, 5 H, H on benzene ring). All data are in agreement with literature values.[2]

(*1R, 2S*)-(-)-2-Phenylcyclohexyl benzyloxyacetate (1-5):[2]
A solution of (-)-*trans*-2-phenylcyclohexanol (0.5 g, 2.8 mmol), benzyloxyacetic acid (0.495 g, 3.0 mmol) and a catalytic amount of *p*-toluenesulfonic acid (*p*-TSA) in 20 mL of toluene was refluxed overnight. The toluene was evaporated *in vacuo* and the reaction mixture was diluted with ether and washed with saturated aqueous $NaHCO_3$. The organic layer was dried over $MgSO_4$, filtered and concentrated *in vacuo* to afford a white solid (0.544 g, 77 %). mp: 52-53 ºC; ^{1}H NMR (400 MHz, $CDCl_3$) δ 1.26-1.63 (m, 4 H, H on C2,C4,C6), 1.76-1.99 (m, 3 H, H on C3,C5,C6), 2.10-2.20 (m, 2 H, H on C6), 2.70 (dt, J = 11.0, 4.1 Hz, 1 H, H on C2), 3.73 (d, J = 16.5 Hz, 1 H, H on acetic acid), 3.84 (d, J = 16.5 Hz, 1 H, H on acetic acid), 4.25 (s, 2 H, H on benzyl group), 5.13 (td, J = 11.0Hz, 4.1 Hz, 1 H, H on C1), 7.16-7.39 (m, 10 H, H on benzene ring). All data are in agreement with literature values.[2]

(*1R, 2S*)-(-)-2-Phenylcyclohexyl hydroxyacetate (1-6):[2]
A mixture of 10 % palladium on carbon (Pd-C) (0.120 g) and (-)-benzyloxyacetate **(1-5)** (0.540 g, 1.66 mmol) in 5.6 mL of THF was stirred overnight at 45 ^{o}C under hydrogen. The reaction mixture was filtered through celite and concentrated *in vacuo* to afford a white solid (0.420 g, 95 %). mp: 59-60 ºC; ^{1}H NMR (300 MHz, $CDCl_3$) δ 1.30-1.66 (m, 4 H, H on C2,C4,C6), 1.78-2.00 (m, 3 H, H on C3,C5,C6), 2.10-2.20 (m, 2 H, H on C6), 2.67 (dt, J = 11.0, 4.2 Hz, 1 H, H on C2), 3.72 (d, J = 17.0 Hz, 1 H, H on acetic acid), 3.93 (d, J = 17.0 Hz, 1 H, H on acetic acid), 5.07 (td, J = 11.0 Hz, 4.2 Hz, 1 H, H on C1), 7.16-7.32 (m, 5 H, H on benzene ring). All data are in agreement with literature values.[2]

(*1R, 2S*)-(-)-2-Phenylcyclohexyl triisopropylsilyloxyacetate (1-7):[2]
To a solution of imidazole (0.285 g, 4.24 mmol) and hydroxy-acetate **(1-6)** (0.407 g, 1.79 mmol) in 8.2 mL of DMF was added chlorotriisopropyl-silane (TIPSCl) (0.52 mL, 2.46 mmol). The reaction was stirred under nitrogen for 24 h, quenched with water, and extracted with ether. The organic layer was washed several times with water and brine, dried over magnesium sulfate, filtered and concentrated in *vacuo*. The oil residue was distilled under reduced pressure to afford colorless oil (0.544 g, 80 %). bp: 195-205 ºC (0.8 mm Hg); ^{1}H NMR (300 MHz, $CDCl_3$) δ 0.94-1.25 (m, 21 H, H on TIPS group),

1.35-1.70 (m, 4 H, H on C2,C4,C6), 1.80-2.05 (m, 3 H, H on C3,C5,C6), 2.10-2.20 (m, 1 H, H on C6), 2.70 (dt, *J* = 11.0 Hz, 4.2 Hz, 1 H, H on C2), 3.91 (d, *J* = 16.5 Hz, 1 H, H on acetic acid), 4.08 (d, *J* = 16.5 Hz, 1 H, H on acetic acid), 5.07 (td, *J* = 11.0, 4.2 Hz, 1 H, H on C1), 7.16-7.30 (m, 5 H, H on benzene ring). All data are in agreement with literature values.[2]

_N_-(4-Methoxyphenyl)-3-methyl-2-butenaldimine (1-8):[2]

To a solution of *p*-anisidine (0.164 g, 1.32 mmol; recrystalized from methanol) and anhydrous Na_2SO_4 (0.592 g, 3.96 mmol) in 6 mL CH_2Cl_2 was added 3-methylbut-2-eneal (0.155 mL, 1.61 mmol) dropwise, and then the reaction mixture was stirred at room temperature for 2 h. The solution was filtered and evaporated to remove the solvent, then put under vacuum to yield imine as yellow, viscous oil, which was immediately used for the synthesis of β-lactam without further purification. ^{1}H NMR (300 MHz, $CDCl_3$) δ 1.95 (s, 3 H, H on CH_3), 2.01 (s, 3 H, H on CH_3), 3.80 (s, 3 H, H on CH_3O group), 6.20 (d, *J* = 9.5 Hz, 1 H, H on C2), 6.89 (d, *J* = 7.0 Hz, 2 H, H on benzene ring), 7.11 (d, *J* = 7.0 Hz, 2 H, H on benzene ring), 8.38 (d, *J* = 9.5 Hz, 1 H, H on C1). All data are in agreement with literature values.[2]

1-*p*-Methoxyphenyl-3-triisopropylsilyloxy-4-(2-methylpropen-2-yl)azetidin-2-one (1-9):[2]

To a solution of diisopropylamine (0.15 mL, 1.06 mmol) in 3.5 mL of THF was added *n*-butyllithium (0.433 mL, 1.082 mmol, 2.5 M in hexanes) at -15 ^{o}C. After stirring for 60 min, the reaction solution was cooled to -85 ^{o}C. A solution of the TIPS-Ester **(1-7)** (0.321 g, 0.820 mmol) in 8 mL THF was slowly added *via* cannula over a period of 1 h. After stirring for an additional hour, a solution of the imine (1.32 mmol in 4.5 mL THF) was carefully added *via* cannula over a period of 2 h. The reaction was stirred at –85 ^{o}C overnight while stirring. Then LiHMDS (0.823 mL, 0.823 mmol, 1M in THF) was added and the reaction was allowed to warm up after 1 h. The reaction was then quenched with saturated aqueous NH_4Cl solution. The aqueous layer was extracted with ethyl acetate and the combined organic layers were washed with brine. The organic layer was then dried over $MgSO_4$ and concentrated *in vacuo*. The residue was then purified by flash column chromatography on silica with hexanes and ethyl acetate to afford desired product **(1-9)** (281 mg, 59 %). ^{1}H NMR (300 MHz, $CDCl_3$) δ 0.97-1.24 (m, 21 H, H on TIPS group), 1.88 (d, *J* = 2.3 Hz, 3 H, H on CH_3), 1.84 (d, *J* = 2.3 Hz, 3 H, H on CH_3), 3.77 (s, 3 H, H on CH_3O group), 4.82 (dd, *J* = 9.9, 5.1 Hz, 1 H, H on C1'), 5.04 (d, *J* = 5.1 Hz, 1 H, H on C4), 5.33 (d, *J* = 9.9 Hz, 1 H, H on C3), 6.84 (d, *J* = 8.7 Hz, 2 H, H on benzene ring), 7.32 (d, *J* = 8.7 Hz, 2 H, H on benzene ring). All data are in agreement with literature values.[2]

3-Triisopropylsilyloxy-4-(2-methylpropen-2-yl)azetidin-2-one (1-10):[2]

To a solution of 1-*p*-methoxyphenyl-3-triisopropylsiloxy-4-(2-methylpropen-2-yl) azetidin-2-one (137 mg, 0.34 mmol) in 12 mL acetonitrile and 9.6 mL water at -10 ^{o}C was added cerium ammonium nitrate (CAN) (0.584 g, 1.19 mmol) in 2.4 mL H_2O dropwise *via* addition funnel. The reaction mixture was allowed to stir for 2 h and then quenched with saturated aqueous Na_2SO_3. The aqueous layer was extracted 3 times with ethyl acetate and the combined organic layers were washed with brine. After drying over

$MgSO_4$ and concentrating *in vacuo*, the residue was purified by flash column chromatography on silica with hexanes and ethyl acetate to yield 3-triisopropylsiloxy-4-(2-methylpropen-2-yl) azetidin-2-one (75.2 mg, 75 %) as white solid. mp: 84.5-86.0 ^oC; ^1H NMR (400 MHz, $CDCl_3$) δ 0.97-1.21 (m, 21 H, H on TIPS group), 1.68 (d, J = 2.3 Hz, 3 H, H on CH_3), 1.19 (d, J = 2.3 Hz, 3 H, H on CH_3), 4.43 (dd, J = 9.5, 4.7 Hz, 1 H, H on C1'), 4.98 (dd, J = 4.7, 2.3 Hz, 1 H, H on C4), 5.31 (d, J = 9.5 Hz, 1 H, H on C3). All data are in agreement with literature values.[2]

1-(*tert*-Butoxycarbonyl)-3-triisopropylsiloxy-4-(2-methylpropen-2-yl)azetidin-2-one (1-11):[2]

To a solution of 3-triisopropylsiloxy-4-(2-methylprop-2-enyl)azetidin-2-one (63.1 mg, 0.210 mmol), triethylamine (0.11 mL, 0.791 mmol) and a catalytic amount of DMAP in 1.5 mL CH_2Cl_2, was added di-*tert*-butyl dicarbonate (50.86 mg, 0.63 mmol) in 1.5 mL of CH_2Cl_2. The reaction mixture was stirred overnight and quenched with H_2O. The reaction mixture was quenched by 10 mL saturated NH_4Cl, and extracted with 10 mL ethyl acetate 3 times and the combined organic layers were washed with brine, dried over $MgSO_4$, and concentrated *in vacuo*. The residue was purified by flash column chromatography on silica with hexanes and ethyl acetate to yield pure 1-(*tert*-butoxycarbonyl)-3-triisopropylsiloxy-4-(2-methyl-prop-2-enyl)-azetidin-2-one (99 mg, 89 %) as a clear oil. ^{1}HNMR (300 MHz, $CDCl_3$) δ 1.02-1.2 (m, 21 H, H on TIPS group), 1.48 (s, 9 H, H on Boc group), 1.77 (d, J = 1.0 Hz, 3 H, H on CH_3), 1.79 (d, J = 1.0 Hz, 3 H, H on CH_3), 4.75 (dd, J = 9.8, 5.6, 1 H, H on C'), 4.98 (d, J = 5.6 Hz, 1 H, H on C4), 5.28 (dd, J = 9.8, 1.0 Hz, 1 H, H on C3). All data are in agreement with literature values.[2]

***N*-(4-Methoxyphenyl)benzaldimine (1-12):**[61]

To a solution of *p*-anisidine (3.16 g, 26.0 mmol; recrystalized from methanol) and anhydrous Na_2SO_4 (11.08 g, 78.0 mmol) in 60 mL CH_2Cl_2 was added benzaldehyde (2.93 mL, 29 mmol) dropwise, and then the reaction mixture was stirred at room temperature for 2 h. The solution was filtered and evaporated to remove the solvent. After recrystallization, *N*-(4-Methoxyphenyl) benzaldimine (5.00 g, 93 %) was obtained as a white solid. ^{1}H NMR (300 MHz, $CDCl_3$) δ 3.84 (s, 3 H), 6.92-6.96 (m, 2 H), 7.23-7.26 (m, 2 H), 7.45-7.48 (m, 3 H), 7.89-7.92 (m, 2 H), 8.49 (s, 1 H). All data are in agreement with literature values.[61]

***cis*-1-*p*-Methoxyphenyl-3-acetoxy-4-phenylazetidin-2-one (1-13):**[61]

To a solution of *N*-(4-methoxyphenyl)benzaldimine (2.185 g, 10 mmol) and triethylamine (2.2 mL, 15.4 mmol) in 45 mL CH_2Cl_2 at –78 °C was added dropwise a solution of acetoxyacetyl chloride (1.963 g, 12 mmol) in 15 mL CH_2Cl_2. The reaction mixture was allowed to warm up to 25 °C over 18 h, and then was diluted with 50 mL CH_2Cl_2. The organic layer was washed with 30 mL H_2O and 30 mL saturated aqueous sodium bicarbonate. The solution was dried over magnesium sulfate, and concentrated *in vacuo*. The residue was purified by flash column chromatography on silica with hexanes and ethyl acetate to yield the desired product (3.512 g, 95 %) as white crystal. ^{1}H NMR (300 MHz, $CDCl_3$) δ 1.68 (s, 3 H, H on acetate group), 3.75 (s, 3 H, H on CH_3O group), 5.34 (d, J = 4.9 Hz, 1 H, H on C4), 5.81(d, J = 4.9 Hz, 1 H, H on C3), 6.81 (d, J = 9.0 Hz, 2 H,

H on PMP group), 7.35-7,26 (m, 7 H, H on benzene group). All data are consistant with literature data.[61]

Enantioselective hydrolysis of β-lactam [(+)-1-13]:[61]
To *cis*-1-*p*-methoxyphenyl-3-acetoxy-4-phenylazetidin-2-one **(1-13)** (2.35 g, 14.6 mmol) suspended in 350 mL 0.2 M sodium phosphate buffer (pH =7.5) and 35 mL acetonitrile was added PS-amano lipase (1.05 g) and the mixture was vigorously stirred at 50 ^{o}C. This reaction was monitored by ^{1}H NMR. After 35 h, the reaction was terminated by extraction of the mixture with ethyl acetate three times (3 x 50 mL). The organic layer was dried over magnesium sulfate, and concentrated *in vacuo*. The residue was purified by flash column chromatography on silica with hexanes and ethyl acetate to give (+)-*cis*-l-(p-methoxyhenyl)-3-acetoxy-4-phenylazetidin-2-one (1.00 g. 43 %) and (-)-*cis*-l-(*p*-methoxyhenyl)- 3-hydroxy-4-phenylazetidin-2-one (1.02 g, 44 %). ^{1}H NMR (300 MHz, $CDCl_3$) δ 1.68 (s, 3 H, H on acetate group), 3.75 (s, 3 H, H on CH_3O group), 5.34 (d, J = 4.9 Hz, 1 H, H on C4), 5.81(d, J = 4.9 Hz, 1 H, H on C3), 6.81 (d, J = 9.0 Hz, 2 H, H on PMP group), 7.35-7.26 (m, 7 H, H on benzene group). All data are consistant with literature data.[61]

(*3R, 4S*)-3-Acetoxy-4-phenylazetidin-2-one (1-15):[45]
To a solution of (+)-*cis*-l-(*p*-methoxyhenyl)-3-acetoxy-4-phenylazetidin-2-one **((+)-1-13)** (0.512 g, 6.50 mmol) in 50 mL acetonitrile and 10 mL water at -10 °C was slowly added a solution of ceric ammonium nitrate (3.06 g, 22.0 mmol) in 50 mL water over a 30-min period. The mixture was stirred for 30 min at -10 °C and quenched with 100 mL of saturated sodium bisulfate. The aqueous layer was extracted with three portions of 50 mL ethyl acetate, and the combined organic layer was washed with brine and concentrated *in vacuo*. The residue was purified by flash column chromatography on silica with hexanes and ethyl acetate to yield the desired product **(1-15)** (0.328 g, 86 %). ^{1}H NMR (300 MHz, $CDCl_3$) δ 1.67 (s, 3 H, H on acetate group), 5.05(d, 1 H, H on C4), 5.87 (dd, J = 2.7Hz, 4.7Hz, 1 H, H on C3), 6.54 (s, exchangeable, 1 H, H on NH), 7.30-7.38 (m, 5 H, H on benzene ring). All data are consistent with literature data.[45]

(*3R, 4S*)-3-Hydroxy-4-phenylazetidin-2-one (1-16):[61]
To a solution of 11 mL THF and 15.6 mL 1 M KOH aqueous solution at 0 °C was added a solution of (*3R, 4S*)-3-acetoxy-4-phenylazetidin-2-one **(1-15)** (0.27 g, 4.53 mmol) in 11 mL of THF. The solution was stirred at 0 °C for 1 h and 40 mL saturated NH_4Cl was added. The mixture was extracted with four portions of 60 mL ethyl acetate and the combined organic layers were dried over sodium sulfate and concentrated *in vacuo*. The residue was purified by flash column chromatography on silica with hexanes and ethyl acetate to yield the desired product (0.190 g, 90 %) as white solid. ^{1}H NMR (300 MHz, $CDCl_3$) δ 2.10 (d, 1 H, H on OH), 4.94 (d, J = 4.7 Hz, 1 H, H on C4), 5.04 (d, J = 4.7 Hz, 1H, H on C3), 6.20 (brs, 1 H, H on NH), 7.25-7.35 (m, 5 H, H on benzene ring). All data are consistent with literature data.[61]

(*3R, 4S*)-3-Ethoxyethoxy-4-phenylazetidin-2-one (1-17):[61]
To a solution of (*3R,4S*)-3-hydroxy-4-phenylazetidin-2-one (0.189 g, 1.16 mmol) in 5 mL THF at 0 °C was added ethyl vinyl ether (0.133 mL, 5.05 mmol) and a catalytic amount

of *p*-toluenesulfonic acid. The mixture was stirred at room temperature for 2 h, diluted with 20 mL of saturated sodium bicarbonate and extracted with four portions of 15 mL ethyl acetate. The combined organic layers were dried over magnesium sulfate and concentrated *in vacuo*. The residue was purified by flash column chromatography on silica with hexanes and ethyl acetate to yield the desired product (0.215 g 79 %) as yellow solid. ^{1}H NMR ($CDC1_3$) δ [0.98 (d, J = 5.4 Hz), 1.05 (d, J = 5.4 Hz)] (3 H), [1.11 (t, J = 7.1 Hz), 1.12 (t, J = 7.1 Hz)] (3 H), [3.16-3.26 (m), 3.31-3.42 (m), 3.59-3.69 (m)] (2 H), [4.47 (q, J = 5.4 Hz), 4.68 (q, J = 5.4 Hz)] (1 H), [4.82 (d, J = 4 .7 Hz), 4.85 (d, J = 4.7 Hz)] (1 H), 5.17-5.21 (m, l H), 6.42 (brs. 1 H). 7.35 (m, 5 H). All data are consistent with literature data.[61]

(±)-1-(4-Methoxyphenyl)-3-acetoxyl-4-(2-methylprop-1-enyl)azetidin-2-one (1-18):[61]
To a mixture of of anhydrous $MgSO_4$ (2.5 g, 30 mmol) and *p*-anisidine (1.28 g, 10.41 mmol) in CH_2Cl_2 (20 mL) was added 3-methylbut-2-enal (1.22 mL, 12.4 mmol) and the mixture was stirred at room temperature for 2 h. The liquid portion in this flask was transferred to another flask, and concentrated *in vacuo*. The residue was dissolved in CH_2Cl_2 (44 mL), triethylamine (2.95 mL, 21.16 mmol) was added, and the solution was cooled to -78 ˚C. To the mixture was added acetoxyacetyl chloride (1.71 mL, 15.87 mmol) and the reaction mixture was warmed up to room temperature overnight. The reaction was quenched with saturated ammonium chloride solution (20 mL) and the resulting mixture was extracted with CH_2Cl_2 (40 mL x 3). The combined organic layers were washed with saturated NH_4Cl solution, water and brine, dried over anhydrous $MgSO_4$, and concentrated *in vacuo*. The residue was purified by flash column chromatography on silica with hexanes and ethyl acetate to yield the desired product (2.52 g, 82 %) as a white solid. mp: 107-109 ^{o}C; ^{1}H NMR (300 MHz, $CDCl_3$) δ 1.70 (s, 3 H, H on CH_3), 1.72 (s, 3 H, H on CH_3), 2.01 (s, 3 H, H on CH_3 of acetate), 3.67 (s, 3 H, H on CH_3 of PMP), 4.83 (dd, J = 9.9 Hz, 4.8 Hz, 1 H, H on CH of isobutenyl), 5.02 (d, J = 9.3 Hz, 1 H, H on C4), 5.67 (d, J = 4.8 Hz, 1 H, H on C3), 6.74 (d, J = 8.9 Hz, 2 H, H on benzene ring), 7.20 (d, J = 8.9 Hz, 2 H, H on benzene ring); ^{13}C NMR (75 MHz, $CDCl_3$) δ 18.3, 20.2, 27.0, 76.1, 114.3, 117.5, 118.4, 130.7, 141.8, 156.4, 161.3, 169.3. All data are consistent with literature data.[61]

Enantioselective hydrolysis of β-lactam [(+)-1-18]:[61]
To a suspension of racemic β-lactam (1.90 g, 6.7 mmol) in 300 mL 0.2 M sodium phosphate buffer (pH = 7.5) and 30 mL acetonitrile was added PS-amano lipase (1.01 g), and the mixture was vigorously stirred at 50 ^{o}C. After 34 h, the ^{1}H NMR showed the conversion of the reaction was 50 %. The reaction was terminated by extraction of the mixture with ethyl acetate (3 x 50 mL). The combined organic layers were washed with water and brine, dried over anhydrous $MgSO_4$, and concentrated *in vacuo*. The residue was purified by flash column chromatography on silica with hexanes and ethyl acetate to yield (*3R,4S*)-l-(4- methoxyhenyl)-3-acetoxy-4-(2-methylprop-1-enyl)-2-one (760 mg, 40 %) and (*3S,4R*)-l -(4-methoxyhenyl)-3-hydroxy-4-(2-methylprop-1-enyl)-2-one (770 mg, 40 %). ^{1}H NMR (300 MHz, $CDCl_3$) δ 1.70 (s, 3 H, H on CH_3), 1.72 (s, 3 H, H on CH_3), 2.01 (s, 3 H, H on CH_3 of acetate), 3.67 (s, 3 H, H on CH_3 of PMP), 4.83 (dd, J = 9.9 Hz, 4.8 Hz, 1 H, H on CH of isobutenyl), 5.02 (d, J = 9.3 Hz, 1 H, H on C4), 5.67 (d, J = 4.8 Hz, 1 H, H on C3), 6.74 (d, J = 8.9 Hz, 2 H, H on benzene ring), 7.20 (d, J = 8.9 Hz, 2 H,

H on benzene ring); ^{13}C NMR (75 MHz, $CDCl_3$) δ 18.3, 20.2, 27.0, 76.1, 114.3, 117.5, 118.4, 130.7, 141.8, 156.4, 161.3, 169.3. All data are consistent with literature data.[61]

(*3R,4S*)-1-(4-Methoxyphenyl)-3-hydroxy-4-(2-methylprop-1-enyl)azetidin-2-one (1-19):[61]

To a solution of 30 mL THF and 30 mL 1 M KOH aqueous solution at 0 °C was added a solution of acetate **((+)-1-18)** (760 mg, 2.63 mmol) in 50 mL of THF. The solution was stirred at 0 °C for 1 h and 100 mL saturated NH_4Cl was added. The mixture was extracted with four portions of 50 mL ethyl acetate. The combined organic layers were dried over $MgSO_4$ and concentrated *in vacuo*. The residue was purified by flash column chromatography on silica with hexanes and ethyl acetate to yield desired product (650 mg, quant.) as white solid. ^{1}H NMR (300 MHz, $CDCl_3$) δ 4.84 (d, J = 4.7 Hz, 1 H, H on C4), 5.04 (d, J = 4.7 Hz, 1 H, H on C3), 7.25-7.35 (m, 5 H, H on benzene ring). All data are consistent with literature data.[61]

1-*p*-Methoxyphenyl-3-triisopropylsilyloxy-4-(2-methylpropen-2-yl)azetidin-2-one (1-9):[61]

To a solution of (*3R,4S*)-1-(4-methoxyphenyl)-3-hydroxy-4-(2-methylprop-1-enyl) azetidin-2-one (697 mg, 2.82 mmol) and DMAP (68 mg, 0.56 mmol) in 10 mL CH_2Cl_2 was added TEA (1.57 mL, 11.4 mmol) and TIPSCl (0.78 mL, 3.67 mmol). After stirring overnight at room temperature, the reaction was then quenched with saturated aqueous NH_4Cl solution. The aqueous layer was extracted with ethyl acetate and the combined organic layers were washed with brine. The organic layer was then dried over $MgSO_4$ and concentrated *in vacuo*. The residue was purified by flash column chromatography on silica with hexanes and ethyl acetate to yield desired product (1.139 g, quant.). ^{1}H NMR (300 MHz, $CDCl_3$) δ 0.97-1.24 (m, 21 H, H on TIPS group), 1.88 (d, J = 2.3 Hz, 3 H, H on CH_3), 1.84 (d, J = 2.3 Hz, 3 H, H on CH_3), 3.77 (s, 3 H, H on CH_3O group), 4.82 (dd, J = 9.9, 5.1 Hz, 1 H, H on C1'), 5.04 (d, J = 5.1 Hz, 1 H, H on C4), 5.33 (d, J = 9.9 Hz, 1 H, H on C3), 6.84 (d, J = 8.7 Hz, 2 H, H on benzene ring), 7.32 (d, J = 8.7 Hz, 2 H, H on benzene ring). All data are in agreement with literature values.[61]

3-Triisopropylsilyloxy-4-(2-methylpropen-2-yl)azetidin-2-one (1-10):[61]

To a solution of 1-*p*-methoxyphenyl-3-triisopropylsiloxy-4-(2-methylpropen-2-yl) azetidin-2-one **(1-9)** (1.13 g, 3.81 mmol) in 100 mL acetonitrile, 20 mL water at -10 ^{o}C was added cerium ammonium nitrate (CAN) (4.83 g, 13.35 mmol) in 80 mL H_2O dropwise *via* addition funnel. The reaction mixture was allowed to stir for 2 h afterwards and then quenched with saturated aqueous Na_2SO_3. The aqueous layer was extracted 3 times with ethyl acetate and the combined organic layers were washed with H_2O and brine. After drying over $MgSO_4$ and concentrating *in vacuo*, the residue was purified by flash column chromatography on silica with hexanes and ethyl acetate to yield desired product (0.54 g, 71 %) as white solid. mp: 84.5-86.0 ^{o}C; ^{1}H NMR (400 MHz, $CDCl_3$) δ 0.97-1.21 (m, 21 H, H on TIPS group), 1.68 (d, J = 2.3 Hz, 3 H, H on CH_3), 1.19 (d, J = 2.3 Hz, 3 H, H on CH_3), 4.43 (dd, J = 9.5, 4.7 Hz, 1 H, H on C1'), 4.98 (dd, J = 4.7, 2.3 Hz, 1 H, H on C4), 5.31 (d, J = 9.5 Hz, 1 H, H on C3). All data are in agreement with literature values.[61]

1-(*tert*-Butoxycarbonyl)-3-triisopropylsiloxy-4-(2-methylpropen-2-yl)azetidin-2-one (1-11):[61]

To a solution of 3-triisopropylsiloxy-4-(2-methylprop-2-enyl)azetidin-2-one **(1-10)** (540 mg, 1.80 mmol), triethylamine (0.94 mL, 2.7 mmol), and a catalytic amount of DMAP in 10 mL of CH_2Cl_2, was added di-*tert*-butyl dicarbonate (435 mg, 1.97 mmol) in 10 mL CH_2Cl_2. The reaction mixture was stirred overnight. The reaction mixture was quenched by 50 mL saturated NH_4Cl, and extracted with 50 mL ethyl acetate 3 times. The combined organic layers were washed with brine, dried over $MgSO_4$, and concentrated *in vacuo*. The residue was purified by flash column chromatography on silica with hexanes and ethyl acetate to yield the desired product (572 mg, 81 %) as clear oil. ^{1}H NMR (300 MHz, $CDCl_3$) δ 1.02-1.2 (m, 21 H, H on TIPS group), 1.48 (s, 9 H, H on Boc group), 1.77 (d, *J* = 1.0 Hz, 3 H, H on CH_3), 1.79 (d, *J* = 1.0 Hz, 3 H, H on CH_3), 4.75 (dd, *J* = 9.8, 5.6, 1 H, H on C'), 4.98 (d, *J* = 5.6 Hz, 1 H, H on C4), 5.28 (dd, *J* = 9.8, 1.0 Hz, 1 H, H on C3). All data are in agreement with literature values.[61]

7-Triethylsilyl-10-deacetylbaccatin III (1-20):[2]

To a solution of 10-deacetyl baccatin III (150 mg, 0.28 mmol) and imidazole (75 mg, 1.028 mmol) in 6.6 mL *N*,*N*-dimethylformamide (DMF) was added chlorotriethylsilane (0.14 mL, 0.83 mmol) dropwise *via* syringe at 0 ^{o}C. The reaction mixture was stirred for 2 h at 0 ^{o}C and diluted with EtOAc (100 mL). The solution was then washed with H_2O (50 mL x 3), brine (50 mL), dried over $MgSO_4$ and concentrated *in vacuo*. The residue was purified by flash column chromatography on silica using hexanes and EtOAc as eluant to give desired product (172 mg, 95 %) as a white solid. ^{1}H NMR (300 MHz, $CDCl_3$) δ 0.56 (m, 6 H), 0.94 (m, 9 H), 1.08 (s, 6 H), 1.59 (d, *J* = 2.5 Hz, 1H), 1.73 (s, 3H), 1.90 (dt, 1 H, H6a), 2.05 (d, *J* = 4.8 Hz, 1H), 2.08 (s, 3 H), 2.24 (s, 1 H), 2.28 (s, 3 H) (OAc), 2.48 (ddd, 1 H, H6b), 3.95 (d, *J* = 7.1 Hz, 1 H, H3), 4.16 (d, *J* = 8.3 Hz, 1 H, H20a), 4.25 (s, 1 H), 4.31 (d, *J* = 8.3 Hz, 1 H, H20b), 4.40 (dd, *J* = 6.4, 10.5 Hz, 1 H, H7), 4.85 (t, 1 H, H13), 4.95 (d, *J* = 8.0 Hz, 1 H, H5), 5.17 (s, 1 H, H10), 5.60 (d, *J* = 7.0 Hz, 1 H, H2), 7.47 (t, *J* = 7.5 Hz, 2 H), 7.60 (t, *J* = 7.5 Hz, 1 H), 8.10 (d, *J* = 7.3 Hz, 2 H); ^{13}C NMR (75 MHz, $CDCl_3$) δ 5.1, 6.7, 9.9, 15.1, 19.5, 22.6, 26.8, 37.2, 38.6, 42.7, 47.0, 57.9, 67.9, 72.9, 74.6, 74.8, 76.5, 78.8, 80.7, 84.2, 87.6, 128.6, 129.4, 130.0, 133.6, 135.1, 141.8, 167.0, 170.7, 210.3. All data are in agreement with literature values.[2]

7-Triethylsilyl-10-cyclopropanecarbonyl-10-deacetylbaccatin III (1-21):[2]

To a solution of 7-TES-10-DAB III (140 mg, 0.21 mmol) in 3.5 mL THF was added 1.0 M LiHMDS in THF (0.25 mL, 0.25 mmol) dropwise *via* syringe at -40 ^{o}C. The mixture was stirred at -40 ^{o}C for 5 min, and then freshly distilled cyclopropanecarbonyl chloride (21 μL, 0.23 mmol) was added dropwise. After 80 min, the reaction was quenched with aqueous saturated NH_4Cl (10 mL) and extracted with CH_2Cl_2 (20 mL x 3). The combined extracts were dried over anhydrous $MgSO_4$ and concentrated *in vacuo*. The residue was purified by flash column chromatography on silica with hexanes and EtOAc to afford desired product (154 mg, 74 %) as white solid. ^{1}H NMR (300 MHz, $CDCl_3$) δ 0.55 (m, 6 H), 0.90 (m, 9 H), 1.00 (s, 3 H), 1.16 (s, 3 H), 1.64 (s, 3 H), 1.73 (m, 1 H), 1.82 (m, 1 H, H6a), 2.14 (s, 3 H), 2.23 (m, 2 H), 2.24 (s, 3 H, OAc), 2.49 (m, 1 H, H6b), 3.84 (d, *J* = 6.9 Hz, 1 H, H3), 4.11 (d, *J* = 8.0 Hz, 1 H, H20a), 4.26 (d, *J* = 8.2 Hz, 1 H, H20b), 4.45 (dd, *J* = 6.7, 10.3 Hz, 1 H, H5), 4.77 (t, *J* = 7.8 Hz, 1 H, H13), 4.92 (d, *J* =

8.6 Hz, 1 H, H5), 5.59 (d, *J* = 7.0 Hz, 1 H, H2), 6.43 (s, 1H, H10), 7.43 (t, *J* = 7.4 Hz, 2 H), 7.56 (t, *J* = 7.6 Hz, 1 H), 8.05 (d, *J* = 7.3 Hz, 2 H). All data are consistent with the reported values.[2]

3'-Dephenyl-3'-(2-methyl-1-propenyl)-7-triethylsilyl-10-cyclopropanecarbonyl-10-deacetyldocetaxel (1-22):[2]

To a solution of 7-TES-10-deacetyl-10-cyclopropanecarbonylbaccatin III (112 mg, 0.15 mmol) and β-lactam (91 mg, 0.23 mmol) in 17 mL dry THF was added LiHMDS (0.23 mL, 1 M in THF, 0.23 mmol) dropwise at -40 ^{o}C. The solution was stirred for 30 min at -40 ^{o}C and then allowed to warm to -25 ^{o}C. The reaction was quenched with aqueous saturated NH_4Cl (5 mL). The aqueous layer was then extracted with CH_2Cl_2 (20 mL x 3). The combined extracts were then dried over anhydrous $MgSO_4$ and concentrated *in vacuo*. The residue was purified by flash column chromatography on silica using hexanes and EtOAc as the eluant to afford desired product (142 mg, 89 %) as white solid. ^{1}H NMR (300 MHz, $CDCl_3$) δ 0.55 (m, 9H), 0.92 (t, *J* = 7.8 Hz, 9 H), 1.20 (m, 24 H), 1.19 (s, 3 H), 1.24 (s, 3 H), 1.34 (s, 9 H), 1.69 (s, 3 H), 1.76 (s, 3 H), 1.80 (s, 3 H), 1.89 (m, 1 H), 2.02 (s, 3 H), 2.36 (s, 3 H), 2.51 (m, 2 H), 3.84 (d, *J* = 6.9 Hz, 1 H), 4.20 (d, *J* = 8.4 Hz, 1 H), 4.30 (d, *J* = 8.4 Hz, 1 H), 4.47 (m, 2 H), 4.77-4.87 (m, 2 H), 4.93 (d, *J* = 8.4 Hz, 1 H), 5.69 (d, *J* = 7.2 Hz, 1 H), 6.09 (t, *J* =9, 1H), 6.49 (s, 1H), 7.46 (t, *J* = 7.5 Hz, 2 H), 7.60 (t, *J* =7.2, 1 H), 8.10 (d, *J* = 6.9 Hz, 2 H). All data are consistent with the reported values.[2]

3'-Dephenyl-3'-(2-methyl-1-propenyl)-10-cyclopropanecarbonyldocetaxel (SB-T-1214, 1-23):[2]

To a solution of 7-triethylsilyl-10-cyclopropanecarbonyldocetaxel (142 mg, 0.13 mmol) in 6 mL pyridine/acetonitrile (1:1) was added dropwise HF/pyridine (70:30, 1.4 mL) at 0 °C, then the mixture was stirred for 17 h at room temperature. The reaction was quenched with aqueous saturated sodium carbonate solution (10 mL). The mixture was then diluted with ethyl acetate (100 mL), washed with aqueous saturated copper sulfate solution (30 mL x 3) and water (30 mL). The combined organic layer was dried over anhydrous magnesium sulfate and concentrated *in vacuo*. The residue was purified by flash column chromatography on silica using hexanes and EtOAc as eluant to afford desired product (92 mg, 90 %). ^{1}H NMR (300 MHz, $CDCl_3$) δ 0.98-1.05 (m, 2 H), 1.13-1.21 (m, 2 H), 1.37 (s, 9 H), 1.42 (m, 1 H), 1.69 (s, 3 H), 1.69-1.1.93(m, 10 H), 1.91 (s, 3 H), 2.06 (s, 3 H), 2.37 (s, 4 H), 2.55 (m, 1 H), 2.63 (d, *J* = 3.9 Hz, 1 H), 3.47 (d, *J* = 6.6 Hz, 1 H), 3.82 (d, *J* = 7.2 Hz, 1 H), 4.21 (m, 2H), 4.33 (d, J = 8.1 Hz, 1 H), 4.43 (m, 1 H), 4.76 (t, *J* = 6, 1 H), 4.85 (d, *J* = 8.4 Hz, 1 H), 4.97 (d, *J* = 9.3 Hz, 1 H), 5.33 (d, *J* = 8.4 Hz, 1 H), 5.68 (d, *J* = 7.2 Hz, 1 H), 6.19 (t, *J* =7.6, 1H), 6.32(s, 1H), 7.49 (t, *J* = 8.1 Hz, 2 H), 7.61 (t, *J* =7.2, 1 H), 8.11 (d, *J* = 8.4 Hz, 2 H). All data are consistent with the reported values.[2]

Chapter II

Synthesis of C3'-Difluorovinyl Taxoid SB-T-12852

§ 2.1. Introduction

Fluorine is a quite unique atom and often introduced into biologically active compounds in medicinal chemistry. A lot of current marketed drugs contain fluorine, as shown in Figure 2-1. Fluorine atom is the second smallest atom with van der waals radius of 1.47 Å, compared with 1.20 Å for hydrogen.[1] Accordingly, the substitution of fluorine for hydrogen would result in minimal steric alterations, *e.g.* carbon-fluorine bond length is 1.39 Å while the length of carbon-oxygen bond is 1.43 Å. As the most electronegative element, fluorine can significantly change the physicochemical properties of the neighboring groups in molecules, *e.g.* density, basicity and/or acidity. The carbon-fluorine bond is at least 14 Kcal/mole stronger than carbon-hydrogen bond, which means carbon-fluorine bond is much less susceptible to metabolic oxidation.[2] Oxidative metabolism by liver enzymes, especially cytochrome P450, often leads to undesirable effects. It has been turned out that introducing a fluorine atom at the active site can greatly increase the metabolic stability by blocking the enzymatic cleavage. Fluorine moieties, *e.g.* trifluoromethyl and difluorovinyl functional groups, can also enhance the lipophilicity of the molecule, resulting in increased hydrophobic binding and membrane permeability. Fluorine also can serve as a unique and valuable tool for *in vitro* and *in vivo* ^{19}F NMR studies of protein structures and drug-protein interactions by taking advantage of the fact that fluorine is virtually absent in the living tissue.[3,4]

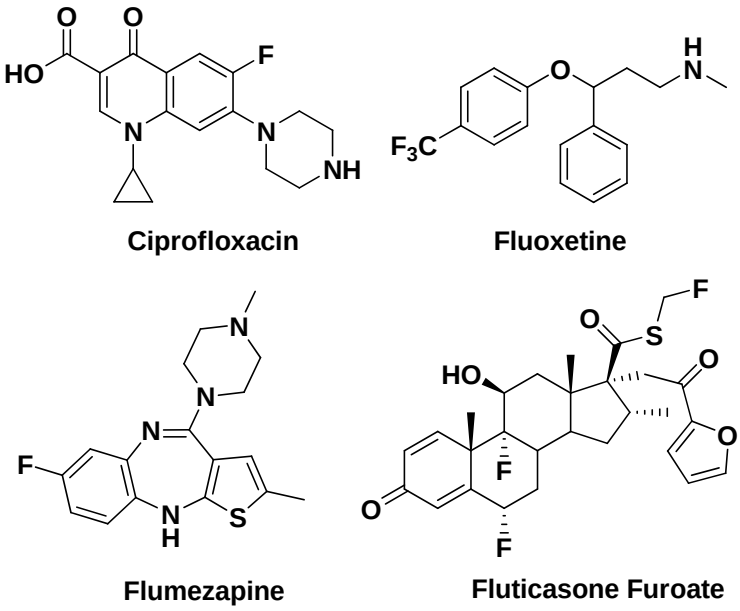

Figure 2-1. Representatives of fluorinated drugs.

Over the past decades, fluorinated β-lactams have attracted significant attention as pharmacophores of numerous pharmacologically active molecules, mainly because the β-lactam skeleton is the core structure of natural and synthetic β-lactam antibiotics.[5] Besides, as an expansion and further application of *β-Lactam Synthon Method* (β-LSM), fluorinated β-lactams could be utilized as versatile synthetic intermediates for the efficient syntheses of fluorinated α-hydroxy-β-amino acids, dipeptides, and fluoro-taxoids, as summarized in Scheme 2-1.[6,7,8]

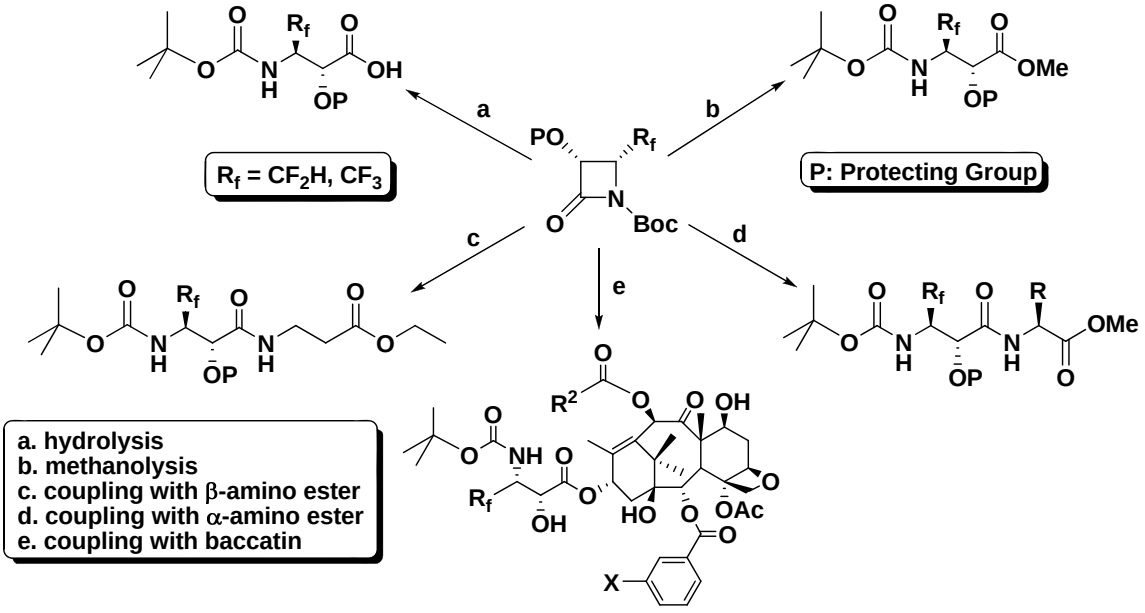

Scheme 2-1. Representative transformations of *N*-*t*-Boc-3-PO-4-R_f-β-lactams.

The introduction of fluorine to novel taxoids *via* the extremely efficient and practical Ojima-Holton protocol has opened a window for extensive structure-activity relationship (SAR) studies of taxoid anticancer agents. The fluorinated 2nd-generation taxoids have been extensively explored by Ojima and coworkers. The novel fluoro-taxoids, SB-T-12842-4 and SB-T-128221-3 (Figure 2-2), were found to possess more than two orders of magnitude higher cytotoxicity than paclitaxel against the drug-resistant cell lines, MCF7-R and LCC6-MDR,and several times higher potency than paclitaxel against the drug-sensitive cell lines, MCF7-S and LCC6-WT(Table 2-1).[7]

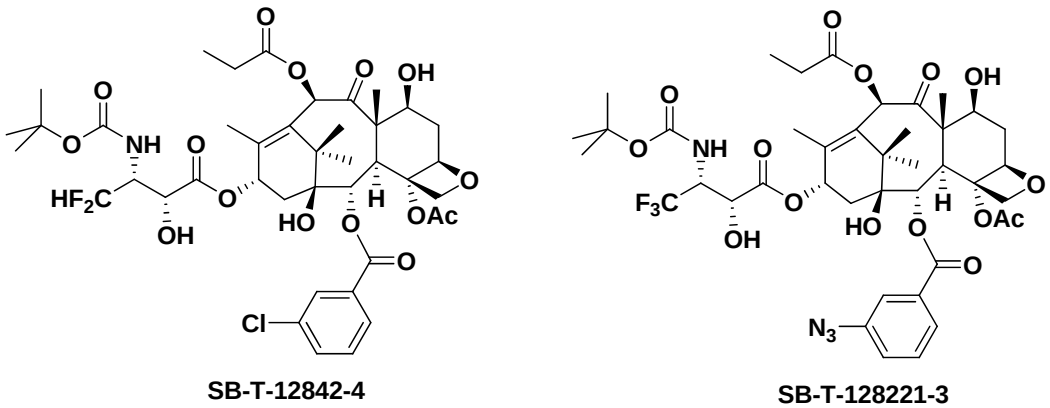

SB-T-12842-4 SB-T-128221-3

Figure 2-2. Structure of **SB-T-12842-4** and **SB-T-128221-3**.

Table 2-1. *In vitro* cytotoxicity (IC_{50} nM)[a] of fluoro-taxoids.[7]

Taxoid	MCF7-S	MCF7-R	R/S[b]	LCC6-WT	LCC6-MDR	R/S[b]	H460	HT-29
Paclitaxel	1.8	484	269	3.4	216	64	5.5	3.6
SB-T-12842-4	0.6	6.4	11	0.6	3.1	5.2	0.3	0.5
SB-T-128221-3	0.4	2.6	6.5	1.2	1.6	1.3	0.2	0.4

[a] The concentration of compound which inhibits 50 % (IC_{50}) of the growth of the human tumor cell line after 72 h drug exposure.
[b] R/S = drug-resistant factor = IC_{50} (drug-resistant cell line)/IC_{50} (drug-sensitive cell line).

Previous metabolism studies on paclitaxel have shown that the para position of the C-3' phenyl, meta position of the C-2 benzoate, C-6 methylene, and C-19 methyl groups are primary sites of hydroxylation by the cytochrome P450 family of enzymes.[2] During the development of novel 2nd-generation taxoids , it was found by our collaborator Dr. Gut that hydroxylation by P450 took place at the methine position of those taxoids containing C3'-isobutyl groups. Accordingly, it is critical to design a series of novel 2nd-generation taxoids with difluorovinyl at the C3' position to avoid metabolic oxidation. This chapter describes the practical large scale syntheses of enantiopure 4-difluorovinyl β-lactam and the corresponding difluorovinyl taxoid **SB-T-12852** (Figure 2-3). The other three difluorovinyl taxoids **SB-T-12851**, **SB-T-12853**, and **SB-T-12854** were synthesized by collaborators Dr. Jin Chen, Mr. Liang Sun, Mr. Xianrui Zhao, Mrs. Yuan Li, Mr. Stephen Chaterpaul and Mrs. Manisha Das.

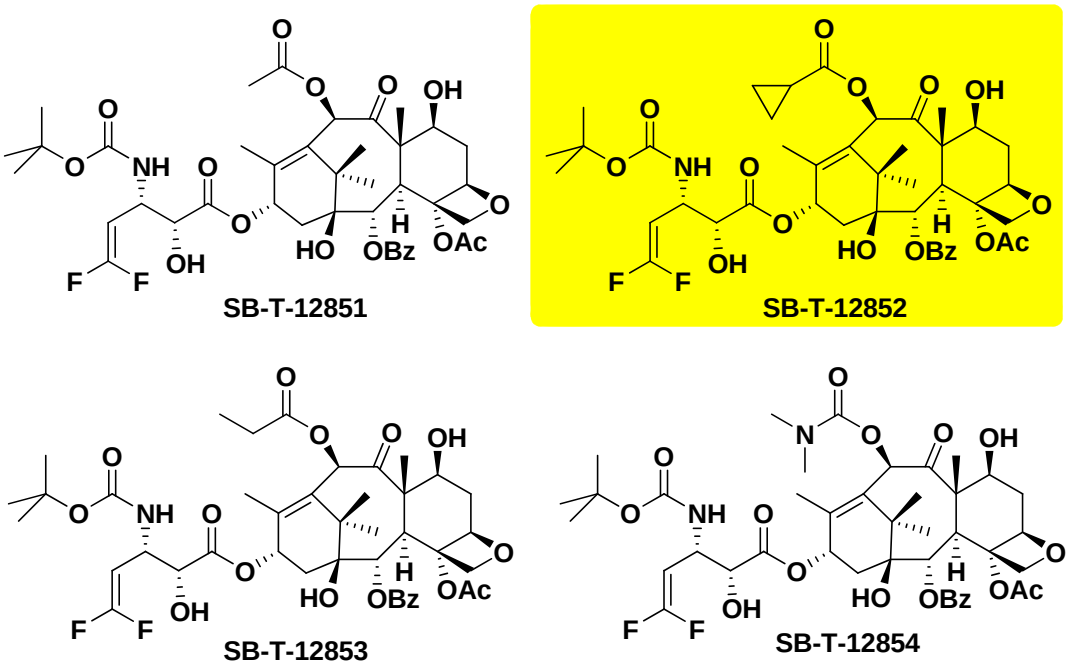

Figure 2-3. Structure of difluorovinyl 2nd-generation taxoids **SB-T-12851**, **SB-T-12852**, **SB-T-12853**, and **SB-T-12854**.

§ 2.2. Results and Discussion

§ 2.2.1. Synthesis of 4-Difluorovinyl β-lactam

Synthesis of enantiopure (*3R,4S*)-*N*-Boc-3-TIPSO-4-difluorovinylazetidin-2-one was accomplished *via* [2+2] ketene-imine cycloaddition followed by kinetic enzymatic resolution, see Chapter 1 for more details.

The TIPS protected *β*-lactam, **(+)-**(3*R*,4*S*)-1-PMP-3-TIPSO-4-(2-methyl-1-propenyl) azetidin-2-one **(1-9)** (see Chapter 1 for synthesis) was first subjected to ozonolysis to give (3*R*,4*S*)-1-PMP-3-TIPSO- 4-formylazetidin-2-one. The resulting aldehyde was then transformed to fluorinated β-lactam, (*3R,4S*)-1-PMP-3-TIPSO-4-difluorovinyl-2-one by Wittig reaction using CBr_2F_2, hexamethylphosphoroustriamide (HMPA) and Zn in THF solution.[9,10] The PMP group was removed with cerium ammonium nitrate (CAN) to afford enantiopure (*3R,4S*)-3-TIPSO-4-difluovinylazetidin-2-one followed by acylation with Boc_2O to yield desired β-lactam (*3R,4S*)-*N*-Boc-3-TIPSO-4-difluorovinyl azetidin-2-one in excellent overall yield (Scheme 2-2).

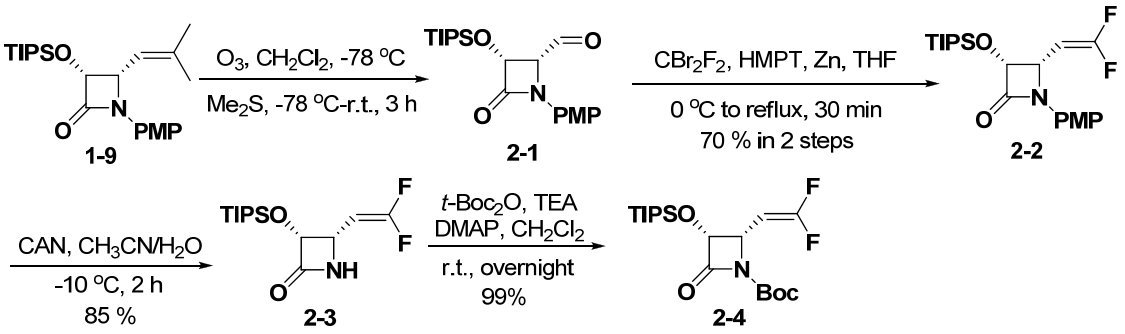

Scheme 2-2. Synthesis of (3*R*,4*S*)-*N*-Boc-3-TIPSO-4-difluorovinylazetidin-2-one.

The mechanism of Wittig reaction was described in Scheme 2-3, including the formation of $[R_3P^+\text{-}CF_2Br]Br^-$ generated *in situ* from the reaction of HMPA and CBr_2F_2 in THF solution. A highly exothermic reaction occured immediately due to the formation of the quasicomplex with zinc and then ylide intermediate was formed. The ylide reacted fast with the aldehyde and yielded the desired difluorovinyl product within a short period of time.[11]

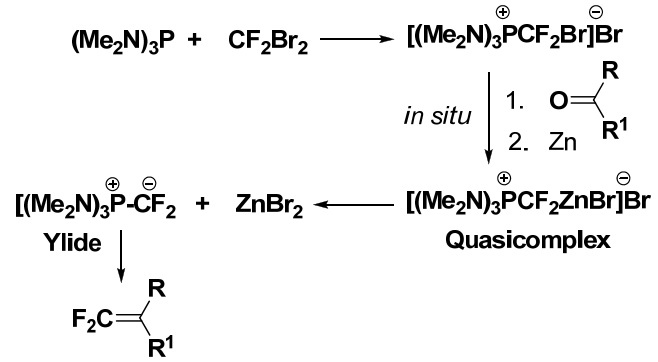

Scheme 2-3. Mechanism of 1,1-difluoroolefins formation.

§ 2.2.2. Synthesis of C3'-Difluorovinyl 2nd-Generation Taxoid SB-T-12852

The synthesis of the modified baccatin core was performed following the regular procedures (C7 TES protection and then C-10 modification) starting from **10-DAB** (see Chapter 1 for synthesis). The ring-opening coupling of β-lactam with proper modified baccatin **(1-21)** was carried out at -40 °C in THF, in the presence of LiHMDS. The subsequent removal of the silyl protecting groups by HF/pyridine gave the corresponding novel C3'-difluorovinyl 2nd-generation taxoids **(SB-T-12852, 2-6)** in good overall yields (Scheme 2-4).

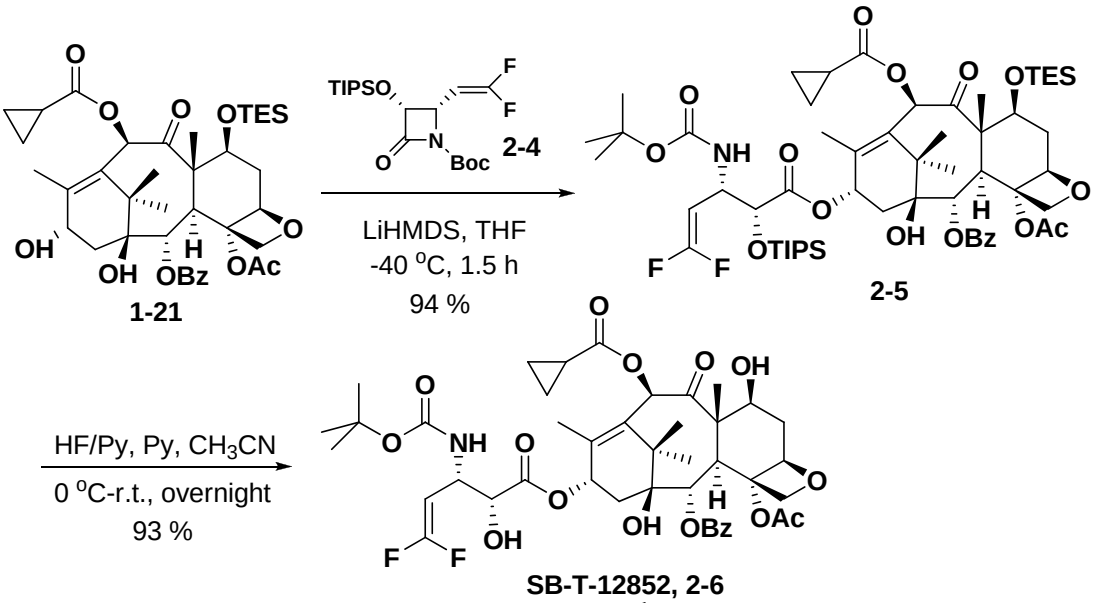

Scheme 2-4. Synthesis of C3'-difluorovinyl 2nd-generation taxoid SB-T-12852.

§ 2.2.3. Biological Evaluation of Difluorovinal Taxoid SB-T-12852

The novel difluorovinyl taxoids **SB-T-12851**, **SB-T-12852**, **SB-T-12853**, and **SB-T-12854** have been previously synthesized by Dr. Larisa Kuzentsova and the biological evaluations was done *in vitro* in the Department of Pharmacology and Therapeutic in Roswell Park Center Institute. Cytotoxicity of these difluorovinyl 2nd-generation taxoids against two types of human breast cancer cell lines, drug sensitive and drug resistant, MCF7-S and MCF7-R respectively, are summarized in table 2-2. The IC_{50} values were determined through 72 h exposure of the fluorinated taxoids to the cancer cells according to the protocol developed by Skehan.[12]

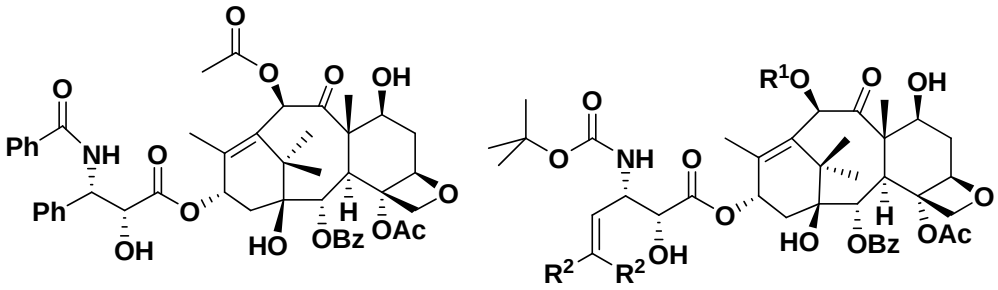

Paclitaxel **C3' difluorovinyl taoxids**

Table 2-2. *In vitro* cytotoxicity (IC_{50} nM) of C3'-difluorovinyl taxoids.

Taxoid	R^1	R^2	MCF7-S (breast)	MCF7-R (breast)	R/S
Paclitaxel			1.7	300	176
SB-T-1213	Et	CH_3	0.18	2.2	12
SB-T-12851	Ac	F	0.14	0.95	6.7
SB-T-12852	*c*-Pr-CO	F	0.17	6.03	35.5
SB-T-12853	Et-CO	F	0.17	1.2	7.06
SB-T-12854	Me_2N-CO	F	0.19	4.27	22.5

According to the IC_{50} values shown in Table 2-2, these C-3' difluorovinyl 2nd-generation taxoids possessed one order of magnitude higher potency than paclitaxel, and comparable cytotoxicity with 2nd-generation taxoid **SB-T-1213,** against the drug-sensitive cell line MCF7-S. Additionally, the cytotoxicity of the fluorinated taxoids is 2-3 orders of magnitude better than paclitaxel and several times higher activity than nonfluoronated 2nd-generation taxoid **SB-T-1213** (except **SB-T-12852, SB-T-12854**), against drug-resistant cell line MCF7-R.

§ 2.3. Experimental Section

General Methods: ^1H, ^{13}C and ^{19}F NMR spectra were measured on a Varian 300, 400, 500, or 600 MHz NMR spectrometer. The melting points were measured on a "Uni-melt" capillary melting point apparatus from Arthur H. Thomas Company, Inc.. Optical rotations were measured on a Perkin-Elmer Model 241 polarimeter. High-resolution mass spectrometric analyses were conducted at the Mass Spectrometry Laboratory, University of Illinois at Urbana-Champaign, Urbana, IL. GC-MS analyses were performed on an Agilent 6890 Series GC system equipped with the HP-5HS capillary column, (50 m X 0.25 mm, 0.25 um) and with the Agilent 5973 network mass selective detector. LC-MS analyses were carried out on an Agilent 1100 Series Liquid Chromatograph Mass Spectrometer. IR spectra were measured on a Shimadzu FTIR-

8400s spectrophotometer. TLC analyses were performed on Merck DC-alufolien with Kieselgel 60F-254 and were visualized with UV light in 10 % sulfuric acid-EtOH or 10 % PMA-EtOH solution. Column chromatography was carried out on silica gel 60 (Merck; 230-400 mesh ASTM). Chemical purity was determined with a Waters HPLC or shimazu HPLC, using a Phenomenex Curosil-B column, employing CH_3CN/water as the solvent system with a flow rate of 1 mL/min. Chiral HPLC analysis for the determination of enantiomeric excess was carried out with a Waters HPLC assembly, comprising Waters M45 solvent delivery system, Waters Model 680 gradient controller, Water M440 detector (at 254 nm) equipped with a Spectra Physics Model SP4270 integrator. The system uses a DAICEL-CHIRACEL OD chiral column (25 x 0.46 cm i.d.), employing hexane/2-propanol as the solvent system with a flow rate of 1.0 ml/min.

Materials: The chemicals were purchased from Sigma Aldrich Company, Fischer Company or Acros Organic Company. 10-Deacetyl baccatin III (DAB) was donated by Indena, SpA, Italy. Dichloromethane and methanol were dried before use by distillation over calcium hydride under nitrogen or argon. Ether and THF were dried before use by distillation over sodium-benzophenone kept under nitrogen or argon. Toluene and benzene were dried by distillation over sodium metal under nitrogen or argon before use. Dry DMF was purchased from EMD chemical company, and used without further purification. PURE SOLVTM, Innovative technology Inc, provided an alternative source of dry toluene, THF, ether, and dichloromethane. The reaction flasks were dried in a 110 ^oC oven and allowed to cool to room temperature in a desiccator over "*Drierite*" (calcium sulfate) and assembled under inert gas nitrogen or argon atmosphere.

1-(4-Methoxy-phenyl)-4-oxo-3-triisopropylsiloxyazetidine-2-carbaldehyde (2-1): Nitrogen was bubbled into a solution of TIPS-protected β-lactam (1.00 g) in CH_2Cl_2 (15 mL) at -78 ^oC for 5 min. O_3 was then bubble into the solution until the color of the solution turned blue. Nitrogen was bubble into the reaction solution again until the blue color disappeared. Me_2S was added and the mixture was warmed to room temperature. The solution was stirred for 3 h at room temperature and the solvent was concentrated *in vacuo*. Ethyl acetate was added to the residue and washed with H_2O and brine, dried over $MgSO_4$. The filtrate was concentrated *in vacuo* to give yellow oil **(2-1)**, which was used directly in next step.

1-(4-Methoxyphenyl)-3-triisopropylsiloxy-4-(2,2-difluoroethenyl)azetidin-2-one (2-2): Dibromodifluoromethane (0.76 mL, 5.08 mmol) and hexamethylphosphorous triamide (1.85 mL, 10.16 mmol) were added to THF (10 mL) at 0 °C. A white precipitate was formed immediately. To a suspension of the aldehyde **(2-1)** (479 mg, 1.27 mmol) and Zn (0.825 g, 12.7 mmol) in THF was poured the white precipitate in a successive manner. The mixture was allowed to reflux for 30 min. The solution was concentrated and the residue was purified by flash chromatography to yield desired product **(2-2)** (440 mg, 75 %). ^1H NMR ($CDCl_3$, 300 MHz): δ 1.08-1.15 (m, 21 H), 3.79 (s, 3 H), 4.54 (ddd, J = 1.5, 6.3, 16.5 Hz, 1 H), 4.83 (m, 1 H), 5.14 (d, J = 5.1 Hz, 1 H), 6.87 (d, J = 9.0 Hz, 2 H), 7.32 (d, J = 9.0 Hz, 2 H); ^{13}C NMR ($CDCl_3$, 75.5 MHz): 12.1, 17.9, 54.1, 55.8, 75.8, 22.1, 76.9, 77.4, 114.8, 118.6, 130.9, 156.7, 164.9; ^{19}F NMR (282 MHz, $CDCl_3$): δ -80.80, -

86.34. HRMS (FAB$^+$, m/z): Calcd. for $C_{21}H_{31}F_2NO_3Si{\cdot}H^+$, 412.2114; Found, 412.2127. All data are consistent with the reported values.[13]

3-Triisopropylsiloxy-4-(2,2-difluoroethenyl)azetidin-2-one (2-3):
To a solution of *N*-PMP-β-lactam **(2-2)** (688 mg, 1.67 mmol) in acetonitrile (50 mL) and H_2O (10 mL), was added dropwise a solution of ceric ammonium nitrate (3.74 g, 6.69 mmol) in water (40 mL). The reaction mixture was stirred at -10 ^oC for 2 h and then quenched by saturated Na_2SO_3 solution (20 mL). The aqueous layer was extracted with EtOAc, and the combined organic layer was washed with H_2O, dried over $MgSO_4$ and concentrated. The residue was purified by flash column chromatography on silica to yield desired product **(2-3)** as yellowish oil (469 mg, 92 %). ^1H NMR ($CDCl_3$, 400 MHz): δ 1.03-1.18 (m, 21 H), 4.51 (ddd, *J* = 1.5, 6.3, 16.5 Hz, 1 H), 4.78 (m, 1 H), 5.04 (dd, *J* = 1.6, 2.4 Hz, 1 H), 6.59 (bs, 1 H); ^{13}C NMR ($CDCl_3$, 100 MHz): 12.1, 17.8, 50.4, 77.1, 79.3, 157.6, 169.4; ^{19}F NMR (282 MHz, $CDCl_3$): δ -82.33, -87.50. All data are consistent with the reported values.[13]

1-(*tert*-Butoxycarbonyl)-3-triisopropylsiloxy-4-(2,2-difluoroethenyl)azetidin-2-one (2-4):
To a solution of *N*-H-4-(2,2-difluorovinyl)-β-lactam **(2-3)** (469 mg, 1.54 mmol), triethylamine (0.75 mL, 4.62 mmol), and DMAP (43 mg, 0.35 mmol) in CH_2Cl_2 (9 mL), was added Boc_2O (398 mg, 1.77 mmol) at room temperature. The reaction mixture was stirred for 18 h. The reaction mixture was diluted with EtOAc and the organic layer was washed with water and brine. The resulting organic solution was dried over $MgSO_4$, and concentrated *in vacuo*. The residue was purified by flash column chromatography on silica to get desired product **(2-4)** as yellow oil (599 mg, 96 %). $[\alpha]_D^{20}$ +24.17 (c 14.4, $CHCl_3$); ^1H NMR (300 MHz, $CDCl_3$) δ 1.04-1.17 (m, 21 H), 1.49 (s, 9 H), 4.49 (ddd, *J* = 1.6, 13.8, 23.7 Hz, 1 H), 4.75 (m, 1 H), 5.04 (d, *J* = 5.7 Hz, 1 H); ^{13}C NMR ($CDCl_3$, 100 MHz): 12.0, 17.8, 28.2, 53.6, 74.5, 77.2, 83.9, 147.9, 158.5, 165.3; ^{19}F NMR (282 MHz, $CDCl_3$): δ -81.20, -85.83. HRMS (FAB$^+$, m/z): Calcd. for $C_{19}H_{33}F_2NO_4SiNa^+$, 428.2039; Found, 428.2050. All data are consistent with the reported values.[13]

3'-Dephenyl-3'-(2,2-difluoroethenyl)-7-triethylsilyl-10-cyclopropanecarbonyl-10-deacetyldocetaxel (2-5):
To a solution of 7-TES-10-deacetyl-10-cyclopropanecarbonylbaccatin **(1-21)** (112 mg, 0.15 mmol) and β-lactam **(2-4)** (91 mg, 0.23 mmol) in 17 mL dry THF was added LiHMDS (0.23 mL, 1 M in THF, 0.23 mmol) dropwise at -40 ^oC. The solution was stirred for 30 min at -40 ^oC and then allowed to warm to -25 ^oC. The reaction was quenched with aqueous saturated NH_4Cl (5 mL). The aqueous layer was then extracted with CH_2Cl_2 (20 mL x 3). The combined extracts were then dried over anhydrous $MgSO_4$ and concentrated *in vacuo*. The residue was purified by flash column chromatography on silica using hexanes and EtOAc to afford the desired product **(2-5)** as a white solid (108 mg, 89 %). ^1H NMR (300 MHz, $CDCl_3$) δ 0.55 (m, 9 H), 0.92 (t, *J* = 7.8 Hz, 9 H), 1.20 (m, 24 H), 1.19 (s, 3 H), 1.24 (s, 3 H), 1.34 (s, 9 H), 1.69 (s, 3 H), 1.76 (s, 3 H), 1.80 (s, 3 H), 1.89 (m, 1 H), 2.51 (m, 2 H), 3.84 (d, *J* = 6.9 Hz, 1 H), 4.20 (d, *J* = 8.4 Hz, 1 H), 4.30 (d, *J* = 8.4 Hz, 1 H), 4.47 (m, 2 H), 4.77-4.87 (m, 2 H), 4.93 (d, *J* = 8.4 Hz, 1 H), 5.69 (d, *J* = 7.2 Hz, 1 H), 6.09 (t, *J* = 9 Hz, 1H), 6.49 (s, 1H), 7.46 (t, *J* = 7.5 Hz,

2 H), 7.60 (t, *J* = 7.2 Hz, 1 H), 8.10 (d, *J* = 6.9 Hz, 2 H). All data are consistent with the reported values.[13]

3'-Dephenyl-3'-(2,2-difluoroethenyl)-10-cyclopropanecarbonyldocetaxel SB-T-12852 (2-6):

To a solution of 7-triethylsilyl-10-cyclopropanecarbonyldocetaxel **(2-5)** (1.09 g, 1.36 mmol) in 40 mL of pyridine/acetonitrile (1:1) was added dropwise HF/pyridine (70:30, 10 mL) at 0 °C, then the mixture was stirred for 17 h at room temperature. The reaction was quenched with aqueous saturated sodium carbonate solution. The mixture was then diluted with ethyl acetate, washed with aqueous saturated copper sulfate solution and water. The organic layer was dried over anhydrous magnesium sulfate and concentrated *in vacuo*. The residue was purified by flash column chromatography on silica using hexanes and EtOAc to afford the desired final product **SB-T-12852 (2-6)** as a white solid (0.760 g, 98 %). ^{1}H NMR (400 MHz, $CDCl_3$) δ 0.98 (m, 2 H, CH_2-*c*-Pr,), 1.13 (m, 2 H, CH_2-*c*-Pr,), 1.15 (s, 3 H), 1.26 (m, 3 H), 1.30 (s, 9 H, Boc), 1.66 (s, 3 H, H19), 1.78 (m, OH, 2 H, CH-*c*-Pr), 1.87 (m, 4 H, H-6b, H18), 2.31 (m, 2 H, H14), 2.38 (s, 3 H, 4-OAc), 2.53 (ddd, *J* = 6.8 Hz, 10.0, 15.2 Hz, 1 H, H6a), 2.59 (d, *J* = 3.2 Hz, 1 H, OH), 3.57 (bs, 1 H, OH), 3.80 (d, *J* = 6.8 Hz, 1 H, H3), 4.17 (d, *J* = 8.4 Hz, 1 H, H20b), 4.28 (m, 2 H), 4.40 (m, 1 H, H7), 4.58 (ddd, *J* = 1.6, 9.6, 24.8 Hz, 1 H), 4.87 (t, *J* = 8.8 Hz, 1 H), 4.97 (m, 2 H, H-5), 5.66 (d, *J* = 7.2 Hz, 1 H, H2), 6.24 (t, *J* = 8.0 Hz, 1 H, H13), 6.29 (s, 1 H, H10), 7.49 (t, *J* = 7.6 Hz, 2 H), 7.60 (t, *J* = 7.6 Hz, 1 H), 8.11 (d, *J* = 7.2 Hz, 2 H). All data are consistent with the reported values.[13]

Chapter III

Biotin-mediated Endocytosis of Fluorescein-labeled Anticancer Agent

§ 3.1. Introduction

§ 3.1.1. Tumor-Targeting Delivery of Cytotoxic Drug

Unlike bacteria or viruses, cancer cells originate from the host and thus do not contain molecular targets that are completely foreign to the host. However, the conventional cancer chemotherapy assumes that tumor cells are more likely to be killed by anticancer drugs because of their much faster cell proliferation.[1] Current representative chemotherapeutic agents, such as paclitaxel, cisplatin, and doxorubin, lack the specificity in killing tumor cells without simultaneously damaging healthy tissue and thus causing severe side effects.[2] This is particularly a serious problem for the treatment of solid tumor because most of the solid tumor cells grow slowly. To secure the target specificity problem of chemotherapeutic agents, development of novel cytotoxic agents and/or their prodrugs with greater selectivity to tumors is an urgent need in cancer chemotherapy. One of the most promising strategies is to tumor-specific deliver the cytotoxic therapeutics by differentiating cancer cells from normal cells. The tumor-specific prodrug with minimal systemic toxicity can be constructed by conjugating a cytotoxic agent to a tumor-targeted molecule, and delivered to malignant tissue cells with subsequent internalization *via* various mechanisms such as endocytosis and transcytosis. The cytotoxic agent is then released from the conjugate and induces cell death. It is conceivable that the next generation of cancer chemotherapy relies on developing tumor-targeting drug delivery system with higher selectivity to tumor cells.

The basic principle of tumor-specific drug delivery is that the prodrug conjugate is initially relatively inactive. However, once bound tightly to the receptors, which are overexpressed on the tumor cell surface, the prodrug is then engulfed *via* receptor-mediated endocytosis pathway. This process involves several steps as illustrated in Figure 3-1.[3] Initially, the prodrug-receptor complex is internalized to form a vesicle coated by clathrin, which is subsequently removed by depolymerization. The formed uncoated vesicle fuses to an endosome and forms another new endosome, which is named "early endosome". In the early endosome, the pH value drops gradually from 7 to 5, resulting in the dissociation of the prodrug from its corresponding receptor. During this point, the endosome is termed "late endosome". In certain cases, receptors, *e.g.* folate receptor, can be recycled to the cell membrane. The prodrug conjugate is further transferred to the lysosome, the cytotoxic drug is released by proteolysis, acid-catalyzed hydrolysis or disulfide cleavage, depending on what kind of linker is applied.

Accordingly, the conjugate is termed as tumor-activated prodrug (TAP), derived from the transportation mechanism.[4]

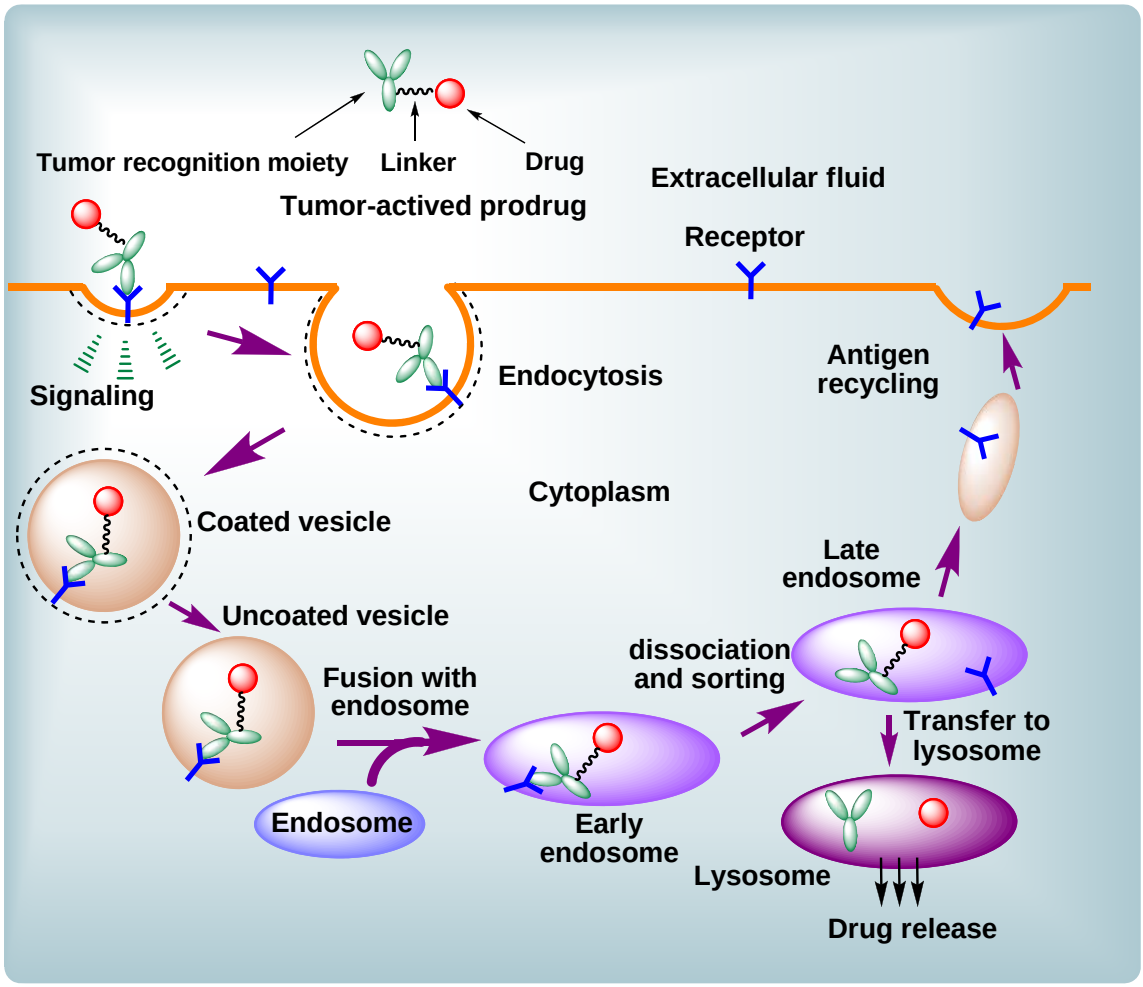

Figure 3-1. Receptor-mediated endocytosis pathway.[3] (Figure was adapted from Ref. 3)

Generally, the tumor-activated prodrug termed as "molecular missile"[5] consists of three parts (Figure 3-2)[3]: (i) tumor recognition moiety (tumor-targeting ligand), (ii) warhead (cytotoxic therapeutics) and (iii) linker. Tumor recognition moiety is the platform that delivers the prodrug conjugate to the targeting site, based on the recognition of specific receptors that are overexpressed on the surface of the tumor cells. Upon binding to the receptors, the tumor-targeting ligand is also responsible for triggering the internalization process *via* endocytosis. Warhead refers to the cytotoxic therapeutics that kills the tumor cell. The role of the linker is to covalently connect the tumor recognition moiety with the warhead to form an inactive prodrug conjugate. Such drug conjugates should be stable and inactive in blood circulation system but restore high potency of original parent drug by activating the cytotoxic warhead inside cancer cells. The efficacy of the prodrug conjugate depends not only on its tumor-targeting selectivity, but also on the cleavable linkers to efficiently release the anticancer therapeutics intracellularly.[5]

Figure 3-2. Tumor-activated prodrug.[3]

It is also essential for the tumor-activated prodrug conjugate to exhibit a good pharmacokinetic profile, a broad therapeutic window and an optimal biodistribution. Additionally, the optimal loading of drug molecules per conjugate is a key parameter for the construction of conjugates. Since only a limited number of receptors are available on the cancer cell surface, a high ratio of drug molecules on a single tumor-specific ligand is preferred. However, previous *in vivo* studies showed that excessive loading caused enhanced immunogenicity and non-specific toxicity in mice.[6] The high loading of hydrophobic toxin molecules also impaired the binding affinity of the tumor recognition ligand.[1]

§ 3.1.2. Tumor Recognition Moiety

In the past few decades, tumor-activated prodrugs have been receiving increased attention for efficacious cancer chemotherapy. The prodrugs can be classified into several groups based on the types of tumor recognition molecule, *e.g.* monoclonal antibody (mAb), polyunsaturated fatty acids, folic acid, biotin, hyaluronic acid and some oligopeptides. (Figure 3-3)[7]

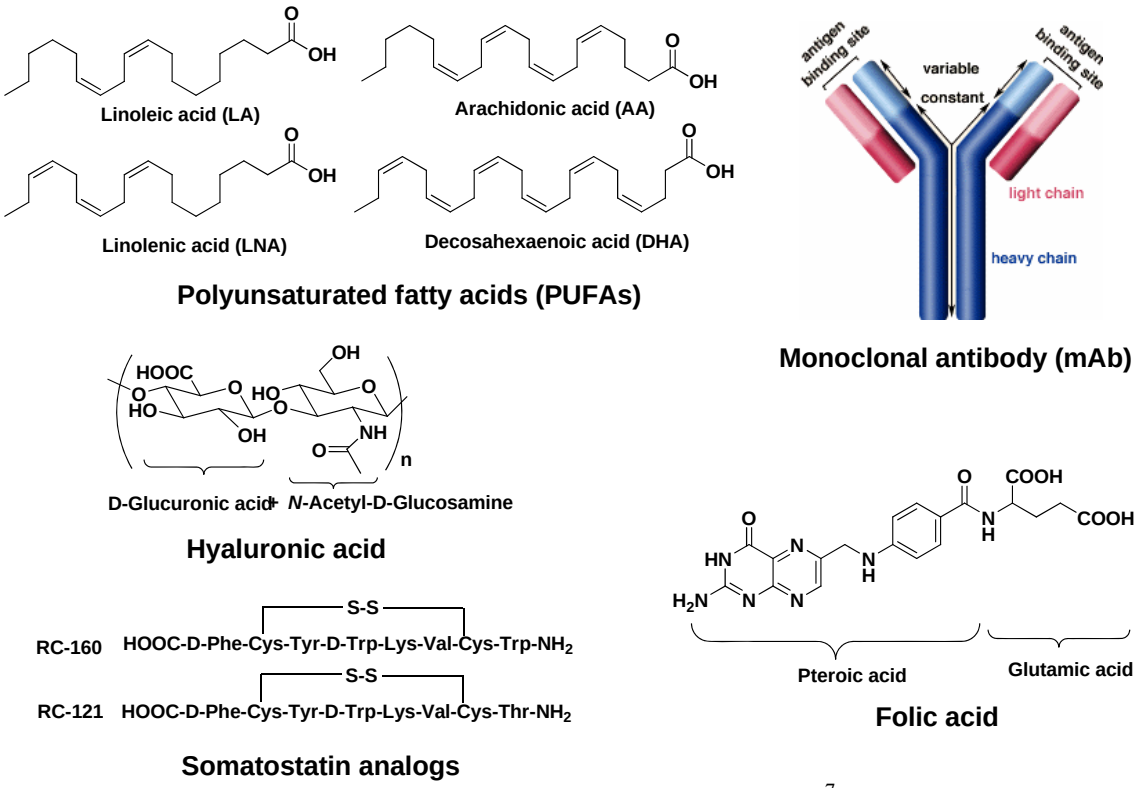

Figure 3-3. Tumor recognition moieties.[7]

The attempted utilization of antibody-based drug conjugates for treatment of cancer can be traced back to early 1900s. Early efforts were not successful due to the technical difficulty in obtaining appropriate antibodies. The pioneering work on discovery of monoclonal antibody by hydridoma technology (Kohler and Milstein, 1975)[3] substantially accelerated the development of mAb-based cancer chemotherapy. The first mAb-drug immunoconjugate approved by the Food and Drug Administration (FDA) for the treatment of cancer diseases was Mylotarg® (gemtuzumab-ozogamicin)[8] in 2000, which combined an anti-CD33 antibody (hP 67.6) with calicheamicin (Figure 3-4), for the treatment of acute myelogenous leukemia (AML). Since then, several other mAb-drug conjugates, including maytansinoid-bearing huC242-DM1,[9] huN901-DM1,[10] MLN2704-DM1,[10] herceptin-DM1,[10] anti-CD44v6 antibody-DM1,[10] BR96–doxorubicin[11] and CTM01-calicheamicin,[12] are currently under human clinical trials.

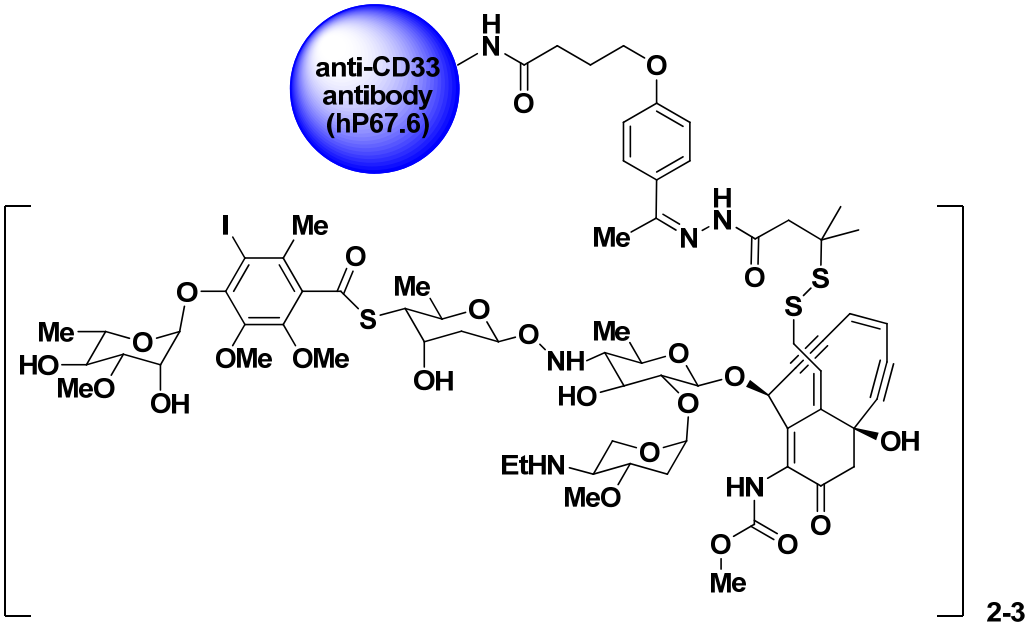

Figure 3-4. Mylotarg® (gemtuzumab-ozogamicin).[8]

In 2001, Bradley *et al.* (Protarga Inc.) successfully developed a docosahexaenoic acid (DHA) conjugate of paclitaxel (Taxoprexin®) by linking DHA to the C-2' position of paclitaxel.[13] Compared with paclitaxel itself, the conjugate exhibited substantially increased antitumor activity and reduced systemic toxicity against the M109 lung tumor xenograft in mice. The conjugate was reported to be stable in blood plasma and high concentrations in tumor cells were maintained for a long period of time, slowly releasing the active cytotoxic agent to kill slowly cycling or residual tumor cells and thus reduce side effects. Consequently, Taxoprexin® was selected as a first-track development drug candidate by FDA and has advanced to human phase III clinical trials. Most recently, Ojima *et al*. have further explored a family of Taxoprexin® analogues (Figure 3-5) comprising cytotoxic warheads, *i.e.* 2nd-generation taxoids and docosahexaenoic acid (DHA) as promising drug candidates. These 2nd-generation taxoids alone exhibited 2-3 orders of magnitude higher activity against drug-resistant cancer cells and tumor xenografts in mice, expressing MDR phenotypes.[14,15,16] The antitumor bioactivities of these tumor-targeting drug conjugates were evaluated against the drug-sensitive A121 human ovarian tumor xenograft and the drug-resistant DLD-1 human colon tumor xenograft in SCID mice.[17] DHA-taxoid conjugates showed excellent antitumor activities against the drug-sensitive A121 ovarian tumor xenograft. The conjugates also exhibited complete regression of the tumor (administration on days 5, 8, and 11) over the duration of experiment for 201 days against the drug-resistant DLD-1 human colon tumor xenograft in all treated animals.[18]

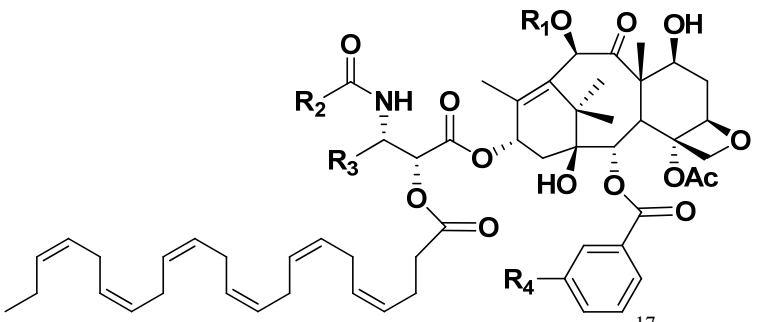

Figure 3-5. DHA-taxoid drug conjugates.[17]

Folic acid belongs to the vitamin B family and participates in the biosynthesis of nucleotide bases. Folic acid can be delivered to epithelial cells through the afore-mentioned receptor-mediated endocytosis pathway.[19] Both of the two membrane-bound folic acid receptors (FR), FR-α and FR-β are 38 kDa and bind folic acid with a high affinity (K_d < 1 nM).[20] FR is overexpressed in several tumors, particularly in ovarian and endometrial cancers. In contrast, the expression of FR in normal tissues is low and restricted to various epithelial cells such as placenta, choroid plexus, lungs, thyroid, and kidneys. Radiolabeling study has shown that [^{3}H] folic acid binds to tumor cells 20-times more than that to normal epithelial cells or fibroblasts.[21] Accordingly, extensive studies have been performed on folate-targeted drug conjugates or formulations. In 2003, Stevens and Lee reported folic acid-containing formulation with entrapped paclitaxel, as illustrated in Figure 3-6.[22] The micelle contained 0.5 % folate-PEG-cholesterol and 59 wt % of paclitaxel. This FR targeted paclitaxel formulation showed significant selectivity against FR-positive KB tumor cells *in vitro*. The IC_{50} value was 18 nM against the FR-positive KB cells, and 1400 nM against the FR-negative glioma cells.

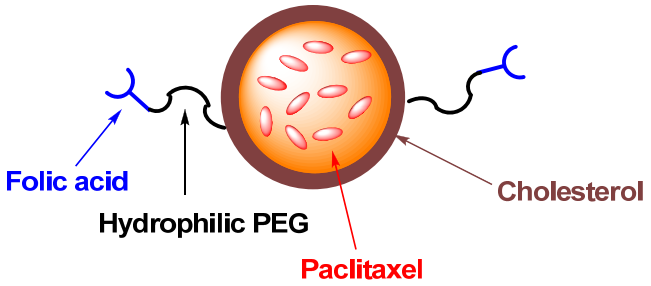

Figure 3-6. Folic acid-guided formulation with entrapped paclitaxel.[22]

Hyaluronic acid or hyaluronan (HA) is a naturally occurring linear negatively charged polysaccharide, which contains two alternating units of D-glucuronic acid (GlcUA) and *N*-acetyl-D-glucosamine (GlcNAc). HA plays pivotal roles in wound healing, cell differentiation, and cell motility. It was reported that HA-binding receptors were overexpressed on various cancer cells, including CD44 (a family of glycoproteins originally associated with lymphocyte activation), RHAMM (the receptors for HA-mediated cell motility) and HARLEC (responsible for receptor-mediated uptake of HA in liver).[23,24] Consequently, the high tumor specificity and exceptional biocompatibility of HA would greatly accelerate the construction of tumor-targeting bioconjugates bearing HA and cytotoxic agents. In 2002, Prestwich *et al.* reported the targeted delivery of

doxorubicin by *N*-(2-hydroxypropyl) methacrylamide (HPMA) copolymer-hyaluronan bioconjugates, where HA was incorporated as the tumor recognition moiety (Figure 3-7).[25] HPMA-HA-DOX bioconjugate demonstrated better internalization and cytotoxicity as compared to non-targeting HMPA-DOX conjugate against human breast cancer (HBL-100), ovarian cancer (SKOV-3), and colon cancer (HCT-116) cells. The IC_{50} value of HPMA–HA–DOX against HBL-100 (breast) cell line was 0.52 μM for 36 wt % loading of HA, which is more than one order of magnitude better than that of non-targeting HMPA–DOX (18.7 μM). It was also found that the systemic toxicity of HMPA–HA–DOX to the primary cells of murine fibroblast was low (IC_{50} =21.2 μM).

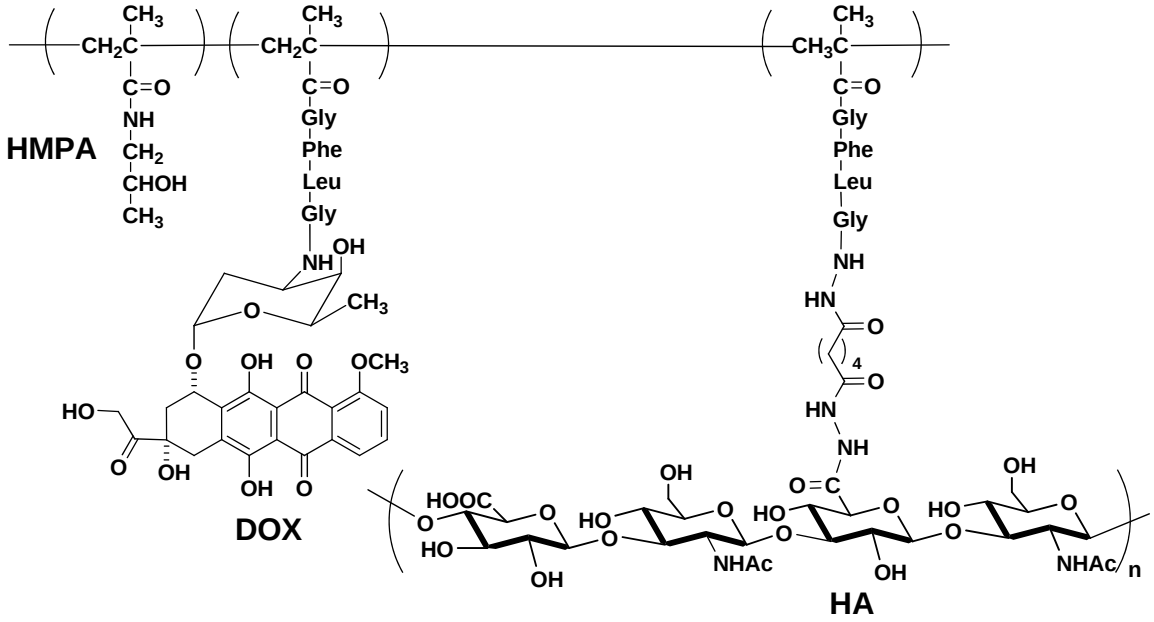

Figure 3-7. Chemical structure of HPMA-HA-DOX bioconjugate.[25]

Peptides with special sequences are also attractive tumor recognition molecules for tumor-specific drug delivery. Somatostatin (SST) is a hormonal neuropeptide and possess high binding affinity to $SSTR_{1–5}$ membrane receptors, which are overexpressed at significantly elevated levels in tumor cells.[26] However, somatostatin has only a short life in plasma, which leads to the development of more stable synthetic somatostatin analogs for therapeutic feasibility in humans. Through screening of combinatorial libraries, octapeptides RC-160 and RC-121 were found to possess similar binding affinities to $SSTR_{1-5}$ membrane receptors with significant improvement in metabolic stability.[27] Nagy *et al.* have explored a tumor-targeting drug delivery platform *via* somatostatin receptor endocytosis. The drug conjugate (AN-238, structure shown in Figure 3-8) was comprised of a somatostatin analogs RC-121 with glutaratelinked 2-pyrrolino-doxorubicin (AN-201, 500–1000 times more cytotoxic than doxorubicin). The antitumor activity assays against MXT murine mammary carcinoma in female BDF mice indicated that inhibition of tumor growth by AN-238 was dose dependent with no systemic toxicity.

In contrast, AN-201 alone at the same dose was highly toxic and did not show any tumor-specific activity.[28]

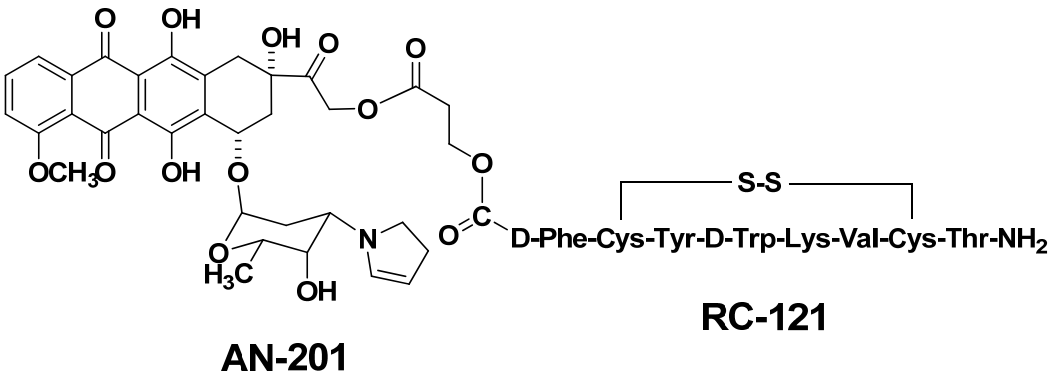

Figure 3-8. Chemical structure of AN-238.[28]

§ 3.1.3. Cytotoxic Agents as Warhead

The selection of an appropriate cytotoxic agent for tumor-targeting drug delivery must meet several criteria. The first criterion is high potency. As only a limited amount of cytotoxic molecules can be loaded onto the tumor recognition molecule without affecting the binding affinity to receptor, highly potent cytotoxic agents are preferred. It has been calculated that the maximum concentration of the drug delivered to a cancer cell through receptor-mediated endocytosis would probably not exceed 10^{-7} M. Accordingly, the toxicity of the warhead should be in the subnanomolar range to be effective in humans.[29,1] The second criterion is the stability of the cytotoxic agent not only in the bloodstream but, more importantly, in the proteolytic and acidic conditions of lysosomes where the cytotoxic agent is released. The third criterion is the lack of immunogenicity. Cytotoxic agents of a large molecular size may be potentially destroyed by the host immune system. The fourth criterion is the presence of proper functional groups, such as hydroxyl, amino, sulfhydryl, carbonyl and carboxyl groups, which can be easily modified to attach to a linker. The fifth criterion is insensitivity towards multi-drug resistance (MDR) or bearing MDR-reversal activity. The cytotoxic agent or its active metabolite should not leak extensively from the cell by efflux mechanism or diffusion. Figure 3-9 summarizs several representative cytotoxic agents commonly used in tumor-targeted drug delivery.[3]

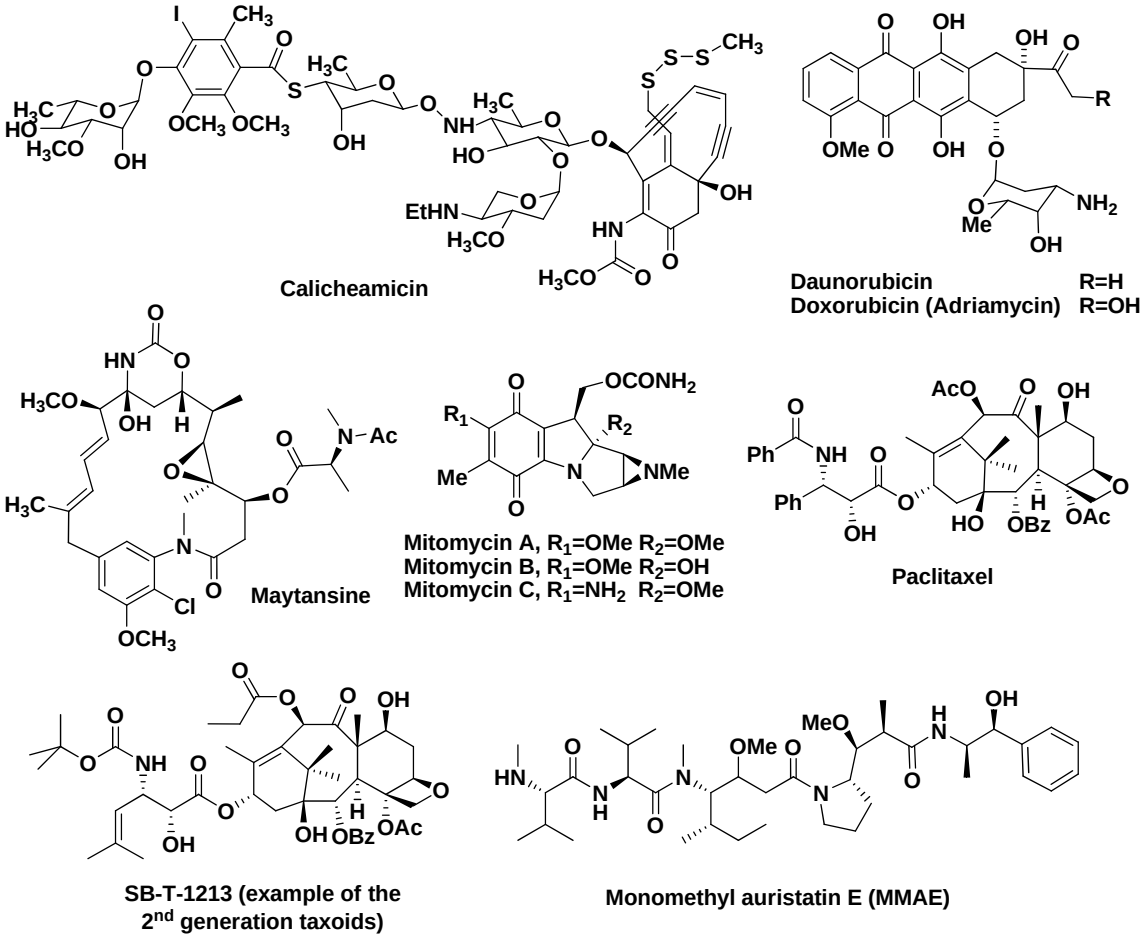

Figure 3-9. Representative cytotoxic agents commonly used in tumor-targeting drug delivery.[3]

Calicheamicin, containing an enediyne with an unusual trisulfide moiety and an iodine atom, is produced by *Micromonospora echinospora calichensis*. Calicheamicin binds to the minor groove of DNA and produces sequence specific DNA breaks.[30] Calicheamicin shows remarkable potency against various tumors and is ~ 4000-fold more active than doxorubicin (adriamycin), with an optimal dose of 0.5 – 1.5 μg/kg.[31,32] Its use as a single-agent chemotherapeutic has been limited because of delayed toxicities, which lead to a very narrow therapeutic window. The unique mechanism of action and extreme potency make calicheamicin a good candidate for immunoconjugates (see § 3.1.2. for details).

Doxorubicin and daunorubicin, isolated from cultures of *Streptomyces peucetius* in 1963 and 1968, respectively, belong to the anthracyclin group of cytotoxic agents.[33] These two drugs gained immediate attention as potent antitumor antibiotics due to their broad-spectrum activity. Numerous immunoconjugates of doxorubicin with mAbs have been investigated (see § 3.1.4. for details).[3]

Maytansine was isolated from the *Maytenus ovatus* plant, and its structure was elucidated in 1972.[34] It is a chlorine-containing macrolactam with an epoxide ring and the initial *in vitro* studies showed median effective (EC_{50}) values in the range of 0.6 - 2 nM.[35] Maytansine is a powerful inhibitor of microtubule assembly. The synthetically

modified maytansine analogue, methyldithio-maytansinoid (DM1), showed 100- to 1000-fold higher cytotoxicity than doxorubicin, methotrexate and vinca alkaloids, with a median inhibitory concentration (IC_{50}) in the picomolar level. DM1 has been explored for mAb-based tumor-targeting therapy by Immunogen (see § 3.1.4. for details).[9]

Mitomycins A, B and C were isolated from the soil bacteria *Streptomyces verticillatus*.[36] Their structures were determined in 1962.[37] The mitomycins form a specific class of antitumor antibiotics and act as DNA alkylating agents.[38,39] Mitomycin C was utilized for the mAb-based tumor-targeting chemotherapy against human gastric cancer and biliary tract carcinoma xenografts in mice.[40,41,42]

Paclitaxel (Taxol®, see Chapter 1 for details) is an antileukaemic and antitumor agent originally isolated from the bark of the Pacific yew tree, *Taxus brevifolia*.[43] The mechanism of action of paclitaxel involves an acceleration of tubulin polymerization and stabilization of the resultant microtubules.[44] The application of paclitaxel in immunoconjugates has not shown significant efficacy *in vivo*.[45,46] The observed inefficacy of mAb-paclitaxel conjugates can be ascribed to insufficient potency, insufficient intracellular release of the drug or unfavourable effects on the mAb function due to the high hydrophobicity of the drug (see § 3.1.4. for details). In addition, paclitaxel is ineffective against drug-resistant cancer cells expressing MDR phenotypes.[47] In sharp contrast, most of the 2nd-generation taxoids developed by Ojima *et al.*,[48,15,49,50,51] *e.g.* SB-T-1213 and SB-T-1214, exhibit one order of magnitude higher potency than that of paclitaxel against drug-sensitive cancer cell lines. They also showed two to three orders of magnitude higher potency than that of paclitaxel against MDR-expressing cell lines. These properties make them highly promising candidates as warheads for efficacious mAb-cytotoxic agent conjugates (see § 3.2.1. for details). Accordingly, the conjugates of the 2nd-generation taxoids with mAbs have been studied. These immunoconjugates show high potency and exceptional tumor-targeting specificity.[2,52,4]

Auristatins are synthetic analogues of dolastatin 10, a pentapeptide isolated from the sea hare *Dolabella auricularia*.[53] The antitumor activity of extracts from *Dolabella auricularia* was discovered in 1972 and after structure elucidation of dolastatin 10,[54] the activity was demonstrated in various tumor models.[55] This class of compounds exerts potent antitumor activities through the inhibition of tubulin polymerization. Auristatins are 100- to 1000-fold more potent than doxorubicin and can be prepared in large quantities. Auristatin E exhibits an average IC_{50} value of 3.2 nM against a diverse panel of human tumor cell lines, including haematological malignancies, melanoma, carcinomas of the lung, stomach, prostate, ovaries, pancreas, breast, colon and kidneys.[56] Another potent dolastatin 10 analogue, monomethyl auristatin E (MMAE), was linked to a mAb and the resulting immunoconjugate exhibited promising antitumor effects against a Karpas 299 lymphoma *in vitro* and *in vivo* (see § 3.1.4. for details).[56]

§ 3.1.4. Linker Pool

Although the linker represents the smallest part of a tumor-activated prodrug conjugate, it has a critical significance in the efficacy of the conjugate. Selection of a suitable linker should meet a few stringent criteria. First, the linker must be stable in circulation, but efficiently cleaved inside cancer cells. The linker for the prodrug conjugates targeting solid tumors require considerable stability, while that targeting

leukemia T-cells can be less stable due to easy access to the target cells. However, a linker that is too stable prevents the toxin release from the conjugate, which would result in substantially decreased or insufficient cytotoxicity. Early work on immunoconjugate involved direct connection of a warhead and a monoclonal antibody (mAb) by the amide bond, which suffered from the insufficient release of the active warhead and led to the development of new generation of cleavable linkers. Second, a linker and a cytotoxic agent should be attached to a tumor recognition moiety under mild chemistry conditions. Third, the linkers should be well exposed so that they can be readily cleaved in cancer cells.

The most frequently used linkers can be categorized into four classes in accordance with the modes of cleavage, *i.e.* (i) acid labile, (ii) proteolytic, (iii) disulfide exchange, and (iv) hydrolytic. Selection of an appropriate linker depends on the type of cancer and the required cytotoxic agent. None of the linkers is universal and each of them has advantages and disadvantages. Specific examples (Figure 3-10) are described in the following sections and the characteristics and applicability of various linkers are discussed as well.

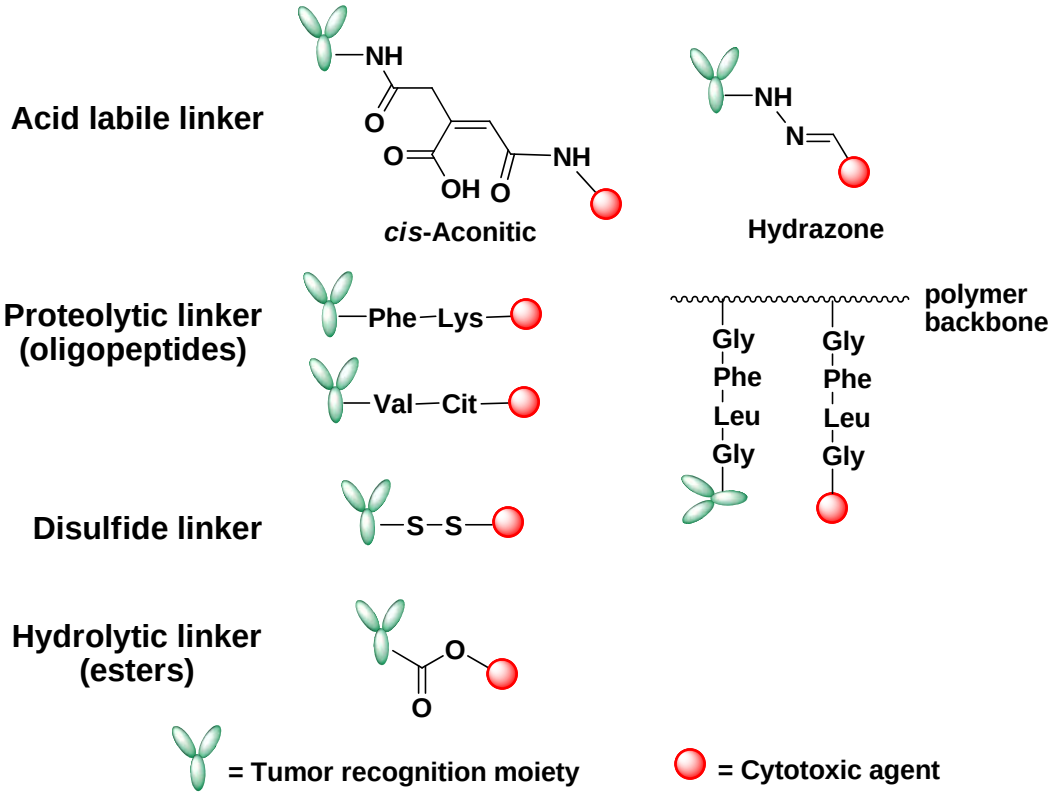

Figure 3-10. Linker pool.[3]

The acid-labile linkers take advantage of the acidic (~ pH 5) conditions in the lysosomes to release the parent toxin *via* non-enzymatic hydrolysis. *cis*-Aconitic and hydrazone linkers have been extensively studied. *cis*-Aconitic acid is one of the first acid-labile linkers used in tumor-specific drug delivery. The very first application of this linker was reported by Shen and Ryser[57] to attach daunorubicin to lysosome. Later, this linker was also used to conjugate daunorubicin to the anti-T-cell mAb by Yang and

Reisfeld[58] as well as Dillman *et al.*[59]. Hydrazone-containing linkers are the most extensively used acid-labile linkers. The therapeutics must have a suitable ketone or aldehyde moiety in order to form hydrazone. Alternatively, the carbonyl groups can be on the tumor-targeting ligand, *e.g.* mAb as well. The hydrazone linker was used for the first time in 1990 to attach doxorubicin to mAb,[60] which exhibited higher release rate under slightly acidic condition than neutral condition. Unfortunately, premature cleavage of the hydrazone linker at physiological pH was also observed,[61] and indicated the instability of this linker during circulation. Doxorubicin was also attached, *via* a hydrazone linker, to a chimeric mAb BR96 (Figure 3-11) that can recognize Lewis Y antigens abundantly expressed on various human carcinomas such as lung, breast and colon. The mAb-drug conjugate containing eight molecules of doxorubicin was rapidly internalized upon binding to the antigen.[1] Complete regressions of human breast, lung and colon carcinomas were observed for xenografts in animal models. However, the phase II clinical trials showed the immunoconjugate was effective only in combination with paclitaxel or docetaxel[62]. To date, vinblastine[63], taxoids[2], doxorubicin[64], daunorubicin,[65] chloambucil[65] and calicheamicin[66] have been used as the cytotoxic agent in tumor-activated prodrug conjugates containing a hydrazone linker.

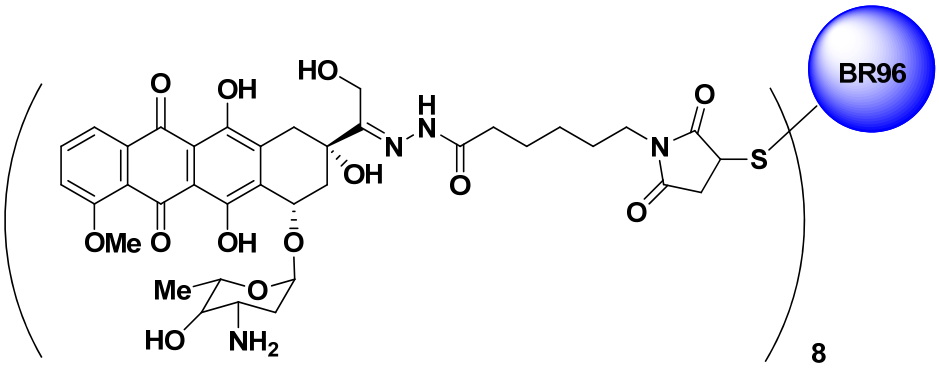

Figure 3-11. BR96-Doxorubicin conjugate.[1]

Complementarity determining region (CDR)-grafted humanized mAb P67.6 targeting CD33 in leukemia cells was linked to calicheamicin *via* a hydrazone linker (Scheme 3-3). The immunoconjugate containing 2-3 molecules of calcheamicin has a rather sophisticated linker system. The lysine residue in mAb was coupled to 4-(4-acetylphenoxy) butanoic acid *via* a stable amide bond. The carbonyl group of the acetophenone moiety was then linked to calicheamicin *via* an alkanoylhydrazone linker serially connected to a disulfide moiety. It has been shown that the hydrazone was the actual cleavage site.[8] However, cleavage by disulfide exchange was insufficient. The *in vitro* assay showed that the conjugate was 2,000 times more potent than the parent drug (calicheamicin). This remarkable activity was also confirmed *in vivo*. After successful human clinical trials, the immunoconjugate, *i.e.* gemtuzumab-ozogamicin (Mylotarg), was approved by the FDA for the treatment of AML in 2000, thus becoming the very first mAb-conjugated anticancer drug in clinical use.[66]

Conjugates delivered to lysosomes in a cancer cell *via* internalization are exposed to many proteases, mostly belonging to the cathepsin family and a number of exopeptidases. A number of short peptide sequences were explored for their utilization as cleavable

linkers. The peptide linker should have 2 to 5 amino acid residues with at least two hydrophobic, preferably aromatic residues.[67] Examples of peptide linkers include tetrapeptide Gly-Phe-Leu-Gly[68] as well as dipeptides Phe-Lys and Val-Cit (Cit = citrulline)[69]. Dipeptide linkers Phe-Lys and Val-Cit have been used for the immunoconjugates of doxorubicin with mAb BR96, with a "self-immolative" spacer (*p*-aminobenzyloxycarbonyl, PABC) inserted between the dipeptide and the warhead. The "self-immolation" is triggered by a proteolytic cleavage of the linker by cathepsin B, which is only present in lysosomes. The half-lives of Phe-Lys-PABC and Val-Cit-PABC linkers were 8 and 240 min, respectively. No cleavage was observed when incubated in fresh human plasma over 7 h. The *in vitro* assay showed potent antigen-specific cytotoxicity of both immunoconjugates with IC_{50} values of 0.15 μM and 0.4 μM, respectively. The dipeptide linker Val-Cit-PABC and mAb BR96 were also employed for the construction of a conjugate with monomethyl auristatin E (MMAE) by Seattle Genetics (Figure 3-12).[56] The *in vitro* cytotoxicity assay of this conjugate against Karpas 299 cell line gave IC_{50} value of 4.5 ng/mL and the specificity ratio (the IC_{50} ratio of nonbinding conjugates to the binding control) of more than 500. The *in vivo* antitumor activity assay against Karpas 299 lymphoma in severe combined immune deficiency (SCID) mice showed that effective dose was 60-times lower than the maximum tolerated dose (MTD). Thus, 35 μg of MMAE component/kg/injection achieved 100 % tumor cure in human Karpas 299 anaplastic large cell lymphoma.

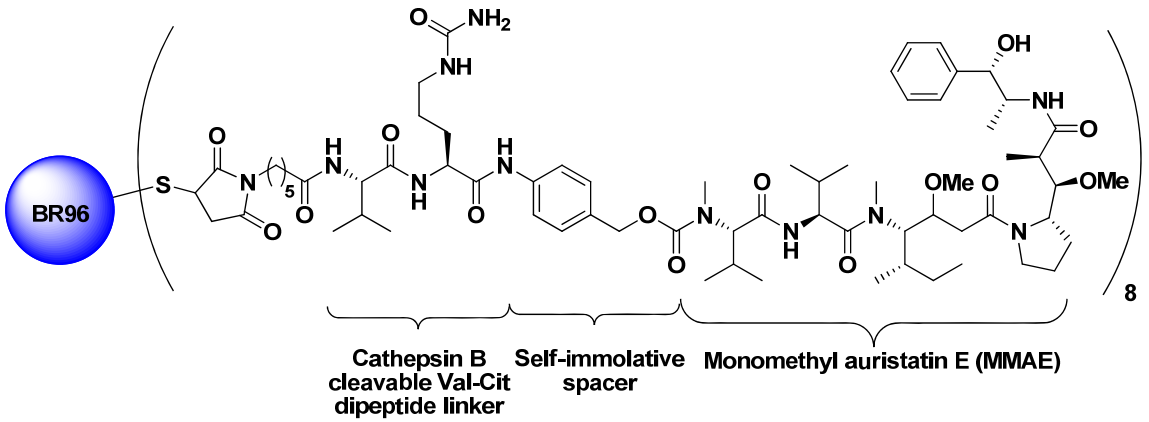

Figure 3-12. BR96-monomethyl auristatin E (MMAE) conjugate.[56]

Disulfide linker is cleaved inside of tumor cells through disulfide exchange with an intracellular thiol such as glutathione. Concentration of glutathione inside of the cell is higher than that in the serum and glutathione also expressed at significantly elevated levels in tumor cells as compared to the normal cell.[70] Considering the stability of the disulfide linker against premature cleavage in circulation, sterically hindered disulfides are commonly used in the construction of prodrugs. The following example provides strong validation that a disulfide linker-containing conjugate has superior efficacy to other linkers against several tumor xenografts including colorectal cancer, pancreatic cancer, gastric cancer, small-cell lung cancer, non-small-cell lung cancer, prostate cancer and breast cancer in preclinical models.[1] Specially designed maytansine derivative DM1 bearing a methyldisulfanyl (MDS) group was attached to a humanized mAb HuC242 (Figure 3-13), which has high binding affinity to CanAg antigen expressed on most

pancreatic, biliary, and colorectal cancer cell membranes.[11] The immunoconjugate bearing a disulfide linker showed remarkable potency and selectivity *in vitro* and *in vivo*. The mAb-DM1 conjugate cured all mice bearing COLO 205 human colon tumor xenografts at much lower dose than the parent drug. Moreover, treatment with the immunoconjugate also produced complete regressions in animals bearing COLO 205 tumor xenografts of large size (260-500 mm^3).[11] A phase I clinical trial on 37 patients with CanAg-expressing solid malignancies observed some responses with the terminal elimination half-life of 41 (+/- 16) hours. A small amount (less than 1 %) of prematurely cleaved maytansinoid DM1 was also detected in the blood.[71]

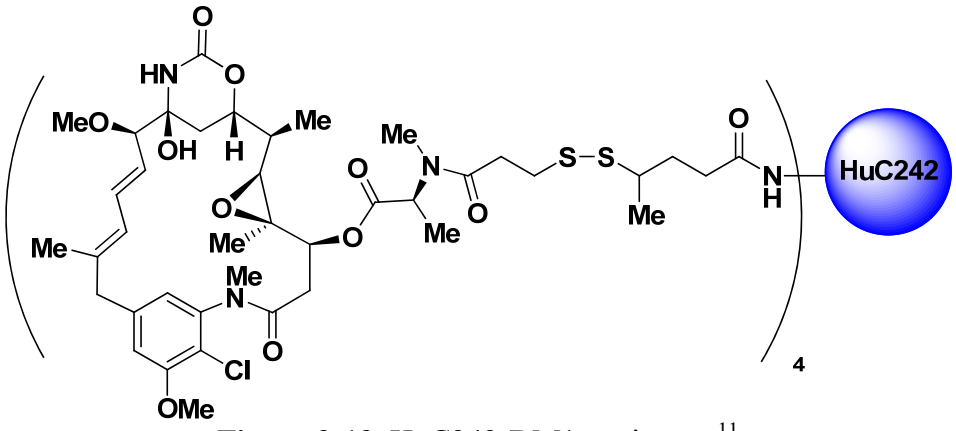

Figure 3-13. HuC242-DM1 conjugate.[11]

Ester linker is cleaved due to pH sensitivity or by lipase-catalyzed hydrolysis *in vivo*. The high lability of this linker limits its use in prodrug construction without proper modification. Thus, in order to circumvent this obstacle, sterically hindered secondary alcohols are used. Safavy *et al.* reported the synthesis and biological evaluation of paclitaxel-C225 (mAb C225 specifically recognizes EGFR) conjugate for tumor-targeting therapy.[46] The conjugate was formed by connecting mAb to the C2'-hydroxyl group of paclitaxel through an ester bond using succinic acid as a spacer (Figure 3-14). *In vitro* treatment with this conjugate induced more apoptosis than free drug alone. However, *in vivo* study showed that there is no difference between the conjugate and C225 in tumor growth inhibition effects. It is very likely that this phenomenon was due to the instability of the ester linker. The same research group also developed a ^{125}I-labeled 3'-OH-paclitaxel-C225 conjugate. Biodistribution and *in vitro* kinetic study confirmed that the conjugate is not stable under physiological conditions with a half-life of ca. 2 h.[72] To improve the systemic stability of the conjugate, the succinic acid moiety in the conjugate was replaced by glutaric acid. The new prodrug showed much better stability and its *in vivo* study also indicated better antitumor activity than the original one.[72]

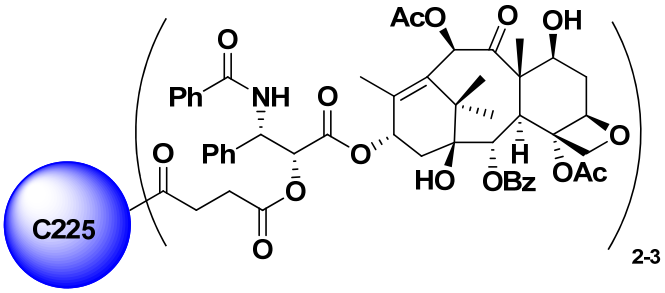

Figure 3-14. C225-paclitaxel conjugates.[46]

§ 3.2. Rational Design of Tumor-specific Prodrug

§ 3.2.1. Previous Achievements of Disulfide-Containing Prodrugs

It has been extensively explored that several types of receptors are particularly overexpressed on the surface of cancer cells. This discovery clearly indicated that tumor cells could be distinguished from normal cells by constructing certain tumor-activated prodrugs with the incorporation of proper tumor recognition moieties. Monoclonal antibody (mAb) has been widely investigated in the past decades as tumor-targeting molecule in efficient drug delivery mainly because of its high binding specificity for tumor-specific receptors. Numerous review articles have been reported in the literature, regarding mAb-mediated drug delivery.[1,11]

Paclitaxel and docetaxel are currently considered as two of the most important drugs in cancer chemotherapy. But they still suffer from the lack of tumor specificity and multidrug resistance (MDR).[73] Additionally, it was calculated that the toxicity of the warhead used in immunoconjugates should be in the subnanomolar range to be effective in humans, considering that the IC_{50} values of paclitaxel and docetaxel were only ~ 10^{-9} M.[1] In sharp contrast, 2nd-generation taxoids developed by Ojima *et al.* possessed one order of magnitude higher potency than that of paclitaxel against drug-sensitive cancer cell lines and two to three orders of magnitude higher potency than that of paclitaxel against MDR-expressing cell lines (See Chapter 1 for details), which enabled them to serve as highly promising drug candidates in mAb-cytotoxic agent conjugates.

It is also crucial to choose an appropriate linker between a taxoid and a mAb. The suitable linker should be stable during the circulation period *in vivo*, but readily cleavable to release taxoid in its active form inside cancer cell. As we have discussed previously (See § 3.1.4. for details), disulfide linkers have superior efficacy to other linkers because of their favorable characteristics.

Recently, our group successfully developed mAb-taxoid conjugates bearing disulfide linkers.[2] The preparation of mAb-taxoid conjugates is illustrated in Scheme 3-1. A 2nd-generation taxoid SB-T-1213 was chosen for the construction of mAb-taxoid conjugate. Structure-activity relationship (SAR) studies clearly demonstrated that cytotoxicity was retained when a 3-MDS-propanoyl group was attached to the C-10 position of the taxoid. The resulting 10-MDS-alkanoyl analog of SB-T-1213, SB-T-12136, was treated with dithiothreitol (DTT) to generate SB-T-12136-SH bearing a free thiol functionality. The mAb, KS61, KS77 and KS78, which specifically bind to human epidermal growth factor

receptor (EGFR), overexpressed in several human squamous cancers such as head, neck, lung, and breast cancers, was also modified with *N*-succinimidyl-4-(2-pyridyldithio)pentanoate (SPP) to attach 4-pyridyldithio (PDT)-pentanoyl groups. Subsequently, the modified mAb was conjugated with SB-T-12136-SH and purified by gel filtration to yield the immunoconjugates. The preliminary analysis of the KS77-taxoid conjugate by matrix-assisted laser desorption ionization time-of-flight (MALDI–TOF) indicated that ~ 4-5 taxoids were loaded per mAb molecule.

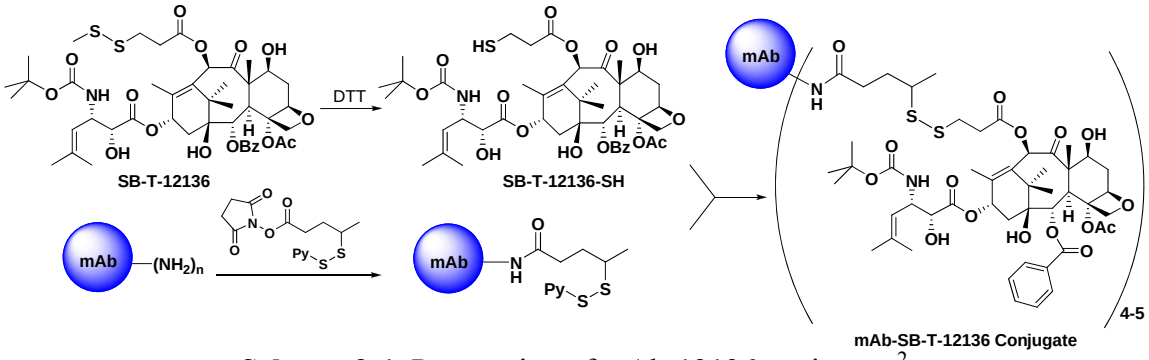

Scheme 3-1. Preparation of mAb-12136 conjugate.[2]

As illustrated in Figure 3-15, these three immunoconjugates exhibited impressive and promising results with specific cytotoxity (IC_{50} = 1.5 x 10^{-9} M) against A431 cancer cells expressing EGFR. However, non-binding immunoconjugate, ***mN901***-SB-T-12136 exhibited no cytotoxicity against the A431 cell line. *In vivo* antitumor activities of two conjugates, KS61-SB-T-12136 and KS77-SB-T-12136, were evaluated against human squamous cancer (A431) xenografts in SCID mice. Both immunoconjugates showed remarkable antitumor activity, with complete inhibition of tumor growth in all the treated animals for the duration of the experiment. Free taxoid SB-T-12136 at the same dose showed no therapeutic effect. Moreover, the immunoconjugates were totally non-toxic to the mice as demonstrated by the absence of any weight loss.[2]

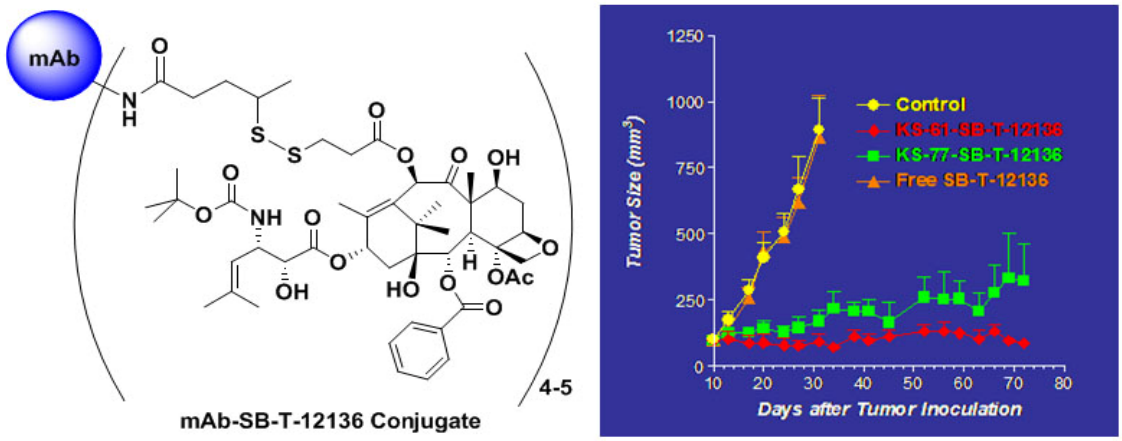

Figure 3-15. Antitumor activity of anti-EGFR mAb-taxoid immunoconjugates against A431 xenografts in SCID mice.[2]

§ 3.2.2. Novel Disulfide Linkers for Efficient Drug Release

Despite the success of 1st-generation mAb-taxoid immunoconjugates, the cytotoxicity of active therapeutics in cancer cell, SB-T-12136-SH, which is a derivative of the original taxoid molecule (SB-T-1213) with the compromised modification at C-10 position to attach the disulfide linker, was 8 times weaker than the parent taxoid (SB-T-1213) and therefore would not be potent enough for clinical use in humans (IC_{50} 0.5-0.8 nM against A431 and MCF7).[2] Accordingly, it is critical to develop 2nd-generation mechanism-based disulfide linkers to release therapeutics in their original form and restore the extremely high cytotoxicity upon internalization to cancer cells. To this aim, several novel disulfide linkers were proposed as shown in Figure 3-16.

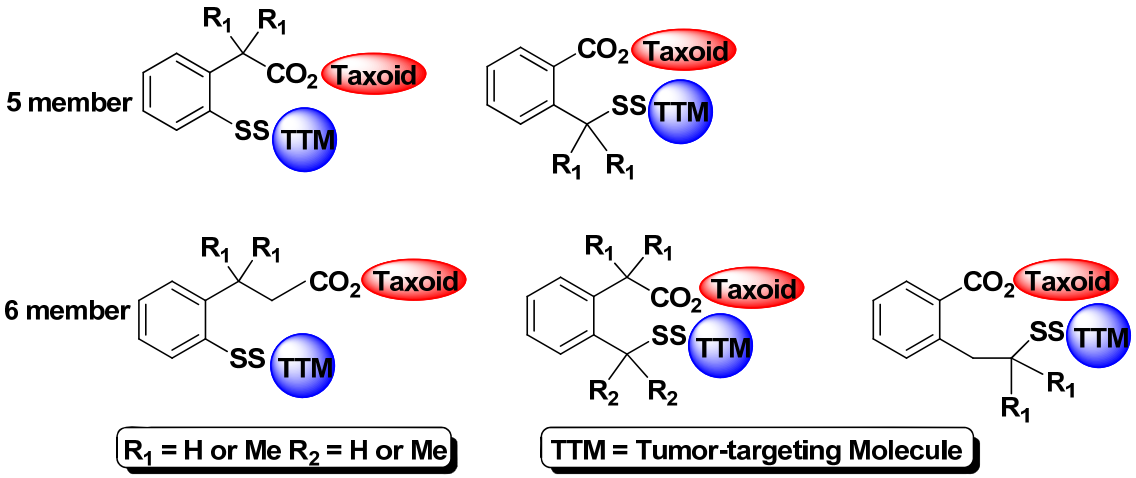

Figure 3-16. Novel disulfide linkers.

This novel class of mechanism-based self-immolative disulfide linker is bifunctional and can be connected to various warheads as well as tumor recognition modules. Once the tumor-activated prodrug conjugate is internalized into the tumor cells specifically, the glutathione-triggered cascade drug release takes place to generate the original anticancer agent. This mechanism-based drug release concept is clearly demonstrated in Figure 3-17. Inside the cancer cells, the disulfide linkage is cleaved by glutathione to generate a sulfhydryl group. The resulting free thiol group will then undergo an intramolecular nucleophilic acyl substitution on the ester moiety to form a 5- or 6-membered ring thiolactone and releasing the taxoid molecule in original active form. Additionally, the presence of a *gem*-dimethyl group will favor this cyclization process. It is essential to note herein that the concentration of glutathione (GSH) in blood plasma is very low (~ 2 μM), while that in tumor tissues is 1,000 times higher (2-8 mM). Also, the concentration of GSH in tumor tissues is 2-10 fold higher level than in normal tissues (10 fold higher in drug-resistant tumors).[70,74,75,76,77] Consequently, these disulfide linkers should be stable in blood circulation, but readily cleavable in tumor tissues and cells.

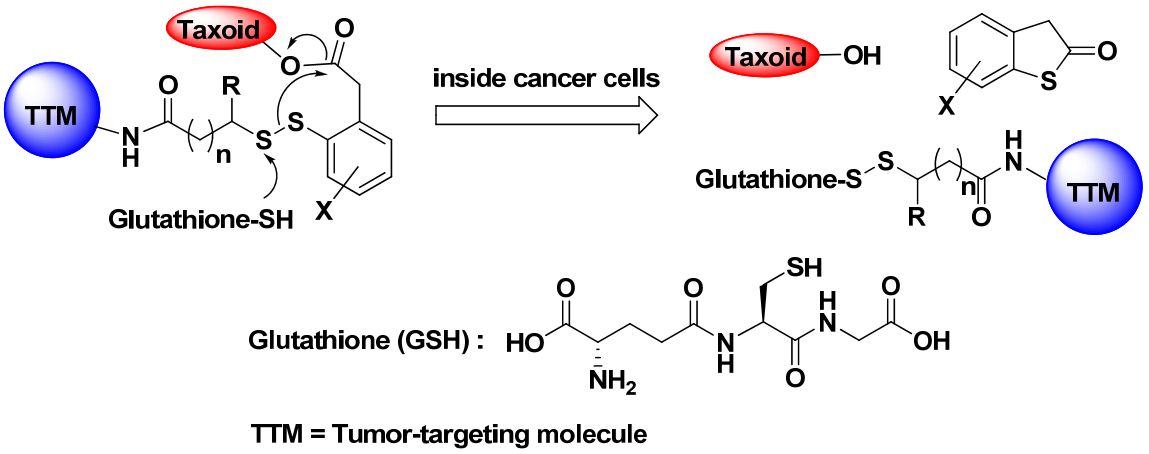

Figure 3-17. Proposed mechanism for 2nd-generation self-immolative disulfide linker.

Model reactions, wherein a *p*-fluorophenol was utilized as an alternative to a real drug and a fluorine tag was also introduced into the aromatic ring, were perform to clarify the mechanism-based release process, *e.g.* the relative reactivity of the disulfide linkers towards a thiol-initiated fragmentation, the substitution effect on the aromatic ring and the release profile under different pH conditions. The incorporation of the fluorine-labeled compound in the model system was to monitor the reaction with ^{19}F NMR.[78] ^{19}F NMR is believed to be a commonly used protocol for dynamic study of complex reaction systems due to the fact that fluorinated tags and their behavior can be easily detected by ^{19}F NMR technique even *in vivo*. Finally, cysteine was used to mimic glutathione in cancer cells. The model reaction was carried out at 37 ^{o}C with acetonitrile as cosolvent in pH 7.4 buffer solution. The progress of this reaction was monitored by time-dependent ^{19}F NMR and the expected intramolecular cyclization went smoothly and completed in about 90 min (Figure 3-18, this work was done by Dr. Ioana Ungreanu).

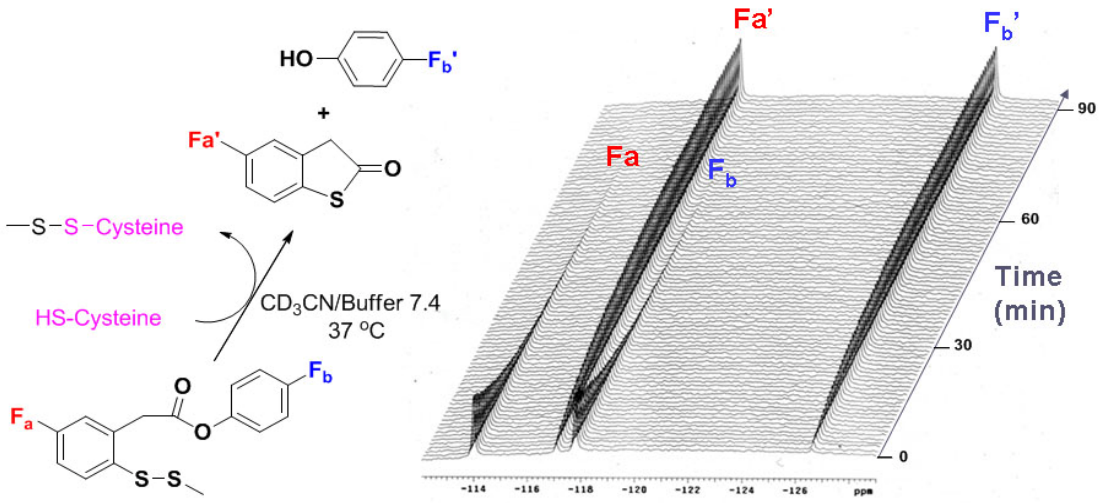

Figure 3-18. Model reaction for the mechanism-based release profile. (This work was done by Dr. Ioana Ungreanu)

With the encouragement of the promising preliminary results, the real therapeutic agent taxoid was applied for the drug release study, as shown in Scheme 3-2. The reaction was performed in a similar manner to the model drug system and monitored by TLC, HPLC and NMR. Time-dependent ^{19}F NMR spectrum clearly indicated the disappearance of the starting material and formation of thiolactone and free taxoid.

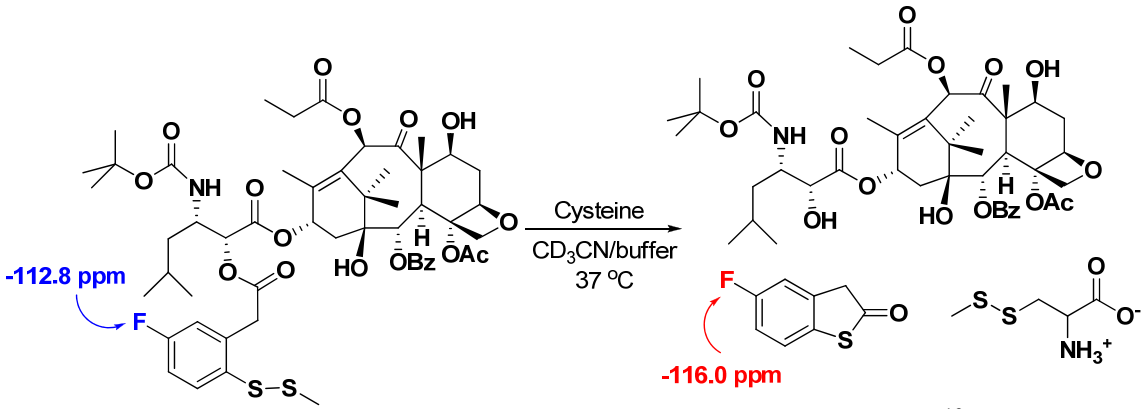

Scheme 3-2. Mechanism-based taxoid release profile monitored by ^{19}F NMR.

Different buffer solutions (pH = 6.0, 7.0, 8.0) were also used to investigate the release profile under different pH conditions. It was found that the reaction completed in 2 h at pH 7, similar to that at pH 8, wherein the reaction finished within 1.5 h. In comparison, the reaction went much slower at pH 6. At pH 6, only 84 % of conjugate was converted to thiolactone and taxoid even after 5 h. (Table 3-1)

Table 3-1. Mechanism-based taxoid release profile with HPLC analysis.

pH	Reaction time
6.0	> 5 h, at 5 h 84 % conversion
7.0	2.0 h
8.0	1.5 h

§ 3.2.3. Biotin as Tumor Recognition Moiety

Biotin (Figure 3-19) also known as vitamin H, is an essential vitamin for all organisms and is found to exist in liver, kidney, pancreas, and milk.[79] Biotin was first isolated from egg yolk in 1936 and later, the chemical structure was elucidated in 1942, which was further confirmed by X-ray crystallography in 1966.[80] Biotin has been found to play an important role in many biological processes, *e.g.* carboxylation, decarboxylation and transcarboxylation.[81] Additionally, the interactions between biotin and the glycoprotein, avidin (a tetrameric protein, with each subunit binding to one biotin molecule) is believed to be one of the strongest noncovalent intereactions ($K_d \sim 10^{-15}$ M).[82] This strong binding affinity lies on the hydrogen bonds between avidin and the heterocyclic structure of biotin. It has been reported that the ureido nitrogens in biotin enable hydrogen bond formation with avidin residues Thr35 and Asn118, while the carbonyl oxygen may interact with Ser16 and Tyr33. A variety of applications have been

achieved from biotin-avidin platform, *e.g.* affinity isolation and purification,[83] diagnostics[84]. Moreover, many biotin labeled biological substrates are now commercially available including peptides, proteins, oligonucleotides, and antibodies.[85]

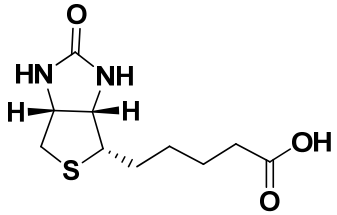

Figure 3-19. Chemical structure of biotin.

The most important characteristic of biotin for our purpose is that it can be applied as tumor recognition molecule in the drug delivery system. Although all living cells require vitamins for survival, the rapidly dividing cancer cells require extra vitamins, *e.g.* vitamin B12, folic acid, biotin and riboflavin to sustain their proliferation. Consequently, these receptors involved in uptake of the vitamins may be overexpressed on these cancer cells and serve as potentially useful biomarkers. In principle, anticancer agents linked to such certain types of vitamins should be highly attractive to tumor cells. The folate receptors have been documented as promising biomarkers for tumor-targeting drug delivery. Numerous reviews have been reported in literature to date.[86,87,88] However, the exploration of biotin receptors for drug delivery has not attracted sufficient attention, mainly because of the lack of biotin receptor structure.[89] In 2004, Russell-Jones *et al.* demonstrated that tumor cells expressing folate or vitamin B-12 receptors also showed a voracious appetite for biotin-containing conjugate (Table 3-2).[79] It is believed that biotin is a growth promoter at the cellular level, and its content in cancer tissues is substantially higher than that in normal tissues. Indeed, it was found that biotin receptors were even more overexpressed than other vitamins, such as folate and vitamin B12 receptors in several different types of cancer cells, including leukemia (L1210FR), ovarian (Ov 2008, ID8), Colon (Colo-26), mastocytoma (P815), lung (M109), renal (RENCA, RD0995), and breast (4T1, JC, MMT06056) cancer cell lines.[90] Consequently, all these findings strongly suggested the benefit of utilizing biotin as tumor recognition moiety and encouraged us to construct a biotin-mediated drug delivery platform, which will be discussed in more detail later in this Chapter.

Table 3-2. Relative uptake of vitamins in various tumor cell lines.[79] (Table was adapted from Ref. 79)

Tumor	Type	Folate	Vitamin B-12	Biotin
O157	Bcell Lymp	+/-	+/-	+/-
BW5147	Lymphoma	+/-	+/-	+/-
B16	Melanoma	-	-	-
LL-2	Lung	-	-	-
HCT-116	Colon Carcinoma	-	-	-
L1210	Leukemia	+/-	+/-	-
L1210FR	Leukemia	++	+	+++
Ov2008	Ovarian	+++	-	++
ID8	Ovarian	+++	-	++
Colo-26	Colon Carcinoma	+-	++	+++
P815	Mastocytoma	+/-	++	+++
M109	Lung	+	+++	+++
RENCA	Renal cell	+	+++	+++
RD995	Renal cell	+	++	+++
4T1	Breast	+	++	+++
JC	Breast	+	++	+++
MMT06056	Breast	+	++	+++

§ 3.2.4. Coupling-Ready Warhead

Since the drug release profiles have been successfully demonstrated in the model system (See § 3.2.2. for details), further efforts on construction of versatile tumor-activated prodrugs have been performed in our laboratory. To this aim, a hetero-bifunctional intermediate involving a novel mechanism-based, self-immolative disulfide linker was proposed, wherein two functional groups ready for further conjugation, carboxylic acid and active ester moiety, *i.e.* hydroxysuccinimide, were installed at the two termini respectively (Figure 3-20).

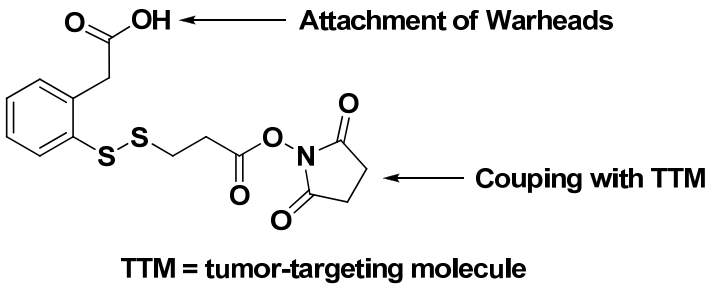

Figure 3-20. Structure of the hetero-bifunctional intermediate.

The carboxylic acid terminus was used for the attachment of any warhead that had a hydroxyl group, *e.g.* 2nd-generation taxoid SB-T-1214 or SB-T-1213, to afford the corresponding "coupling-ready warhead" construct. Subsequently, any tumor-targeting

molecule (TTM) bearing amine residues can ready couple with the active ester moiety to form an amide linkage using the standard peptide coupling protocol. Accordingly, it was believed that the construction of various tumor-targeting drug conjugates will proceed smoothly on the basis of the afore-mentioned coupling-ready warhead. Some examples are described in Figure 3-21.

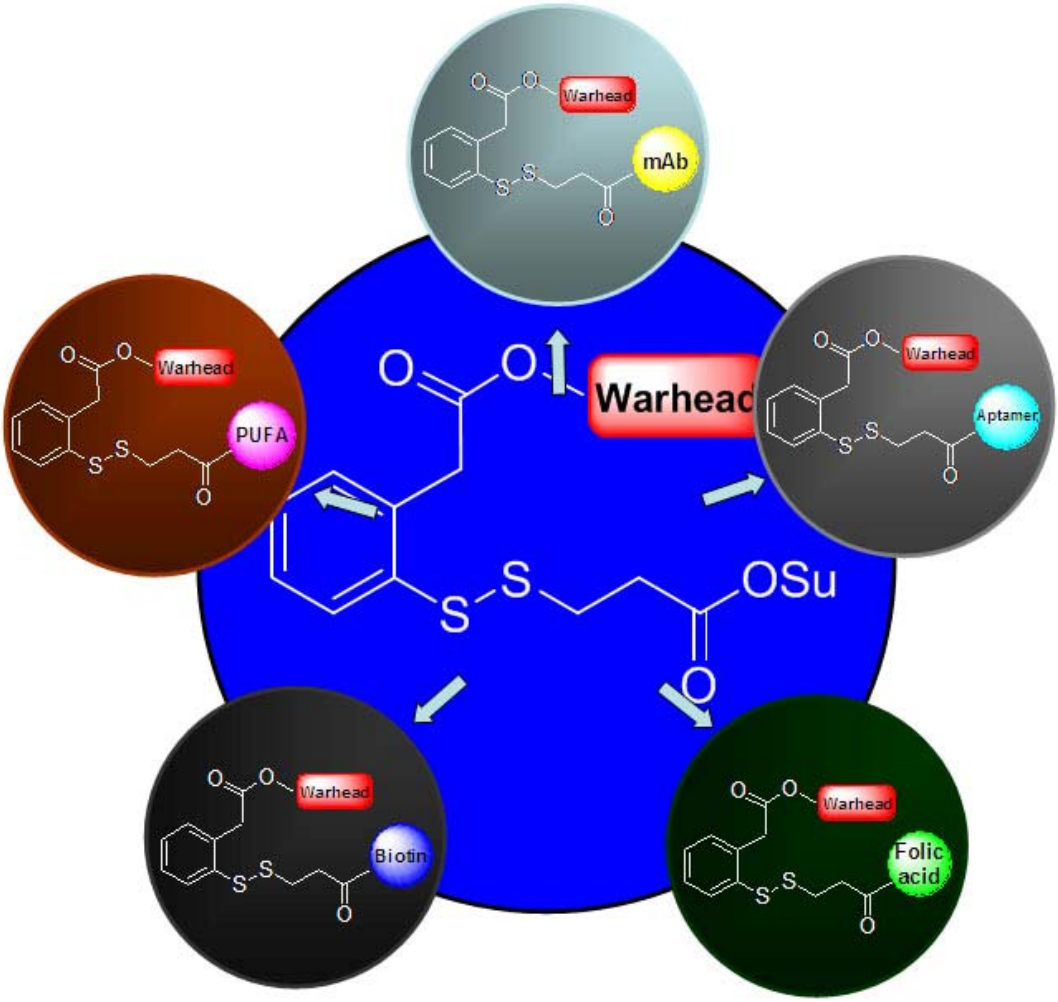

Figure 3-21. Examples of tumor-targeting drug conjugates bearing novel self-immolative disulfide linkers.

§ 3.2.5. Fluorescent Probes for Evaluation of Intracellular Drug Release

Fluorescent molecules responsive to the intracellular environment of cells have proven to be indispensable for the rapid detection of essential elements in biological sciences, drug discovery and delivery system, as illustrated in Figure 3-22.[91,92,93,94,95]

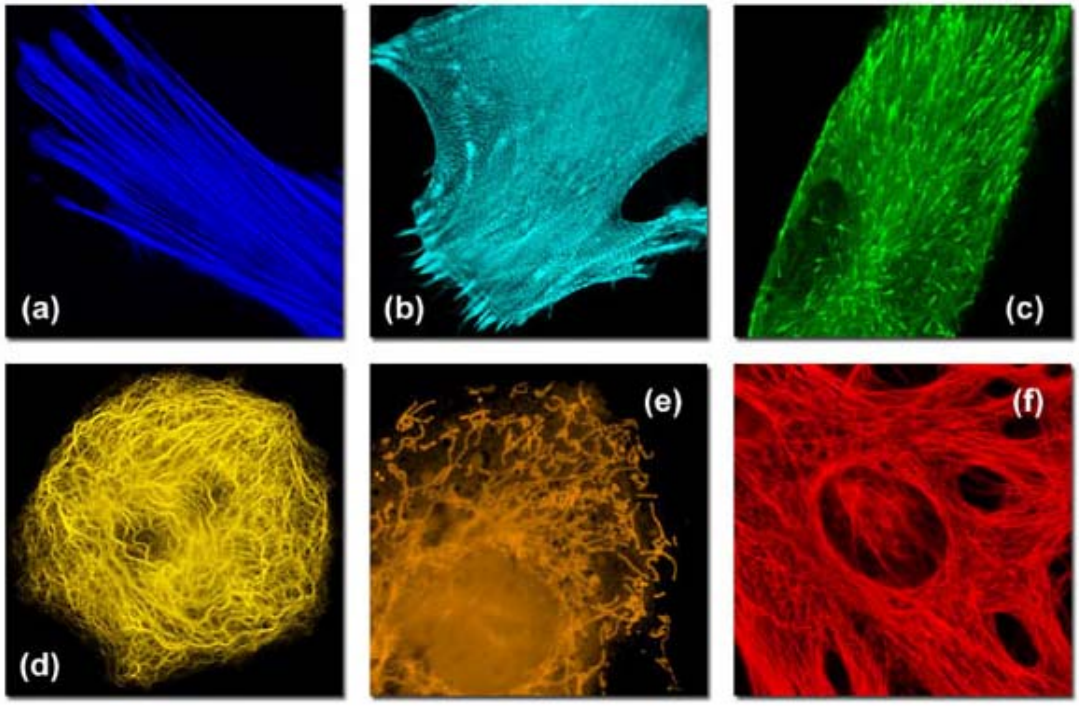

Figure 3-22. Subcellular localization of fusion genes highlight organelles of interest with new colors: (a) Azurite-actin targets the filamentous actin network; (b) alpha-actinin-mTFP1 bestows a cyan emission to focal adhesions and cytoskeletal elements; (c) YPET fused to the microtubule end-binding protein EB-3 tracks the growth of microtubules; (d) Kusabira Orange reveals cytokeratin intermediate filaments; (e) tandem-dimer Tomato fused to a mitochondrial targeting sequence helps visualize mitochondria; (f) mPlum highlights the vimentin filamentous network with emission in the deep red region of the spectrum. (Figure was adapted from http://www.rdmag.com/images/0704/0704Microscopy image lrg.jpg)

With proof-of-concept for readily available fluorophore dyes capable of detecting intracellular organic biomolecules, we turned our attention to fluorescein and coumarin derivatives due to their high quantum yields and water solubility (Figure 3-23).

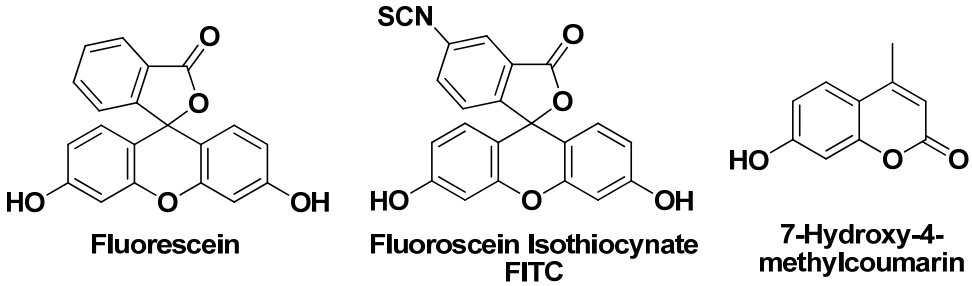

Figure 3-23. Commonly used fluorescent probes: fluorescein and coumarin derivatives.

A set of fluorescent and fluorogenic probes, *i.e.* (a) biotin-FITC **(3-49)**, (b) biotin-linker-coumarin **(3-53)** and (c) biotin-linker-SB-T-1214-fluorescein conjugate **(3-64)**

(Figure 3-24) were proposed to monitor in real-time the receptor-mediated endocytosis process and clarify controlled drug release mechanism with confocal fluorescence microscopy (CFM).

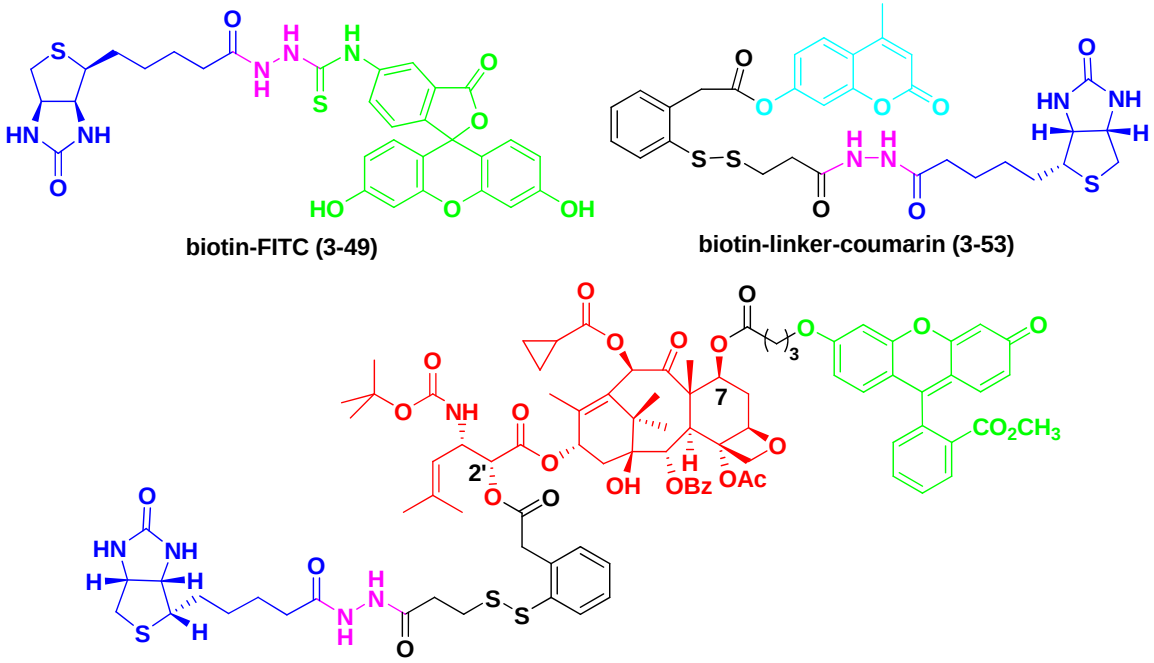

Figure 3-24. Fluorescent and flurogenic probes for the internalization and drug release.

The attachment of fluorescent probe "fluorescein isothiocyanate (FITC)" to the tumor-targeting moiety, *i.e.* biotin afforded biotin-FITC conjugate **(3-49)**, which would allow us to elucidate cellular uptake of the tumor-targeting molecule *via* receptor-mediated endocytosis pathway. To demonstrate the efficacy of the mechanism-based self-immolative disulfide linker, a fluorogenic probe "biotin-linker-coumarin conjugate **(3-53)**" was also proposed, wherein a coumarin derivative was introduced as a profluorophore whereas "lighting up" upon the action of endogenous thiol, such as glutathione (GSH). The presence of fluorogenic moieties has served as model drugs for sensitively probing drug release activities. The conjugate was initially nonfluorescent when the electron-donating group, *i.e.* phenolic group, on the coumarin unit, was attached to the disulfide linker *via* an ester bond.[96] However, once the disulfide linker was cleaved by endogenous thiol, glutathione in particular, an intramolecular cyclization took place and unmasked a highly fluorescent free coumarin that could be readily detected, as described in Figure 3-25.

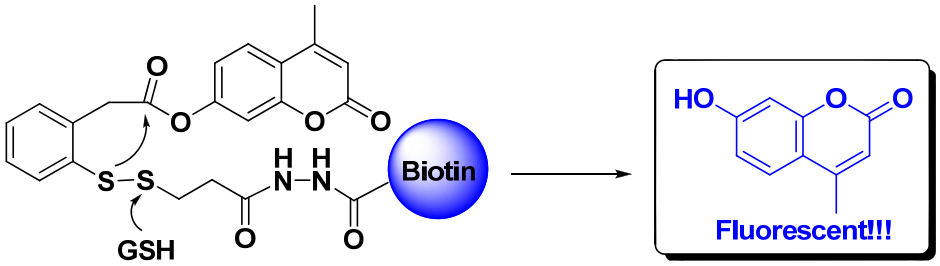

Figure 3-25. Intracellular release of coumarin from fluorogenic probe biotin-linker-coumarin conjugate **(3-53)**.

Fluorescent paclitaxel derivatives have been applied to the study on cellular microtubules, as well as the mechanisms of microtubule assembly and stabilization by paclitaxel.[97,98,95] Figure 3-26 depicts the fluorescence microscopy images of permealized and fixed H-460 cells by FITC-labeled (A) and rhodamine-labeled paclitaxel (B) staining.

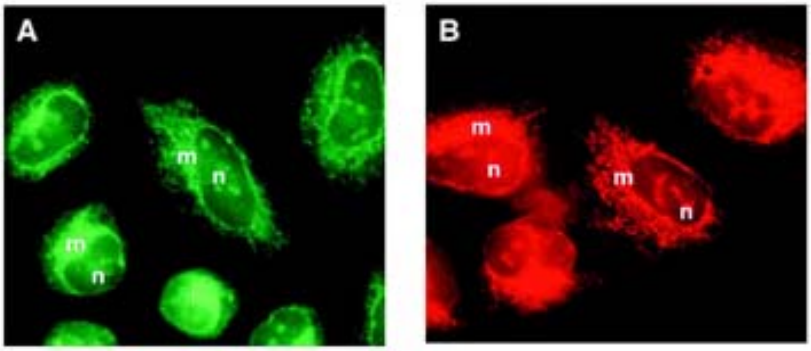

Figure 3-26. The fluorescence microscopy images of permealized and fixed H-460 cells by FITC-labeled (A) and rhodamine-labeled paclitaxel (B) staining; m = microtubule organizing center; n = nucleus.[97] (Figure was adapted from Ref. 97)

On the basis of previous literature, the biotin-linker-SB-T-1214-fluorescein conjugate **(3-64)** was constructed to validate the receptor-mediated endocytosis of the whole prodrug conjugate and taxoid release processes. Figure 3-27 illustrates a detailed plausible receptor-mediated endocytosis process and drug release mechanism with biotin as the tumor-targeting module. Once localized at the tumor site, the biotin-linker-SB-T-1214-fluorescein conjugate **(3-64)** bound to its complementary receptor on the tumor cell surface and is further internalized. Subsequently, the disulfide linkage was cleaved by endogenous disulfide-reducing peptides, such as glutathione (GSH), which was reported at elevated levels in cancer cells,[70] to generate a sulfhydryl group. The resulting thiol then underwent a nucleophilic acyl substitution of the ester moiety, forming a 5-membered ring thiolactone and thereby releasing the taxoid in original form to restore its high potency. Since fluorescein-labeled taxoid was applied in this study to monitoring the intramolecular cyclization process, the freed fluorescent taxoid should bind to the target protein, microtubules, in the cancer cells and render possible to real-time visualize the fluorescent microtubule network where the taxoid had localized.

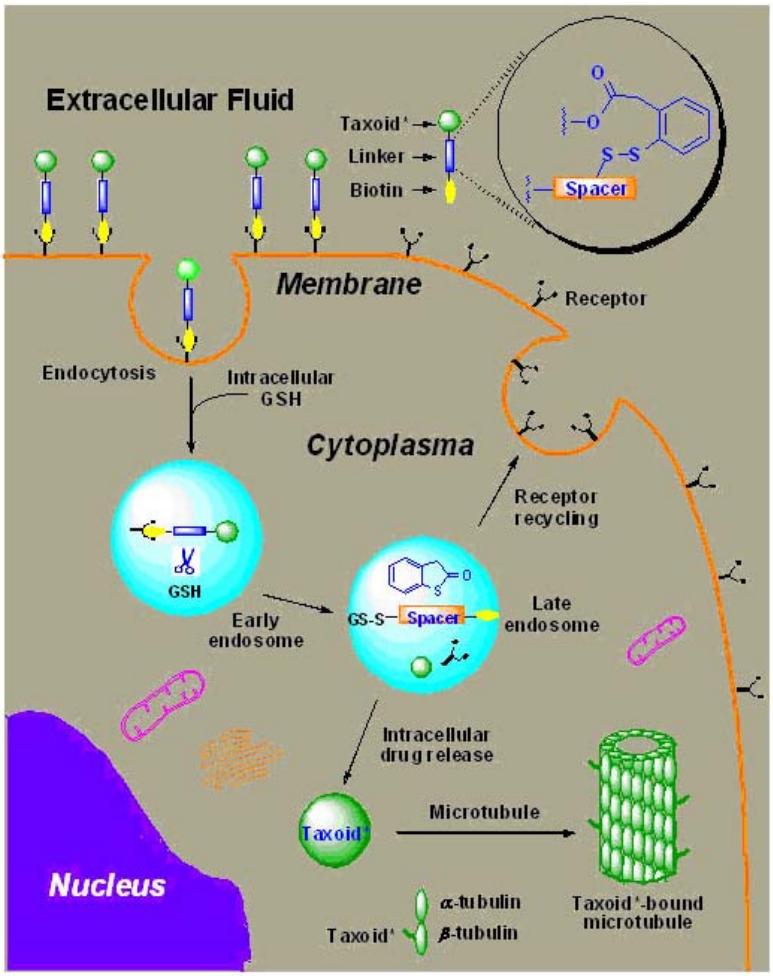

Figure 3-27. Receptor-mediated endocytosis of the whole drug conjugate and the taxoid release mechanism: (A) the biotin-taxoid conjugates are first delivered to the tumor cells by receptor-mediated endocytosis; and (B) the drugs are released intracellularly by cleavage of the disulfide bond using glutathione (GSH).

§ 3.3. Results and Discussion

§ 3.3.1. A New Class of Disulfide Linkers

Despite the promising achievements of mechanism-based drug release traced by time-dependent ^{19}F NMR, there are still a lot of details to be clarified in our disulfide-containing system, *e.g.* the relative reactivity of the disulfide linkers towards a thiol-initiated fragmentation, the substitution effect on the aromatic ring and the release profile under different pH conditions. Accordingly, a systematic kinetic study, wherein a *p*-fluoro-phenol was used as an alternative to a real drug for simplicity, was performed towards the understanding of the drug release processes. Glutathione was utilized to mimic the reducing biological environment *in vitro*. All the model reactions were carried

out at 37 ^{o}C and pH 7.4 conditions. This project was carried out in collaboration with Dr. Jin Chen, Mr. Xianrui Zhao, Dr. Stanislav Jaracz and Mrs. Manisha Das.

§ 3.3.1.1. Synthesis of Disulfide-Containing Linkers

Initially, the relative activity of disulfide linkers with variable lengths was investigated, as shown in Figure 3-28.

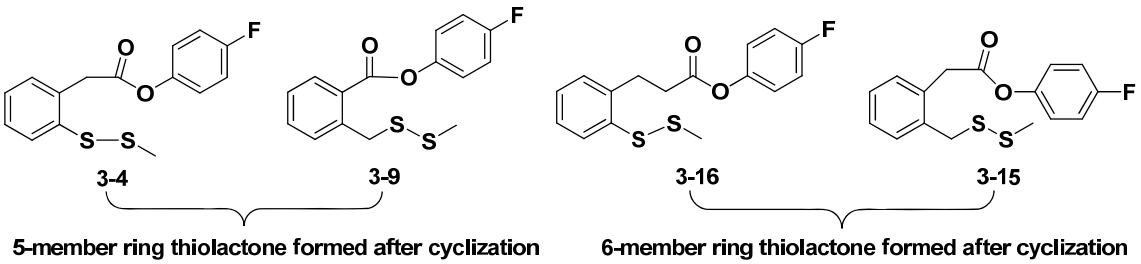

Figure 3-28. Structure of disulfide linkers with variable lengths.

The disulfide linker **(3-4)** has been proven to be the most successful substrate in our model study system. Its synthetic route is illustrated in Scheme 3-3. First, oxidation of benzo[b]thiophen-2-ylboronic acid with H_2O_2 in ethanol gave the 5-member ring thiolactone **(3-1)**, which was then hydrolyzed to yield the corresponding product **(3-2)** bearing a free sulfhydryl group. Methyl methanethiosulfonate was used in thiol-disulfide exchange reaction to afford methyl disulfide **(3-3)**, followed by esterification with *p*-fluorophenol and DIC/DMAP protocol to give the final product **(3-4)** in good overall yield.

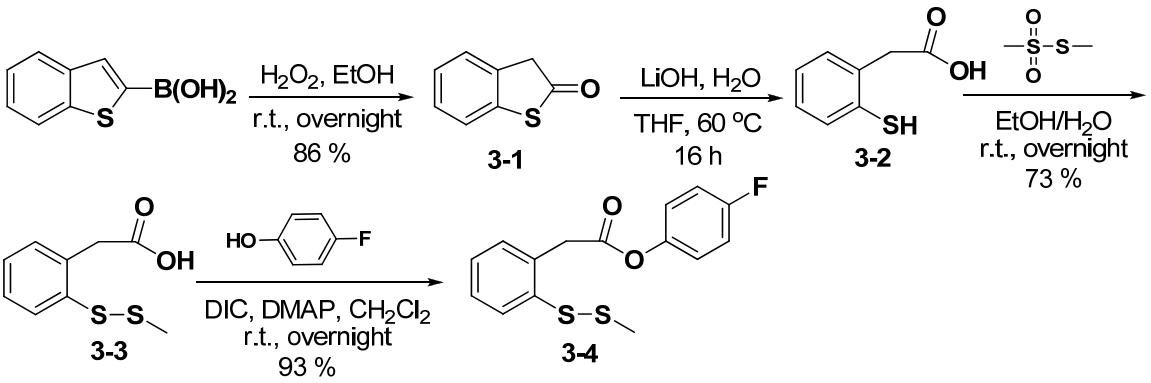

Scheme 3-3. Synthesis of 4-fluorophenyl 2-(2-(methyldisulfanyl)phenyl)acetate **(3-4)**.

The strategic synthesis of disulfide linker **(3-9)** is illustrated in Scheme 3-4. Starting from the bromination of the commercially available methyl 2-methylbenzoate with *N*-bromosuccinimide provided 2-bromomethylbenzoic acid methyl ester **(3-5)** in 94 % yield, which further reacted with thiourea in acetone under reflux conditions to give thiouronium salt **(3-6)**. The subsequent hydrolysis step was performed using potassium hydroxide in methanol/water solvent system to yield 2-mercaptomethyl benzoic acid **(3-7)**

in excellent yield, which underwent methyl disulfide formation **(3-8)** and esterification to afford the desired disulfide linker **(3-9)**.

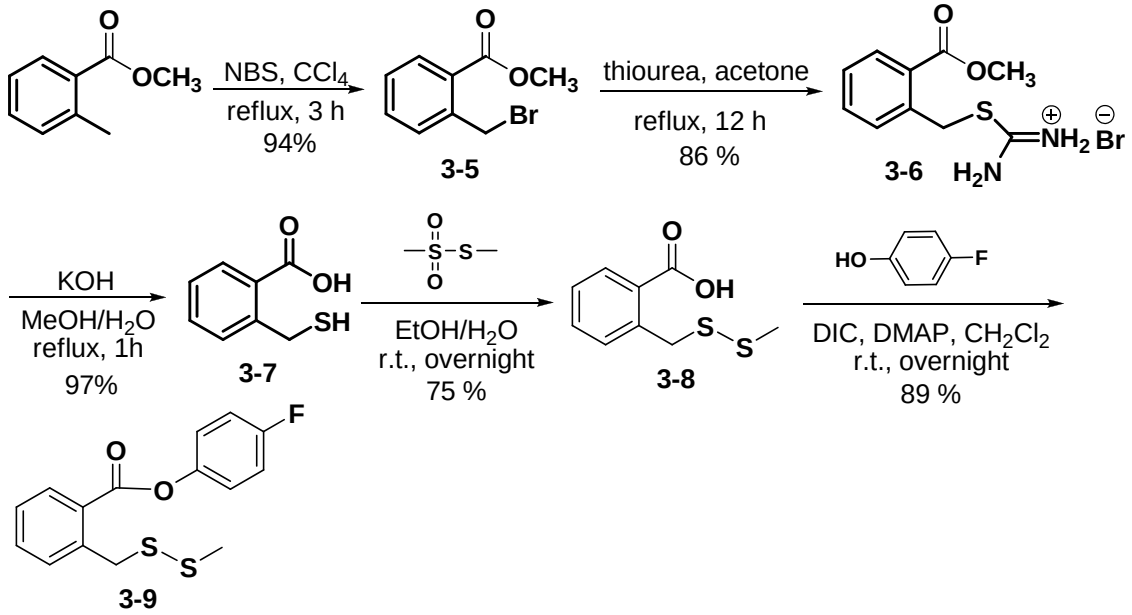

Scheme 3-4. Synthesis of 4-fluorophenyl 2-((methyldisulfanyl)methyl)benzoate **(3-9)**.

Preparation of disulfide linker **(3-15)** started from ring-opening hydrolysis of isochroman-3-one with hydrobromic acid in acetic acid, giving the corresponding product 2-bromomethylphenylacetic acid **(3-10)**. Protection of the carboxylic acid moiety with sulfuric acid in methanol yielded the corresponding methyl ester **(3-11)**, which was treated with thiourea and further basic hydrolysis readily furnished thiol substrate **(3-13)**. Final disulfide linker **(3-15)** was obtained after methyl disulfide formation **(3-14)** and esterification in a similar manner as that mentioned above (Scheme 3-5).

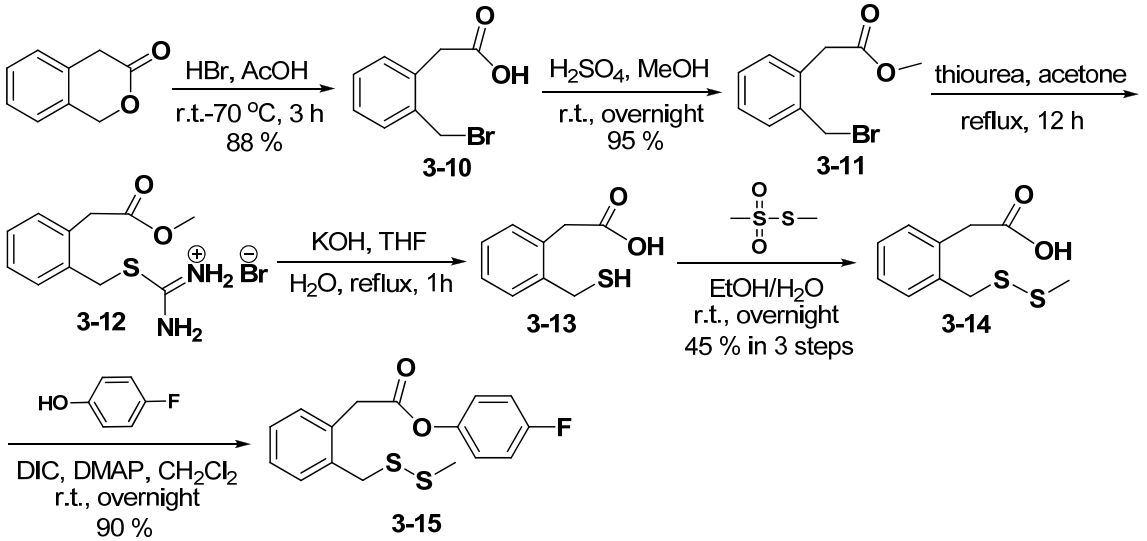

Scheme 3-5. Synthesis of 4-fluorophenyl 2-(2-((methyldisulfanyl)methyl)phenyl)acetate **(3-15)**.

Cyclization reactions are extremely critical components in organic synthesis (Scheme 3-6). The *gem*-dimethyl effect, also termed as Thorpe-Ingold effect was first reported by Beesley, Thorpe and Ingold in 1916 to accelerate cyclization rate by a *gem*-dialkyl moiety located on the framework of the acyclic carbon backbone.[99,100,101,102,103,104,105,106] A common application of this effect is the presence of a quaternary carbon, *e.g.* a *gem*-dimethyl group, in an alkyl chain, to increase the reaction rate of cyclization.

Dehydration and Anhydride Formation:

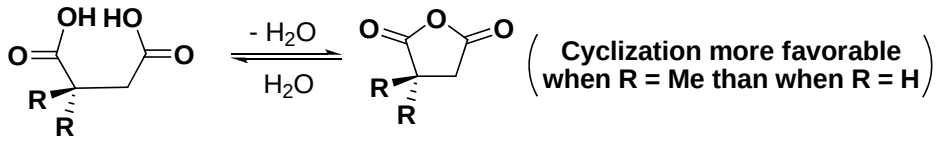

Olefin Metathesis:

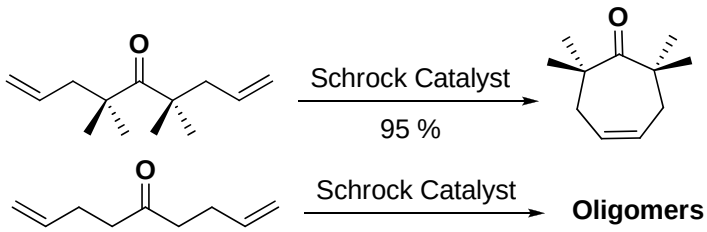

[2+2] Photocyclization:

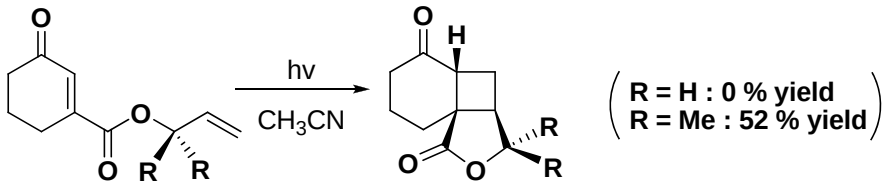

Intramolecular Diels-Alder Reactions:

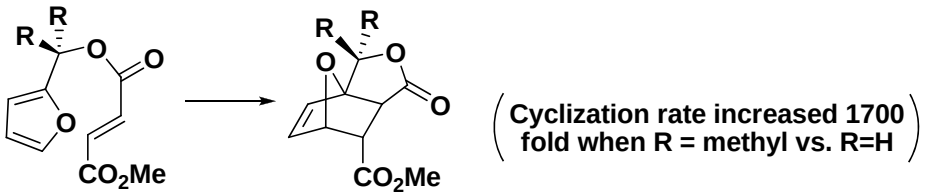

Scheme 3-6. Utilization the *gem*-dimethyl effect to facilitate organic synthesis.

The *gem*-dimethyl effect has also been widely used as a convenient means of constructing complicated macrocyclic molecules because of the expected minor perturbations in reactivity (Figure 3-29).

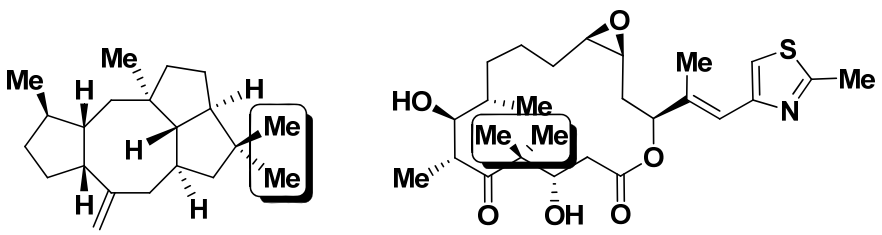

Figure 3-29. Utilization of the *gem*-dimethyl effect to construct complicated macrocyclic molecules.

The postulation for afore-mentioned rate acceleration in cyclization was attributed to the decrease in angle between the two reacting termini when the *gem*-dimethyl functionality was located on the framework of the acyclic carbon backbone (Figure 3-30). This compression would subsequently result in positioning two reacting termini closer to each other and increase the cyclization rate.

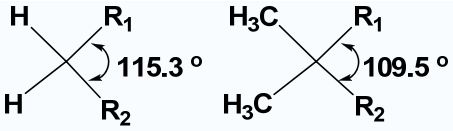

Figure 3-30. Decreasing in angle between the two reacting termini when the *gem*-dimethyl functionality was introduced.

In our attempts to elucidate the mechanism-based release process, we believed that the incorporation of *gem*-dimethyl effect may facilitate the intramolecular cyclization and thereby accelerate the drug release. Accordingly, a set of disulfide linkers bearing a *gem*-dimethyl functionality on the benzilic position was proposed, as illustrated in Figure 3-31.

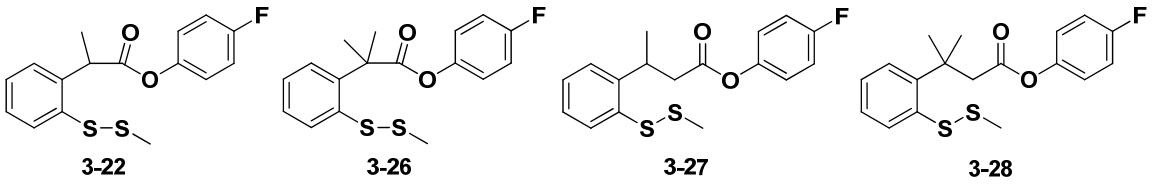

Figure 3-31. Structure of disulfide linkers with a *gem*-mono/dimethyl functionality on the benzilic position.

The synthesis of 4-fluorophenyl 2-(2-(methyldisulfanyl)phenyl)propanoate **(3-22)** was performed in a convenient way (Scheme 3-7). The thiolactone **(3-1)** was initially condensed with diphenylformamidine in boiling ether solution to afford phenylimino thiolaction **(3-17)**, which subsequently underwent a basic hydrolysis in aqueous ethanol to yield the aldehyde **(3-18)**. The transformation from aldehyde to monomethyl-substituted thiolactone **(3-19)** was performed under reductive conditions, *i.e.* sodium

borohydride in acetic acid. Further basic hydrolysis, methyl disulfide formation and ester condensation should give the desired product 4-fluorophenyl 2-(2-(methyldisulfanyl)-phenyl)propanoate **(3-22)**.

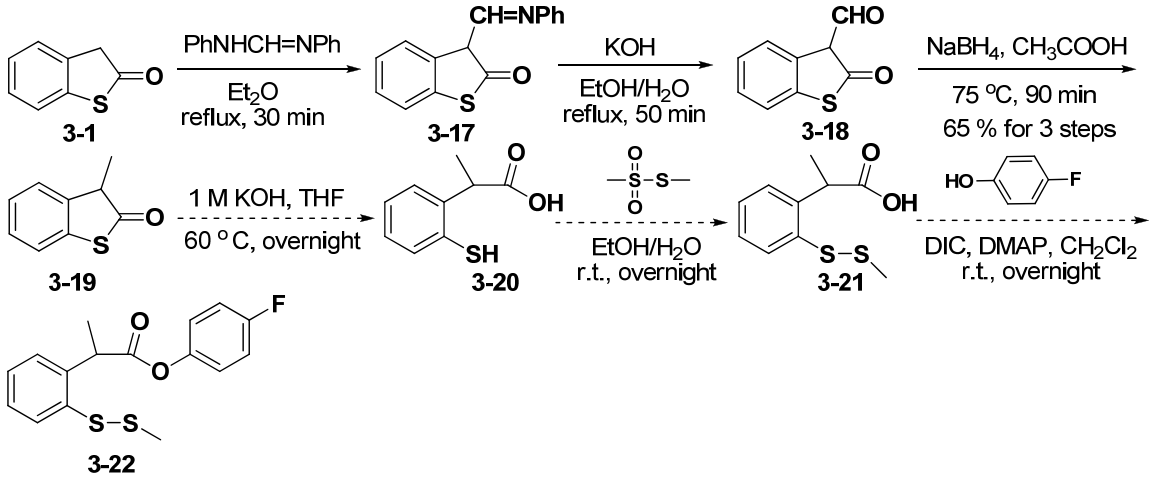

Scheme 3-7. Synthesis of 4-fluorophenyl 2-(2-(methyldisulfanyl)phenyl)propanoate **(3-22)**.

The attempt towards the synthesis of dimethyl substituted disulfide linker **(3-26)** was also carried out from the thiolactone **(3-1)**, which was treated with potassium *tert*-butoxide and iodomethane to introduce the dimethyl functionality to the benzilic position **(3-23)**. Further reactions, including basic hydrolysis, methyl disulfide formation and ester condensation will be performed to provide the desired dimethyl substituted disulfide linker 4-fluorophenyl 2-methyl-2-[2-(methyldisulfanyl)phenyl]propanoate **(3-26)**, as shown in Scheme 3-8.

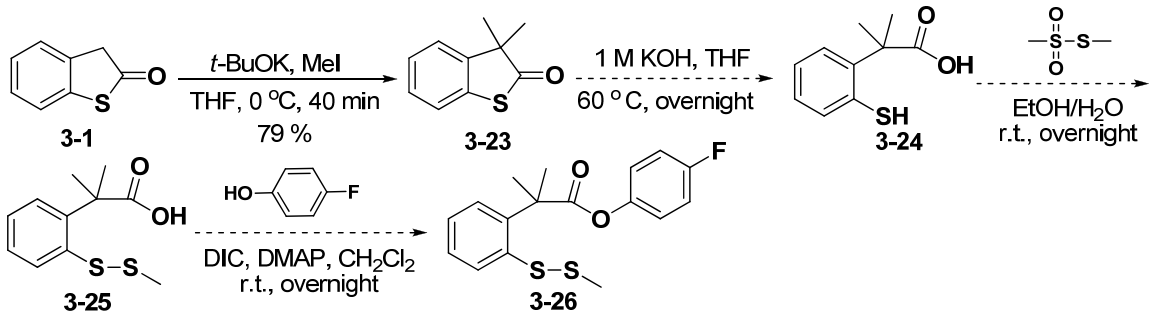

Scheme 3-8. Synthesis of 4-fluorophenyl 2-methyl-2-[2-(methyldisulfanyl)phenyl]propanoate **(3-26)**.

Other efforts towards the kinetic study of the mechanism-based drug release such as the substitution effect on the aromatic ring and the comparison of the polarities of different disulfide bonds have also been performed by Dr. Stanislav Jaracz (Figure 3-32) and Mrs. Manisha Das (Figure 3-33), respectively.

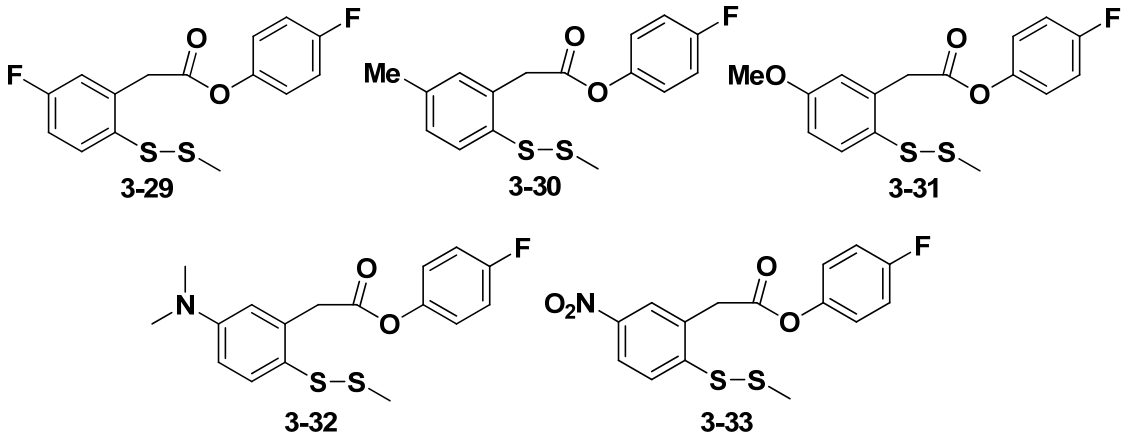

Figure 3-32. Structure of disulfide linkers with substituents on aromatic ring.

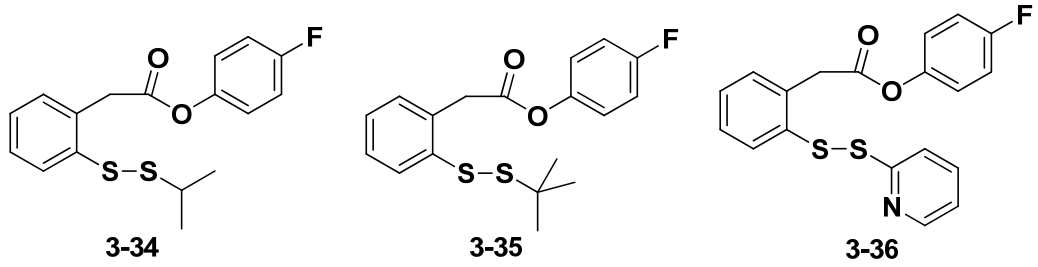

Figure 3-33. Structure of disulfide linkers with different S-S bonds.

Meanwhile, the strategic synthesis of coupling-ready warhead **(3-40)** was also explored. The original synthetic route is illustrated in Scheme 3-9. 3-Mercapto-propanoic acid reacted with 2, 2'-bipyridyl disulfide to give 3-(2-pyridyldithio)propanoic acid **(3-37)**. The resulting carboxylic acid **(3-37)** was then converted to the corresponding active ester **(3-38)** by condensation with *N*-hydroxysuccinimide. The thiol-disulfide exchange reaction between a free sulfhydryl derivative **(3-2)** and the pyridine disulfide substrate **(3-38)** yielded the hetero-bifunctional intermediate **(3-39)**, which was further attached to the 2^{nd}-generation taxoid, SB-T-1214 **(1-23)**, under the standard coupling conditions (DIC/ DMAP) to provide the desired coupling-ready warhead conjugate **(3-40)**.

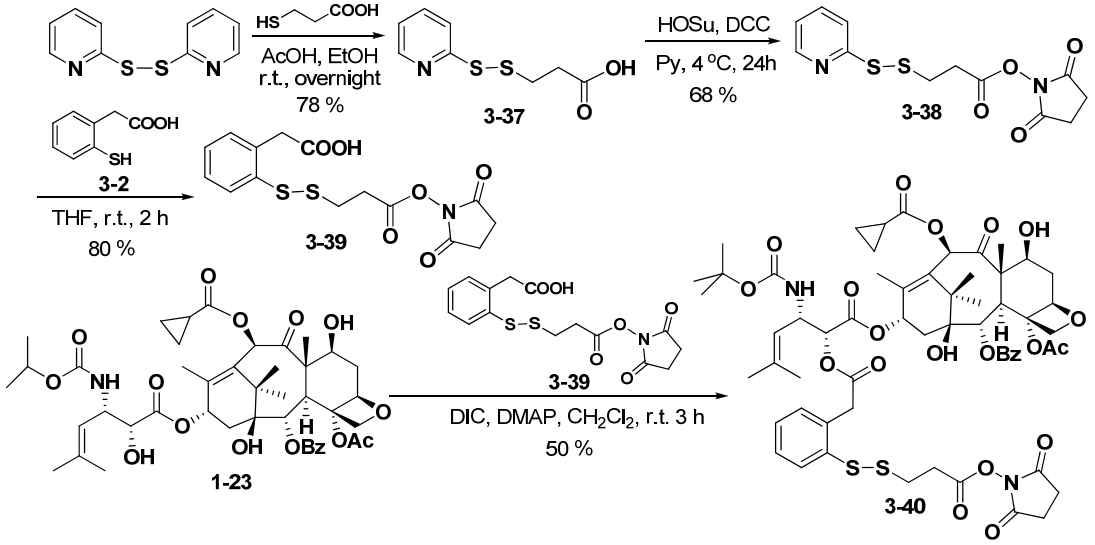

Scheme 3-9. Original synthetic route towards the coupling-ready warhead conjugate **(3-40)**.

Unfortunately, the final coupling step suffered from low yield and hard separation from the reaction mixtures. This may be ascribed to the presence of DMAP, which caused partial loss of the active ester. The possible optimization of this synthesis was to revise the synthetic strategy, wherein the protection of the carboxylic acid in substrate **(3-37)** took place before the conjugation with taxoid. Accordingly, an allyl-ester group was employed in the first trial, as described in Scheme 3-10.

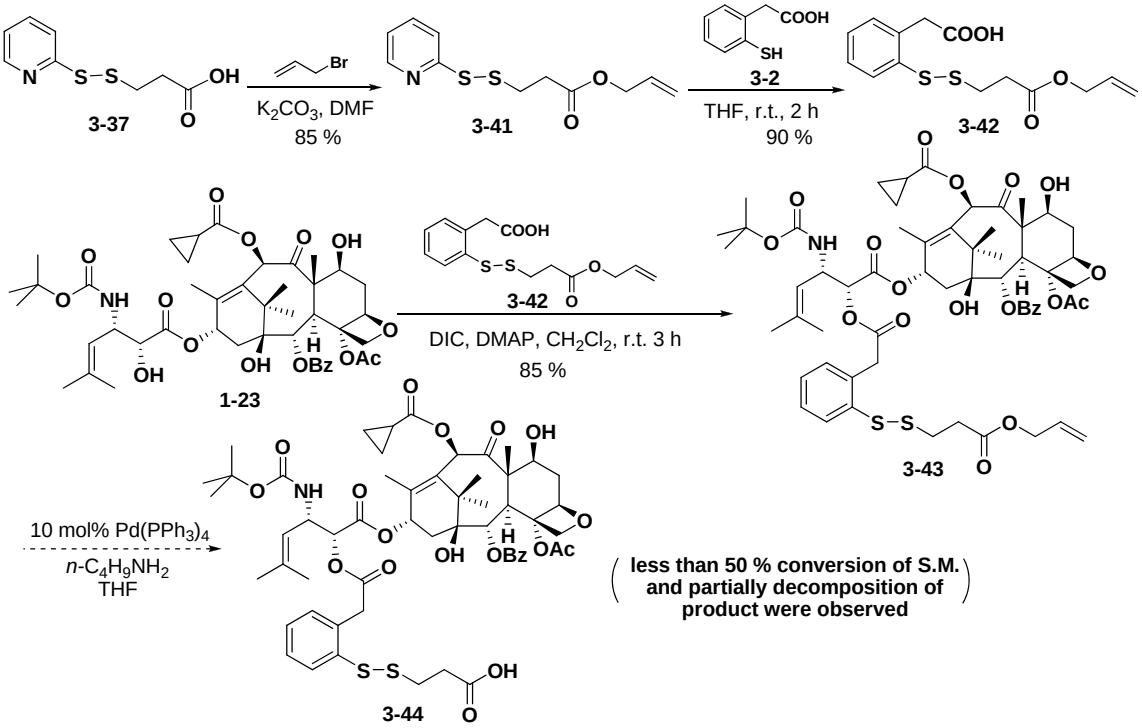

Scheme 3-10. Utilization of an allyl-ester protecting group in the synthesis towards the coupling-ready warhead conjugate.

As shown in Scheme 3-46, the coupling reaction between the disulfide linker unit **(3-42)** and SB-T-1214 **(1-23)** proceeded smoothly in good yield. Nevertheless, the low conversion of the starting material **(3-43)** (less than 50 % conversion) and the partial decomposition of the product were observed in the last deprotection step. This failure made it unfeasible for the smooth synthesis of the coupling-ready warhead conjugate. Another attempt, wherein the triisopropylsilyl (TIPS) ester was applied as the protecting group to mask the carboxylic acid in substrate **(3-37)**, was explored and proved to be a highly efficient synthetic route towards the coupling-ready warhead construct, without any unexpected side reactions and purification difficulties (Scheme 3-11). With this protocol, the coupling-ready warhead construct can readily be conjugated with any tumor targeting molecules bearing the amino functionality to provide versatile tumor-activated prodrugs.

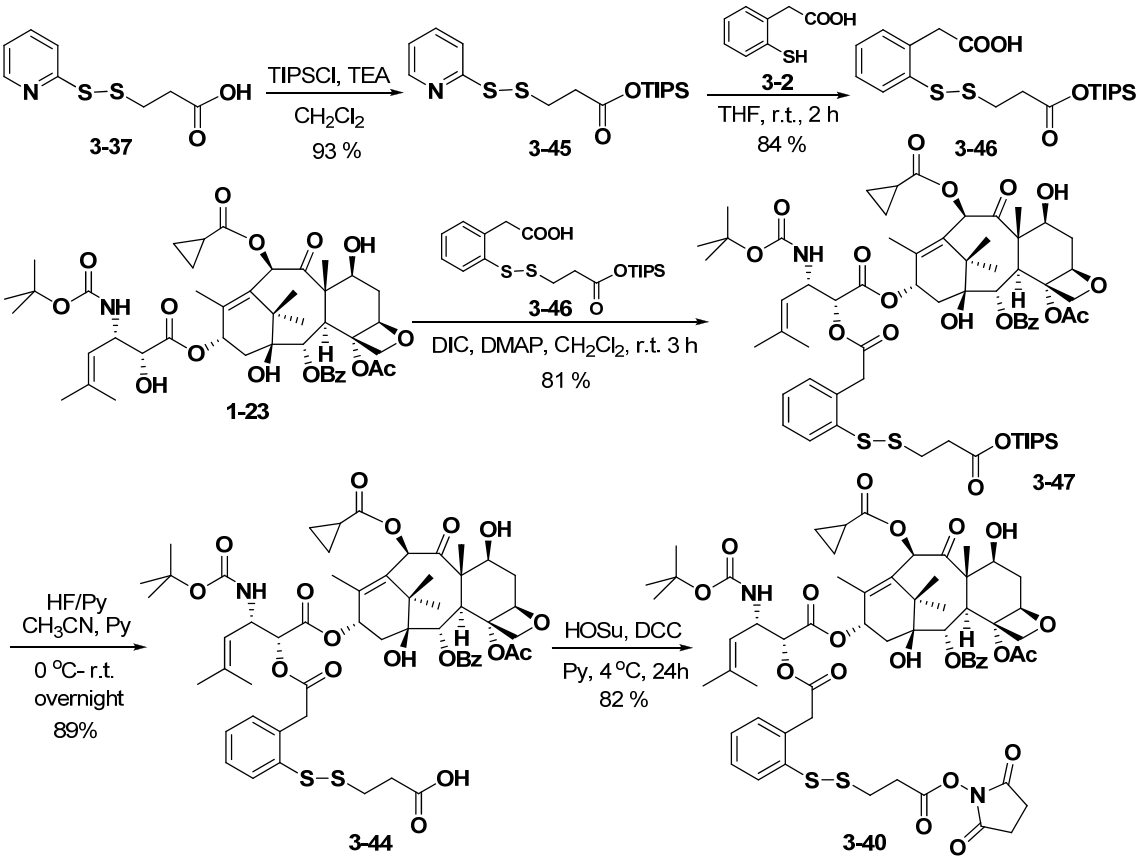

Scheme 3-11. Synthesis of the coupling-ready warhead conjugate **(3-40)** using TIPS-ester protecting group.

§ 3.3.1.2. Kinetic Study of Model Drug Release Profile

To date, the disulfide linker **(3-4)** has been proven to be the most promising candidate to trigger mechanism-based drug release, *via* thiol disulfide exchange reaction, fast intramolecular cyclization to form the thiolactone, and the release of the free *p*-fluorophenol or taxoid. To further understand the characteristics of this self-immolative disulfide linker, a series of systematic kinetic studies were performed in our laboratory,

including reaction rate constant determination and pH-dependent drug release profile by Dr. Jin Chen.

The reaction rate constant was determined based on HPLC assay as shown in Scheme 3-12. The reaction was carried out in the presence of 100 equivalents of glutathione, pH 7.4 buffer, at 37 °C to mimic biological conditions. Acetonitrile was used as the co-solvent to improve the poor solubility of the substrate.

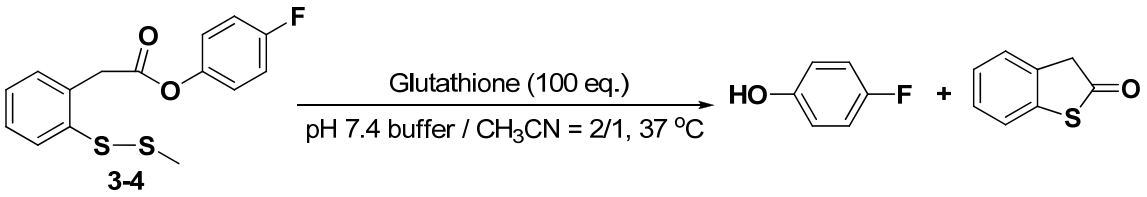

Scheme 3-12. Model reaction for rate constant determination using disulfide linker **(3-4)**.

Subsequently, the rate constant was calculated according to rate law, rate = -d[A]/dt = k[A][B]. When B is in large excess, rate = -d[A]/dt = q[A], wherein q = k[B]. As shown in Figure 3-34 (C), ln(A) exhibited a linear relationship with time course, which indicated that this reaction was considered a pseudo-first order reaction. Consequently, $\ln(A_t) = \ln(A_0)-qt$, $q = 6.1\times10^{-2}$ min^{-1}, half time $t_{1/2} = 11.4$ min.

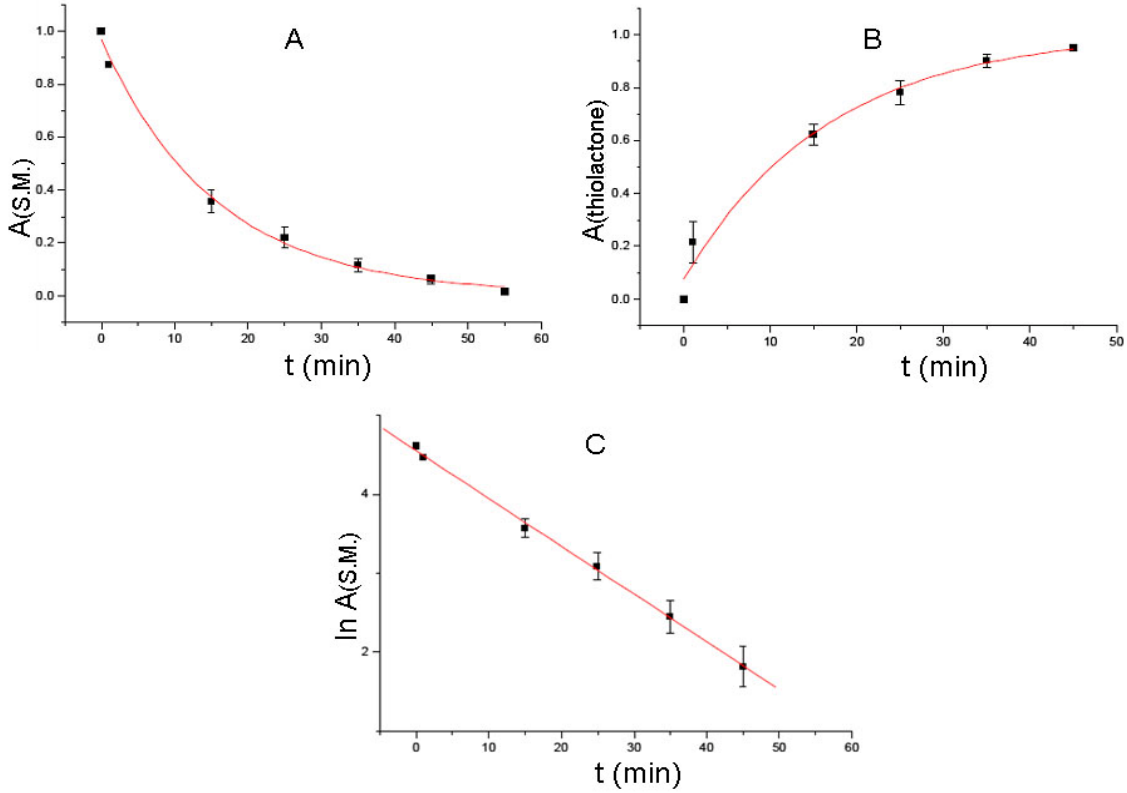

Figure 3-34. Measurement of model drug release rate constant for disulfide linker **(3-4)**.

In sharp contrast, in the case of disulfide linker **(3-9)** and **(3-15)** bearing S-S bond at the benzilic position, both reactions were extremely slow with incomplete conversion even after days (Scheme 3-13).

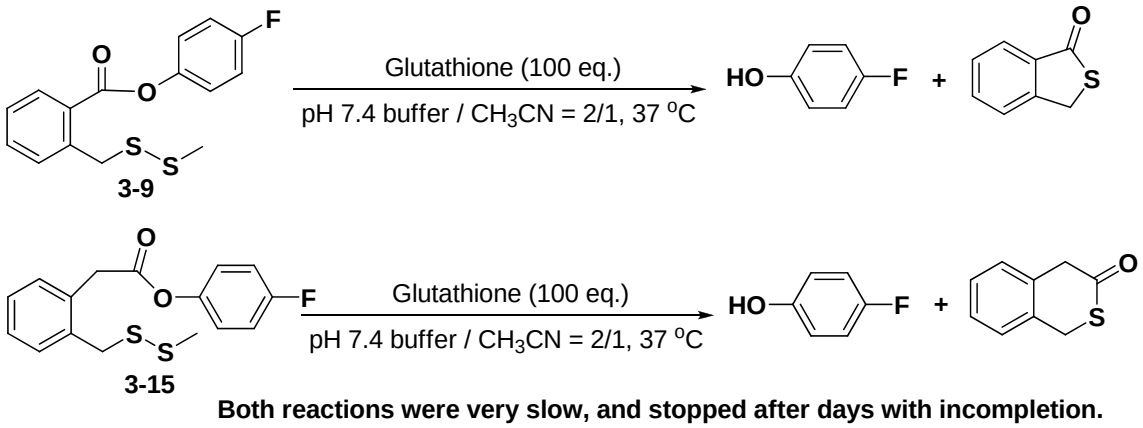

Scheme 3-13. Model reaction for drug release with different thiol-initiated fragmentation.

The pH-dependent drug release profile was also assayed with disulfide linker **(3-4)** in a similar manner (Figure 3-35). It is essential to explore this reaction under different pH conditions, since the pH in physiological environment is 7.4, while that in tumor tissues is usually lower than 7. As expected, the reaction was faster at pH 10.0 (green) than that under physiological conditions at pH 7.4 (red). Encouragingly, the release rate is only slightly decreased at pH 5.0 (blue) than that at pH 7.4 (red).

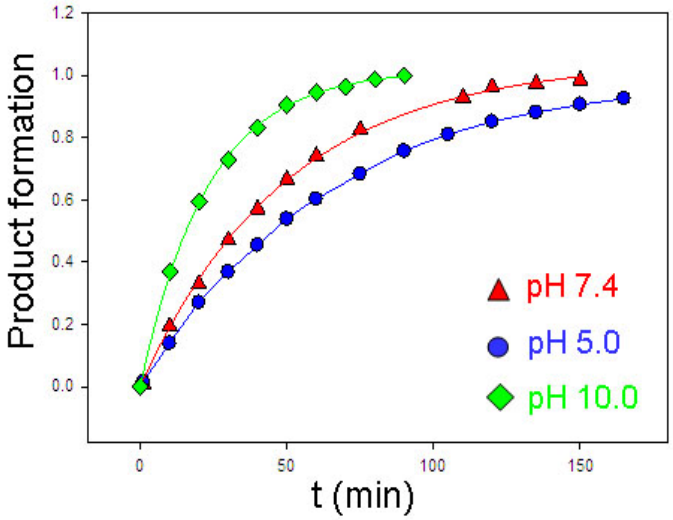

Figure 3-35. Measurement of pH-dependent drug release profile for disulfide linker **(3-4)**.

A preliminary evaluation of *gem*-dimethyl effect with disulfide linker **(3-28)** is illustrated in Scheme 3-14 and Figure 3-36. The rate constant (q) and release half time ($t_{1/2}$) were also calculated according to the rate law: $q = 9.6\times10^{-3}$ min^{-1} and $t_{1/2} = 72.1$ min, respectively.

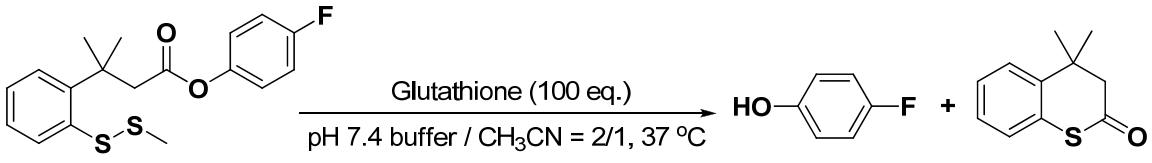

3-28

Scheme 3-14. Model reaction of disulfide linker **(3-28)** with a *gem*-dimethyl functionality at the benzilic position.

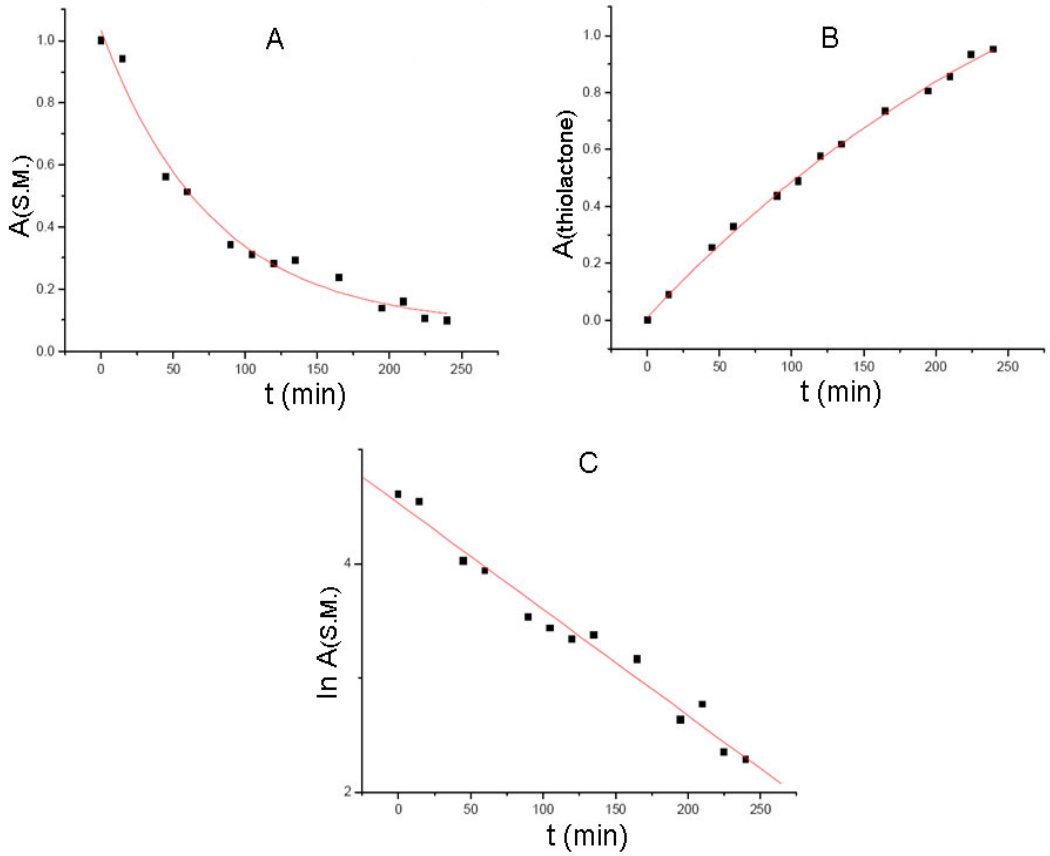

Figure 3-36. Measurement of *gem*-dimethyl effect on drug release for disulfide linker **(3-28)**.

The substituent effects on the aromatic ring of the disulfide linker are described in Scheme 3-15. These substituents included H, F, Me, OMe, NMe_2, NO_2. The reactions were carried out in the presence of 100 equivalents of glutathione, pH 7.4 buffer, at 37 ^oC to mimic biological conditions. Acetonitrile was applied as the co-solvent to improve the poor solubility of the substrates.

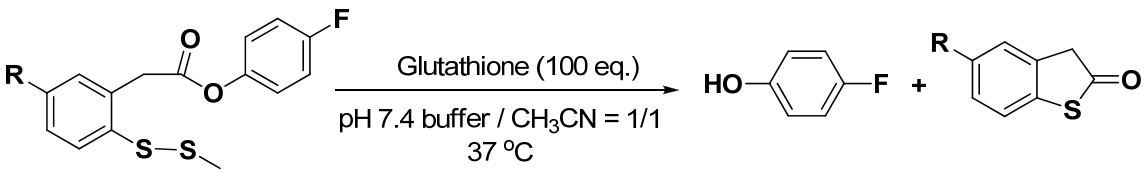

3-4 R = H
3-29 R = F
3-30 R = Me
3-31 R = OMe
3-32 R = NMe_2
3-33 R = NO_2

Scheme 3-15. Model reactions for substituent effect comparison.

Preliminary results, wherein R = H, Me and OMe, are summarized in Table 3-3. The release rate decreased in the following order, R = H > R = OMe > R = Me. Presently, it would be very difficult to make a convincible conclusion on the exact intrinsic characteristics of mechanism-based drug release profile without extensive exploration of other substituents. Figure 3-37 describes the drug release profile only when R = OMe for simplicity.

Table 3-3. Substituent effects on the aromatic ring for drug release.

	Reaction Rate Constant (q, min^{-1})	Release Half Time ($t_{1/2}$, min)
R = H	6.1×10^{-2}	11.4
R = OMe	2.6×10^{-2}	22.6
R = Me	1.5×10^{-2}	46.2

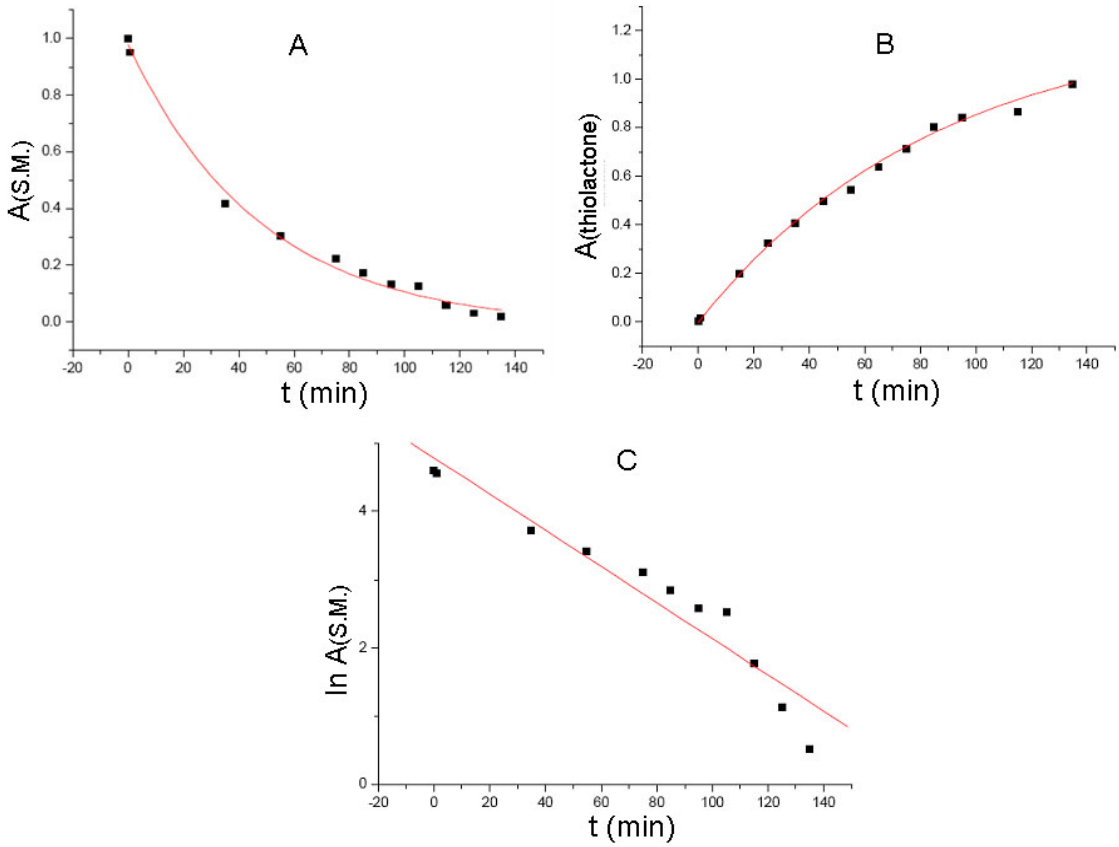

Figure 3-37. Measurement of substituent effect on drug release for disulfide linker **(3-31)**.

Disulfide bonds with different polarities and steric hindrance environments may also significantly affect the thiol disulfide exchange reaction. Accordingly, an *iso*-propyl functionalized disulfide linker **(3-34)** was employed for comparison (Scheme 3-16). It was observed that this reaction was sluggish with only trace amounts of thiolactone formation even after 40 h. Another two disulfide linker substrates **(3-35)** and **(3-36)** with *tert*-butyl and pyridinyl substituents, respectively, are still under investigation.

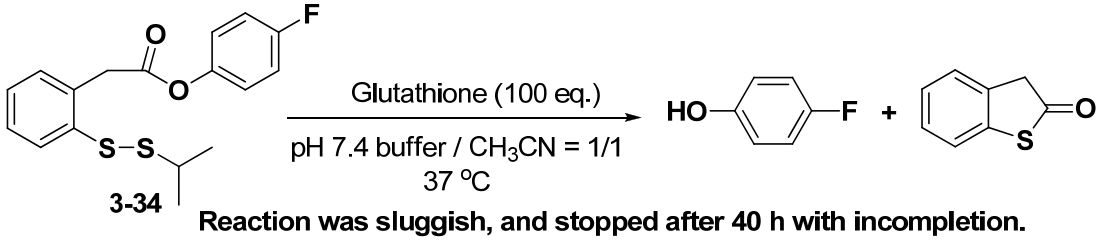

Scheme 3-16. Model reaction for S-S bond polarity comparison using the disulfide linker **(3-34)**.

§ 3.3.2. Fluorescence-Tagged Molecular Probes

A set of novel fluorescent molecular probes have been designed and synthesized to clarify the interaction between the tumor-targeting molecule and its receptor(s) on the cell

membrane, the internalization and real-time distribution of the conjugate, as well as the mechanism-based drug release profile *in vitro*. Significant progress in the investigation of monitoring these events has been achieved by confocal fluorescence microscopy (CFM) with leukemia cells overexpressing biotin receptors (L1210FR).

§ 3.3.2.1. Synthesis of Fluorescence-Tagged Molecular Probes

The first fluorescent probe biotin-FITC conjugate **(3-49)** was synthesized *via* attachment of fluorescein isothiocyanate (FITC) to biotin hydrazide **(3-48)**, which was initially converted from biotin through esterification and hydrazine substitution (Scheme 3-17).

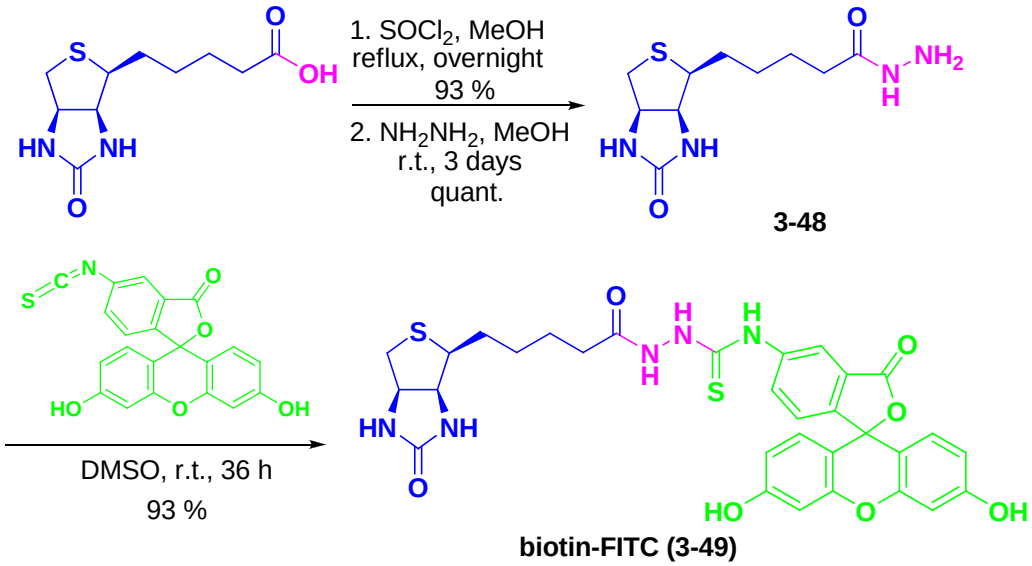

Scheme 3-17. Synthesis of biotin-FITC conjugate **(3-49)**.

The synthetic route of the second fluorogenic probes **(3-53)** is illustrated in Scheme 3-18. Triisopropylsilyl (TIPS) ester protected disulfide linker unit **(3-46)** was coupled with 7-hydroxy-4-methylcoumarin to provide coumarin-linker conjugate **(3-50)**, followed by the deprotection of the TIPS ester group and activation with *N*-hydroxysuccinimide to yield the active ester **(3-52)**. The attachment of biotin hydrazide **(3-48)** to the self-immolative disulfide linker derivative **(3-52)** afforded the desired product, biotin-linker-coumarin conjugate **(3-53)**.

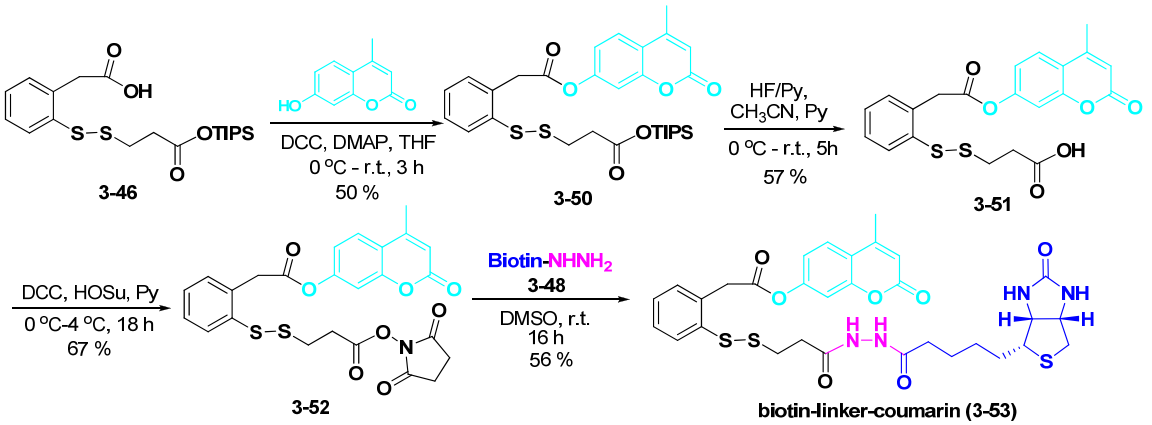

Scheme 3-18. Synthesis of biotin-linker-coumarin conjugate **(3-53)**.

The synthesis of biotin-linker-SB-T-1214-fluorescein **(3-64)** is shown in three steps in Scheme 3-55, 3-56 and 3-57. Commercially available fluorescein was first converted to methyl ester **(3-54)**, followed by Mitsunobu coupling with 4-hydroxy-butyric acid *tert*-butyl ester **(3-55)**, which was obtained through the reduction of 4-*tert*-butoxy-4-oxobutanoic acid with borane dimethylsulfide, to give protected fluorescein derivative **(3-56)**. Deprotection of the *tert*-butyl group afforded 2-[6-(3-carboxy-propoxy)-3-oxo-3H-xanthen-9-yl]benzoic acid methyl ester **(3-57)** (Scheme 3-19).

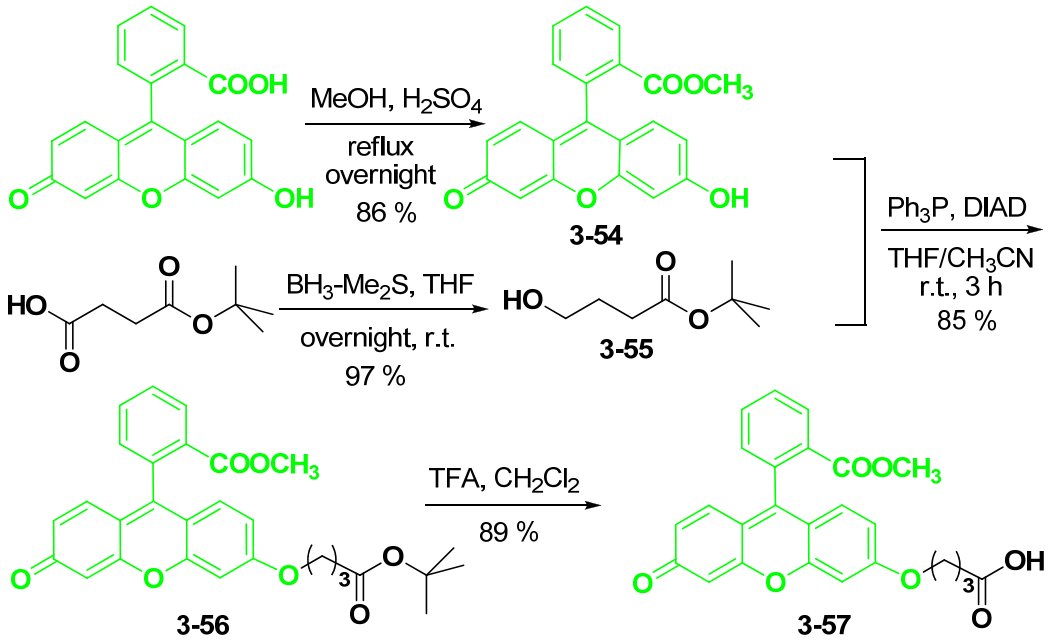

Scheme 3-19. Modification of fluorescein moiety.

Scheme 3-20 illustrates the installation of fluorescein unit **(3-57)** onto the 2nd-generation taxoid, SB-T-1214 **(1-23)**. The free C-2' hydroxy group of SB-T-1214 was first protected by *tert*-butyldimethylsilyl (TBDMS) group **(3-58)**, followed by C-7 modification with carboxylic acid tethered fluorescein unit **(3-57)** to give the protected

fluorescein-SB-T-1214 conjugate **(3-59)**. Deprotection of TBDMS, provided the desired fluorescein-SB-T-1214 conjugate **(3-60)**.

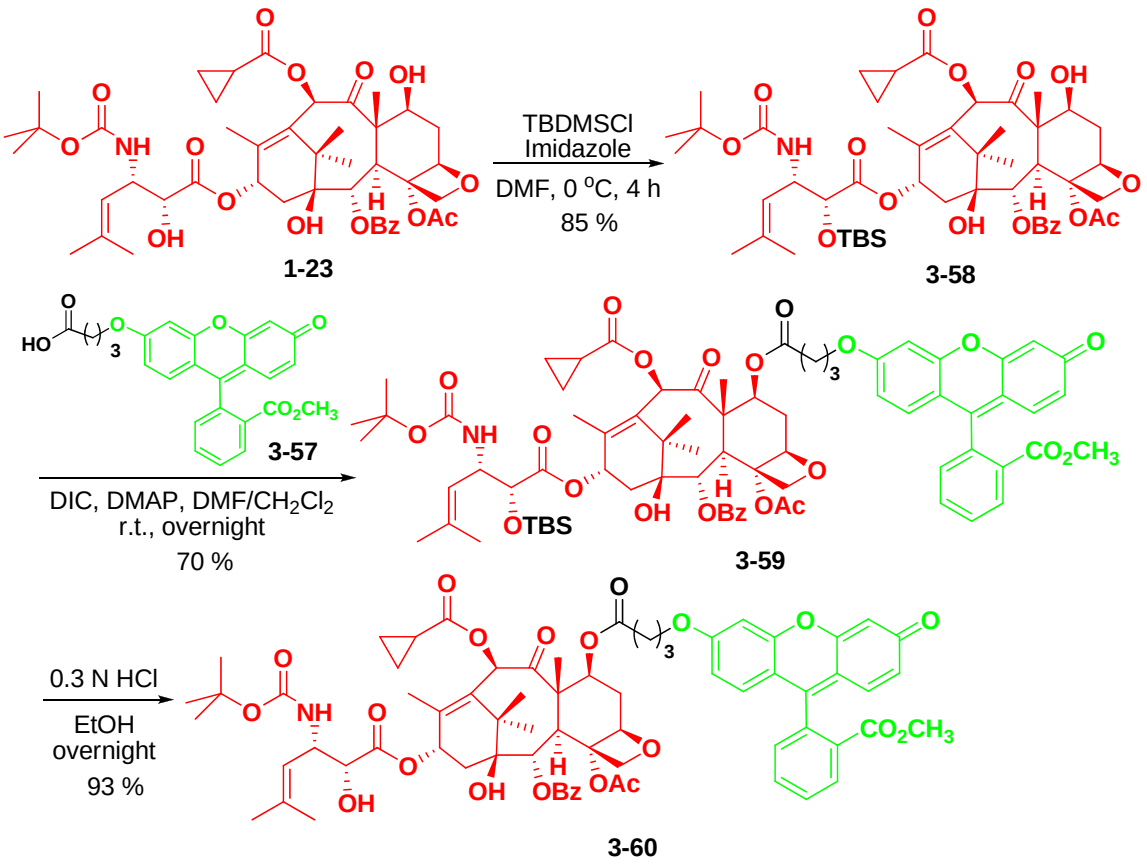

Scheme 3-20. Installation of fluorescein unit **(3-57)** onto SB-T-1214 **(1-23)**.

Subsequently, the resulting fluorescein-SB-T-1214 conjugate **(3-60)** was coupled with mono-TIPS ester of the disulfide linker carboxylic acid **(3-46)** to afford a TIPS-protected linker-SB-T-1214-flurorescein conjugate **(3-61)**. The TIPS ester protecting group was then removed by HF-pyridine to give the linker-SB-T-1214-flurorescein conjugate **(3-62)**. The resulting carboxylic acid group in **(3-63)** was transformed to the corresponding activated ester **(3-63)** using *N*-hydroxysuccinimide (HO-Su)/DIC, which was then directly reacted with biotin hydrazide **(3-48)** to provide the biotin-linker-SB-T-1214-fluorescein conjugate **(3-64)** in reasonable overall yield (Scheme 3-21).

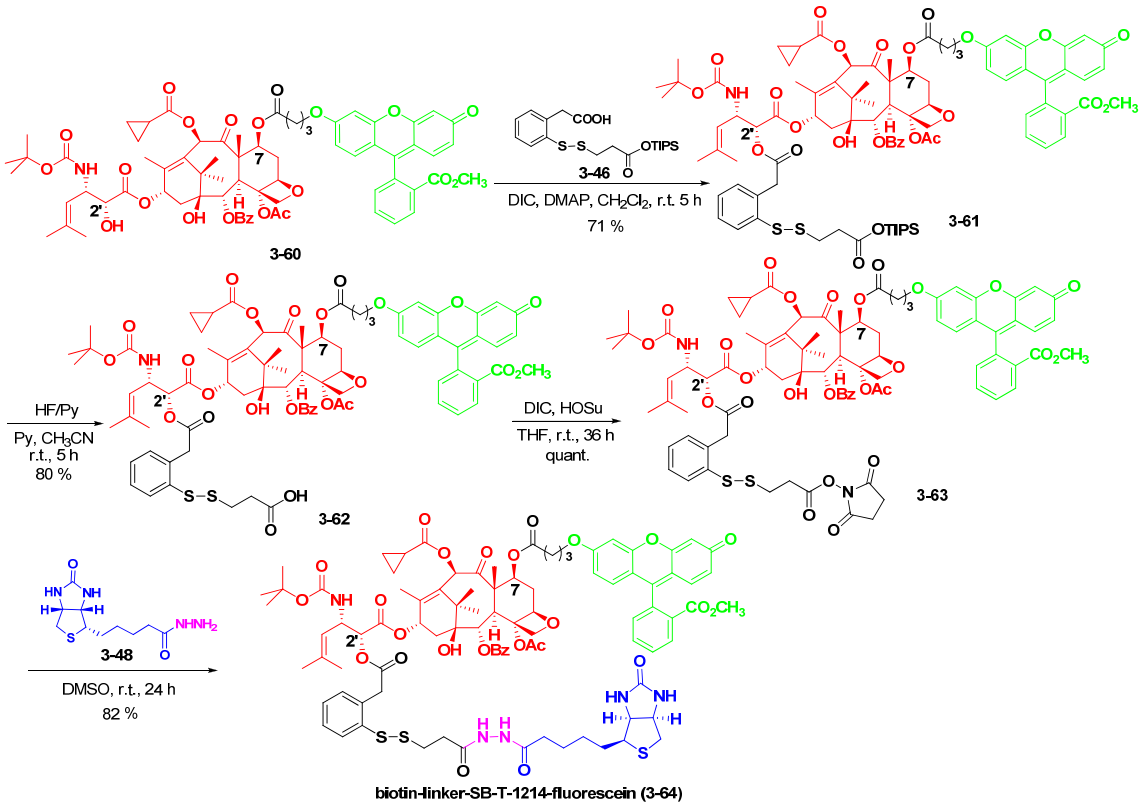

Scheme 3-21. Synthesis of the biotin-linker-SB-T-1214-fluorescein conjugate **(3-64)**.

With the use of same protocol, biotin-linker-SB-T-1214 **(3-65)**, wherein no fluorescein tag was attached to the warhead, was synthesized for *in vitro* cytotoxicity assay study, as shown in Scheme 3-22.

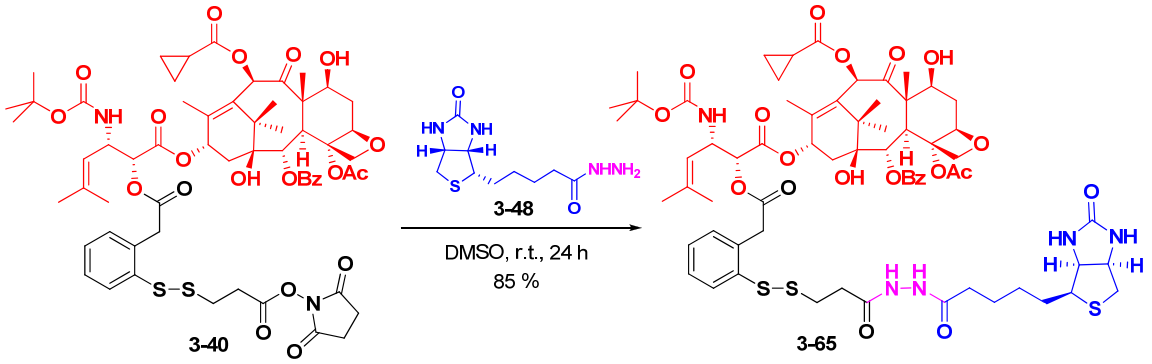

Scheme 3-22. Synthesis of biotin-linker-SB-T-1214 conjugate **(3-65)**.

§ 3.3.2.2. *In Vitro* Evaluation of Fluorescence-Tagged Molecular Probes

A preliminary study on the cellular uptake of the tumor recognition moiety, *i.e.* biotin, was assayed *in vitro* with leukemia cancer cells (L1210FR) by CFM under different conditions. Initially, certain parameters such as conjugate concentration and incubation time were examined. Figure 3-38 demonstrates the concentration-dependent

uptake of biotin-FITC conjugate **(3-49)**. In sharp contrast, a dramatic enhancement in fluorescent intensity was observed when the conjugate concentration was increased from 10 nM (Figure 3-38 (B)) to 100 nM (Figure 3-38 (C)). In comparison to the case of 100 nM, the fluorescence was saturated when 1 μM was applied (Figure 3-38 (D)), which indicated the fact that 100 nM was a suitable incubation concentration for further studies.

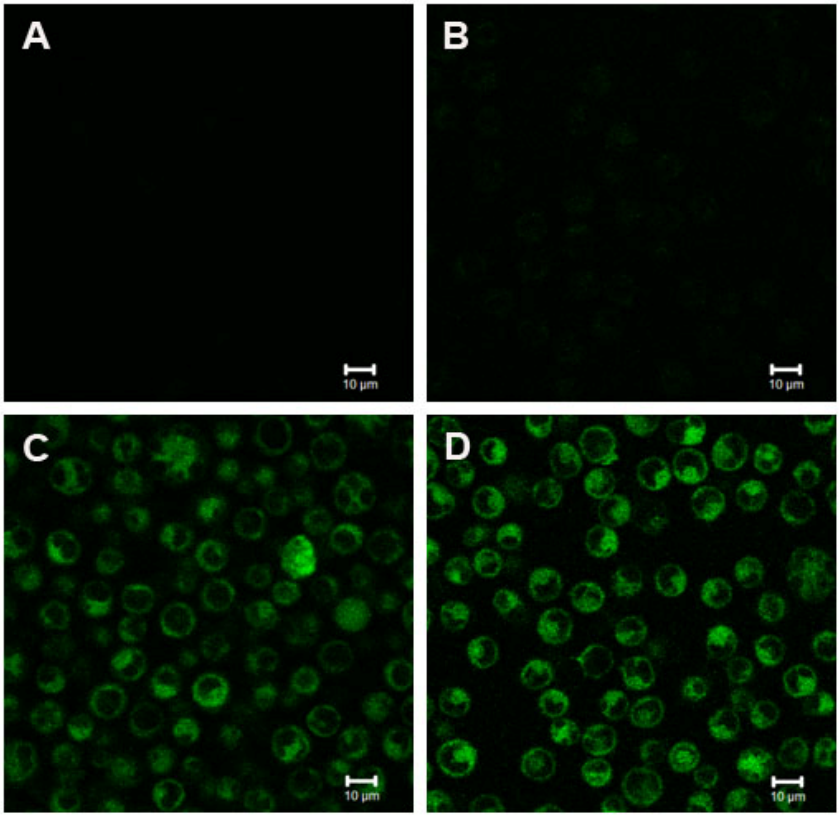

Figure 3-38. Concentration-dependent cellular uptake of biotin-FITC conjugate **(3-49)**: (A) DMSO as control, 37 ^{o}C, 3 h; (B) 10 nM, 37 ^{o}C, 3 h; (C) 100 nM, 37 ^{o}C, 3 h; (D) 1 μM, 37 ^{o}C, 3 h.

Subsequently, the time-dependent CFM analysis confirmed the uptake of the biotin-FITC conjugate **(3-49)** into leukemia cancer cells within hours. As depicted in Figure 3-39, the cells were incubated with biotin-FITC (100 nM) at 37 ^{o}C and photographed at time period of 5 min, 10 min, 15 min, 30 min, 1 h and 3 h. The presence of intense fluorescence in Figure 3-39 (F), wherein the L1210FR cells were incubated with biotin-FITC (100 nM) at 37 ^{o}C for 3 h, clearly indicated that 3 h was a sufficient time period for incubation.

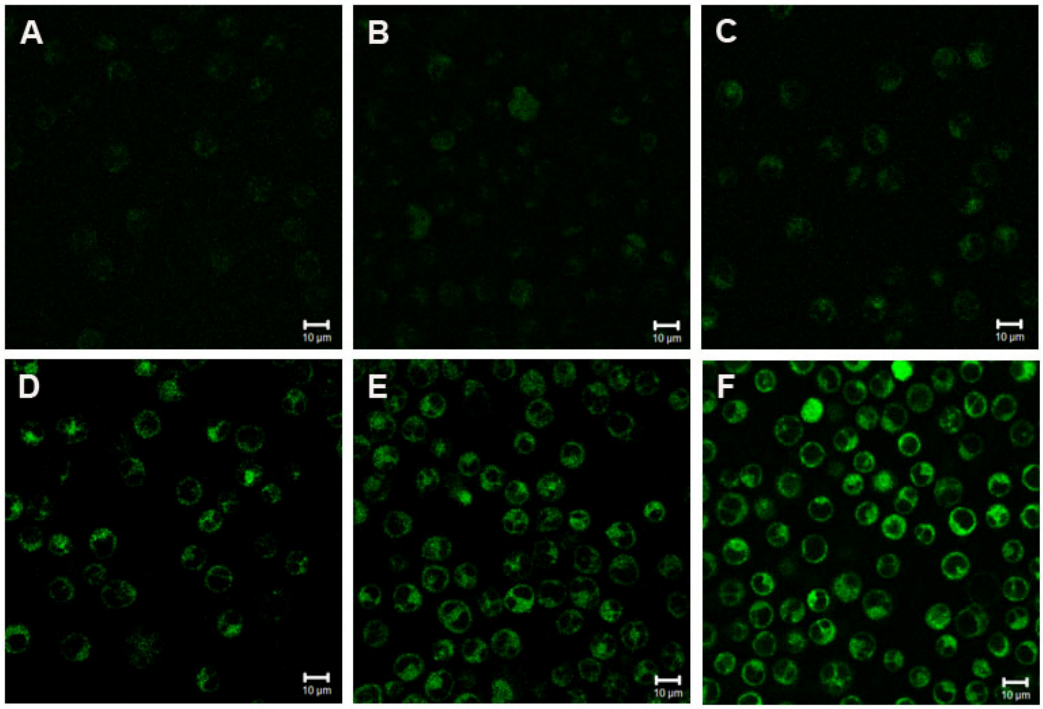

Figure 3-39. Time-dependent cellular uptake of biotin-FITC conjugate **(3-49)**: (A) 100 nM, 37 ^{o}C, 5 min; (B) 100 nM, 37 ^{o}C, 10 min; (C) 100 nM, 37 ^{o}C, 15 min; (D) 100 nM, 37 ^{o}C, 30 min; (E) 100 nM, 37 ^{o}C, 1 h; (F) 100 nM, 37 ^{o}C, 3 h.

Nevertheless, the conclusion that the uptake of biotin conjugate into the cells relied on the receptor-mediated endocytosis pathway cannot be addressed through this straightforward occurrence alone. A systematic study was carried out to verify the biotin internalization pathway in L1210FR cells (Figure 3-40). It was well known that the endocytosis process was an energy dependent uptake[107] and that endocytosis could inhibited at lower temperature, *e.g.* 4 ^{o}C or in the presence of the metabolism inhibitor, such as NaN_3.[106]. When L1210FR cells were incubated with biotin-FITC conjugate **(3-49)** (100 nM, 3 h) at 4 ^{o}C or in the presence of 0.05 % NaN_3 at 37 ^{o}C, a remarkable decrease of fluorescence inside the cells was detected, compared to that at 37 ^{o}C (without the addition of NaN_3). This observation clearly indicated that biotin was internalized into the cell by means of an endocytosis pathway. Additionally, L1210FR cells pretreated with excess biotin molecules (2 mM) yielded far less fluorescence than that incubated with biotin-FITC conjugate **(3-49)** alone (100 nM, 37 ^{o}C, 3 h). The lack of fluorescence validated the receptor-mediated endocytosis of biotin-FITC conjugate **(3-49)** since the treatment of excess biotin blocked the binding site on cell surface and hindered the internalization of conjugate. Additionally, flow cytometry data on average of 10,000 treated live cells also supported this observation. Conclusively, these evidences strongly suggest that biotin was a good candidate to serve as a tumor-targeting module.

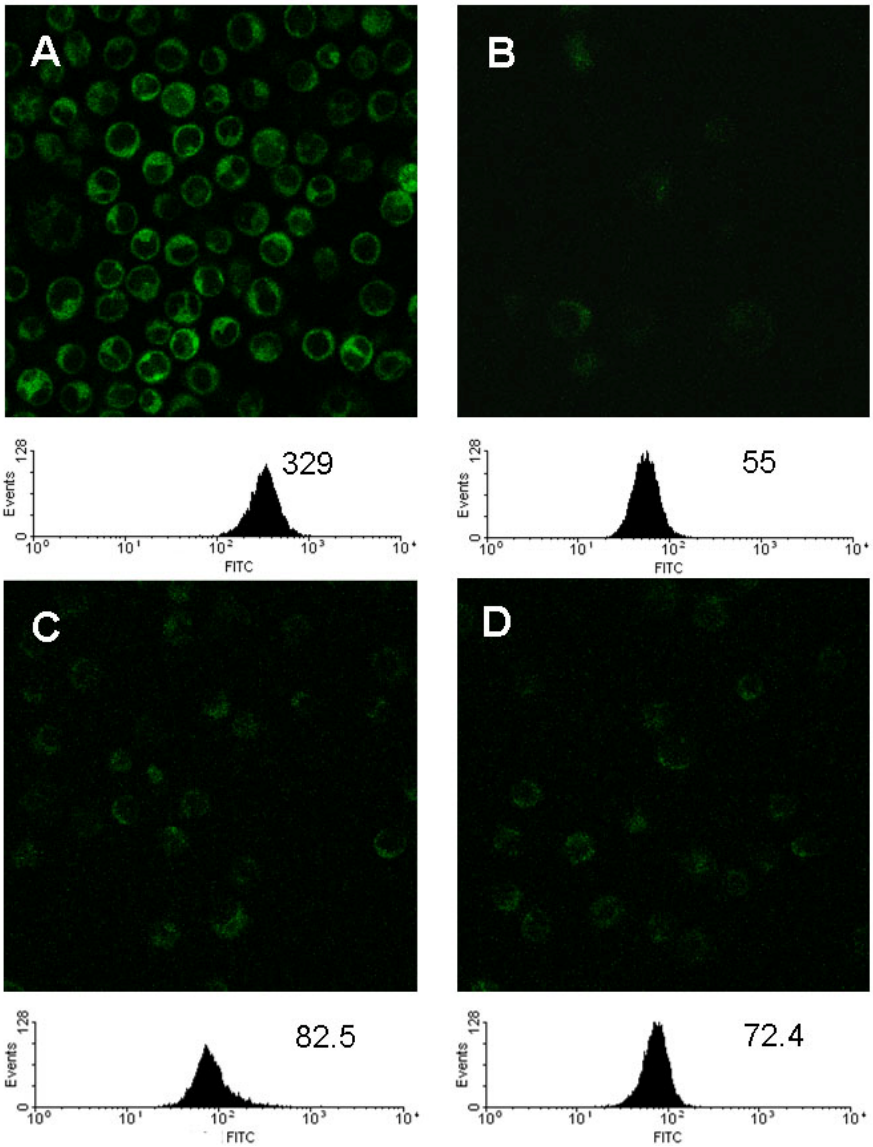

Figure 3-40. Confocal fluorescent images and the flow cytometry analysis of L1210FR cells after incubation with biotin-FITC **(3-49)** under different conditions: (A) 100 nM, 37 ^{o}C, 3 h; (B) 100 nM, 4 ^{o}C, 3 h; (C) 100 nM, 37 ^{o}C, 0.05 % NaN_3, 3 h; (D) 100 nM, 37 ^{o}C, 3 h, pretreated with excess biotin (2 mM).

With the aim of demonstrating the efficacy of the mechanism-based self-immolative disulfide linker, a fluorogenic probe, biotin-linker-coumarin **(3-53)** was designed and synthesized, wherein a coumarin derivative was incorporated as a profluorophore to take the place of the warhead. The presence of fluorogenic moieties has been widely utilized as model drugs for sensitively probing drug release activities.[108] In our effort, the fluorogenic probe became fluorescent only when it was converted to the free coumarin structure. The conjugate was initially nonfluorescent when the electron-donating group, *i.e.* phenolic group, on the coumarin, was attached to the disulfide linker.[96] Once the linker was treated with glutathione mono ethyl ester (GSH-OEt), a disulfide exchange reaction occurred, followed by intramolecular cyclization, which freed a highly

fluorescent coumarin that could be readily detected. It has been reported that GSH-OEt can be internalized into cells and generate GSH inside the cell.[109] Figure 3-41 (A) confirms that fluorescent coumarin was indeed liberated from the biotin-linker-coumarin conjugate **(3-53)** *via* the thiol disulfide exchange reaction. The conjugate (1 μM) was initially incubated with L1210FR cells at 37 ^{o}C for 3 h. After washing thoroughly with phosphate buffered saline (PBS), the cells were treated with GSH-OEt (2 mM) and incubated for another 2 h at 37 ^{o}C to trigger the coumarin release. The late addition of GSH-OEt was meant to determine if release of coumarin from the conjugate could be accelerated by a disulfide exchange reaction and whether an intramolecular cyclization mechanism was involved as proposed. It was worthy of note that there may be sufficient glutathione supply in animal models, tumor tissues and cells to cleave the disulfide linkage and trigger the drug release in longer period of time. A control experiment (Figure 3-41 (B)), wherein GSH-OEt was not added, was also performed to eliminate the possibility of extracellular hydrolysis of the conjugate and simultaneous coumarin uptake. Not surprisingly, the coumarin release was also detected in the absence of additional GSH-OEt, but the afore-mentioned fluorescence was much weaker, which may be attributed to the lack of sufficient amounts of glutathione in the cultured cells in 3 h period.

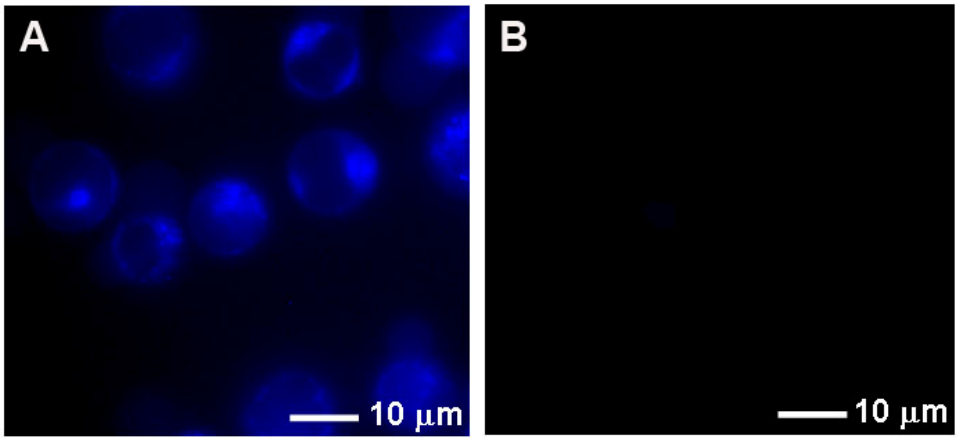

Figure 3-41. (A) Epifluorescent image of L1210FR cells that are initially incubated with biotin-linker-coumarin **(3-53)**, in its non-fluorescent form, followed by treatment with GSH-OEt to cleave the disulfide bond and activate the dye to fluoresce in blue; (B) Epifluorescent image of L1210FR cells after incubation with biotin-linker-coumarin **(3-53)** in its non-fluorescent form.

Encouraged by these promising results, the third fluorescent probe, biotin-linker-SB-T-1214-fluorescein conjugate **(3-64)**, was synthesized and assayed in the same manner, with respect to cellular uptake and the corresponding release mechanism inside the cancer cells. It was worth noting herein that high potency of the anticancer drug for drug delivery was a very important criterion. Toxicity of the anticancer agent should be in the sub-nanomolar range as expected (See § 3.1.3. for details). In this sense, a 2nd-generation taxoid, SB-T-1214 **(1-23)** was chosen as the warhead due to its excellent bioactivity (See § 3.1.3. for details). SB-T-1214 **(1-23)** possessed one order of magnitude higher potency than that of paclitaxel and docetaxel against drug-sensitive cancer cell lines, and 2-3

orders of magnitude higher potency as compared with their parent compounds against drug-resistant cell lines expressing MDR phenotypes. To covalently conjugate biotin to the anticancer drug, a self-immolative disulfide linker, which had been reported to be stable in circulation, but efficiently cleaved inside cancer cells,[110,111] was introduced to form an initially inactive prodrug conjugate. L1210FR cells were initially exposed to the biotin-linker-SB-T-1214-fluorescein conjugate **(3-64)**, (20 μM) at 37 ^{o}C for 2 h, followed by treatment with GSH-OEt (2 mM) and incubation for another 1 h (washing off the cells before addition of GSH-OEt). Figure 3-42 (A) depicts the microtubule networks after release of fluorescent taxoid. It can be clearly observed from the CFM image that the microtubule networks appeared to be bundled after treatment with GSH-OEt. Fluorescein-SB-T-1214 conjugate **(3-60)** was also incubated with L1210FR cells for control (Figure 3-42 (B)). As depicted in Figure 3-42 (A) and Figure 3-42 (B), the fluorescent cellular network of microtubules displayed after release of fluorescent taxoid from the biotin-linker-SB-T-1214-fluorescein conjugate **(3-64)**, and the direct treatment with the fluorescein-SB-T-1214 conjugate **(3-60)** illuminated the same microtubule skeleton. This result clearly demonstrated that the fluorescent taxoid was successfully released as expected. It should be noted that the intracellular glutathione in the leukemia cells (L1210FR) would also be able to cleave the disulfide linkage with much longer incubation time, but the endogenous glutathione level in cancer cells varies due to the significant difference in the physiological conditions in the actual leukemia or solid tumors. Accordingly, the extracellular addition of excess GSH-OEt was beneficial for a rapid visualization of the drug release inside the leukemia cells. This acceleration is evident by comparing Figure 3-42 (A) and Figure 3-42 (C).

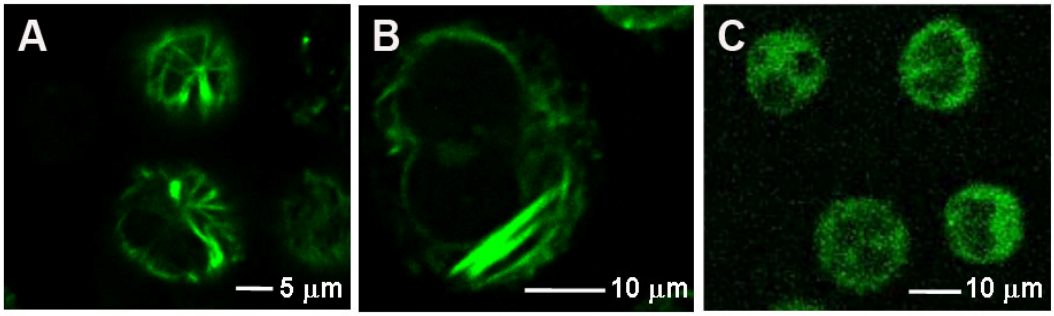

Figure 3-42. (A) Confocal fluorescent image of L1210FR cells that was initially incubated with prodrug biotin-linker-SB-T-1214-fluorescein conjugate **(3-64)** (20 μM at 37 ^{o}C for 2 h) , followed by treatment of GSH-OEt (2 mM at 37 ^{o}C for 1 h) to release the fluorescent taxoid and thereby visualize the fluorescent-labeled microtubule networks in the cells; (B) Confocal fluorescent image of L1210FR cells after incubation with fluorescein-SB-T-1214 conjugate **(3-60)** for control (20 μM at 37 ^{o}C for 2 h); (C) Confocal fluorescent image of L1210FR cells after incubation with prodrug biotin-linker-SB-T-1214-fluorescein conjugate **(3-64)** (20 μM at 37 ^{o}C for 2 h).

To elucidate the specificity of the biotin-mediated endocytosis, two other cell lines, the mouse leukemia L1210 cell line and the WI38 noncancerous human embryonic lung fibroblast cell line, were chosen to compare with L1210FR cell line. Both the L1210 and WI38 cell line lack the biotin receptors overexpressed on their surfaces. Accordingly, biotin-linker-SB-T-1214-fluorescein **(3-64)** was expected to be internalized into

L1210FR cells with much higher selectivity, as compared with L1210 and WI38 cells. Figure 3-43 (A) did show much stronger fluorescence in L1210FR cells than that in L1210 cells (Figure 3-43 (B)) and WI38 cells (Figure 3-43 (C)) upon incubation with biotin-linker-SB-T-1214-fluorescein **(3-64)** under the same conditions.

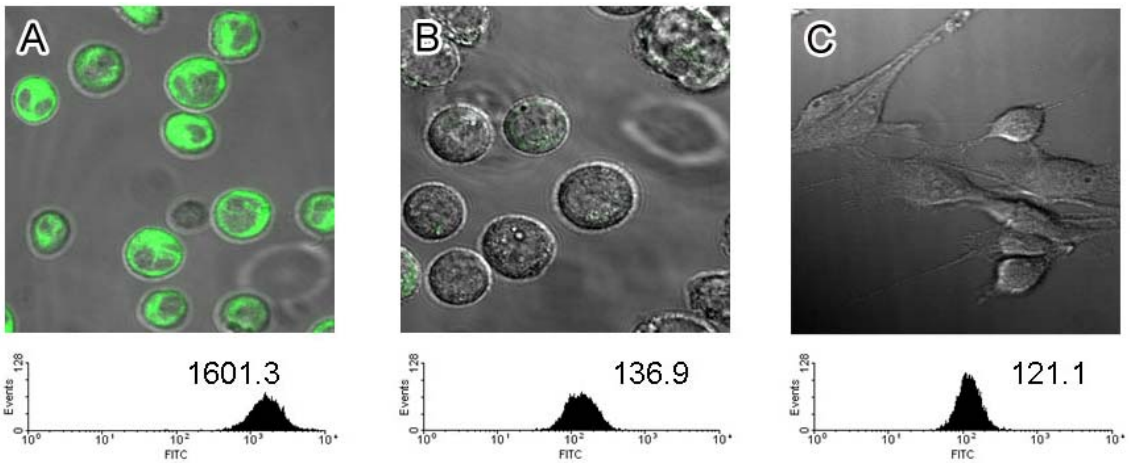

Figure 3-43. CFM images and the flow cytometry analysis of different types of cells after incubation with biotin-linker-SB-T-1214-fluorescein **(3-64)** at the final concentration of 20 μM at 37 ^{o}C for 2 h: (A) L1210FR that overexpresses biotin receptors; (B) L1210; and (C) WI38 noncancerous human embryonic lung fibroblast cells.

The mechanism investigation with fluorescent molecular probes has suggested that the guided molecular missile was able to efficiently deliver the active therapeutic drug to the target, *via* receptor-mediated endocytosis and intracellular release of the therapeutic drug through cleavage of the self-immolative disulfide linker and thiolactonization. Further efforts on the *in vitro* cytotoxicity evaluation of biotin-linker-SB-T-1214 **(3-65)** was also performed using a MTT assay against L1210FR (leukemia) cancer cell line. Paclitaxel and the parent taxoid SB-T-1214 **(1-23)** were assayed as well for comparison. The IC_{50} values of these compounds are summarized in Table 3-4. Interestingly, when the self-immolative disulfide linker was attached to C2'-OH of taxoid, the resulting biotin-linker-SB-T-1214 **(3-65)** showed higher potency (IC_{50} 8.8 nM) than that of parent SB-T-1214 (IC_{50} 10.1 nM), which was one order of magnitude more potent than paclitaxel (IC_{50} 121 nM). It is apparent that the internalization was enhanced by receptor-mediated endocytosis and the drug release was efficient with endogenous GSH during longer incubation time (72 h) applied to the MTT assay. Accordingly, it is reasonable to conclude that such a prodrug conjugate generally serves as an effective prodrug candidate since attachment of the disulfide linker unit to the C-2' hydroxyl group on the taxoid would render it practically non-cytotoxic in circulation. Once at the tumor site, the presence of a high concentration of intracellular GSH could then efficiently trigger the release of the free drug in its fully active form and thereby restore its original potency.

Table 3-4. *In vitro* cytotoxicity of taxol, taxoid (SB-T-1214, **1-23**) and biotin-linker-SB-T-1214 **(3-65)**.

	taxol	taxoid (SB-T-1214)	biotin-linker-SB-T-1214
IC_{50},* nM	121	10.1	8.8
Standar Error, nM	14.0	1.31	0.54

*: The concentration of compound that inhibits 50 % of the growth of cancer cell line after 72 h of drug exposure.

In another control experiment, the mouse leukemia L1210 cells and the WI38 noncancerous human embryonic lung fibroblast cells were treated with biotin-linker-SB-T-1214 **(3-65)**. After 72 h incubation, the IC_{50} value of biotin-linker-SB-T-1214 **(3-65)** against both L1210 cells and WI38 cells were 522 nM and 570 nM, respectively, as shown in Table 3-5.

Table 3-5. IC_{50} value of the biotin-linker-SB-T-1214 **(3-65)** against different cell lines.

Cell Line	L1210FR	L1210	WI38
IC_{50},* nM	8.8	522	570

*: The concentration of compound that inhibits 50 % of the growth of cancer cell line after 72 h of drug exposure.

§ 3.4. Experimental Section

General Methods: ^{1}H and ^{13}C NMR spectra were measured on a Varian 300, 400, 500, or 600 MHz NMR spectrometer. High-resolution mass spectrometric analyses were conducted at the Mass Spectrometry Laboratory, University of Illinois at Urbana-Champaign, Urbana, IL. GC-MS analyses were performed on an Agilent 6890 Series GC system equipped with the HP-5HS capillary column, (50 m X 0.25 mm, 0.25 um) and with the Agilent 5973 network mass selective detector. LC-MS analyses were carried out on an Agilent 1100 Series Liquid Chromatograph Mass Spectrometer. Infrared spectra were obtained on a Nexus 670 (Thermo Nicolet) equipped with a single reflectance ZnSe ATR accessory, a KBr beam splitter, and a DTGS KBr detector. UV-vis spectra were recorded on a UV1 (Thermo Spectronic) spectrometer. TLC analyses were performed on Merck DC-alufolien with Kieselgel 60F-254 and were visualized with UV light, iodine chamber, 10 % sulfuric acid-EtOH or 10 % PMA-EtOH solution. The staining agent on TLC for biotin derivatives was 4-*N,N*-Dimethylamino-cinnamaldehyde ethanol solution. Column chromatography was carried out on silica gel 60 (Merck; 230-400 mesh ASTM). Chemical purity was determined with a Waters HPLC or shimazu HPLC, using a Phenomenex Curosil-B column, employing CH_3CN/water as the solvent system with a flow rate of 1 mL/min. Dark room, aluminum foil, and inert nitrogen atmosphere were applied when necessary.

Materials: The chemicals were purchased from Sigma Aldrich Company, Fischer Company or Acros Organic Company. Dichloromethane and methanol were dried before use by distillation over calcium hydride under nitrogen or argon. Ether and THF were dried before use by distillation over sodium-benzophenone kept under nitrogen or argon. Toluene and benzene were dried by distillation over sodium metal under nitrogen or argon before use. Dry DMF was purchased from EMD chemical company, and used without further purification. PURE SOLVTM, Innovative technology Inc, provided an alternative source of dry toluene, THF, ether, and dichloromethane. The reaction flasks were dried in a 110 ^{o}C oven and allowed to cool to room temperature in a desiccator over "*Drierite*" (calcium sulfate) and assembled under inert gas nitrogen or argon atmosphere.

3H-Benzo[b]thiophen-2-one (3-1)[112]:
To a solution of benzo[b]thiophen-2-ylboronic acid (3.09 g, 17.0 mmol) in EtOH (30 mL) was added hydrogen peroxide (30 %, 5.6 mL) dropwise. The color changed from pink to red. After stirring for 8 h, the solution was carefully evaporated under vacuum. Then the crude residue was diluted by water, and extracted by $CHCl_3$ three times. The organic layers were combined and dried over $MgSO_4$. After removal of the solvent and column purification, the title compound (2.25 g, 86 %) was obtained. ^{1}H NMR (300 MHz, $CDCl_3$): δ 3.98 (s, 2 H), 7.2-7.4 (m, 4 H). The data were in accordance with reported values.[112]

(2-Mercaptophenyl)acetic acid (3-2):
To a solution of thiolactone **(3-1)** (310 mg, 2.00 mmol) in THF (10 mL) was added LiOH hydrate (508 mg, 12.0 mmol) in H_2O (10 mL) at 60 ^{o}C. After stirring for 16 h and cooling to room temperature, the solution was diluted with H_2O (2 mL) and diethyl ether (10 mL). The pH was adjusted to 2 by aqueous HCl (2 M). The organic layer was separated, washed with saturated NaCl, and dried over Na_2SO_4. After the solvent was removed in vacuum, pure product (302 mg, 90 %) was obtained under column. ^{1}H NMR (400 MHz, $CDCl_3$): δ 3.49 (s, 1 H, S-H), 3.83 (s, 2 H), 7.18-7.29 (m, 3 H), 7.41 (m, 1 H), 10.10 (b, 1 H). ^{13}C NMR (75 MHz, $CDCl_3$): δ 39.85, 126.94, 128.25, 130.74, 131.00, 132.41, 133.33, 176.16.

Methyl 2-bromomethylbenzoate (3-5)[113]:
To a solution of *ortho*-methylcarboxylate (1.90 g, 12.6 mmol) in CCl_4 (32 mL), containing catalytic amount of benzoylperoxide (20 mg) was added *N*-bromosuccinimide (2.32 g, 12.6 mmol). The reaction mixture was heated at reflux temperature until the starting material completely disappeared. The reaction was cooled to 10 ^{o}C and filtered. The filtrate was concentrated under reduced pressure and purified by silica gel chromatography to get yellow oil in 94 % yield (2.7 g). ^{1}H NMR ($CDCl_3$, 400 MHz): δ 3.95 (s, 3 H, MeOCO), 4.96 (s, 2 H, CH_2Br), 7.38 (t, 1 H, J = 10.8 Hz, arom), 7.48 (m, 2 H, arom), 7.97 (d, 1 H, J = 11.2 Hz, arom). All data were consistent with literature.[113]

Methyl 2-benzoate thiouronium salt (3-6)[114]:
Methyl 2-bromomethylbenzoate **(3-5)** (2.58 g, 11.3 mmol) and thiourea (953 mg, 12.4 mmol) in dry acetone (11 mL) was refluxed overnight. The precipitate was filtered, collected and dried under reduced pressure to get white solid 2.97 g (86 %). ^{1}H NMR

(D_2O, 400 MHz): δ 3.81 (s, 3 H, MeOCO), 4.57 (s, 2 H, CH_2), 7.38 (m, 2 H, arom), 7.49 (t, 2 H, *J* = 7.6 Hz, arom), 7.87 (d, 1 H, *J* = 8.0 Hz, arom). All data consistent with literature.[114]

2-Mercaptomethylbenzoic acid (3-7)[114]:
Thiouronium salt **(3-6)** (921 mg, 3.02 mmol) was refluxed for 1 hour in 12 mL of 2 N KOH of aqueous/methanol solution (1:1). After complete disappearance of starting materials, methanol was removed by reduced pressure. The aqueous solution was cooled down to ambient temperature, acidified with 1 N HCl solution, and extracted with ether. The combined organic layers were dried with $MgSO_4$ and concentrated. The residue was purified by recrystallization from MeOH/hexane solution to get yellowish solid 492 mg (97 %). ^{1}H NMR (CDCl3, 400 MHz): δ 2.13 (t, *J* = 8.0 Hz, 1 H, SH), 4.96 (d, *J* = 8.4 Hz, 2 H, CH_2), 7.36 (m, 2 H, arom), 7.54 (t, *J* = 8.0 Hz, 2 H, arom), 8.11 (d, 1 H, *J* = 7.6 Hz, arom). All data were consistent with literature.[114]

2-Methyldisulfanylmethylbenzoic acid (3-8):
To a solution of 2-mercaptomethyl-benzoic acid **(3-7)** (488 mg, 2.90 mmol) in dry ether (83 mL) and triethylamine (1.03 mL, 6.38 mmol) was added dropwise methyl methanethiosulfonate (282 μL, 2.9 mmol) with stirring at 0 ^{o}C. The reaction mixture was allowed to warm to room temperature. After overnight stirring, TLC was checked for consumption of starting material and conversion to product. After work up with acid-base extraction, the combine organic layers were dried over $MgSO_4$ and purified by flash chromatography on silica gel to get 355 mg (75 %) of desired product as white solid. ^{1}H NMR (CD_3OD, 300 MHz): δ 2.04 (s, 3 H, S-Me), 4.34 (s, 2 H, CH_2), 7.32-7.46 (m, 3 H, arom), 7.95 (d, 1 H, *J* = 7.8 Hz, arom). ^{13}C NMR (CD_3OD, 75.5 MHz) δ 22.2, 41.07, 127.4, 129.9, 131.4, 131.8, 131.9, 140.3, 169.4.

2-Methyldisulfanylmethylbenzoic acid 4-fluorophenyl ester (3-9):
To a solution of 2-methyldisulfanylmethyl-benzoic acid **(3-8)** (51 mg, 0.24 mmol), DMAP (176 mg, 1.44 mmol), and *p*-fluorophenol (108 mg, 0.96 mmol) in dichloromethane (1.2 mL) was added DIC (223 μL, 1.44 mmol). The reaction mixture was stirred for 18 h at 40 ^{o}C. The precipitate was filtered and washed with dichloromethane (30 mL) and the filtrate was washed with a aqueous saturated sodium bicarbonate solution, dried over anhydrous magnesium sulfate, and then concentrated *in vacuo.* The residue was purified on a silica gel column chromatography using hexane/ethyl acetate to give oil 42 mg (89 %). ^{1}H NMR ($CDCl_3$, 400 MHz): δ 2.08 (s, 3 H, s-Me), 4.36 (s, 2 H, CH_2), 6.97 (m, 1 H, arom), 7.09-7.23 (m, 4 H, arom), 7.45 (m, 2 H, arom), 7.54 (t, 1 H, *J* = 6.3 Hz, arom), 8.19 (d, 1 H, *J* = 9.3 Hz, arom). ^{13}C NMR ($CDCl_3$, 100 MHz) δ 23.5, 41.7, 116.4 (d, *J* = 23.5), 123.4 (d, *J* = 9.1), 127.9, 128.4, 131.9, 132.2, 132.3, 133.0, 140.9, 146.8, 159.4, 161.8, 165.8. ^{19}F NMR, ($CDCl_3$, 282 MHz): δ –117.01 (dd, *J* = 9.0, 12.4 Hz).

***o*-Bromomethylphenylacetic Acid (3-10):**
A solution of isochroman-3-one (976.1 mg, 6.6 mmol) in 8.13 mL of a 33 % solution of hydrobromic acid in acetic acid was maintained at room temperature for two hours and then at 70 ^{o}C for an hour. Dilution with cold water (20 mL) and filtration afforded the

acid **(3-10)** (1.25 g, 83 %) which was air dried and used crude in the following reaction. ^{1}H NMR ($CDCl_3$, 400 MHz) δ 3.84 (s, 2 H), 4.56 (s, 2 H), 7.29 (m, 4 H), 11.2 (s, 1 H). ^{13}C NMR ($CDCl_3$, 100 MHz) δ 31.77, 38.11, 128.51, 129.50, 130.97, 131.60, 132.78, 136.62, 176.93.

Methyl 2-bromomethylphenylacetate (3-11):
40 % sulfuric acid in absolute methanol (0.75 mL) was added to *o*-bromomethylphenylacetic acid **(3-10)** (300 mg, 1.31 mmol). The reaction mixture was stirred at room temperature for 3 hours. Methanol was removed under vacuum. The reaction residue was then diluted with EtOAc, and washed with sodium bicarbonate, water and brine. The organic layer was dried over $MgSO_4$, filtered and concentrated. The crude product was purified by column chromatography on silica gel (hexanes:EtOAc = 15:1) to give desired product **(3-11)** (255 mg, 80 %) as a clear oil. ^{1}H NMR ($CDCl_3$, 400 MHz) δ 3.68 (s, 3 H), 3.80 (s, 2 H), 4.58 (s, 2 H), 7.26 (m, 4 H); ^{13}C NMR ($CDCl_3$, 100 MHz) δ 31.83, 38.19, 52.26, 128.05, 129.23, 130.76, 131.31, 133.38, 136.39, 171.40.

Thiouronium salt (3-12):
Methyl 2-bromomethylphenylacetate (**3-11**) (238 mg, 0.979 mmol) and thiourea (83 mg, 1.08 mmol) in 0.93 mL of abs. acetone were refluxed for 12 h. Acetone was removed under vacuum and the reaction residue was dissolved in water. After centrifuge, the clear water solution was collected and water was removed under vacuum. The product, thiouronium salt **(3-12)** was provided as a white solid (70 %). ^{1}H NMR (D_2O, 300 MHz) δ 3.65 (s, 3 H), 3.82 (s, 2 H), 4.37 (s, 2 H), 7.32 (m, 4 H). ^{13}C NMR (D_2O, 100 MHz) δ 33.48, 37.99, 53.08, 128.75, 129.57, 130.92, 132.00, 132.04, 133.44, 170.61, 174.87.

2-Hydrosulfanylmethylphenylacetic acid (3-13):
Thiouronium salt **(3-12)** (194 mg) was refluxed for 1 h in 2 N KOH (water solution 1.4 mL) and THF (1.4 mL). The reaction mixture was cooled down to room temp. The THF was removed under reduced pressure. The resulting aqueous solution was washed with ether. The aqueous layer was acidified with 1 N HCl, and extracted with EtOAc 3 times. The combined organic lays were dried with anhydrous magnesium sulfate to afforded 2-hydrosulfanylmethylphenylacetic acid **(3-13)** as a white solid (95 %). ^{1}H NMR ($CDCl_3$, 300 MHz) δ 1.80 (t, J = 7.2 Hz, 1 H), 3.85 (s, 2 H), 3.88 (s, 2 H), 7.36 (m, 4 H).

(2-Methyldisulfanylmethylphenyl)acetic acid (3-14):
To a solution of thiol **(3-13)** (104 mg, 0.570 mmol) in H_2O (0.67 mL) and EtOH (2.7 mL) was added methyl methanethiosulfonate (79 mg, 0.630 mmol). After stirring for 20 h, the reaction mixture was diluted with ether and washed with 1 *N* KOH twice. The water layers were combined and acidified to pH 2 with 5 *N* HCl. This solution was extracted with CH_2Cl_2 3 times. The organic layers were combined, dried over anhydrous $MgSO_4$, filtered, and concentrated *in vacuo*. The crude product was purified by column chromatography on silica gel (hexanes:EtOAc = 8:1) to give desired product **(3-14)** (88.4 mg, 68 %) as a white solid. ^{1}H NMR ($CDCl_3$, 400 MHz) δ 2.10 (s, 2 H), 3.84 (s, 2 H), 3.99 (s, 2 H), 7.26 (m, 4 H), 11.76 (br, 1 H). ^{13}C NMR ($CDCl_3$, 100 MHz) δ 23.16, 38.50, 40.67, 127.97, 128.31, 131.38, 131.43, 132.45, 135.83, 178.16.

4-Fluorophenyl (2-methyldisulfanylmethylphenyl)acetate (3-15):
To a solution of acid **(3-14)** (80 mg, 0.344 mmol) and DMAP (294 mg, 2.41 mmol) in CH_2Cl_2 (3 mL) was added DIC (0.373 mL, 2.41 mmol), and 4-fluorobenzyl alcohol (217 mg, 1.72 mmol). The reaction mixture was stirred for 2 h, and then concentrated *in vacuo*. Purification by column chromatography on silica gel using hexans/EtOAc (10/1) afforded the desired ester **(3-15)** in 90 % yield. ^{1}H NMR (300 MHz, $CDCl_3$): δ 2.11 (s, 3 H), 4.03 (s, 2 H), 4.07 (s, 2 H), 7.04 (m, 4 H), 7.35 (m, 4 H). ^{13}C NMR (75 MHz, $CDCl_3$): δ 23.13, 38.66, 40.80, 116.09, 116.33, 123.07, 127.96, 128.39, 131.37, 131.47, 132.50, 135.78, 146.71, 159.20, 161.63, 169.98. ^{19}F NMR (282 Hz, $CDCl_3$): δ -117.04.

3-[(Phenylimino)methyl]benzo[*b*]thiophen-2(3*H*)-one (3-17):
A mixture of thiolactone **(3-1)** (300 mg, 2 mmol) and *N,N'*-diphenylformamidine (390 mg, 2 mmol) in ether (3 mL) was reflux for 30 min under N_2. The chilled mixture was dried *in vacuo* to remove the ether and used directly in the next step.

2-Oxo-2,3-dihydrobenzo[*b*]thiophene-3-carbaldehyde (3-18):
The resulting compound **(3-17)** and potassium hydroxide (1.50 g, 26.0 mmol) were dissolved in water (6 mL) and ethanol (3 mL). The mixture was heated under reflux for 50 min. The solution was then diluted with water and acidified with hydrochloric acid to pH 2, followed by extraction with CH_2Cl_2 3 times. The organic layers were combined, dried over anhydrous $MgSO_4$, filtered, and concentrated *in vacuo* to yield the crude product aldehyde **(3-18)**, which was used without purification in the next step.

3-Methylbenzo[*b*]thiophen-2(3*H*)-one (3-19):
The resulting aldehyde **(3-18)** was dissolved in 5 mL glacial acetic acid. To the resulting solution was carefully added sodium borohydride (377 mg, 10.2 mmol) in the form of a pellet. Gas evolved upon the addition. The reaction mixture was gradually warmed to 75 ^{o}C for 30 min. Another portion of pelletized sodium borohydride (377 mg, 10.2 mmol) was added to the transparent reaction mixture that resulted. The temperature was maintained at 75 ^{o}C for an additional 60 min. After a total reaction time of 90 min, the reaction mixture was gradually cooled to room temperature, diluted with 50 mL of distilled water, and extracted with three 20 mL portions of diethyl ether. The combined organic layers were washed with three 45 mL portions of 5 % sodium bicarbonate, thoroughly dried over anhydrous magnesium sulfate, filtered by gravity, and concentrated *in vacuo*. The desired product mono methyl substituted thiolactone **(3-19)** was obtained after column chromatography on silica gel (213 mg, 65 % for 3 steps). ^{1}H NMR (300 MHz, $CDCl_3$): δ 1.55 (d, J = 7.2 Hz, 3 H), 3.84 (q, J = 7.2 Hz, 1 H), 7.24-7.37 (m, 4 H).

3,3-Dimethylbenzo[*b*]thiiphen-2(3*H*)-one (3-23):
To a solution of thiolactone **(3-1)** (300 mg, 2.00 mmol) in THF (10 mL) was added potassium *tert*-butoxide (2.24 g, 20.0 mmol) and iodo methane (2.86 g, 20.0 mmol) at 0 ^{o}C. The mixture was stirred for 40 min and solvent was removed *in vacuo*. The resulting residue was purified by column chromatography to yield the desired product **(3-23)** (178 mg, 79 %). ^{1}H NMR (300 MHz, $CDCl_3$): δ 1.55 (s, 6 H), 7.24-7.53 (m, 4 H). ^{13}C NMR (75 MHz, $CDCl_3$): δ 26.25, 55.52, 122.94, 123.62, 126.40, 128.10, 133.58, 144.33, 209.82.

3-(2-Pyridyldithio)propionic acid (3-37)[115]:
2,2'-Bipyridyl disulfide (3.75 g, 17.0 mmol) was dissolved in 15 mL of ethanol (99.5 %), and 0.4 mL of glacial acetic acid was added. The solution was stirred vigorously, and 0.9 g (8.50 mmol) of 3-mercaptopropionic acid in 5 mL of ethanol was added dropwise. The reaction mixture was allowed to stir at room temperature for 12 h. Solvent was then removed by evaporation. The residue was purified on a neutral alumina column with methylene chloride-ethanol-glacial acetic acid to yield desired product **(3-37)** (1.30 g, 78 %). ^{1}H NMR (300 MHz, $CDCl_3$) δ 2.79 (t, *J* = 6.9 Hz, 2 H), 3.06 (t, *J* = 6.9 Hz, 2 H), 7.14 (m, 1 H), 7.66 (m, 1 H), 8.48 (dd, *J* = 3.3, 1.2 Hz, 1 H), 10.4 (br, 1 H). ^{13}C NMR (75 MHz, $CDCl_3$): δ 33.8, 34.1, 120.5, 121.2, 137.4, 149.4, 159.2, 176.1. All data are consistent with the reported values.[115]

2,5-Dioxopyrrolidin-1-yl 3-(2-pyridyldithio)propanoate (3-38)[115]:
A solution of 3-(2-pyridyldithio)propionic acid **(3-37)** (200 mg, 0.929 mmol) in pyridine (1.4 mL) was treated with *N*-hydroxysuccinimide (110 mg, 0.929 mmol) and DCC (767 mg, 3.72 mmol). The contents were stirred at 0 ^{o}C for 2 hours and then kept in refrigerator (4-7 ^{o}C) for overnight. The reaction mixture was filtered through celite and washed with small amounts of cold dichloromethane (remove DCU). Pyridine was removed under reduced pressure. Toluene was added to the mixture to help remove pyridine. The above work up step was repeated twice until most of the DCU and pyridine were removed. The residue was taken up in a minimum volume and purified on a silica column with 2:1 hexanes-ethyl acetate. The resulting residue was dried under vacuum to give desired product **(3-38)** (180 mg, 68 % yield). ^{1}H NMR (400 MHz, $CDCl_3$) δ 2.84 (s, 4 H), 3.0-3.1 (m, 4 H), 7.20 (m, 1 H), 7.67 (m, 2 H), 8.50 (m, 1 H). ^{13}C NMR (75 MHz, $CDCl_3$): δ 25.5, 30.8, 32.7, 119.9, 121.0, 137.3, 149.7, 159.0, 166.9, 168.9. All data are consistent with the reported values.[115]

2,5-Dioxopyrrolidin-1-yl 3-(2-hydroxycarbonylmethylphenyldisulfanyl)propaneate (3-39):
To a solution of 2,5-dioxopyrrolidin-1-yl 3-(2-pyridyldithio)propanoate **(3-38)** (50 mg, 0.160 mmol) in THF (1.2 mL) was added (2-mercapto-phenyl)acetic acid **(3-2)** (18 mg, 0.107 mmol) in THF (0.6 mL) dropwise. After stirring for 1.5 h, the solvent was removed under vacuum. The resulting product **(3-39)** (32 mg, 80 %) was obtained after column (hexane/ethyl acetate). ^{1}H NMR (400 MHz, $CDCl_3$) δ 2.89 (s, 4 H), 3.01 (m, 2 H), 3.08 (m, 2 H), 3.95 (s, 2 H), 7.33 (m, 3 H), 7.83 (m, 1 H).

SB-T-1214-linker-OSu conjugate (3-40):
A mixture of SB-T-1214 **(1-23)** (20 mg, 0.0234 mmol), DMAP (1 mg, 0.0094 mmol), DIC (10 μL, 0.056 mmol) and disulfide linker **(3-39)** (10 mg, 0.0281 mmol) were dissolved in dichloromethane (0.86 mL). The solution was stirred for 4 h at room temperature and the product was purified on a silica column with eluent hexane and ethyl acetate (1:1) to give the conjugate **(3-40)** (10 mg) in 50 % yield. ^{1}H NMR (400 MHz, $CDCl_3$) δ 1.13 (s, 3 H, H16), 1.14 (s, 3 H, H17), 1.25 (s, 4 H, H10 cyclopropane), 1.34 (s, 9 H, Boc), 1.66 (s, 3 H, H19), 1.71 (s, 1 H, cyclopropane), 1.75 (s, 6 H, isobutenyl), 1.82 (s, 1 H, OH), 1.86 (m, 1 H, H6a), 1.91 (s, 3 H, H18), 2.31 (s, 1 H, H 6), 2.33 (s, 1 H, OH), 2.37 (s, 3 H, OAc), 2.60 (m, 2 H, H 14), 2.83 (s, 4 H, OSu), 2.87 (d, *J* =6 Hz, 2 H, CH_2-

CO_2Su), 2.97 (d, J =6 Hz, 2 H, S-CH_2), 3.80 (d, J = 7.2 Hz, 1 H, H3), 4.17 (s, 2 H, Ph-CH_2-CO_2), 4.19 (d, J = 8.7 Hz, 1 H, H20a), , 4.30 (d, J = 8.7 Hz, 1 H, H20b), 4.43 (dd, J = 10.6, 6.6 Hz, 1 H, H7), 4.9-5.0 (m, 4 H, H3', H4'isobutenyl, H5, H2'), 5.19 (s, 1 H, NH), 5.66 (d, J = 7.2 Hz, 1 H, H2), 6.17 (t, J = 8.7 Hz, 1 H, H13), 6.29 (s, 1 H, H10), 7.34 (m, 3 H, Ph linker), 7.47 (t, J = 7.5 Hz, 2 H, Bz), 7.60 (t, J = 7.3 Hz, 1 H, Bz), 7.80 (d, J = 7.2 Hz, 1 H, Ph linker), 8.10 (d, J = 7.4 Hz, 2 H, Bz). ^{13}C NMR (100 MHz, $CDCl_3$): δ 1.22, 9.32, 9.53, 9.75, 13.21, 13.90, 15.00, 18.75, 19.32, 22.42, 22.63, 23.69, 25.80, 25.94, 26.91, 28.44, 29.90, 30.86, 32.84, 33.54, 35.67, 35.95, 43.40, 45.84, 49.20, 58.71, 64.56, 72.05, 72.37, 75.05, 75.45, 75.66, 76.62, 79.51, 80.07, 81.22, 84.70, 120.15, 128.57, 128.85, 129.20, 129.51, 130.38, 131.03, 131.27, 132.12, 132.76, 133.82, 136.70, 138.16, 143.58, 155.13, 166.58, 167.21, 168.39, 169.20, 169.86, 171.19, 175.30, 204.30. HRMS (FAB) *m/z* calcd for $C_{60}H_{72}N_2O_{20}S_2 \cdot H^+$: 1205.4198. Found: 1205.4188 (Δ = -0.8 ppm).

[2-(3-Allyloxy-3-oxopropyl)disulfanyl]phenyl acetic acid (3-42):
To a solution of allyl 3-(pyridi-2-yldisulfanyl)propanoate **(3-41)** (46 mg, 0.180 mmol) in THF (6 mL) was added (2-mercapto-5-methoxy-phenyl)-acetic acid (32 mg, 0.190 mmol) in THF (3 mL) dropwise. After stirring for 3 h, the solvent was removed under vacuum. The residue was purified by flash column chromatography with hexanes and ethyl acetate to give desired product **(3-42)** (50 mg, 90 %). ^{1}H NMR (300 MHz, $CDCl_3$): δ 2.76 (t, J = 6.9 Hz, 2 H), 2.96 (t, J = 6.9 Hz, 2 H), 3.85 (s, 2 H), 4.56 (d, J = 6.0 Hz, 2H), 5.34 (m, 2 H), 5.96 (m, 1 H), 7.28 (m, 3 H), 7.77 (d, J = 8.4 Hz, 1H). ^{13}C NMR (75 MHz, $CDCl_3$): δ 32.9, 33.7, 38.9, 65.5, 118.5, 127.9, 128.4, 130.5, 131.0, 131.8, 133.6, 136.7, 171.3, 176.7

SB-T-1214-linker-allyl ester conjugate (3-43):
A mixture of SB-T-1214 **(1-23)** (75 mg, 0.088 mmol), DMAP (2 mg, 0.034 mmol) and 2-(2-((3-(allyloxy)-3-oxopropyl)disulfanyl)phenyl)acetic acid **(3-42)** (29 mg, 0.093 mmol) was dissolved in dichloromethane (4.2 mL). DIC (26 μL, 0.170 mmol) was added to the mixture, and the solution was stirred for 18 h at room temperature. The residue was purified on flash column using hexanes and ethyl acetate to give desired product **(3-43)** (85 mg, 85 %). ^{1}H NMR (300 MHz, $CDCl_3$) δ 1.13 (s, 3 H), 1.14 (s, 3 H), 1.25 (s, 4 H), 1.34 (s, 9 H), 1.66 (s, 3 H), 1.71 (s, 1 H), 1.75 (s, 6 H), 1.82 (s, 1 H), 1.86(m, 1 H), 1.91 (s, 3 H), 2.31 (s, 1 H), 2.33 (s, 1 H), 2.37 (s, 3 H), 2.60 (m, 2 H), 2.87 (d, J = 6 Hz, 2 H), 2.97 (d, J = 6 Hz, 2 H), 3.80 (d, J = 7.2 Hz, 1 H), 4.17 (s, 2 H), 4.19 (d, J = 8.7 Hz, 1 H), 4.30 (d, J = 8.7 Hz, 1 H), 4.43 (dd, J = 10.6, 6.6 Hz, 1 H), 4.56 (d, J = 6.0 Hz, 2H), 4.9-5.0 (m, 4 H), 5.19 (s, 1 H), 5.34 (m, 2 H), 5.66 (d, J = 7.2 Hz, 1 H), 5.96 (m, 1 H), 6.17 (t, J = 8.7 Hz, 1 H), 6.29 (s, 1 H), 7.34 (m, 3 H), 7.47 (t, J = 7.5 Hz, 2 H), 7.60 (t, J = 7.3 Hz, 1 H), 7.80 (d, J = 7.2 Hz, 1 H), 8.10 (d, J = 7.4 Hz, 2 H)

Tri*iso*propylsilyl 3-(pyridin-2-yldisulfanyl)propanoate (3-45):
To a solution of 3-(2-pyridyldithio)-propionic acid **(3-37)** (562 mg, 2.60 mmol) and triethylamine (TEA, 0.60 mL, 4.20 mmol) in CH_2Cl_2 (10 mL) was added chlorotri*iso*propylsilane (TIPS-Cl, 0.75 mL, 3.40 mmol) dropwise at 0 ^{o}C. After stirring at room temperature for 1 h, the reaction mixture was diluted with ether and washed with $NaHCO_3$ (aq, s) and brine. The desired product **(3-45)** (900 mg, 93 %) was obtained after chromatography. ^{1}H NMR (400 MHz, $CDCl_3$): δ 1.05 (d, J = 7.2 Hz, 18 H), 1.29 (m,

3H), 2.80 (t, *J* = 7.2 Hz, 2 H), 3.04 (t, *J* = 7.2 Hz, 2 H), 7.09 (m, 1 H), 7.66 (m, 2 H), 8.45 (d, *J* = 8.4 Hz, 1 H). ^{13}C NMR (100 MHz, $CDCl_3$): δ 12.07, 17.93, 34.04, 35.51, 119.94, 120.92, 137.26, 149.84, 160.13, 171.61.

2-[(3-Oxo-3-tri*iso*propylsilyloxypropyl)disulfanyl]phenyl acetic acid (3-46):
To a solution of TIPS ester **(3-45)** (900 mg, 2.40 mmol) in THF (10 mL) was added (2-mercapto-phenyl)acetic acid **(3-2)** (407 mg, 2.40 mmol) in THF (6 mL) dropwise at 0 ^{o}C. After stirring for 2-3 h, the solvent was removed *in vacuo*. The desired product **(3-46)** (868 mg, 84 %) was obtained as oil after column purification. ^{1}H NMR (300 MHz, $CDCl_3$): δ 1.22 (d, *J* = 7.2 Hz, 18 H), 1.31 (m, 3H), 2.76 (t, *J* = 6.9 Hz, 2 H), 2.92 (t, *J* = 6.9 Hz, 2 H), 3.90 (s, 2 H), 7.28 (m, 3 H), 7.77 (d, *J* = 8.4 Hz, 1 H). ^{13}C NMR (75 MHz, $CDCl_3$): δ 12.05, 17.93, 33.78, 35.53, 39.09, 128.23, 128.62, 131.06, 131.18, 134.00, 137.00, 171.85, 176.55.

SB-T-1214-linker-TIPS ester conjugate (3-47):
A mixture of SB-T-1214 **(1-23)** (42 mg, 0.049 mmol), DMAP (1 mg, 0.010 mmol) and 2-(2-((3-oxo-3-(tri*iso*propylsilyloxy)propyl)disulfanyl)phenyl)acetic acid **(3-46)** (22 mg, 0.051 mmol) were dissolved in dichloromethane (2.5 mL). DIC (9.2 µL, 0.059 mmol) was added to the mixture, and the solution was stirred for 4 h at room temperature, concentrated, and the residue was purified by flash column chromatography on silica with hexanes and ethyl acetate to give desired product **(3-47)** (85 mg, 85 %). ^{1}H NMR (300 MHz, $CDCl_3$) δ 1.13 (s, 3 H), 1.14 (s, 3 H), 1.25 (s, 4 H), 1.22 (d, *J* = 7.2 Hz, 18 H), 1.31 (m, 3H), 1.34 (s, 9 H), 1.66 (s, 3 H), 1.71 (s, 1 H), 1.75 (s, 6 H), 1.82 (s, 1 H), 1.86(m, 1 H), 1.91 (s, 3 H), 2.31 (s, 1 H), 2.33 (s, 1 H), 2.37 (s, 3 H), 2.60 (m, 2 H), 2.87 (d, *J* = 6 Hz, 2 H), 2.97 (d, *J* = 6 Hz, 2 H), 3.80 (d, *J* = 7.2 Hz, 1 H), 4.17 (s, 2 H), 4.19 (d, *J* = 8.7 Hz, 1 H), , 4.30 (d, *J* = 8.7 Hz, 1 H), 4.43 (dd, *J* = 10.6, 6.6 Hz, 1 H), 4.9-5.0 (m, 4 H), 5.19 (s, 1 H), 5.66 (d, *J* = 7.2 Hz, 1 H), 6.17 (t, *J* = 8.7 Hz, 1 H), 6.29 (s, 1 H), 7.34 (m, 3 H), 7.47 (t, *J* = 7.5 Hz, 2 H), 7.60 (t, *J* = 7.3 Hz, 1 H), 7.80 (d, *J* = 7.2 Hz, 1 H), 8.10 (d, *J* = 7.4 Hz, 2 H). ^{13}C NMR (75 MHz, $CDCl_3$): δ 1.22, 9.32, 9.53, 9.75, 13.21, 13.90, 15.00, 18.75, 19.32, 22.42, 22.63, 23.69, 25.80, 25.94, 26.91, 28.44, 29.90, 30.86, 32.84, 33.54, 35.67, 35.95, 43.40, 45.84, 49.20, 58.71, 64.56, 72.05, 72.37, 75.05, 75.45, 75.66, 76.62, 79.51, 80.07, 81.22, 84.70, 120.15, 128.57, 128.85, 129.20, 129.51, 130.38, 131.03, 131.27, 132.12, 132.76, 133.82, 136.70, 138.16, 143.58, 155.13, 166.58, 167.21, 168.39, 169.20, 169.86, 171.19, 175.30, 204.30.

SB-T-1214-linker-carboxylic acid conjugate (3-44):
To a solution of TIPS protected conjugate **(3-47)** (50 mg) in 2 mL of pyridine/acetonitrile (1:1) was added dropwise HF/pyridine (70:30, 0.5 mL) at 0°C, then the mixture was stirred for 12 h at room temperature. The mixture was then diluted with ethyl acetate (30 mL), washed with aqueous saturated copper sulfate solution (30 mL x 3) and water (30 mL), dried over anhydrous magnesium sulfate and concentrated *in vacuo* and purified by flash column chromatography on silica to afford desired compound **(3-44)** (39 mg, 89 %). ^{1}H NMR (300 MHz, $CDCl_3$) δ 1.13 (s, 3 H), 1.14 (s, 3 H), 1.25 (s, 4 H), 1.34 (s, 9 H), 1.66 (s, 3 H), 1.71 (s, 1 H), 1.75 (s, 6 H), 1.82 (s, 1 H), 1.86(m, 1 H), 1.91 (s, 3 H), 2.31 (s, 1 H), 2.33 (s, 1 H), 2.37 (s, 3 H), 2.60 (m, 2 H), 2.87 (d, *J* = 6 Hz, 2 H), 2.97 (d, *J* = 6 Hz, 2 H), 3.80 (d, *J* = 7.2 Hz, 1 H), 4.17 (s, 2 H), 4.19 (d, *J* = 8.7 Hz, 1 H), , 4.30 (d, *J* =

8.7 Hz, 1 H), 4.43 (dd, *J* = 10.6, 6.6 Hz, 1 H), 4.9-5.0 (m, 4 H), 5.19 (s, 1 H), 5.66 (d, *J* = 7.2 Hz, 1 H), 6.17 (t, *J* = 8.7 Hz, 1 H), 6.29 (s, 1 H), 7.34 (m, 3 H), 7.47 (t, *J* = 7.5 Hz, 2 H), 7.60 (t, *J* = 7.3 Hz, 1 H), 7.80 (d, *J* = 7.2 Hz, 1 H), 8.10 (d, *J* = 7.4 Hz, 2 H).

SB-T-1214-Linker-OSu (3-40):
To a solution of SB-T-1214-linker-carboxylic acid conjugate **(3-44)** (107 mg, 0.090 mmol) and HOSu (14 mg, 0.135 mmol) in 0.25 mL pyridine was added DCC (24 mg, 0.11 mmol) at 0 ^{o}C. After stirring for 24 h at 4 ^{o}C, the solution was filtered and evaporated. The residue was purified by flash column chromatography on silica, which offered the desired product **(3-40)** (117 mg, quant.). ^{1}H NMR (400 MHz, $CDCl_3$) δ 1.13 (s, 3 H, H16), 1.14 (s, 3 H, H17), 1.25 (s, 4 H, H10 cyclopropane), 1.34 (s, 9 H, Boc), 1.66 (s, 3 H, H19), 1.71 (s, 1 H, cyclopropane), 1.75 (s, 6 H, isobutenyl), 1.82 (s, 1 H, OH), 1.86(m, 1 H, H6a), 1.91 (s, 3 H, H18), 2.31 (s, 1 H, H 6), 2.33 (s, 1 H, OH), 2.37 (s, 3 H, OAc), 2.60 (m, 2 H, H 14), 2.83 (s, 4 H, OSu), 2.87 (d, *J* =6 Hz, 2 H, CH_2-CO_2Su), 2.97 (d, *J* =6 Hz, 2 H, S-CH_2), 3.80 (d, *J* = 7.2 Hz, 1 H, H3), 4.17 (s, 2 H, Ph-CH_2-CO_2), 4.19 (d, *J* = 8.7 Hz, 1 H, H20a), , 4.30 (d, *J* = 8.7 Hz, 1 H, H20b), 4.43 (dd, *J* = 10.6, 6.6 Hz, 1 H, H7), 4.9-5.0 (m, 4 H, H3', H4'isoButenyl, H5, H2'), 5.19 (s, 1 H, NH), 5.66 (d, *J* = 7.2 Hz, 1 H, H2), 6.17 (t, *J* = 8.7 Hz, 1 H, H13), 6.29 (s, 1 H, H10), 7.34 (m, 3 H, Ph linker), 7.47 (t, *J* = 7.5 Hz, 2 H, Bz), 7.60 (t, *J* = 7.3 Hz, 1 H, Bz), 7.80 (d, *J* = 7.2 Hz, 1 H, Ph linker), 8.10 (d, *J* = 7.4 Hz, 2 H, Bz). ^{13}C NMR (100 MHz, $CDCl_3$): δ 1.22, 9.32, 9.53, 9.75, 13.21, 13.90, 15.00, 18.75, 19.32, 22.42, 22.63, 23.69, 25.80, 25.94, 26.91, 28.44, 29.90, 30.86, 32.84, 33.54, 35.67, 35.95, 43.40, 45.84, 49.20, 58.71, 64.56, 72.05, 72.37, 75.05, 75.45, 75.66, 76.62, 79.51, 80.07, 81.22, 84.70, 120.15, 128.57, 128.85, 129.20, 129.51, 130.38, 131.03, 131.27, 132.12, 132.76, 133.82, 136.70, 138.16, 143.58, 155.13, 166.58, 167.21, 168.39, 169.20, 169.86, 171.19, 175.30, 204.30. HRMS (FAB) *m/z* calcd for $C_{60}H_{72}N_2O_{20}S_2 \cdot H^+$: 1205.4198. Found: 1205.4188 (Δ = -0.8 ppm).

Biotin hydrazide (3-48)[116]:
To a suspension solution of biotin (300 mg, 1.23 mmol) in MeOH (3 mL) was added $SOCl_2$ (0.30 mL, 4.00 mmol), and the solution was stirred overnight at room temperature, which resulted a clear solution. After evaporation at reduced pressure, the crude biotin methyl ester (296 mg) was obtained as a white solid with 93 % yield. ^{1}H NMR (300 MHz, $CDCl_3$): δ 1.4-1.7 (m, 6 H), 2.34 (t, *J* = 7.2 Hz, 2 H), 2.76 (d, *J* = 13.2 Hz, 1 H), 2.91 (dd, *J* = 13.2, 4.8 Hz, 1 H), 3.17 (m, 1 H), 3.67 (s, 3 H), 4.32 (m, 1 H), 4.52 (m, 1 H), 5.08 (s, 1 H), 5.37 (s, 1 H). All data were in agreement with literature values.[116]
The biotin methyl ester was dispersed in MeOH (2.5 mL), and hydrazine (0.30 mL, 10.0 mmol) was added. After 16 h, the solution was evaporated and diluted with water. The aqueous layer was washed with chloroform three times. The solvent was removed under vacuum and the desired biotin hydrazide **(3-48)** (296 mg) was obtained as white solid with 99 % yield. ^{1}H NMR (400 MHz, D_2O): δ 1.40 (m, 2 H), 1.5-1.7 (m, 4 H), 2.3 (t, *J* = 7.2 Hz, 2 H), 2.8 (d, *J* = 13.2 Hz, 1 H), 3.0 (dd, *J* = 13.2, 4.8 Hz, 1 H), 3.4 (m, 1 H), 4.4 (m, 1 H), 4.6 (m, 1 H). ^{13}C NMR (100 MHz, D_2O): δ 25.0, 27.8, 28.0, 33.6, 39.9, 55.5, 60.5, 62.3, 165.6, 175.8. All data were in agreement with literature values.[116]

Biotin-FITC conjugate (3-49):
To a solution of biotin hydrazide **(3-48)** (52 mg, 0.200 mmol) in dimethylsulfoxide (DMSO, 1 mL) was added fluorescein isothiocynate (FITC, 130 mg, 0.300 mmol). The yellow solution was stirred for 36 h at room temperature. The desired compound **(3-49)** (120 mg, 93 %) was obtained after column purification. HRMS (ESI): $C_{31}H_{30}N_5O_7S_2^+$ ($M + H^+$) *calc*. 647.1581; found 648.1587. Purity was determined to be 93.1 % by Waters Nova-Pak® (CH_3CN/H_2O = 20/80, flow rate at 1 mL/min, retention time at 3.30 min, UV 254 nm) and 90.3 % by Phenomenex® (CH_3CN/H_2O = 20/80, flow rate at 1 mL/min, retention time at 5.67 min, UV 254 nm). ^{1}H NMR (300 MHz, CD_3OD): δ 1.4-1.8 (m, 6 H), 2.35 (t, *J* = 7.5 Hz, 2 H), 2.68 (d, *J* = 12.9 Hz, 1 H), 2.90 (dd, *J* = 12.9, 4.8 Hz, 1 H), 3.20 (m, 1 H), 4.29 (m, 1 H), 4.47 (m, 1 H), 6.57 (m, 2 H), 6.67 (m, 2 H), 6.76 (m, 2 H), 7.15 (d, *J* = 8.4 Hz, 1 H), 7.87 (dd, *J* = 8.4, 1.8 Hz, 1 H), 8.13 (d, *J* = 1.8 Hz, 1 H). ^{13}C NMR (100 MHz, CD_3OD): δ 26.27, 29.63, 29.90, 34.69, 41.21, 57.09, 61.74, 63.45, 103.70, 111.71, 113.96, 121.83, 125.60, 128.82, 130.54, 133.60, 142.36, 150.27, 154.38, 161.71, 166.16, 170.98, 175.77, 184.16.

3-[2-(4-Methyl-2-oxo-2H-1-benzopyran-7-yloxycarbonylmethyl)-phenyldisulfanyl]-propionic acid triisopropylsilyl ester (3-50):
To a solution of 2-[(3-oxo-3-tri*iso*propylsilyloxypropyl)disulfanyl]phenyl acetic acid **(3-46)** (113 mg, 0.26 mmol), 4-dimethylaminopyridine (DMAP, 16 mg, 0.13 mmol) and 7-hydroxy-4-methylcoumarin (142 mg, 0.78 mmol) in tetrahydrofuran (THF, 2 mL) was added dicyclohexylcarbodiimide (DCC, 56 mg, 0.26 mmol) at 0 ^{o}C. After 3 h, the precipitate was filtered off, and the desired product **(3-50)** (80 mg, 50 %) was obtained after silica gel column chromatography purification (hexane:ethyl acetate = 8:1). Rotamers were found in NMR by using either $CDCl_3$ or CD_3OD or DMSO-d^6. ^{1}H NMR (400 MHz, $CDCl_3$): δ 1.22 (m, 18 H), 1.31 (m, 3H), 2.40-2.42 (m, 3 H), 2.77 (t, *J* = 7.2 Hz, 1.6 H), 2.96 (t, *J* = 6.8 Hz, 1.6 H), 3.04 (m, 0.8 H), 3.90 (s, 0.4 H), 4.14 (s, 1.6 H), 6.25 (m, 1 H), 7.04-7.12 (m, 2 H), 7.20-7.33 (m, 3 H), 7.56 (m, 1 H), 7.80 (d, *J* = 8.4 Hz, 1H). ^{13}C NMR (100 MHz, $CDCl_3$): δ 12.02, 17.90, 18.85 (CH_3), 33.84, 35.43, 39.53, 110.50, 114.69, 118.03, 118.16, 125.50, 128.54, 128.76, 131.31, 131.33, 133.87, 136.75, 152.01, 153.28, 154.30, 160.58, 168.97, 171.51. Some other peaks may belong to the rotamer: 17.85 (TIPS CH_3), 32.88, 34.02, 40.93 (linker, Ar-CH_2), 114.75, 118.12, 125.55, 127.99, 128.29, 134.87, 136.58, 153.01, 169.67, 170.72.

3-[2-(4-Methyl-2-oxo-2H-1-benzopyran-7-yloxycarbonylmethyl)-phenyldisulfanyl]-propionic acid (3-51):
To a solution of TIPS ester protected coumarin derivative **(3-50)** (105 mg, 0.18 mmol) in pyridine (1.6 mL) and acetonitrile (1.6 mL) was added HF/Py (70 % weight, 0.80 mL) at 0 ^{o}C. After stirring for 5 h, the solution was diluted with EtOAc and washed with water, $CuSO_4$ (aq, s) and brine. The desired product **(3-51)** (40 mg, 57 %) was obtained after further purification by silica gel column chromatography (Hex:EA = 1:1.5). Again, rotamers were found in NMR by using $CDCl_3$. ^{1}H NMR (400 MHz, $CDCl_3$): δ 2.43 (m, 3 H), 2.77 (t, *J* = 7.2 Hz, 1.4 H), 2.95 (t, *J* = 7.2 Hz, 1.4 H), 3.04 (m, 1.2 H), 3.90 (s, 0.7 H), 4.14 (s, 1.3 H), 6.26 (m, 1 H), 7.04-7.12 (m, 2 H), 7.20-7.33 (m, 3 H), 7.56 (d, *J* = 8.4 Hz, 1 H), 7.80 (m, 1H). ^{13}C NMR (100 MHz, $CDCl_3$): δ 18.86 (HMC CH_3), 32.84, 33.69, 39.51 (linker, Ph-CH_2), 110.51, 114.64, 118.10, 118.19, 125.56, 128.56, 128.83, 131.04,

131.42, 133.71, 136.53, 152.21, 153.27, 154.25, 160.80, 169.03, 176.88. Some other peaks may belong to the rotamer: 32.89, 34.06, 39.10, 110.54, 114.72, 118.10, 125.55, 128.36, 128.71, 130.78, 131.34, 133.91, 136.69152.16, 153.00, 160.73, 169.75, 176.52.

3-[2-(4-Methyl-2-oxo-2H-1-benzopyran-7-yloxycarbonylmethyl)-phenyldisulfanyl]-propionic acid 2,5-dioxo-pyrrolidin-1-yl ester (3-52):

To a solution of carboxylic acid **(3-51)** (40 mg, 0.093 mmol) and *N*-hydroxysuccinimide (HOSu, 11 mg, 0.093 mmol) in DCM (0.25 mL) and pyridine (0.25 mL) was added DCC (20 mg, 0.098 mmol) at 0 ^{o}C. After stirring for 18 h, the solvent was evaporated, and the residue was further purified by silica gel column chromatography, which gave the desired product **(3-52)** (33 mg, 67 %). ^{1}H NMR (300 MHz, $CDCl_3$): δ 2.42 (m, 3 H), 2.81-2.85 (s and s, 4 H), 3.02 (m, 4 H), 4.0-4.2 (s and s, 2 H), 6.25 (m, 1 H), 7.04-7.12 (m, 2 H), 7.20-7.33 (m, 3 H), 7.56 (d, J = 8.4 Hz, 1 H), 7.80 (m, 1 H).

4-Methyl-2-oxo-2H-chromen-7-yl 2-[(3-(2-biotinylhydrazinyl)-3-oxopropyl)disul-fanyl]phenyl acetate (3-53):

To a solution of active ester **(3-52)** (75 mg, 0.14 mmol) in DMSO (1 mL) was added biotin hydrazide **(3-48)** (33 mg, 0.13 mmol). After stirring for 16 h at room temperature, the solution was subjected to silica gel column chromatography directly (DCM:MeOH = 10:1). And the title compound **(3-53)** (48 mg, 56 %) was obtained as white powder. HRMS (ESI): $C_{31}H_{35}N_4O_7S_3^+$ (M + H^+) *calc.* 671.1662; found 671.1674. Purity was determined as 94.8 % by Waters Nova-Pak® (CH_3CN/H_2O = 70/30, flow rate at 0.5 mL/min, retention time at 2.91 min) and 95.3 % by Phenomenex® (CH_3CN/H_2O = 70/30, flow rate at 0.5 mL/min, retention time at 6.71 min). ^{1}H NMR (300 MHz, CD_3OD): δ 1.4-1.8 (m, 6 H, biotin side chain), 2.25 (t, J = 7.2 Hz, 2 H, biotin), 2.48 (m, 3 H, HMC), 2.65-2.73 (m, 3 H, biotin (1) and linker (2)), 2.90 (m, 1 H, biotin), 3.0 (m, 2 H, linker), 3.20 (m, 1 H, biotin), 3.86 and 4.21 (s, 2 H, integrations were 0.78 and 1.24, respectively, linker), 4.27(m, 1 H, biotin), 4.45 (m, 1 H, biotin), 6.32 (m, 1 H, HMC), 7.15 (m, 2 H, linker), 7.2-7.4 (m, 3 H, linker (1) and HMC (2)), 7.78 (m, 2 H, linker (1) and HMC (1)). ^{13}C NMR (100 MHz, DMSO-d^6): δ 18.16 (HMC), 25.02, 28.01, 28.08 (25.1-28.1 biotin), 32.68, 32.92 (linker two carbons), 33.41 (biotin), 38.57 (linker, Ar-CH_2), 39.86 (biotin), 55.39, 59.19, 61.04 (55.4-61.0 biotin), 109.85, 113.85, 117.69, 118.19, 126.58 (109.8-126.6 HMC), 127.59, 128.67, 130.15, 131.63, 133.78, 136.15 (127.6-136.2 linker), 152.76, 152.90, 153.55, 159.58 (152.8-159.6 HMC), 162.71 (biotin), 168.82 (amide), 169.64 (amide), 170.90 (ester). Some other peaks may belong to the rotamer: 32.57, 37.83, 109.97, 113.81, 117.62, 118.30, 126.46, 127.88, 128.14, 130.69, 136.29, 152.68, 152.92, 153.50, 159.57, 162.67, 168.19, 169.64 and 171.00.

Methyl 2-(6-hydroxy-3-oxo-3H-xanthen-9-yl)benzoate (3-54):

Concentrated sulfuric acid (1.5 mL) was added dropwise to a suspension of fluorescein (2.00 g, 6.00 mmol) in methanol (6 mL). The resulting suspension was refluxed for 14 h. The mixture was then cooled, and diluted with EtOAc (100 mL). The organic layer was washed with 5 % aqueous sodium bicarbonate three times, water and brine. After drying over $MgSO_4$ and filtering, the solvent was removed *in vacuo* and dried with vacuum to yield the desired product methyl 2-(6-hydroxy-3-oxo-3H-xanthen-9-yl)benzoate **(3-54)** as a red solid (1.88 g, 85 %). ^{1}H NMR (300 MHz, CD_3OD): δ 3.60 (s, 3 H), 6.66 (dd, J =

9.2, 2.0 Hz, 2 H), 6.74 (d, *J* = 1.5 Hz, 2 H), 7.00 (d, *J* = 9.2 Hz, 2 H), 7.43 (d, *J* = 7.6 Hz, 1 H), 7.79 (td, *J* = 7.2, 1.4 Hz, 1 H), 7.84 (td, *J* = 7.2, 1.4 Hz, 1 H), 8.29 (d, *J* = 7.4 Hz, 1 H).

***tert*-Butyl 4-hydroxybutanoate (3-55):**
To a solution of 4-*tert*-butoxy-4-oxobutanoic acid (2.12 g, 12.2 mmol) in dry THF (18 mL) at 0 ^{o}C was added BH_3•Me_2S (2.0 M, 6.55 mL, 13.1 mmol) dropwise. After stirring at room temperature for 24 h, the solution was diluted with EtOAc (100 mL) and washed with water and brine. The organic layer was dried over $MgSO_4$, and concentrated *in vacuo* to give the desired product 4-hydroxybutanoic acid *tert*-butyl ester **(3-55)** as colorless liquid (1.92 g, 98 %). ^{1}H NMR (300 MHz, $CDCl_3$): δ 1.41 (s, 9 H), 1.82 (m, 2 H), 2.31 (t, *J* = 6.3 Hz, 2 H), 2.50 (bs, 1 H), 3.64 (t, *J* = 6.3 Hz, 2 H). ^{13}C NMR (75 MHz, $CDCl_3$): δ 27.78, 27.98, 32.31, 61.97, 80.43, 173.41.

Methyl 2-(6-(4-*tert*-butoxy-4-oxobutoxy)-3-oxo-3H-xanthen-9-yl)benzoate (3-56):
To a suspension of methyl 2-(6-hydroxy-3-oxo-3H-xanthen-9-yl)benzoate **(3-54)** (200 mg, 0.58 mmol), 4-hydroxybutanoic acid *tert*-butyl ester **(3-55)** (278 mg, 1.74 mmol) and triphenylphosphine (454 mg, 1.74 mmol) in 50 % THF/CH_3CN (4 mL) was added diethyl azodicarboxylate (0.33 mL, 1.74 mmol). The mixture was stirred for 3 h and then concentrated *in vacuo*. The residue was purified on a silica gel column chromatography using 5 % methanol in dichloromethane as the eluant to give the desired product methyl 2-(6-(4-*tert*-butoxy-4-oxobutoxy)-3-oxo-3H-xanthen-9-yl)benzoate **(3-56)** as an orange solid (197 mg, 70 %). ^{1}H NMR (300 MHz, $CDCl_3$): δ 1.45 (s, 9 H), 2.17 (m, 2 H), 2.42 (t, *J* = 6.3 Hz, 2 H), 3.65 (s, 3 H), 4.18 (t, *J* = 6.3 Hz, 2 H), 6.66 (dd, *J* = 9.2, 2.0 Hz, 2 H), 6.74 (d, *J* = 1.5 Hz, 2 H), 7.00 (d, *J* = 9.2 Hz, 2 H), 7.43 (d, *J* = 7.6 Hz, 1 H), 7.79 (td, *J* = 7.2, 1.4 Hz, 1 H), 7.84 (td, *J* = 7.2, 1.4 Hz, 1 H), 8.29 (d, *J* = 7.4 Hz, 1H). ^{13}C NMR (75 MHz, $CDCl_3$): δ 24.70, 28.42, 32.04, 52.68, 68.04, 80.91, 101.15, 106.04, 113.96, 115.09, 117.84, 129.13, 130.47, 130.59, 130.85, 131.41, 132.30, 132.43, 132.98, 134.92, 150.43, 154.52, 159.22, 163.63, 165.88, 172.44, 185.92.

Methyl 2-[6-(3-hydroxycarbonylpropyl)-3H-xanthen-9-yl]benzoate (3-57):
To a solution of protected fluorescein **(3-56)** (230 mg, 0.471 mmol) in 2.3 mL of dichloromethane was added dropwise TFA (2.3 mL). The mixture was stirred at room temperature for 2 h. Diethyl ether was added to precipitate out the product. The upper ether layer was removed and the precipitate was dried *in vacuo*. The crude product was purified on a silica gel column chromatography using 3 % methanol in dichloromethane as the eluant to give the desired product **(3-57)** as an orange solid (215 mg, 94 % yield). ^{1}H NMR ($CDCl_3$, 300 MHz) δ 2.28 (m, 2 H), 2.68 (t, 2 H), 3.69 (s, 3 H), 4.40 (t, 2 H), 7.37 (m,7 H), 7.89 (m, 2 H), 8.42 (d, *J* = 7.5 Hz, 1 H), 12.26 (s, br, 1 H).

2'-*tert*-Butyldimethylsilyl-SB-T-1214 (3-58):
To a flask containing SB-T-1214 **(1-23)** (343 mg, 0.400 mmol), *tert*-butyldimethylsilyl chloride (TBDMS-Cl, 302 mg, 2.00 mmol) and imidazole (273 mg, 4.00 mmol) was added dry *N*,*N*-dimethylformamide (DMF, 0.54 mL). After stirring at room temperature for 4 h, the mixture was diluted with EtOAc (90 mL), and was washed with water and brine. After evaporation of the solvent, the desired product (330 mg, 85 %) was isolated

by silica gel column chromatography (Hex:EA = 2.5:1) as white solid. ^{1}H NMR (300 MHz, $CDCl_3$): δ 0.080 (s, 3 H), 0.12 (s, 3 H), 0.98-1.05 (m, 2 H), 1.13-1.21 (m, 2 H), 1.15 (s, 3H), 1.26 (s, 3H), 1.35 (s, 9 H), 1.37 (s, 9 H), 1.66 (s, 3 H), 1.74-1.79 (m, 8 H), 1.86 (m, 1 H), 1.87 (s, 3 H), 2.2-2.4 (m, 2 H), 2.41 (s, 3 H), 2.55 (m, 1 H), 2.58 (d, *J* = 3.9 Hz, 1 H), 3.81 (d, *J* = 7.2 Hz, 1 H), 4.17 (d, *J* = 8.1 Hz, 1 H), 4.23 (d, *J* = 3.6 Hz, 1 H), 4.30 (d, *J* = 8.1 Hz, 1 H), 4.40 (m, 1 H), 4.78 (m, 2 H), 4.95 (d, *J* = 7.8 Hz, 1 H), 5.21 (d, *J* = 8.4 Hz, 1 H), 5.65 (d, *J* = 7.2 Hz, 1 H), 6.19 (t, *J* = 7.2 Hz, 1 H), 6.28 (s, 1 H), 7.49 (t, *J* = 8.1 Hz, 2 H), 7.61 (t, *J* = 7.2 Hz, 1 H), 8.11 (d, *J* = 8.4 Hz, 2 H).

7-Fluorescein-SB-T-1214-2'-TBDMS (3-59):
To a solution of SB-T-1214-2'-TBDMS **(3-58)** (120 mg, 0.124 mmol), DMAP (15 mg, 0.124 mmol) and fluorescein derivative **(3-57)** (107 mg, 0.247 mmol) in DCM (5 mL) and DMF (2 mL) was added diisopropylcarbodiimide (DIC, 0.038 mL, 0.248 mmol) at room temperature. The solution was stirred overnight and the crude product was purified on a silica gel column chromatography (2 % MeOH in DCM) to afford 7-fluorescein-SB-T-1214-2'-TBDMS **(3-59)** (116 mg, 70 %) as orange solid. ^{1}H NMR (300 MHz, $CDCl_3$): 0.07 (s, 3 H), 0.10 (s, 3 H), 0.92 (s, 9 H), 0.99 (m, 2 H), 1.06 (m, 2 H), 1.16 (s, 3 H), 1.22 (s, 3 H), 1.34 (s, 9 H), 1.66 (m, 1 H), 1.73 (s, 3 H), 1.77 (s, 3 H), 1.79 (s, 3 H), 1.93 (s, 3 H), 2.09 (m, 2 H), 2.15 (m, 1 H), 2.29 (m, 1 H), 2.40 (s, 3 H), 2.46 (m, 2 H), 2.57 (m, 2 H), 3.61 (s, 3 H), 3.69 (s, 1 H), 3.95 (d, *J* = 6.8 Hz, 1 H), 4.10 (m, 2 H), 4.17 (d, *J* = 8.4 Hz, 1 H), 4.23 (d, *J* = 3.2 Hz, 1 H), 4.30 (d, *J* = 8.4 Hz, 1 H), 4.74 (m, 1 H), 4.80 (m, 1 H), 4.93 (d, *J* = 8.8 Hz, 1 H), 5.22 (d, *J* = 8.0 Hz, 1 H), 5.60 (dd, *J* = 10.8, 7.2 Hz, 1 H), 5.66 (d, *J* = 6.8 Hz, 1 H), 6.13 (t, *J* = 8.8 Hz, 1 H), 6.29 (s, 1 H), 6.49 (s, 1 H), 6.54 (d, *J* = 10 Hz, 1 H), 6.73 (m, 1 H), 6.86 (m, 2 H), 6.96 (t, *J* = 2.4 Hz, 1 H), 7.28 (d, *J* = 7.2 Hz, 1 H), 7.46 (t, *J* = 8.0 Hz, 2 H), 7.64 (m, 3 H), 8.08 (d, *J* = 8.8 Hz, 2 H), 8.22 (m, 1 H).

7-Fluorescein-SB-T-1214-2'-OH (3-60):
7-Fluorescein-SB-T-1214-2'-TBDMS **(3-59)** (38 mg, 0.0275 mmol) was dissolved in hydrochloric acid in ethanol (1 %, 2.4 mL). After the mixture was stirred at room temperature overnight, the reaction was diluted with ethyl acetate, washed with $NaHCO_3$ and water. The organic layer was dried over anhydrous $MgSO_4$, filtered and concentrated *in vacuo.* The crude product was purified on a silica gel column chromatography (2 % MeOH in DCM) to afford 7-fluorescein-SB-T-1214-2'-OH **(3-60)** (24 mg, 93 %) as orange solid. ^{1}H NMR (300 MHz, $CDCl_3$): 0.9l (m, 2 H), 1.08 (m, 2 H), 1.18 (s, 3 H), 1.24 (s, 3 H), 1.35 (s, 9 H), 1.68 (m, 1 H), 1.73 (s, 3 H), 1.77 (s, 3 H), 1.81 (s, 3 H), 2.02 (s, 3 H), 2.10 (m, 2 H), 2.20 (m, 1 H), 2.33 (m, 1 H), 2.38 (s, 3 H), 2.42 (m, 2 H), 2.57 (m, 2 H), 3.62 (s, 3 H), 3.97 (d, *J* = 6.8 Hz, 1 H), 4.13 (m, 2 H), 4.17 (d, *J* = 8.4 Hz, 1 H), 4.27 (d, *J* = 3.2 Hz, 1 H), 4.31 (d, *J* = 8.4 Hz, 1 H), 4.77 (m, 1 H), 4.95 (m, 2 H), 5.35 (d, *J* = 8.0 Hz, 1 H), 5.67 (m, 2 H), 6.13 (t, *J* = 8.8 Hz, 1 H), 6.32 (s, 1 H), 6.56 (s, 1 H), 6.60 (d, *J* = 10 Hz, 1 H), 6.74 (m, 1 H), 6.89 (m, 2 H), 7.15 (t, *J* = 2.4 Hz, 1 H), 7.29 (d, *J* = 7.2 Hz, 1 H), 7.48 (t, *J* = 8.0 Hz, 2 H), 7.64 (m, 3 H), 8.09 (d, *J* = 8.8 Hz, 2 H), 8.24 (m, 1 H).

7-Fluorescein-SB-T-1214-2'-linker-CO_2TIPS (3-61):
To a solution of 7-fluorescein-SB-T-1214-2'-OH **(3-60)** (84 mg, 0.066 mmol), disulfide liner **(3-46)** (34 mg, 0.079 mmol) and DMAP (8 mg, 0.066 mmol) in DCM was added

DIC (0.020 mL, 0.132 mmol) at 0 °C. The reaction was stopped after 4 h with incomplete conversion when side reaction was observed on TLC. The desired product **(3-61)** (65 mg, 71 %) was purified by silica gel column chromatography. ^{1}H NMR (300 MHz, $CDCl_3$): δ 0.98-1.05 (m, 2 H), 1.07 (d, *J* = 6.9 Hz, 18 H), 1.13-1.21 (m, 2 H), 1.15 (s, 3 H), 1.26 (s, 3 H), 1.29 (m, 3 H), 1.35 (s, 9 H), 1.62 (m, 2 H), 1.65 (s, 3 H), 1.67 (s, 3 H), 1.72 (m, 1 H), 1.75 (s, 3 H), 1.92 (s, 3 H), 2.12 (m, 2 H), 2.24 (m, 2 H), 2.32 (s, 3 H), 2.41 (m, 2 H), 2.52 (m, 1 H), 2.72 (t, *J* = 6.6 Hz, 2 H), 2.91 (t, *J* = 6.6 Hz, 2 H), 3.58 (d, *J* = 0.9 Hz, 3 H), 3.87 (m, 2 H), 4.02-4.14 (m, 4 H), 4.26 (d, *J* = 8.4 Hz, 1 H), 4.7-4.9 (m, 4 H), 5.04 (d, *J* = 8.4 Hz, 1 H), 5.55 (dd, *J* = 10.5, 6.9 Hz, 1 H), 5.63 (d, *J* = 6.9 Hz, 1 H), 6.11 (t, *J* = 7.2 Hz, 1 H), 6.25 (s, 1 H), 6.41 (s, 1 H), 6.47 (d, *J* = 9.9 Hz, 1 H), 6.68 (dd, *J* = 9.0, 2.1 Hz, 1 H), 6.80 (m, 2 H), 6.92 (t, *J* = 2.1 Hz, 1 H), 7.27 (m, 4 H), 7.43 (t, *J* = 7.8 Hz, 2 H), 7.54-7.73 (m, 4 H), 8.06 (d, *J* = 8.4 Hz, 2 H), 8.19 (dd, *J* = 8.1, 1.5 Hz, 1 H).

7-Fluorescein-SB-T-1214-2'-linker-CO_2H (3-62):
To a solution of 7-fluorescein-SB-T-1214-2'-linker-CO_2TIPS **(3-61)** (65 mg, 0.039 mmol) in pyridine (1 mL) and CH_3CN (1 mL) was added HF/Py (70 % wt, 0.50 mL) at 0 °C. After stirring for 5 h at room temperature, the solution was diluted with EtOAc, and washed thoroughly with $CuSO_4$ (aq, s) several times, then with water and brine. The organic layer was dried and evaporated. The residue was further purified by silica gel column chromatography, which gave desired product (43 mg, 80 %) as yellow powder. MS (ESI): $C_{81}H_{88}NO_{24}S_2^+$ (M + H^+) *calc.* 1522.5, found 1522.4; $C_{81}H_{87}NNaO_{24}S_2^+$ (M + Na^+) *calc.* 1544.5, found 1544.4. ^{1}H NMR (300 MHz, $CDCl_3$): δ 0.98-1.05 (m, 2 H), 1.13-1.21 (m, 8 H), 1.35 (s, 9 H), 1.62 (m, 2 H), 1.72-1.78 (m, 10 H), 1.97 (s, 3 H), 2.12 (m, 2 H), 2.3-2.6 (m, 8 H), 2.68 (t, *J* = 6.9 Hz, 2 H), 2.95 (m, 2 H), 3.62 (d, *J* = 0.9 Hz, 3 H), 3.94 (m, 2 H), 4.02-4.25 (m, 4 H), 4.33 (d, *J* = 8.7 Hz, 1 H), 4.90-4.97 (m, 4 H), 5.12 (d, *J* = 8.4 Hz, 1 H), 5.58 (dd, *J* = 10.5, 6.9 Hz, 1 H), 5.69 (d, *J* = 6.9 Hz, 1 H), 6.17 (t, *J* = 7.2 Hz, 1 H), 6.28 (s, 1 H), 6.58-6.62 (m, 2 H), 6.74 (dd, *J* = 9.0, 2.1 Hz, 1 H), 6.88 (m, 2 H), 7.03 (t, *J* = 1.8 Hz, 1 H), 7.27 (m, 4 H), 7.43 (t, *J* = 7.8 Hz, 2 H), 7.54-7.73 (m, 4 H), 8.06 (d, *J* = 8.4 Hz, 2 H), 8.19 (dd, *J* = 8.1, 1.5 Hz, 1 H).

7-Fluorescein-SB-T-1214-2'-linker-OSu (3-63):
To a solution of carboxylic acid **(3-62)** (43 mg, 0.028 mmol) and HOSu (16 mg, 0.14 mmol) in THF was added DCC (14 mg, 0.068 mmol) at 0 °C. After stirred for 36 h at room temperature, the solution was filtered and evaporated. The residue was purified by silica gel column chromatography, which gave the desired product **(3-63)** (48 mg, quant.). MS (ESI): $C_{85}H_{91}N_2O_{26}S_2^+$ (M + H^+) *calc.* 1619.5, found 1619.5; $C_{85}H_{90}N_2NaO_{26}S_2^+$ (M + Na^+) *calc.* 1641.5, found 1641.5 (M+Na). ^{1}H NMR (300 MHz, $CDCl_3$): δ 0.98-1.05 (m, 2 H), 1.13-1.21 (m, 8 H), 1.34 (s, 9 H), 1.62 (m, 2 H), 1.72-1.78 (m, 10 H), 1.97 (s, 3 H), 2.12 (m, 2 H), 2.3-2.6 (m, 8 H), 2.83 (s, 4 H), 3.02 (m, 4 H), 3.62 (d, *J* = 0.9 Hz, 3 H), 3.94 (m, 2 H), 4.02-4.25 (m, 4 H), 4.33 (d, *J* = 8.7 Hz, 1 H), 4.90-4.97 (m, 4 H), 5.12 (d, *J* = 8.4 Hz, 1 H), 5.57 (dd, *J* = 10.5, 6.9 Hz, 1 H), 5.67 (d, *J* = 6.9 Hz, 1 H), 6.17 (t, *J* = 7.2 Hz, 1 H), 6.28 (s, 1 H), 6.45 (d, *J* = 2.1 Hz, 1 H), 6.52 (dd, *J* = 9.6, 1.8 Hz, 1 H), 6.72 (dd, *J* = 9.0, 2.4 Hz, 1 H), 6.85 (m, 2 H), 6.96 (t, *J* = 2.4 Hz, 1 H), 7.27 (m, 4 H), 7.47 (t, *J* = 7.8 Hz, 2 H), 7.54-7.73 (m, 4 H), 8.09 (d, *J* = 8.4 Hz, 2 H), 8.24 (dd, *J* = 8.1, 1.5 Hz, 1 H).

Biotin-linker-SB-T-1214-fluorescein (3-64):
To a solution of active ester **(3-63)** (45 mg, 0.022 mmol) in DMSO was added biotin hydrazide **(3-48)** (5.4 mg, 0.020 mmol) at room temperature. After stirring for 24 h, the solution was loaded onto silica gel column chromatography directly. The desired product **(3-64)** (24 mg, 82 %) was obtained after column. HRMS (ESI): $C_{91}H_{103}N_5O_{25}S_3^+$ ($M + H^+$) *calc.* 1762.6177, found 1762.6162. Purity was determined to be 91.9 % by Waters Nova-Pak® (CH_3CN/H_2O = 40/60, flow rate at 1 mL/min, retention time at 3.57 min) and 96.6 % by Phenomenex® (CH_3CN/H_2O = 40/60, flow rate at 1 mL/min, retention time at 7.13 min, UV 220 nm). ^{1}H NMR (300 MHz, $CDCl_3$): δ 0.80-1.10 (m, 4 H, cyclopropyl(2) and biotin(2)), 1.13-1.41 (m, 21 H, biotin (4), cyclopropyl(2), C17(3), C16(3) and Boc(9)), 1.5-1.8 (m, 12 H, OH, cyclopropyl(1), C6(1), C5'(6) and C19(3)), 1.95 (s, 3 H, C18), 2.1-2.74 (m, 15 H, tether(2 at 2.10 ppm), biotin(2 at 2.26 ppm), Ac(3), C6(1), C14(2), tether(2), biotin (1 at 2.60 ppm) and linker(2)), 2.85 (m, 1 H, biotin), 2.95 (m, 2 H, linker), 3.10 (m, 1 H, biotin), 3.62 (d, *J* = 1.2 Hz, 3 H, OCH_3), 3.94-4.20 (m, 6 H, C3(1), linker(2), C20(1) and tether (2)), 4.33 (m, 2 H, C20(1) and biotin(1)), 4.47 (m, 1 H, biotin), 4.90-5.2 (m, 5 H, C2', C3', C4', C5 and NH at taxoid), 5.59 (dd, *J* = 10.5, 6.9 Hz, 1 H, C7), 5.68 (d, *J* = 6.9 Hz, 1 H, C2), 5.83 (s, 1 H, urea NH at biotin), 6.16 (t, *J* = 7.2 Hz, 1 H, C13), 6.28 (s, 1 H, C10), 6.54 (d, *J* = 1.5 Hz, 1 H, fluorescein), 6.62 (dd, *J* = 9.6, 1.8 Hz, 1 H, fluorescein), 6.66 (br, 1 H, urea NH at biotin), 6.75 (dd, *J* = 9.0, 2.4 Hz, 1 H, fluorescein), 6.88 (m, 2 H, fluorescein), 7.02 (t, *J* = 2.1 Hz, 1 H, fluorescein), 7.27-7.35 (m, 4 H, fluorescein(1) and linker(3)), 7.43 (t, *J* = 7.8 Hz, 2 H, taxoid), 7.54-7.73 (m, 4 H, taxoid(1), fluorescein(2) and linker(1)), 8.06 (d, *J* = 8.4 Hz, 2 H, taxoid), 8.19 (dd, *J* = 8.1, 1.5 Hz, 1 H, fluorescein), 9.13 (br, 1 H, hydrazide), 9.31 (br, 1 H, hydrazide). ^{13}C NMR (100 MHz, $CDCl_3$): δ 8.98, 11.05, 13.05, 14.68, 18.73, 21.58, 22.60, 23.88, 25.28, 25.62, 25.95, 26.45, 27.96, 28.08, 28.45, 30.48, 33.16, 33.44, 33.45, 35.63, 38.90, 40.62, 43.45, 47.04, 49.21, 52.61, 55.66, 56.19, 60.57, 62.08, 68.25, 71.71, 71.99, 74.76, 75.14, 75.23, 76.49, 78.82, 80.09, 80.92, 84.07, 100.92, 105.64, 114.70, 114.89, 117.43, 119.94, 128.20, 128.81, 129.12, 129.47, 129.92, 130.33, 130.45, 130.68, 131.31, 132.57, 132.87, 133.61, 133.80, 134.70, 136.81, 138.32, 141.72, 152.16, 154.83, 155.38, 159.50, 164.19, 164.80, 165.71, 166.92, 168.64, 169.89, 170.05, 170.64, 172.03, 172.15, 172.81, 173.05, 185.82, 202.61.

Cell culture: L1210FR cell line was received as a gift from Dr. Gregory Russell-Jones[79] (Access Pharmaceuticals Australia Pty Ltd., Targeted Delivery, Unit 5, 15-17 Gibbes St, Chatswood, NSW, Sydney 2067, Australia). L1210FR cells were grown in RPMI-1640 cell culture medium (Invitrogen) in the absence of folate receptor (FR) supplemented with 10 % fetal bovine serum (FBS). Prior to incubation, the cells were collected by centrifugation at 1000 rpm for 6 min and resuspended in RPMI medium without FR at a cell density of 5×10^5 cells/mL.

Incubation of cells with the biotin-FITC conjugate (3-49):
The cell suspension (1 mL) was added to microtube. The biotin-FITC conjugate **(3-49)** (10 μL) in DMSO was added to the microtube at a final concentration of 100 nM and incubated at 37 ^{o}C for 3 h. After incubation, the cells were washed with phosphate buffered saline (PBS) and collected by centrifugation twice, and resuspended in 100 μL phosphate buffered saline (PBS) for imaging.

Low temperature incubation of cells with the biotin-FITC conjugate (3-49):
The incubation of L1210FR with the biotin-FITC conjugate **(3-49)** was carried out in the cold room at ~ 4 ^{o}C. The isolation and washing of the cells were achieved as described above.

Blocking the receptors on L1210FR cells with excess biotin:
Before incubation with the biotin-FITC conjugate **(3-49)**, the cells were treated with biotin at a final concentration of 2 mM for 1 h.

Incubation of cells with the biotin-linker-coumarin conjugate (3-53):
The cell suspension (1 mL) was added to microtube. The biotin-linker-coumarin conjugate **(3-53)** (10 μL) in DMSO was added to the microtube at a final concentration of 1 μM. After incubation at 37 ^{o}C for 3 h, the cells were washed twice with phosphate buffered saline (PBS) to remove excess conjugates and resuspended in the medium. DMSO (10 μL) was then added to the suspension as a control and incubated for another 2 h. After incubation, the cells were washed with phosphate buffered saline (PBS) and collected by centrifugation twice, and resuspended in 100 μL phosphate buffered saline (PBS) for imaging.

Release of the coumarin in L1210FR cells:
The biotin-linker-coumarin conjugate **(3-53)** (10 μL) in DMSO was added to 1 mL of cells in a microtube at a final concentration of 1 μM. After incubation at 37 ^{o}C for 3 h, the cells were washed twice with phosphate buffered saline (PBS) to remove excess conjugates and resuspended in the medium. Glutathione ethyl ester (GSH-OEt) (10 μL) was then added to the suspension at a final concentration of 2 mM and incubated for another 2 h. The excess GSH-OEt was removed by washing twice with phosphate buffered saline (PBS) and the cells were resuspended in 100 μL phosphate buffered saline (PBS) before imaging.

Incubation of cells with the biotin-linker-SB-T-1214-fluorescein conjugate (3-64):
The cell suspension (1 mL) was added to microtube. The conjugates (10 μL) in DMSO were added to the microtube at a final concentration of 20 μM. After incubation at 37 ^{o}C for 2 h, the cells were washed twice with phosphate buffered saline (PBS) to remove excess conjugates and resuspended in the medium. DMSO (10 μL) was then added to the suspension as a control and incubated for another 1 h. After incubation, the cells were washed with phosphate buffered saline (PBS) and collected by centrifugation twice, and resuspended in 100 μL phosphate buffered saline (PBS) for imaging.

Release of the taxoid, SB-T-1214 in L1210FR cells:
The conjugates (10 μL) in DMSO were added to 1 mL of cells in the microtube at a final concentration of 20 μM. After incubation at 37 ^{o}C for 2 h, the cells were washed twice with phosphate buffered saline (PBS) to remove excess conjugates and resuspended in the medium. Glutathione monoester (GSH-OEt) (10 μL) was then added to the suspension at a final concentration of 2 mM and incubated for another 1 h. The excess GSH-OEt was removed by washing twice with phosphate buffered saline (PBS) and the cells were resuspended in 100 μL phosphate buffered saline (PBS) before imaging.

Confocal microscopy imaging of the treated cells:
All the confocal images were taken immediately after the incubation and washing steps. 100 μL of the cell suspension was transferred to the bottom-glass dish using micropipette and imaged by a Zeiss LSM 510 confocal microscope.

Flow cytometry fluorescent measurements of the cells:
Flow cytometry analysis was performed immediately after the incubation and washing steps. Cells were resuspended in 0.5 mL of PBS and analyzed using a flow cytometer, FACSCalibur, operating at a 488 nm excitation wavelength and detecting emission wavelengths with a 530/30 nm bandpass filter. At least 10,000 cells were counted for each experiment using CellQuest 3.3 software (Becton Dickinson) and the distribution of FITC fluorescence was analyzed using WinMDI 2.8 freeware (Joseph Trotter, Scripps Research Institute).

***In vitro* cytotoxicity assay:**
The cytotoxicity of biotin-linker-SB-T-1214 **(3-65)** was quantitatively evaluated *in vitro* on leukemia mouse cell line L1210FR and the measurement was performed with the well-established MTT (3-(4,5-dimethylthiazolyl)-2,5-diphenyl-2H-tetrazolium bromide) cell proliferation assay on the L1210FR cell line. Another two drugs, taxol and 2^{nd}-generation taxoid, SB-T-1214 **(1-23)** were also assayed as control. The cell suspension was cultured and incubated at a concentration of $\sim 2 \times 10^4$ in each well of a 96-well plate. For the adhesive cell type, the cells were allowed to reseed to the bottom of the plates overnight and the fresh medium were added to each well upon removal of the old medium. Cells were subsequently treated with 10 μL of the biotin-linker-SB-T-1214 **(3-65)** dispersion in medium at different final concentrations ranging from 0.1 to 100 nM for 3 days. After spinning down the cells and removal of the old medium, the fresh medium containing MTT (*e.g.* 100 μL of 0.5 mg/mL) was added and incubated at 37 ^{o}C for 4 h. The resulting medium was then removed and the as-produced insoluble violet formazan crystals, which were the product of the mitochondrial reduction of MTT by succinic dehydrogenase, were further dissolved using 0.1 N HCl in isopropanol with 10 % Triton X-100 to give a violet solution. The spectrophotometrical absorbance measurement of each well in the 96-well plate was performed at 570 nm and gave a direct estimate of cell viability and activity. The viability of the cells was plotted as a function of concentration and the cytotoxicity of biotin-linker-SB-T-1214 **(3-65)** was also determined by the IC_{50} value, which was defined as the drug concentration inducing 50 % of the cells death. Finally, the IC_{50} value from the viability-concentration curve was calculated with the software Sigma Plot.

Chapter IV

Functionalized SWNT (*f*-SWNT) as Transporter for Tumor-targeting Drug Delivery

§ 4.1. Introduction

§ 4.1.1. Nanomedicine

A nanometer is one-billionth of a meter (10^{-9} m) and a sheet of paper is about 100,000 nanometers thick. The last decades have witnessed the rapid development of novel materials within the nano scale (nanomaterials), including inorganic and organic materials. To date, nanotechnology has been playing an important role in many industrial and academic researches. The application of nanotechnology to healthcare is referred as nanomedicine, which is the latest achievement in the medical field. Recently, extensive efforts in "nanomedicine" have been focused on novel diagnostic and therapeutic modalities, *e.g.* the 2005 allocation of $144 million by the National Cancer Institute (NCI) for nanomedicine.[1] The history of nanomedicine can date back to 1965, when the first example of liposomes were reported by Bangham and coworkers.[2] Novel nanotechnology applications to healthcare have been extensively explored at many levels including: (1) disease diagnosis; (2) disease imaging; (3) drug delivery. Several excellent reviews on these subjects have been reported in literature.[3,4,5,6] The most representative nano platforms include liposomes,[7] polymeric nanoparticles,[5] quantum dots,[8] gold nanoparticles,[9] magnetic nanoparticles,[10] carbon nanotubes,[11] dendrimers,[12] nucleic acid based nanoconstructs,[13] and engineered viral nanoparticles.[14]. The applications of nanoscale materials to healthcare are summarized in Table 4-1.[15]

Table 4-1. Applications of nanomaterials to healthcare.[15] (Table is adapted from Ref. 15)

Nanomaterials	Size	Toxicity	Status	Application
Liposome	100-200 nm	Low	Clinical use	Delivery
Polymer	~ 200 KDa	Low	Clinical use	Delivery
Dendrimer	2-6 nm	Variable	Phase I	Delivery
Gold nanoparticle	2-4 nm	Low	Commercial	Delivery/Treatment
Magnetic nanoparticle	~ 100 nm	Low	Research	Delivery/Imaging
Quantum dot	2-10 nm	Toxic	Commercial	Delivery/Imaging
Single-walled carbon nanotube	1-2 nm diameter Variable length	Variable	Research	Delivery
Multi-walled carbon nanotube	20-25 nm diameter Variable length	Variable	Research	Delivery
Virus	30-100 nm	High	Phase II	Delivery
Nanowire	Variable length/diameter	N/A	Research	Sensing

The principal reason for the successful utilization of nanomaterials is often referred to the "*enhanced permeability and retention (EPR) effect*", termed by Maeda *et al.* in 1986.[16] Many low molecular weight drugs usually rapidly enter all types of cells by random diffusion through the cell membrane. This lack of selectivity decreases their availability at the desired target tissue and sometimes causes undesirable side effects. Cellular uptake is rapid so that the therapeutic effect is not extended over a period of time, while glomerular filtration can rapidly remove the drugs from the bloodstream. Accordingly, in order to achieve effective tumor-specific drug delivery, it is essential to recognize the morphological and physiological differences between malignant and normal tissues (Figure 4-1).[17] Since the rapid proliferation of cancer cells requires quick formation of new blood vessels, the tumor vasculature exhibits a defective vascular architecture. These defects allow large molecules or nano scale materials to readily enter the extravascular space in tumors. On the other hand, the suppressed lymphatic drainage in the tumor interstitium enhances the retention time of large molecules inside the tumors.[18] Since the accumulation of macromolecules, including plasma proteins in tumors, does not require a specific receptor, the EPR effect is passive in nature and termed as "passive tumor-targeting effect".[19]

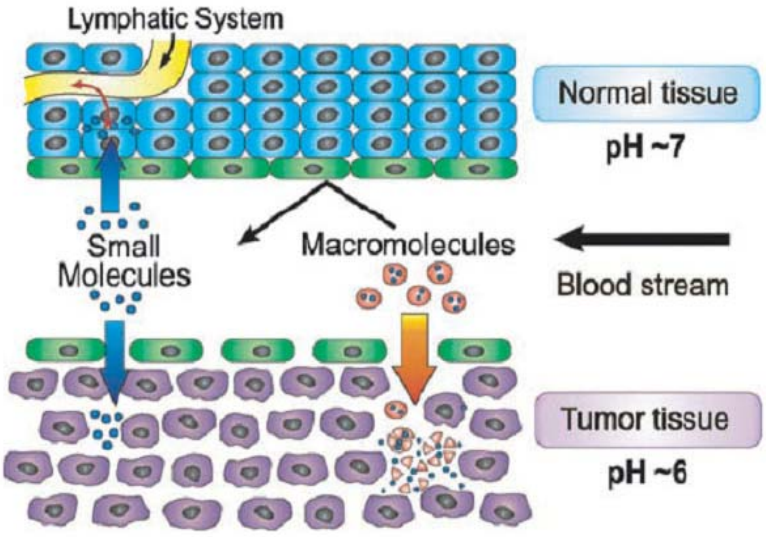

Figure 4-1. Physiological characteristics of normal and tumor tissues.[17] (Figure is adapted from Ref. 17)

To date, a number of multi-functional nanoparticles are in various stages of preclinical and clinical development. One excellent example of the nanomedicine application was Abraxane (ABI-007, invented by American Pharmaceutical Partners), which was a novel cremophor-free formulation of paclitaxel. Abraxane was a 130 nm nanoparticle formed through the assembly of paclitaxel-bound natural human serum albumin. It was approved by FDA in 2005 as second line treatment of breast cancer.[20] In this case, human serum albumin was employed as a stabilizer instead of the traditional excipients, polyoxyethylated castor oil and alcohol. Abraxane was generated by high-pressure homogenization of paclitaxel in the presence of human serum albumin, resulting in a nanoparticle colloidal suspension.[21] The ultrasonic irradiation process caused tremendous local heat and pressure, which resulted in the formation of superoxide ions that crosslinked the albumin by oxidizing the sulfhydryl residues. The anticancer agent, paclitaxel, was then encapsulated into the albumin-contained aqueous solution. The concentration of paclitaxel was increased to 2-10 mg/mL in normal saline.[22] Clinical studies have shown that Abraxane almost (1) doubled the therapeutic response rate; (2) increased time to disease progression; (3) enhanced overall survival in patients with breast cancer.[20] Additionally, in the absence of regular excipient cremophor, the risk of causing hypersensitivity reactions decreased significantly, and patients administrated with Abraxane would avoid premedication.[23] Scientists from American Pharmaceutical Partners suggested that an albumin-binding protein, known as "gp60" or "albondin", on endothelial cells within the microvasculature of tissue may be responsible for rapid binding and transportation of albumin-bound paclitaxel from the bloodstream, across the blood vessel endothelial cells, into the underlying tumor tissue space.[24] Once in tumor interstitium, albumin-drug complex binds to SPARC (secreted protein, acidic and rich in cysteine) and rapidly internalizes into tumor cells *via* a non-lysosomal pathway. This transendothelial transportation mechanism may in part be responsible for the efficient delivery of the anticancer drug, paclitaxel (Figure 4-2).[25] The enhancement in accumulation of Abraxane in tumors may also in part be attributed to passive enhanced permeability and retention (EPR) effect.[1]

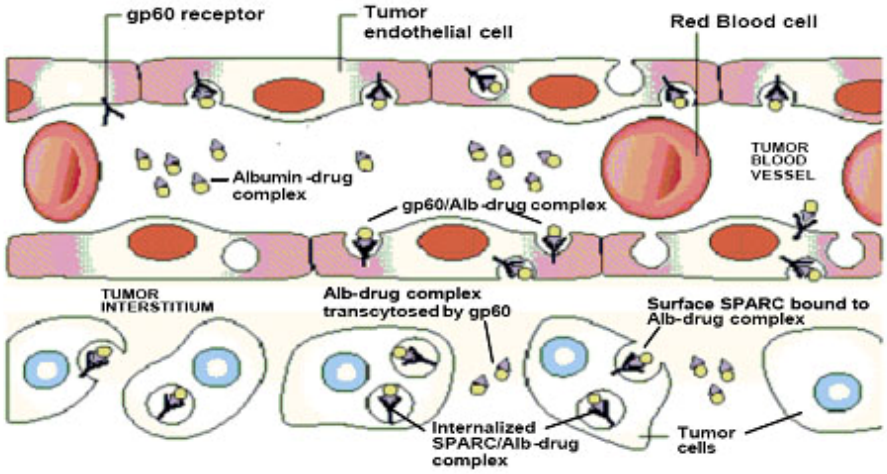

Figure 4-2. Transendothelial transportation mechanism of Abraxane delivery.[25] (Figure is adapted from Ref. 25)

Other nanoscale imaging platforms have also been explored and are currently under pre-clinical or clinical trials. The most characterized system is iron oxide nanoparticles with magnetic resonance imaging (MRI) for enhanced resolution imaging and nanocrystal quantum dots with fluorescent microscopy imaging for molecular or cellular imaging applications. Monocrystalline iron oxide (Combidex, Advanced Magnetics, in the United States and Sinerem, Guerbet, in the Netherlands)[26] is significantly more sensitive for detection of prostate cancer lymph node metastasis as compared to conventional MRI and is in late stage clinical evaluation.[27] The lymphotropic superparamagnetic nanoparticles were measured as 2 to 3 nm on average and the mean overall size of the particles coated with 10 KDa dextrans was about 28 nm. Figure 4-3 outlines the mechanism of action of lymphotropic superparamagnetic nanoparticles for MRI detection. These long-circulating nanoparticles were first systemically injected, followed by the drainage through blood vessel and the access into the lymphatic vessel. Disturbances in lymph flow finally lead to abnormal patterns of accumulation of lymphotropic superparamagnetic nanoparticles, which can be detected by MRI.[27] The authors[27] suggested that lymphotropic superparamagnetic nanoparticles have a significant enhancement in sensitivity than conventional MRI and the MRI with magnetic nanoparticles allowed the detection of usually undetectable lymph-node metastases in patients with prostate cancer.

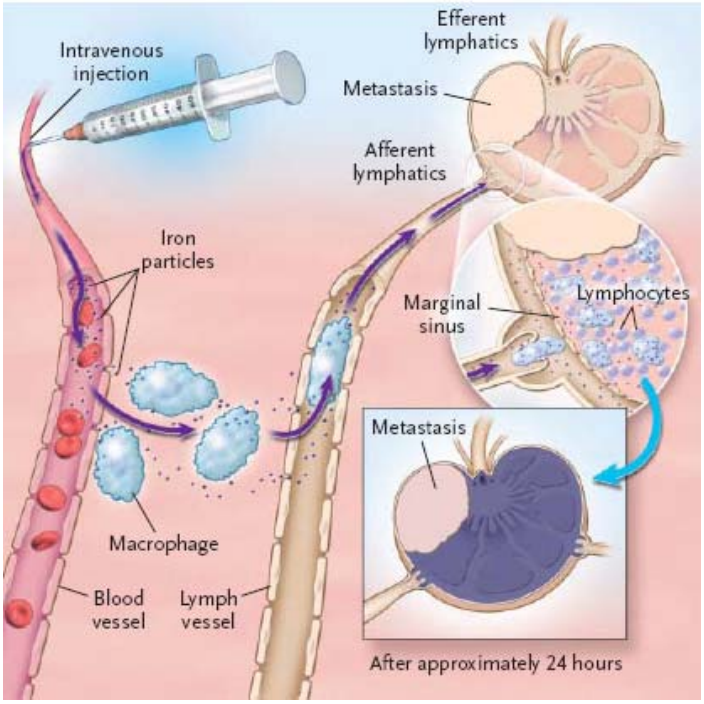

Figure 4-3. Mechanism of action of lymphotropic superparamagnetic nanoparticles.[27] (Figure is adapted from Ref. 27)

Semiconductor quantum dots (QDs) represent another promising platform for fluorescent imaging in molecular profiling of single cells and tissue specimens.[28] Quantum dots are tiny fluorescent particles within the nano scale (2-10 nm, Figure 4-4), which are composed of a core of hundreds to thousands of atoms of group II and VI elements (*e.g.* cadmium, technetium, zinc, and selenide) or group III (*e.g.* tantalum) and V elements (*e.g.* indium).[29]

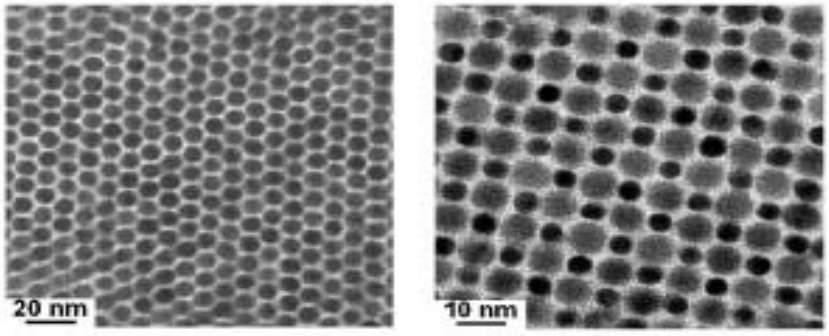

Figure 4-4. Transmission electron microscopy (TEM) images of semiconductor quantum dots.[30] (Figure is adapted from http://chemistry.uchicago.edu/fac/talapin.shtml)

Quantum dots with cadmium selenide core and zinc sulfide shell, coated with the capping ligand (Trioctylphosphine Oxide, TOPO) and an amphiphilic polymer, have been considered to be the most practical biological fluorescent probe for both *in vitro* and *in vivo* cellular imaging (Figure 4-5). Considerable interest over the past 20 years have been attracted on the utilization of the unique optical properties of quantum dots in

comparison with traditional organic dyes.[31]

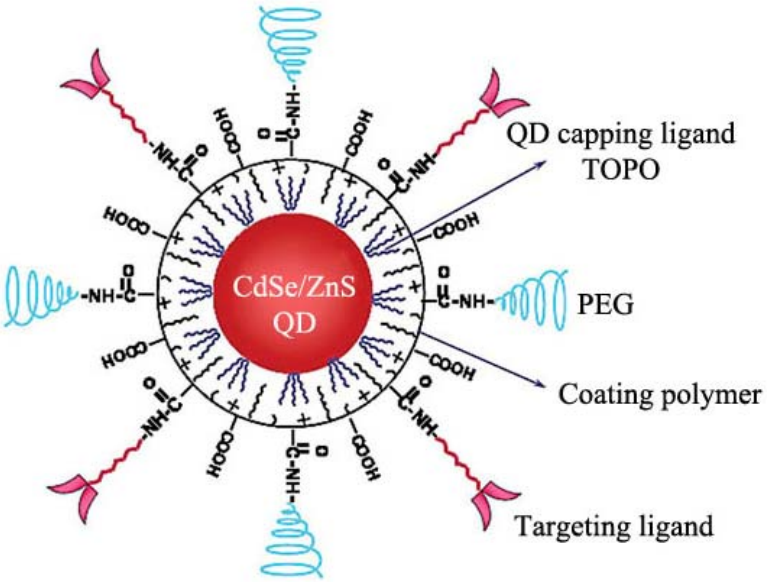

Figure 4-5. Structure of a multifunctional QD probe.[31] (Figure is adapted from Ref. 31)

By varying the size and composition of quantum dots, the tunable emission wavelengths from blue to near infrared can be achieved. Figure 4-6 shows ten distinguishable emission colors (from left to right: blue to red) of ZnS capped CdSe quantum dots excited with a near-UV lamp, and the maximum emission wavelengths are located at 443, 473, 481, 500, 518, 543, 565, 587, 610, and 655 nm, respectively.[32] The typical organic dye species usually have much broader and asymmetric emission profiles. Conversely, the narrow and symmetric emission characteristics of QDs offer simultaneous labeling and detection when multiple analytes are desired.[33] In comparison with regular organic dyes, QDs exhibit advantageous high absorption molar absorptivities and broad absorption spectra, resulting in the efficient excitation of QD-based fluorophores.[34] Studies on comparing the "brightness" and "photostability" of ZnS-capped CdSe QDs to that of rhodamine 6G molecules indicate that QDs are approximately 20 times brighter and 100-200 times more stable than rhodamine 6G molecules.[35]

Figure 4-6. Ten distinguishable emission colors of CdSe/ZnS QDs.[32] (Figure is adapted from Ref. 32)

Due to advantageous properties, which are not available with traditional organic dyes and fluorescent proteins, preclinical trials have demonstrated that quantum dots may be effective for intra-operative investigating genes, proteins and drug targets in single cells, tissue specimens and even in living animals. Figure 4-7 (A) exhibits the detailed cell skeleton structures taken by confocal fluorescent microscopy (CFM).[36] Microtubules in mouse NIH-3T3 fibroblast cells are clearly labeled with polymer-protected QD-streptavidin fluorescent probe (red fluorescence). Early *in vitro* histological application of QDs focused on the use of QDs to target tumor vasculatures guided by peptides and the QD probes were able to escape clearance by the reticuloendothelial system.[37] Most recently, Nie and coworkers reported the *in vivo* behavior of a novel series of multifunctional QD probes, including their biodistribution, nonspecific uptake, cellular toxicity and pharmacokinetics, for simultaneous targeting and imaging of tumors in live animals, as shown in Figure 4-7 (B).[31] QD probes can also be delivered to tumors through the active targeting mechanism (receptor-mediated endocytosis) under *in vivo* conditions. Figure 4-7 (C) clearly illustrates molecular targeting and *in vivo* imaging of a prostate tumor in mouse with QD-antibody conjugates, which are capable of targeting a prostate-specific membrane antigen (PSMA).

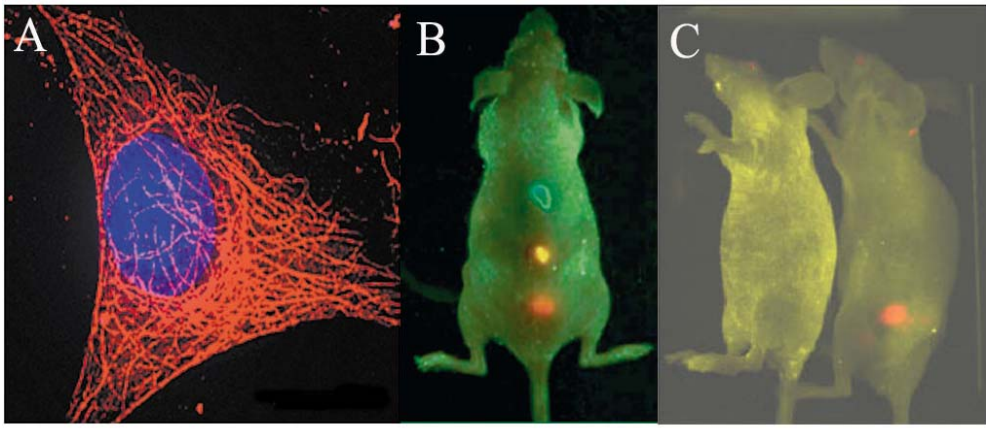

Figure 4-7. Fluorescence micrographs of QD-stained cells and tissues: (A) Microtubules in NIH-3T3 cells labeled with red color QDs.[36] (Figure is adapted from Ref. 36) (B) *In vivo* simultaneous imaging of multicolor QD-encoded microbeads injected into a live mouse.[31] (Figure is adapted from Ref. 31) (C) Molecular targeting and *in vivo* imaging of a prostate tumor in mouse using a QD–antibody conjugate.[31] (Figure is adapted from Ref. 31)

Despite the promising biomedical utilization and applications of nanomaterials, lack of confidence sometimes lies on their systemic toxicity and severe side effects. Numerous efforts on such toxicological and pharmacological assessment are in urgent need for further pharmaceutical development and FDA approval. From this point of view, it is unfair to consider nanomedicine more harmful than any cytotoxic drugs currently on clinical trials. It is believed that nanomedicine will radically change the common ways and develop innovative strategies of diagnosis, prevention and treatment of diseases.

§ 4.1.2. Carbon Nanotubes (CNTs)

Carbon nanotubes (CNTs) were first discovered by Iijima *et al.* in 1991[38], immediately following the invention of fullerene (also known as C_{60}).[39] Different from other classes of organic or inorganic tubes, CNTs exhibit extremely promising potential applications in materials science and medicine, due to their special electronic, mechanical, and structural properties.[40] The composition of CNTs are graphitic sheets, rolled into a cylindrical shape (see Figure 4-8).

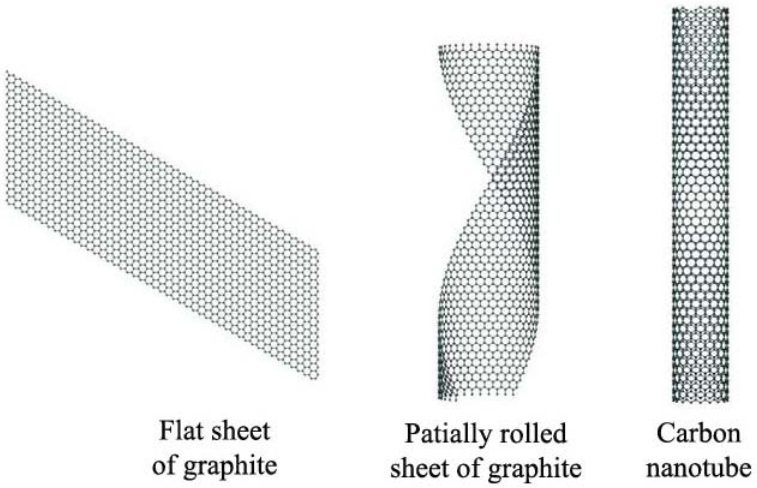

Fiure 4-8. Different structures of graphite. (Figure is adapted from http://www.ewels.info/img/science/nano.html)

Commercial quantities of size controllable carbon nanotubes can be prepared by arc discharge,[41] laser ablation,[42,43] chemical vapor deposition (CVD)[44] and high pressure carbon monoxide (HiPCO).[45] The length of the nanotube is in the size of micrometers with diameters up to 100 nm (Figure 4-9). Nanotubes can be categorized as single-walled nanotubes (SWNTs, diameter: 1-2 nm) and multi-walled nanotubes (MWNTs, diameter: 10-100 nm) or metallic nanotubes and semiconducting nanotubes.

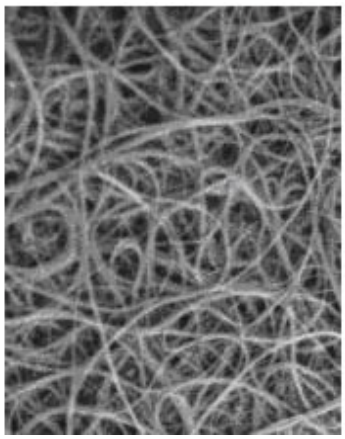

Figure 4-9. SEM image of carbon nanotubes (CNTs). (Figure is adapted from http://www.helixmaterial.com/product.html)

Carbon nanotubes possess very interesting physicochemical properties,[46,47] *e.g.* ordered structure with high aspect ratio, ultralight weight, high mechanical strength, high electrical conductivity, high thermal conductivity, metallic or semi-metallic behavior and high surface area. These extraordinary properties make them potentially useful and attractive candidates in diverse applications, such as molecular electronics, biosensors, gas storage, field-emission devices, catalyst supports, fillers in polymer matrixes, probes for scanning probe microscopy and many others.[48,49,50] Recently, there is an increasing interest in exploring pharmacological properties and applications of carbon nanotubes in nanomedicine. Both exhaustive and critical reports have been reviewed in the literature.[51] The most widespread studies of CNTs to date have concentrated on the safety and toxicological responses. The state-of-the-art application of this nano platform ranges from detection at molecular level to diagnosis of genetic or biological diseases and delivery of a variety of therapeutic agents.[52,53,54]

§ 4.1.2.1. Toxicity and Pharmacological Studies of CNT

The toxicity and pharmacological profile of these nanomaterials, *e.g.* nanoparticles and carbon nanotubes, have been the most pressing tasks in nanomedicine. However, results from numerous biological evaluations are still controversial.[55] Generally, the harmful effects of nanomedicine arise from two predominant factors: high surface area and intrinsic toxicity of the surface.[56] The total surface area of nano scale material mainly depend on their bundling and degree of aggregation in solution, which varies from different administration formulations and functionalization. In vitro studies concerning intrinsic toxicity have suggested that carbon nanotubes covalently functionalized with phenyl-SO_3H or phenyl-$(COOH)_2$ exhibited less cytotoxic effects than aqueous dispersions of surfactants stabilized pristine carbon nanotubes.[57] The cytotoxicity of surface modified carbon nanotube was reported to be further decreased with enhancing of the degree of functionalization.[57] Consequently, the toxicity of carbon nanotubes is likely dependent on the extent of aggregation and the density of the surface functional groups. Concerning the in vivo tissue tolerance and toxicity assessment, to date, most efforts have been primarily focused on the interaction between CNT and the tissues of live organisms. A summary of all studies reported in the literature so far using in vivo investigations of CNT is presented in Table 4-2.[58] As more confidence and knowledge gaining from previous experience on how to handle CNT, more efforts have been made on *in vivo* evaluation for therapeutic aim and other biomedical applications.

Table 4-2. *In vivo* toxicity studies on different types of carbon nanotubes (CNTs).[58]

CNT	Amount	Model	Toxicity	Ref.
Pristine Arc-CNT	25 mg/ Kg	Male dunkin Hartley guiea pigs	Not induce any abnormalities of pulmonary function or measurable inflammation	59
Pristine Laser SWNT	1 and 5 mg/Kg	Male Crl:CD® (SD)IGS BR Rats	Exposure to the high dose produced mortality within 24 h post-instillation. Pulmonary inflammation with non-dose-dependent granulomas.	60
Raw and purified HiPCO CNT and Arc-CNT	0.1 and 0.5 mg/mouse	Male mice B6C3F1	Induced dose-dependent epithelioid granulomas. Mortality was observed with the high dose.	61
MWNT	0.5, 2 and 5 mg/rat	Female Sprague-Dawley rats	Not ground MWNT accumulate in the airways. Ground MWNTs were cleared more rapidly. Both MWNT have induced inflammatory and fibrotic reactions. Also both have caused pulmonary lesions at 2 months.	62
Metal-free HiPCO SWNT	0-40 μg/mouse	Female C57BL/6 mice	Rapid progressive fibrosis and granulomas. Dose-dependent increase in expiratory time. Increased pulmonary resistance.	63
Purified open SWNT and MWNT	50 μg/ml	Wistar–Kyotorats	Accelerated time and the rate of development of carotid artery thrombosis.	64

Regarding the pharmacological profiles, *i.e.* biodistribution and pharmacokinetics of carbon nanotubes, up to now, only two research groups have carried out the systematic studies and both were performed on water soluble CNTs. Wang *et al.*[65] applied ^{125}Iodine-labeled multiple hydroxylated SWNTs (^{125}I-SWNTs-OH) for their study with different administration routes to male KM mice (intraperitoneal injection, subcutaneous injection, stomach incubation and intravenous injection), and they suggested that the ^{125}I-SWNTs-OH distributed quickly throughout the whole body with preferred accumulation in the stomach, kidneys and bone. The biodistribution was reported to be not significantly influenced by the administration routes. From the most important safety point of view, 94 % of the ^{125}I-SWNTs-OH was excreted into the urine and 6 % in the

feces. Excitingly, no tissue damage or distress was observed. Most recently, another research group led by Pantarotto and Bianco intravenously administrated female BALB/c mice with another type of water soluble functionalized CNTs. These CNTs were modified *via* 1, 3-dipolar cycloaddition reaction and functionalized with diethylentriaminepentaacetic acid (DTPA) chelating ligand for radio-labeled ^{111}Indium ([^{111}In] DTPA-CNTs).[66] The biodistribution profiles of [^{111}In] DTPA-CNTs showed an affinity to kidneys, muscle, skin, bone and blood. The maximum blood circulation half time was determined to be 3.5 h and these tubes were quickly cleared from all tissues.

§ 4.1.2.2. Surface Chemistry of CNT

As we discussed in § 4.1.2.1, pristine carbon nanotubes are totally insoluble in all kinds of solvents, leading to high degree of aggregation in biological environment, which will generate some health concerns and hinder their integration into biological systems. Accordingly, it is extremely critical to develop efficient and practical approaches for the preparation of water soluble CNTs, which can be employed in several biological applications, especially drug delivery.[11] The functionalized CNTs (*f*-CNTs) can be obtained either by non-covalent or covalent modification on CNTs. The surface chemistry of CNTs has been extensively explored and several excellent reviews have been reported in literature.[67,68] Supramolecular complexes between CNTs and peptides,[69,70] proteins,[71] polysaccharides,[72,73] phospholipids,[74] oligonucleotides[75,76] and different types of polymers[77,78,79] have been realized and these macromolecules were able to wrap around the tubes and increase their solubility (Figure 4-10).

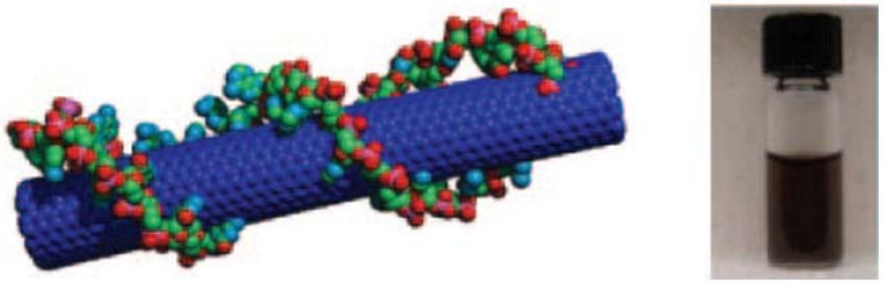

Figure 4-10. CNT wrapped with macromolecules and a photo of DNA-functionalized SWNT solution in H_2O.[80] (Picture is adapted from Ref. 80)

An alternative way of constructing functionalized CNT (*f*-CNTs) is chemical modification around the sidewalls and the end parts of the nanotubes,[68,67] including acid oxidation,[81,82] fluorination,[83] Bingel reaction,[84,85] nucleophilic addition,[46,86] ozonation,[87,88,89] nitrene cycloaddition,[90] diazotization,[91] dichlorocarbene addition,[92] alkylation,[93] hydrogenation,[94] radical addition,[95] and 1,3-dipolar cycloaddtion[96,97]. Scheme 4-1 summarizes several functionalization reactions of CNTs.[67]

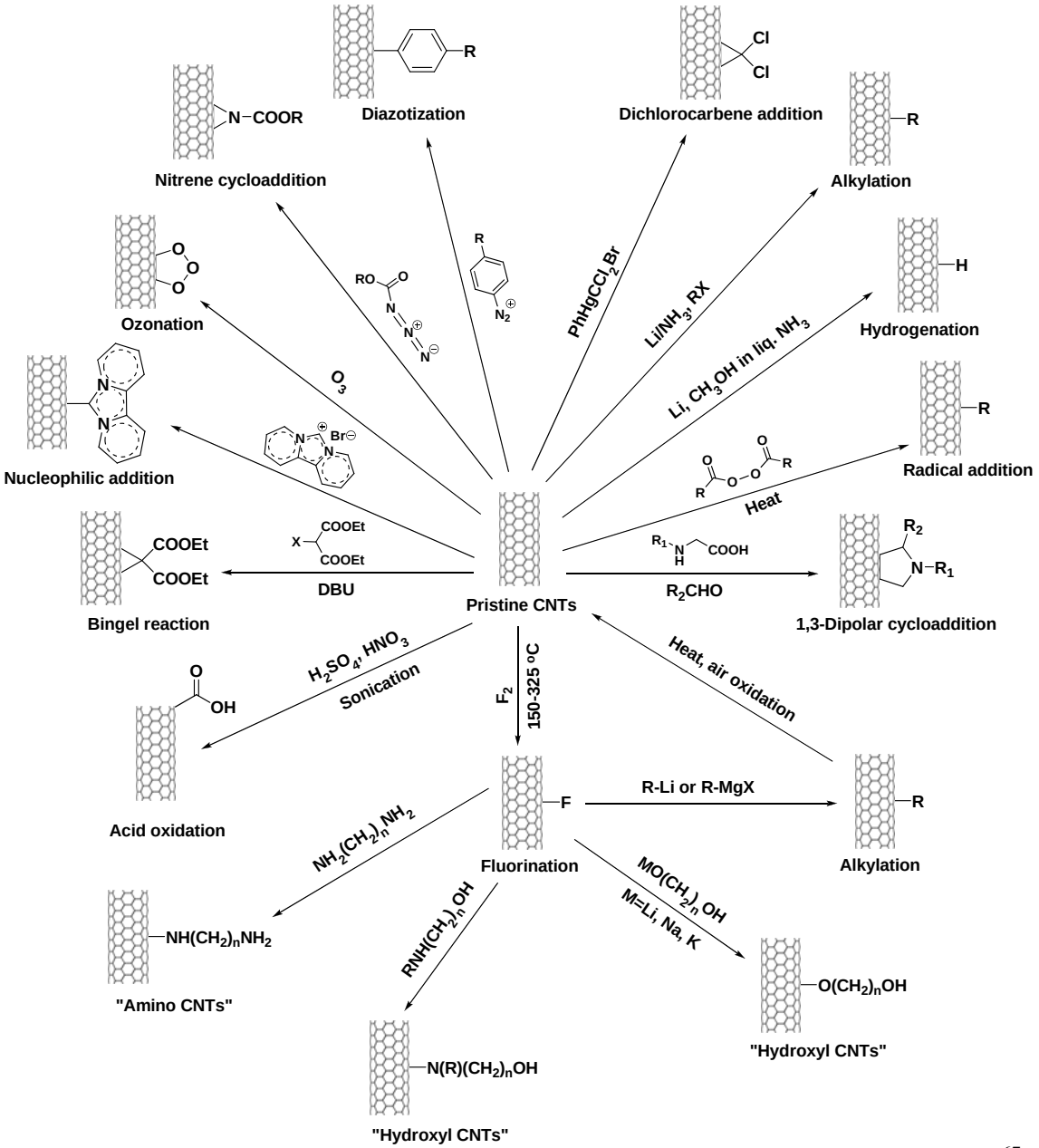

Scheme 4-1. Chemical modification around the sidewalls and the end parts of CNTs.[67] (Scheme is adapted from Ref. 67 with proper modification)

At this time, acid oxidation and 1,3-dipolar cycloaddtion were the two most valuable methodologies to obtain carbon nanotubes soluble in water or organic solvent for particular interests. Acid oxidation was originally applied for the purification of raw CNTs, which generally contained impurities, *i.e.* amorphous carbon and catalyst nanoparticles. The treatment of CNTs with strong oxidative acid (combination of HNO_3 and H_2SO_4) induced the opening of the end tips as well as the formation of holes on the sidewalls of CNTs, producing nanotube fragments modified with carboxylic acid groups.[82] Consequently, amidation or esterification of oxidized nanotubes terminated with carboxylic acids, would thus become one of the most standard ways to produce

either lipophilic[92] or hydrophilic[98] carbon nanotubes. 1,3-Dipolar cycloaddition developed by Prato and Bianco,[96,97] was another simple way to promote the efficient functionalization of CNTs. During the reaction, the azomethine ylides, were generated *in situ* by the condensation reaction between glycine derivatives and aldeydes, which then underwent successful 1,3-dipolar cycloaddition to the graphitic surface, forming pyrrolidine rings. The resulting amine-functionalized CNTs were particularly useful for the covalent attachment of molecules, such as amino acids,[99] peptides,[100] nucleic acids[101] and therapeutic agents[102]. Currently, the rational functionalizaion of CNTs in a predictive manner is still a vital subject for manipulating the properties of these unique nanostructures, such as solubility, biocompatibility, toxicity and many others.

§ 4.1.3. Functionalized CNT as Drug delivery Platform

Prior work on functionalization of carbon nanotubes (CNTs) on their external surface has promoted the utilization of *f*-CNTs as novel family of nanovectors for efficient delivery of diverse types of therapeutic molecules. Indeed, CNTs have served as highly effective and efficient transport media to carry a wide range of molecules across membranes into living cells. Single-walled carbon nanotubes (SWNTs) noncovalently tethered to biomolecules, either proteins or genes have been delivered into cells through endocytosis, as shown in Figure 4-11.[103,104,105,106] The transportation mechanism exploration of fluorescein-labeled SWNTs (SWNT-biotin-SA, structure shown on the left in Figure 4-11) in HL-60 cell was investigated in the presence of the endosome marker FM 4-64 (red fluorescence), which was reported to specifically stain the endosomes *via* endocytosis uptake.[107] Kam *et al.*[105] claimed that the red fluorescence caused by FM 4-64 and the green fluorescence by nanotube conjugates in the endosome regions completely overlapped with each other, which provided the direct evidence for the endocytosis cellular uptake pathway of protein-SWNT conjugates.

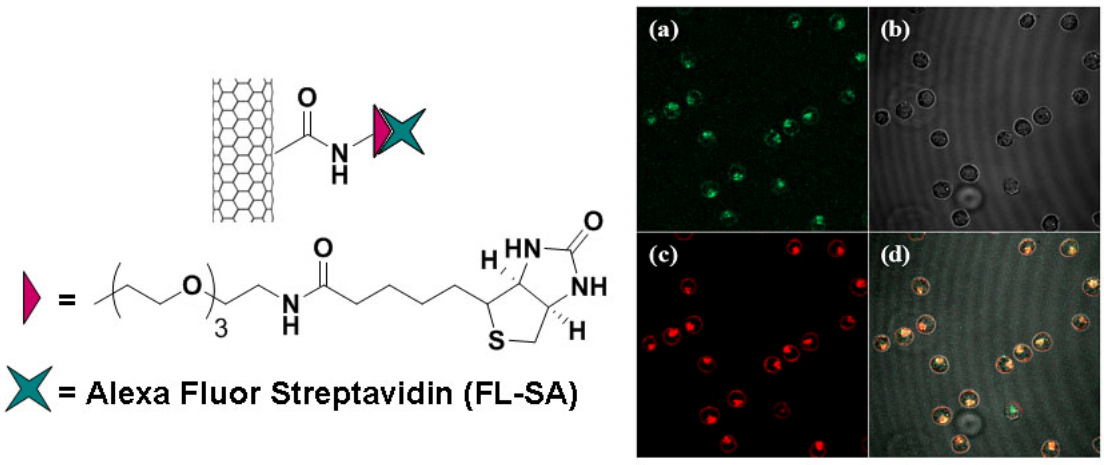

Figure 4-11. Confocal fluorescent microscopy images of dual staining of endosomes in HL-60 cells revealed the endocytosis mechanism of fluorescein-labeled SWNTs (SWNT-biotin-SA, on the left). (a) Green fluorescent SWNT-biotin-SA (0.05 mg/mL, 37 ^{o}C, 1 h) inside cells; (b) bright- field image of cells; (c) red endosomes inside cells stained by red endosome marker FM 4-64; and (d) overlap of (a)-(c).[105] (Figure is adapted from Ref. 105)

More recently, Feazell *et al.* reported the attachment of platinum(IV) complexes to the surface of amine-functionalized soluble SWNTs (Scheme 4-2), with the mediation of phospholipids, to deliver these anticancer drugs to tumor cells.[108] Platinum(IV) complexes, *c*,*c*,*t*-[$Pt(NH_3)_2Cl_2(OEt)(O_2CCH_2CH_2CO_2H)$] served as prodrugs with almost no toxicity to cells. Once the water soluble prodrug conjugates were internalized into the cancer cells through endocytosis, dissociation of the active platinum(II) species was facilitated *via* reduction in a low pH environment in cancer cells and displayed a significantly enhanced cytotoxicity profile compared with the untethered complexes.

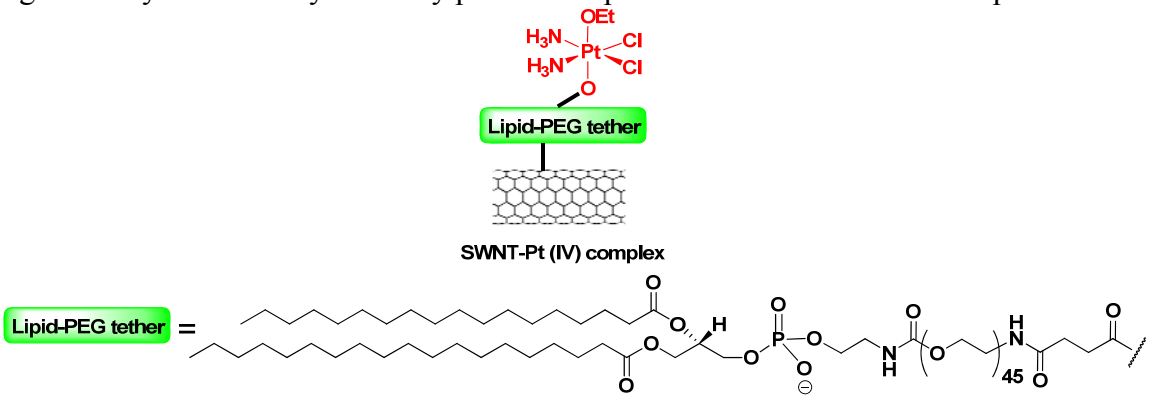

Scheme 4-2. Structure of the SWNT-Pt(IV) complex bearing phospholipids-PEG conjugate.[108]

In contrast, SWNTs covalently functionalized by small molecules through carboxylic acid sites localized at either their ends, defect sites, or sidewalls, *e.g.* amino acids,[109] oligopeptides,[110] and antibiotics,[102] have all previously been transported into different types of cells through energy-independent intercession of appropriately functionalized CNTs (Scheme 4-3).[111]

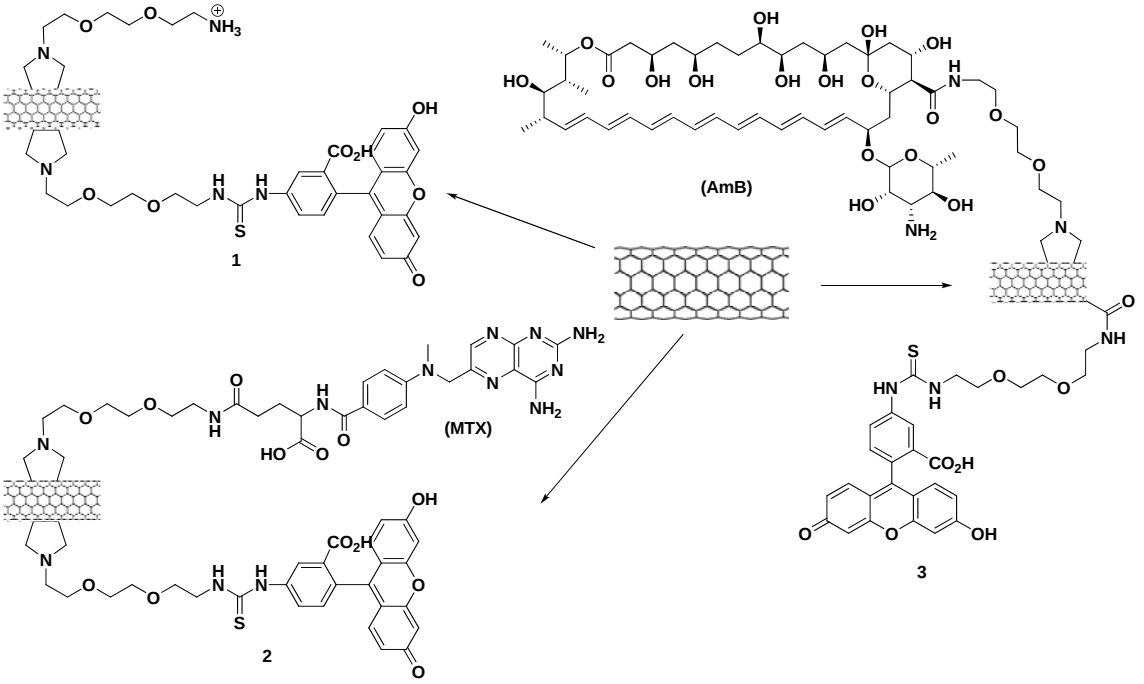

Scheme 4-3. Structure of some chemically functionalized SWNTs *via* 1,3-dipolar cycloaddition.[111]

In order to elucidate the intracellular localization of *f*-CNTs, Prato, Bianco *et al.* suggested that *f*-CNTs distributed in the perinuclear region in human alveolar epithelial (A549) cells. This behavior was reasonably different from that of *f*-CNTs coated with macromolecules as those polymers or biomacromolecules layered at the CNTs surface would inevitably manipulate the interactions with cells and the intracellular transport kinetics. Additionally, they observed uptake and internalization of *f*-CNTs *via* non-endocytosis mechanism. The incubation of *f*-CNTs with Jurkat cells was carried out in the presence of sodium azide (NaN_3) at 4 ^oC, which was commonly used to inhibit endocytosis process. They claimed that there was no significant change between the cells with and without NaN_3 treatment, which clearly indicated that energy-independent intercession took place during the cellular uptake of *f*-CNTs (Figure 4-12). They ascribed such discrepancies in contrast to previous dated reported by Dai *et al.* (Figure 4-11) to the substantial difference in the characteristics of the *f*-CNT surface construction. It was expected that energy-dependent cellular endocytosis occurred when proteins, single-stranded oligonucleotides or other macromolecules wrapped *f*-CNTs was used.[106]

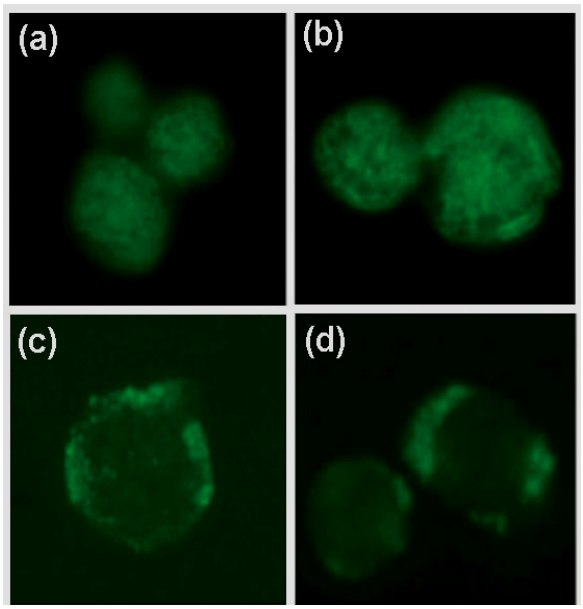

Figure 4-12. Epifluorescence images of Jurkat cells incubated with *f*-CNTs: (a) *f*-CNT **1** (0.5 μg/mL), 37 ^{o}C, 16 h, in the presence of NaN_3; (b) *f*-CNT **2** (5 μg/mL), 37 ^{o}C, 16 h, in the presence of NaN_3; (c) *f*-CNT **3** (20 μg/mL), 4 ^{o}C, 1 h; and (d) *f*-CNT **3** (20 μg/mL), 37 ^{o}C, 1 h, in the presence of NaN_3.[111]

Despite the promising results that *f*-CNTs are able to cross cell membranes easily and to deliver peptides, proteins, and nucleic acids into cells,[11] it may be more appropriate for practical anticancer treatment if functionalized CNTs can not only transport drugs, but also target tumor cells (as opposed to normal cells) in a highly specific manner by recognizing specific biomarkers on the tumor cell surface under physiological pH conditions. The combination of two tumor-targeting modalities, active receptor-mediated endocytosis (See Chapter 3 for details) and passive EPR (enhanced permeability and retention) effects has become a new approach toward efficient drug delivery. Such a strategy would minimize systemic toxicity, which is the cause of undesirable side effects in conventional chemotherapy. This objective is fundamentally associated with the rational design of a biocompatible nanotube-based drug delivery device. In fact, some biocompatible nanoscale drug delivery cargoes have been explored based on this principle. Figure 4-13 shows biodegradable dendrimeric and polymeric drug delivery platforms, which can take advantage of EPR effect of their own, and further increases the therapeutic index through receptor-mediated uptake *via* specific interactions between receptors on the cell surface and targeting moieties therein.

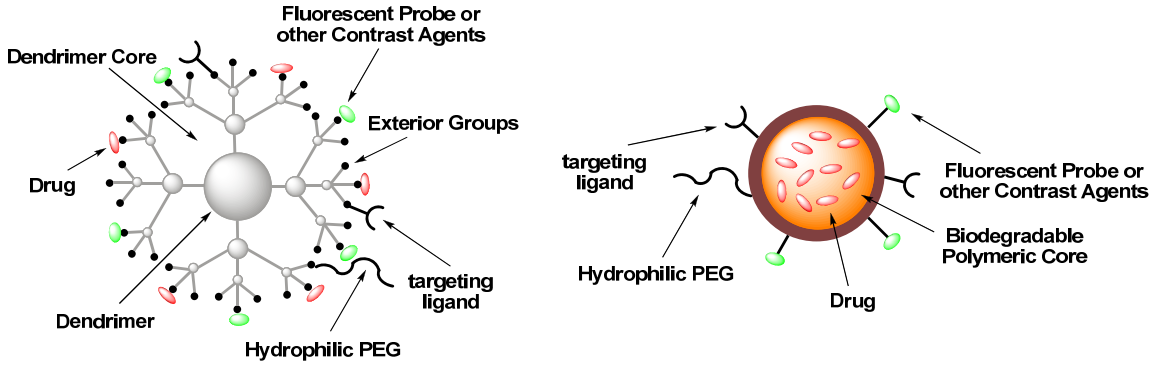

Figure 4-13. Biodegradable dendrimeric and polymeric drug delivery platforms.

Expectantly, with the effort performed in many laboratories, we are able to envisage full applications of this novel material in the future, to vaccine and drug delivery, gene transfer, and immunopotentiation.

§ 4.2. Results and Discussion

§ 4.2.1. Rational Design of *f*-SWNT as Transporter for Drug Delivery

The practical use of functional nanomaterials for biomedical purposes is of great interest. The utilization of functionalized carbon nanotubes (*f*-CNTs) as novel drug delivery vectors for efficient delivery of therapeutic molecules has been attracting increasing attention in the past few years.[102] With the aim of enhancing the selectivity and efficacy of anticancer drug molecules to tumor tissues, a novel SWNT-based tumor-targeting drug delivery system (DDS) was developed in our laboratory. The conventional tumor-targeting drug delivery system was a prodrug conjugate formed *via* connecting a tumor recognition moiety and a cytotoxic warhead directly or through suitable linker (See Chapter 3 for details). However, the monovalent binding between a prodrug and a given receptor would result in the rapidly diffusion of the conjugates into healthy tissues. Consequently, the conjugates would be distributed evenly within the body and relatively small amounts of the drugs would reach the target site.[17] Unlike traditional drug delivery system, the chemical fictionalization of tumor recongnition moieties at the end tips of SWNTs may potentially exhibit polyvalent effects (Figure 4-14), in addition to the EPR effect. Besides, the unique one-dimensional structure may facilitate SWNTs leaking out from blood microvessels to reach cancer cells through vascular and interstitial barriers.

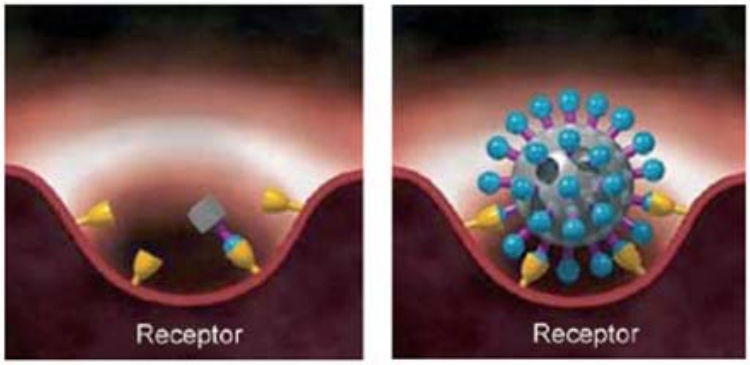

Figure 4-14. Monovalent binding of a drug (left) *versus* polyvalent binding of a virus (right) on a cell surface.[17] (Figure is adapted from Ref. 17)

Accordingly, the SWNTs were simultaneously functionalized with a tumor-targeting module recognizing tumor cell specific receptors and with a prodrug component of a cytotoxic agent. This SWNT-based tumor-targeting drug delivery system (DDS) presents a model drug carrier platform for tumor-targeted drug conjugate and combines three key features: (a) use of functionalized carbon nanotubes as the biocompatible platform technology for potential diagnostics and therapeutic drug delivery (amplification of tumor-targeting drug delivery *via* the potential EPR effect associated with nano-scale materials), (b) incorporation of prodrug modules of antitumor agents, that are activated to the active cytotoxic form inside the tumor cells upon internalization, followed by *in situ* drug release, and (c) simultaneous attachment of tumor-recognition modules onto the nanotube and enhancement of internalization efficacy *via* possible multivalent ligand-receptor interactions at the tumor cell surface. This SWNT-based tumor-targeting conjugate is a multi-functional, multi-component drug delivery system, possessing not only the receptor recognition modules, *i.e.* biotin, at the nanotube end parts, which can recognize the biotin receptors overexpressed on the exterior of the tumor cell surface, but also the prodrug modules on the nanotube sidewalls, comprised of 2nd-generation taxoid antitumor agents and the highly efficient self-immolative disulfide linkers, which are stable in blood plasma but readily cleaved by intracellular thiols, *e.g.* glutathione, to release a highly cytotoxic anticancer agent inside the cancer cells (See Chapter 3 for details). This drug delivery system integrates the advantages of tumor-targeting drug delivery and enhanced permeability and retention (EPR) effect associated with nanomaterials.

To demonstrate the specificity and efficacy of this SWNT-based tumor-targeting drug delivery system (DDS), three fluorescently labeled SWNT-conjugates (Scheme 4-4), were designed and subjected to monitor the receptor-mediated endocytosis and drug release process inside the cancer cells (L1210FR leukemia cell line) by confocal fluorescence microscopy (CFM).

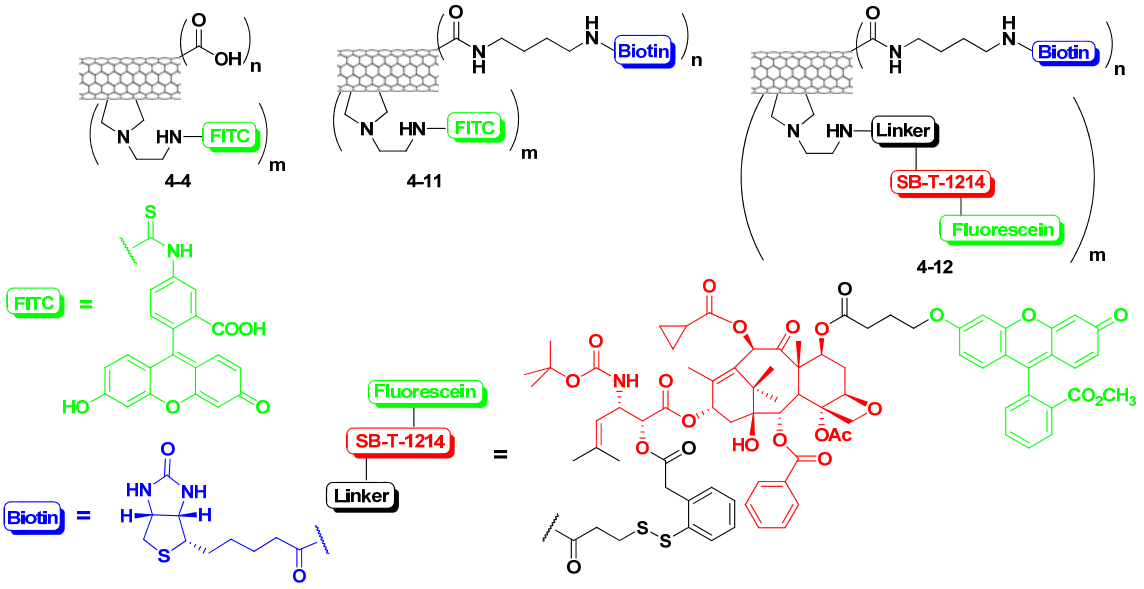

Scheme 4-4. Structures of three fluorescently labeled *f*-SWNT-based conjugates: SWNT-FITC **(4-4)**, biotin-SWNT-FITC **(4-11)**, and biotin-SWNT-linker-SB-T-1214-fluorescein **(4-12)**.

As shown in Scheme 4-4, SWNT-FITC conjugates **(4-4)** and biotin-SWNT-FITC **(4-11)** are labeled with fluorescein isothiocyanate (FITC) to track the internalization of SWNT with or without biotin into the tumor cells, respectively. The construction of biotin-SWNT-linker-SB-T-1214-fluorescein conjugate **(4-12)** was to envisage the receptor-mediated endocytosis and intracellular drug release. Figure 4-15 illustrates the three key steps involved in the activation of the nanotube-based DDS. First, the biotin-SWNT-linker-SB-T-1214 conjugate is internalized into the tumor cells through receptor-mediated endocytosis. The biotin moieties covalently attached to the ends of the SWNT efficiently recognizes the biotin receptors overexpressed on the tumor cell surfaces. The presence of multiple biotin moieties, localized at the ends of the SWNT, would enhance the internalization of the conjugate *via* increased probability for receptor binding or *via* multivalent binding.[112] Second, the active drug is released through cleavage of the disulfide bond in the linker moiety (connecting taxoids to SWNTs) by endogenous thiols such as glutathione (GSH). The disulfide bond is readily cleaved by GSH (or other intracellular thiols) to generate a sulfhydryl group, which subsequently undergoes a thiolactonization process to form benzothiophen-2-one and regenerates a free taxoid in its active form. Concentrations of GSH are typically 1-2 μM in circulating human blood plasma, but are in the range of 2-8 mM in tumor tissue.[113,114] Thus, the adventitious activation of the cytotoxic drug warhead should be minute at best in blood circulation, whereas the activation process would be facile in tumor cells. Third, the released taxoid binds to microtubules, inhibiting cell mitosis at the G2/M stage by stabilizing microtubules, which triggers signaling to induce apoptosis.[115,116]

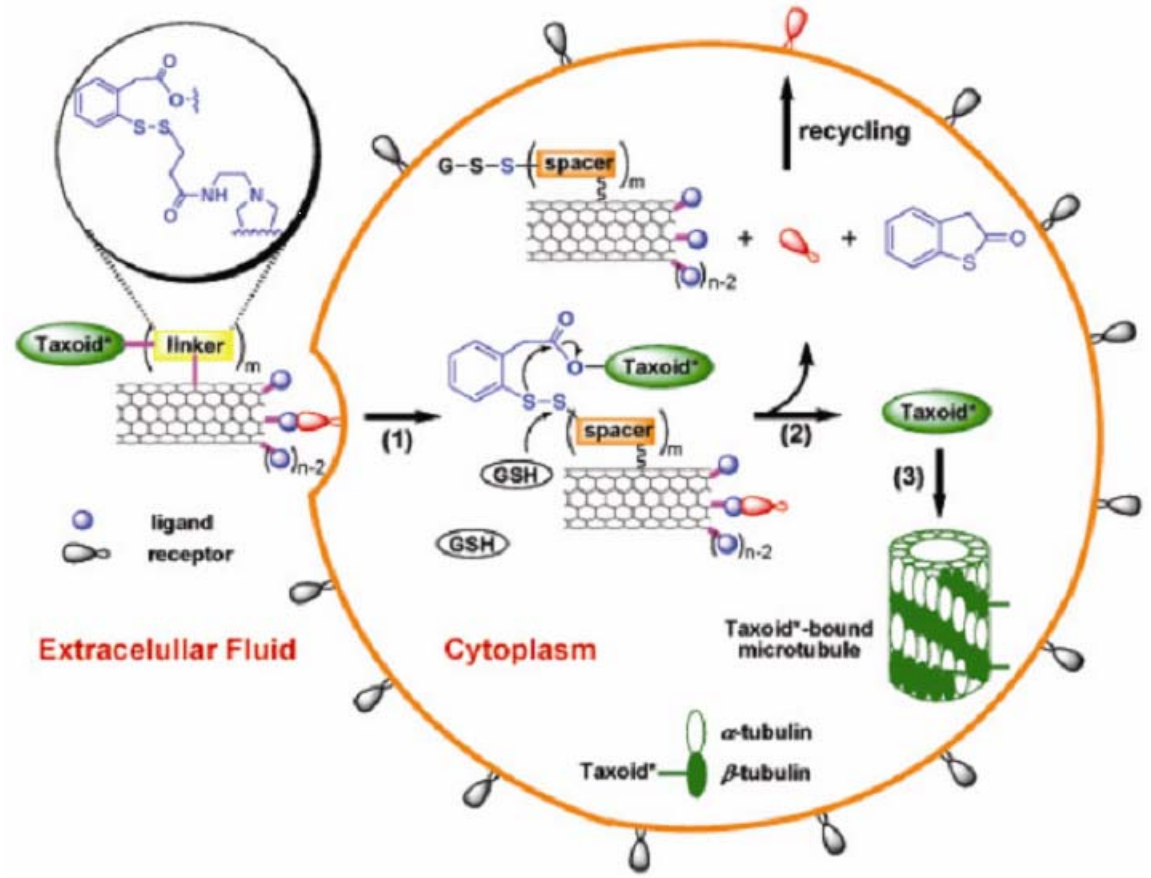

Figure 4-15. Schematic illustration of three key steps involved in the tumor-targeting drug delivery of biotin-SWNT-taxoid conjugate **(4-12)**: (a) internalization of the whole conjugate *via* receptor-mediated endocytosis; (2) drug release through cleavage of the disulfide linker moiety by intracellular thiol, *e.g.* GSH; (3) binding of the free taxoid molecules to tubulins/microtubules, forming stabilized microtubules that block cell mitosis and trigger apoptosis. [*Note:* Since each taxoid molecule is fluorescently labeled with fluorescein, the internalized conjugate **(4-12)** present in the cytoplasm and the taxoid-bound microtubules is fluorescent.]

§ 4.2.2. Syntheses and Structure Characterization of *f*-SWNT-based Conjugate

Initially, it was essential to establish the selective chemical functionalization of single-walled carbon nanotube (SWNTs) at the defective sides and side wall. Scheme 4-5 illustrates the synthetic pathway to SWNT-FITC conjugate **(4-4)** from the commercially available pristine HiPCO SWNT.

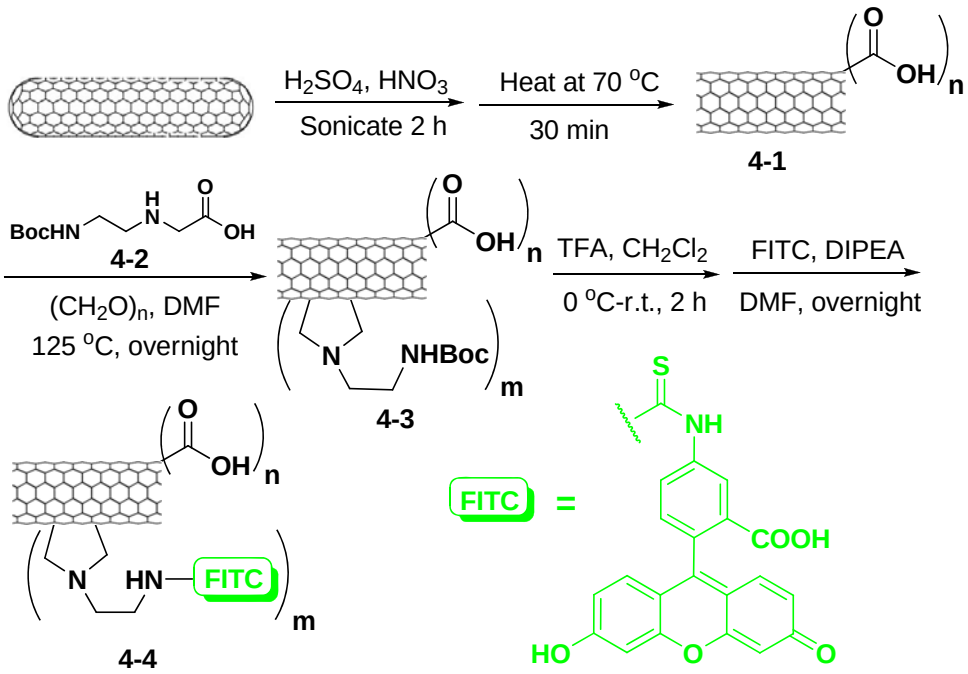

Scheme 4-5. Synthesis of SWNT-FITC conjugate **(4-4)**.

A batch of pristine SWNTs was first purified by oxidation in concentrated H_2SO_4:HNO_3 (3:1 by volume) with sonication for 2 h, followed by reflux at 70 °C for 30 min to remove the impurities containing in SWNT formed, such as amorphous carbon and metal nanoparticles and generated the defective sites mainly at the end parts of the nanotubes **(4-1)**.[82] Figures 4-16 (A) and 4-16 (B) illustrate the transmission electron microscopy (TEM) images of the pristine SWNTs and acid-oxidized SWNTs **(4-1)**. Figure 4-16 (C) shows the AFM image of the oxidized SWNTs **(4-1)** with ~ 3 nm in diameter and ~ 250 nm in length. The ends and defective sites on the side walls of the oxidized SWNTs **(4-1)** were functionalized with carboxylic acid and carboxylate groups, whose presence were confirmed by ATR IR spectroscopy, showing expected relevant peaks at 3400, 1703 and 1630 cm^{-1} (Figure 4-16 (D)).

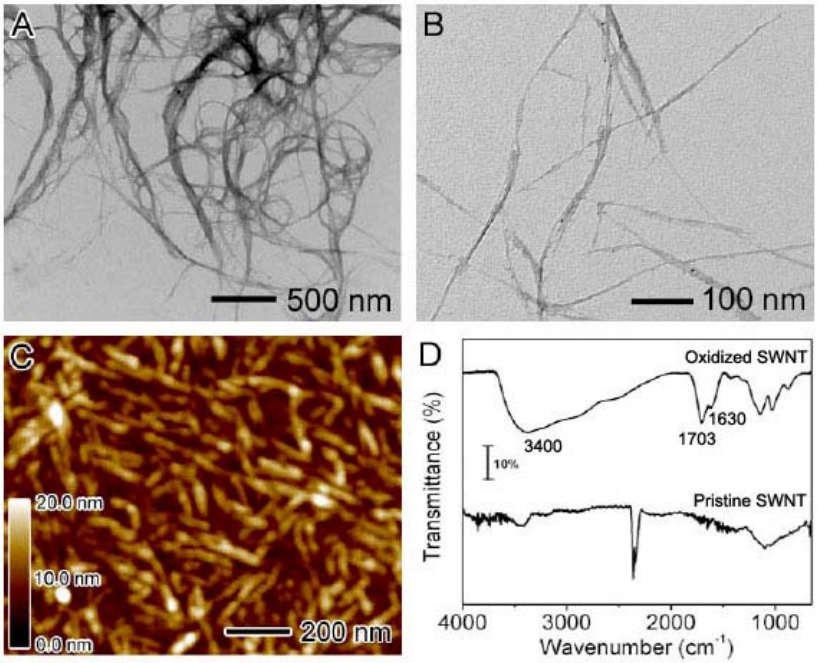

Figure 4-16. TEM images of (A) pristine SWNTs; (B) acid-oxidized SWNTs **(4-1)**; (C) AFM image of the acid-oxidized SWNTs **(4-1)**, and (D) ATR-IR spectrum of acid-oxidized SWNTs **(4-1)**. [Note: the peak at 2349 cm^{-1} was attributed to the asymmetric stretch mode of the CO_2 molecules in the atmosphere.]

Subsequently, the tube sidewalls were functionalized with amine moieties **(4-2)** through 1,3-dipolar cycloaddition of *in situ* generated azomethine ylide.[109] The extent of amine loading was estimated to be 0.5 and 0.2 mmol per gram at the ends/defective sites and the sidewalls of SWNTs, respectively, by means of the Kaiser test.[117] SWNT-FITC conjugate **(4-4)** was obtained from functionalized SWNT **(4-3)** by attaching the fluorescein isothiocyanate (FITC) groups to its sidewall through deprotection of the Boc group and the addition of FITC. The presence of FITC groups was characterized by UV-visible spectroscopy with the absorption peaks at 450 and 480 nm (Figure 4-17).

The biotin-SWNT-FITC conjugate **(4-11)** was prepared from functionalized SWNT **(4-3)** by introducing the biotin moiety through the standard peptide coupling protocol (Scheme 4-6). The carboxylic acids in *f*-SWNT conjugate **(4-3)** were coupled with mono-protected diamines **(4-5)**, followed by the deprotection of phthalimide with hydrazine and further attachment of biotin succinic active ester **(4-8)** to afford the biotin-SWNT conjugate **(4-9)**. The final product "biotin-SWNT-FITC **(4-11)**" was obtained in the same manner as that used for the synthesis of SWNT-FITC conjugate **(4-4)** (Scheme 4-6). Similarly, the presence of FITC and biotin was confirmed by UV-visible and ATR IR spectroscopy, as shown in Figure 4-17 and Figure 4-18.

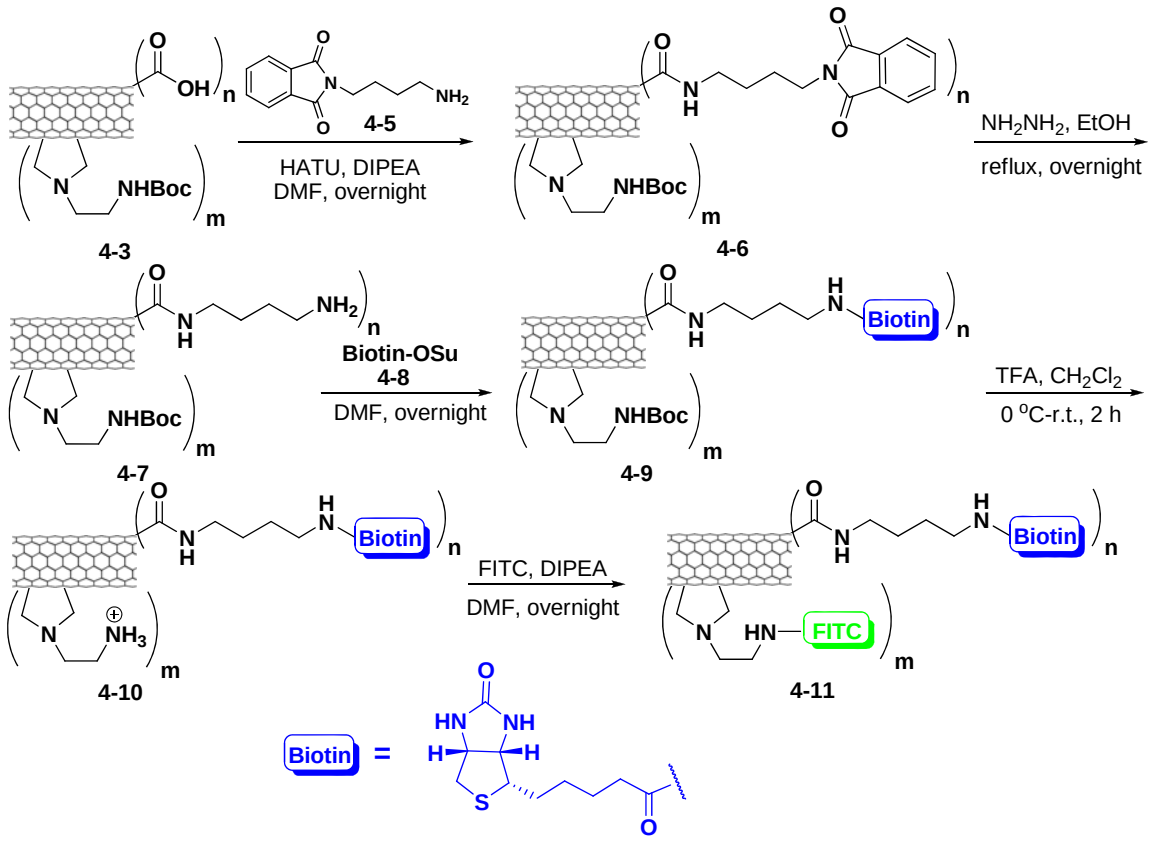

Scheme 4-6. Synthesis of biotin-SWNT-FITC conjugate **(4-11)**.

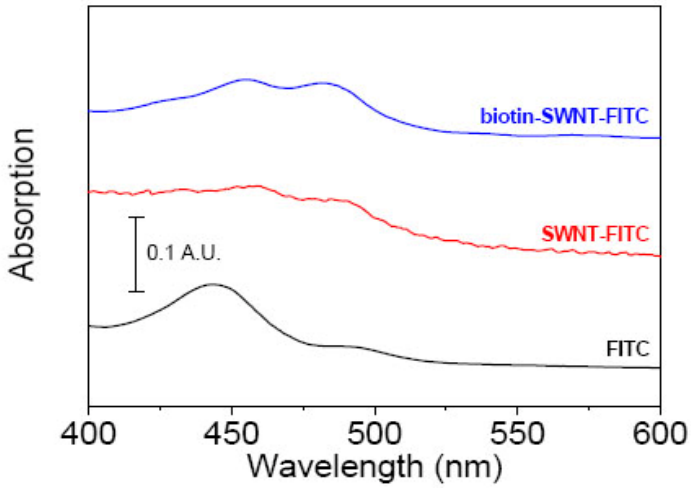

Figure 4-17. UV-visible spectra of SWNT-based conjugates: SWNT-FITC **(4-4)** (red) and biotin-SWNT-FITC **(4-11)** (blue).

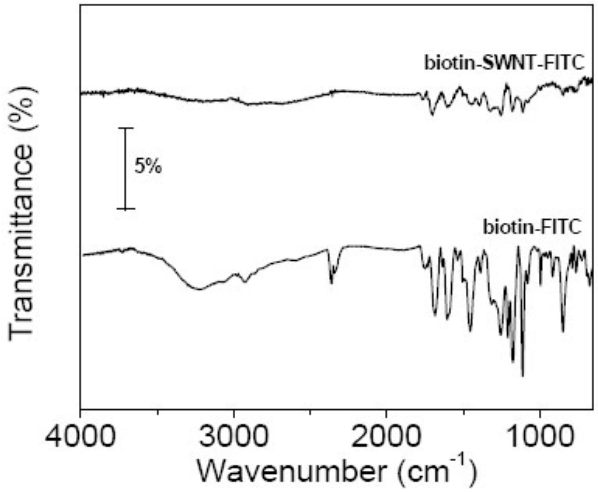

Figure 4-18. ATR-IR spectra of biotin-SWNT-FITC conjugate **(4-11)**.

The biotin-SWNT-linker-SB-T-1214-fluorescein **(4-12)** was prepared from functionalized SWNT **(4-10)** by coupling the succinic ester form of fluorescein-labeled taxoid-linker moiety **(3-63)** with the amine located at the sidewall of SWNTs, through the standard peptide coupling reaction (Scheme 4-7). In principle, these coupling reagents were used in large excess and should proceed quantitatively to give a maximum of 714 biotin modules (at the ends and the defective sites on the side walls) and 285 taxoid modules (on the side walls themselves) per SWNT (based on the mass of a carbon nanotube with 1 μm in length and 1 nm in diameter estimated as 2.2×10^{-18} g).[118] Therefore, biotin-SWNT-linker-SB-T-1214-fluorescein **(4-12)** of 100 μg/mL was estimated to contain taxoid molecules of 13.9 μM.

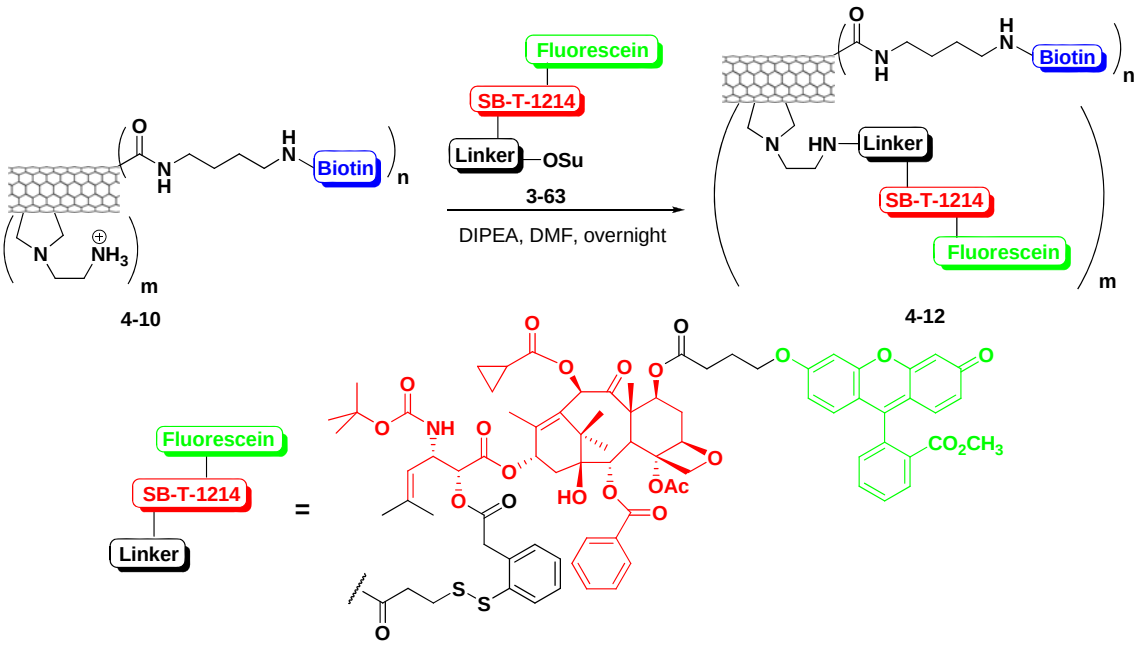

Scheme 4-7. Synthesis of biotin-SWNT-linker-SB-T-1214-fluorescein **(4-12)**.

The biotin-SWNT-linker-SB-T-1214-fluorescein **(4-12)** was further characterized by UV-visible spectroscopy (Figure 4-19). The peak at ~ 280 nm can be attributed, from sum of absorption, to taxoid (SB-T-1214) molecules and the dye molecules (fluorescein), while absorption peaks at 455, 485 and 524 nm are characteristic of fluorescein.

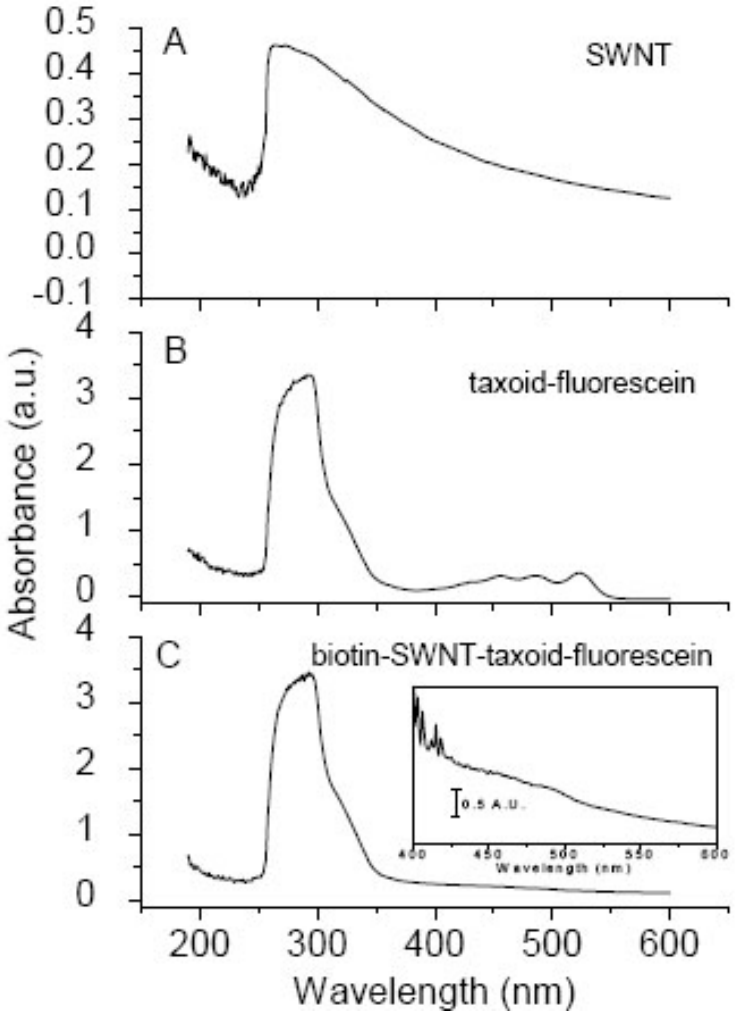

Figure 4-19. UV-visible spectra of SWNT and its conjugates: (A) acid-oxidized SWNTs **(4-1)**; (B) fluorescein-SB-T-1214 conjugate **(3-60)**; and (C) biotin-SWNT-linker-SB-T-1214-fluorescein **(4-12)** and the blow-up spectrum in the inset showing the absorption peak of the conjugate **(4-12)** at the region between 400-600 nm.

It was also worthy of note that the solubility of the functionalized SWNTs **(4-4, 4-11 and 4-12)** in dichloromethane was greatly enhanced as compared with pristine tubes, as shown in Figure 4-20.

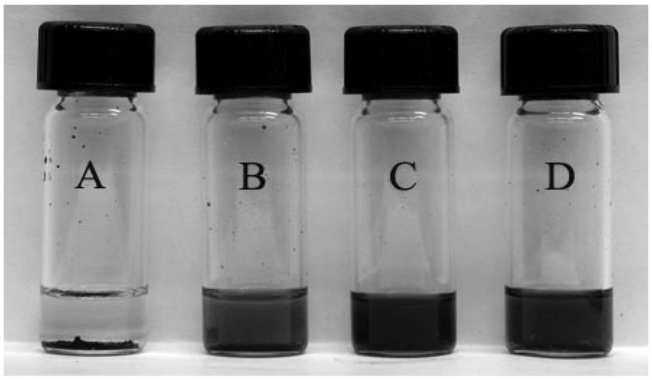

Figure 4-20. Photographs of vials containing (A) pristine SWNT; (B) FITC-SWNT conjugate **(4-4)**; (C) biotin-SWNT-FITC conjugate **(4-11)** and (D) biotin-SWNT-taxoid-fluorescein conjugate **(4-12)** in CH_2Cl_2.

§ 4.2.3. Biological Evaluation of *f*-SWNT-based Conjugate

To demonstrate the specificity and efficacy of the SWNT-based DDS, we designed and synthesized three fluorescently labeled SWNT-conjugates **(4-4, 4-11, and 4-12)**. Conjugates **(4-4)** and **(4-11)** were labeled with fluorescein isothiocyanate (FITC). The resulting fluorescent conjugates, SWNT-FITC **(4-4)** and biotin-SWNT-FITC **(4-11)**, were used to track the internalization of SWNT and biotin-SWNT, respectively, into the tumor cells. Biotin-SWNT-linker-SB-T-1214-fluorescein **(4-12)** was the designed fluorescent molecular probe of the SWNT-based DDS for the receptor-mediated endocytosis and intracellular drug release.

First, we examined cellular uptake of SWNT-FITC **(4-4)** and biotin-SWNT-FITC (**4-11**) with a leukemia cell line, L1210FR (Figure 4-21), which was known to overexpress biotin receptors on its surface.[119,120] DMSO (Figure 4-21 (A)) and oxidized SWNT **(4-1)** (Figure 4-21 (B)) were employed as control. Figures 4-21 (C) and 4-21 (D) depicted confocal fluorescence microscopy (CFM) images of L1210FR cells after treatment with 10 μg/mL (final concentration) of SWNT-FITC **(4-4)** and biotin-SWNT-FITC **(4-11)** conjugates, respectively, for 3 h at 37 ^{o}C. The treated leukemia cells were washed with phosphate buffered saline (PBS) to remove excess fluorescent probes in extracellular medium. L1210FR cells treated with biotin-SWNT-FITC **(4-11)** yielded far more intense fluorescence than those incubated with SWNT-FITC **(4-4)**. This observation can be attributed to the remarkably increased permeability of conjugate **(4-11)** into the cancer cells because of the highly effective interaction of biotin and its receptors on the leukemia cells.

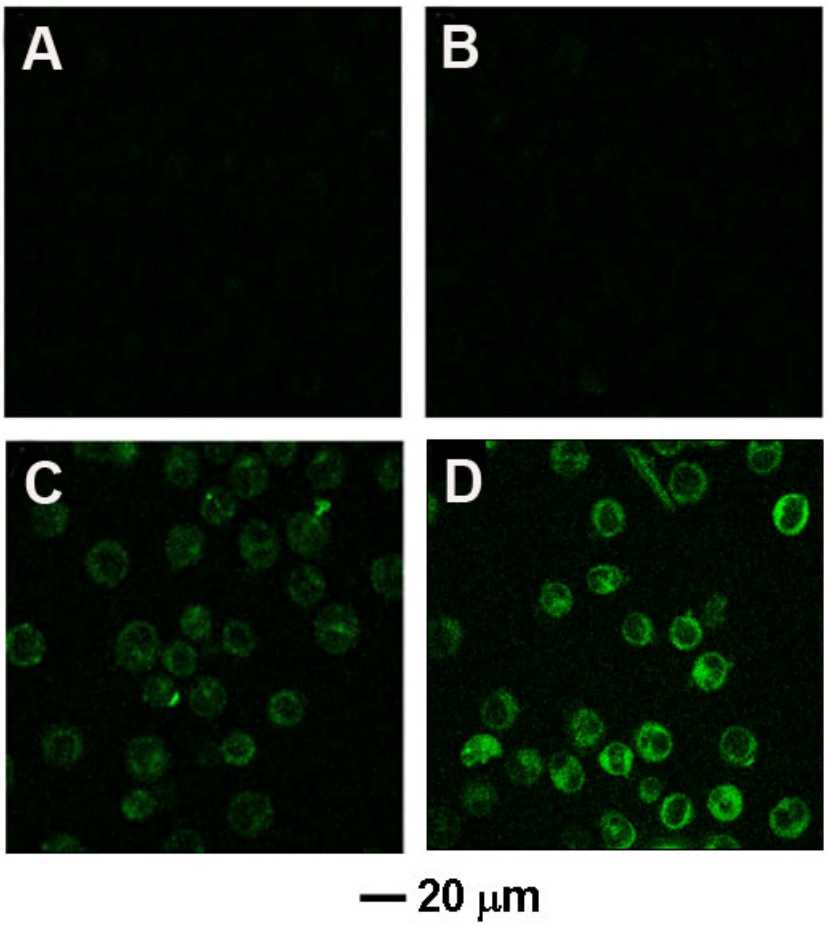

Figure 4-21. CFM images of L1210FR cells: (A) DMSO; (B) oxidized SWNT **(4-1)**, with the final concentration of 10 μg/mL at 37 ^{o}C for 3 h; (C) SWNT-FITC conjugate **(4-4)**, with the final concentration of 10 μg/mL at 37 ^{o}C for 3 h; (D) biotin-SWNT-FITC conjugate **(4-11)**, with the final concentration of 10 μg/mL at 37 ^{o}C for 3 h.

Flow cytometry data (Figure 4-22) on average of 10,000 treated live cells also supported this observation, *i.e.* the fluorescence intensity increased substantially in the order of pristine SWNT (purple line), SWNT-FITC conjugate **(4-4)** (blue line) and biotin-SWNT-FITC **(4-11)** (red line).

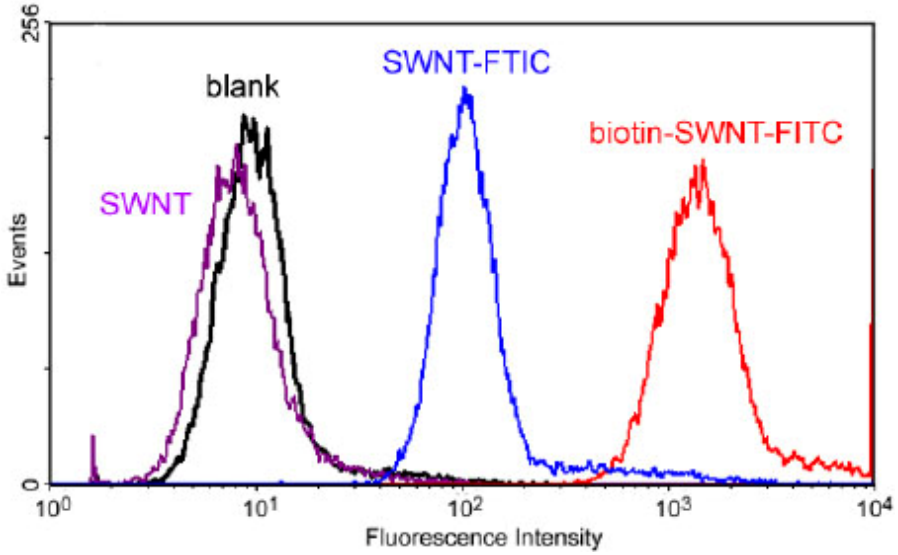

Figure 4-22. Comparison of fluorescence intensities of L1210FR cells by flow cytometry upon treatment with pristine SWNT (purple line), SWNT-FITC conjugate **(4-4)** (blue line) and biotin-SWNT-FITC **(4-11)** (red line) with the final concentration of 10 μg/mL at 37 °C for 3 h, in each case. Background, *i.e.* data for untreated cells, was plotted in black.

The mechanism of internalization of SWNTs into cells has not been fully established. It has been proposed that SWNTs wrapped with proteins or genes can be internalized into cells *via* endocytosis,[106] whereas SWNTs functionalized with small molecules tended to act as nanoneedles that can pierce cell membranes, thereby allowing for their diffusion into cells.[111] Endocytosis is known to be energy dependent and can be blocked at low temperature or in the presence of the metabolism inhibitor, such as NaN_3.[106] To probe the mechanism of cellular uptake in the SWNT conjugates, the L1210FR cells were incubated with SWNT-FITC conjugate **(4-4)** at 4 ^oC or in the presence of 0.05 % NaN_3 for comparison with the uptake at 37 ^oC. It was clearly demonstrated that the SWNT-FITC conjugate **(4-4)** was able to transverse the cell membrane at low temperature (Figure 4-23 (B)) or in the presence of 0.05 % NaN_3 (Figure 4-23 (C)) for 3 h incubation. Similar fluorescence intensity was visualized after incubation without (Figure 4-23 (A)) or with 0.05 % NaN_3 presence (Figure 4-23 (C)). A slightly decreased, *i.e.* 2 times, in the fluorescence intensity was observed at low temperature (Figure 4-23 (B)), compared with that at 37 ^oC, due to the temperature effect of diffusion process. The flow cytometry analysis on 10,000 cells was also in agreement with these findings. Accordingly, the internalization of SWNT itself to the cells was temperature-related, but energy-independent.

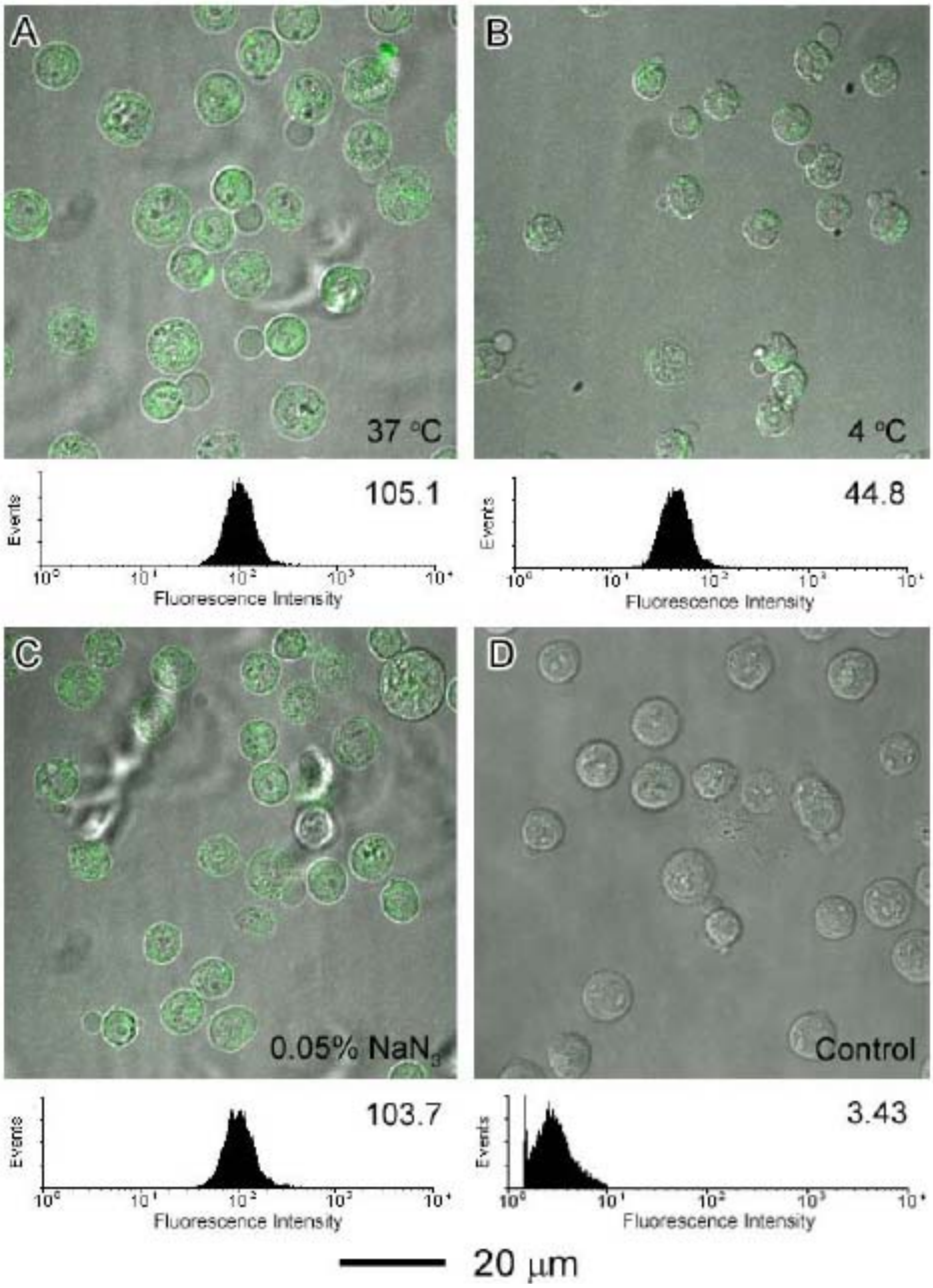

Figure 4-23. CFM images and the flow cytometry analysis of L1210FR cells after incubation with SWNT-FITC conjugate **(4-4)** at the final concentration of 10 μg/mL under different conditions for 3 h: (A) at 37 ^{o}C for 3 h; (B) at 4 ^{o}C; and (C) at 37 ^{o}C in the presence of 0.05 % NaN_3. (D) CFM images and flow cytometry data of L1210FR cells after treatment with oxidized SWNT at the same concentration at 37 ^{o}C for 3 h as the control experiment.

The biotin uptake is known to be temperature and energy-dependent receptor mediated endocytosis.[121,122] To examine the mechanism of the cellular uptake of the biotin-conjugate **(4-11)**, L1210FR cells that overexpressed biotin receptors on their surface were incubated with biotin-SWNT-FITC conjugate **(4-11)** under different

conditions. The fluorescence intensity of cells incubated at 4 ^{o}C (Figure 4-24 (B)) decreased by one order of magnitude as compared with that treated at 37 ^{o}C (Figure 4-24 (A)). It was implied that the internalization of the biotin-SWNT-FITC conjugate **(4-11)** was hindered at low temperature. This observation was not only caused by the temperature effect on the SWNT internalization, but also on the endocytosis of the biotin functionalities. Figure 4-24 (C) illustrates that the fluorescence intensity decreased dramatically in the presence of 0.05 % NaN_3, indicating that endocytosis of biotin conjugates was energy-dependent and can be blocked by the NaN_3. To further verify the nature of the internalization of biotin-SWNT-FITC conjugate **(4-11)** as that of receptor-mediated endocytosis, L1210FR cells were incubated with excess biotin to saturate accessible biotin receptors on the surfaces of the leukemia cells, and then treated with biotin-SWNT-FITC conjugate **(4-11)** at 37 ^{o}C for 3 h. The CFM image in Figure 4-24 (D) clearly indicates a drastic reduction in the fluorescence intensity, as compared with that observed in the absence of excess biotin (Figure 4-24 (A)). These results confirmed that the receptor-mediated endocytosis was by far the predominant mechanism of internalization, with nanotube diffusion as a contributing, albeit relatively minor pathway to the observed data.

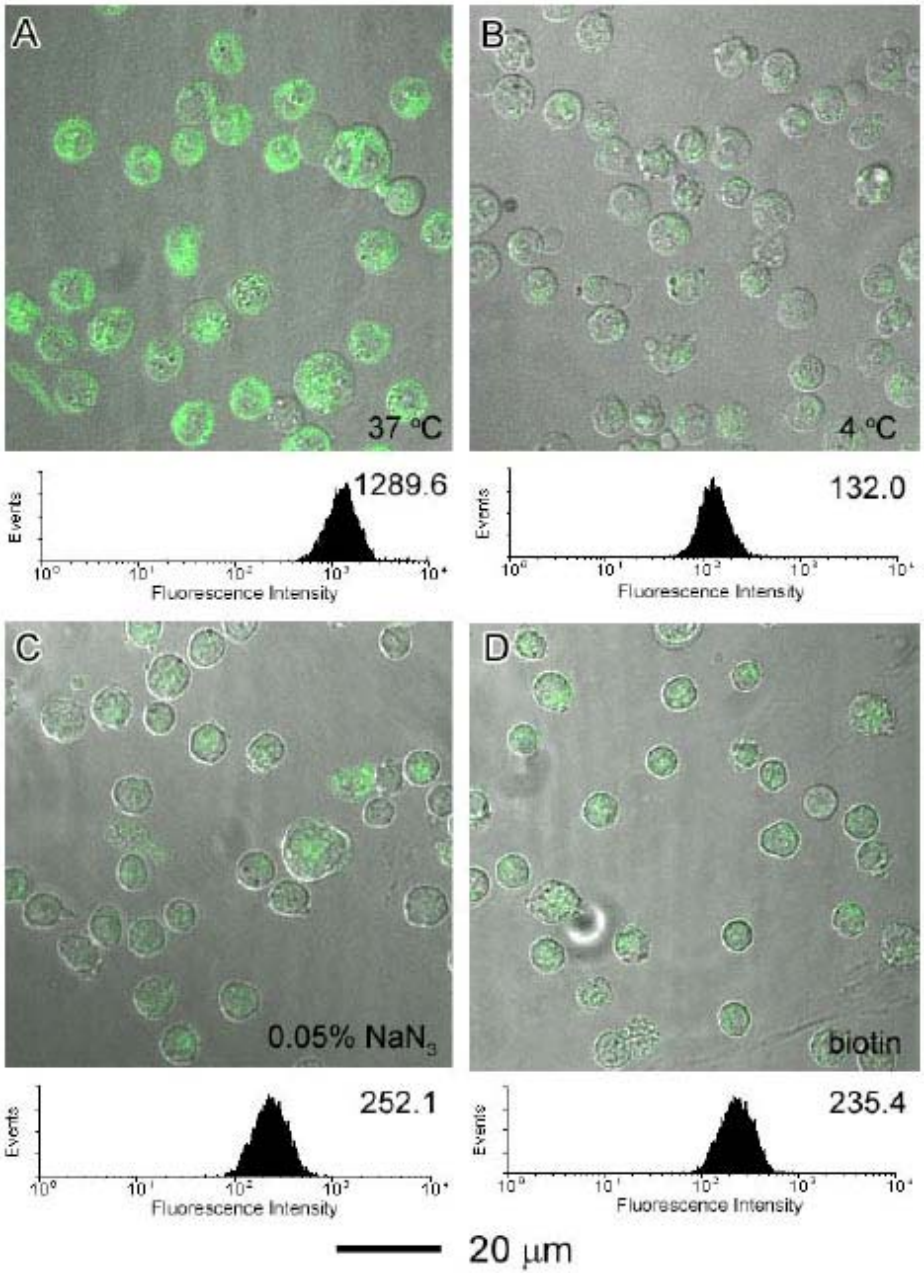

Figure 4-24. CFM images and the flow cytometry analysis of L1210FR cells after incubation with biotin-SWNT-FITC conjugate **(4-11)** at the final concentration of 10 μg/mL under different conditions for 3 h: (A) at 37 ^{o}C; (B) at 4 ^{o}C; (C) at 37 ^{o}C with the presence of 0.05 % NaN_3; (D) at 37 ^{o}C after pretreatment with excess biotin.

Building upon the promising results with biotin-SWNT-FITC **(4-11)** as a potentially versatile vehicle for tumor-targeting drug delivery, we investigated the efficacy of biotin-SWNT-linker-SB-T-1214-fluorescein **(4-12)** for cellular uptake and drug release inside leukemia cells. Initially, we incubated conjugate **(4-12)** with L1210FR cells at 50 μg/mL concentration for 3 h at 37 ^{o}C and washed the treated cells with PBS. As Figure 4-25 (A) shows, the internalization of conjugate **(4-12)** was confirmed by the bright fluorescence of the L1210FR cells observed by CFM. Subsequently, the leukemia cells were treated

with glutathione ethyl ester for an additional 2 h at 37 ^{o}C in order to secure the cleavage of the disulfide linkage covalently connecting the taxoid to the biotin-SWNT moiety. The resulting fluorescein-labeled taxoid released from the conjugate inside the leukemia cells should bind to tubulin/microtubule which was the target protein of the drug. In fact, as clearly shown in Figure 4-25 (B), the fluorescent taxoid did bind to the target protein to light up the large bundles of microtubules, which provided ultimate proof of the designed drug release. It should be noted that the intracellular glutathione in the leukemia cells should be able to cleave the disulfide linkage with much longer incubation time, but the endogenous glutathione level in cancer cells varied due to the significant difference in the physiological conditions between the cultivated cancer cells and those in actual leukemia or solid tumors. Accordingly, the extracellular addition of excess glutathione ethyl ester was beneficial for a rapid visualization of the drug release inside the leukemia cells. This acceleration was evident by comparing Figure 4-25 (A) and Figure 4-25 (B).

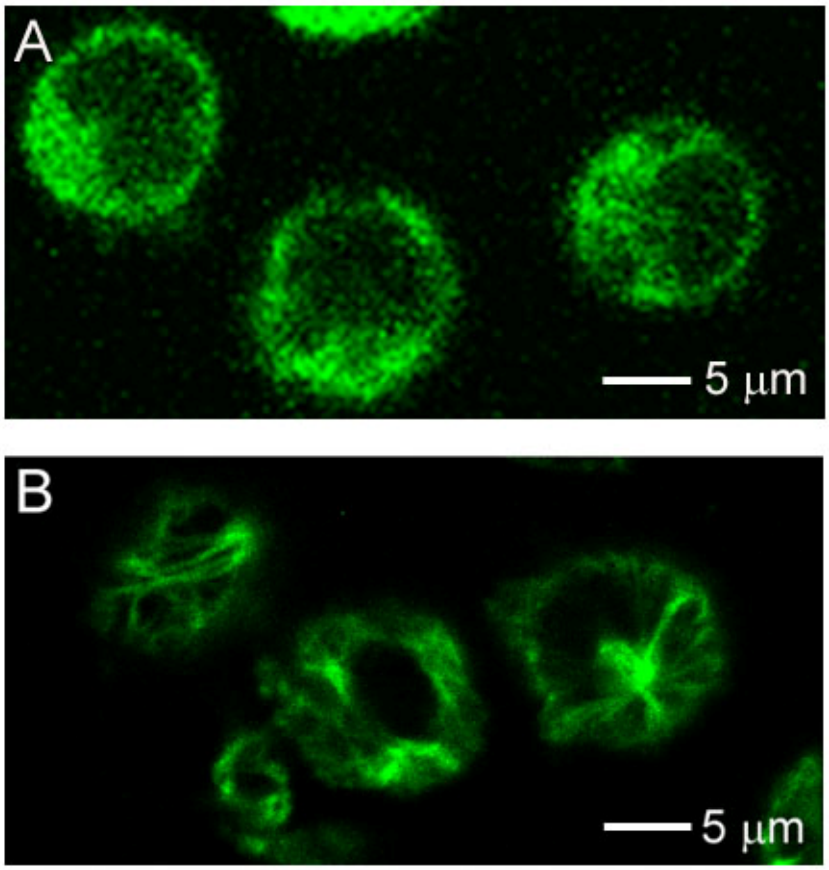

Figure 4-25. CFM images of L1210FR cells treated with biotin-SWNT-SB-T-1214-fluorescein **(4-12)** (final concentration: 50 μg/mL) at 37 ^{o}C for 3 h, incubated before (A) and after (B) the addition of glutathione ethyl ester (GSH-OEt, at the final concentration of 2 mM at 37 ^{o}C for additional 2 h). The image (B) clearly demonstrates the fluorescent microtubule networks generated by the binding of the fluorescent taxoid, SB-T-1214-fluorescein, after cleavage of the disulfide bond in the linker by either GSH or GSH-OEt.

To elucidate the specificity of the biotin-SWNT-SB-T-1214-fluorescein **(4-12)** to cells that overexpressed biotin receptors on their surface, two other cell lines, the mouse leukemia L1210 cell line and the WI38 noncancerous human embryonic lung fibroblast cell line, were chosen to compare with L1210FR cell line. Both the L1210 and WI38 cell line lack the biotin receptors overexpressing on their surface. Accordingly, biotin-SWNT-SB-T-1214-fluorescein **(4-12)** was expected to be readily internalized into L1210FR cells as compared with L1210 and WI38 cells. Figure 4-26 (A) shows a much stronger fluorescence intensity in L1210FR cells than that in L1210 cells (Figure 4-26 (B)) and WI38 cells (Figure 4-26 (C)) upon incubation with biotin-SWNT-SB-T-1214-fluorescein **(4-12)** under the same conditions.

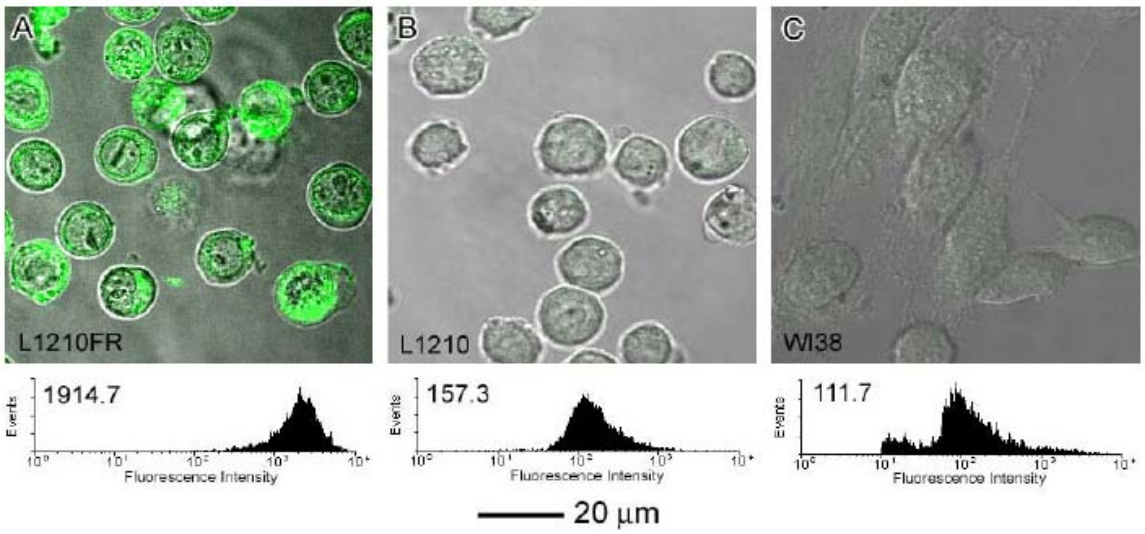

Figure 4-26. CFM images and the flow cytometry analysis of different types of cells after incubation with biotin-SWNT-SB-T-1214-fluorescein **(4-12)** at the final concentration of 50 μg/mL at 37 ^{o}C for 3 h: (A) L1210FR that overexpress biotin receptors; (B) L1210; and (C) WI38 noncancerous human embryonic lung fibroblast cells.

Cytotoxicity of biotin-SWNT-SB-T-1214-fluorescein **(4-12)** against these three cell lines were also performed by the MTT assay. After 72 h incubation, the IC_{50} value of biotin-SWNT-SB-T-1214-fluorescein conjugate **(4-12)** against the L1210FR cell line was 0.36 μg/mL, whereas that against L1210 and WI38 cell lines were 39.5 μg/mL and more than 50 μg/mL, respectively, as shown in Figure 4-27 and summarized in Table 4-3. (According to the previous calculation, 0.36 μg/mL of biotin-SWNT-SB-T-1214-fluorescein **(4-12)** corresponds to 50.0 nM taxoid.) In the control experiments, the IC_{50} value of acid-oxidized SWNT **(4-1)**, SWNT-FITC conjugate **(4-4)** and biotin-SWNT-FITC conjugate **(4-11)**, were more than 100 μg/mL. These combined findings suggest that the cytotoxicity of biotin-SWNT-SB-T-1214-fluorescein **(4-12)** is only caused by the successful release of taxoid molecules. In addition, biotin-SWNT-SB-T-1214-fluorescein conjugate **(4-12)** is more toxic against L1210FR cell line than fluorescein-SB-T-1214 conjugate **(3-60)** (87.1 nM) and biotin-linker-SB-T-1214-fluorescein conjugate **(3-64)** (81.7 nM). Such an increase in cytotoxicity of biotin-SWNT-SB-T-1214-fluorescein conjugate **(4-12)** may be caused by not only the recognition moieties, biotin molecules,

but also the transportation carrier, SWNT. It is worthy noting that the taxoid molecules appear to be fully released by the GSH inside the L1210FR cells after 72 h incubation.

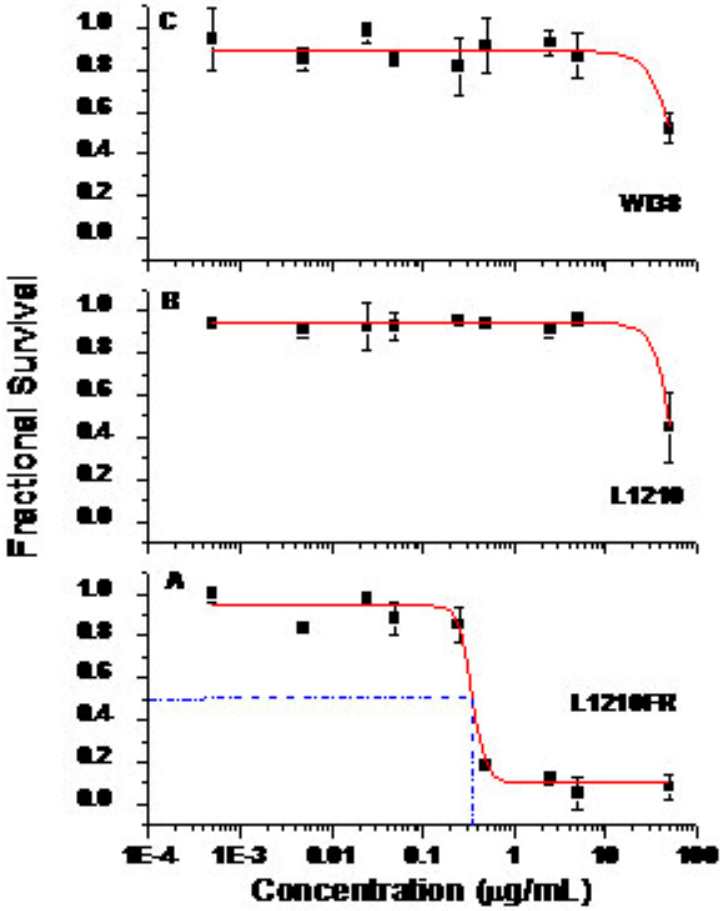

Figure 4-27. Results of MTT cytotoxicity assay of biotin-SWNT-SB-T-1214-fluorescein conjugate **(4-12)** on different cell lines: (A) L1210FR; (B) L1210; and (C) WI38 human noncancerous cell line.

Table 4-3. IC_{50} value of the biotin-SWNT-SB-T-1214-fluorescein conjugate **(4-12)** against different cell lines.

Cell Line	L1210FR	L1210	WI38
IC_{50} (µg/mL)	0.36	39.5	> 50
IC_{50} (SB-T-1214)	50.0 nM	5.49 µM	> 6.95 µM

§ 4.3. Experimental Section

§ 4.3.1 Syntheses of Functionalized SWNTs

General Methods: ^{1}H and ^{13}C NMR spectra were measured on a Varian 300, 400, 500, or 600 MHz NMR spectrometer. High-resolution mass spectrometric analyses were conducted at the Mass Spectrometry Laboratory, University of Illinois at Urbana-Champaign, Urbana, IL. GC-MS analyses were performed on an Agilent 6890 Series GC system equipped with the HP-5HS capillary column, (50 m X 0.25 mm, 0.25 um) and with the Agilent 5973 network mass selective detector. LC-MS analyses were carried out on an Agilent 1100 Series Liquid Chromatograph Mass Spectrometer. Infrared spectra were obtained on a Nexus 670 (Thermo Nicolet) equipped with a single reflectance ZnSe ATR accessory, a KBr beam splitter, and a DTGS KBr detector. UV-vis spectra were recorded on a UV1 (Thermo Spectronic) spectrometer. TLC analyses were performed on Merck DC-alufolien with Kieselgel 60F-254 and were visualized with UV light, iodine chamber, 10 % sulfuric acid-EtOH or 10 % PMA-EtOH solution. The staining agent on TLC for biotin derivatives was 4-*N,N*-Dimethylamino-cinnamaldehyde ethanol solution. Column chromatography was carried out on silica gel 60 (Merck; 230-400 mesh ASTM). Chemical purity was determined with a Waters HPLC or shimazu HPLC, using a Phenomenex Curosil-B column, employing CH_3CN/water as the solvent system with a flow rate of 1 mL/min. Dark room, aluminum foil, and inert nitrogen atmosphere were applied when necessary.

Materials: The chemicals were purchased from Sigma Aldrich Company, Fischer Company or Acros Organic Company. Dichloromethane and methanol were dried before use by distillation over calcium hydride under nitrogen or argon. Ether and THF were dried before use by distillation over sodium-benzophenone kept under nitrogen or argon. Toluene and benzene were dried by distillation over sodium metal under nitrogen or argon before use. Dry DMF was purchased from EMD chemical company, and used without further purification. PURE SOLVTM, Innovative technology Inc, provided an alternative source of dry toluene, THF, ether, and dichloromethane. The reaction flasks were dried in a 110 ^{o}C oven and allowed to cool to room temperature in a desiccator over "*Drierite*" (calcium sulfate) and assembled under inert gas nitrogen or argon atmosphere.

Oxidized SWNT (4-1):[82]
Pristine SWNTs (10 mg) were oxidized to yield a functionalized SWNT **(4-1)** using 5 mL of a 3:1 (v/v) concentrated H_2SO_4 and HNO_3 solution by sonicating at 40 ^{o}C for 2 h, followed by heating at 70 ^{o}C for 30 min.[82] The reaction mixture was diluted to 200 mL with water and filtered through a 0.2 μm polycarbonate membrane. The product **(4-1)** was then washed extensively with water until the pH reached neutral conditions and further oven dried at 120 ^{o}C under vacuum for 2 h (9 mg, 90 % yield).

2-(*tert*-Butoxycarbonylamino)ethylamino acetic acid (4-2):
To a solution of ethane-1,2-diamine (6 g, 100 mmol) in CH_2Cl_2 (60 mL) was added di-*tert*-butyl dicarbonate (2.18 g, 10 mmol) in CH_2Cl_2 (10 mL) dropwise with an additional

funnel at 0 ^{o}C. The mixture was stirred for 2 h and then concentrated *in vacuo*. The resulting residue was diluted with EtOAc and washed with water and brine. The organic layer was then dried over anhydrous magnesium sulfate and concentrated *in vacuo*. The crude product was a colorless oil and used directly in the next step without further purification.

To a solution of as-prepared mono-protected amine (480 mg, 3 mmol) in 1,4-dioxane (2 mL) at 0 ^{o}C was added a solution of benzyl bromoacetate (766 mg, 1 mmol) in 1,4-dioxane (3 mL) over a period of 1 h, and the reaction mixture was stirred overnight. The solvent was then evaporated under reduced pressure, and the residue was diluted with water (20 mL) and extracted with ethyl acetate three times. The combined organic phase was dried over $MgSO_4$, and the solvent was removed under vacuum. The crude residue was purified by chromatography to afford the desired product, benzyl 2-(2-(*tert*-butoxycarbonylamino)ethylamino)acetate as colorless oils (220 mg, 70 %). ^{1}H NMR (300 MHz, $CDCl_3$) δ 1.50 (s, 9 H), 2.03 (bs, 1 H), 2.79 (t, J = 5.9 Hz, 2 H), 3.26 (m, 2 H), 3.52 (s, 2H), 5.15 (bs, 1 H), 5.23 (s, 2 H), 7.43 (m, 5 H). ^{13}C NMR (75 MHz, $CDCl_3$): δ 28.7, 40.4, 49.0, 50.7, 66.9, 86.2, 128.7, 128.8, 128.9, 135.9, 156.5, 172.6.

To a methanol solution (7 mL) of benzyl protected acetate (220 mg, 0.714 mmol) was added 7.0 mg of 10 % Pd/C, and the mixture was stirred under a hydrogen atmosphere for 24 h. The catalyst was removed by filtration on celite, and the solvent was evaporated. The pure product was triturated in diethyl ether to give the desired product 2-(2-(*tert*-butoxycarbonylamino)ethylamino)acetic acid **(4-2)** as a white solid and used directly in the next steps.

SWNT-FITC conjugate (4-4):

To a suspension of oxidized SWNT **(4-1)** (15 mg) in DMF (5 mL) was added *N*-(2-*N*-Boc-ethyl) glycine **(4-2)** (70 mg, 0.32 mmol) and paraformaldehyde (47 mg, 1.57 mmol). The reaction mixture was subsequently heated overnight at 125 ^{o}C under a N_2 atmosphere. Excess amino acid **(4-2)** and paraformaldehyde were removed by filtration. The resulting residue was further purified by precipitation with methanol/ether 5 times (4/1, 12 mL/3 mL) and dried under vacuum to afford product **(4-3)** (11 mg, 73 % yield). The resulting functionalized SWNT **(4-3)** was treated with 2 mL of TFA/CH_2Cl_2 (1:1) and then stirred at room temperature for 2 h. The solvent was evaporated *in vacuo*. Crude product was purified by washing with several aliquots of methanol and diethyl ether 5 times (4/1, 12 mL/3 mL), and subsequent drying under vacuum. The amount of loading of functional groups per gram was estimated *via* a quantitative Kaiser test.[117] To a solution of functionalized SWNTs obtained above (10 mg, 1.8 μmol, based on the loading calculated using the quantitative Kaiser test) in 1 mL of DMF, a solution of FITC (50 mg, 0.13 mmol) and DIPEA (0.1 mL) in 1 mL of DMF was added. The mixture was then stirred overnight at room temperature. Upon solvent removal, the resulting SWNT-FITC **(4-4)** was reprecipitated 5 times from methanol/ether (4/1, 12 mL/3 mL) and finally dried under vacuum for 5 h to give the pure conjugate **(4-4)** (7 mg, 70 % yield).

***N*-(4-(Aminobutyl)phthalimide (4-5):**

To a solution of *N*-(4-(bromobutyl)phthalimide (1.0 g, 3.5 mmol) in 10 mL of DMF was added sodium azide (290 mg, 4.4 mmol). The reaction mixture was then allowed to stir for 5 h under nitrogen at room temperature. The solvent was removed *in vacuo* to yield a

white semisolid, which was further dissolved in water and extracted with three 50 mL portions of ethyl acetate. The combined organic layers were dried over anhydrous magnesium sulfate and filtered, and the solvent was removed to afford *N*-(4-azidobutyl)phthalimide (760 mg, 88 %) as a white amorphous powder, which was used directly in the next reaction without further purification. ^{1}H NMR (300 MHz, CDCl3) δ 1.6-1.68 (m, 2 H), 1.74-1.82 (m, 2 H), 3.41 (t, *J* = 7.2 Hz, 2 H), 3.83 (t, *J* = 7.2 Hz, 2 H), 7.71-7.73 (m, 2 H), 7.87-7.95 (m, 2 H).
The resulting *N*-(4-azidobutyl)phthalimide (760 mg, 3.1 mmol) was dissolved in 50 mL of ethanol along with 100 mg of 10% Pd/C. The suspension was hydrogenated for 12 h. The reaction mixture was then filtered, and the filtrate was concentrated *in vacuo* to yield *N*-(4-aminobutyl)phthalimide **(4-5)** as an amorphous white solid (620 mg, 92 %) and was sufficiently pure to use in the next reaction.

Biotin-SWNT-FITC conjugate (4-11):
A solution of functionalized SWNT **(4-3) (**20 mg), *N*-(4-aminobutyl)phthalimide (**4-5**) (100 mg, 0.46 mmol), DIPEA (0.3 mL), and HATU (175 mg, 0.46 mmol) in 2 mL of anhydrous DMF was stirred at room temperature for 3 h. An excess of amine **(4-5)** was removed by washing 5 times with methanol/ether (4/1, 12 mL/3 mL) to afford modified SWNT **(4-6)**. A mixture of 10 mg of modified SWNT **(4-6)** and of hydrazine hydrate (25%, 0.2 mL) in 5 mL of ethanol was heated overnight under reflux under a nitrogen atmosphere. The resulting phthalhydrazide was removed by dialysis to yield amine-functionalized SWNT **(4-7)**. The loading of amine groups per gram was estimated using the quantitative Kaiser test.[117] Amine-functionalized SWNT **(4-7)** (10 mg, 5 μmol, based on the loading calculated with the quantitative Kaiser test) and *N*-succinimidyl ester of biotin **(4-8)** (110 mg, 0.32 mmol) were suspended in 3 mL of anhydrous DMSO. The resulting suspension was stirred overnight at room temperature. Excess *N*-succinimidyl ester of biotin **(4-8)** was removed by dialysis to yield biotin-*N*-Boc-SWNT conjugate **(4-9)** (10 mg, quant.). SWNT conjugate **(4-9)** was treated with 2 ml of TFA/CH_2Cl_2 (1:1) and the reaction mixture was stirred at room temperature for 2 h. Upon evaporation of the solvent *in vacuo*, the crude product was washed with methanol/ether 5 times (4/1, 12 mL/3 mL) and dried under vacuum to give the biotin-amine-SWNT conjugate **(4-10)**. To a suspension of the resulting biotin-amine-SWNT conjugate **(4-10)** (10 mg, 1.8 μmol, based on the loading calculated with the quantitative Kaiser test) in 2 ml of anhydrous DMF was added FITC (50 mg, 0.13 mmol) and DIPEA (0.1 mL). The resulting mixture was stirred overnight at room temperature. The excess of FITC was removed by washing 5 times with methanol/ether (4/1, 12 mL/3 mL), and the resulting product was dried at room temperature under vacuum for a few hours to afford biotin-SWNT-FITC conjugate biotin-amine-SWNT conjugate **(4-11)** (7.5 mg, 75 % yield).

Biotin-SWNT-linker-SB-T-1214-fluorescein (4-12):
To a suspension of biotin-amine-SWNT **(4-10)** (10 mg, 1.8 μmol, based on the loading calculated with the quantitative Kaiser test) in 4 mL of anhydrous DMF was added *N*-succinimidyl ester of linker-taxoid-fluorescein **(3-63)** (160 mg, 0.099 mmol) and DIPEA (0.1 mL). The resulting mixture was stirred overnight at room temperature. Excess taxoid derivatives **(3-63)** was removed by washing 5 times with methanol/ether (4/1, 12 mL/3 mL) and the product was ultimately dried at room temperature under vacuum for 5

h to afford biotin-SWNT-linker-SB-T-1214-fluorescein **(4-12)** (6 mg, 60 % yield).

§ 4.3.2 Confocal Microscopy, Flow Cytometry and Cytotoxicity Analysis

Cell culture: The L1210FR cell line was received as a gift from Dr. Gregory Russell-Jones (Access Pharmaceuticals Australia Pty Ltd., Targeted Delivery, Unit 5, 15-17 Gibbes St, Chatswood, NSW, Sydney 2067, Australia). L1210FR cells were grown in a RPMI-1640 cell culture medium (Gibco) in the absence of folic acid (FA) supplemented with 10 % fetal bovine serum (FBS) and 1 % Penicillin and Streptomycin. Prior to incubation, the cells were collected by centrifugation at 1000 rpm for 6 min and resuspended in RPMI medium without FBS at a cell density of 5×10 cells/mL.

Incubation of cells with SWNT-FITC (4-4) and biotin-SWNT-FITC (4-11):
The cell suspension (1 mL) was initially added to a microtube. The nanotube conjugates (10 μL) in DMSO were then inserted to the microtube to provide for a final concentration of 10 μg/mL and the resultant suspension was incubated at 37 ^{o}C for 3 h. After incubation, the cells were washed with PBS, collected by centrifugation twice, and resuspended in PBS at the desired concentration for further analysis.

Low temperature incubation of cells with SWNT-FITC (4-4) and biotin-SWNT-FITC (4-11):
The incubation of L1210FR with conjugates, SWNT-FITC **(4-4)** and biotin-SWNT-FITC **(4-11)**, was carried out in a cold room at 4 ^{o}C for 3 h. The isolation and washing of the cells were achieved, as described above.

Saturation of the biotin receptors on surface of L1210FR cells with excess biotin molecules:
Prior to incubation with the conjugate, biotin-SWNT-FITC **(4-11)**, and the cells were treated with 2 mM of biotin (at final concentration) for 1 h.

Incubation of cells with biotin-SWNT-linker-SB-T-1214-fluorescein (4-12):
The cell suspension (1 mL) was initially added to a microtube. The biotin-SWNT-SB-T-1214-fluorescein conjugate **(4-12)** (10 μL) in DMSO was subsequently added to the microtube at a final concentration of 50 μg/mL. After incubation at 37 ^{o}C for 3 h, the cells were washed twice with PBS to remove excess conjugates and resuspended in the medium. DMSO (10 μL) was then added to the suspension as a control and incubated for another 2 h. After incubation, the cells were washed with PBS, collected by centrifugation twice, and resuspended in 100 μL PBS prior to imaging.

Release of the drug molecule, taxoid, to L1210FR cells:
The biotin-SWNT-linker-SB-T-1214-fluorescein conjugate **(4-12)** (10 μL), in DMSO was added to 1 mL of cells in the microtube to yield a final concentration of 50 μg/mL. After incubation at 37 ^{o}C for 3 h, the cells were washed twice with PBS to remove excess conjugates and resuspended in the medium. Glutathione ethyl ester (10 μL) was then added to the suspension at a final concentration of 2 mM and incubated for another 2 h.

The excess glutathione ethyl ester was removed by washing twice with PBS and the cells were then resuspended in 100 μL PBS prior to imaging.

Confocal microscopy imaging of the cells:
All of the confocal images were taken immediately after the incubation and washing steps. 100 μL of the cell suspension was transferred to the bottom-glass dish using a micropipette. Confocal fluorescence microscopy (CFM) was performed using a Zeiss LSM 510 META NLO two-photon laser scanning confocal microscope system, operating at a 488 nm excitation wavelength and detecting emission wavelengths using a 505-550 nm bandpass filter. Images were captured with a C-Apochromat 63×/1.2 Water (corr.) objective and a Plan-Apochromat 100×/1.45 oil objective. Data were analyzed using LSM 510 META software.

Flow cytometry fluorescent measurements of the cells:
Flow cytometry analysis was performed immediately after the incubation and washing steps. Cells were resuspended in 0.5 mL of PBS and analyzed using a flow cytometer, FACSCalibur, operating at a 488 nm excitation wavelength and detecting emission wavelengths with a 530/30 nm bandpass filter. At least 10,000 cells were counted for each experiment using CellQuest 3.3 software (Becton Dickinson) and the distribution of FITC fluorescence was analyzed using WinMDI 2.8 freeware (Joseph Trotter, Scripps Research Institute).

Cytotoxicity evaluation of biotin-SWNT-linker-SB-T-1214-fluorescein (4-12):
The cells were harvested, collected, and resuspended in 100 μL at a concentration of 2 x 10^4 cells per well in 96-well plates. For the adhesive cell type, the cells were allowed to reseed to the bottom of the plates overnight and the fresh medium were added to each well upon removal of the old medium. The SWNT conjugates were diluted to a series of concentration in medium with FBS as stock solution. The stock solution containing biotin-SWNT-linker-SB-T-1214-fluorescein **(4-12)** (10 μL) was added to each of the wells in the 96-well plates and the cells cultured for 3 days. At the end of this time, the number of viable cells each wells was determined by a quantitative colorimetric staining assay using a tetrazolium salt (MTT, Sigma Chemical Co.). The inhibitory concentration (IC_{50}) of each compound was determined, as the concentration required inhibiting 50 % of the growth of the L1210FR cells.

§ 4.4. Perspective: Combination Chemotherapy

In contemporary usage, the expression combination chemotherapy refers to the simultaneous administration of two or more therapeutics to treat a single disease. The past few years have witnessed a great progress of combination chemotherapy in cancer treatment and it has been stated that chemotherapeutic agents are generally more effective when given in combination in many cases.[123] The rationale for combination chemotherapy is to combine two or more drugs that work by different mechanisms of action at their optimal doses respectively to avoid intolerable side effects. Thereby, it is able to decrease the likelihood that resistant cancer cells will develop (Figure 4-28). In

comparison to mono-chemotherapy, combination chemotherapy displays several significant advantages, *e.g.* lower treatment failure rate, lower case-fatality ratios, slower development of resistance and consequently, less money needed for the development of new drugs.[124]

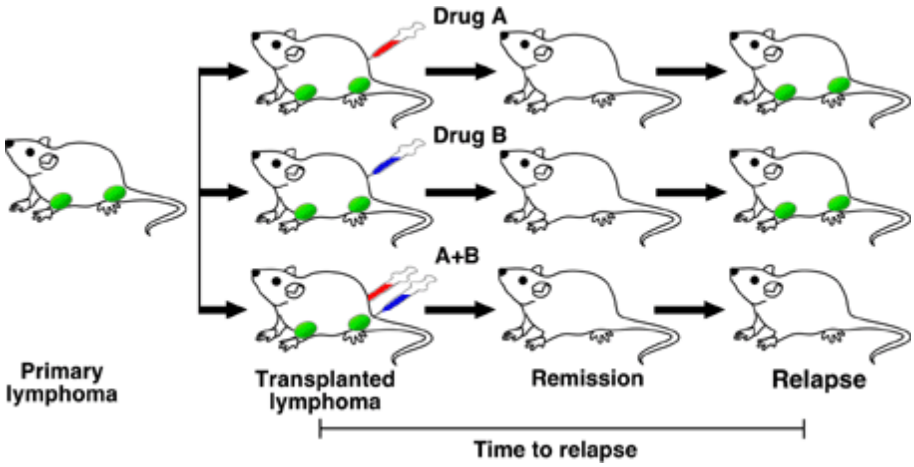

Figure 4-28. A two-drug combination therapy leads to the complete remission of a mouse model of B-cell lymphoma in all of the treated animals. In contrast, animals treated with either drug alone (rapamycin or doxorubicin) rarely experienced complete remission. (Figure is adapted from http://www.cshl.edu/public/releases/combotherapy.html)

Although combination chemotherapy has demonstrated promising results in clinical trials,[125] recent clinical data have underlined the complexity of their pharmacokinetics-formulation relationships.[126] The 2nd-generation combination chemotherapy currently emerging in an attempt to further enhance activity and circumvent resistance is to utilize the biocompatible nanoscale platforms, *e.g.* polymer and carbon nanotube. The use of polymer-drug conjugates in combination chemotherapy has been documented as an important opportunity to enhance tumor response rates[125] and provided an ideal platform for the delivery of a cocktail of drugs simultaneously. Figure 4-29 shows a recently reported model complex *N*-(2-hydroxypropyl)methacrylamide copolymer-aminoglutethimide-doxorubincin (HPMA copolymer-AGM-DOX) for combination chemotherapy.[127] It was suggested that the conjugate containing both drugs exhibited markedly enhanced cytotoxicity and a synergistic benefit compared with mixtures of polymer conjugates containing only aminoglutethimide (AGM), or only doxorubincin (DOX). Complex cellular mechanisms appear to be responsible for the increased antitumor activity of HPMA copolymer-AGM-DOX *in vitro*. This conjugate caused a significant decrease in the expression of the anti-apoptotic protein Bcl-2, whereas the HPMA copolymer-DOX alone had no effect on Bcl-2 in MCF-7 and MCF-7ca cells, indicating that combining AGM and DOX leaded to a synergistic effect that induced apoptosis. Hence, these observations of increasing activity *via* combination polymer indicate the significance and feasibility of constructing other nanoscale drug conjugates, *i.e.* SWNT-base drug delivery platform for efficient combination chemotherapy.

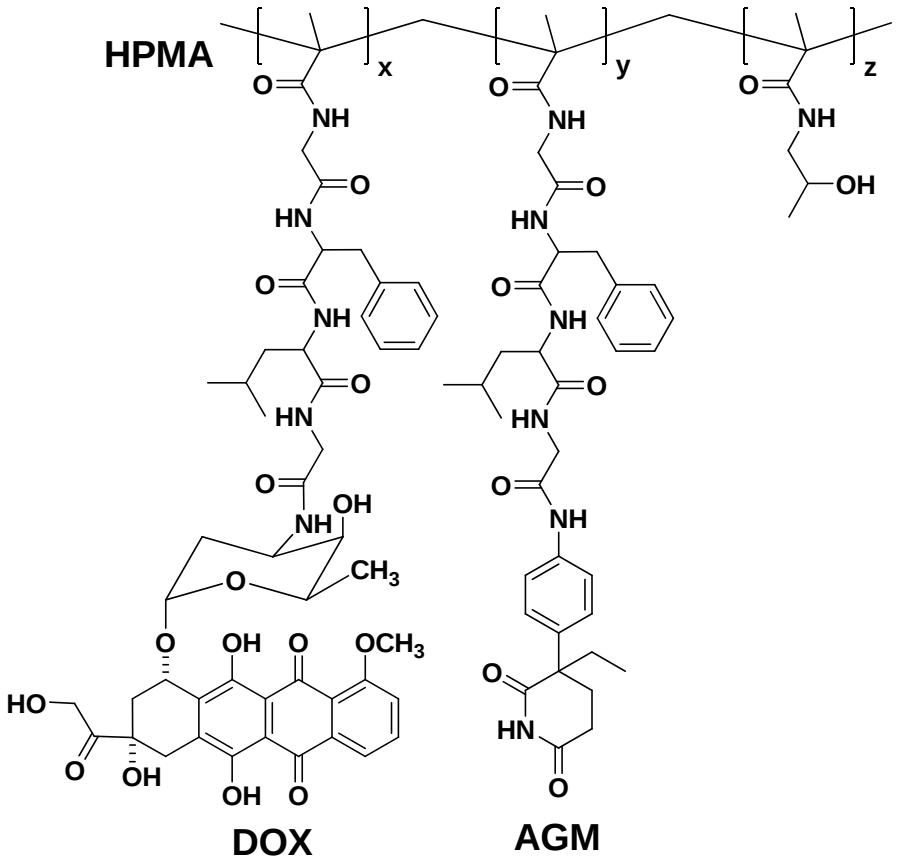

Figure 4-29. Structure of HPMA copolymer-AGM-DOX conjugate as an example of polymer-drug combination chemotherapy.[127]

References

References for Chapter I:

1. Jemal, A.; Siegel, R.; Ward, E.; Murray, T.; Xu, J.; Smigal, C.; Thun Michael, J. Cancer statistics, 2006. *CA Cancer J. Clin.*, **2006**, *56*, 106-130.
2. Wu, X. Design, synthesis and biological evaluation of tumor-targeting taxane-based anticancer agents and mdr modulators. Ph.D. Dissertation, State University of New York at Stony Brook, Stony Brook, **2003**.
3. Georg, G. I.; Boge, T. C.; Cheruvallath, Z. S.; Clowers, J. S.; Harriman, G. C. B.; Hepperle, M.; Park, H. The medicinal chemistry of taxol. *Taxol: Science and Applications*, **1995**, 317-375.
4. Wani, M. C.; Taylor, H. L.; Wall, M. E.; Coggon, P.; McPhail, A. T. Plant Antitumor Agents. VI. The Isolation and Structure of Taxol, a Novel Antileukemic and Antitumor Agent from *Taxus brevifolia*. *J. Am. Chem. Soc.*, **1971**, *93*, 2325-2327.
5. Kumar, N. Taxol-Induced Polymerization of Purified Tubulin. *J. Biol. Chem.*, **1981**, *256*, 10435-10441.
6. Schiff, P. B.; Fant, J.; Horwitz, S. B. Promotion of Microbubule Assembly *in vitro* by Taxol. *Nature*, **1979**, *277*, 665-667.
7. Schiff, P. B.; Horwitz, S. B. Taxol Stabilizes Microtubules in Mouse Fibroblast Cells. *Proc. Natl. Acad. Sci., U. S. A.*, **1980**, *77*, 1561-1565.
8. Schiff, P. B.; Horwitz, S. B. Taxol assembles tubulin in the absence of exogenous guanosine 5'-triphosphate or microtubule-associated proteins. *Biochemistry*, **1981**, *20*, 3247-3252.
9. Blume, E. Government moves to increase taxol supply. *J. Natl. Cancer Inst.*, **1991**, *83*, 1054-1056.
10. Nicolaou, K. C.; Dai, W.-M.; Guy, R. K. Chemistry and Biology of Taxol. *Angew. Chem. Int. Ed. Engl.*, **1994**, *33*, 15-44.
11. Holton, R. A.; Somoza, C.; Kim, H.-B.; Liang, F.; Biediger, R. J.; Boatman, P. D.; Shindo, M.; Smith, C. C.; Kim, S.; Nadizadeh, H.; Suzuki, Y.; Tao, C.; Vu, P.; Tang, S.; Zhang, P.; Murthi, K. K.; Gentile, L. N.; Liu, J. H. First Total Synthesis of Taxol. 1. Functionalization of the B Ring. *J. Am. Chem. Soc.*, **1994**, *116*, 1597-1598.
12. Holton, R. A.; Kim, H.-B.; Somoza, C.; Liang, F.; Biediger, R. J.; Boatman, P. D.; Shindo, M.; Smith, C. C.; Kim, S.; Nadizadeh, H.; Suzuki, Y.; Tao, C.; Vu, P.; Tang, S.; Zhang, P.; Murthi, K. K.; Gentile, L. N.; Liu, J. H. First Total Synthesis of Taxol. 2. Completion of the C and D Rings. *J. Am. Chem. Soc.*, **1994**, *116*, 1599-1600.
13. Nicolaou, K. C.; Nantermet, P. G.; Ueno, H.; Guy, R. K.; Couladouros, E. A.; Sorensen, E. J. Total Synthesis of Taxol. 1. Retrosynthesis, Degradation, and Reconstitution. *J. Am. Chem. Soc.*, **1995**, *117*, 624-633.
14. Nicolaou, K. C.; Liu, J.-J.; Yang, Z.; Ueno, H.; Sorensen, E. J.; Claiborne, C. F.; Guy, R. K.; Hwang, C.-K.; Nakada, M.; Nantermet, P. G. Total Synthesis of Taxol. 2. Construction of A and C Ring Intermediates and Initial Attempts to

Construct the ABC Ring System. *J. Am. Chem. Soc.*, **1995**, *117*, 634-644.
15. Nicolaou, K. C.; Yang, Z.; Liu, J. J.; Nantermet, P. G.; Claiborne, C. F.; Renaud, J.; Guy, R. K.; Shibayama, K. Total Synthesis of Taxol. 3. Formation of Taxol's ABC Ring Skeleton. *J. Am. Chem. Soc.*, **1995**, *117*, 645-652.
16. Nicolaou, K. C.; Ueno, H.; Liu, J.-J.; Nantermet, P. G.; Yang, Z.; Renaud, J.; Paulvannan, K.; Chadha, R. Total Synthesis of Taxol. 4. The Final Stages and Completion of the Synthesis. *J. Am. Chem. Soc.*, **1995**, *117*, 653-659.
17. Danishefsky, S.; Masters, J.; Young, W.; Link, J.; Snyder, L.; Magee, T.; Jung, D.; Isaacs, R.; Bornmann, W.; Alaimo, C.; Coburn, C.; Di Grandi, M. Total Synthesis of Baccatin III and Taxol. *J. Am. Chem. Soc.*, **1996**, *118*, 2843-2859.
18. Wender, P. A.; Mucciaro, T. P. A New and Practical Approach to the Synthesis of Taxol and Taxol Analogues: The Pinene Path. *J. Am. Chem. Soc.*, **1992**, *114*, 5878-5879.
19. Wender, P. A.; Badham, N. F.; Conway, S. P.; Floreancig, P. E.; Glass, T. E.; Houze, J. B.; Krauss, N. E.; Lee, D.; Marquess, D. G.; McGrane, P. L.; Meng, W.; Natchus, M. G.; Shuker, A. J.; Sutton, J. C.; Taylor, R. E. The Pinene Path to Taxanes. 6. A Concise Stereocontrolled Synthesis of Taxol. *J. Am. Chem. Soc.*, **1997**, *119*, 2757-2758.
20. Morihira, K.; Nishimori, T.; Kusama, H.; Horiguchi, Y.; Kuwajima, I.; Tsuruo, T. Synthesis of C-ring aromatic taxoids and evaluation of their multi-drug resistance reversing activity. *Bioorg. Med. Chem. Lett.*, **1998**, *8*, 2973-2976.
21. Mukaiyama, T.; Shiina, I.; Iwadare, H.; Saitoh, M.; Nishimura, T.; Ohkawa, N.; Sakoh, H.; Nishimura, K.; Tani, Y.-I.; Hasegawa, M.; Yamada, K.; Saitoh, K. Asymmetric total synthesis of taxol. *Chem. - Eur. J.*, **1999**, *5*, 121-161.
22. Ojima, I.; Chakravarty, S.; Inoue, T.; Lin, S.; He, L.; Horwitz, S. B.; Kuduk, S. D.; Danishefsky, S. J. A Common Pharmacophore for Cytotoxic Natural Products that Stabilize Microtubules. *Proc. Natl. Acad. Sci. USA*, **1999**, *96*, 4256-4261.
23. Denis, J. N.; Greene, A. E.; Guenard, D.; Gueritte-Voegelein, F.; Mangatal, L.; Potier, P. Highly efficient, practical approach to natural taxol. *J. Am. Chem. Soc.*, **1988**, *110*, 5917-5919.
24. Denis, J.-N.; Correa, A.; Greene, A. E. An Improved Synthesis of the Taxol Side Chain and of RP 56976. *J. Org. Chem.*, **1990**, *55*, 1957-1959.
25. Denis, J.-N.; Correa, A.; Greene, A. E. Direct, Highly Efficient Synthesis from (*S*)-(+)-Phenylglycine of the Taxol and Taxotere Side Chains. *J. Org. Chem.*, **1991**, *56*, 6939-6942.
26. Holton, R. A.; Biediger, R. J.; Boatman, D. Semisynthesis of taxol and taxotere. *Taxol: Science and Applications*, **1995**, 97-121.
27. Ojima, I. β-Lactam Synthon Method - Enantiomerically Pure β–Lactams as Synthetic Intermediates. In *The Organic Chemistry of β–Lactam Antibiotics*, Georg, G. I., Ed. VCH Publishers: New York, 1992; pp 197-255.
28. Ojima, I.; Zucco, M.; Duclos, O.; Kuduk, S. D.; Sun, C.-M.; Park, Y. H. *N*-Acyl-3-hydroxy-β-lactams as Key Intermediates for Taxotere and Its Analogs. *Bioorg. Med. Chem. Lett.*, **1993**, *3*, 2479-2482.
29. Commercon, A.; Bezard, D.; Bernard, F.; Bourzat, J. D. Improved protection and esterification of a precursor of the Taxotere and taxol side chains. *Tetrahedron Lett.*, **1992**, *33*, 5185-5188.

30. Kingston, D. G. I.; Chaudhary, A. G.; Gunatilaka, A. A. L.; Middleton, M. L. Synthesis of Taxol from Baccatin III via an Oxazoline Intermediate. *Tetrahedron Lett.*, **1994**, *35*, 4483-4484.
31. Guenard, D.; Gueritte-Voegelein, F.; Potier, P. Taxol and taxotere: discovery, chemistry, and structure-activity relationships. *Acc. Chem. Res.*, **1993**, *26*, 160-167.
32. Kingston, D. G. I. Recent Advances in the Chemistry and Structure-Activity Relationships of Paclitaxel. In *Taxane Anticancer Agents: Basic Science and Current Status; ACS Symp. Ser. 583*, Georg, G. I.; Chen, T. T.; Ojima, I.; Vyas, D. M., Eds. American Chemical Society: Washington, D. C., 1995; pp 203-216.
33. Ojima, I.; Lin, S.; Wang, T. Recent advances in the medicinal chemistry of taxoids with novel β-amino acid side chains. *Curr. Med. Chem.*, **1999**, *6*, 927-954.
34. Kingston, D. G. I.; Samaramayake, G.; Ivey, C. A. The Chemistry of Taxol, a Clinically Useful Anticancer Agent. *J. Nat. Prod.*, **1990**, *53*, 1-12.
35. Georg, G. I.; Cheruvallath, Z. S.; Harriman, G. C. B.; Hepperle, M.; Park, H. An Efficient Semisynthesis of Taxol from (3*R*,4*S*)-*N*-Benzoyl-3-[(*t*-butyldimethylsilyl)oxy]-4-phenyl-2-azetidinone and 7-(Triethylsilyl)baccatin III. *Bioorg. Med. Chem. Lett.*, **1993**, *3*, 2467-2470.
36. Miller, L. A.; Ratnam, K.; Payne, D. J. β-Lactamase-inhibitor combinations in the 21st century: current agents and new developments. *Curr. Opin. Pharmacol.*, **2001**, *1*, 451-458.
37. Fueloep, F. The Chemistry of 2-Aminocycloalkanecarboxylic Acids. *Chem. Rev.*, **2001**, *101*, 2181-2204.
38. Fulop, F.; Bernath, G.; Pihlaja, K. Synthesis, stereochemistry and transformations of cyclopentane-, cyclohexane-, cycloheptane-, and cyclooctane-fused 1,3-oxazines, 1,3-thiazines, and pyrimidines. *Adv. Heterocycl. Chem.*, **1998**, *69*, 349-477.
39. Rosenblum, S. B.; Huynh, T.; Afonso, A.; Davis, H. R., Jr.; Yumibe, N.; Clader, J. W.; Burnett, D. A. Discovery of 1-(4-Fluorophenyl)-(3R)-[3-(4-fluorophenyl)-(3S)-hydroxypropyl]-(4S)-(4-hydroxyphenyl)-2-azetidinone (SCH 58235): A Designed, Potent, Orally Active Inhibitor of Cholesterol Absorption. *J. Med. Chem.*, **1998**, *41*, 973-980.
40. Ojima, I. Recent Advances in β-Lactam Synthon Method. *Acc. Chem. Res.*, **1995**, *28*, 383-389 and references cited therein.
41. Koppel, G. A. The synthesis of the β-lactam function. *Chem. Heterocycl. Compd.*, **1983**, *42*, 219-441.
42. Palomo, C.; Aizpurua, J. M.; Ganboa, I.; Oiarbide, M. Asymmetric synthesis of .beta.-lactams by Staudinger ketene-imine cycloaddition reaction. *Eur. J. Org. Chem.*, **1999**, 3223-3235.
43. Miller, M. J. Hydroxamate approach to the synthesis of .beta.-lactam antibiotics. *Acc. Chem. Res.*, **1986**, *19*, 49-56.
44. Hegedus, L. S. Synthesis of Amino Acids and Peptides Using Chromium Carbene Complex Photochemistry. *Acc. Chem. Res.*, **1995**, *28*, 299-305.
45. Brieva, R.; Crich, J. Z.; Sih, C. J. Chemoenzymatic Synthesis of the C-13 Side Chain of Taxol: Optically-Active 3-Hydroxy-4-phenyl β-Lactam Derivatives. *J. Org. Chem.*, **1993**, *58*, 1068-1075.

46. Schwartz, A.; Madan, P.; Whitesell, J. K.; Lawrence, R. M. Lipase-catalyzed kinetic resolution of alcohols via chloroacetate esters: (-)-(1R,2S)-trans-2-phenylcyclohexanol and (+)-(1S,2R)-trans-2-phenylcyclohexanol. *Org. Synth.*, **1990**, *69*, 1-9.
47. Whitesell, J. K.; Lawrence, R. M. Practical Enzymatic Resolution of Chiral Auxiliaries Enantiomerically Pure t*rans-2*-Phenylcyclohexanol and t*rans-2*-(a–Cumyl)cyclohexanol. *Chimia*, **1986**, *40*, 318-321.
48. Holton, R. A. Method for Preparation of Taxol Using Oxazinone. *U.S. Patent*, **1991**, 5,175,315.
49. Jiao, L.; Liang, Y.; Xu, J. Origin of the Relative Stereoselectivity of the b-Lactam Formation in the Staudinger Reaction. *J. Am. Chem. Soc.*, **2006**, *128*, 6060-6069.
50. Verweij, J.; Clavel, M.; Chevalier, B. Paclitaxel (Taxol) and Docetaxel (Taxotere): Not Simply Two of a Kind. *Ann. Oncol.*, **1994**, *5*, 495-505.
51. Ojima, I. Chemistry of Taxoid Antitumor Agents at the Biomedical Interface. *7th International Kyoto Conference on Organic Chemistry, Kyoto, Japan, November 10-14,*, **1997**, *Abstracts*, IL-19.
52. Ojima, I. Science of Taxol. *Farumashia*, **2003**, *39*, 49-53.
53. Ojima, I.; Bounaud, P.-Y.; Takeuchi, C.; Pera, P.; Bernacki, R. J. New taxanes as highly efficient reversal agents for multi-drug resistance in cancer cells. *Bioorg. Med. Chem. Lett.*, **1998**, *8*, 189-194.
54. Ojima, I.; Duclos, O.; Zucco, M.; Bissery, M.-C.; Combeau, C.; Vrignaud, P.; Riou, J. F.; Lavelle, F. Synthesis and Structure-Activity Relationships of New Antitumor Taxoids. Effects of Cyclohexyl Substitution at the C-3' and/or C-2 of Taxotere (Docetaxel). *J. Med. Chem.*, **1994**, *37*, 2602-2608.
55. Ojima, I.; Fenoglio, I.; Park, Y. H.; Sun, C.-M.; Appendino, G.; Pera, P.; Bernacki, R. J. Synthesis and Structure-Activity Relationships of Novel Nor-Seco Analogs of Taxol and Taxotere. *J. Org. Chem.*, **1994**, *59*, 515-517.
56. Ojima, I.; Geney, R.; Ungureanu, I. M.; Li, D. Medicinal chemistry and chemical biology of new generation taxane antitumor agents. *IUBMB Life*, **2002**, *53*, 269-274.
57. Ojima, I.; Kuduk, S. D.; Pera, P.; Veith, J. M.; Bernacki, R. J. Synthesis of and Structure-Activity Relationships of Non-Aromatic Taxoids. Effects of Alkyl and Alkenyl Ester Groups on Cytotoxicity. *J. Med. Chem.*, **1997**, *40*, 279-285.
58. Ojima, I.; Kuduk, S. D.; Slater, J. C.; Gimi, R. H.; Sun, C. M.; Chakravarty, S.; Ourevich, M.; Abouabdellah, A.; Bonnet-Delpon, D.; J.-P., B.; Veith, J. M.; Pera, P.; Bernacki, R. J. Synthesis, Biological Activity, and Conformational Analysis of Fluorine-Containing Taxoids. In *"Biomedical Frontiers of Fluorine Chemistry" ACS Symp. Ser. 639*, Ojima, I.; McCarthy, J. R.; Welch, J. T., Eds. American Chemical Society: Washington, D. C., 1996; pp 228-243.
59. Ojima, I.; Slater, J. C.; Michaud, E.; Kuduk, S. D.; Bounaud, P.-Y.; Vrignaud, P.; Bissery, M.-C.; Veith, J.; Pera, P.; Bernacki, R. J. Syntheses and Structure-Activity Relationships of the Second Generation Antitumor Taxoids. Exceptional Activity against Drug-Resistant Cancer Cells. *J. Med. Chem.*, **1996**, *39*, 3889-3896.
60. Ojima, I.; Slater, J. S.; Kuduk, S. D.; Takeuchi, C. S.; Gimi, R. H.; Sun, C.-M.; Park, Y. H.; Pera, P.; Veith, J. M.; Bernacki, R. J. Syntheses and Structure-

Activity Relationships of Taxoids Derived from 14β-Hydroxy-10-deacetylbaccatin III. *J. Med. Chem.*, **1997**, *40*, 267-278.

61. Holton, R. A. Method for Preparation of Taxol. *Eur. Pat. Appl.*, **1990**, US Patent, **1992**, 5,175,315; EP 400,971, 1990: *Chem. Abstr.* **1990**, *114*, 164568q.
62. Ojima, I.; Habus, I.; Zhao, M.; Zucco, M.; Park, Y. H.; Sun, C. M.; Brigaud, T. New and efficient approaches to the semisynthesis of taxol and its C-13 side chain analogs by means of b-lactam synthon method. *Tetrahedron*, **1992**, *48*, 6985-7012.

References for Chapter II:

1. Bondi, A. van der Waals volumes and radii. *J. Phys. Chem.*, **1964**, *68*, 441-451.
2. Boehm, H.-J.; Banner, D.; Bendels, S.; Kansy, M.; Kuhn, B.; Mueller, K.; Obst-Sander, U.; Stahl, M. Fluorine in medicinal chemistry. *ChemBioChem*, **2004**, *5*, 637-643.
3. O'Hagan, D.; Schaffrath, C.; Cobb, S. L.; Hamilton, J. T. G.; Murphy, C. D. Biochemistry: Biosynthesis of an organofluorine molecule. *Nature*, **2002**, *416*, 279.
4. Martino, R.; Subira, M. Invasive fungal infections in hematology: new trends. *Ann. Hematol.*, **2002**, *81*, 233-243.
5. Page, M. I. The mechanisms of reactions of β-lactam antibiotics. *Acc. Chem. Res.*, **1984**, *17*, 144-151.
6. Ojima, I.; Delaloge, F. Syntheses of Norstatine, Its Analogs, Dipeptide Isosteres by Means of β-Lactam Synthon Method. In *Peptidomimetics Protocols*, Kazmierski, W. M., Ed. Humana Press: Totowa, 1997; p137-160.
7. Kuznetsova, L.; Ungureanu, I. M.; Pepe, A.; Zanardi, I.; Wu, X.; Ojima, I. Trifluoromethyl- and difluoromethyl-β-lactams as useful building blocks for the synthesis of fluorinated amino acids, dipeptides, and fluoro-taxoids. *J. Fluorine Chem.*, **2004**, *125*, 487-500.
8. Ojima, I. Recent Advances in β-Lactam Synthon Method. *Acc. Chem. Res.*, **1995**, *28*, 383-389 and references cited therein.
9. Yamazaki, T.; Hiraoka, S.; Sakamoto, J.; Kitazume, T. Mesyloxy-group migration as the stereoselective preparation method of various functionalized olefins and its reaction mechanism. *Org. Lett.*, **2001**, *3*, 743-746.
10. Lim, M. H.; Kim, H. O.; Moon, H. R.; Chun, M. W.; Jeong, L. S. Synthesis of Novel D-2'-Deoxy-2'-C-difluoromethylene-4'-thiocytidine as a Potential Antitumor Agent. *Org. Lett.*, **2002**, *4*, 529-531.
11. Bhadury, P. S.; Palit, M.; Sharma, M.; Raza, S. K.; Jaiswal, D. K. Fluorinated phosphonium ylides: versatile in situ Wittig intermediates in the synthesis of hydrofluorocarbons. *J. Fluorine Chem.*, **2002**, *116*, 75-80.
12. Skehan, P.; Storeng, R.; Scudiero, D.; Monks, A.; McMahon, J.; Vistica, D.; Warren, J. T.; Bokesch, H.; Kenney, S.; Boyd, M. R. New Colorimetric Cytotoxicity Assay for Anticancer-Drug Screening. *J. Nat. Cancer Inst.*, **1990**, *82*, 1107-1112.
13. Ojima, I.; Slater, J. S.; Kuduk, S. D.; Takeuchi, C. S.; Gimi, R. H.; Sun, C.-M.; Park, Y. H.; Pera, P.; Veith, J. M.; Bernacki, R. J. Syntheses and Structure-Activity Relationships of Taxoids Derived from 14β-Hydroxy-10-deacetylbaccatin III. *J. Med. Chem.*, **1997**, *40*, 267-278.

References for Chapter III:

1. Chari, R. V. J. Targeted delivery of chemotherapeutics: tumor-activated prodrug therapy. *Adv. Drug Deliv. Rev.*, **1998**, *31*, 89-104.
2. Ojima, I.; Geng, X.; Wu, X.; Qu, C.; Borella, C. P.; Xie, H.; Wilhelm, S. D.; Leece, B. A.; Bartle, L. M.; Goldmacher, V. S.; Chari, R. V. J. Tumor-Specific Novel Taxoid-Monoclonal Antibody Conjugates. *J. Med. Chem.*, **2002**, *45*, 5620-5623.
3. Chen, J.; Jaracz, S.; Zhao, X.; Chen, S.; Ojima, I. Antibody-cytotoxic agent conjugates for cancer therapy. *Expert Opin. Drug Deliv.*, **2005**, *2*, 873-890.
4. Wu, X.; Ojima, I. Tumor specific novel taxoid-monoclonal antibody conjugates. *Curr. Med. Chem.*, **2004**, *11*, 429-438.
5. Ojima, I. Guided molecular missiles for tumor-targeting chemotherapy-case studies using the second-generation taxoids as warheads. *Acc. Chem. Res.*, **2008**, *41*, 108-119.
6. Hamblett, K. J.; Senter, P. D.; Chace, D. F.; Sun, M. M. C.; Lenox, J.; Cerveny, C. G.; Kissler, K. M.; Bernhardt, S. X.; Kopcha, A. K.; Zabinski, R. F.; Meyer, D. L.; Francisco, J. A. Effects of drug loading on the antitumor activity of a monoclonal antibody drug conjugate. *Clin. Cancer Res.*, **2004**, *10*, 7063-7070.
7. Jaracz, S.; Chen, J.; Kuznetsova, L. V.; Ojima, I. Recent advances in tumor-targeting anticancer drug conjugates. *Bioorg. Med. Chem.*, **2005**, *13*, 5043-5054.
8. Hamann, P. R.; Hinman, L. M.; Beyer, C. F.; Lindh, D.; Upeslacis, J.; Flowers, D. A.; Bernstein, I. An anti-CD33 antibody-calicheamicin conjugate for treatment of acute myeloid leukemia. Choice of linker. *Bioconjugate Chem.*, **2002**, *13*, 40-46.
9. Liu, C. N.; Tadayoni, B. M.; Bourret, L. A.; Mattocks, K. M.; Derr, S. M.; Widdison, W. C.; Kedersha, N. L.; Ariniello, P. D.; Goldmacher, V. S.; Lambert, J. M.; Blattler, W. A.; Chari, R. V. J. Eradication of large colon tumor xenografts by targeted delivery of maytansinoids. *Proc. Nat. Acad. Sci. U.S.A.,* **1996**, *93*, 8618-8623.
10. Lam, L.; Lam, C.; Li, W. H.; Cao, Y. Recent advances in drug-antibody immunoconjugates for the treatment of cancer. *Drugs Future*, **2003**, *28*, 905-910.
11. Saleh, M. N.; LoBuglio, A. F.; Trail, P. A. Monoclonal antibody-based immunoconjugate therapy of cancer: studies with BR96-doxorubicin. *Basic Clin. Oncol.*, **1998**, *15*, 397-416.
12. Gillespie, A. M.; Broadhead, T. J.; Chan, S. Y.; Owen, J.; Farnsworth, A. P.; Sopwith, M.; Coleman, R. E. Phase I open study of the effects of ascending doses of the cytotoxic immunoconjugate CMB-401 (hCTMO1-calicheamicin) in patients with epithelial ovarian cancer. *Ann. Oncol.*, **2000**, *11*, 735-741.
13. Bradley, M. O.; Webb, N. L.; Anthony, F. H.; Devanesan, P.; Witman, P. A.; Hemamalini, S.; Chander, M. C.; Baker, S. D.; He, L.; Horwitz, S. B.; Swindell, C. S. Tumor targeting by covalent conjugation of a natural fatty acid to paclitaxel. *Clin. Cancer Res.*, **2001**, *7*, 3229-3238.
14. Ojima, I.; Lin, S.; Wang, T. Recent advances in the medicinal chemistry of taxoids with novel b-amino acid side chains. *Curr. Med. Chem.*, **1999**, *6*, 927-954.
15. Ojima, I.; Wang, T.; Miller, M. L.; Lin, S.; Borella, C. P.; Geng, X.; Pera, P.; Bernacki, R. J. Syntheses and Structure-Activity Relationships of New Second-

Generation Taxoids. *Bioorg. Med. Chem. Lett.*, **1999**, *9*, 3423-3428.

16. Lin, S.; Geng, X.; Qu, C.; Tynebor, R.; Gallagher, D. J.; Pollina, E.; Rutter, J.; Ojima, I. Synthesis of highly potent second-generation taxoids through effective kinetic resolution coupling of racemic .beta.-lactams with baccatins. *Chirality*, **2000**, *12*, 431-441.
17. Kuznetsova, L.; Chen, J.; Sun, L.; Wu, X.; Pepe, A.; Veith, J. M.; Pera, P.; Bernacki, R. J.; Ojima, I. Syntheses and evaluation of novel fatty acid-second-generation taxoid conjugates as promising anticancer agents. *Bioorg. Med. Chem. Lett.*, **2006**, *16*, 974-977.
18. Geney, R.; Chen, J.; Ojima, I. Recent advances in the new generation taxane anticancer agents. *Med. Chem.*, **2005**, *1*, 125-139.
19. Anderson, R. G. W.; Kamen, B. A.; Rothberg, K. G.; Lacey, S. W. Potocytosis: sequestration and transport of small molecules by caveolae. *Science*, **1992**, *255*, 410-411.
20. Elnakat, H.; Ratnam, M. Distribution, functionality and gene regulation of folate receptor isoforms: implications in targeted therapy. *Adv. Drug Deliv. Rev.*, **2004**, *56*, 1067-1084.
21. Weitman, S. D.; Lark, R. H.; Coney, L. R.; Fort, D. W.; Frasca, V.; Zurawski, V. R., Jr.; Kamen, B. A. Distribution of the folate receptor GP38 in normal and malignant cell lines and tissues. *Cancer Res.*, **1992**, *52*, 3396-3401.
22. Stevens, P. J.; Lee, R. J. A folate receptor-targeted emulsion formulation for paclitaxel. *Anticancer Res.*, **2003**, *23*, 4927-4931.
23. Huang, L.; Grammatikakis, N.; Yoneda, M.; Banerjee, S. D.; Toole, B. P. Molecular characterization of a novel intracellular hyaluronan-binding protein. *J. Biol. Chem.*, **2000**, *275*, 29829-29839.
24. Ponta, H.; Sherman, L.; Herrlich, P. A. CD44: From adhesion molecules to signalling regulators. *Nat. Rev. Mol. Cell Biol.*, **2003**, *4*, 33-45.
25. Luo, Y.; Bernshaw, N. J.; Lu, Z.-R.; Kopecek, J.; Prestwich, G. D. Targeted delivery of doxorubicin by HPMA copolymer-hyaluronan bioconjugates. *Pharm. Res.*, **2002**, *19*, 396-402.
26. Orlando, C.; Raggi, C. C.; Bianchi, S.; Distante, V.; Simi, L.; Vezzosi, V.; Gelmini, S.; Pinzani, P.; Smith, M. C.; Buonamano, A.; Lazzeri, E.; Pazzagli, M.; Cataliotti, L.; Maggi, M.; Serio, M. Measurement of somatostatin receptor subtype 2 mRNA in breast cancer and corresponding normal tissue. *Endocr. Relat. Cancer*, **2004**, *11*, 323-332.
27. Weckbecker, G.; Raulf, F.; Stolz, B.; Bruns, C. Somatostatin analogs for diagnosis and treatment of cancer. *Pharmacol. Ther.*, **1993**, *60*, 245-264.
28. Nagy, A.; Schally, A. V.; Halmos, G.; Armatis, P.; Cai, R.-Z.; Csernus, V.; Kovacs, M.; Koppan, M.; Szepeshazi, K.; Kahan, Z. Synthesis and biological evaluation of cytotoxic analogs of somatostatin containing doxorubicin or its intensely potent derivative, 2-pyrrolinodoxorubicin. *Proc. Nat. Acad. Sci. U.S.A.*, **1998**, *95*, 1794-1799.
29. Moody, T. W.; Czerwinski, G.; Tarasova, N. I.; Michejda, C. J. VIP-ellipticine derivatives inhibit the growth of breast cancer cells. *Life Sci.*, **2002**, *71*, 1005-1014.
30. Nicolaou, K. C.; Ogawa, Y.; Zuccarello, G.; Kataoka, H. DNA cleavage by a

synthetic mimic of the calicheamicin-esperamicin class of antibiotics. *J. Am. Chem. Soc.*, **1988**, *110*, 7247-7248.

31. Lee, M. D.; Dunne, T. S.; Siegel, M. M.; Chang, C. C.; Morton, G. O.; Borders, D. B. Calichemicins, a novel family of antitumor antibiotics. 1. Chemistry and partial structure of calichemicin g1I. *J. Am. Chem. Soc.*, **1987**, *109*, 3464-3466.
32. Lee, M. D.; Dunne, T. S.; Chang, C. C.; Ellestad, G. A.; Siegel, M. M.; Morton, G. O.; McGahren, W. J.; Borders, D. B. Calichemicins, a novel family of antitumor antibiotics. 2. Chemistry and structure of calichemicin g1I. *J. Am. Chem. Soc.*, **1987**, *109*, 3466-3468.
33. Dimarco, A.; Valentine, L.; Scarpina.Bm; Dasdia, T.; Soldati, M.; Gaetani, M.; Orezzi, P.; Silvestrini, R. Daunomycin New Antibiotic of Rhodomycin Group. *Nature*, **1964**, *201*, 706-707.
34. Kupchan, S. M.; Komoda, Y.; Thomas, G. J.; Smith, R. M.; Bryan, R. F.; Haltiwan.Rc; Karim, A.; Court, W. A.; Gilmore, C. J. Tumor Inhibitors .73. Maytansine, a Novel Antileukemic Ansa Macrolide from Maytenus-Ovatus. *J. Am. Chem. Soc.,* **1972**, *94*, 1354-1356.
35. Wolpert-DeFilippes, M. K.; Adamson, R. H.; Cysyk, R. L.; Johns, D. G. Initial Studies on Cytotoxic Action of Maytansine, a Novel Ansa Macrolide. *Biochem. Pharmacol.*, **1975**, *24*, 751-754.
36. Hata, T.; Sano, Y.; Sugawara, R.; Matsumae, A.; Kanamori, K.; Shima, T.; Hoshi, T. Mitomycin, a new antibiotic from Streptomyces. I. *J. Antibiot.*, **1956**, *9*, 141-146.
37. Webb, J. S.; Cosulich, D. B.; Fulmor, W.; Mowat, J. H.; Broschard, R. W.; Pidacks, C.; Williams, R. P.; Lancaster, J. E.; Wolfe, C. F.; Patrick, J. B.; Meyer, W. E. Structures of Mitomycins a, B and C and Porfiromycin .1. *J. Am. Chem. Soc.*, **1962**, *84*, 3185-3187.
38. Keyes, S. R.; Heimbrook, D. C.; Fracasso, P. M.; Rockwell, S.; Sligar, S. G.; Sartorelli, A. C. Chemotherapeutic attack of hypoxic tumor cells by the bioreductive alkylating agent mitomycin C. *Adv. Enzyme Regul.*, **1985**, *23*, 291-307.
39. Li, V.-S.; Choi, D.; Tang, M.-s.; Kohn, H. Concerning In Vitro Mitomycin-DNA Alkylation. *J. Am. Chem. Soc.*, **1996**, *118*, 3765-3766.
40. Manabe, Y.; Tsubota, T.; Haruta, Y.; Kataoka, K.; Okazaki, M.; Haisa, S.; Nakamura, K.; Kimura, I. Production of a monoclonal antibody-mitomycin C conjugate, utilizing dextran T-40, and its biological activity. *Biochem. Pharmacol.*, **1985**, *34*, 289-291.
41. Tanaka, J.-I.; Sato, E.; Saito, Y.; Kusano, T.; Koyama, K. Preparation of a conjugate of mitomycin C and anti-neural cell adhesion molecule monoclonal antibody for specific chemotherapy against biliary tract carcinoma. *Surg. Today*, **1998**, *28*, 1217-1220.
42. Li, S.; Zhang, X.; Zhang, S.; Chen, X.; Chen, L.; Shu, Y.; Zhang, J.; Fan, D. Preparation of antigastric cancer monoclonal antibody MGb2-mitomycin C conjugate with improved antitumor activity. *Bioconjugate Chem.*, **1990**, *1*, 245-250.
43. Wani, M. C.; Taylor, H. L.; Wall, M. E.; Coggon, P.; McPhail, A. T. Plant Antitumor Agents. VI. The Isolation and Structure of Taxol, a Novel

Antileukemic and Antitumor Agent from *Taxus brevifolia*. *J. Am. Chem. Soc.*, **1971**, *93*, 2325-2327.

44. Kumar, N. Taxol-Induced Polymerization of Purified Tubulin. *J. Biol. Chem.*, **1981**, *256*, 10435-10441.
45. Guillemard, V.; Saragovi, H. U. Taxane-antibody conjugates afford potent cytotoxicity, enhanced solubility, and tumor target selectivity. *Cancer Res.*, **2001**, *61*, 694-699.
46. Safavy, A.; Bonner, J. A.; Waksal, H. W.; Buchsbaum, D. J.; Gillespie, G. Y.; Khazaeli, M. B.; Arani, R.; Chen, D.-T.; Carpenter, M.; Raisch, K. P. Synthesis and Biological Evaluation of Paclitaxel-C225 Conjugate as a Model for Targeted Drug Delivery. *Bioconjugate Chem.*, **2003**, *14*, 302-310.
47. Ojima, I. Science of Taxol. *Farumashia*, **2003**, *39*, 49-53.
48. Ojima, I.; Slater, J. C.; Michaud, E.; Kuduk, S. D.; Bounaud, P.-Y.; Vrignaud, P.; Bissery, M.-C.; Veith, J.; Pera, P.; Bernacki, R. J. Syntheses and Structure-Activity Relationships of the Second Generation Antitumor Taxoids. Exceptional Activity against Drug-Resistant Cancer Cells. *J. Med. Chem.*, **1996**, *39*, 3889-3896.
49. Ojima, I.; Slater, J. S.; Kuduk, S. D.; Takeuchi, C. S.; Gimi, R. H.; Sun, C.-M.; Park, Y. H.; Pera, P.; Veith, J. M.; Bernacki, R. J. Syntheses and Structure-Activity Relationships of Taxoids Derived from 14β-Hydroxy-10-deacetylbaccatin III. *J. Med. Chem.*, **1997**, *40*, 267-278.
50. Ojima, I.; Kuduk, S. D.; Pera, P.; Veith, J. M.; Bernacki, R. J. Synthesis of and Structure-Activity Relationships of Non-Aromatic Taxoids. Effects of Alkyl and Alkenyl Ester Groups on Cytotoxicity. *J. Med. Chem.*, **1997**, *40*, 279-285.
51. Ojima, I.; Lin, S. Efficient Asymmetric Syntheses of β-Lactams Bearing a Cyclopropane or an Epoxide Moiety and Their Application to the Syntheses of Novel Isoserines and Taxoids. *J. Org. Chem.*, **1998**, *63*, 224-225.
52. Ojima, I.; Geney, R.; Ungureanu, I. M.; Li, D. Medicinal chemistry and chemical biology of new generation taxane antitumor agents. *IUBMB Life*, **2002**, *53*, 269-274.
53. Pettit, G. R.; Kamano, Y.; Herald, C. L.; Tuinman, A. A.; Boettner, F. E.; Kizu, H.; Schmidt, J. M.; Baczynskyj, L.; Tomer, K. B.; Bontems, R. J. The isolation and structure of a remarkable marine animal antineoplastic constituent: dolastatin 10. *J. Am. Chem. Soc.*, **1987**, *109*, 6883-5.
54. Pettit, G. R.; Singh, S. B.; Hogan, F.; Lloyd-Williams, P.; Herald, D. L.; Burkett, D. D.; Clewlow, P. J. Antineoplastic agents. Part 189. The absolute configuration and synthesis of natural (-)-dolastatin 10. *J. Am. Chem. Soc.*, **1989**, *111*, 5463-5465.
55. Madden, T.; Tran, H. T.; Beck, D.; Huie, R.; Newman, R. A.; Pusztai, L.; Wright, J. J.; Abbruzzese, J. L. Novel marine-derived anticancer agents: a phase I clinical, pharmacological, and pharmacodynamic study of dolastatin 10 (NSC 376128) in patients with advanced solid tumors. *Clin. Cancer Res.*, **2000**, *6*, 1293-1301.
56. Doronina, S. O.; Toki, B. E.; Torgov, M. Y.; Mendelsohn, B. A.; Cerveny, C. G.; Chace, D. F.; DeBlanc, R. L.; Gearing, R. P.; Bovee, T. D.; Siegall, C. B.; Francisco, J. A.; Wahl, A. F.; Meyer, D. L.; Senter, P. D. Development of potent monoclonal antibody auristatin conjugates for cancer therapy. *Nat. Biotechnol.*,

2003, *21*, 778-784.

57. Shen, W. C.; Ryser, H. J. P. Cis-Aconityl Spacer between Daunomycin and Macromolecular Carriers - a Model of Ph-Sensitive Linkage Releasing Drug from a Lysosomotropic Conjugate. *Biochem. Biophys. Res. Commun.*, **1981**, *102*, 1048-1054.
58. Yang, H. M.; Reisfeld, R. A. Pharmacokinetics and Mechanism of Action of a Doxorubicin- Monoclonal Antibody 9.2.27 Conjugate Directed to a Human-Melanoma Proteoglycan. *J. Nat. Cancer Inst.*, **1988**, *80*, 1154-1159.
59. Dillman, R. O.; Johnson, D. E.; Shawler, D. L.; Koziol, J. A. Superiority of an Acid-Labile Daunorubicin Monoclonal Antibody Immunoconjugate Compared to Free Drug. *Cancer Res.*, **1988**, *48*, 6097-6102.
60. Greenfield, R. S.; Kaneko, T.; Daues, A.; Edson, M. A.; Fitzgerald, K. A.; Olech, L. J.; Grattan, J. A.; Spitalny, G. L.; Braslawsky, G. R. Evaluation Invitro of Adriamycin Immunoconjugates Synthesized Using an Acid-Sensitive Hydrazone Linker. *Cancer Res.*, **1990**, *50*, 6600-6607.
61. Kaneko, T.; Willner, D.; Monkovic, I.; Knipe, J. O.; Braslawsky, G. R.; Greenfield, R. S.; Vyas, D. M. New hydrazone derivatives of Adriamycin and their immunoconjugates - a correlation between acid stability and cytotoxicity. *Bioconjugate Chem.*, **1991**, *2*, 133-141.
62. Wahl, A. F.; Donaldson, K. L.; Mixan, B. J.; Trail, P. A.; Siegall, C. B. Selective tumor sensitization to taxanes with the mAb-drug conjugate cBR96-doxorubicin. *Int. J. Cancer*, **2001**, *93*, 590-600.
63. Apelgren, L. D.; Zimmerman, D. L.; Briggs, S. L.; Bumol, T. F. Antitumor-Activity of the Monoclonal-Antibody Vinca Alkaloid Immunoconjugate Ly203725 (Ks1/4-4-Desacetylvinblastine-3- Carboxhydrazide) in a Nude-Mouse Model of Human Ovarian-Cancer. *Cancer Res.*, **1990**, *50*, 3540-3544.
64. Trail, P. A.; Willner, D.; Knipe, J.; Henderson, A. J.; Lasch, S. J.; Zoeckler, M. E.; TrailSmith, M. D.; Doyle, T. W.; King, H. D.; Casazza, A. M.; Braslawsky, G. R.; Brown, J.; Hofstead, S. J.; Greenfield, R. S.; Firestone, R. A.; Mosure, K.; Kadow, K. F.; Yang, M. B.; Hellstrom, K. E.; Hellstrom, I. Effect of linker variation on the stability, potency, and efficacy of carcinoma-reactive BR64-doxorubicin immunoconjugates. *Cancer Res.*, **1997**, *57*, 100-105.
65. Griffiths, G. L.; Hansen, H. J.; Goldenberg, D. M.; Lundberg, B. B. Anti-CD74 immunoconjugates and their therapeutic and diagnostic uses. *U.S. Patent*, 219,203 A1, 20041104, **2004**.
66. Hamann, P. R.; Hinman, L. M.; Hollander, I.; Beyer, C. F.; Lindh, D.; Holcomb, R.; Hallett, W.; Tsou, H. R.; Upeslacis, J.; Shochat, D.; Mountain, A.; Flowers, D. A.; Bernstein, I. Gemtuzumab ozogamicin, a potent and selective anti-CD33 antibody-calicheamicin conjugate for treatment of acute myeloid leukemia. *Bioconjugate Chem.*, **2002**, *13*, 47-58.
67. Dyba, M.; Tarasova, N. I.; Michejda, C. J. Small molecule toxins targeting tumor receptors. *Curr. Pharm. Des.*, **2004**, *10*, 2311-2334.
68. Rejmanova, P.; Kopecek, J.; Duncan, R.; Lloyd, J. B. Stability in Rat Plasma and Serum of Lysosomally Degradable Oligopeptide Sequences in N-(2-Hydroxypropyl) Methacrylamide Copolymers. *Biomaterials*, **1985**, *6*, 45-48.
69. Dubowchik, G. M.; Radia, S.; Mastalerz, H.; Walker, M. A.; Firestone, R. A.;

Dalton King, H.; Hofstead, S. J.; Willner, D.; Lasch, S. J.; Trail, P. A. Doxorubicin immunoconjugates containing bivalent, lysosomally-cleavable dipeptide linkages. *Bioorg. Med. Chem. Lett.*, **2002**, *12*, 1529-1532.

70. Zheng, Z.-B.; Zhu, G.; Tak, H.; Joseph, E.; Eiseman, J. L.; Creighton, D. J. N-(2-Hydroxypropyl)methacrylamide copolymers of a glutathione (GSH)-activated glyoxalase I inhibitor and DNA alkylating agent: synthesis, reaction kinetics with GSH, and in vitro antitumor activities. *Bioconjugate Chem.*, **2005**, *16*, 598-607.
71. Tolcher, A. W.; Ochoa, L.; Hammond, L. A.; Patnaik, A.; Edwards, T.; Takimoto, C.; Smith, L.; de Bono, J.; Schwartz, G.; Mays, T.; Jonak, Z. L.; Johnson, R.; DeWitte, M.; Martino, H.; Audette, C.; Maes, K.; Chari, R. V. J.; Lambert, J. M.; Rowinsky, E. K. Cantuzumab mertansine, a maytansinoid immunoconjugate directed to the CanAg antigen: A phase I, pharmacokinetic, and biologic correlative study. *J. Clin. Oncol.*, **2003**, *21*, 211-222.
72. Safavy, A.; Georg, G. I.; Vander Velde, D.; Raisch, K. P.; Safavy, K.; Carpenter, M.; Wang, W.; Bonner, J. A.; Khazaeli, M. B.; Buchsbaum, D. J. Site-specifically traced drug release and biodistribution of a paclitaxel-antibody conjugate toward improvement of the linker structure. *Bioconjugate Chem.*, **2004**, *15*, 1264-1274.
73. Ojima, I.; Bounaud, P.-Y.; Pera, P.; Bernacki, R. J. Discovery and development of new taxanes as highly efficient reversal agents for multi-drug resistance in cancer cells. *Ann. Oncol.*, **1998**, *9*, 557.
74. Cook, J. A.; Pass, H. I.; Iype, S. N.; Friedman, N.; DeGraff, W.; Russo, A.; Mitchell, J. B. Cellular glutathione and thiol measurements from surgically resected human lung tumor and normal lung tissue. *Cancer Res.*, **1991**, *51*, 4287-4294.
75. Blair, S. L.; Heerdt, P.; Sachar, S.; Abolhoda, A.; Hochwald, S.; Cheng, H.; Burt, M. Glutathione metabolism in patients with non-small cell lung cancers. *Cancer Res.*, **1997**, *57*, 152-155.
76. Kosower, N. S. The glutathione status of cells. *Int. Rev. Cytol.*, **1978**, *54*, 109-160.
77. Britten, R. A.; Green, J. A.; Warenius, H. M. Cellular glutathione (GSH) and glutathione S-transferase (GST) activity in human ovarian tumor biopsies following exposure to alkylating agents. *Int. J. Radiat. Oncol., Biol., Phys.*, **1992**, *24*, 527-531.
78. Ojima, I. Use of fluorine in the medicinal chemistry and chemical biology of bioactive compounds - a case study on fluorinated taxane anticancer agents. *ChemBioChem*, **2004**, *5*, 628-635.
79. Russell-Jones, G.; McTavish, K.; McEwan, J.; Rice, J.; Nowotnik, D. Vitamin-mediated targeting as a potential mechanism to increase drug uptake by tumors. *J. Inorg. Biochem.*, **2004**, *98*, 1625-1633.
80. De Clercq, P. J. Biotin: A Timeless Challenge for Total Synthesis. *Chem. Rev.*, **1997**, *97*, 1755-1792.
81. Kluger, R. Ionic intermediates in enzyme-catalyzed carbon-carbon bond formation: patterns, prototypes, probes, and proposals. *Chem. Rev.*, **1990**, *90*, 1151-1169.
82. Corona, C.; Bryant, B. K.; Arterburn, J. B. Synthesis of a Biotin-Derived Alkyne for Pd-Catalyzed Coupling Reactions. *Org. Lett.*, **2006**, *8*, 1883-1886.
83. Wilchek, M.; Bayer, E. A. The avidin-biotin complex in bioanalytical applications.

Anal. Biochem., **1988**, *171*, 1-32.
84. Diamandis, E. P.; Christopoulos, T. K. The biotin-(strept)avidin system: principles and applications in biotechnology. *Clin. Chem.*, **1991**, *37*, 625-636.
85. Boerman Otto, C.; van Schaijk Frank, G.; Oyen Wim, J. G.; Corstens Frans, H. M. Pretargeted radioimmunotherapy of cancer: progress step by step. *J. Nucl. Med.*, **2003**, *44*, 400-411.
86. Lu, Y.; Low, P. S. Folate-mediated delivery of macromolecular anticancer therapeutic agents. *Adv. Drug Deliv. Rev.*, **2002**, *54*, 675-693.
87. Lu, Y.; Sega, E.; Leamon, C. P.; Low, P. S. Folate receptor-targeted immunotherapy of cancer: mechanism and therapeutic potential. *Adv. Drug Deliv. Rev.*, **2004**, *56*, 1161-1176.
88. Leamon, C. P.; Reddy, J. A. Folate-targeted chemotherapy. *Adv. Drug Deliv. Rev.*, **2004**, *56*, 1127-1141.
89. Na, K.; Lee, T. B.; Park, K.-H.; Shin, E.-K.; Lee, Y.-B.; Choi, H.-K. Self-assembled nanoparticles of hydrophobically-modified polysaccharide bearing vitamin H as a targeted anti-cancer drug delivery system. *Eur. J. Pharm. Sci.*, **2003**, *18*, 165-173.
90. Russell-Jones, G.; McEwan, J. Amplification of biotin-mediated targeting. *PCT Int. Appl.*, 045647, 20040603, **2004**.
91. Errington, R. J.; Ameer-Beg, S. M.; Vojnovic, B.; Patterson, L. H.; Zloh, M.; Smith, P. J. Advanced microscopy solutions for monitoring the kinetics and dynamics of drug-DNA targeting in living cells. *Adv. Drug Deliv. Rev.*, **2004**, *57*, 153-167.
92. Watson, P.; Jones, A. T.; Stephens, D. J. Intracellular trafficking pathways and drug delivery: fluorescence imaging of living and fixed cells. *Adv. Drug Deliv. Rev.*, **2004**, *57*, 43-61.
93. White, N. S.; Errington, R. J. Fluorescence techniques for drug delivery research: theory and practice. *Adv. Drug Deliv. Rev.*, **2004**, *57*, 17-42.
94. Gumbleton, M.; Stephens, D. J. Coming out of the dark: the evolving role of fluorescence imaging in drug delivery research. *Adv. Drug Deliv. Rev.*, **2004**, *57*, 5-15.
95. Evangelio, J. A.; Abal, M.; Barasoain, I.; Souto, A. A.; Lillo, M. P.; Acuna, A. U.; Amat-Guerri, F.; Andreu, J. M. Fluorescent taxoids as probes of the microtubule cytoskeleton. *Cell Motil. Cytoskeleton*, **1998**, *39*, 73-90.
96. Zhu, Q.; Uttamchandani, M.; Li, D.; Lesaicherre, M. L.; Yao, S. Q. Enzymatic Profiling System in a Small-Molecule Microarray. *Org. Lett.*, **2003**, *5*, 1257-1260.
97. Rao, C. S.; Chu, J.-J.; Liu, R.-S.; Lai, Y.-K. Synthesis and evaluation of [14C]-labeled and fluorescent-tagged paclitaxel derivatives as new biological probes. *Bioorg. Med. Chem.*, **1998**, *6*, 2193-2204.
98. Guy, R. K.; Scott, Z. A.; Sloboda, R. D.; Nicolaou, K. C. Fluorescent taxoids. *Chem. Biol.*, **1996**, *3*, 1021-1031.
99. Ingold, C. K. The conditions underlying the formation of unsaturated and of cyclic compounds from halogenated open-chain derivatives. I. Products derived from a-halogenated glutaric acids. *J. Chem. Soc., Trans.*, **1921**, *119*, 305-329.
100. Ingold, C. K.; Sako, S.; Thorpe, J. F. Influence of substituents on the formation and stability of heterocyclic compounds. I. Hydantoins. *J. Chem. Soc., Trans.*,

1922, *121*, 1177-1198.
101. Allinger, N. L.; Zalkow, V. Conformational analysis. IX. gem-Dimethyl effect. *J. Org. Chem.*, **1960**, *25*, 701-704.
102. Blagoeva, I.; Kurtev, B.; Pozharliev, I. b-Ureido acids and dihydrouracils. II. Linear free energy-steric strain energy relations for the gem-dimethyl effect. Acid-catalyzed ring closure of methyl-substituted 3-ureidopropionic acids. *J. Chem. Soc., Perkin Trans. 2: Phys. Org. Chem.*, **1979**, 1115-1122.
103. Kirby, A. J. Effective molarities for intramolecular reactions. *Adv. Phys. Org. Chem.*, **1980**, *17*, 183-278.
104. Valter, R. E. Electronic and steric effects in heterolytic reactions of intramolecular cyclization. *Usp. Khim.*, **1982**, *51*, 1374-1397.
105. Mandolini, L. Intramolecular reactions of chain molecules. *Adv. Phys. Org. Chem.*, **1986**, *22*, 1-111.
106. Verevkin, S. P.; Kuemmerlin, M.; Beckhaus, H. D.; Galli, C.; Ruechardt, C. Geminal substituent effects. Part 16. Do alkoxycarbonyl substituents stabilize small cycloalkane rings? *Eur. J. Org. Chem.*, **1998**, *1998*, 579-584.
107. Kam, N. W. S.; Liu, Z.; Dai, H. Carbon nanotubes as intracellular transporters for proteins and DNA: an investigation of the uptake mechanism and pathway. *Angew. Chem. Intl. Ed.*, **2006**, *45*, 577-581.
108. Pires, M. M.; Chmielewski, J. Fluorescence Imaging of Cellular Glutathione Using a Latent Rhodamine. *Org. Lett.*, **2008**, *10*, 837-840.
109. Hong, R.; Han, G.; Fernandez, J. M.; Kim, B.-j.; Forbes, N. S.; Rotello, V. M. Glutathione-Mediated Delivery and Release Using Monolayer Protected Nanoparticle Carriers. *J. Am. Chem. Soc.*, **2006**, *128*, 1078-1079.
110. Jones, L. R.; Goun, E. A.; Shinde, R.; Rothbard, J. B.; Contag, C. H.; Wender, P. A. Releasable Luciferin-Transporter Conjugates: Tools for the Real-Time Analysis of Cellular Uptake and Release. *J. Am. Chem. Soc.*, **2006**, *128*, 6526-6527.
111. Yang, J.; Chen, H.; Vlahov, I. R.; Cheng, J.-X.; Low, P. S. Evaluation of disulfide reduction during receptor-mediated endocytosis by using FRET imaging. *Proc. Natl. Acad. Sci. U.S.A.*, **2006**, *103*, 13872-13877.
112. Bordwell, F. G.; Fried, H. E. Heterocyclic aromatic anions with 4n + 2.pi.-electrons. *J. Org. Chem.*, **1991**, *56*, 4218-4223.
113. Pal, R.; Murty, K. V. S. N.; Mal, D. A convenient synthesis of aromatic thiolactones. *Synth. Commun.*, **1993**, *23*, 1555-1560.
114. Vegh, D.; Morel, J.; Decroix, B.; Zalupsky, P. A new convenient method for preparation of condensed aromatic and heterocyclic thiolactones. *Synth. Commun.*, **1992**, *22*, 2057-2061.
115. Chari, R. V. J.; Widdison, W. C. Process for preparation of cytotoxic conjugates of maytansinoids and cell binding agents. 6441163, 20020827, **2002**.
116. Wilchek, M.; Bayer, E. A. Biotin-containing reagents. *Methods Enzymol.*, **1990**, *184*,123-138.

References for Chapter IV:

1. Farokhzad, O. C.; Langer, R. Nanomedicine: Developing smarter therapeutic and diagnostic modalities. *Adv. Drug Deliv. Rev.*, **2006**, *58*, 1456-1459.
2. Bangham, A. D.; Standish, M. M.; Watkins, J. C. Diffusion of univalent ions across the lamellae of swollen phospholipids. *J. Mol. Biol.*, **1965**, *13*, 238-252.
3. Ferrari, M. Cancer nanotechnology: opportunities and challenges. *Nat. Rev. Cancer*, **2005**, *5*, 161-171.
4. Brannon-Peppas, L.; Blanchette, J. O. Nanoparticle and targeted systems for cancer therapy. *Adv. Drug Deliv. Rev.*, **2004**, *56*, 1649-1659.
5. Langer, R. Drug delivery and targeting. *Nature*, **1998**, *392*, 5-10.
6. Jain, K. K. Editorial: targeted drug delivery for cancer. *Technol. Cancer Res. Treat.*, **2005**, *4*, 311-313.
7. Cavalcanti, L. P.; Konovalov, O.; Torriani, I. L.; Haas, H. Drug loading to lipid-based cationic nanoparticles. *Nucl. Instrum. Meth. B,* **2005**, *238*, 290-293.
8. Smith, A. M.; Gao, X.; Nie, S. Quantum dot nanocrystals for in vivo molecular and cellular imaging. *Photochem. Photobiol.,* **2004**, *80*, 377-385.
9. Han, G.; Ghosh, P.; Rotello, V. M. Functionalized gold nanoparticles for drug delivery. *Nanomedicine*, **2007**, *2*, 113-123.
10. McCarthy, J. R.; Kelly, K. A.; Sun, E. Y.; Weissleder, R. Targeted delivery of multifunctional magnetic nanoparticles. *Nanomedicine*, **2007**, *2*, 153-167.
11. Bianco, A.; Hoebeke, J.; Kostarelos, K.; Prato, M.; Partidos, C. D. Carbon nanotubes: On the road to deliver. *Curr. Drug Deliv.*, **2005**, *2*, 253-259.
12. Jain, N. K.; Asthana, A. Dendritic systems in drug delivery applications. *Expert Opin. Drug Deliv.*, **2007**, *4*, 495-512.
13. Yevdokimov, Y. M.; Skuridin, S. G.; Nechipurenko, Y. D.; Zakharov, M. A.; Salyanov, V. I.; Kurnosov, A. A.; Kuznetsov, V. D.; Nikiforov, V. N. Nanoconstructions based on double-stranded nucleic acids. *Int. J. Biol. Macromol.*, **2005**, *36*, 103-115.
14. Singh, P.; Destito, G.; Schneemann, A.; Manchester, M. Canine parvovirus-like particles, a novel nanomaterial for tumor targeting. *J. Nanobiotechnol.*, **2006**, *4*, 2.
15. Pathak, P.; Katiyar, V. K. Multi-functional nanoparticles and their role in cancer drug delivery - a review. *Online J. Nanotechnol.*, **2007**, *3*, No pp given.
16. Maeda, H.; Matsumura, Y.; Oda, T.; Sasamoto, K. Cancer selective macromolecular therapeusis: tailoring of an antitumor protein drug. *Am. Chem. Soc. Symp.*, **1986**, 353-382.
17. Haag, R.; Kratz, F. Polymer therapeutics: concepts and applications. *Angew. Chem. Int. Ed.*, **2006**, *45*, 1198-1215.
18. Maeda, H.; Sawa, T.; Konno, T. Mechanism of tumor-targeted delivery of macromolecular drugs, including the EPR effect in solid tumor and clinical overview of the prototype polymeric drug SMANCS. *J. Controlled Release*, **2001**, *74*, 47-61.
19. Luo, Y.; Bernshaw, N. J.; Lu, Z.-R.; Kopecek, J.; Prestwich, G. D. Targeted delivery of doxorubicin by HPMA copolymer-hyaluronan bioconjugates. *Pharm. Res.*, **2002**, *19*, 396-402.

20. Harries, M.; Ellis, P.; Harper, P. Nanoparticle albumin-bound paclitaxel for metastatic breast cancer. *J. Clin. Oncol.*, **2005**, *23*, 7768-7771.
21. Grinstaff, M. W.; Soon-Shiong, P.; Wong, M.; Sandford, P. A.; Suslick, K. S.; Desai, N. P. Methods for the preparation of pharmaceutically active agents for in vivo delivery. 5665382, 19950607, **1997**.
22. Ibrahim, N. K.; Desai, N.; Legha, S.; Soon-Shiong, P.; Theriault, R. L.; Rivera, E.; Esmaeli, B.; Ring, S. E.; Bedikian, A.; Hortobagyi, G. N.; Ellerhorst, J. A. Phase I and pharmacokinetic study of ABI-007, a cremophor-free, protein-stabilized, nanoparticle formulation of paclitaxel. *Clin. Cancer Res.*, **2002**, *8*, 1038-1044.
23. Damascelli, B.; Cantu, G.; Mattavelli, F.; Tamplenizza, P.; Bidoli, P.; Leo, E.; Dosio, F.; Cerrotta, A. M.; Di Tolla, G.; Frigerio, L. F.; Garbagnati, F.; Lanocita, R.; Marchiano, A.; Patelli, G.; Spreafico, C.; Ticha, V.; Vespro, V.; Zunino, F. Intraarterial chemotherapy with polyoxyethylated castor oil free paclitaxel, incorporated in albumin nanoparticles (ABI-007): Phase I study of patients with squamous cell carcinoma of the head and neck and anal canal: preliminary evidence of clinical activity. *Cancer*, **2001**, *92*, 2592-2602.
24. John, T. A.; Vogel, S. M.; Tiruppathi, C.; Malik, A. B.; Minshall, R. D. Quantitative analysis of albumin uptake and transport in the rat microvessel endothelial monolayer. *Am. J. Physiol.*, **2003**, *284*, 187-196.
25. Desai, N. Nanoparticle albumin bound (nab) technology: A nanotechnology platform for biologically interactive drug delivery and targeting. *Abstracts of Papers, 234th ACS National Meeting, Boston, MA, United States, August 19-23, 2007*, **2007**, ORGN-069.
26. Shen, T.; Weissleder, R.; Papisov, M.; Bogdanov, A., Jr.; Brady, T. J. Monocrystalline iron oxide nanocompounds (MION): physicochemical properties. *Magn. Reson. Med.*, **1993**, *29*, 599-604.
27. Harisinghani Mukesh, G.; Barentsz, J.; Hahn Peter, F.; Deserno Willem, M.; Tabatabaei, S.; van de Kaa Christine, H.; de la Rosette, J.; Weissleder, R. Noninvasive detection of clinically occult lymph-node metastases in prostate cancer. *New Engl. J. Med.*, **2003**, *348*, 2491-2499.
28. Gao, X.; Nie, S. Molecular profiling of single cells and tissue specimens with quantum dots. *Trends Biotechnol.*, **2003**, *21*, 371-373.
29. Alivisatos, A. P. Semiconductor clusters, nanocrystals, and quantum dots. *Science*, **1996**, *271*, 933-937.
30. Talapin, D. V.; Rogach, A. L.; Kornowski, A.; Haase, M.; Weller, H. Highly Luminescent Monodisperse CdSe and CdSe/ZnS Nanocrystals Synthesized in a Hexadecylamine-Trioctylphosphine Oxide-Trioctylphosphine Mixture. *Nano Lett.*, **2001**, *1*, 207-211.
31. Gao, X.; Cui, Y.; Levenson, R. M.; Chung, L. W. K.; Nie, S. In vivo cancer targeting and imaging with semiconductor quantum dots. *Nat. Biotechnol.*, **2004**, *22*, 969-976.
32. Han, M.; Gao, X.; Su, J. Z.; Nie, S. Quantum-dot-tagged microbeads for multiplexed optical coding of biomolecules. *Nat. Biotechnol.*, **2001**, *19*, 631-635.
33. Rosenthal, S. J. Bar-coding biomolecules with fluorescent nanocrystals. *Nat. Biotechnol.*, **2001**, *19*, 621-622.

34. Murray, C. B.; Norris, D. J.; Bawendi, M. G. Synthesis and characterization of nearly monodisperse CdE (E = sulfur, selenium, tellurium) semiconductor nanocrystallites. *J. Am. Chem. Soc.*, **1993**, *115*, 8706-8715.
35. Chan, W. C. W.; Nile, S. Quantum dot bioconjugates for ultrasensitive nonisotopic detection. *Science,* **1998**, *281*, 2016-2018.
36. Wu, X.; Liu, H.; Liu, J.; Haley, K. N.; Treadway, J. A.; Larson, J. P.; Ge, N.; Peale, F.; Bruchez, M. P. Immunofluorescent labeling of cancer marker Her2 and other cellular targets with semiconductor quantum dots. *Nat. Biotechnol.*, **2003**, *21*, 41-46.
37. Akerman, M. E.; Chan, W. C. W.; Laakkonen, P.; Bhatia, S. N.; Ruoslahti, E. Nanocrystal targeting in vivo. *Proc. Nat. Acad. Sci. U. S. A.*, **2002**, *99*, 12617-12621.
38. Iijima, S. Helical microtubules of graphitic carbon. *Nature*, **1991**, *354*, 56-58.
39. Kraetschmer, W.; Lamb, L. D.; Fostiropoulos, K.; Huffman, D. R. Solid C60: a new form of carbon. *Nature*, **1990**, *347*, 354-358.
40. Ajayan, P. M.; Ebbesen, T. W.; Ichihashi, T.; Iijima, S.; Tanigaki, K.; Hiura, H. Opening carbon nanotubes with oxygen and implications for filling. *Nature*, **1993**, *362*, 522-525.
41. Ebbesen, T. W.; Ajayan, P. M. Large-scale synthesis of carbon nanotubes. *Nature*, **1992**, *358*, 220-222.
42. Guo, T.; Nikolaev, P.; Rinzler, A. G.; Tomanek, D.; Colbert, D. T.; Smalley, R. E. Self-Assembly of Tubular Fullerenes. *J. Phys. Chem.*, **1995**, *99*, 10694-10697.
43. Guo, T.; Nikolaev, P.; Thess, A.; Colbert, D. T.; Smalley, R. E. Catalytic growth of single-walled nanotubes by laser vaporization. *Chem. Phys. Lett.*, **1995**, *243*, 49-54.
44. Jose-Yacaman, M.; Miki-Yoshida, M.; Rendon, L.; Santiesteban, J. G. Catalytic growth of carbon microtubules with fullerene structure. *Appl. Phys. Lett.*, **1993**, *62*, 657-659.
45. Chiang, I. W.; Brinson, B. E.; Huang, A. Y.; Willis, P. A.; Bronikowski, M. J.; Margrave, J. L.; Smalley, R. E.; Hauge, R. H. Purification and Characterization of Single-Wall Carbon Nanotubes (SWNTs) Obtained from the Gas-Phase Decomposition of CO (HiPco Process). *J. Phys. Chem. B*, **2001**, *105*, 8297-8301.
46. Hirsch, A. Functionalization of single-walled carbon nanotubes. *Angew. Chem. Int. Ed.*, **2002**, *41*, 1853-1859.
47. Banerjee, S.; Kahn, M. G. C.; Wong, S. S. Rational chemical strategies for carbon nanotube functionalization. *Chem. Eur. J.*, **2003**, *9*, 1898-1908.
48. Baughman, R. H.; Zakhidov, A. A.; de Heer, W. A. Carbon nanotubes-the route toward applications. *Science*, **2002**, *297*, 787-792.
49. Dresselhaus, M. S.; Dresselhaus, G.; Avouris, P.; Editors. Carbon Nanotubes Synthesis, Structure, Properties, and Applications. *Top. Appl. Phys.,* **2001**, *80,* 447.
50. Ajayan, P. M. Nanotubes from Carbon. *Chem. Rev.*, **1999**, *99*, 1787-1799.
51. Kostarelos, K.; Lacerda, L.; Partidos, C. D.; Prato, M.; Bianco, A. Carbon nanotube-mediated delivery of peptides and genes to cells: Translating nanobiotechnology to therapeutics. *J. Drug Deliv. Sci. Technol.*, **2005**, *15*, 41-47.
52. Bianco, A.; Kostarelos, K.; Prato, M. Applications of carbon nanotubes in drug delivery. *Curr. Opin. Chem. Biol.*, **2005**, *9*, 674-679.

53. Pastorin, G.; Kostarelos, K.; Prato, M.; Bianco, A. Functionalized carbon nanotubes: Towards the delivery of therapeutic molecules. *J. Biomed. Nanotechnol.*, **2005**, *1*, 133-142.
54. Bianco, A. Carbon nanotubes for the delivery of therapeutic molecules. *Expert Opin. Drug Deliv.*, **2004**, *1*, 57-65.
55. Lam, C.-w.; James, J. T.; McCluskey, R.; Arepalli, S.; Hunter, R. L. A Review of Carbon Nanotube Toxicity and Assessment of Potential Occupational and Environmental Health Risks. *Crit. Rev. Toxicol.*, **2006**, *36*, 189-217.
56. Donaldson, K.; Stone, V.; Tran, C. L.; Kreyling, W.; Borm, P. J. A. Nanotoxicology. *Occup. Environ. Med.*, **2004**, *61*, 727-728.
57. Sayes, C. M.; Liang, F.; Hudson, J. L.; Mendez, J.; Guo, W.; Beach, J. M.; Moore, V. C.; Doyle, C. D.; West, J. L.; Billups, W. E.; Ausman, K. D.; Colvin, V. L. Functionalization density dependence of single-walled carbon nanotubes cytotoxicity in vitro. *Toxicol. Lett.*, **2006**, *161*, 135-142.
58. Lacerda, L.; Bianco, A.; Prato, M.; Kostarelos, K. Carbon nanotubes as nanomedicines: From toxicology to pharmacology. *Adv. Drug Deliv. Rev.*, **2006**, *58*, 1460-1470.
59. Huczko, A.; Lange, H.; Calko, E.; Grubek-Jaworska, H.; Droszcz, P. Physiological testing of carbon nanotubes: are they asbestos-like? *Fullerene Sci. Technol.*, **2001**, *9*, 251-254.
60. Warheit, D. B.; Laurence, B. R.; Reed, K. L.; Roach, D. H.; Reynolds, G. A. M.; Webb, T. R. Comparative Pulmonary Toxicity Assessment of Single-wall Carbon Nanotubes in Rats. *Toxicol. Sci.*, **2004**, *77*, 117-125.
61. Lam, C.-W.; James, J. T.; McCluskey, R.; Hunter, R. L. Pulmonary Toxicity of Single-Wall Carbon Nanotubes in Mice 7 and 90 Days After Intratracheal Instillation. *Toxicol. Sci.*, **2004**, *77*, 126-134.
62. Muller, J.; Huaux, F.; Moreau, N.; Misson, P.; Heilier, J.-F.; Delos, M.; Arras, M.; Fonseca, A.; Nagy, J. B.; Lison, D. Respiratory toxicity of multi-wall carbon nanotubes. *Toxicol. Appl. Pharmacol.*, **2005**, *207*, 221-231.
63. Shvedova, A. A.; Kisin, E. R.; Mercer, R.; Murray, A. R.; Johnson, V. J.; Potapovich, A. I.; Tyurina, Y. Y.; Gorelik, O.; Arepalli, S.; Schwegler-Berry, D.; Hubbs, A. F.; Antonini, J.; Evans, D. E.; Ku, B.-K.; Ramsey, D.; Maynard, A.; Kagan, V. E.; Castranova, V.; Baron, P. Unusual inflammatory and fibrogenic pulmonary responses to single-walled carbon nanotubes in mice. *Am. J. Physiol.*, **2005**, *289*, 698-708.
64. Radomski, A.; Jurasz, P.; Alonso-Escolano, D.; Drews, M.; Morandi, M.; Malinski, T.; Radomski, M. W. Nanoparticle-induced platelet aggregation and vascular thrombosis. *Br. J. Pharmacol.*, **2005**, *146*, 882-893.
65. Wang, H.; Wang, J.; Deng, X.; Sun, H.; Shi, Z.; Gu, Z.; Liu, Y.; Zhao, Y. Biodistribution of carbon single-wall carbon nanotubes in mice. *J. Nanosci. Nanotechnol.*, **2004**, *4*, 1019-1024.
66. Singh, R.; Pantarotto, D.; Lacerda, L.; Pastorin, G.; Klumpp, C.; Prato, M.; Bianco, A.; Kostarelos, K. Tissue biodistribution and blood clearance rates of intravenously administered carbon nanotube radiotracers. *Proc. Nat. Acad. Sci. U. S. A.*, **2006**, *103*, 3357-3362.

67. Banerjee, S.; Hemraj-Benny, T.; Wong, S. S. Covalent surface chemistry of single-walled carbon nanotubes. *Adv. Mater.*, **2005**, *17*, 17-29.
68. Tasis, D.; Tagmatarchis, N.; Bianco, A.; Prato, M. Chemistry of Carbon Nanotubes. *Chem. Rev.*, **2006**, *106*, 1105-1136.
69. Dieckmann, G. R.; Dalton, A. B.; Johnson, P. A.; Razal, J.; Chen, J.; Giordano, G. M.; Munoz, E.; Musselman, I. H.; Baughman, R. H.; Draper, R. K. Controlled Assembly of Carbon Nanotubes by Designed Amphiphilic Peptide Helices. *J. Am. Chem. Soc.*, **2003**, *125*, 1770-1777.
70. Wang, S.; Humphreys, E. S.; Chung, S.-Y.; Delduco, D. F.; Lustig, S. R.; Wang, H.; Parker, K. N.; Rizzo, N. W.; Subramoney, S.; Chiang, Y.-M.; Jagota, A. Peptides with selective affinity for carbon nanotubes. *Nat. Mater.*, **2003**, *2*, 196-200.
71. Chen, R. J.; Zhang, Y.; Wang, D.; Dai, H. Noncovalent sidewall functionalization of single-walled carbon nanotubes for protein immobilization. *J. Am. Chem. Soc.*, **2001**, *123*, 3838-3839.
72. Kim, O. K.; Je, J.; Baldwin, J. W.; Kooi, S.; Pehrsson, P. E.; Buckley, L. J. Solubilization of Single-Wall Carbon Nanotubes by Supramolecular Encapsulation of Helical Amylose. *J. Am. Chem. Soc.*, **2003**, *125*, 4426-4427.
73. Star, A.; Steuerman, D. W.; Heath, J. R.; Stoddart, J. F. Starched carbon nanotubes. *Angew. Chem. Int. Ed.,* **2002**, *41*, 2508-2512.
74. Kam, N. W. S.; Liu, Z.; Dai, H. Functionalization of Carbon Nanotubes via Cleavable Disulfide Bonds for Efficient Intracellular Delivery of siRNA and Potent Gene Silencing. *J. Am. Chem. Soc.*, **2005**, *127*, 12492-12493.
75. Zheng, M.; Jagota, A.; Semke, E. D.; Diner, B. A.; McLean, R. S.; Lustig, S. R.; Richardson, R. E.; Tassi, N. G. DNA-assisted dispersion and separation of carbon nanotubes. *Nat. Mater.*, **2003**, *2*, 338-342.
76. Zheng, M.; Jagota, A.; Strano, M. S.; Santos, A. P.; Barone, P.; Chou, S. G.; Diner, B. A.; Dresselhaus, M. S.; McLean, R. S.; Onoa, G. B.; Samsonidze, G. G.; Semke, E. D.; Usrey, M.; Walls, D. J. Structure-Based Carbon Nanotube Sorting by Sequence-Dependent DNA Assembly. *Science*, **2003**, *302*, 1545-1548.
77. O'Connell, M. J.; Boul, P.; Ericson, L. M.; Huffman, C.; Wang, Y.; Haroz, E.; Kuper, C.; Tour, J.; Ausman, K. D.; Smalley, R. E. Reversible water-solubilization of single-walled carbon nanotubes by polymer wrapping. *Chem. Phys. Lett.*, **2001**, *342*, 265-271.
78. Star, A.; Stoddart, J. F.; Steuerman, D.; Diehl, M.; Boukai, A.; Wong, E. W.; Yang, X.; Chung, S.-W.; Choi, H.; Heath, J. R. Preparation and properties of polymer-wrapped single-walled carbon nanotubes. *Angew. Chem. Int. Ed.,* **2001**, *40*, 1721-1725.
79. Wang, J.; Musameh, M.; Lin, Y. Solubilization of carbon nanotubes by nafion toward the preparation of amperometric biosensors. *J. Am. Chem. Soc.*, **2003**, *125*, 2408-2409.
80. Kam, N. W. S.; O'Connell, M.; Wisdom, J. A.; Dai, H. Carbon nanotubes as multifunctional biological transporters and near-infrared agents for selective cancer cell destruction. *Proc. Nat. Acad. Sci. U. S. A.*, **2005**, *102*, 11600-11605.

81. Ivanov, V.; Fonesca, A.; Nagy, J. B.; Lucas, A.; Lambin, P.; Bernaerts, D.; Zhang, X. B. Catalytic production and purification of nanotubules having fullerene-scale diameters. *Carbon*, **1995**, *33*, 1727-1738.
82. Liu, J.; Rinzler, A. G.; Dai, H.; Hafner, J. H.; Bradley, R. K.; Boul, P. J.; Lu, A.; Iverson, T.; Shelimov, K.; Huffman, C. B.; Rodriguez-Macias, F.; Shon, Y.-S.; Lee, T. R.; Colbert, D. T.; Smalley, R. E. Fullerene pipes. *Science,* **1998**, *280*, 1253-1256.
83. Nakajima, T.; Kasamatsu, S.; Matsuo, Y. Synthesis and characterization of fluorinated carbon nanotube. *Eur. J. Solid State Inorg. Chem.*, **1996**, *33*, 831-840.
84. Coleman, K. S.; Bailey, S. R.; Fogden, S.; Green, M. L. H. Functionalization of Single-Walled Carbon Nanotubes via the Bingel Reaction. *J. Am. Chem. Soc.*, **2003**, *125*, 8722-8723.
85. Worsley, K. A.; Moonoosawmy, K. R.; Kruse, P. Long-range periodicity in carbon nanotube sidewall functionalization. *Nano Lett.*, **2004**, *4*, 1541-1546.
86. Holzinger, M.; Vostrowsky, O.; Hirsch, A.; Hennrich, F.; Kappes, M.; Weiss, R.; Jellen, F. Sidewall functionalization of carbon nanotubes. *Angew. Chem. Int. Ed.*, **2001**, *40*, 4002-4005.
87. Banerjee, S.; Wong, S. S. Rational Sidewall Functionalization and Purification of Single-Walled Carbon Nanotubes by Solution-Phase Ozonolysis. *J. Phys. Chem. B*, **2002**, *106*, 12144-12151.
88. Banerjee, S.; Hemraj-Benny, T.; Balasubramanian, M.; Fischer, D. A.; Misewich, J. A.; Wong, S. S. Ozonized single-walled carbon nanotubes investigated using NEXAFS spectroscopy. *Chem. Commun.*, **2004**, 772-773.
89. Banerjee, S.; Wong, S. S. Demonstration of Diameter-Selective Reactivity in the Sidewall Ozonation of SWNTs by Resonance Raman Spectroscopy. *Nano Lett.*, **2004**, *4*, 1445-1450.
90. Holzinger, M.; Abraham, J.; Whelan, P.; Graupner, R.; Ley, L.; Hennrich, F.; Kappes, M.; Hirsch, A. Functionalization of Single-Walled Carbon Nanotubes with (R-)Oxycarbonyl Nitrenes. *J. Am. Chem. Soc.,* **2003**, *125*, 8566-8580.
91. Bahr, J. L.; Yang, J.; Kosynkin, D. V.; Bronikowski, M. J.; Smalley, R. E.; Tour, J. M. Functionalization of carbon nanotubes by electrochemical reduction of aryl diazonium salts: A bucky paper electrode. *J. Am. Chem. Soc.*, **2001**, *123*, 6536-6542.
92. Chen, J.; Hamon, M. A.; Hu, H.; Chen, Y.; Rao, A. M.; Eklund, P. C.; Haddon, R. C. Solution properties of single-walled carbon nanotubes. *Science,* **1998**, *282*, 95-98.
93. Liang, F.; Sadana, A. K.; Peera, A.; Chattopadhyay, J.; Gu, Z.; Hauge, R. H.; Billups, W. E. A Convenient Route to Functionalized Carbon Nanotubes. *Nano Lett.*, **2004**, *4*, 1257-1260.
94. Pekker, S.; Salvetat, J. P.; Jakab, E.; Bonard, J. M.; Forro, L. Hydrogenation of Carbon Nanotubes and Graphite in Liquid Ammonia. *J. Phys. Chem. B*, **2001**, *105*, 7938-7943.
95. Peng, H.; Alemany, L. B.; Margrave, J. L.; Khabashesku, V. N. Sidewall Carboxylic Acid Functionalization of Single-Walled Carbon Nanotubes. *J. Am. Chem. Soc.*, **2003**, *125*, 15174-15182.

96. Georgakilas, V.; Kordatos, K.; Prato, M.; Guldi, D. M.; Holzinger, M.; Hirsch, A. Organic functionalization of carbon nanotubes. *J. Am. Chem. Soc.,* **2002**, *124*, 760-761.
97. Tagmatarchis, N.; Prato, M. Functionalization of carbon nanotubes via 1,3-dipolar cycloadditions. *J. Mater. Chem.*, **2004**, *14*, 437-439.
98. Sun, Y.-P.; Zhou, B.; Henbest, K.; Fu, K.; Huang, W.; Lin, Y.; Taylor, S.; Carroll, D. L. Luminescence anisotropy of functionalized carbon nanotubes in solution. *Chem. Phys. Lett.*, **2002**, *351*, 349-353.
99. Bianco, A.; Prato, M. Can carbon nanotubes be considered useful tools for biological applications? *Adv. Mater.*, **2003**, *15*, 1765-1768.
100. Pantarotto, D.; Partidos, C. D.; Hoebeke, J.; Brown, F.; Kramer, E.; Briand, J.-P.; Muller, S.; Prato, M.; Bianco, A. Immunization with Peptide-Functionalized Carbon Nanotubes Enhances Virus-Specific Neutralizing Antibody Responses. *Chem. Biol.*, **2003**, *10*, 961-966.
101. Pantarotto, D.; Singh, R.; McCarthy, D.; Erhardt, M.; Briand, J.-P.; Prato, M.; Kostarelos, K.; Bianco, A. Functionalized carbon nanotubes for plasmid DNA gene delivery. *Angew. Chem. Int. Ed.*, **2004**, *43*, 5242-5246.
102. Wu, W.; Wieckowski, S.; Pastorin, G.; Benincasa, M.; Klumpp, C.; Briand, J.-P.; Gennaro, R.; Prato, M.; Bianco, A. Targeted delivery of amphotericin B to cells by using functionalized carbon nanotubes. *Angew. Chem. Int. Ed.*, **2005**, *44*, 6358-6362.
103. Gao, L.; Nie, L.; Wang, T.; Qin, Y.; Guo, Z.; Yang, D.; Yan, X. Carbon nanotube delivery of the GFP gene into mammalian cells. *ChemBioChem*, **2006**, *7*, 239-242.
104. Kam, N. W. S.; Dai, H. Carbon nanotubes as intracellular protein transporters: Generality and biological functionality. *Journal of the American Chemical Society*, **2005**, *127*, 6021-6026.
105. Kam, N. W. S.; Jessop, T. C.; Wender, P. A.; Dai, H. Nanotube molecular transporters: internalization of carbon nanotube-protein conjugates into mammalian cells. *J. Am. Chem. Soc.*, **2004**, *126*, 6850-6851.
106. Kam, N. W. S.; Liu, Z.; Dai, H. Carbon nanotubes as intracellular transporters for proteins and DNA: an investigation of the uptake mechanism and pathway. *Angew. Chem. Int. Ed.*, **2006**, *45*, 577-581.
107. Vida, T. A.; Emr, S. D. A new vital stain for visualizing vacuolar membrane dynamics and endocytosis in yeast. *J. Cell Biol.*, **1995**, *128*, 779-792.
108. Feazell, R. P.; Nakayama-Ratchford, N.; Dai, H.; Lippard, S. J. Soluble Single-Walled Carbon Nanotubes as Longboat Delivery Systems for Platinum(IV) Anticancer Drug Design. *J. Am. Chem. Soc.*, **2007**, *129*, 8438-8439.
109. Georgakilas, V.; Tagmatarchis, N.; Pantarotto, D.; Bianco, A.; Briand, J.-P.; Prato, M. Amino acid functionalization of water soluble carbon nanotubes. *Chem. Commun.*, **2002**, 3050-3051.
110. Pantarotto, D.; Partidos, C. D.; Graff, R.; Hoebeke, J.; Briand, J.-P.; Prato, M.; Bianco, A. Synthesis, Structural Characterization, and Immunological Properties of Carbon Nanotubes Functionalized with Peptides. *J. Am. Chem. Soc.*, **2003**, *125*, 6160-6164.
111. Kostarelos, K.; Lacerda, L.; Pastorin, G.; Wu, W.; Wieckowski, S.; Luangsivilay, J.; Godefroy, S.; Pantarotto, D.; Briand, J.-P.; Muller, S.; Prato, M.; Bianco, A.

Cellular uptake of functionalized carbon nanotubes is independent of functional group and cell type. *Nat. Nanotechnol.*, **2007**, *2*, 108-113.

112. Hong, S.; Leroueil, P. R.; Majoros, I. J.; Orr, B. G.; Baker, J. R.; Banaszak Holl, M. M. The Binding Avidity of a Nanoparticle-Based Multivalent Targeted Drug Delivery Platform. *Chem. Biol.*, **2007**, *14*, 107-115.
113. Zheng, Z.-B.; Zhu, G.; Tak, H.; Joseph, E.; Eiseman, J. L.; Creighton, D. J. N-(2-Hydroxypropyl)methacrylamide copolymers of a glutathione (GSH)-activated glyoxalase I inhibitor and DNA alkylating agent: synthesis, reaction kinetics with GSH, and in vitro antitumor activities. *Bioconjugate Chem.*, **2005**, *16*, 598-607.
114. Meister, A. Metabolism and transport of glutathione and other g-glutamyl compounds. Funct. Glutathione: Biochem., Physiol., Toxicol., Clin. Aspects, *Karolinska Inst. Nobel Conf., 5th*, **1983**, 1-22.
115. Jordan, M. A.; Ojima, I.; Rosas, F.; Distefano, M.; Wilson, L.; Scambia, G.; Ferlini, C. Effects of Novel Taxanes SB-T-1213 and IDN5109 on Tubulin Polymerization and Mitosis. *Chem. Biol.*, **2002**, *9*, 93-101.
116. Nogales, E.; Wolf, S. G.; Khan, I. A.; Luduena, R. F.; Downing, K. H. Structure of tubulin at 6.5 A and location of the taxol-binding site. *Nature*, **1995**, *375*, 424-427.
117. Sarin, V. K.; Kent, S. B. H.; Tam, J. P.; Merrifield, R. B. Quantitative monitoring of solid-phase peptide synthesis by the ninhydrin reaction. *Anal. Biochem.*, **1981**, *117*, 147-157.
118. Zhu, Y.; Peng, A. T.; Carpenter, K.; Maguire, J. A.; Hosmane, N. S.; Takagaki, M. Substituted carborane-appended water-soluble single-wall carbon nanotubes: new approach to boron neutron capture therapy drug delivery. *J. Am. Chem. Soc.*, **2005**, *127*, 9875-9880.
119. Russell-Jones, G.; McTavish, K.; McEwan, J.; Rice, J.; Nowotnik, D. Vitamin-mediated targeting as a potential mechanism to increase drug uptake by tumors. *J. Inorg. Biochem.*, **2004**, *98*, 1625-1633.
120. Russell-Jones, G.; McEwan, J. Amplification of biotin-mediated targeting. 2004045647, 20031121, **2004**.
121. Balamurugan, K.; Vaziri, N. D.; Said, H. M. Biotin uptake by human proximal tubular epithelial cells: cellular and molecular aspects. *Am. J. Physiol. Renal Physiol.*, **2005**, *288*, 823-831.
122. Becker, J. M.; Wilchek, M.; Katchalski, E. Irreversible Inhibition of Biotin Transport in Yeast by Biotinyl-p-nitrophenyl Ester. *Proc. Nat. Acad. Sci. U. S. A.*, **1971**, *68*, 2604-2607.
123. Broxterman, H. J.; Georgopapadakou, N. H. Anticancer therapeutics: "addictive" targets, multi-targeted drugs, new drug combinations. *Drug Resist. Updat.*, **2005**, *8*, 183-197.
124. Vicent, M. J. Polymer-Drug Conjugates as Modulators of Cellular Apoptosis. *AAPS J.*, **2007**, *9*, 200-207.
125. Herzog, T.; Barret, R. J.; Edwards, R.; Oldham, F. B. Phase II study of paclitaxel poliglumex (PPX)/carboplatin (C) for 1st line induction and maintenance therapy of stage III/IV ovarian or primary peritoneal carcinoma. *J. Clin. Oncol.*, **2005**, *23*, 16 S.

126. Kabanov, A. V. Polymer genomics: an insight into pharmacology and toxicology of nanomedicines. *Adv. Drug Deliv. Rev.*, **2006**, *58*, 1597-1621.
127. Vicent, M. J.; Greco, F.; Nicholson, R. I.; Paul, A.; Griffiths, P. C.; Duncan, R. Polymer therapeutics designed for a combination therapy of hormonedependent cancer. *Angew. Chem. Int. Ed.*, **2005**, *44*, 4061-4066.

Appendices

A1. Appendix Chapter I 165

A2. Appendix Chapter II 169

A3. Appendix Chapter III 172

^{1}H NMR Spectrum of **1-8**

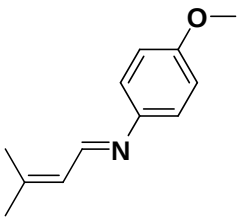

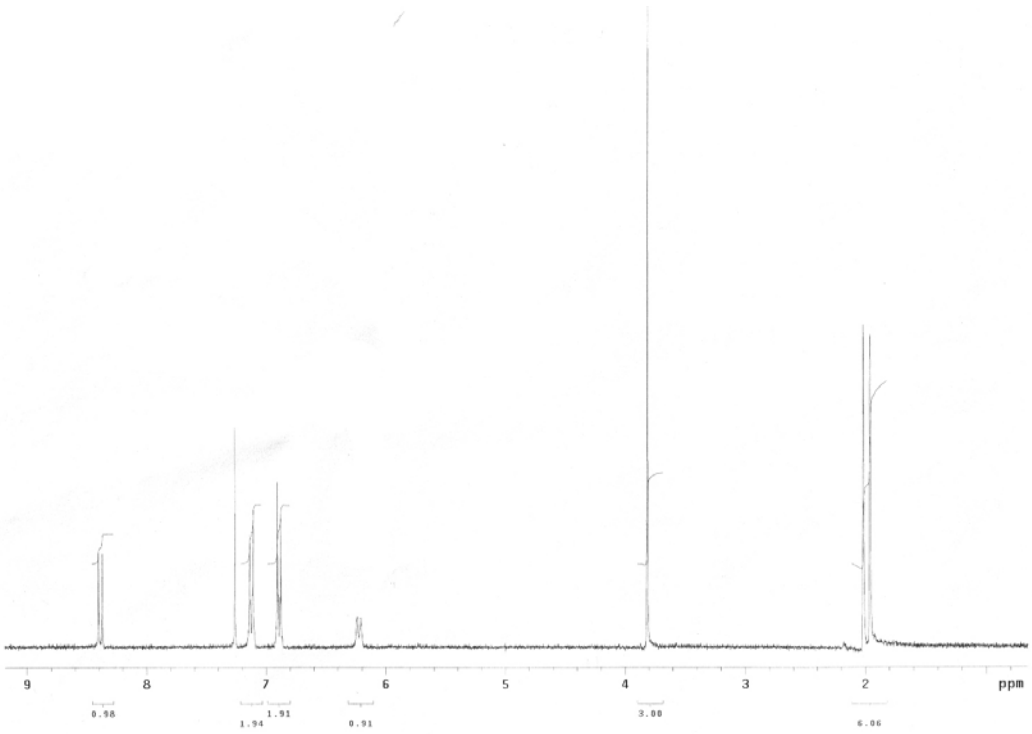

^{1}H NMR Spectrum of **1-9**

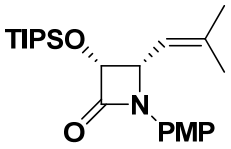

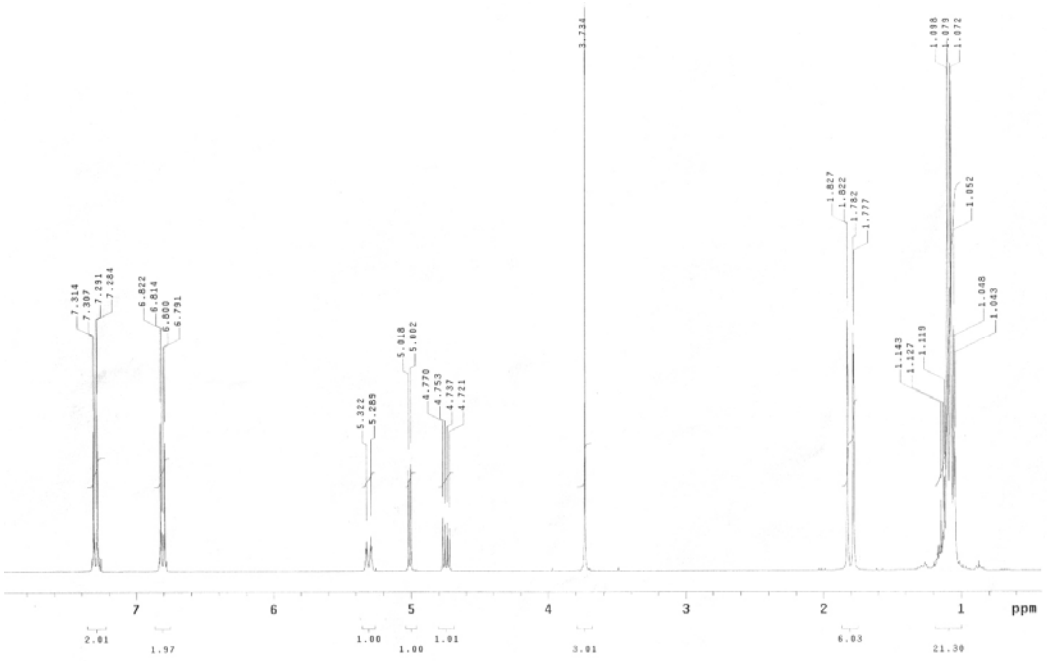

^{1}H NMR Spectrum of **1-23 (SB-T-1214)**

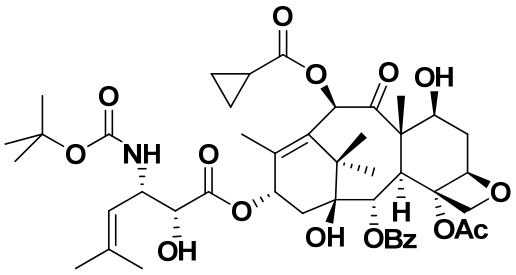

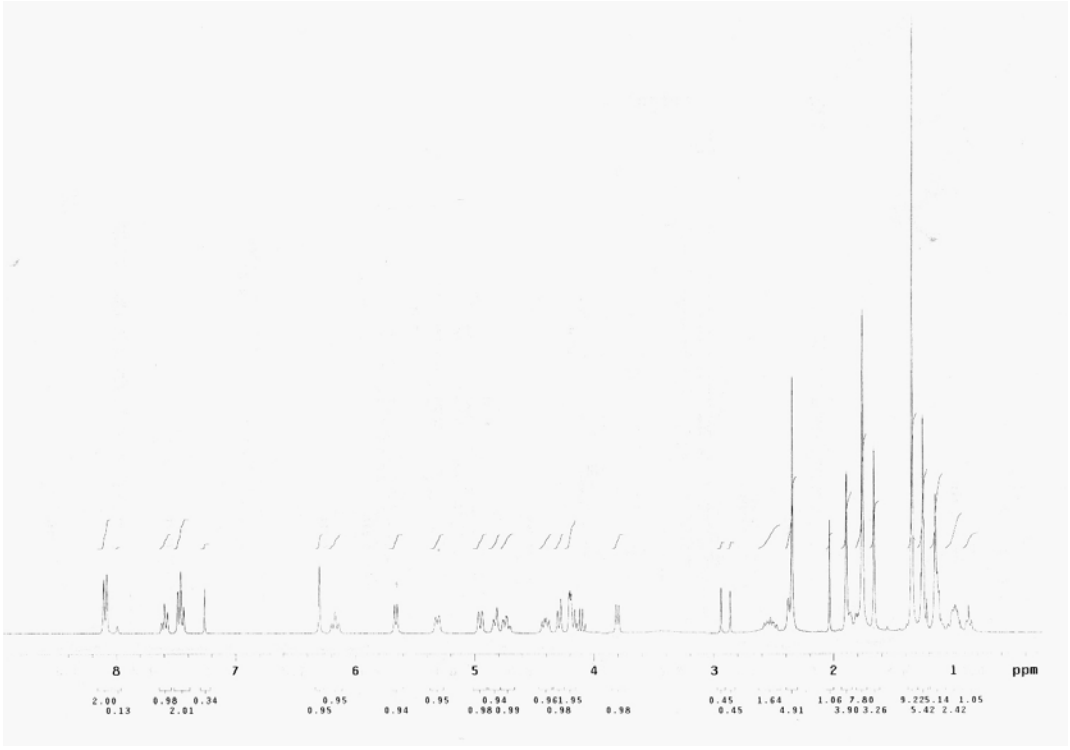

^{13}C NMR Spectrum of **1-23 (SB-T-1214)**

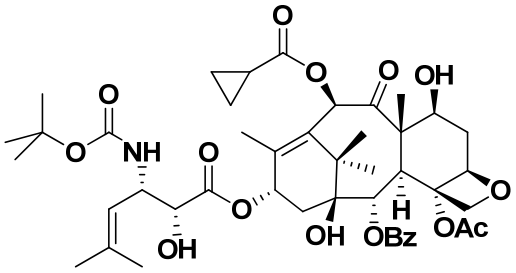

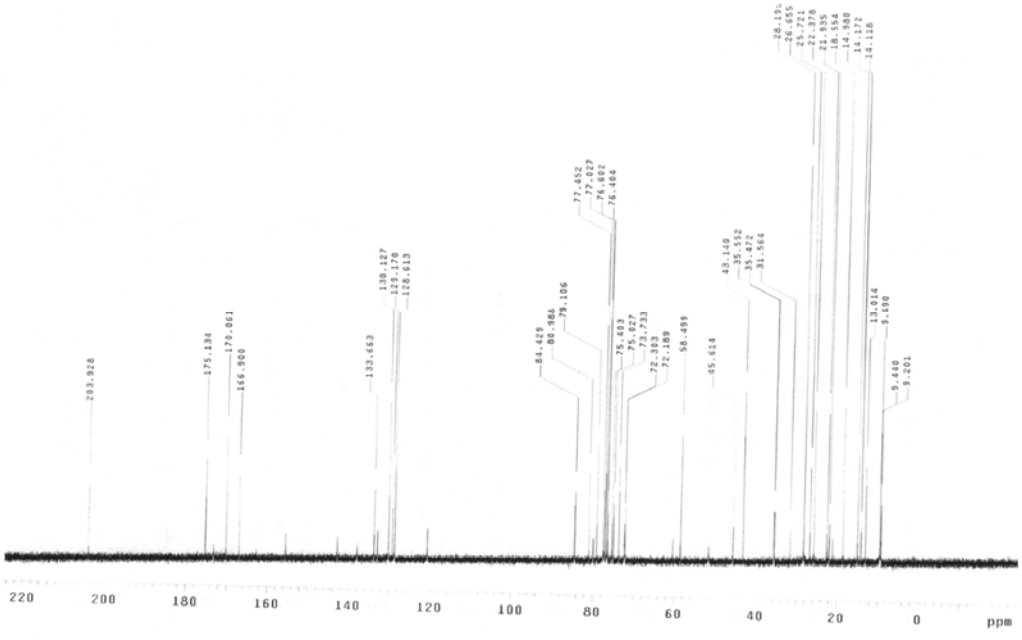

^{1}H NMR Spectrum of **2-2**

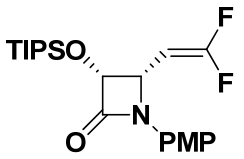

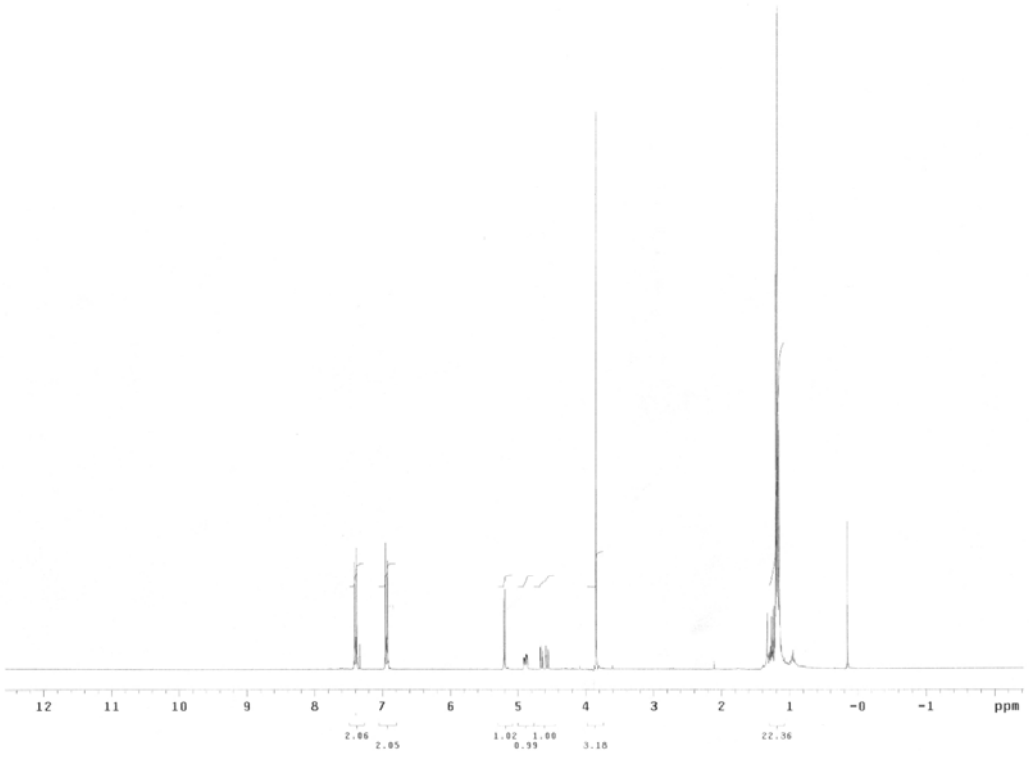

^{1}H NMR Spectrum of **2-5**

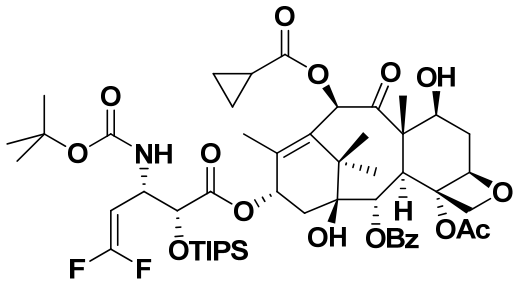

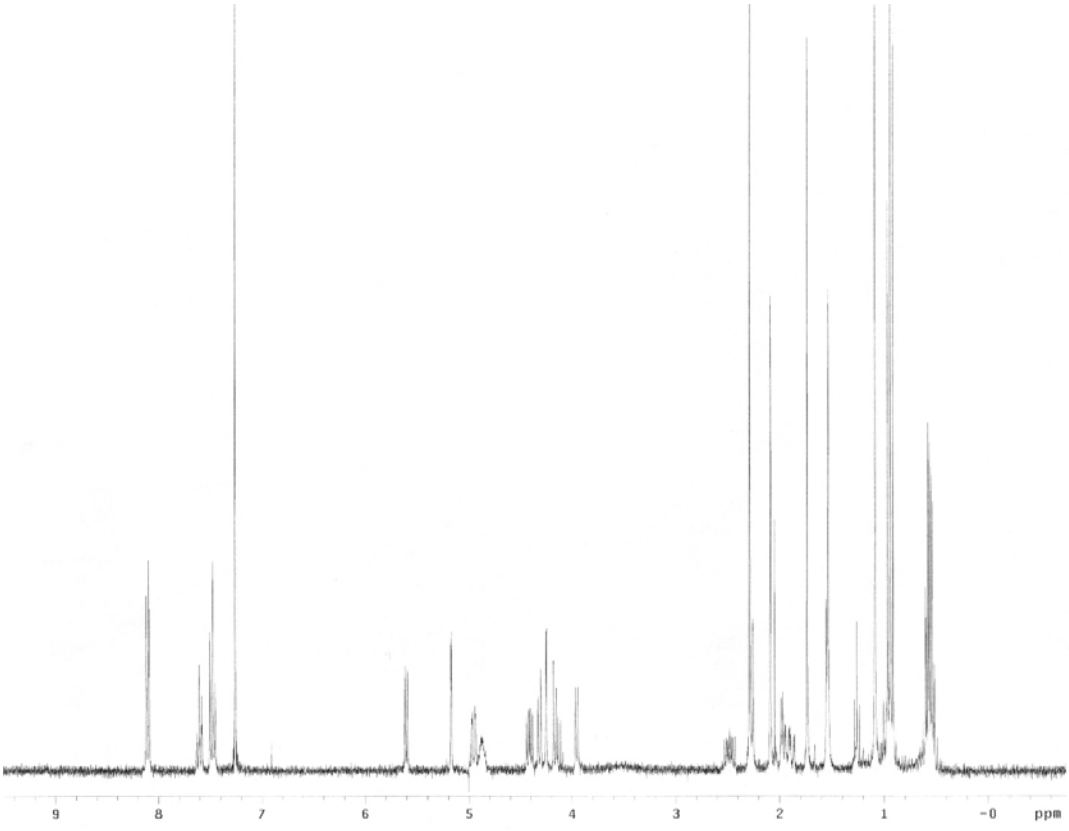

^{1}H NMR Spectrum of **2-6 (SB-T-12852)**

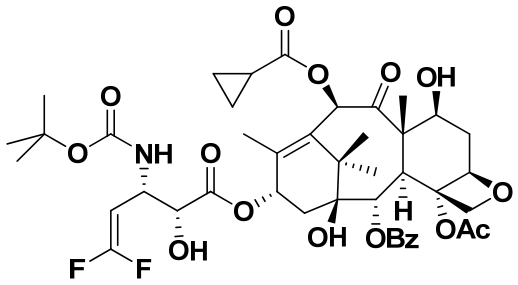

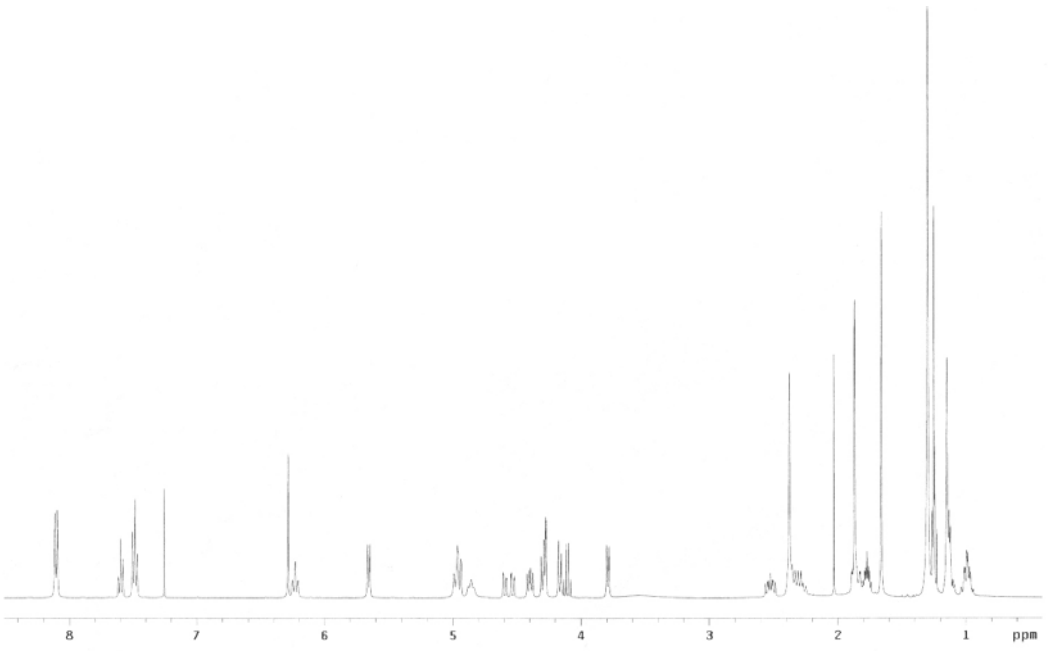

^{1}H NMR Spectrum of **3-1**

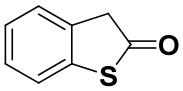

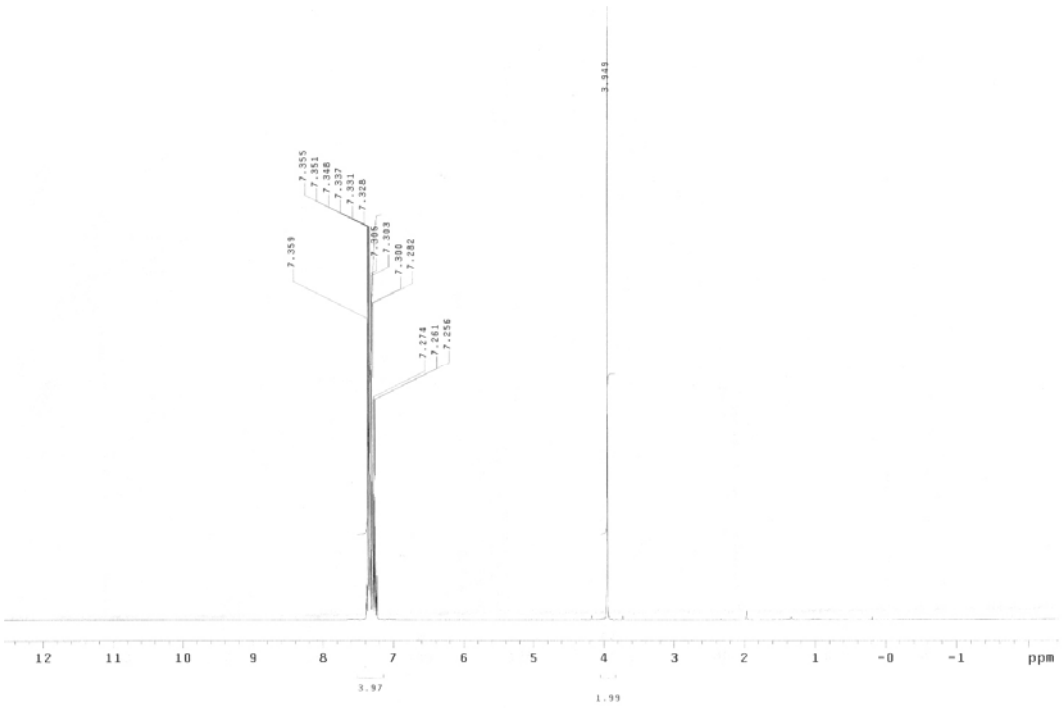

^{13}C NMR Spectrum of **3-1**

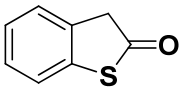

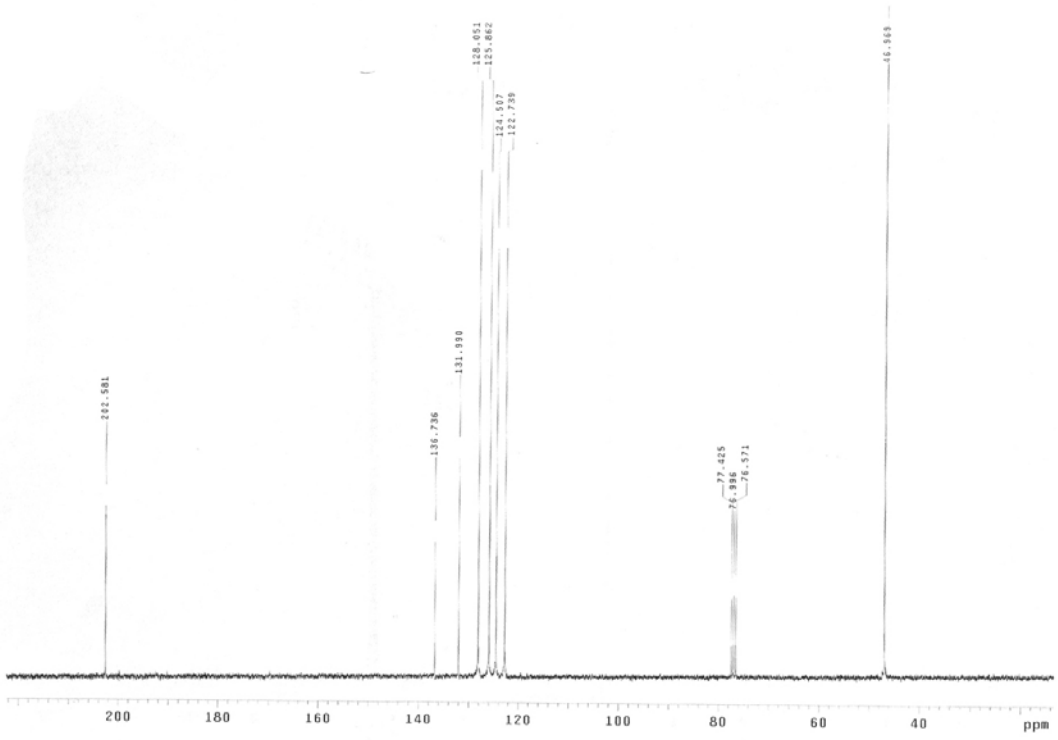

^{1}H NMR Spectrum of **3-2**

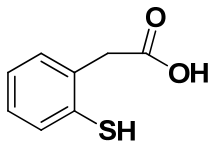

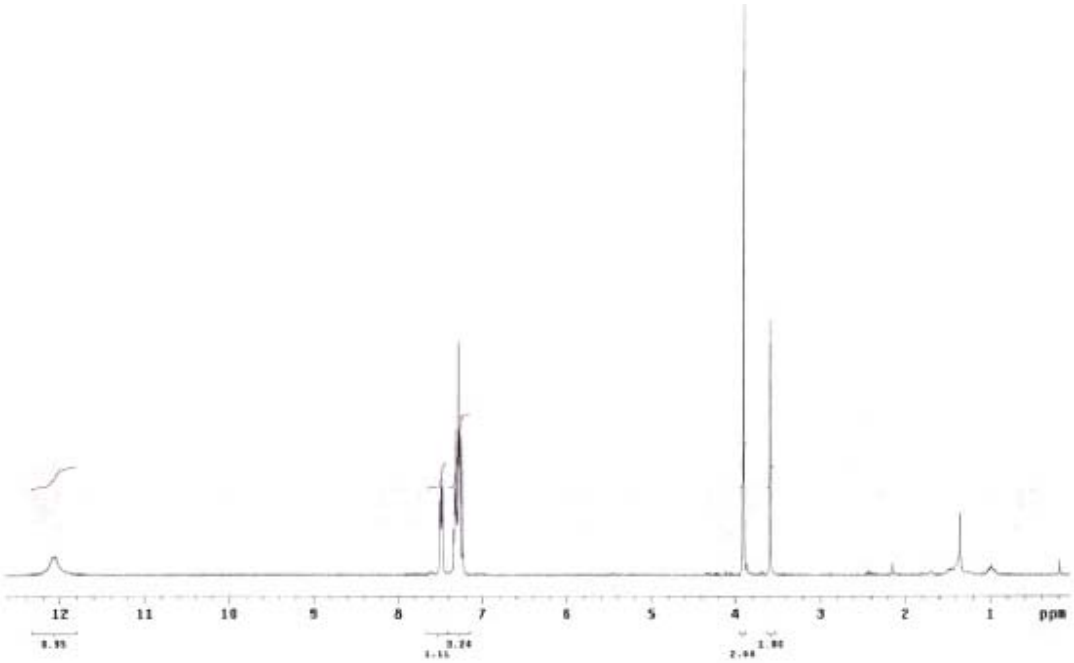

^{1}H NMR Spectrum of **3-5**

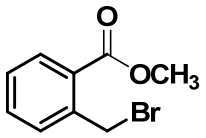

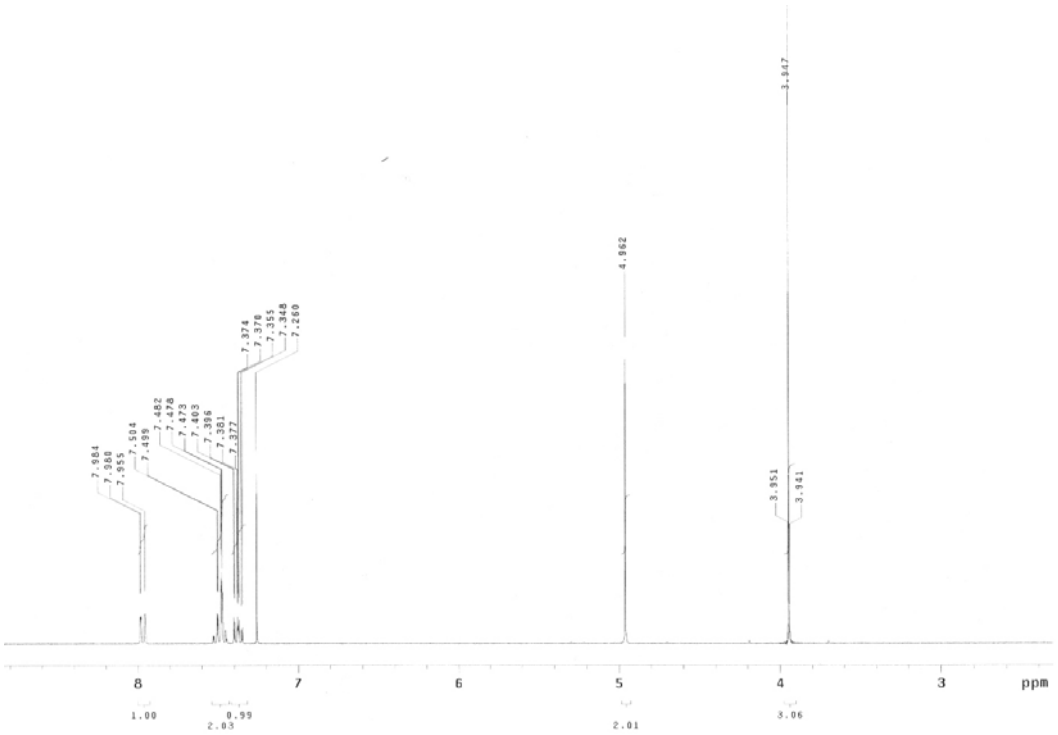

^{1}H NMR Spectrum of **3-7**

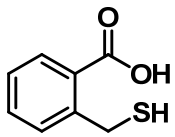

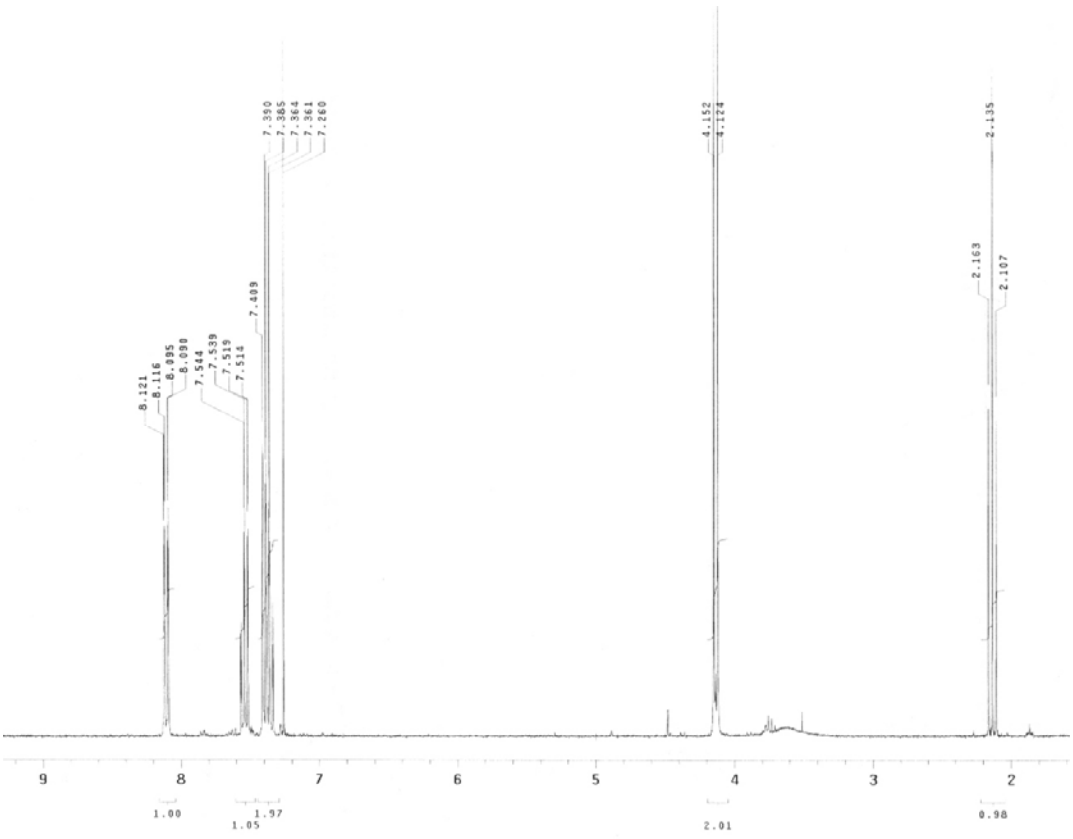

^{1}H NMR Spectrum of **3-8**

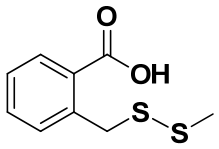

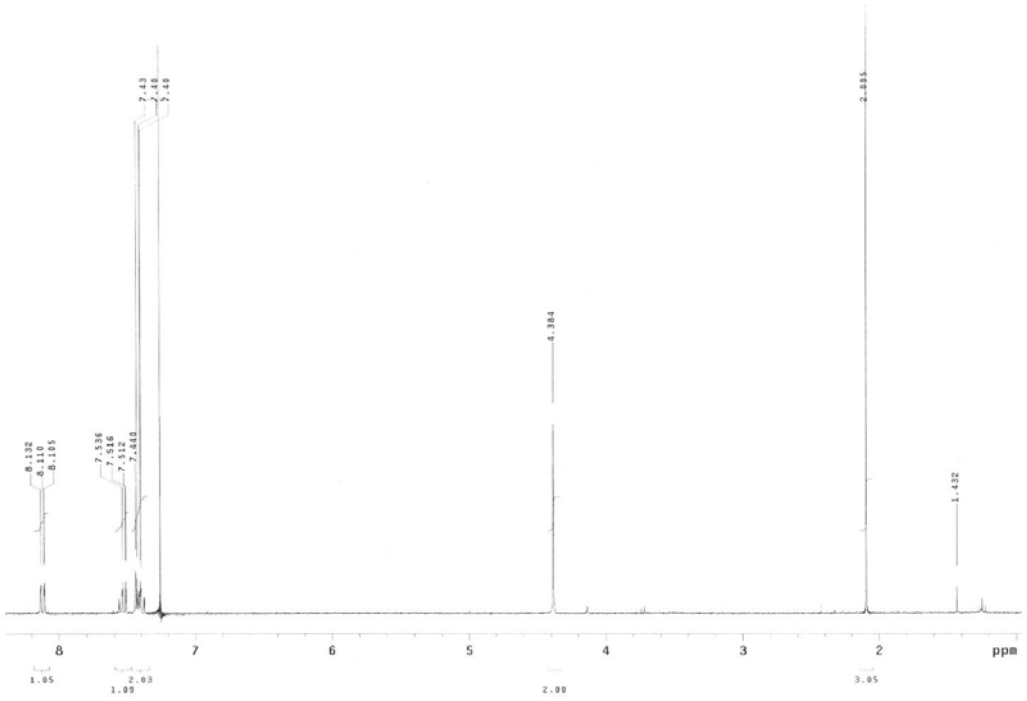

^{1}H NMR Spectrum of **3-9**

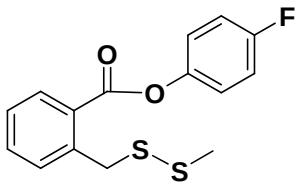

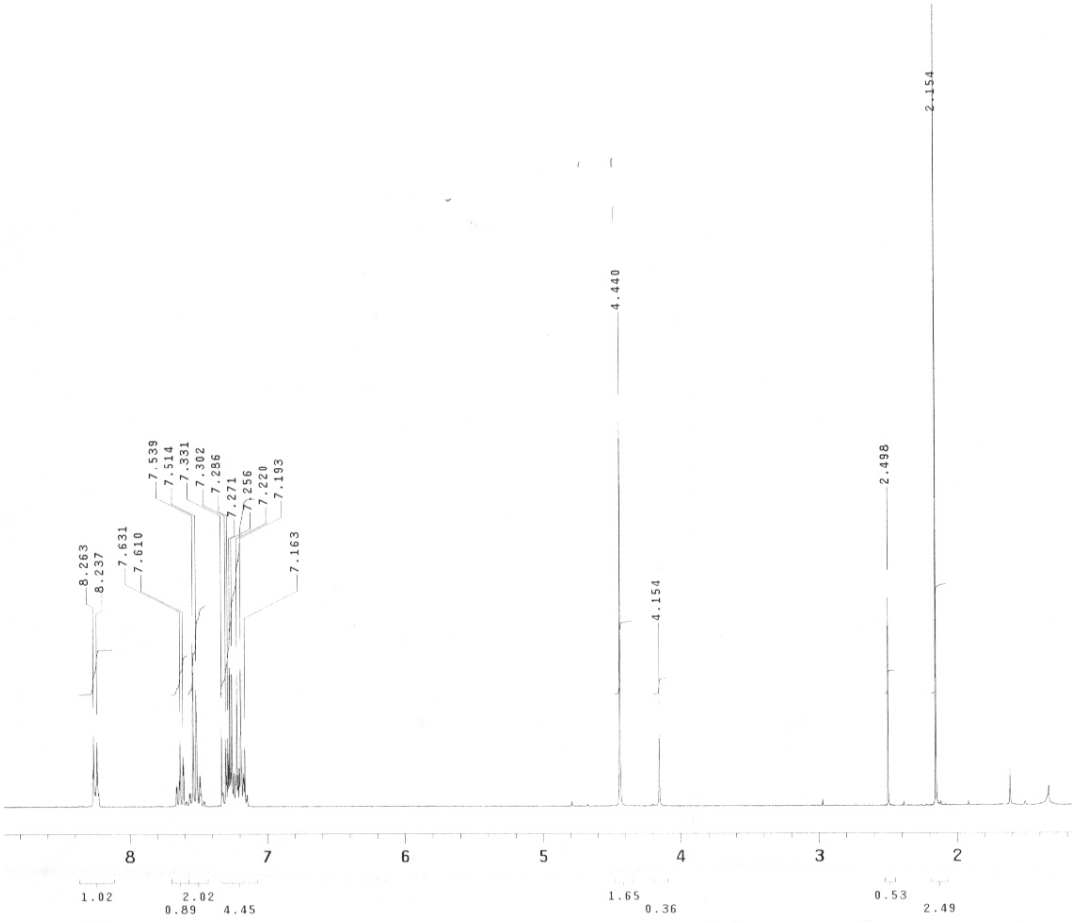

^{19}F NMR Spectrum of **3-9**

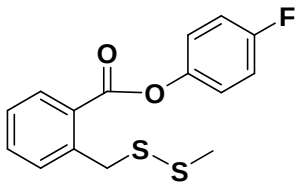

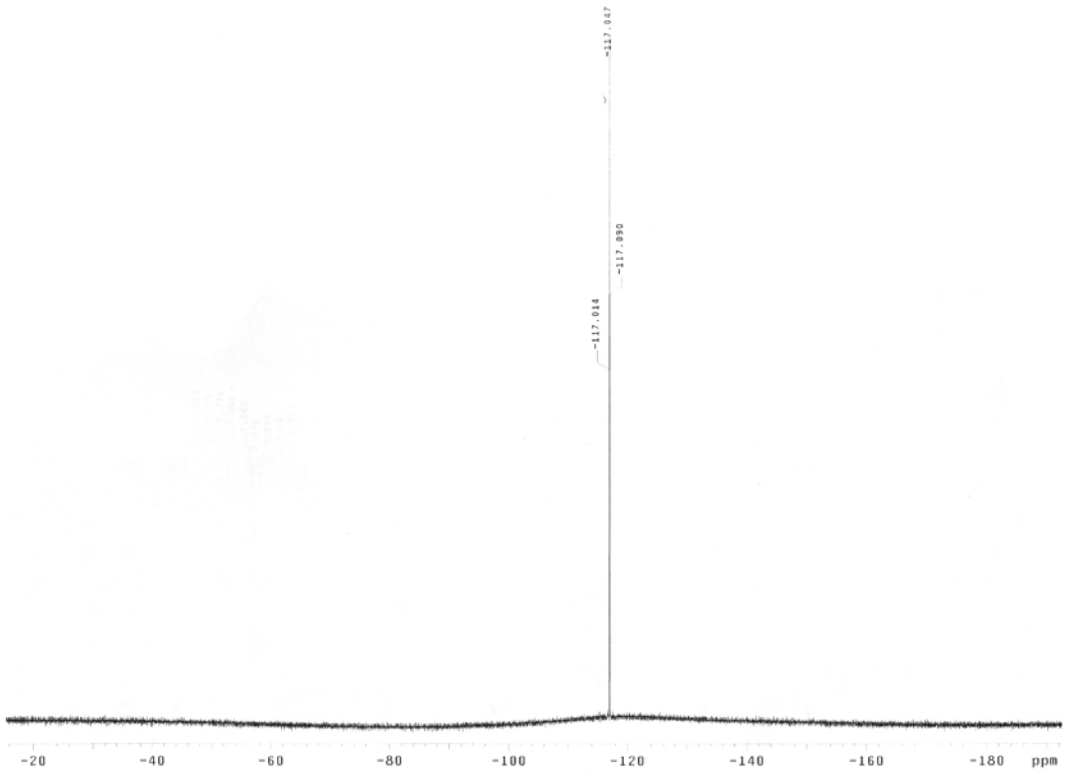

^{1}H NMR Spectrum of **3-10**

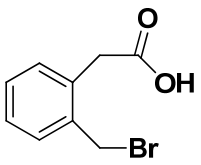

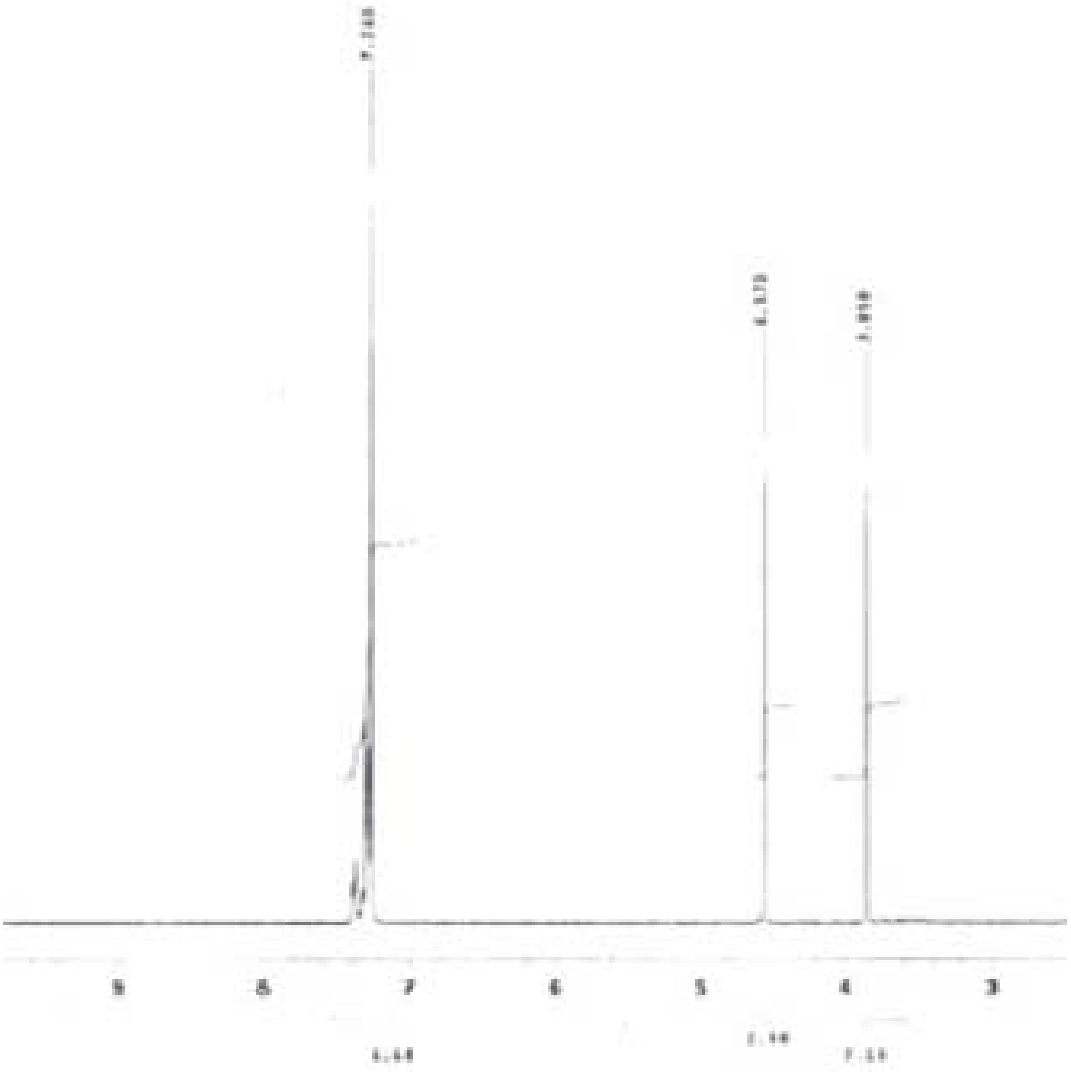

^{13}C NMR Spectrum of **3-10**

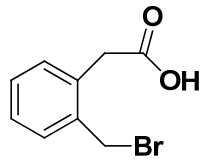

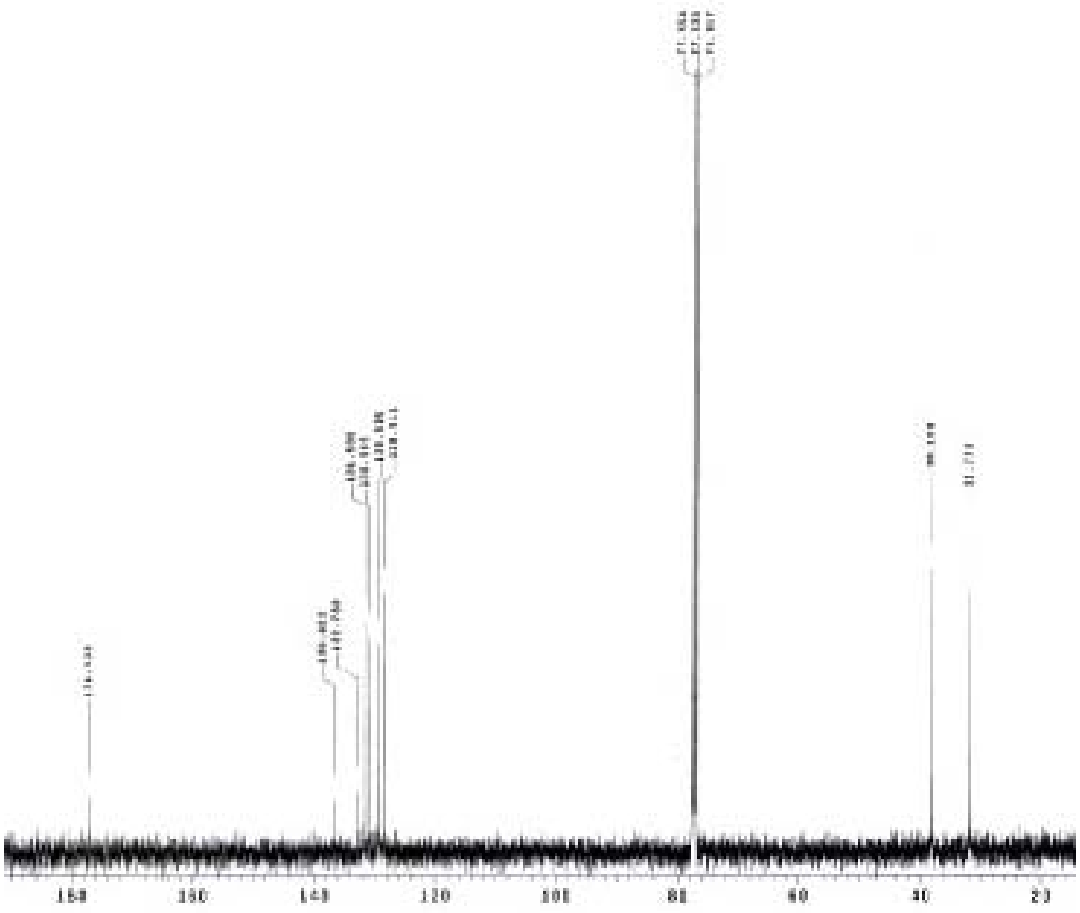

^{1}H NMR Spectrum of **3-11**

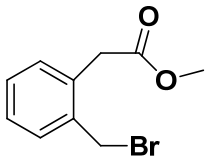

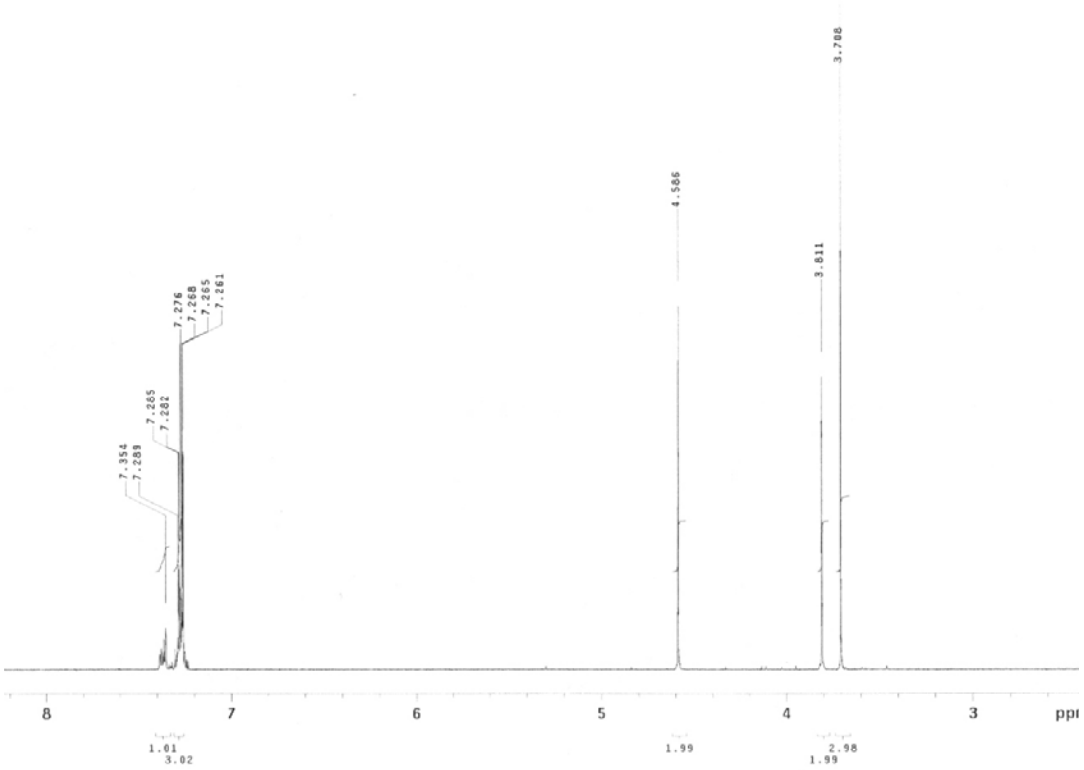

^{13}C NMR Spectrum of **3-11**

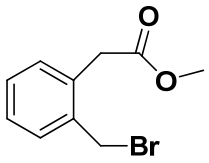

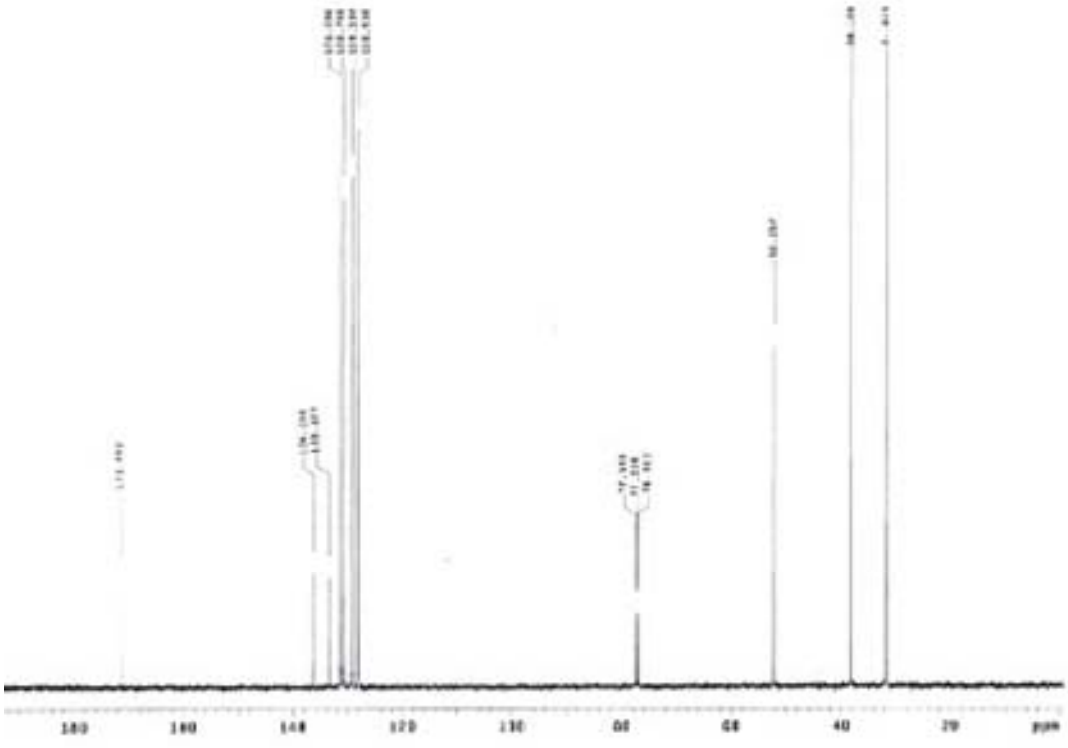

^{1}H NMR Spectrum of **3-12**

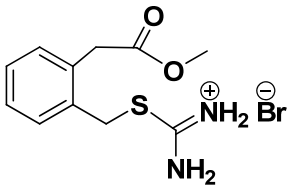

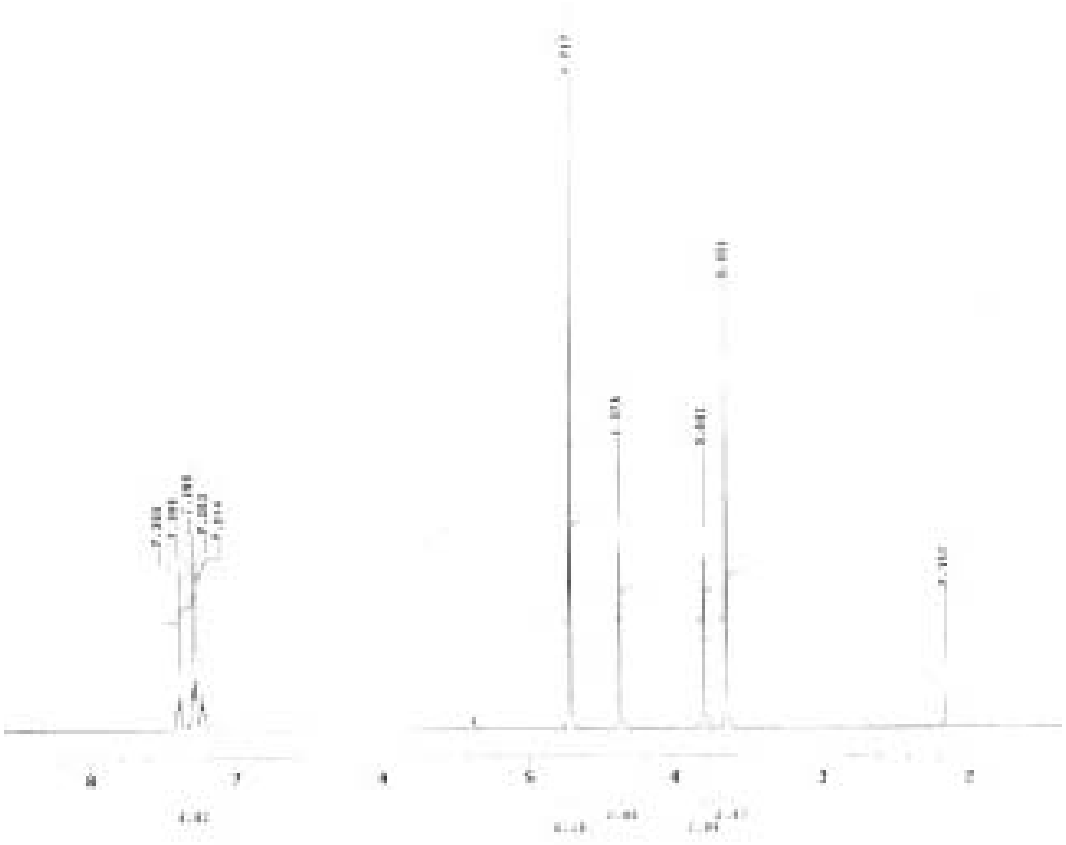

^{13}C NMR Spectrum of **3-12**

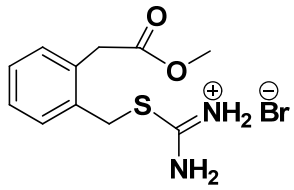

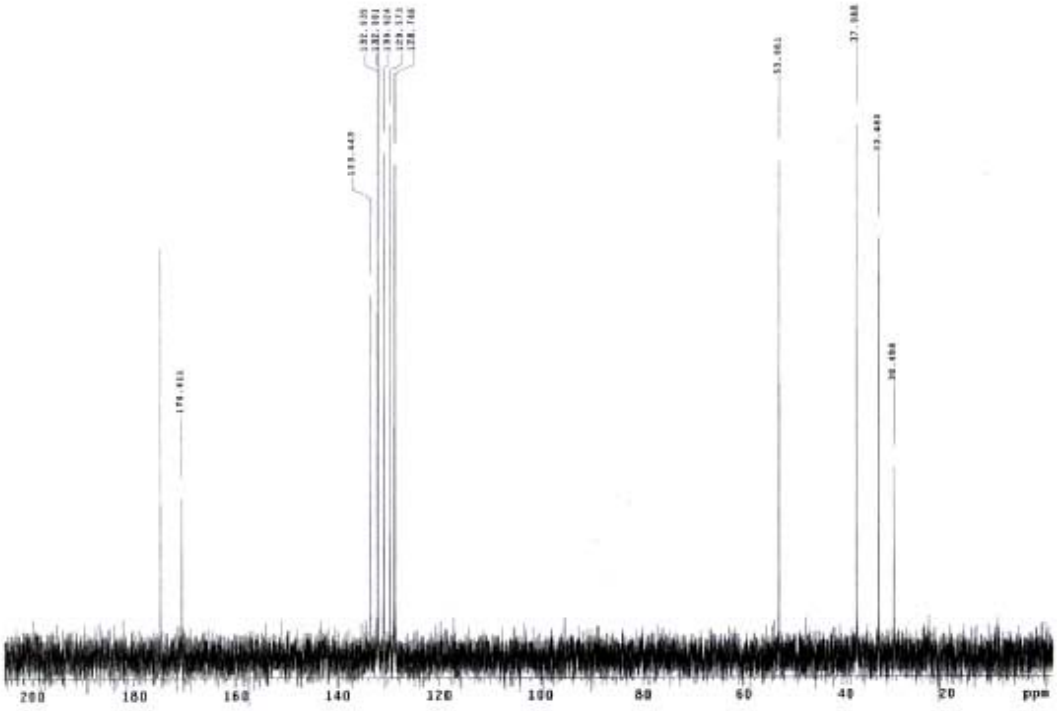

^{1}H NMR Spectrum of **3-13**

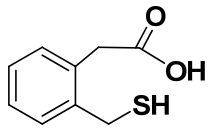

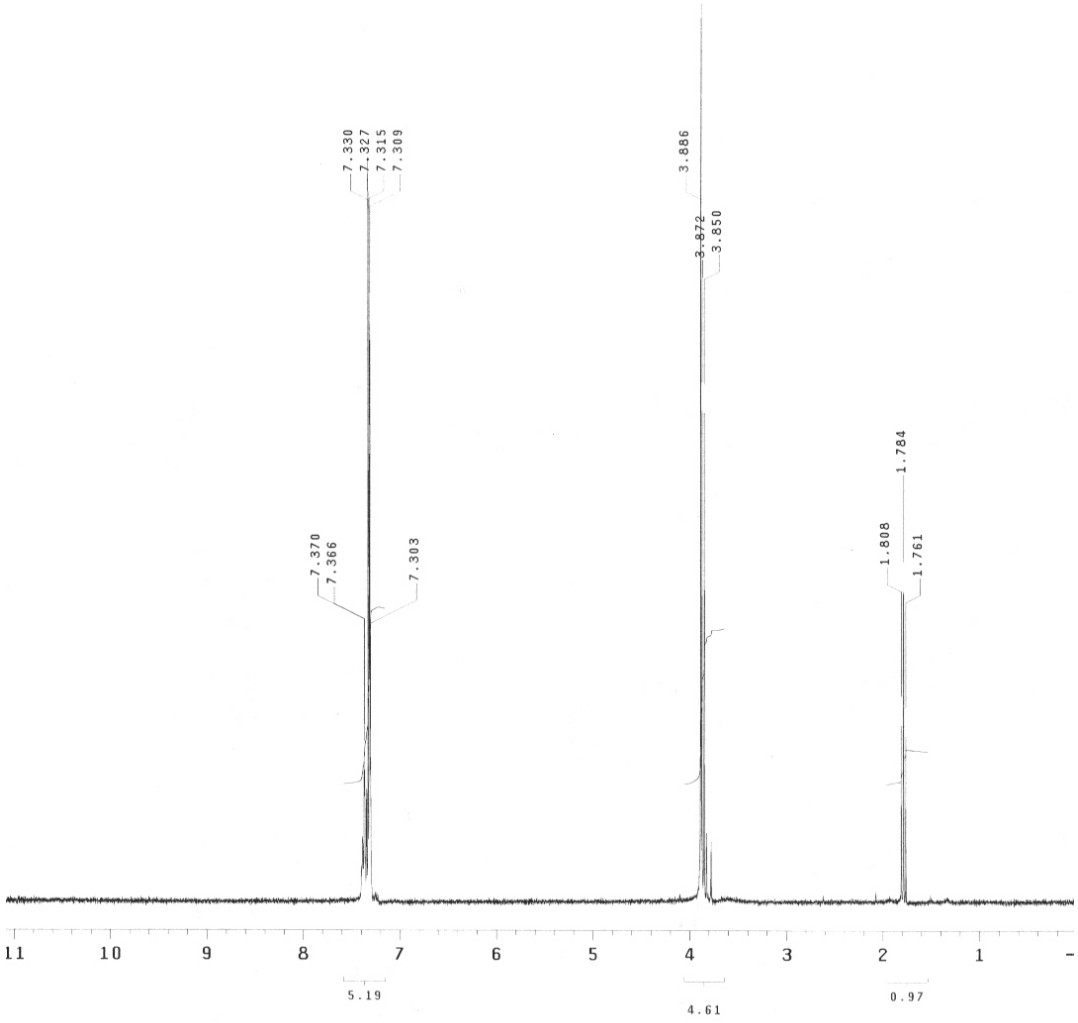

^{1}H NMR Spectrum of **3-14**

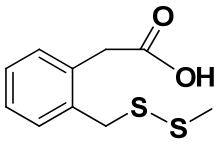

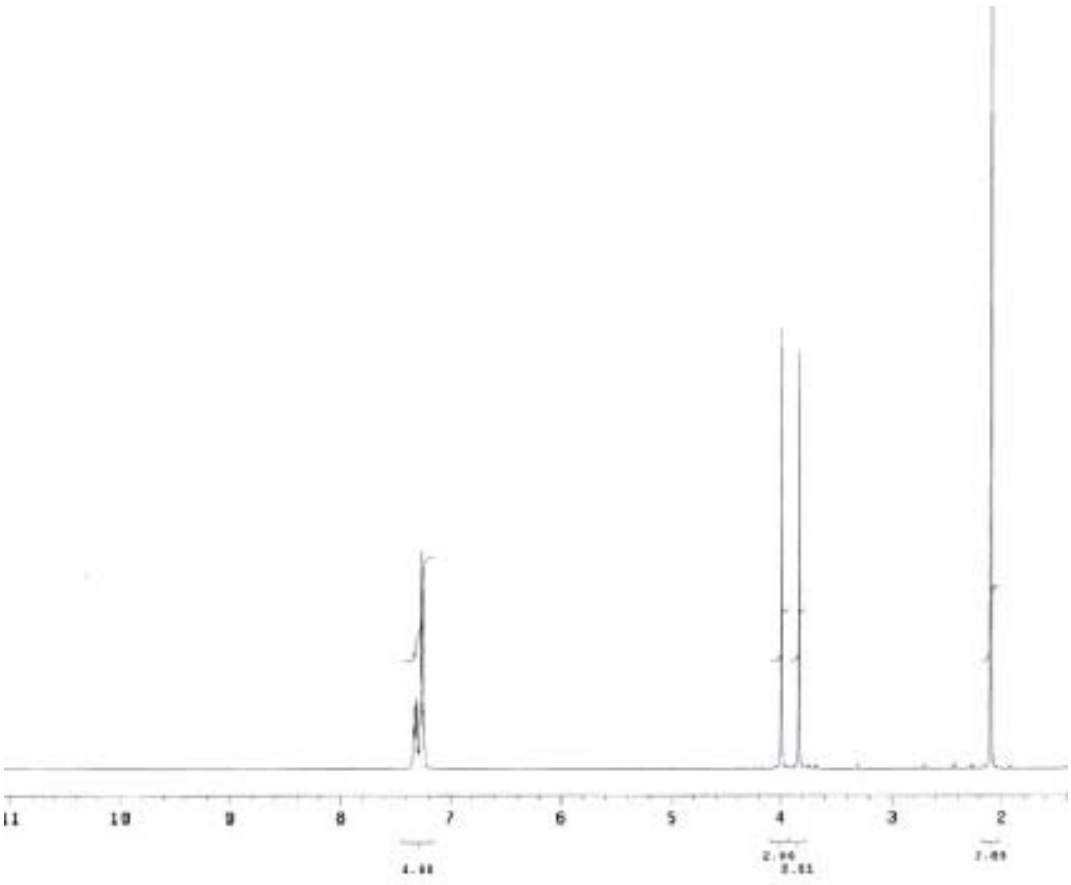

^{13}C NMR Spectrum of **3-14**

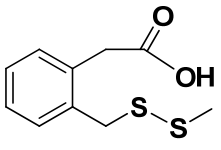

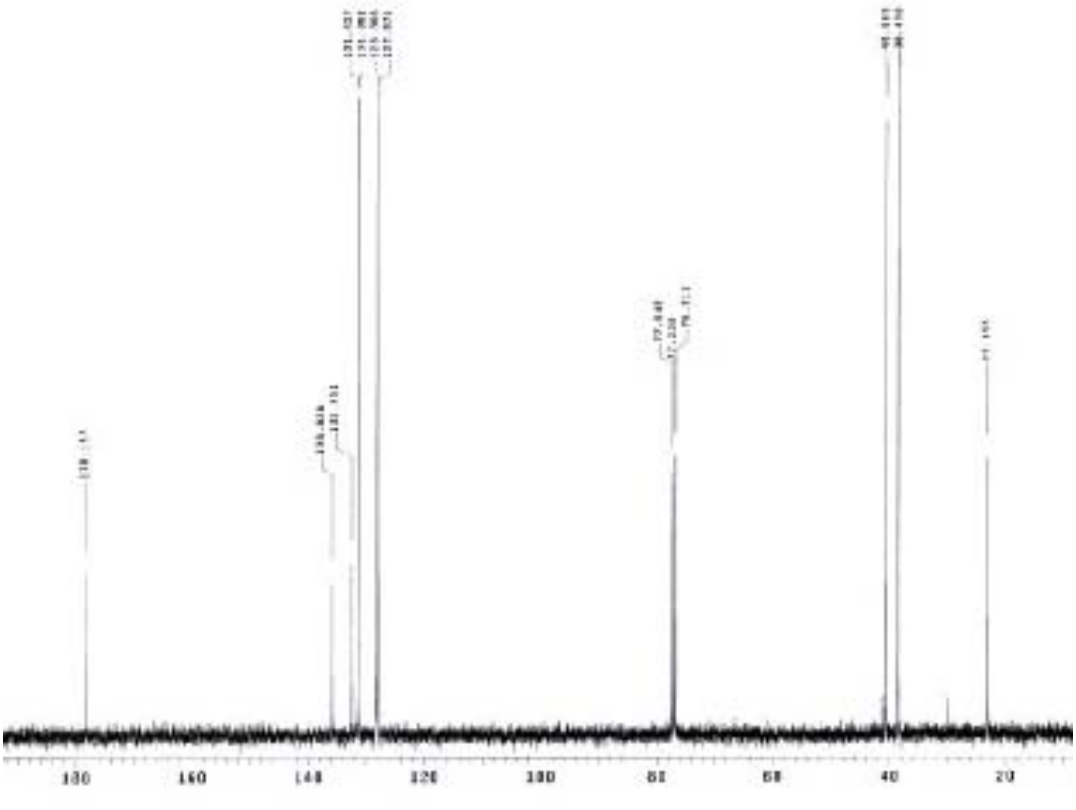

^{1}H NMR Spectrum of **3-15**

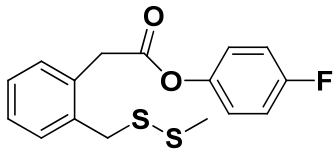

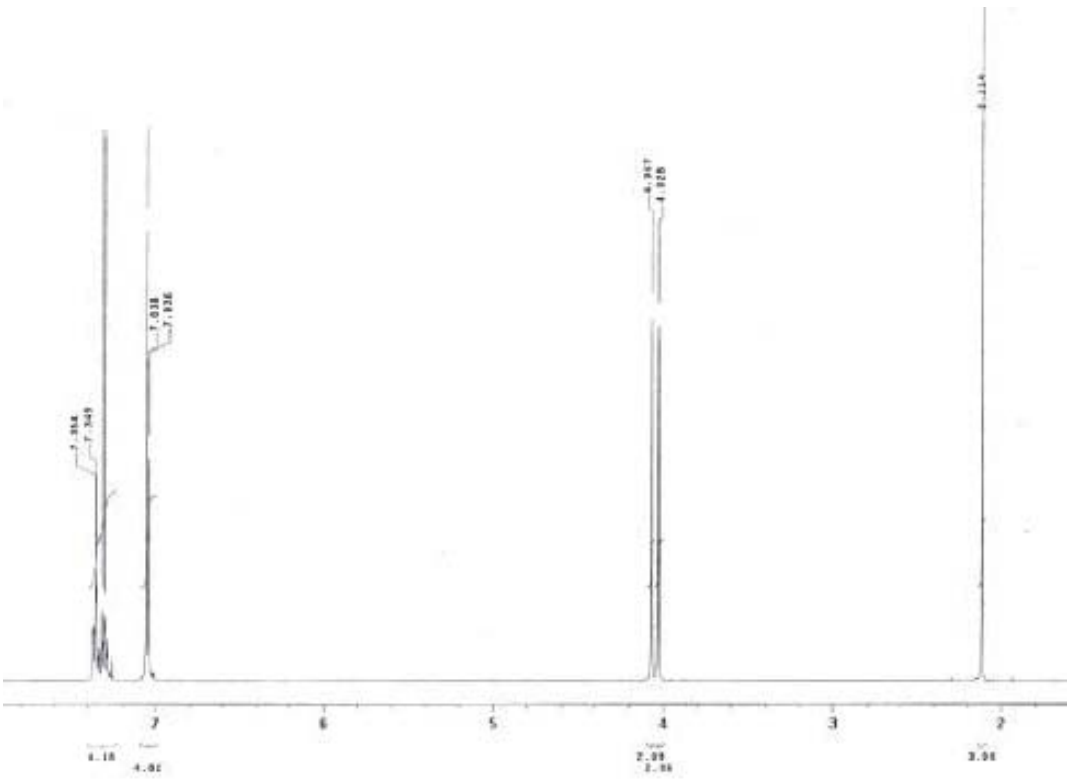

^{13}C NMR Spectrum of **3-15**

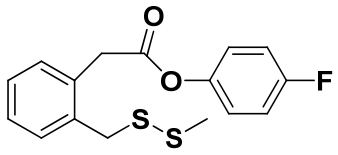

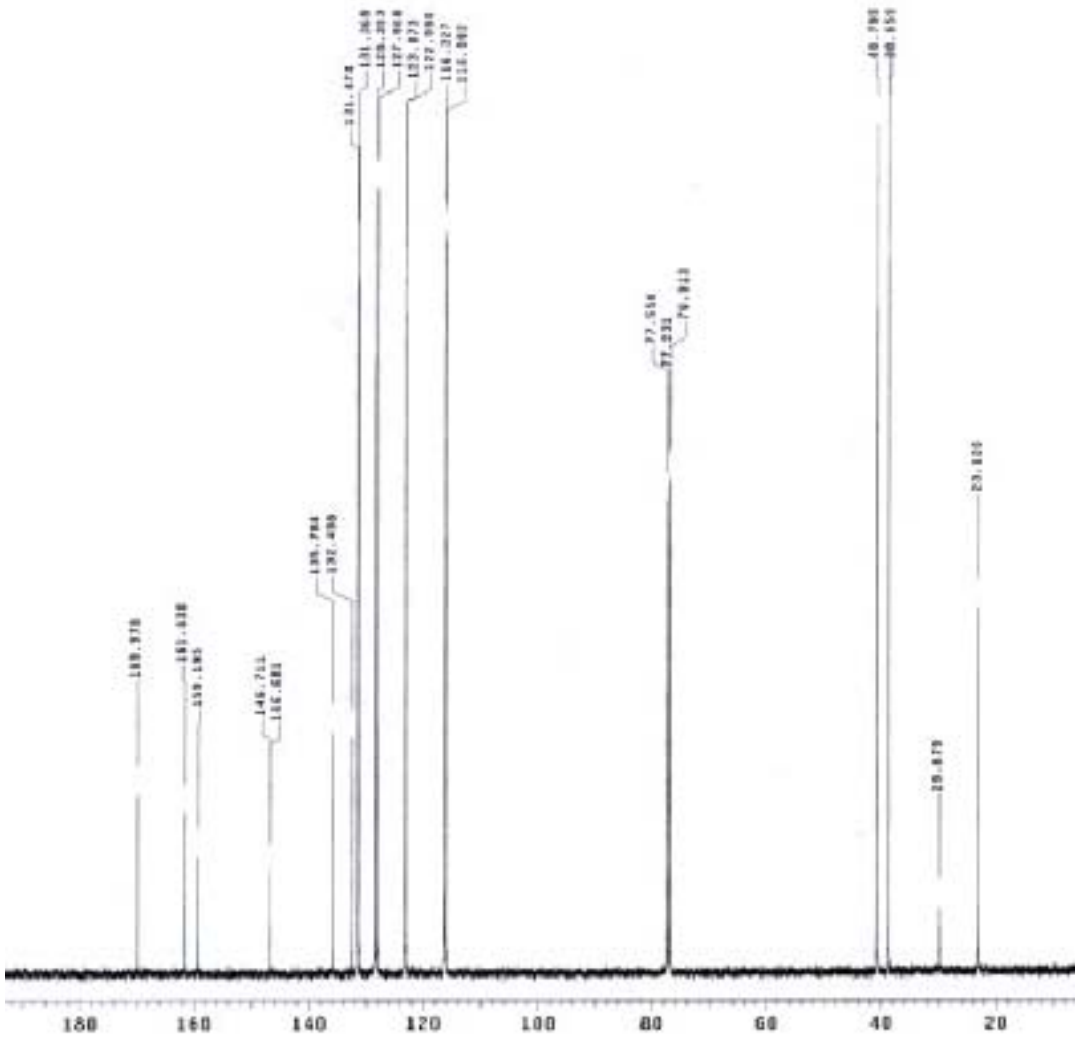

^{19}F NMR Spectrum of **3-15**

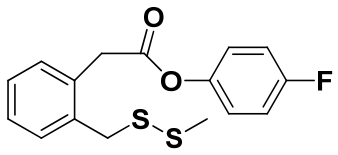

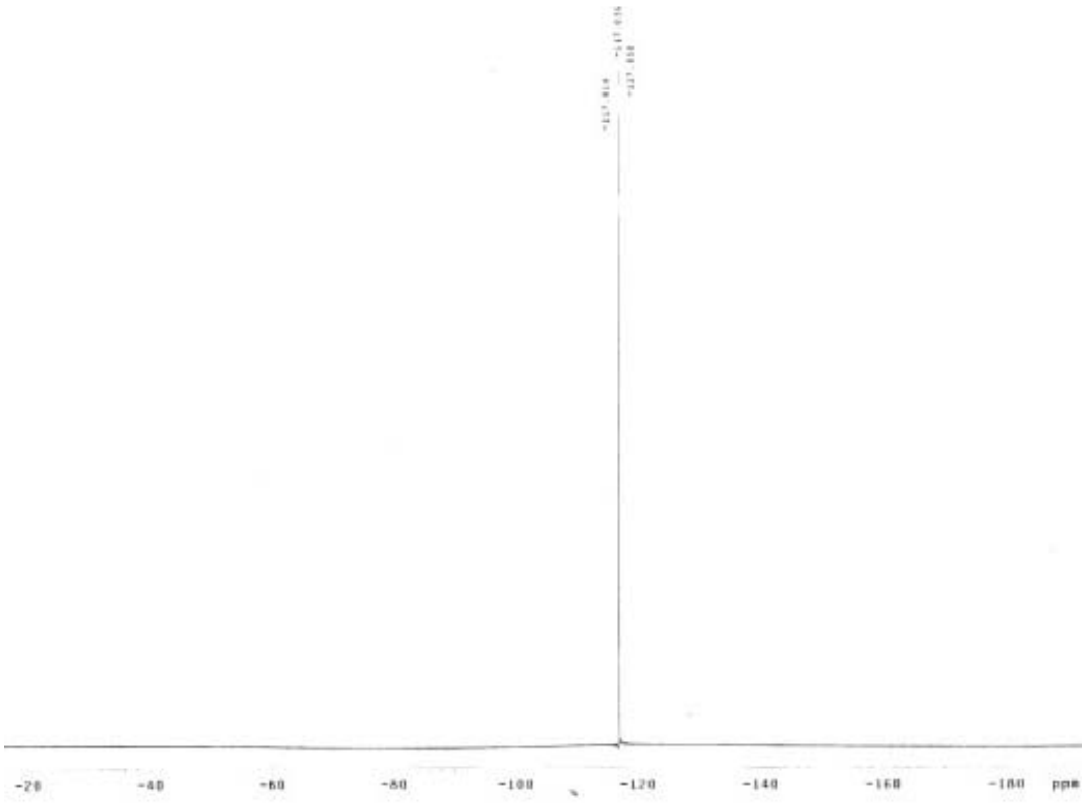

^{1}H NMR Spectrum of **3-23**

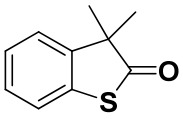

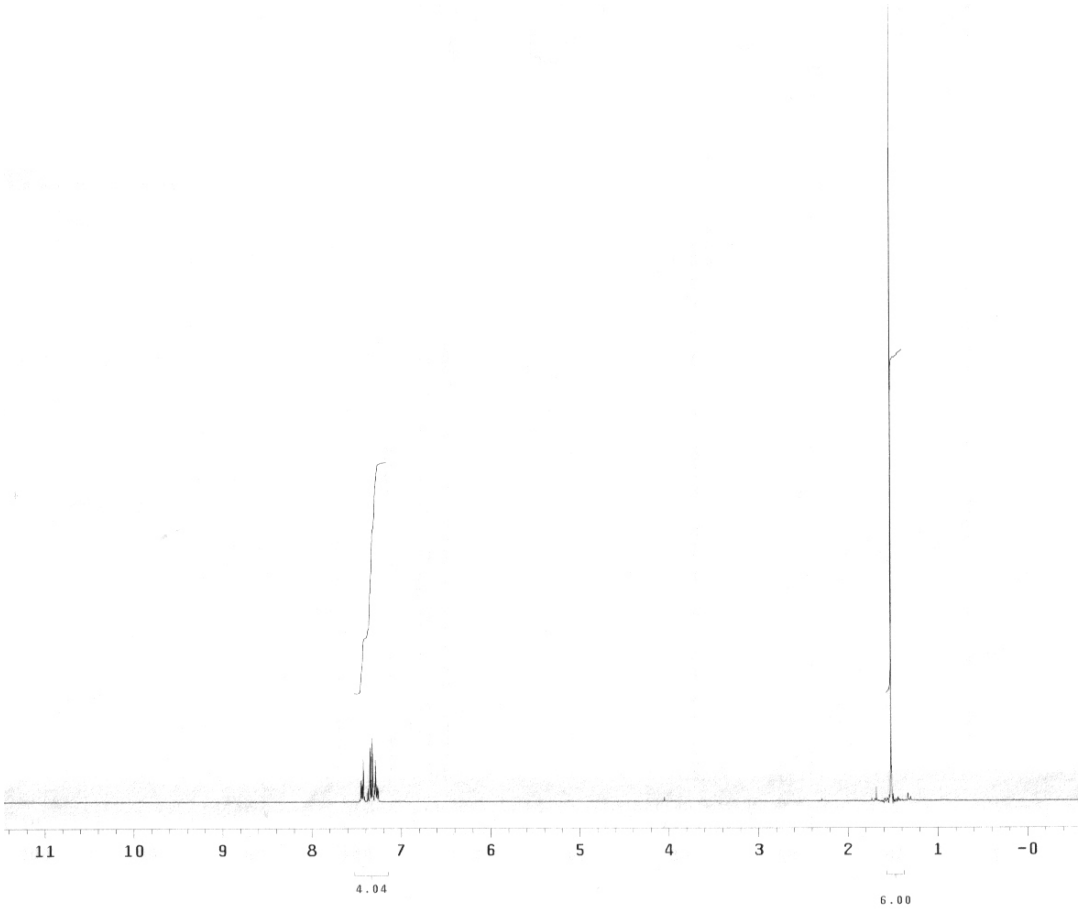

^{13}C NMR Spectrum of **3-23**

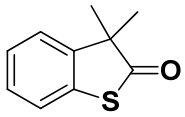

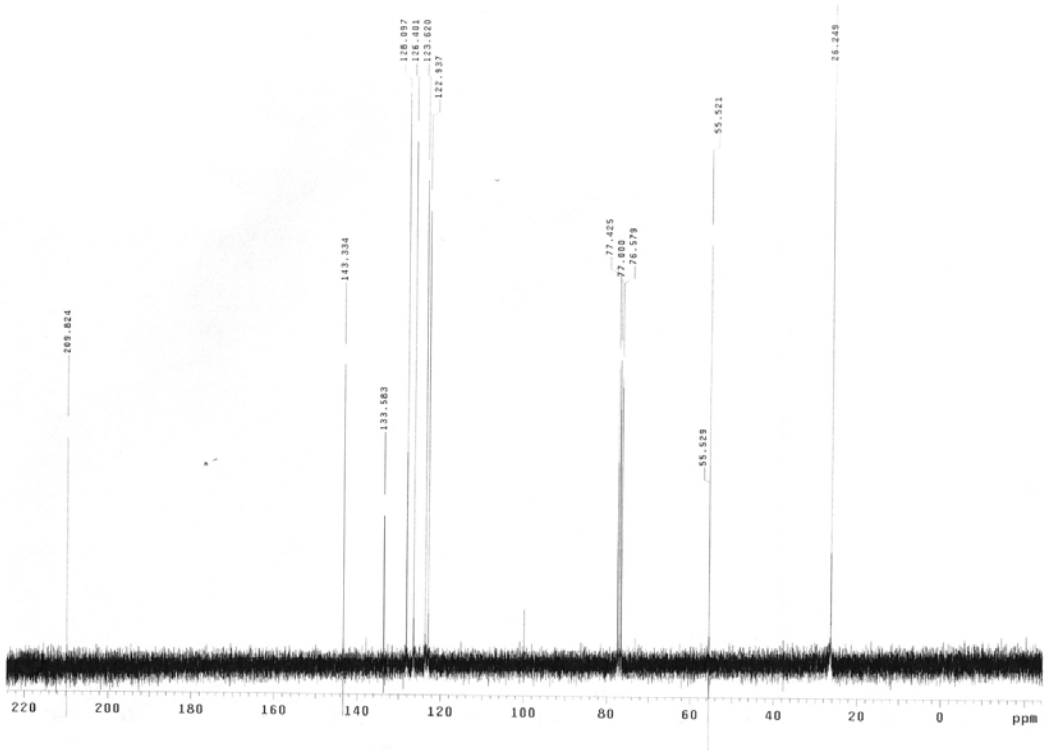

^{1}H NMR Spectrum of **3-37**

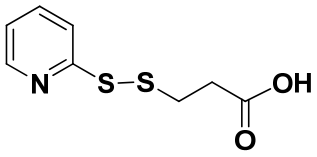

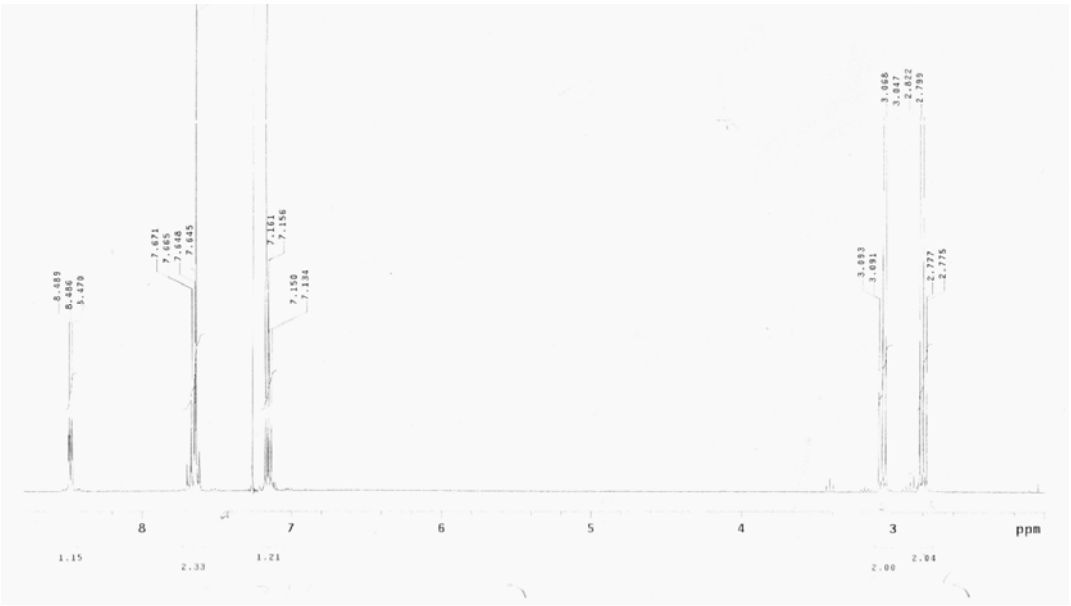

^{1}H NMR Spectrum of **3-38**

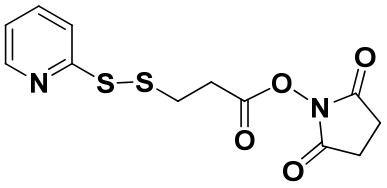

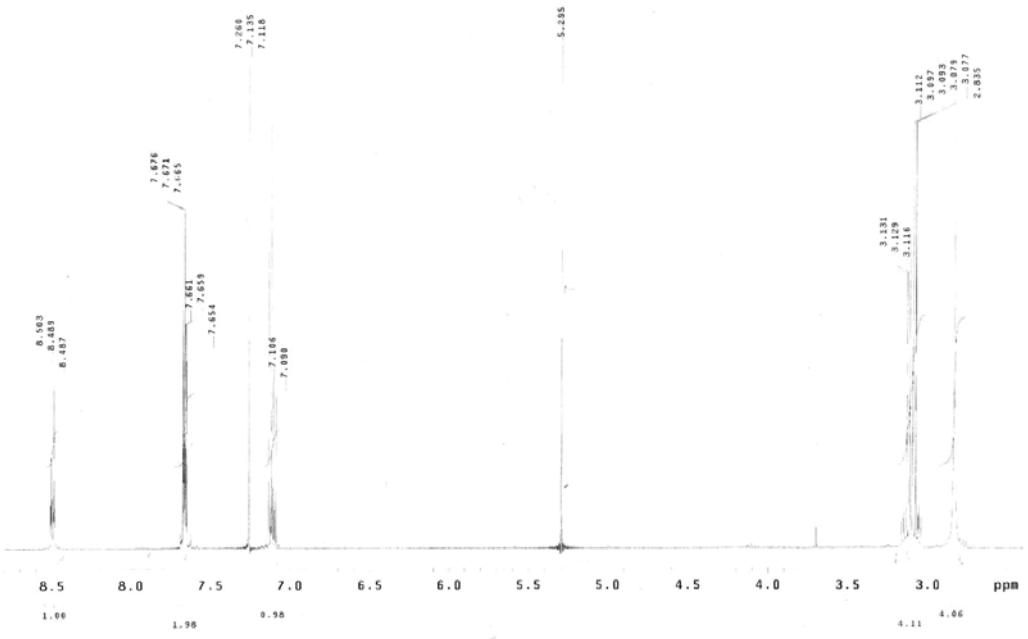

^{1}H NMR Spectrum of **3-39**

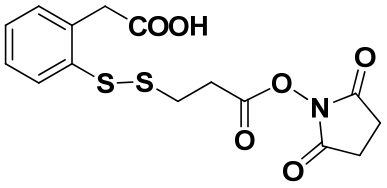

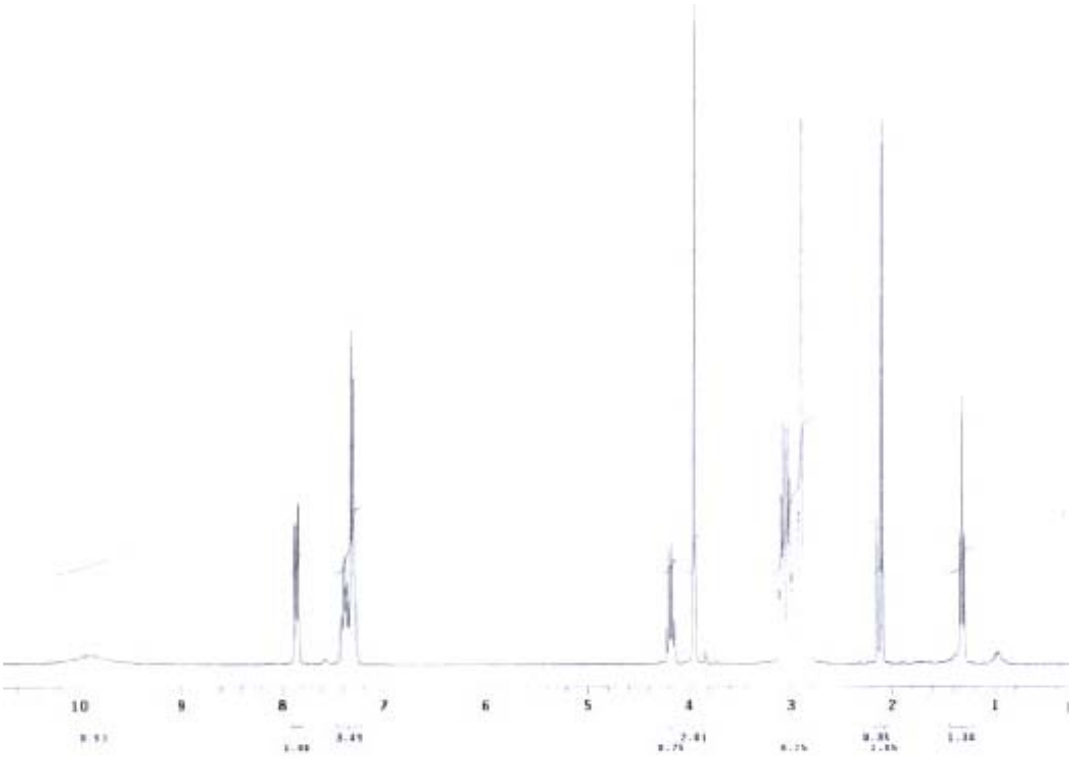

^{1}H NMR Spectrum of **3-40**

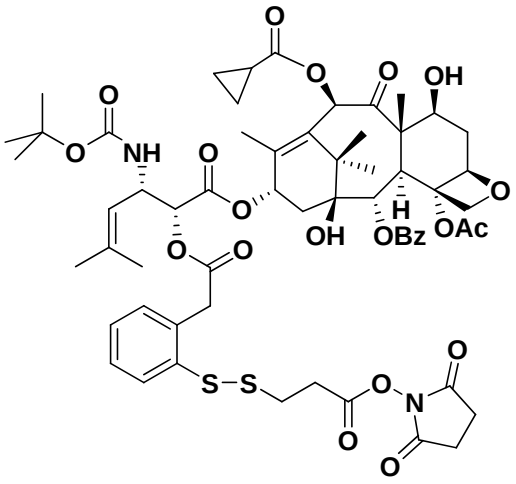

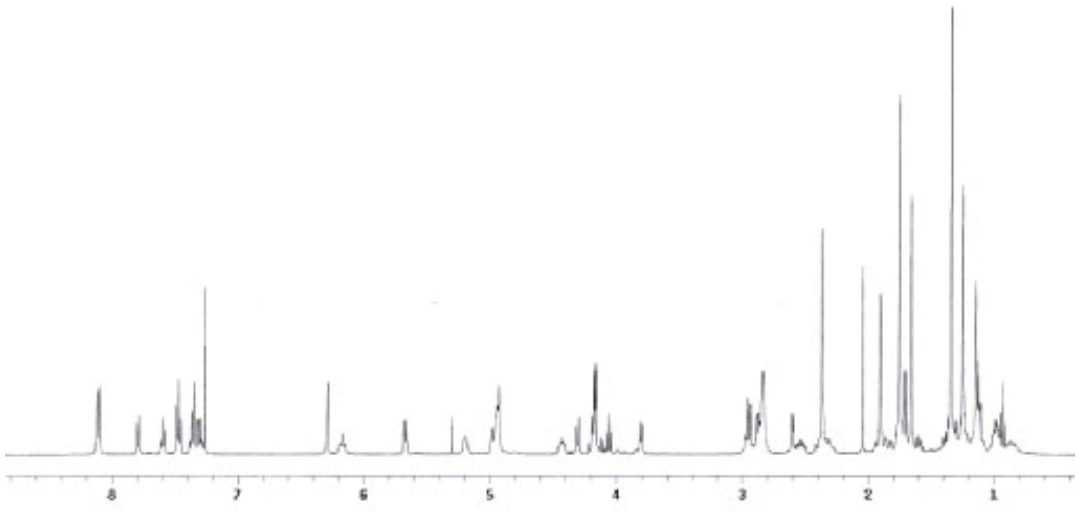

^{13}C NMR Spectrum of **3-40**

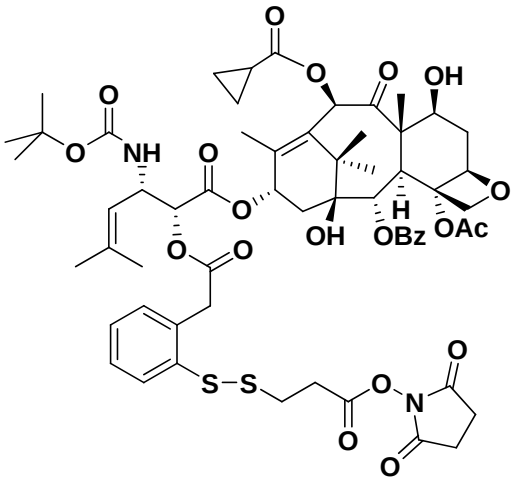

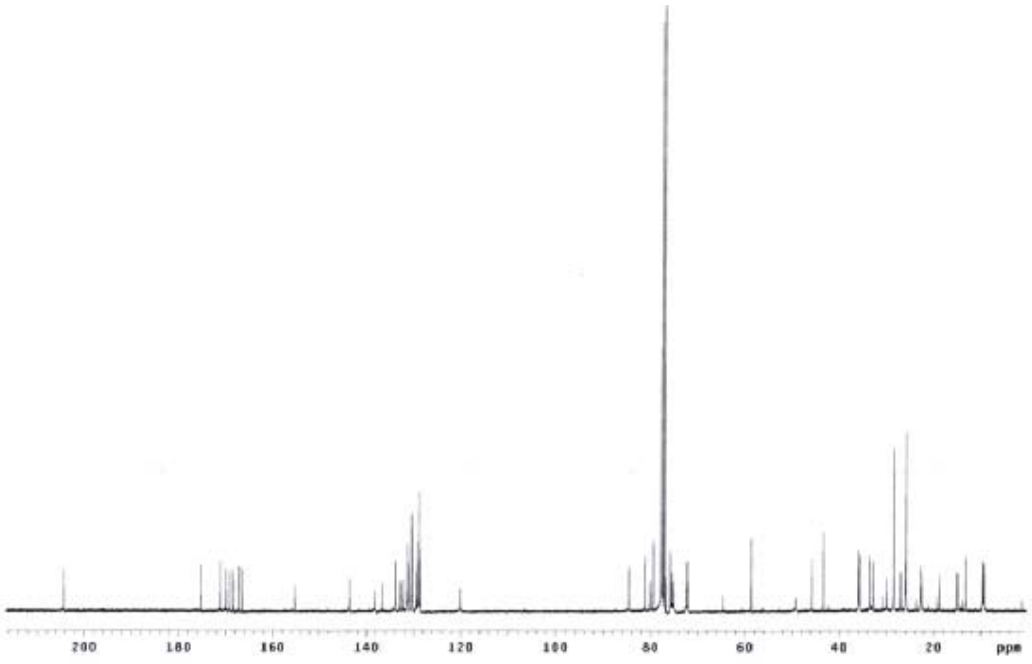

^{1}H NMR Spectrum of **3-42**

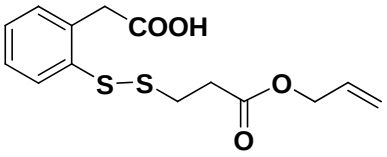

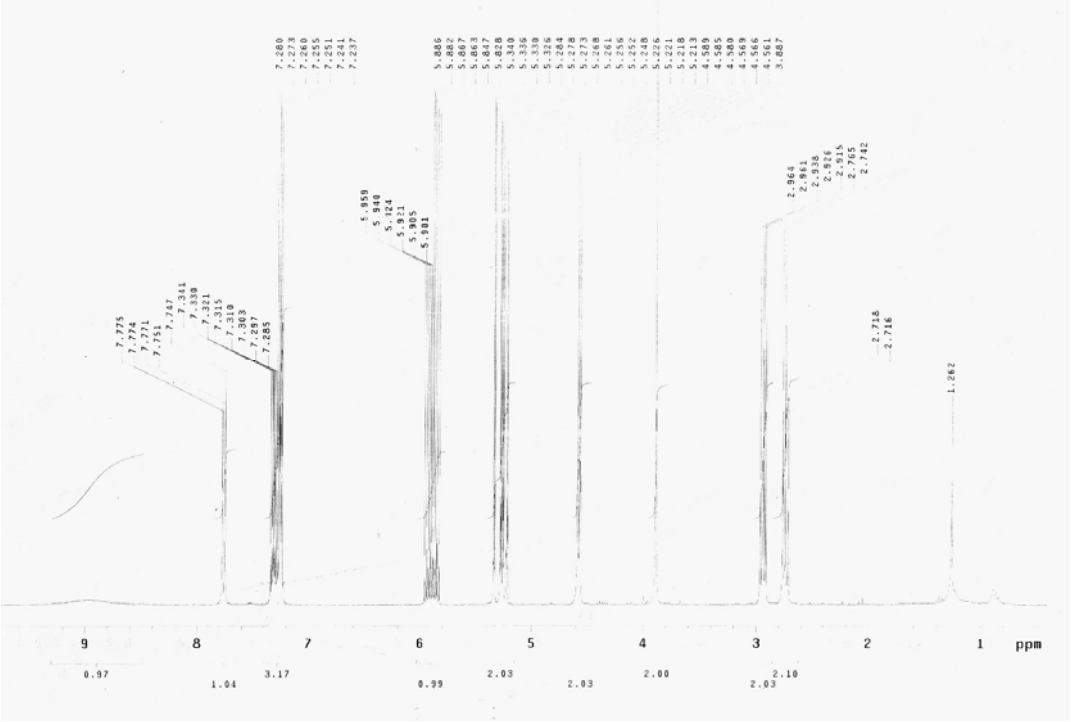

^{1}H NMR Spectrum of **3-42**

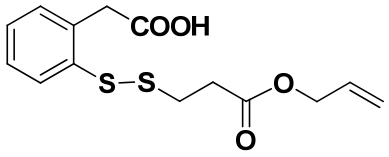

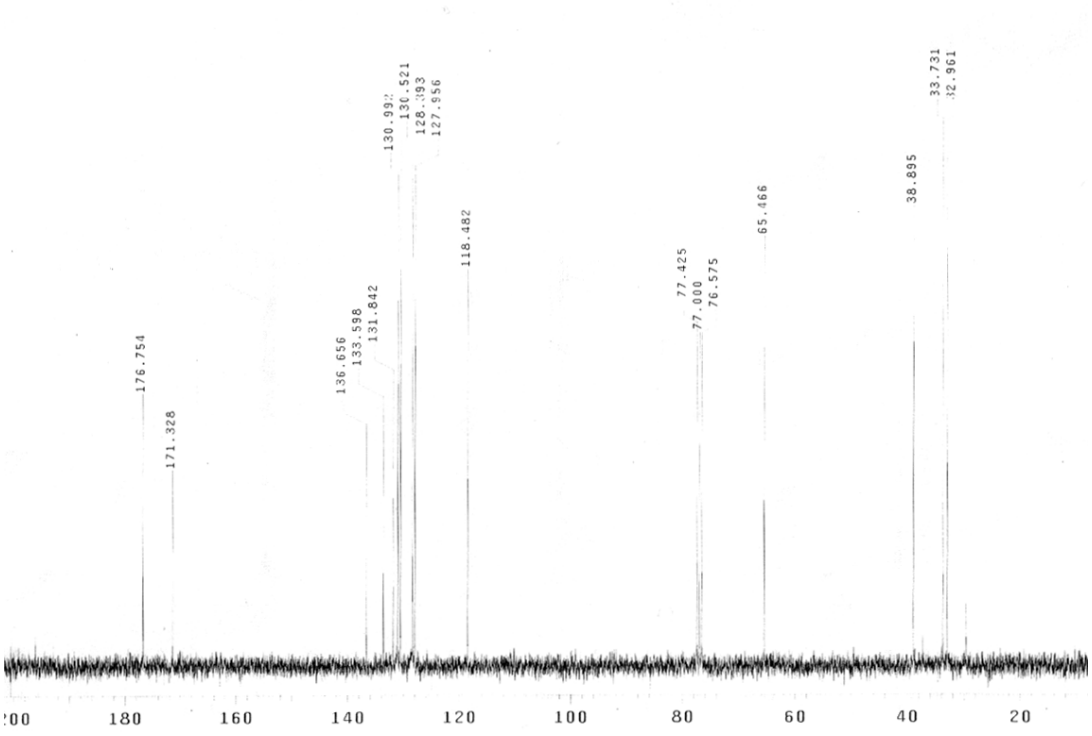

^{1}H NMR Spectrum of **3-43**

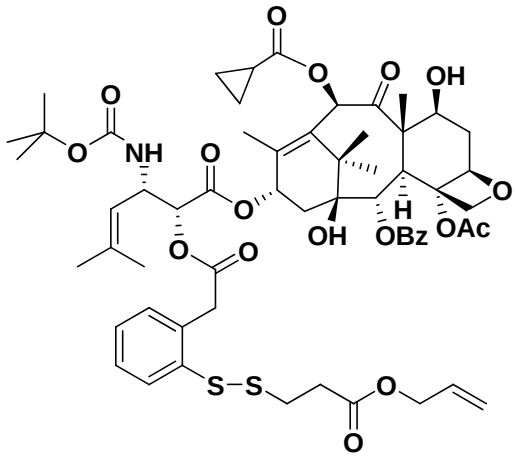

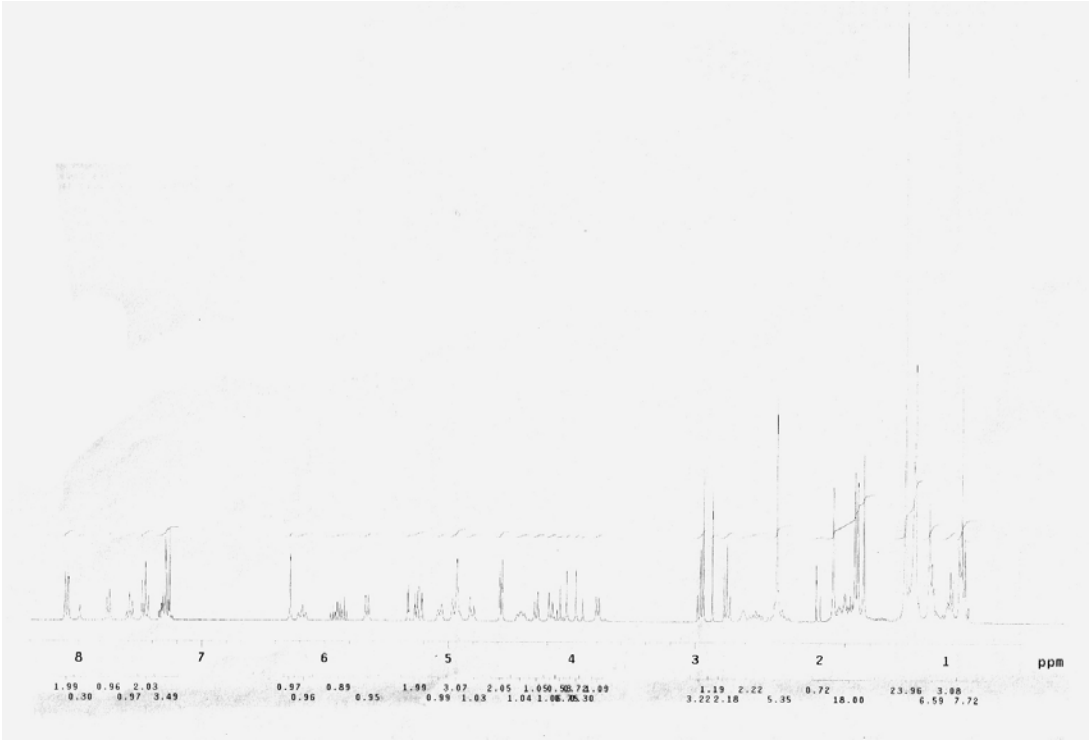

^{13}C NMR Spectrum of **3-43**

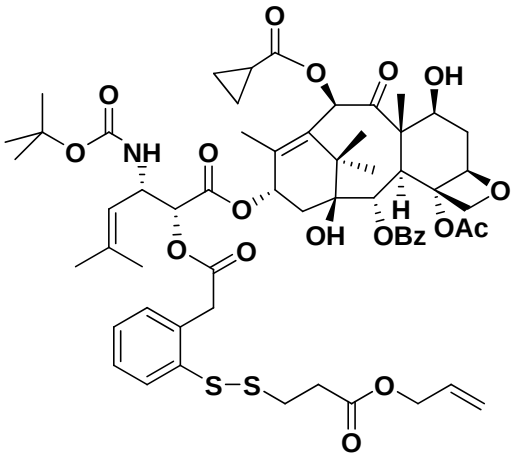

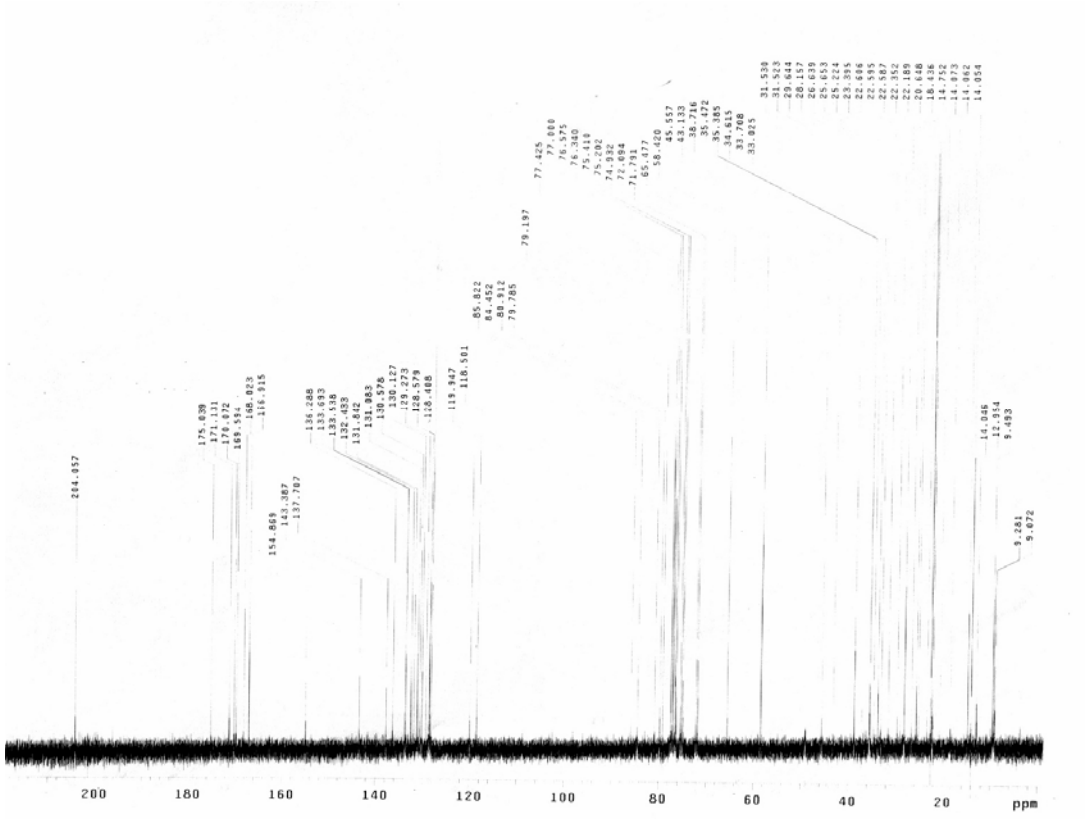

^{1}H NMR Spectrum of **3-44**

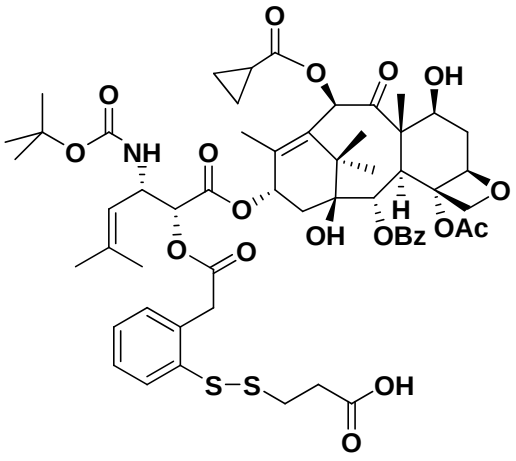

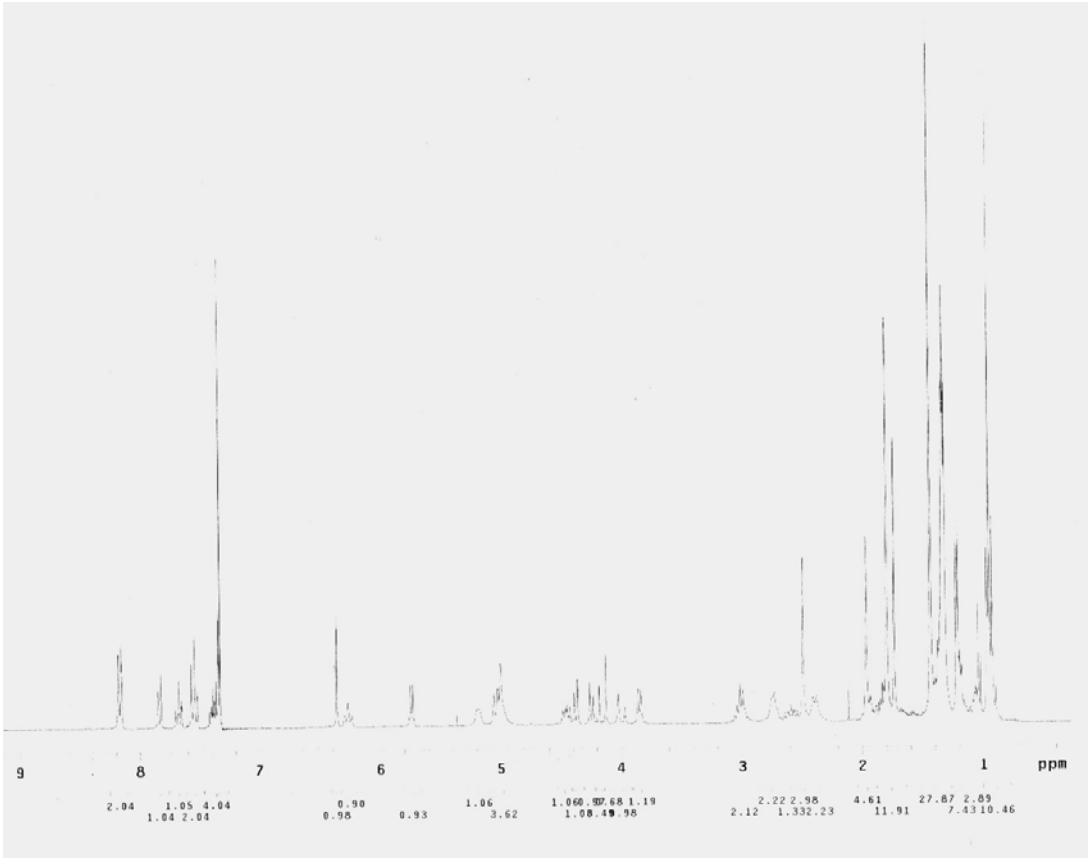

^{13}C NMR Spectrum of **3-44**

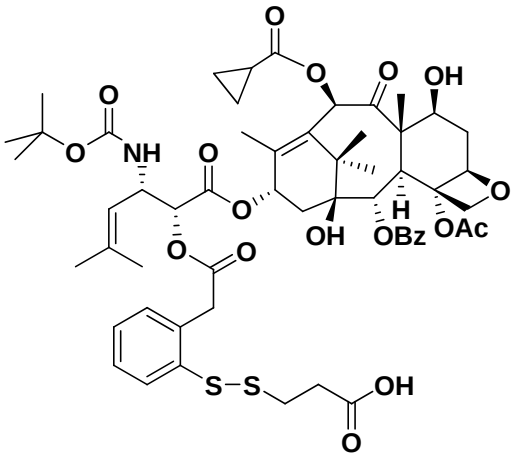

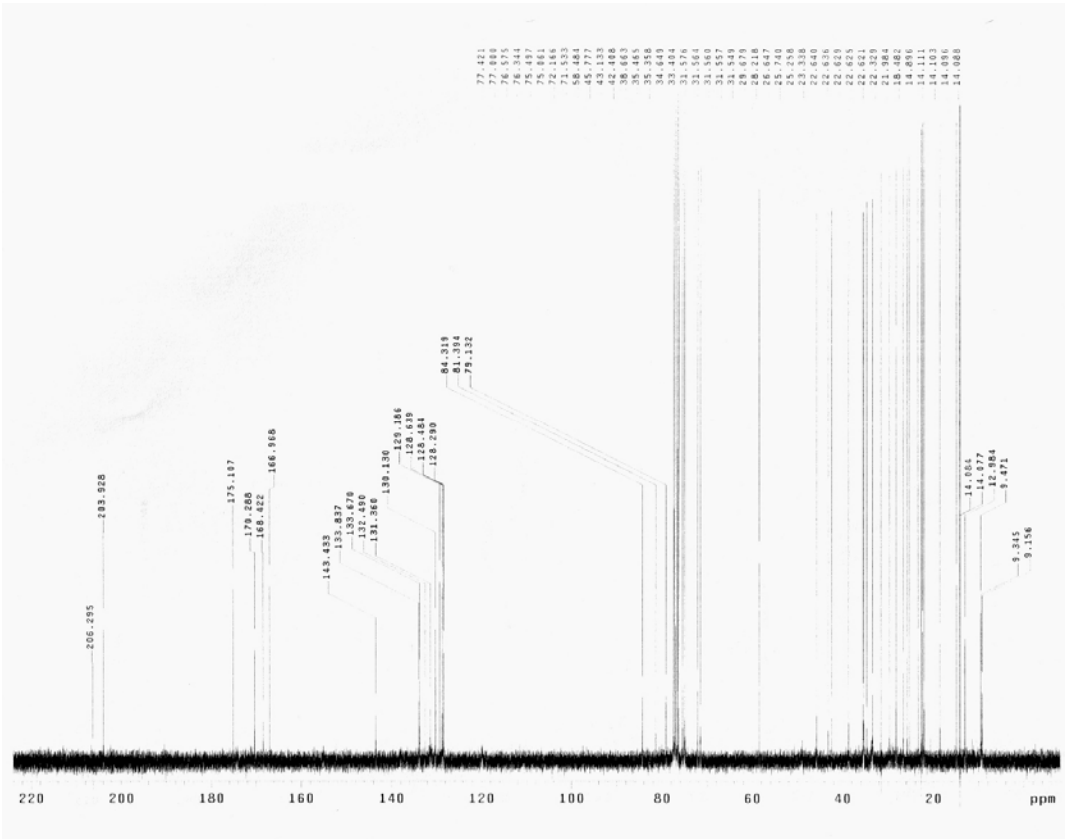

^{1}H NMR Spectrum of **3-45**

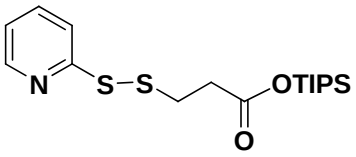

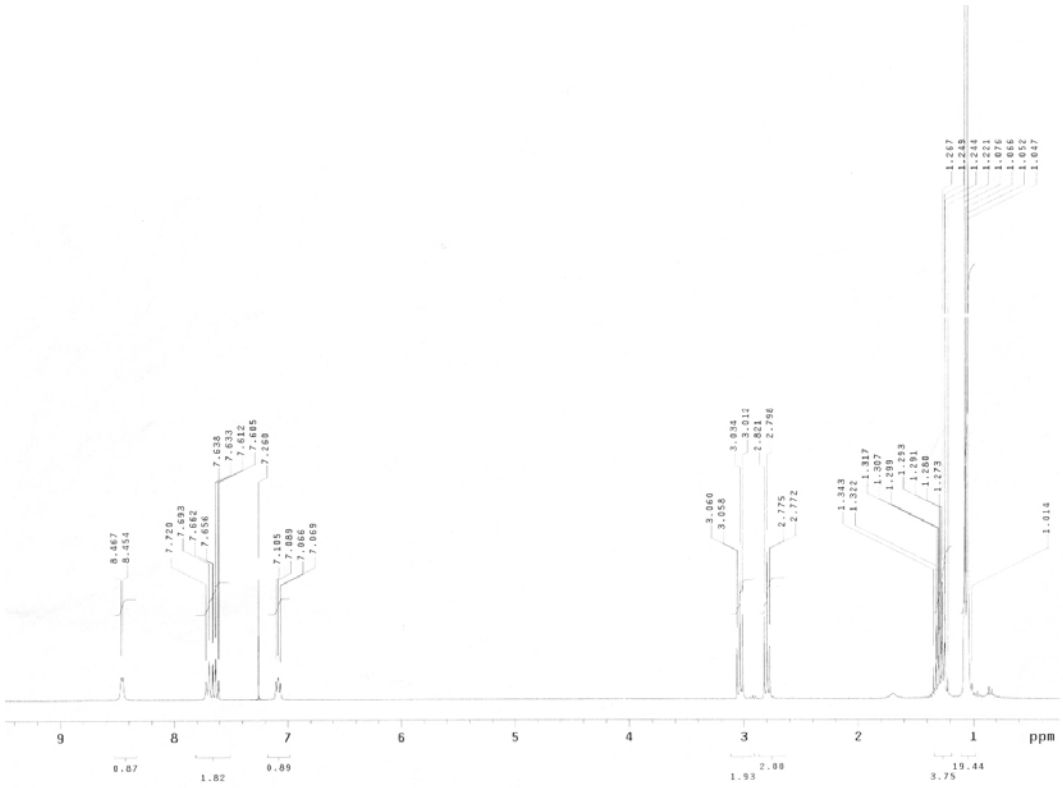

^{13}C NMR Spectrum of **3-45**

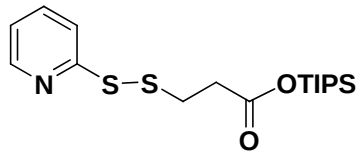

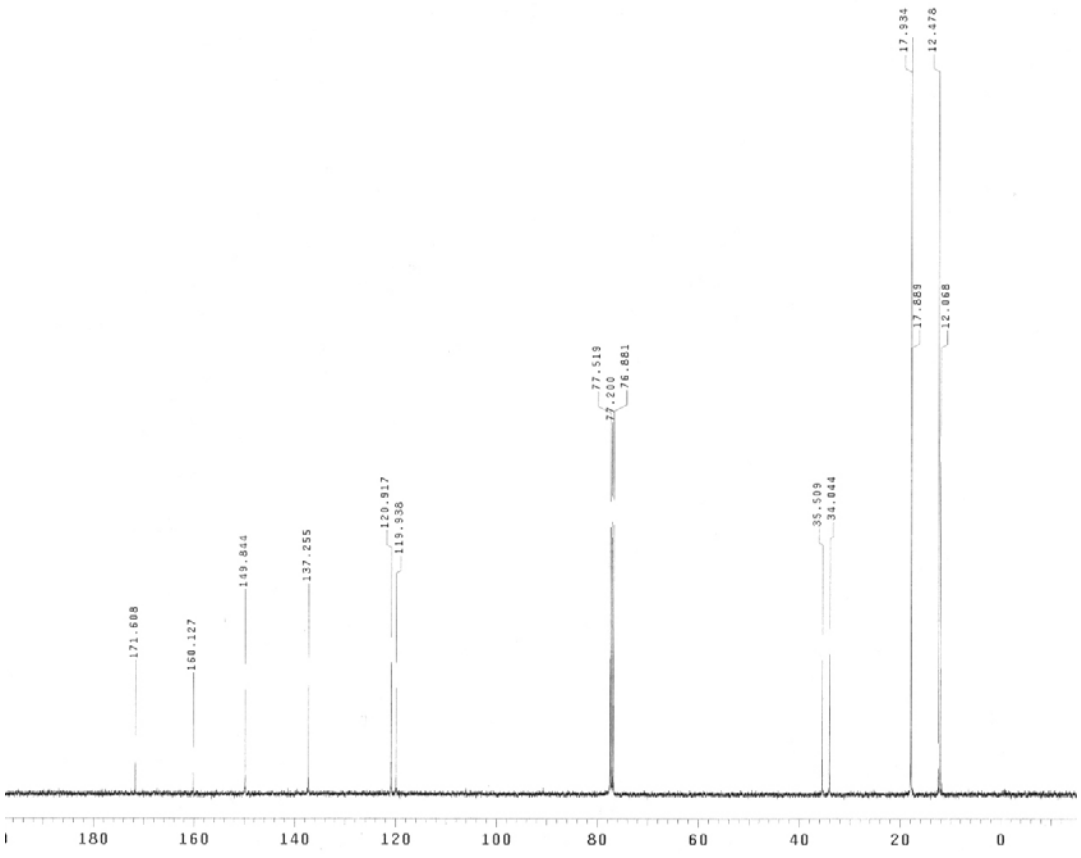

^{1}H NMR Spectrum of **3-46**

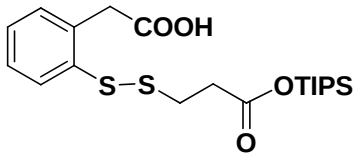

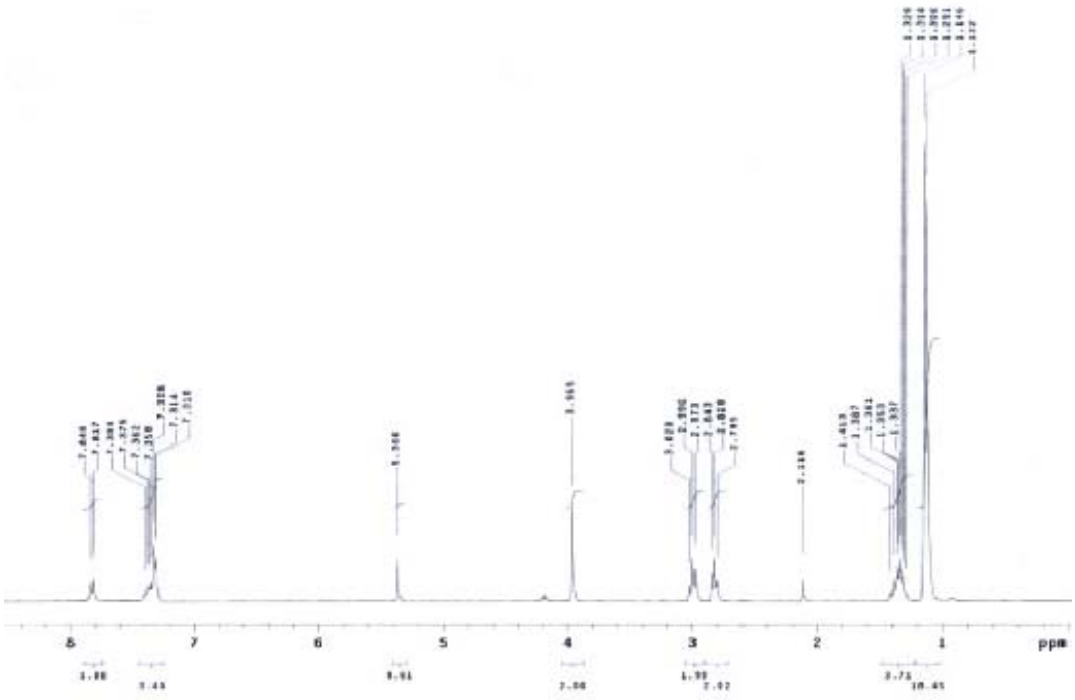

^{13}C NMR Spectrum of **3-46**

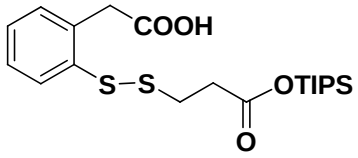

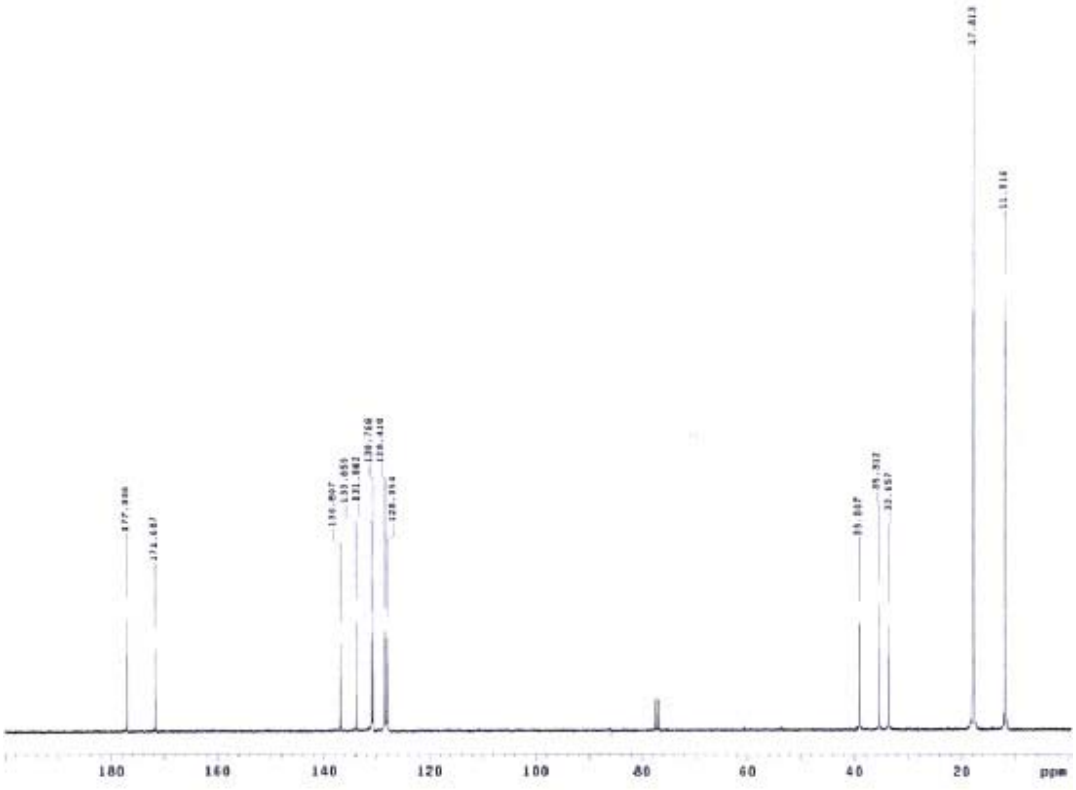

^{1}H NMR Spectrum of **3-47**

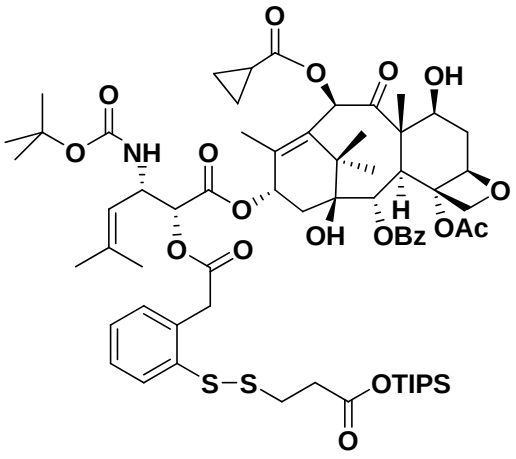

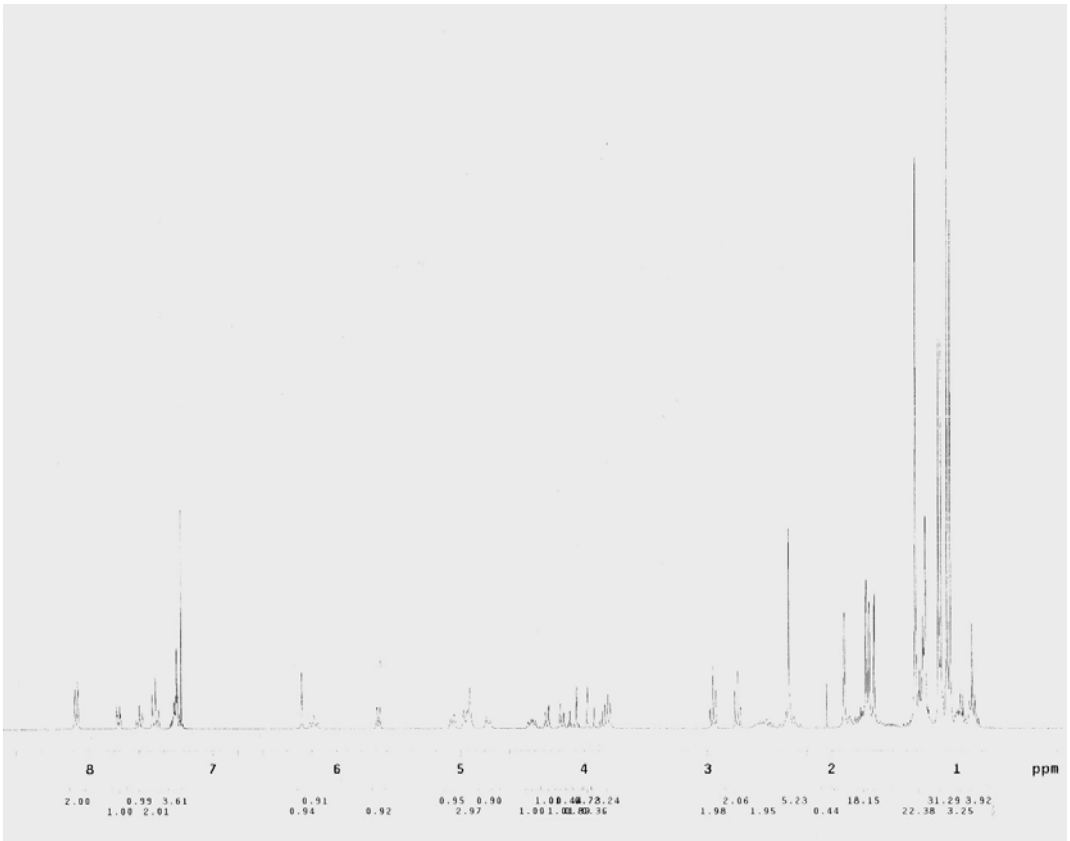

^{1}H NMR Spectrum of **3-48**

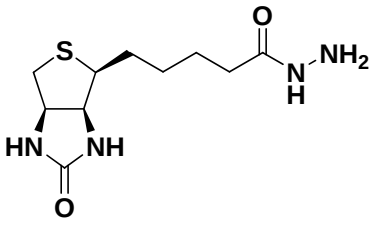

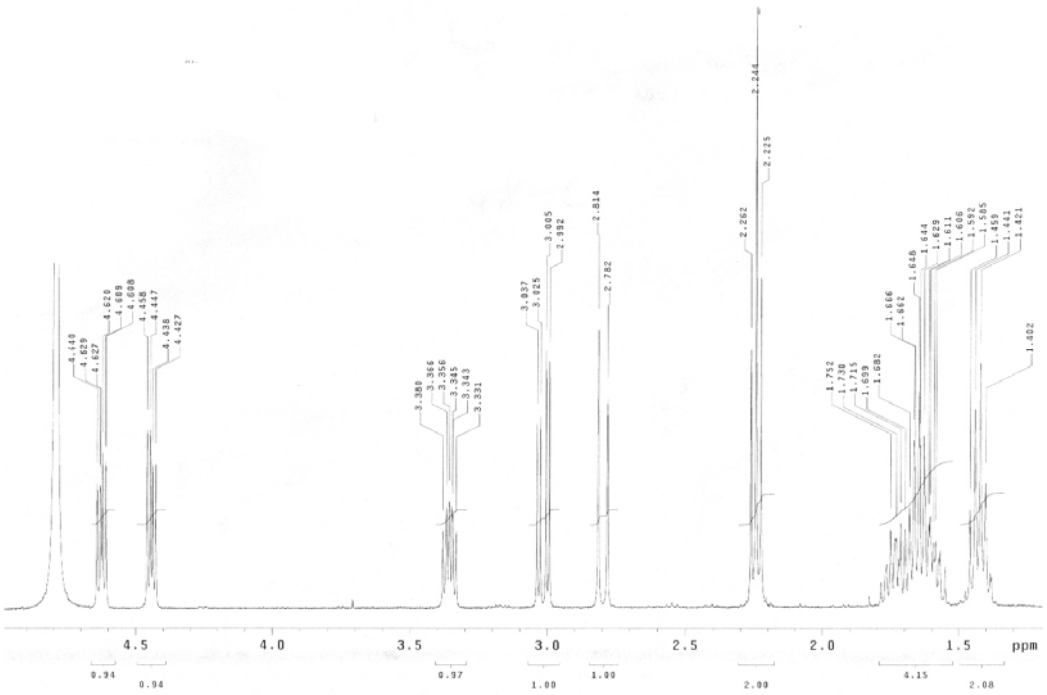

^{13}C NMR Spectrum of **3-48**

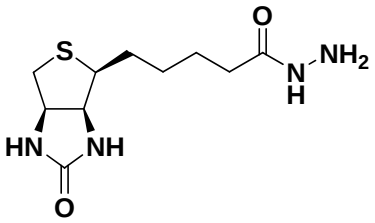

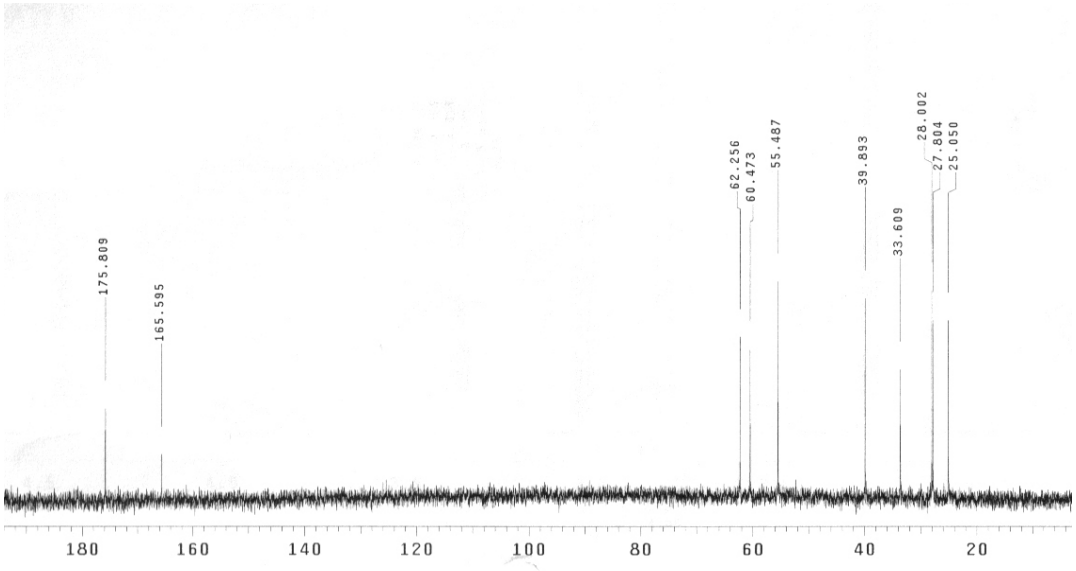

^{1}H NMR Spectrum of **3-49**

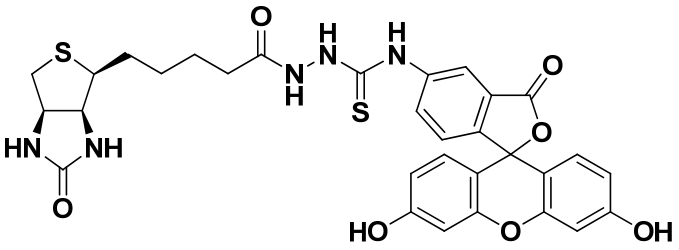

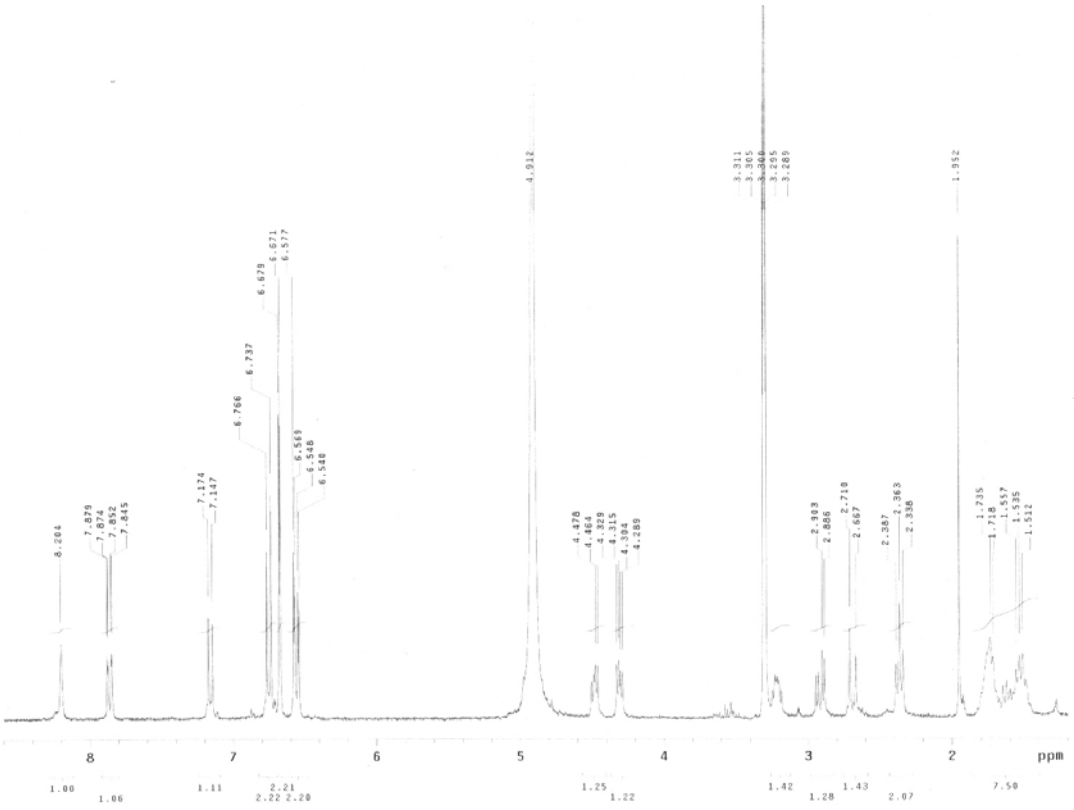

^{13}C NMR Spectrum of 3-49

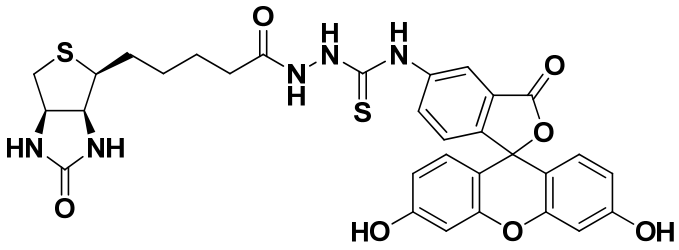

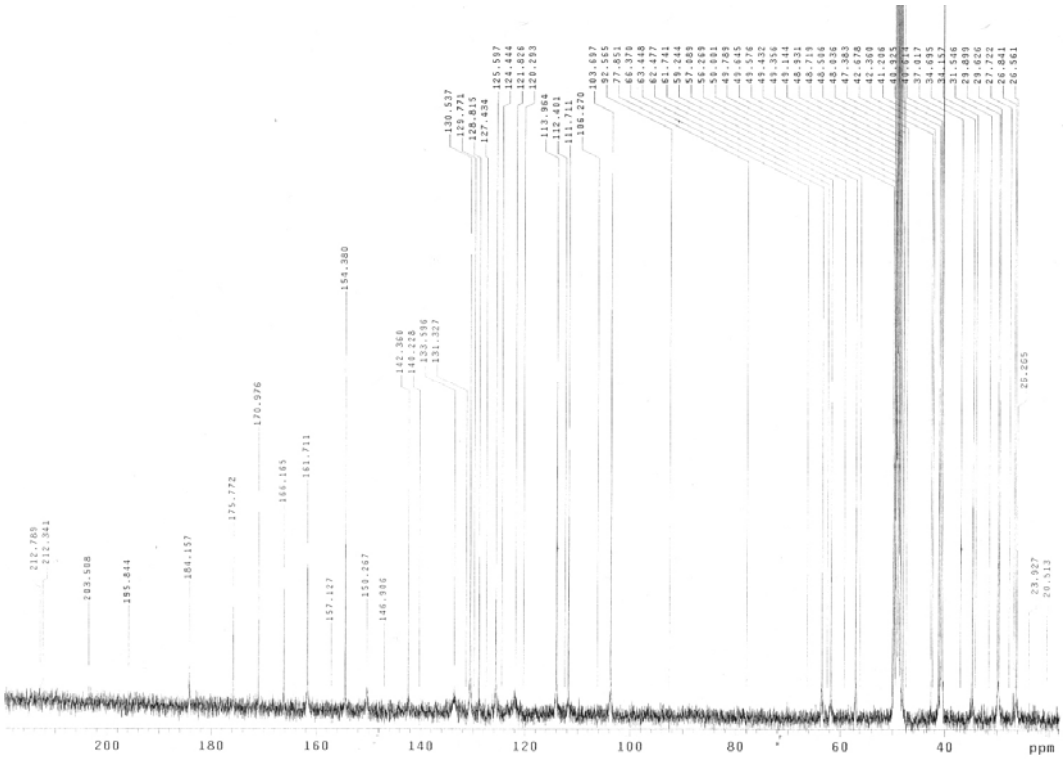

^{1}H NMR Spectrum of **3-50**

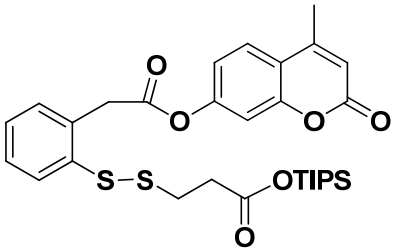

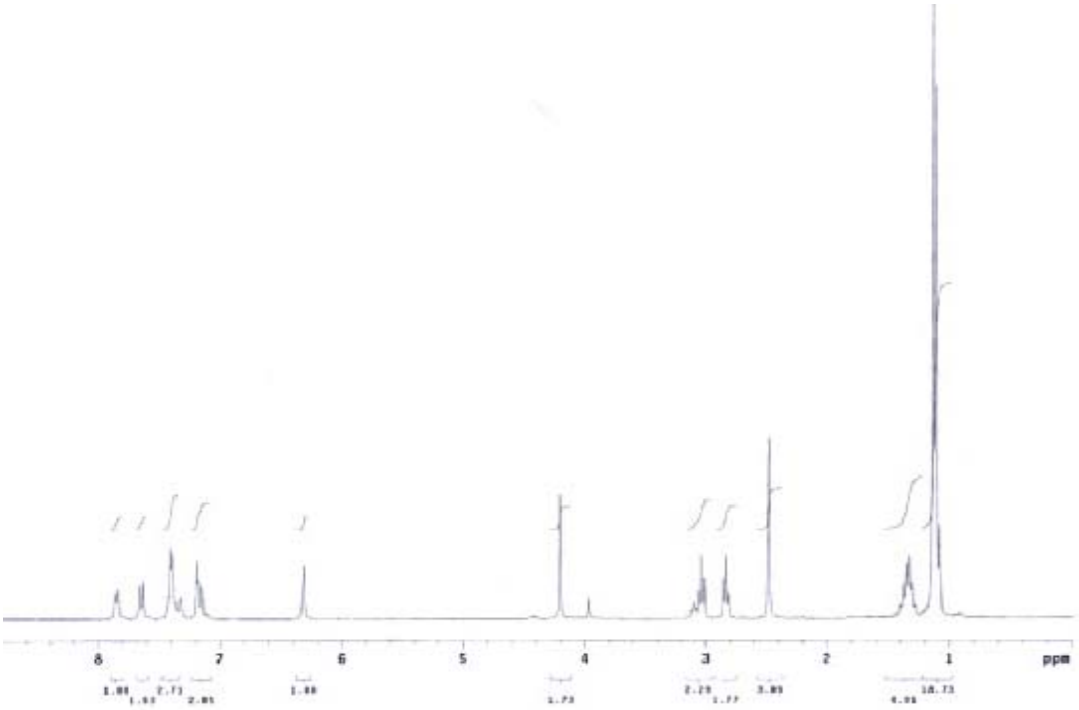

^{1}H NMR Spectrum of **3-51**

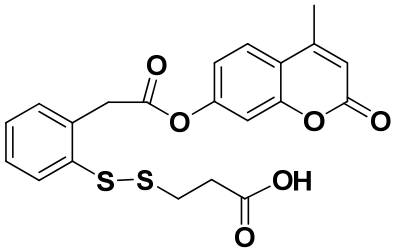

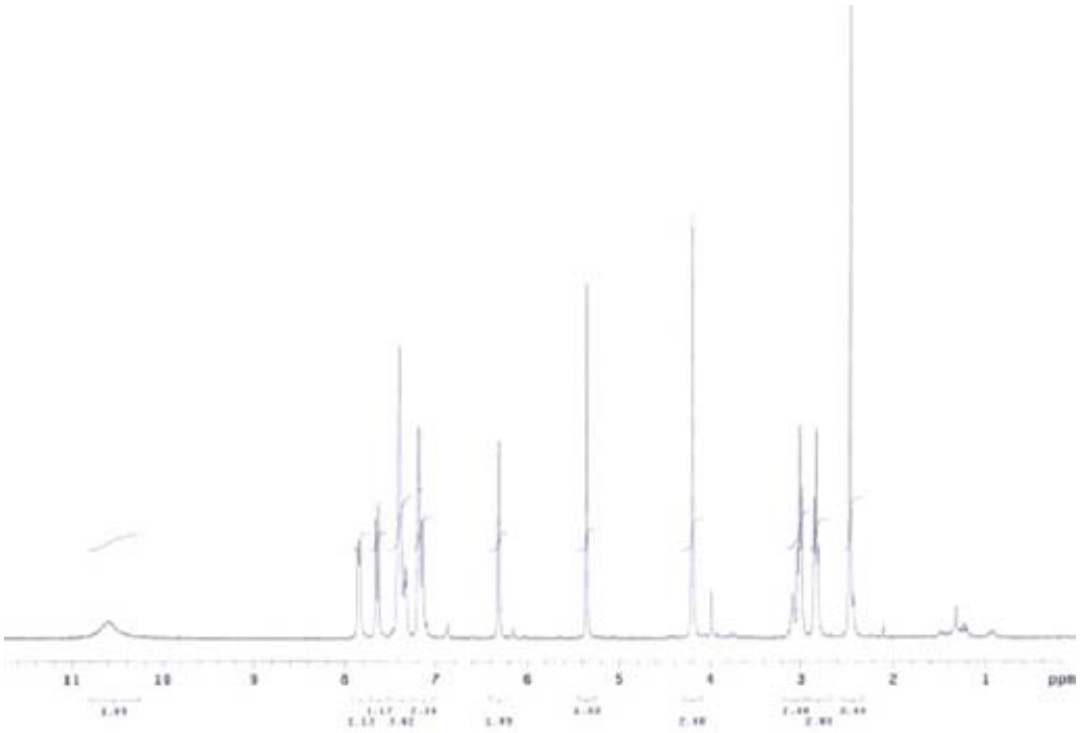

^{13}C NMR Spectrum of **3-51**

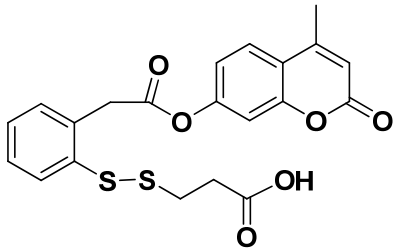

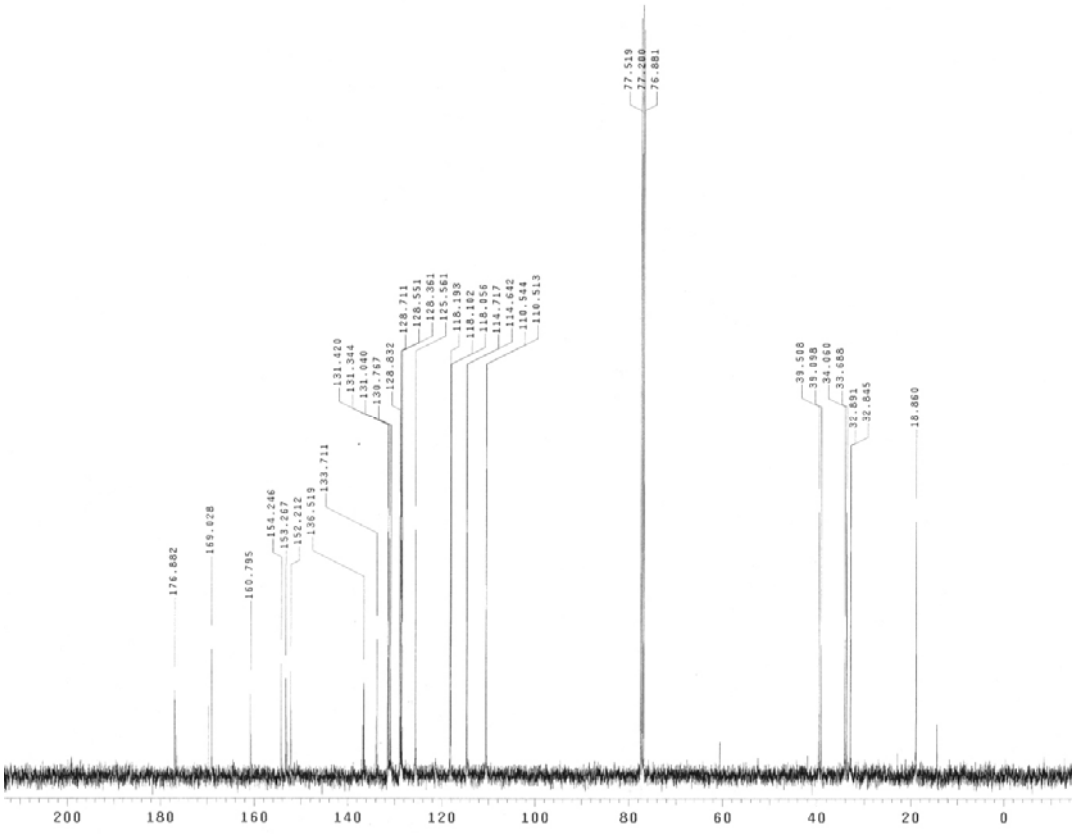

^{1}H NMR Spectrum of **3-52**

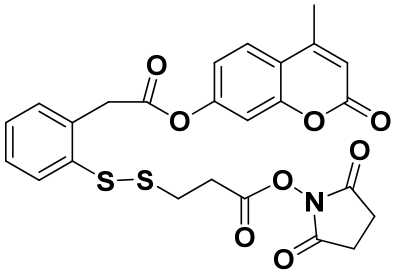

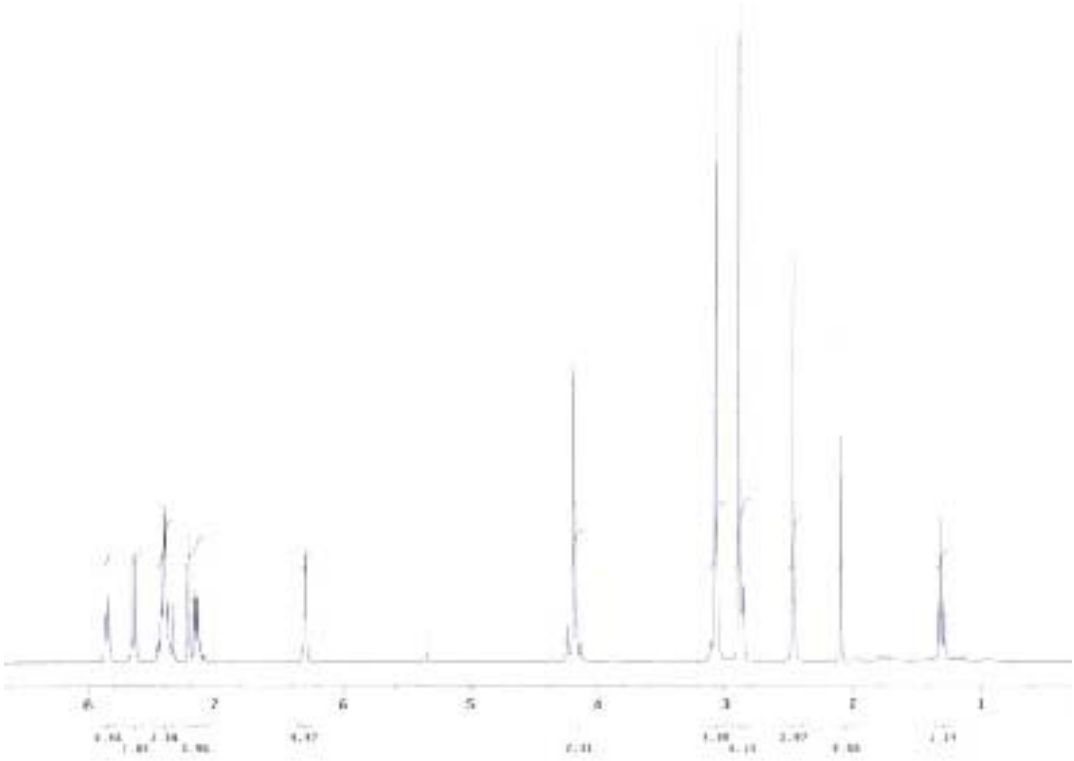

^{1}H NMR Spectrum of **3-53**

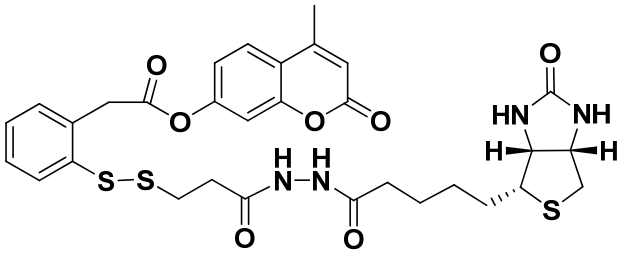

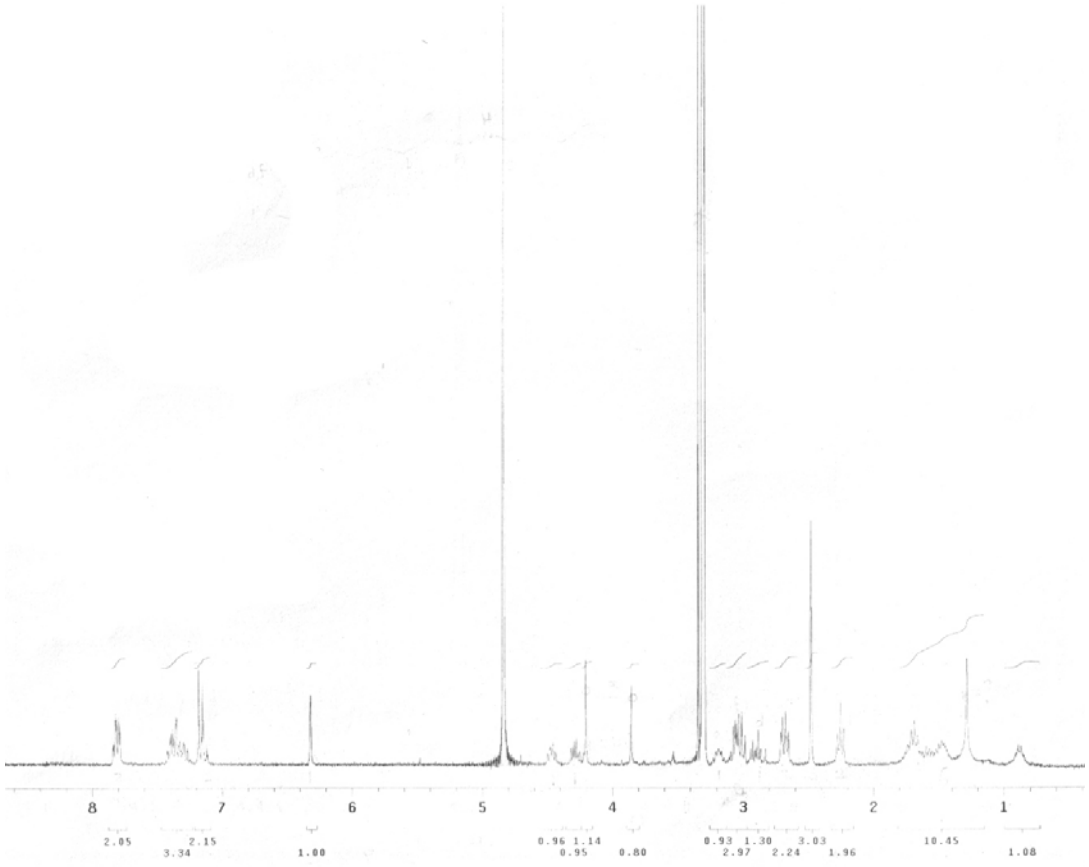

^{1}H NMR Spectrum of **3-54**

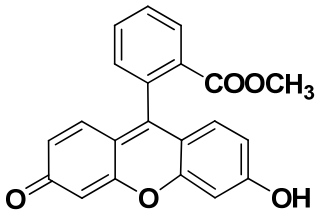

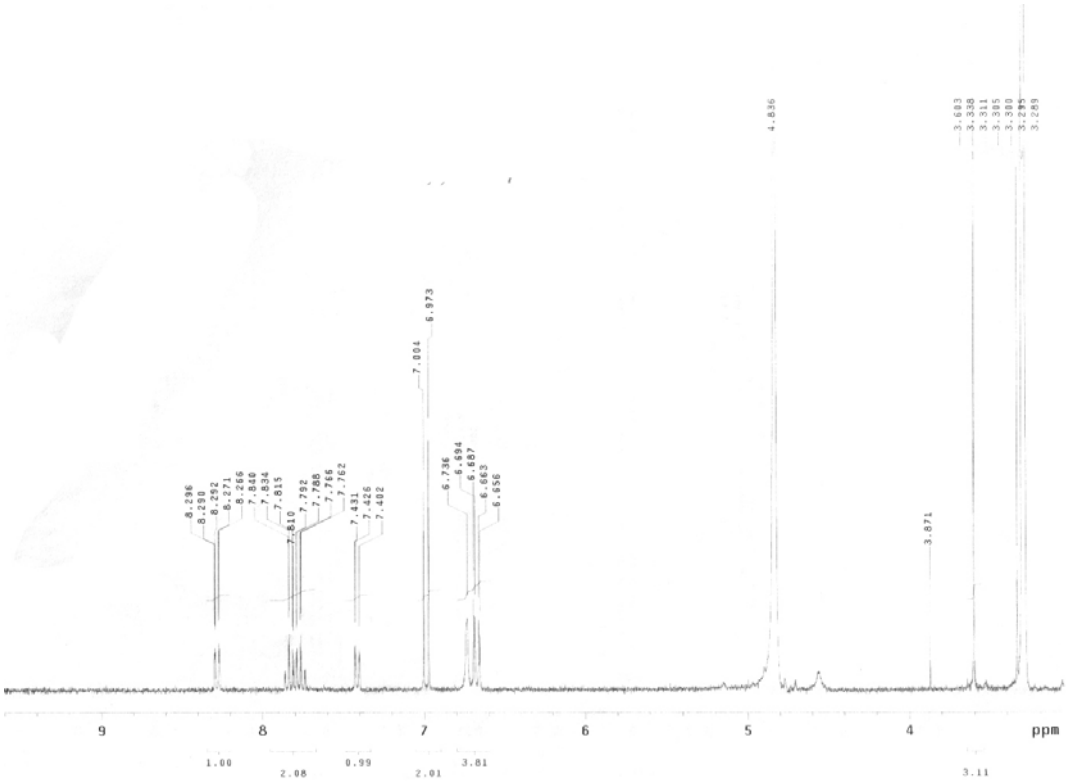

^{13}C NMR Spectrum of **3-54**

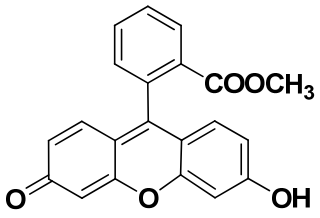

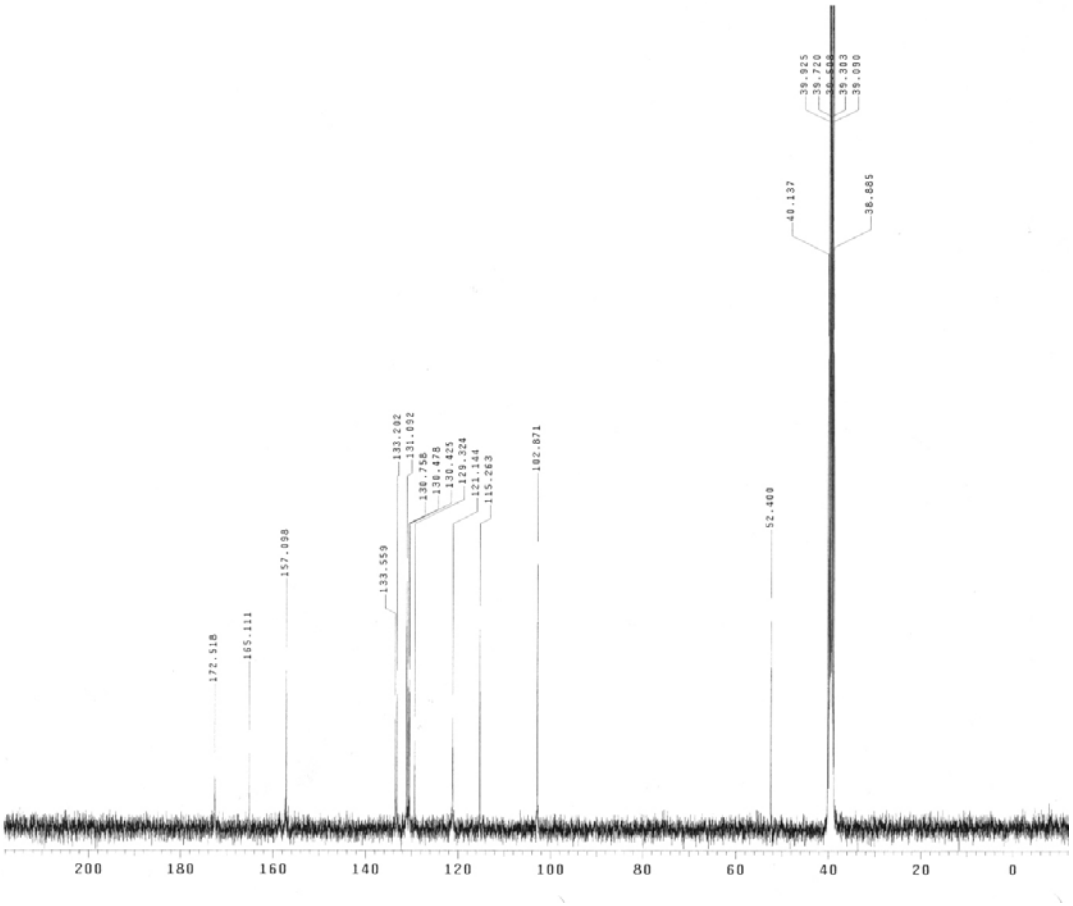

^{1}H NMR Spectrum of **3-55**

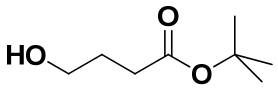

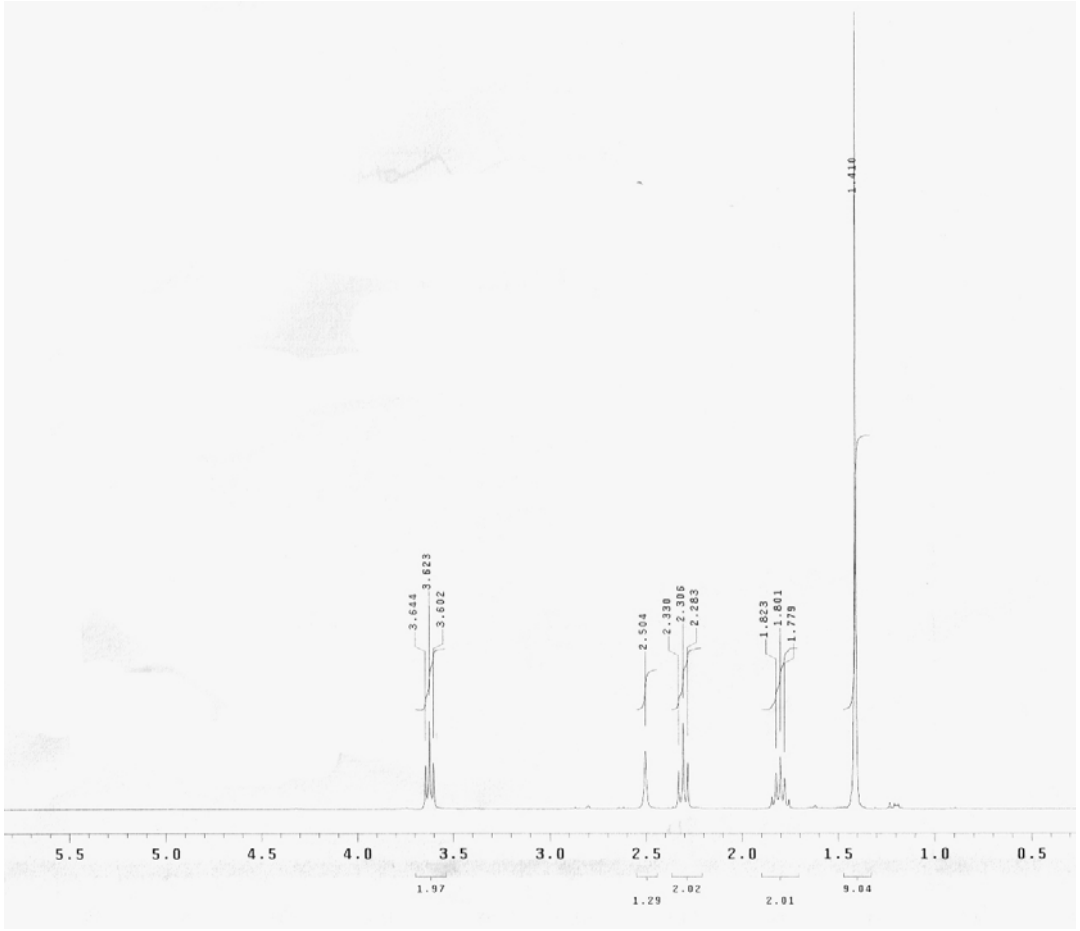

^{13}C NMR Spectrum of **3-55**

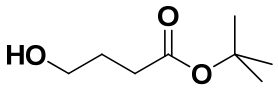

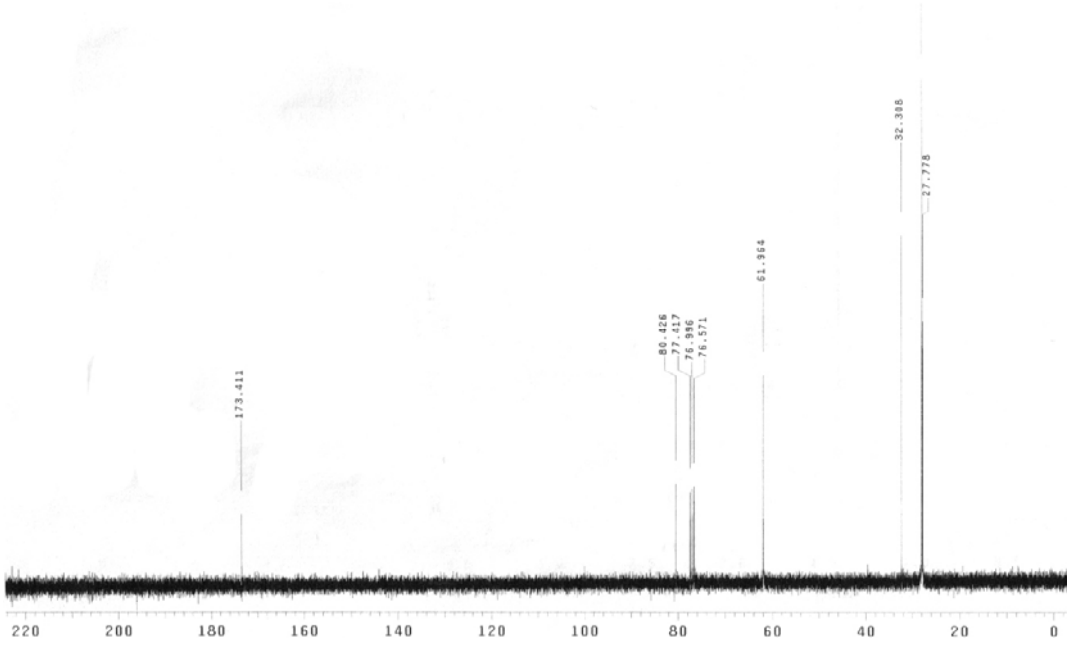

^{1}H NMR Spectrum of **3-56**

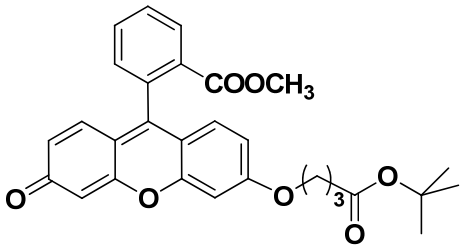

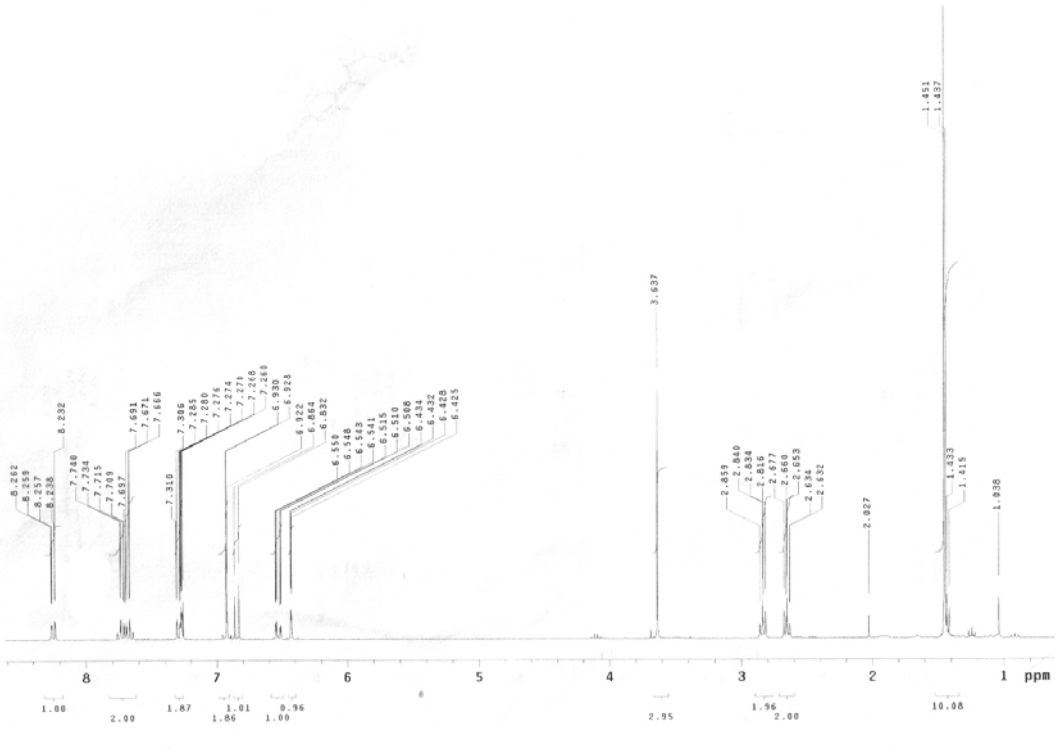

^{13}C NMR Spectrum of **3-56**

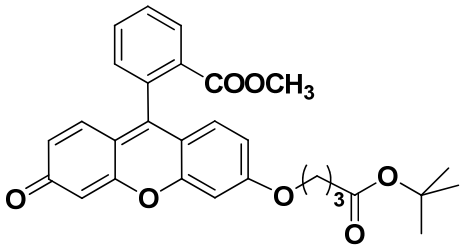

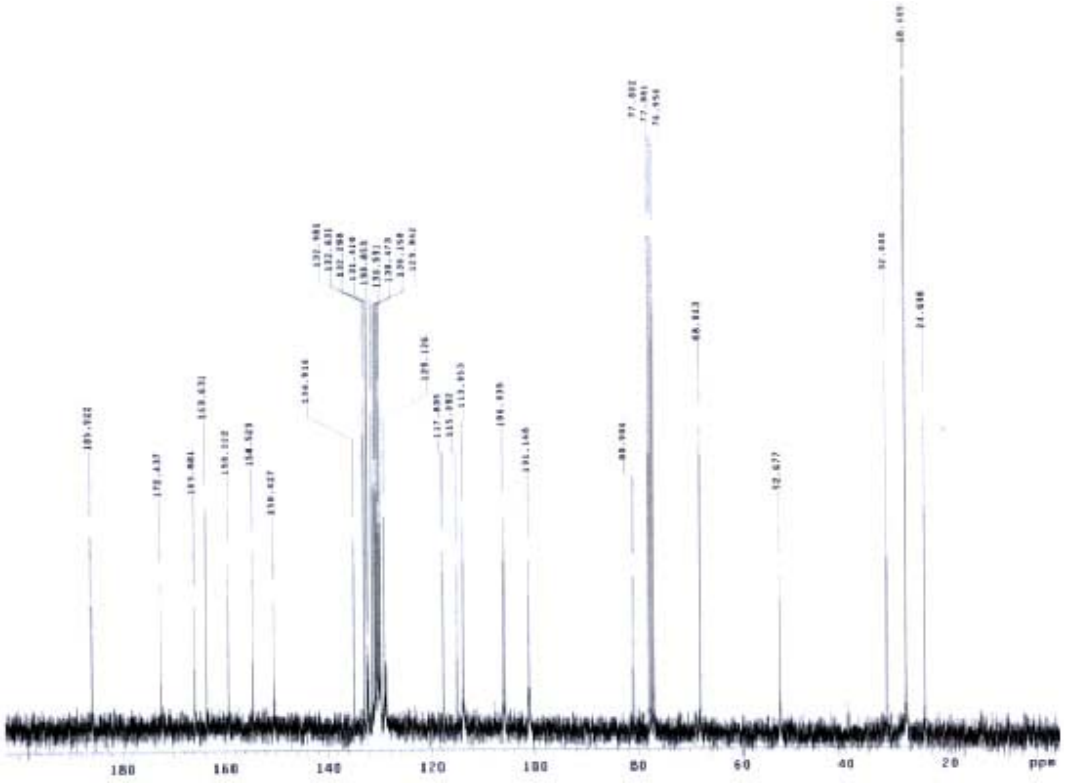

^{1}H NMR Spectrum of **3-57**

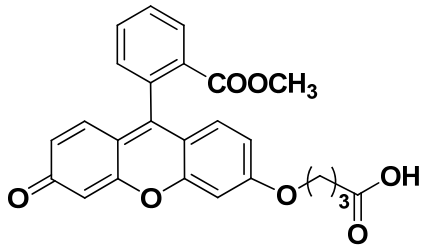

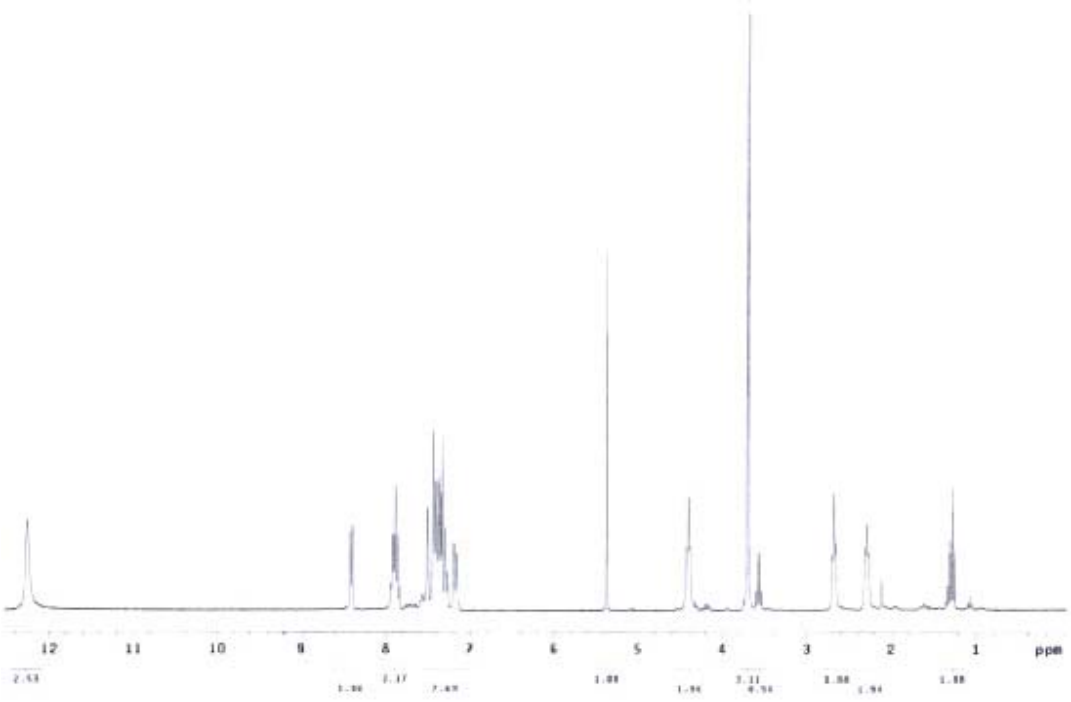

^{1}H NMR Spectrum of **3-58**

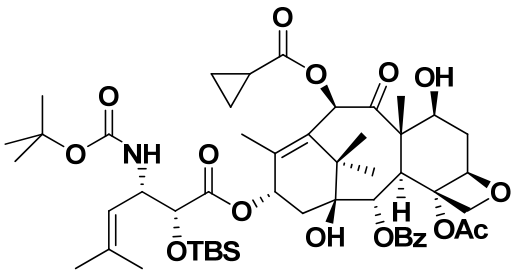

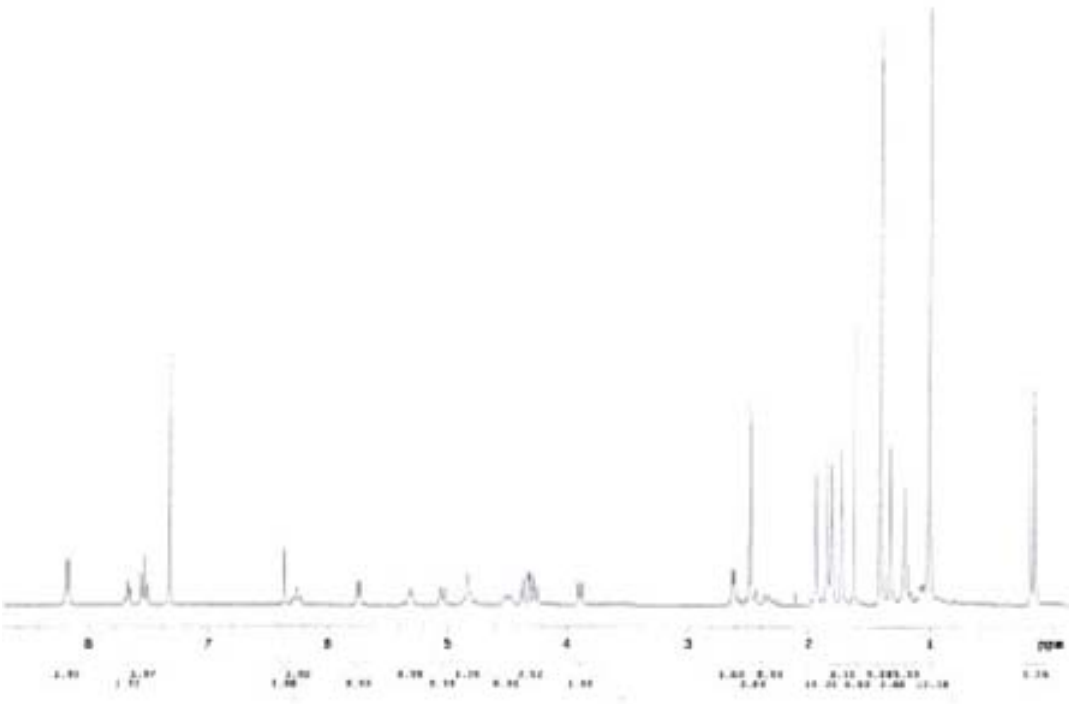

^{1}H NMR Spectrum of **3-59**

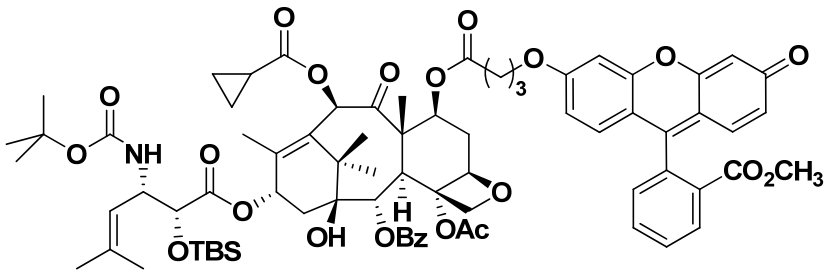

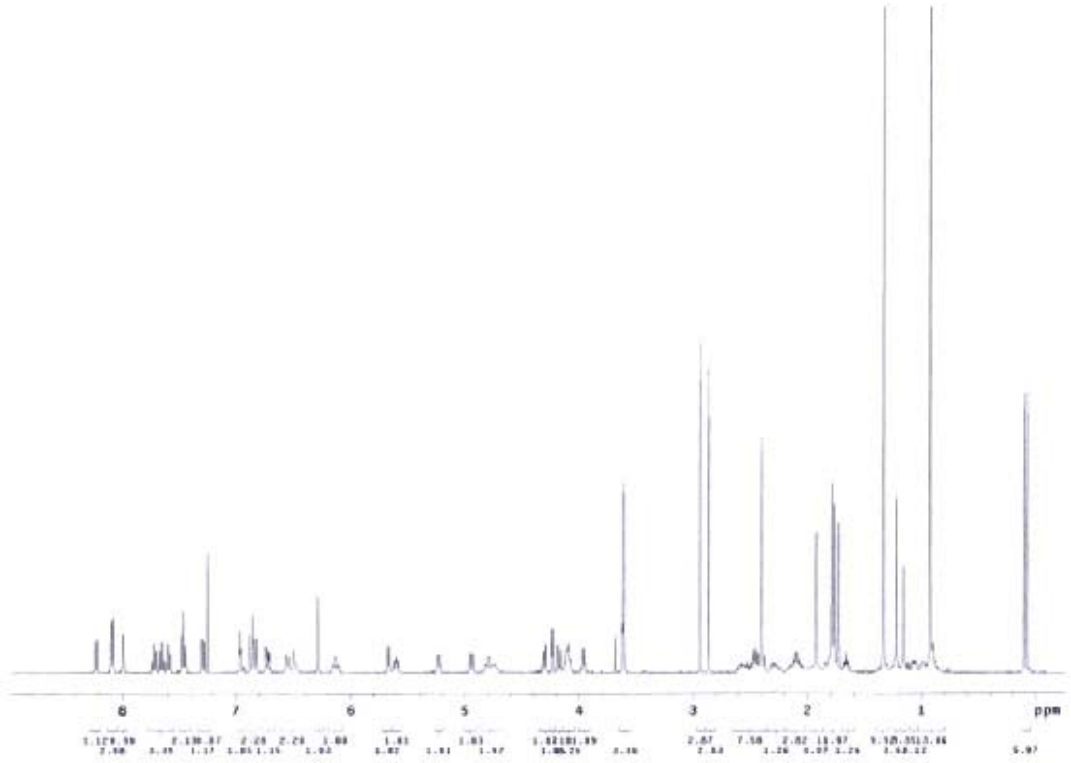

^{1}H NMR Spectrum of **3-60**

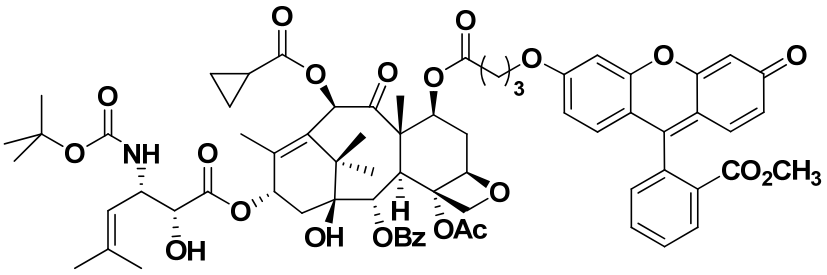

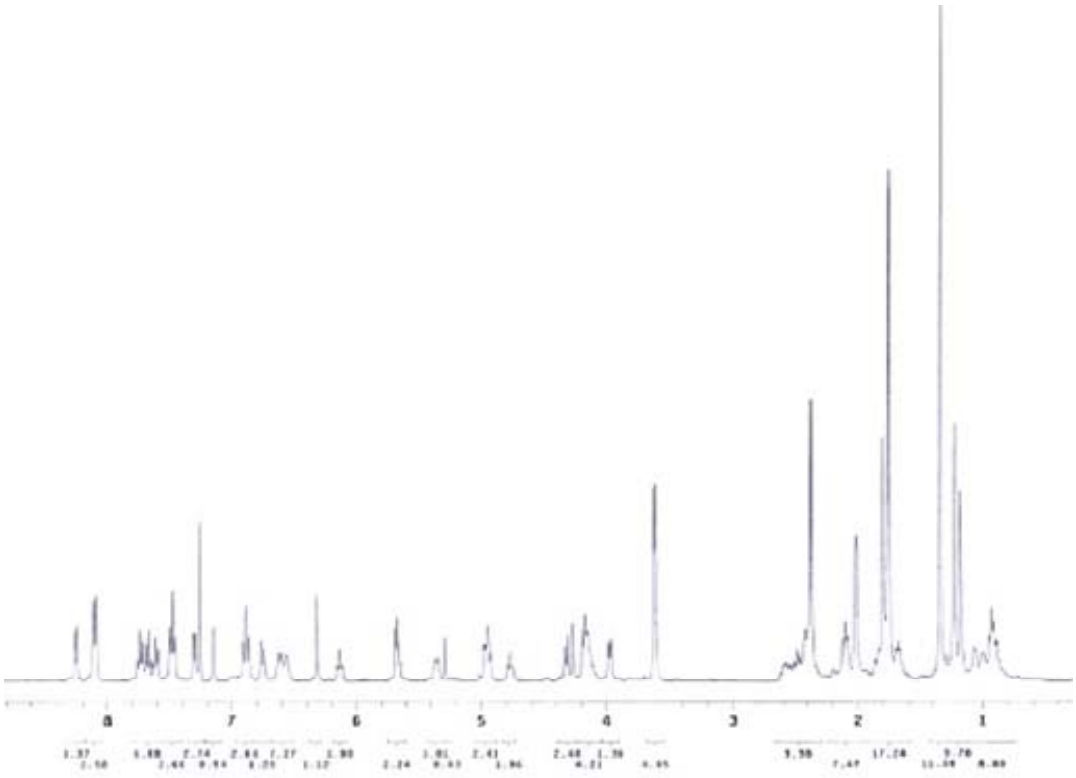

^{1}H NMR Spectrum of **3-62**

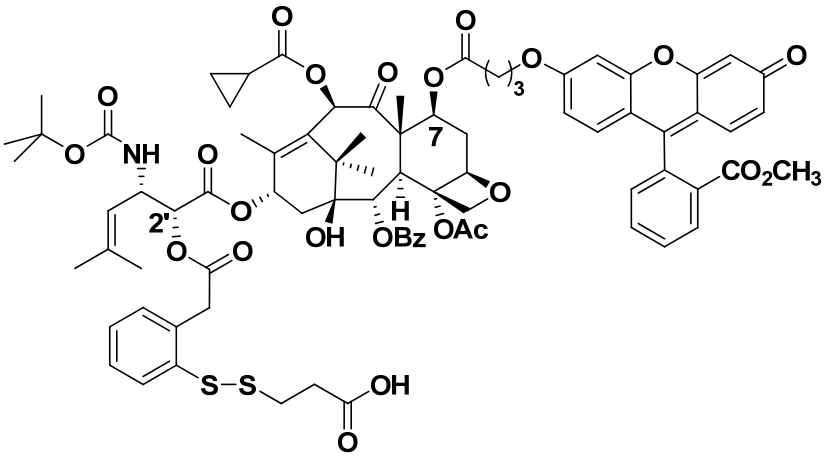

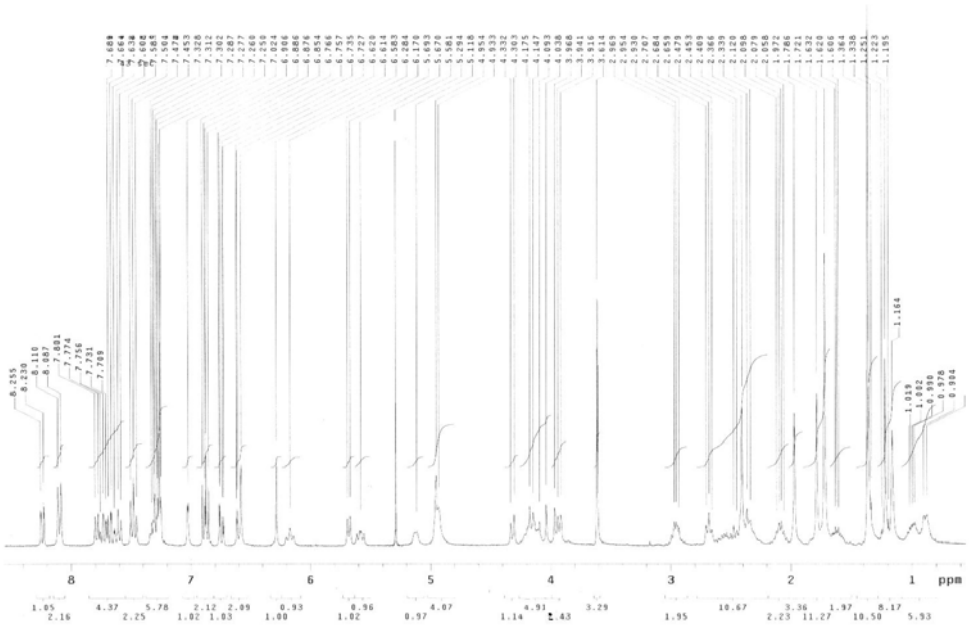

[1]H NMR Spectrum of **3-63**

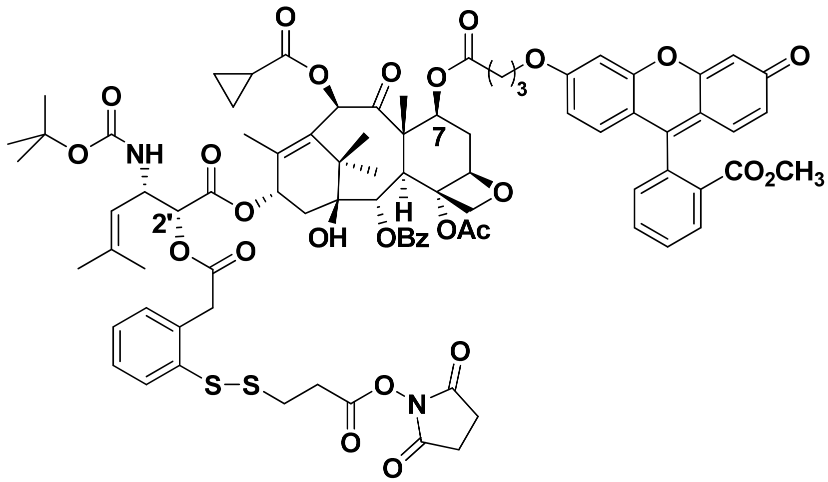

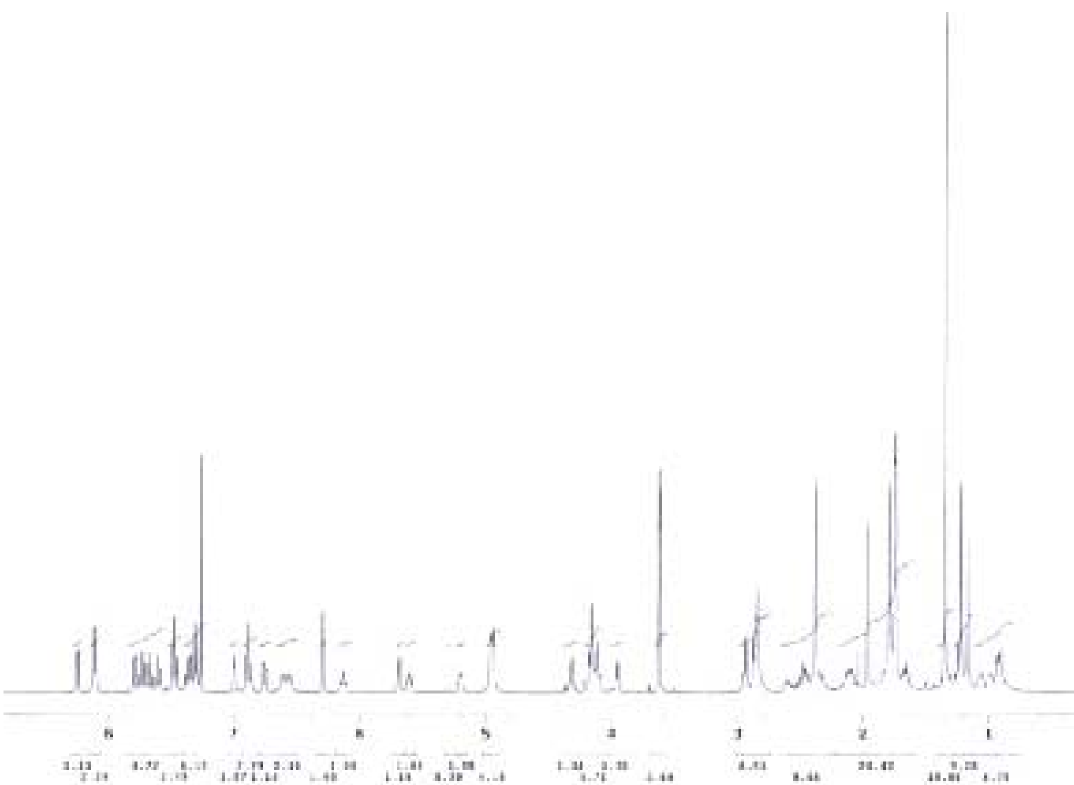

^{1}H NMR Spectrum of **3-64**

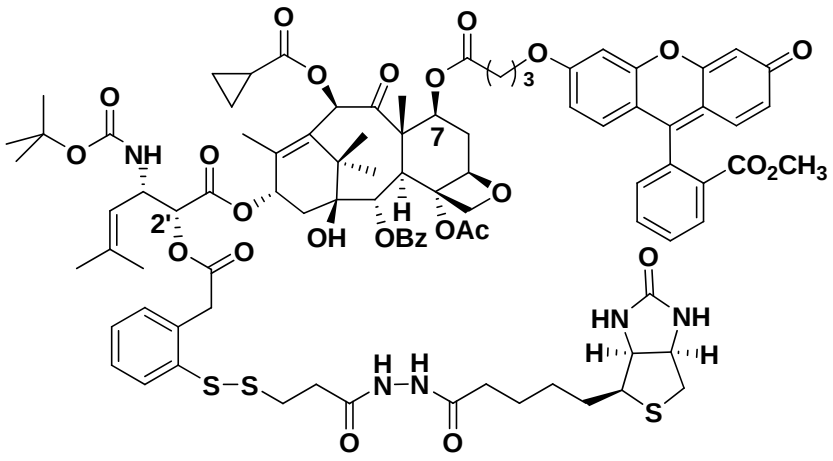

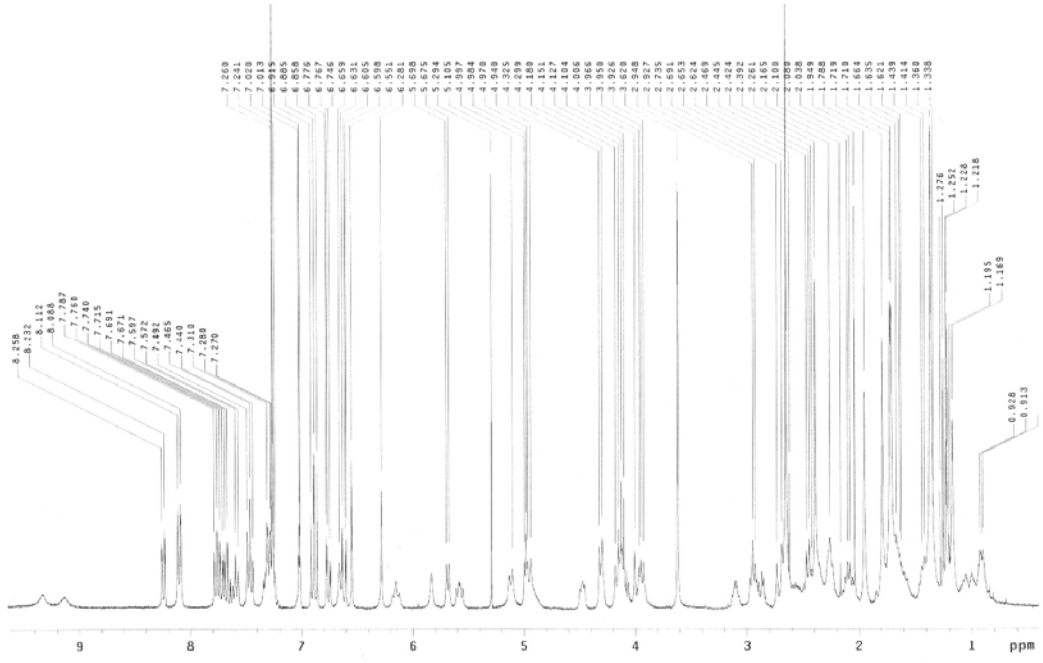

^{1}H NMR Spectrum of **3-65**